НАЦІОНАЛЬНА АКАДЕМІЯ НАУК УКРАЇНИ
ІНСТИТУТ МОЛЕКУЛЯРНОЇ БІОЛОГІЇ І ГЕНЕТИКИ

Кваліфікаційна наукова робота, підготовлена у формі доповіді за сукупністю наукових статей

ШАЛАК В'ЯЧЕСЛАВ ФЕДОРОВИЧ

УДК 577.112; 577.217.535

ДИСЕРТАЦІЯ

СТРУКТУРНО-ФУНКЦІОНАЛЬНА ОРГАНІЗАЦІЯ МАКРОМОЛЕКУЛЯРНИХ КОМПЛЕКСІВ І ЇХ КОМПОНЕНТІВ АПАРАТУ ЕЛОНГАЦІЇ ТРАНСЛЯЦІЇ У ССАВЦІВ

03.00.03 – Молекулярна біологія
Біологічні науки

Подається на здобуття наукового ступеня доктора біологічних наук

Дисертація містить результати власних досліджень. Використання ідей, результатів і текстів інших авторів мають посилання на відповідне джерело
_____ В.Ф. Шалак

Київ – 2025

АНОТАЦІЯ

Шалак В.Ф. Структурно-функціональна організація макромолекулярних комплексів і їх компонентів апарату елонгації трансляції у ссавців. – Кваліфікаційна наукова робота на правах рукопису, підготовлена у формі доповіді за сукупністю наукових статей.

Дисертація на здобуття наукового ступеня доктора біологічних наук за спеціальністю 03.00.03 - Молекулярна біологія. – Інститут молекулярної біології і генетики НАН України, Київ, 2025.

У дисертаційній роботі представлено широкомасштабні дослідження просторової структури і особливостей функціонування компонентів двох основних макромолекулярних комплексів, що працюють на дорибосомному етапі трансляції ссавців. Комплекс факторів елонгації eEF1B містить субодиниці eEF1Bα, eEF1Bβ і eEF1Bγ, що забезпечують обмін гуанінового нуклеотиду на молекулах eEF1A1 або eEF1A2, формуючи лабільний комплекс eEF1H. Комплекс аміноацил-тРНК синтетаз, які забезпечують синтез аміноацил-тРНК, містить 9 ферментів та 3 додаткових білка p18, p38, p43.

Метою роботи було з'ясування особливостей структурної організації і функціональної активності комплексів факторів елонгації трансляції eEF1B та eEF1H, та їх окремих компонентів, а також функціональних особливостей білка p43 – компонента макромолекулярного комплексу аміноацил-тРНК синтетаз ссавців.

У роботі було використано сукупність різноманітних **методів** для проведення **експериментальних досліджень** у галузі сучасної молекулярної біології і біохімії. Робота з рекомбінантною ДНК полягала у створені генетичних конструкцій, які потім експресували в бактеріях або в клітинах вищих еукаріот. Для створення генетичних конструкцій використовували стандартні молекулярно-біологічні методи, зокрема ПЛР ампліфікацію, рестрикцію і лігування ДНК фрагментів у відповідні вектори, аналіз рестрикційних фрагментів методом електрофорезу в агарозному гелі. Синтез цільових рекомбінантних білків перевіряли в екстрактах трансформованих бактерій або трансфікованих клітин

ссавців методом електрофорезу в поліакриламідному гелі за умов денатурації та/або вестерн-блот аналізом. Очищення цільових рекомбінантних білків з бактеріальних екстрактів проводили із застосуванням афінної та іон-обмінної хроматографії, а також гель фільтрації. Препарати нативних білків-паралогів eEF1A1 та eEF1A2 виділяли з печінки і м'язів кроля, відповідно, з використанням комбінації різних видів хроматографії, а саме аніон- і катіон-обмінної, гідроксилапатиту і гель фільтрації. Активність очищених eEF1A1 та eEF1A2 визначали в реакції [^{3}H]ГДФ/ГДФ обміну і трансляції полі(У) матриці очищеними 80S рибосомами у присутності [^{14}C]фенілаланіл-тРНК і фактора елонгації eEF2. Активність аміноацил-тРНК синтетаз визначали в реакції аміноацилювання тРНК у присутності відповідних [^{3}H] або [^{14}C] мічених амінокислот. Активність факторів обміну гуанінового нуклеотиду (eEF1Bα і eEF1Bβ) визначали по кінетиці [^{3}H]ГДФ/ГДФ обміну на молекулі eEF1A1 чи eEF1A2. Олігомерний стан досліджуваних білків і білкових комплексів визначали за допомогою гель фільтрації і аналітичного ультрацентрифугування. Формування білкових комплексів визначали за допомогою гель фільтрації і агарозного гель електрофорезу за нативних умов. Утворення комплексів між білками і радіоактивно міченою тРНК спостерігали за допомогою методу затримки в поліакриламідному гелі. Картування сайтів взаємодії між білками проводили з використанням різних вкорочених форм білків-партнерів, а також за допомогою методу воднево-дейтерієвого обміну (HDX) з наступним мас-спектрометричним аналізом пептидів. Вміст елементів вторинної структури N-кінцевого домену eEF1Bβ вимірювали за допомогою кругового дихроїзму. Внутрішньоклітинну локалізацію цільових білків злитих з зеленим флуоресцентним білком (GFP) визначали методом конфокальної мікроскопії живих клітин в культурі. Знаходження білків в цитоплазматичній і мітохондріальній фракціях підтверджували методом субклітинного фракціонування клітин з наступним вестерн-блот аналізом.

Просторові моделі білків створювали у програмі Modeller, після чого ці моделі вдосконалювали в ModRefiner і перевіряли на web-сервері MolProbity з подальшим їх покращенням на сервері з мінімізації енергії YASARA.

Молекулярний докінг між білками eEF1Bβ та eEF1Bγ проводили на web-сервері PatchDock. Симетричний докінг між мономерами eEF1Bβ моделювали на web-сервері SymmDock.

Отримані експериментальні результати виявили низку нових аспектів структурно-функціональної організації компонентів апарату трансляції ссавців зокрема відмінності просторової організації високо гомологічних білків-паралогів eEF1A1 та eEF1A2, неканонічних взаємодій фактора елонгації eEF1A1, четвертинної організації комплексу eEF1B, подвійної функціональної ролі білка p43 макромолекулярного комплексу аміноацил-тРНК синтетаз.

Вперше встановлено, що фактор елонгації трансляції eEF1A1 в ГДФ-зв'язаній формі має видовжену конформацію в розчині з радіусом гірації 5.2±0.2 нм, що більш ніж в 2 рази більше обрахованого радіусу гірації кристалографічної структури його білка-паралога eEF1A2 в комплексі з ГДФ.

Вперше розшифровано кристалічну структуру фактора елонгації трансляції eEF1A2, який складається з трьох доменів і має близьку до сферичної просторову конформацію. Встановлено, що іони Mg^{2+} не впливають на реакцію обміну гуанінового нуклеотиду на молекулі eEF1A2.

Вперше показано, що eEF1A1 у ГДФ-зв'язаній формі може утворювати неканонічний потрійний комплекс з деацильованою тРНК і четвертинний комплекс з фенілаланіл-тРНК синтетазою, а також збільшує початкову швидкість реакції, яку каталізує метіоніл-тРНК синтетаза.

Вперше виявлено взаємодію трансляційно-контрольованого білка пухлин (TCTP) з факторами елонгації трансляції eEF1A1 і субодиницею eEF1Bβ. Зв'язування TCTP з eEF1A1 призводить до зниження швидкості реакції як спонтанного, так і eEF1Bβ-опосередкованого обміну гуанінового нуклеотиду на молекулі eEF1A1.

Вперше детально досліджено структурну організацію факторів елонгації eEF1Bα, eEF1Bβ і eEF1Bγ, які утворюють макромолекулярний комплекс eEF1B. Визначено сайти взаємодії між субодиницями eEF1Bα і eEF1Bγ, eEF1Bβ і eEF1Bγ, і встановлено, що мотив «лейцинова застібка» eEF1Bβ відповідає за тримеризацію цього білка, а також всього комплексу eEF1B, який має структурну організацію

типу $(\alpha\beta\gamma)_3$. Показано, що eEF1B$(\alpha\beta\gamma)_3$ здатен зв'язувати до шести молекул eEF1A2, відповідно до кількості GEF-доменів в ньому.

Вперше розкрито механізм стимуляції активності eEF1Bα субодиницею eEF1Bγ при утворенні комплексу між ними. Конформація N-кінцевого домену eEF1Bα частково перешкоджає взаємодії eEF1A з GEF-доменом, що знижує швидкість обміну гуанінового нуклеотиду. Зв'язування N-кінцевих доменів eEF1Bα і eEF1Bγ усуває цей інгібіторний ефект.

Встановлено, що N-кінцевий домен білка p43 макромолекулярного комплексу аміноацил-тРНК синтетаз взаємодіє з аргініл-тРНК синтетазою. Показано, що p43 не впливає на каталітичні параметри аргініл-тРНК синтетази і не збільшує її спорідненість до відповідної тРНК. Отже, білок p43 не є кофактором для цього ферменту.

Встановлено, що інкубація макромолекулярного комплексу аміноацил-тРНК синтетаз з каспазою 7 *in vitro* призводить до розщеплення його p43 компоненту на два фрагменти. Його С-кінцевий фрагмент, який вивільняється з комплексу, є ідентичним EMAPII і здатен викликати хемотаксис моноцитів. Розщеплення p43 призводить до втрати його тРНК-зв'язувальної властивості.

Вперше виявлено, що індукція апоптозу в клітинах призводить до появи і вивільнення з клітин іншого протеолітичного фрагменту білка p43, названого p43(ARF), який на 40 амінокислот довший ніж EMAPII. Показано, що обидва p43(ARF) і EMAPII не індукували експресію Е-селектину на ендотеліальних клітинах (HUVEC), тоді як повнорозмірний p43 таку індукцію викликав. Протеоліз білка p43 дозволяє уникнути активації ендотеліальних клітин і, як наслідок, можливого розвитку запальної реакції в організмі.

Вперше ідентифіковано новий трансляційний продукт гена, який кодує білок p43. Цей продукт має мітохондріальну локалізацію і є на 9 амінокислот довшим ніж цитоплазматична ізоформа p43. Кількість мітохондріальної ізоформи складає приблизно 2% від загальної кількості p43 в клітині.

Ключові слова: тРНК, аміноацил-тРНК синтетази, G-білки, фактори обміну гуанінового нуклеотиду (GEF), фактори елонгації трансляції, мультибілкові

комплекси, білок-білкові взаємодії, білок-нуклеїнові взаємодії, цитокіни, EMAPII, клітинні сигнальні шляхи, канцерогенез, експресія генів, апоптоз.

SUMMARY

Shalak V.F. Structural and functional organization of the macromolecular complexes and their components of the mammalian translation elongation apparatus. This qualifying scientific work is a manuscript that is based on a collection of the author's scientific articles.

The thesis for the Degree of Doctor of Biological Sciences in Molecular Biology (03.00.03). – Institute of Molecular Biology and Genetics, National Academy of Science of Ukraine. Kyiv, 2025.

This thesis presents a large-scale study of structural organization and functional properties of the components of two major macromolecular complexes that operate at the pre-ribosomal stage of mammalian translation. The eEF1B elongation factor complex contains the eEF1Bα, eEF1Bβ, and eEF1Bγ subunits, which ensure the exchange of guanine nucleotide on eEF1A1 or eEF1A2 molecules, forming the transient eEF1H complex. The aminoacyl-tRNA synthetase complex, which performs the synthesis of aminoacyl-tRNAs, contains 9 enzymes and 3 auxiliary proteins p18, p38, p43.

The **aim of the study** was to elucidate the structural organization and functional activity of the eEF1B and eEF1H translation elongation factor complexes and their individual components, as well as the functional features of the p43 protein of the mammalian macromolecular aminoacyl-tRNA synthetase complex.

A set of different methods was used to conduct experimental research in the field of modern molecular biology and biochemistry. The work with recombinant DNA aimed to create the genetic constructs for expression either in bacteria or in higher eukaryotic cells. For this purpose, standard molecular biology methods were used, including PCR amplification, restriction and ligation of the DNA fragments into appropriate vectors, and analysis of the restriction patterns by agarose gel electrophoresis. The synthesis of the target recombinant proteins was checked in the extracts of transformed bacteria or

transfected mammalian cells by polyacrylamide gel electrophoresis under denaturing conditions and/or Western-blot analysis. Purification of the target recombinant proteins from bacterial extracts was performed by using affinity and ion exchange chromatography, as well as gel filtration. The native eEF1A1 and eEF1A2 paralog proteins were isolated from rabbit liver and muscle, respectively, using a combination of different types of chromatography, namely anion- and cation-exchange chromatography, hydroxylapatite, and gel filtration. The activity of the purified eEF1A1 and eEF1A2 proteins was determined in the [^{3}H]GDP/GDP exchange reaction and by translation of the poly(U)-programed 80S ribosomes in the presence of [^{14}C]phenylalanyl-tRNA and elongation factor eEF2. The activity of aminoacyl-tRNA synthetases was determined in the tRNA amino acylation reaction in the presence of the corresponding [^{3}H] or [^{14}C]-labeled amino acids. The activity of the guanine nucleotide exchange factors (eEF1Bα and eEF1Bβ) was estimated by the kinetics of [^{3}H]GDP/GDP exchange on the eEF1A1 or eEF1A2 molecule. The oligomeric state of the studied proteins and protein complexes was assessed by gel filtration and analytical ultracentrifugation. The formation of protein complexes was detected by gel filtration and agarose gel electrophoresis under native conditions. The complex formation between proteins and radiolabeled tRNA was observed by the polyacrylamide gel retardation method. Mapping of the interaction sites between proteins was performed using various truncated forms of the protein-partners and by the method of the hydrogen-deuterium exchange (HDX) followed by mass-spectrometry. The content of secondary structure elements of the eEF1Bβ N-terminal domain was measured by circular dichroism. The intracellular localization of target proteins fused to the green fluorescent protein (GFP) was determined by confocal microscopy of the living cells in culture. The presence of proteins in the cytoplasmic and mitochondrial fractions was confirmed by subcellular fractionation of cells followed by the Western-blot analysis.

Spatial models of proteins were created in the Modeller program, after which these models were improved in ModRefiner and checked on the MolProbity web server, followed by their improvement on the YASARA energy minimization server. Molecular docking between eEF1Bβ and eEF1Bγ proteins was performed on the PatchDock web

server and symmetric docking between eEF1Bβ monomers – on the SymmDock web server.

The obtained experimental results revealed a number of new aspects of the structural and functional organization of the components of mammalian translation apparatus, including differences in the spatial organization of the highly homologous eEF1A1 and eEF1A2 protein-paralogs, non-canonical interactions of the elongation factor eEF1A1, quaternary organization of the eEF1B complex, and the dual functional role of the p43 protein involved into macromolecular complex of aminoacyl-tRNA synthetases.

For the first time, it has been found that the translation elongation factor eEF1A1 in the GDF-bound form has an elongated conformation in solution with a radius of gyration 5.2±0.2 nm, which is more than 2 times larger than the radius of gyration of its eEF1A2 paralog.

The crystal structure of the translation elongation factor eEF1A2, which has a three-domain fold and a spherical-like spatial conformation, has been deciphered for the first time. It has been found that Mg^{2+} ions do not affect the guanine nucleotide exchange reaction on the eEF1A2 molecule.

For the first time, it has been demonstrated that eEF1A1 in the GDP-bound state can form a non-canonical ternary complex with deacylated tRNA and a quaternary complex with phenylalanyl-tRNA synthetase, and it also increases the initial rate of reaction catalyzed by methionyl-tRNA synthetase.

For the first time, the interaction of the translationally controlled tumor protein (TCTP) with the translation elongation factors eEF1A1 and eEF1Bβ subunit has been revealed. The binding of TCTP to eEF1A1 leads to a decrease of the reaction rate of both spontaneous and eEF1Bβ-mediated guanine nucleotide exchange on the eEF1A1 molecule.

The structural organization of the elongation factors eEF1Bα, eEF1Bβ and eEF1Bγ, which form the eEF1B macromolecular complex, has been studied in detail for the first time. The sites of interaction between eEF1Bα and eEF1Bγ, eEF1Bβ and eEF1Bγ have been identified, and it has been found that the “leucine zipper” motif of eEF1Bβ is responsible for the trimerization of this protein, as well as the entire eEF1B

complex, which has a structural organization of the $(\alpha\beta\gamma)_3$ type. It has been shown that eEF1B$(\alpha\beta\gamma)_3$ is able to bind up to six eEF1A2 molecules, according to the number of GEF domains in the complex.

For the first time, the mechanism of eEF1Bγ-mediated stimulation of eEF1Bα activity upon a complex formation between them has been revealed. The conformation of the N-terminal domain of eEF1Bα partially prevents the interaction of eEF1A with the GEF domain, which reduces the rate of guanine nucleotide exchange. Binding of the N-terminal domains of eEF1Bα and eEF1Bγ eliminates this inhibitory effect.

We have established that the p43 N-terminal domain interacts with arginyl-tRNA synthetase. We have shown that p43 does not affect the catalytic parameters of arginyl-tRNA synthetase and does not increase its affinity for the cognate tRNA. Thus, the p43 protein is not a cofactor for this enzyme.

We have shown that incubation of the macromolecular complex of aminoacyl-tRNA synthetases with caspase 7 *in vitro* leads to cleavage of its p43 component into two fragments. The resulting C-terminal fragment, identified as EMAPII, is released from the complex and exhibits cytokine-like activity in a monocyte chemotaxis assay, while the N-terminal fragment remains within the complex. Cleavage of p43 leads to the loss of its tRNA-binding property.

For the first time, it has been found that the induction of apoptosis in U937 cells leads to the appearance and release of another proteolytic fragment of p43 protein, named p43(ARF), which is 40 amino acids longer than EMAPII. It has been demonstrated that both p43(ARF) and EMAPII do not induce E-selectin expression in endothelial cells (HUVECs), whereas full-length p43 does. Proteolysis of p43 protein in apoptotic cells prevents activation of endothelial cells and, consequently, possible development of an inflammatory response in organism.

For the first time, a new translational product of the p43-encoding gene has been identified. It has mitochondrial localization and is 9 amino acids longer than the cytoplasmic isoform of p43. The amount of the mitochondrial isoform is approximately 2% of the total amount of p43 in the cell.

Keywords: tRNA, aminoacyl-tRNA synthetases, G-proteins, guanine nucleotide exchange factors (GEFs), translation elongation factors, multiprotein nanocomplexes, protein-protein interactions, protein-nucleic acid interactions, cytokines, EMAPII, cell signaling pathways, carcinogenesis, gene expression, apoptosis.

СПИСОК ОПУБЛІКОВАНИХ ПРАЦЬ ЗА ТЕМОЮ ДИСЕРТАЦІЇ

Основні наукові результати дисертації, опубліковані у фахових виданнях, які входять до першого і другого квартилів **(Q1** і **Q2)** відповідно до класифікації SCImago Journal and Country Rank або Journal Citation Reports:

1. Budkevich TV, Timchenko AA, Tiktopulo EI, Negrutskii BS, **Shalak VF**, Petrushenko ZM, Aksenov VL, Willumeit R, Kohlbrecher J, Serdyuk IN, El'skaya AV. (2002). Extended conformation of mammalian translation elongation factor 1A in solution. *Biochemistry*. 41(51):15342-9. doi:10.1021/bi026495h. (*Дисертантом особисто проведено очищення препаративних кількостей фактора елонгації трансляції eEF1A1 і визначено його функціональну активність in vitro різними тестами*).
2. Crepin T, **Shalak VF**, Yaremchuk AD, Vlasenko DO, McCarthy A, Negrutskii BS, Tukalo MA, El'skaya AV. (2014). Mammalian translation elongation factor eEF1A2: X-ray structure and new features of GDP/GTP exchange mechanism in higher eukaryotes. *Nucleic Acids Res*. 42(20):12939-48. doi:10.1093/nar/gku974. (*Дисертантом особисто проведено частину експериментальних досліджень, зокрема підготовку білка для кристалізації, експерименти по обміну гуанінового нуклеотиду, аналіз та інтерпретування отриманих результатів та їх підготовку до публікації*).
3. Petrushenko ZM, Budkevich TV, **Shalak VF**, Negrutskii BS, El'skaya AV. (2002). Novel complexes of mammalian translation elongation factor eEF1A*GDP with uncharged tRNA and aminoacyl-tRNA synthetase. Implications for tRNA channeling. *Eur J Biochem*. 269(19):4811-8. doi:10.1046/j.1432-1033.2002.03178.x. (*Дисертантом особисто проведено очищення препаративних кількостей*

фактора елонгації трансляції eEF1A1 і фенілаланіл-тРНК синтетази і визначено їх функціональну активність in vitro).

4. Kaminska M, **Shalak V**, Mirande M. (2001). The appended C-domain of human methionyl-tRNA synthetase has a tRNA-sequestering function. *Biochemistry.* 40(47):14309-16. doi:10.1021/bi015670b. (*Дисертантом особисто отримано високо очищений препарат фактора елонгації трансляції eEF1A1 проведено серію експериментів по взаємодії цього білка з метіоніл-тРНК синтетазою*).
5. Cans C, Passer BJ, **Shalak V**, Nancy-Portebois V, Crible V, Amzallag N, Allanic D, Tufino R, Argentini M, Moras D, Fiucci G, Goud B, Mirande M, Amson R, Telerman A. (2003). Translationally controlled tumor protein acts as a guanine nucleotide dissociation inhibitor on the translation elongation factor eEF1A. *Proc Natl Acad Sci U S A.* 100(24):13892-7. doi:10.1073/pnas.2335950100. (*Дисертантом особисто проведено частину експериментальних досліджень, зокрема експерименти по обміну гуанінового нуклеотиду, білок-білкові взаємодії (pull-down) аналіз та імуноблотинг, інтерпретування отриманих результатів та їх підготовку до публікації*).
6. Trosiuk TV, **Shalak VF**, Szczepanowski RH, Negrutskii BS, El'skaya AV. (2016). A non-catalytic N-terminal domain negatively influences the nucleotide exchange activity of translation elongation factor 1Bα. *FEBS J.* 283(3):484-97. doi:10.1111/febs.13599. (*Дисертант керував виконанням загального обсягу експериментальних досліджень, а також особисто виконав частину експериментальної роботи, аналіз та інтерпретування отриманих результатів, оформлення статті*).
7. Bondarchuk TV, Lozhko DM, **Shalak VF**, Fatalska A, Szczepanowski RH, Dadlez M, Negrutskii BS, El'skaya AV. (2019). The protein-binding N-terminal domain of human translation elongation factor 1Bβ possesses a dynamic α-helical structural organization. *Int J Biol Macromol*. 126:899-907. doi:10.1016/j.ijbiomac.2018.12.220 (*Дисертант керував виконанням загального обсягу експериментальних досліджень, а також особисто виконав частину експериментальної роботи, аналіз та інтерпретування отриманих результатів, оформлення статті*).

8. Bondarchuk TV, **Shalak VF**, Lozhko DM, Fatalska A, Szczepanowski RH, Liudkovska V, Tsuvariev OY, Dadlez M, El'skaya AV, Negrutskii BS. (2022). Quaternary organization of the human eEF1B complex reveals unique multi-GEF domain assembly. *Nucleic Acids Res.* 50(16):9490-9504. doi: 10.1093/nar/gkac685. (*Дисертант керував виконанням загального обсягу експериментальних досліджень, а також особисто виконав частину експериментальної роботи, аналіз та інтерпретування отриманих результатів, оформлення статті*).
9. Guigou L, **Shalak V**, Mirande M. (2004). The tRNA-interacting factor p43 associates with mammalian arginyl-tRNA synthetase but does not modify its tRNA aminoacylation properties. *Biochemistry*. 43(15):4592-600. doi10.1021/bi036150e. (*Дисертантом особисто проведено частину експериментальних досліджень, зокрема, очищення ферментів і вимірювання їх каталітичних характеристик, аналіз та інтерпретування отриманих результатів*).
10. **Shalak V**, Kaminska M, Mitnacht-Kraus R, Vandenabeele P, Clauss M, Mirande M. (2001). The EMAPII cytokine is released from the mammalian multisynthetase complex after cleavage of its p43/proEMAPII component. *J Biol Chem*. 276(26):23769-76. doi:10.1074/jbc. (*Дисертантом особисто проведено основні експериментальні дослідження з мультисинтетазним комплексом мишей, рекомбінантним білком p43 мишей і людини, аналіз результатів та їх підготовку до публікації*).
11. **Shalak V**, Guigou L, Kaminska M, Wautier MP, Wautier JL, Mirande M. (2007). Characterization of p43(ARF), a derivative of the p43 component of multiaminoacyl-tRNA synthetase complex released during apoptosis. *J Biol Chem.* 282(15):10935-43. doi:10.1074/jbc.M611737200 (*Дисертантом особисто проведено основну частину експериментальних досліджень, зокрема всю роботу з культурами клітин, імуноблотинг, взаємодію білків з мРНК, активацію ендотеліальних клітин, аналіз та інтерпретування отриманих результатів та їх підготовку до публікації*).
12. **Shalak V**, Kaminska M, Mirande M. (2009). Translation initiation from two in-frame AUGs generates mitochondrial and cytoplasmic forms of the p43 component of the multisynthetase complex. *Biochemistry.* 48(42):9959-68. doi:10.1021/bi901236g

(*Дисертантом особисто проведено більшу частину експериментальних досліджень, зокрема створення ДНК конструкцій, трансфекцію клітин і конфокальну мікроскопію, субклітинне фракціонування, аналіз та інтерпретування отриманих результатів та їх підготовку до публікації*).

Наукові праці, які засвідчують апробацію матеріалів дисертації:

1. **V. Shalak,** J.C. Robinson, P. Vandenabeele and M. Mirande. The p43 component of the multisynthetase complex is a precursor of the EMAP II cytokine. 18th International tRNA Workshop - "tRNA 2000". 2000. April 8-12. Queen's College, Cambrige, UK. *Публікація тез, постерна доповідь.*
2. M. Kaminska, **V. Shalak,** J.C. Robinson, P. Kerjan and M. Mirande. From protein synthesis to apoptosis. The p43 component of the multisynthetase complex: a molecular switch. 18th International tRNA Workshop - "tRNA 2000". 2000. April 8-12, Queen's College, Cambrige, UK. *Публікація тез, усна доповідь.*
3. M. Kaminska, **V. Shalak** and M. Mirande. Human methiony-tRNA synthetase is a processive enzyme. Asilomar Conference on Aminoacyl-tRNA synthetases in Biology, Medicine & Evolution. 2002. January 13-18. Pacific grove, CA, USA. *Публікація тез, постерна доповідь.*
4. M. Kaminska, M. Francin, **V. Shalak** and M. Mirande. Role of the general RNA-binding domains appended to mammalian aminoacyl-tRNA synthetases. 19th International tRNA Workshop. 2002. April 6-1. Shanghai, China. *Публікація тез, усна доповідь.*
5. **Vyacheslav Shalak**, Ludovic Guigou and Marc Mirande. The p43 subunit of the multi-aminoacyl-tRNA synthetase complex: structure and function. 20th International tRNA Workshop. 2003. October 2-7. Banz, Germany. *Публікація тез, постерна доповідь.*
6. **V. Shalak**, M.-P. Golinelli-Cohen, Ludovic Guigou and Marc Mirande. La machinerie traductionnele et l'apoptose: function duale d'un cofacteur des aminoacyl-tRNA synthetases. 5éme Rencontre sifrARN "ARN, le nouveau monde". 2004. Octobre 10 - 13. Arcachon, France. *Публікація тез, усна доповідь.*
7. **V. F. Shalak**, A.V. El'skaya, M. Mirande. The multi-aminoacyl-tRNA synthetase complex: link between protein synthesis and apoptosis. 5th Parnas Conference

"Molecular mechanisms of Cellular Signaling". 2005. April 26-29. Kyiv. Ukraine. *Публікація тез, усна доповідь.*

8. M. Kaminska, **V. Shalak**, S. Havrylenko, L. Guigou, R. Freguja and M. Mirande. Human aminoacyl-tRNA synthetases: role of the eukaryotic-specific, protein-protein and protein-RNA interaction domains. aaRS2008. International conference on aminoacyl-tRNA synthetase: from basic mechanisms to systems biology. September 7-11. 2008. Veyrier du Lac, France. *Публікація тез, постерна доповідь.*
9. V. V. Liudkovska, **V.F. Shalak**. Complex of translation elongation factors (eEF-1H): in vitro reconstitution from recombinant proteins. International life sciences' students' conference. August 19-23. 2009. Kyiv, Ukraine. *Публікація тез, усна доповідь.*
10. **V. Shalak**, V. Liudkovska, A. Timchenko, B. Negrutskii. Interaction between subunits of translation elongation factor 1B: two approaches to study their complexes in vitro. X Український біохімічний з'їзд. 13-17 вересня. 2010. м. Одеса, Україна. *Публікація тез, усна доповідь.*
11. Trosiuk T.V**., Shalak V. F.** Construction and expression of deletion mutants of translation elongation factors eEF1Bα, eEF1Bβ, eEF1Bγ. VII conference of Young Scientists of the Institute of Molecilar Biology and Genetics NAS of Ukraine. 28-29 May 2013. Kyiv, Ukraine. *Публікація тез, усна доповідь.*
12. Trosiuk T.V., **Shalak V. F.** The interaction of truncated forms of translation elongation factor eEF1Bγ with eEF1Bα and eEF1Bβ. VIII Conference of Young Scientists of Molecular Biology and Genetics NAS of Ukraine Dedicated to 90th anniversary of P.G. Kostyuk. 20-21 May 2014. Kyiv, Ukraine. *Публікація тез, усна доповідь.*
13. Trosiuk T.V., **Shalak V. F.** Dissection of translation elongation factor eEF1Bγ: creation of deletion mutants to study its interaction with protein partners in vitro. XI Український біохімічний конгрес. 6-10 жовтня 2014 р. м. Київ. *Публікація тез, усна доповідь*.
14. **V. Shalak**, R. Szczepanowski, L. Kapustian, J. Debski, L. Porubleva, T. Trosiuk, A. Nehelia, I. Shrubkovskij, M. Dadlez, M. Bochtler, B. Negrutskii. COMBIOM in

research of translation elongation factors. Combiom Final Scientific Meeting. 16-17 April 2015. Kyiv, Ukraine. *Публікація тез, усна доповідь.*

15. Bondarchuk T.V., **Shalak V.F.** Leucine-zipper motif is responsible for the multimerization of translation elongation factor 1Bβ. International Conference for the Young Scientists (CYS-2015), 21-25 September 2015, Kyiv, Ukraine. *Публікація тез, усна доповідь.*
16. Bondarchuk T. V., **Shalak V.F.** Structural and functional features of translation elongation factor 1B alpha. 41st FEBS congress "Molecular and systems biology for a better life", September 03-08, 2016, Ephesus/Kusadasi, Turkey. *Публікація тез, постерна доповідь.*
17. **В'ячеслав Шалак**, Тетяна Бондарчук. Неглобулярні білки з неструктурованими ділянками: точне визначення молекулярної маси, агрегатного стану і локалізації неструктурованих ділянок. XII Відкрита конференція молодих вчених ІМБГ НАН України. 15-16 травня 2018 року. м. Київ. *Публікація тез, ключова доповідь*.
18. T.V. Bondarchuk, **V.F. Shalak**, A. Fatalska, D.M. Lozhko, R.H. Shchepanovskyi, M. Dadlez, B.S. Negrutskii, A.V. El'skaya. The new model of structural organization of the human translation elongation complex eEF1B. XII Український біохімічний конгрес. 30 вересня-4 жовтня 2019 р. м. Тернопіль. Україна. *Публікація тез, усна доповідь.*

ЗМІСТ

ПЕРЕЛІК ОСНОВНИХ УМОВНИХ ПОЗНАЧЕНЬ

eEF1A – фактор елонгації трансляції 1А еукаріот, під загальною назвою якого об'єднано два паралоги **eEF1A1** і **eEF1A2**

eEF1B – комплекс факторів елонгації трансляції 1В еукаріот, до якого входять субодиниці α, β і γ.

eEF1Bα –субодиниця **α** фактора елонгації трансляції 1В еукаріот

eEF1Bβ –субодиниця **β** фактора елонгації трансляції 1В еукаріот

eEF1Bγ –субодиниця **γ** фактора елонгації трансляції 1В еукаріот

eEF1H – важка форма факторів елонгації трансляції 1 еукаріот, до складу якої входить комплекс eEF1B та паралоги eEF1A1 або eEF1A2

p43 – білок з молекулярною масою 43кДа у складі мультибілкового комплексу аміноацил-тРНК синтетаз

p43(ARF) – фрагмент білка p43, який утворюється і вивільняється з клітин під час апоптозу (apoptosis released factor).

EMAPII – протеїн (II), який активує ендотеліальні клітини і моноцити

p38 – білок з молекулярною масою 38 кДа у складі мультибілкового комплексу аміноацил-тРНК синтетаз

p18 – білок з молекулярною масою 18 кДа у складі мультибілкового комплексу аміноацил-тРНК синтетаз

ARS – аміноацил-тРНК синтетази

ValRS – валіл-тРНК синтетаза

ArgRS – аргініл-тРНК синтетаза

MetRS – метіоніл-тРНК синтетаза

тРНК – транспортна рибонуклеїнова кислота

ГДФ – гуанозин дифосфат

ГТФ – гуанозин трифосфат

GEF-домен – функціональний домен, який прискорює обмін гуанінового

нуклеотиду на молекулі **eEF1A**

кДа – кілодальтон

TCTP – трансляційно-контрольований білок пухлин

HUVEC – первинні ендотеліальні клітини пупкової вени людини

U937 – клітинна лінія про-моноцитів

HDX-MS – воднево-дейтерієвий обмін з мас-спектрометричним аналізом

ВСТУП

Актуальність теми. Апарат біосинтезу білка в еукаріотичній клітині є просторово і структурно компартменталізованим, що забезпечує високу ефективність його функціонування. Однією з характерних особливостей вищих еукаріотів є існування двох стабільних трансляційних мультибілкових комплексів, що містять аміноацил-тРНК синтетази (ARS) та фактори елонгації трансляції (eEF) (*Gomez et al., 2020, Le Sourd et al,. 2006*). Найбільший з цих комплексів має у своєму складі дев'ять аміноацил-тРНК синтетаз і три додаткових білка, названих p43, p38 і p18 (*Mirande et al., 1985*). До іншого стабільного комплексу входять валіл-тРНК синтетаза (VRS) і фактори елонгації трансляції α, β і γ групи eEF1B (*Bec et al., 1994*). Окрім цього, вважається, що в клітині певна кількість молекул комплексу eEF1B може існувати окремо. eEF1B і VRS-eEF1B можуть утворювати лабільні комплекси (відповідно eEF1H і VRS-eEF1H) при взаємодії з фактором eEF1A – ключовим G-білком циклу елонгації трансляції (*Sasikumar et al., 2012*). Існує два високогомологічних (97%) варіанти цього білка eEF1A1 і eEF1A2, які кодуються різними генами (*Lund et al., 1993*). Експресія їх є тканиноспеціфічною (*Lee et al., 1992, Knudsen et al., 1993*) і змінюється в процесі ембріонального розвитку організму (*Chambers et al., 1998*). eEF1A2 синтезується в нейронах, міоцитах і кардіоміоцитах, тоді як eEF1A1 – у всіх інших клітинах (*Kahns et al., 1998*). Було повідомлено, що eEF1A2 може виступати в ролі онкогену при розвитку раку яєчника і легенів (*Anand et al., 2002, Jia et al., 2021*). Важливо, що синтез цього білка не спостерігається в здорових тканинах цих органів. Окрім цього, відомо, що білки-паралоги eEF1A залучені до інших "нетрансляційних" процесів, як то перебудова цитоскелету, клітинний цикл, апоптоз, аутофагія, вірусна інфекція та інші, а також можуть бути пов'язаними з розвитком деяких патологічних станів організму (*детально розглянуто Negrutskii et al., 2023*). Отже, ґрунтовні дослідження відмінностей структурної організації eEF1A1 і eEF1A2 є необхідними як для чіткого розуміння їх ролі в процесі білкового синтезу, так і для аналізу потенційних механізмів виконання ними численних неканонічних функцій, а також для висвітлення їх участі в патологічних процесах, які можуть бути специфічними для кожного паралога.

Функція комплексу eEF1B в трансляції полягає у відновленні активної ГТФ-зв'язаної конформації факторів eEF1A1 і eEF1A2, необхідної для взаємодії з аміноацил-тРНК (*Merrick & Nyborg,* 2000, *Le Sourd et al., 2006*). Відомо, що субодиниці eEF1Bα і eEF1Bβ відповідають за ГДФ/ГТФ обмін, тоді як eEF1Bγ є структурним компонентом цього комплексу (*Andersen et al., 2003, Le Sourd et al,. 2006*). Важливо зазначити, що субодиниця eEF1Bγ підсилює активність eEF1Bα в 2-4 рази при утворенні комплексу між ними, але механізм такого впливу залишався невідомим (*Janssen et al., 1988, Bec et al., 1994*). Необхідно також зауважити, що у комплексі eEF1B з валіл-тРНК синтетазою може відбуватися безпосередня передача (channeling) валіл-тРНК від ферменту до eEF1A1*GTP з утворенням відповідного потрійного комплексу (*Negrutskii et al., 1999*).

На сьогоднішній день, структура макромолекулярного комплексу аміноацил-тРНК синтетаз, комплексів eEF1H, eEF1B і VRS-eEF1B є достеменно невизначеними. Це також стосується структури і функції їх окремих компонентів, зокрема субодиниць eEF1Bα, eEF1Bβ і eEF1Bγ, паралогів eEF1A1 і eEF1A2, які продовжують знаходитись у фокусі досліджень різних наукових груп у світі.

Білки макромолекулярного комплексу аміноацил-тРНК синтетаз p43, p38 і p18, окрім структурної ролі, можуть виконувати додаткові неканонічні функції. Зокрема, білок p43, крім того, що безпосередньо взаємодіє з аргініл- і глютамініл-тРНК синтетазами в комплексі (*Quevillon et al, 1999, Robinson et al, 2000, Fu et al., 2014*), може бути попередником прозапального цитокіну EMAPII (*Quevillon et al, 1997*), який, як повідомляється, впливає на активацію моноцитів і ендотеліальних клітин (*Kao et al.,1992*). Однак, молекулярні механізми вивільнення біологічно активних білків (або фрагментів білків) з макромолекулярного комплексу аміноацил-тРНК синтетаз залишаються нез'ясованими. Очевидно, що розуміння цих механізмів є важливим як з точки зору фундаментальної науки, так і прикладної біомедичної галузі.

Зв'язок роботи з науковими програмами, планами, темами. Дисертаційна робота відповідає основному плану фундаментальних досліджень, які проводились в лабораторії білкового синтезу, а після її реорганізації - у відділі структурної та функціональної протеоміки Інституту молекулярної біології і

генетики НАН України за такими бюджетними темами: «Роль неканонічних взаємодій компонентів трансляційного апарату в організації білкового синтезу у вищих еукаріотів» (2.2.4.9; №0101U009211, 2002–2005 рр), «Особливості функціонування та множинність форм фактора елонгації трансляції 1 вищих еукаріотів» (2.2.4.9, №0105U005340, 2006–2010 рр.), «Дослідження трансляційних нанокомплексів та їх компонентів» (2.2.4.9; №0110U000693, 2011–2015 рр), «Дослідження факторів елонгації трансляції ссавців у біосинтезі білка та інших клітинних процесах» (2.2.4.9, №0115U003744, 2016 - 2020 рр) та «Структурні та функціональні дослідження факторів елонгації трансляції вищих евкаріотів» (2.2.4.9; №0120U102238, 2021-2025 рр).

Мета дослідження: з'ясування особливостей структурної організації і функціональної активності комплексів факторів елонгації трансляції eEF1B та eEF1H, та їх окремих компонентів, а також функціональних особливостей білка p43 – компонента макромолекулярного комплексу аміноацил-тРНК синтетаз ссавців.

Завдання дослідження:

1. Охарактеризувати просторову організацію фактора елонгації трансляції eEF1A1 і його комплексу з деацильованою тРНК в розчині методом малокутового розсіювання нейтронів.
2. Встановити структуру фактора елонгації трансляції eEF1A2 методом рентген-структурного аналізу і визначити особливості реакції обміну гуанінового нуклеотиду на цьому білку.
3. Виявити утворення неканонічного комплексу і взаємодії фактора елонгації трансляції eEF1A1 з деацильованою тРНК, фенілаланіл- і метіоніл-тРНК синтетазами.
4. Визначити вплив трансляційно-контрольованого білка пухлин (TCTP) на активність фактора елонгації трансляції eEF1A1 в реакції обміну гуанінового нуклеотиду.
5. З'ясувати структурну організацію і функціональні особливості факторів елонгації трансляції eEF1Bα, eEF1Bβ і eEF1Bγ, які утворюють макромолекулярний комплекс eEF1B.

6. Визначити сайти взаємодії між eEF1Bα, eEF1Bβ і eEF1Bγ і побудувати модель просторової організації макромолекулярного комплексу eEF1B.
7. Охарактеризувати взаємодію білка p43 з аргініл-тРНК синтетазою і визначити його вплив на активність цього ферменту.
8. Визначити вплив каспази 7 на білок p43 в складі макромолекулярного комплексу аміноацил-тРНК синтетаз *in vitro*.
9. Охарактеризувати протеолітичний фрагмент білка p43, який утворюється і вивільняється з клітин U937 в процесі апоптозу.
10. Визначити внутрішньоклітинну локалізацію довгої ізоформи білка p43.

Об'єкт дослідження – фактори елонгації трансляції eEF1A1 і eEF1A2 вищих еукаріот, комплекс eEF1B людини, який складається з eEF1Bα, eEF1Bβ і eEF1Bγ субодиниць, білок p43 макромолекулярного комплексу аміноацил-тРНК синтетаз.

Предмет дослідження – особливості структурної організації факторів елонгації трансляції eEF1A1 і eEF1A2, їх функціональна активність, взаємодія з тРНК і білками-партнерами, просторова організація і функціональна активність комплексу eEF1B факторів елонгації трансляції і його окремих компонентів. Функція білка p43 макромолекулярного комплексу аміноацил-тРНК синтетаз в трансляції і його роль як попередника цитокін-подібних сигнальних молекул.

Методи дослідження включають підходи генної інженерії (сайт-спрямований мутагенез і клонування кДНК фрагментів, створення генетичних конструкцій для синтезу цільових білків і репортерних конструкцій), молекулярно-біологічні підходи (ПЛР, електрофорез ДНК в агарозному гелі, створення штамів-продуцентів на основі бактерій, дріжджів і клітин людини, вестерн-блот, *in vitro* та *in vivo* pull-down), біохімічні підходи (афінна, іонообмінна хроматографія білків, гель фільтрація, визначення активності ферментів в реакції аміноацилювання тРНК, визначення активності факторів елонгації трансляції в реакції обміну гуанінових нуклеотидів, *in vitro* трансляція, визначення цитокінової активності білків, електрофорез білків в нативних і денатуруючих умовах), біофізичні (рентген-структурний аналіз, аналітичне ультрацентрифугування білків, воднево-дейтерієвий обмін, круговий дихроїзм, спектрометрія), підходи клітинної біології

(культивування і трансфекція клітин в культурі, конфокальна мікроскопія), математичні підходи (моделювання просторової структури білків і білкових комплексів), статистичні підходи для кількісної обробки результатів з метою оцінки достовірності відмінностей (t - критерій Стьюдента).

Наукова новизна отриманих результатів. Вперше встановлено, що фактор елонгації трансляції eEF1A1 в ГДФ-зв'язаній формі має видовжену конформацію в розчині на відміну від його білка-паралога eEF1A2.

Вперше розшифровано кристалічну структуру фактора елонгації трансляції eEF1A2 і встановлено, що іони Mg^{2+} не впливають на реакцію обміну гуанінового нуклеотиду на цьому факторі.

Вперше показано, що eEF1A1 у ГДФ-зв'язаній формі може утворювати неканонічний потрійний комплекс з деацильованою тРНК і четвертинний комплекс з фенілаланіл-тРНК синтетазою, а також збільшує початкову швидкість реакції, яку каталізує метіоніл-тРНК синтетаза. Виявлено взаємодію трансляційно-контрольованого білка пухлин (TCTP) з факторами елонгації трансляції eEF1A1 і субодиницею eEF1Bβ, що призводить до зниження швидкості реакції як спонтанного обміну, так і eEF1Bβ-опосередкованого обміну гуанінового нуклеотиду на молекулі eEF1A1.

Вперше детально досліджено структурну організацію факторів елонгації eEF1Bα, eEF1Bβ і eEF1Bγ, які утворюють макромолекулярний комплекс eEF1B. Визначено сайти взаємодії між субодиницями eEF1Bα і eEF1Bγ, eEF1Bβ і eEF1Bγ, і встановлено, що структурний мотив типу «лейцинова застібка» eEF1Bβ відповідає за тримеризацію цього білка, а також всього комплексу eEF1B, який має структурну організацію типу $(\alpha\beta\gamma)_3$. Показано, що eEF1B$(\alpha\beta\gamma)_3$ здатен зв'язувати до шести молекул eEF1A2, відповідно до кількості GEF-доменів в ньому. Вперше розкрито механізм стимуляції активності eEF1Bα субодиницею eEF1Bγ при утворенні комплексу між ними.

Встановлено, що N-кінцевий домен білка p43 макромолекулярного комплексу аміноацил-тРНК синтетаз взаємодіє з аргініл-тРНК синтетазою. Показано, що p43 не впливає на каталітичні параметри аргініл-тРНК синтетази і

не збільшує її спорідненість до відповідної тРНК. Отже, білок p43 не є кофактором для цього ферменту.

Доведено, що інкубація макромолекулярного комплексу аміноацил-тРНК синтетаз з каспазою 7 *in vitro* призводить до розщеплення його p43 компоненту на два фрагменти. Його С-кінцевий фрагмент, який вивільняється з комплексу, є ідентичним EMAPII і здатен викликати хемотаксис моноцитів. Розщеплення p43 призводить до втрати його тРНК-зв'язувальної властивості.

Вперше виявлено, що індукція апоптозу в клітинах U937 призводить до появи і вивільнення з клітин іншого протеолітичного фрагменту білка p43, названого p43(ARF), який на 40 амінокислот довший ніж EMAPII. Показано, що обидва p43(ARF) і EMAPII не індукували експресію Е-селектину в ендотеліальних клітинах (HUVEC), тоді як повнорозмірний p43 таку індукцію викликав.

Вперше ідентифіковано новий трансляційний продукт гена, який кодує білок p43. Цей продукт має мітохондріальну локалізацію і є на 9 амінокислот довшим, ніж цитоплазматична ізоформа p43.

Практичне значення отриманих результатів. Результати представлені в дисертаційній роботі не тільки розширюють і поглиблюють сучасні теоретичні уявлення про функціонування апарату трансляції вищих еукаріот, але і мають практичне значення. Перш за все, розуміння відмінностей структурної організації і функціональної активності високогомологічних (97%) білків-паралогів eEF1A1 і eEF1A2 є важливим для розробки специфічних інгібіторів для eEF1A2, який вважається прото-онкогенним білком або eEF1A1, що є важливим компонентом системи розмноження РНК-вірусів. Окрім цього, існування взаємодії eEF1A1 і eEF1Bβ з трансляційно-контрольованим білком пухлин (TCTP) також пов'язує фактори елонгації трансляції з процесом злоякісної трансформації клітини. Така взаємодія може бути ще однією мішенню для розробки лікарських засобів нового покоління. Важливо зауважити, що білок p43 високомолекулярного комплексу аміноацил-тРНК синтетаз є попередником цитокін-подібних молекул, які можуть грати роль певних сигналів, що забезпечують ефективне видалення апоптозних клітин імунною системою, уникаючи розвитку запального процесу. Використання таких цитокін-подібних молекул може бути перспективним для зменшення

запального процесу в організмі. Матеріали дисертаційної роботи містять новітню наукову інформацію і, отже, використовуються в лекціях для навчання студентів і аспірантів різних біологічних спеціальностей, які слухають загальний чи спеціальний курс(и) з молекулярної біології, зокрема «Структура рибосом, етапи і регуляція біосинтезу білка», «Регуляція експресії генів на рівні трансляції».

Особистий внесок здобувача. Автором було проведено аналіз наукової літератури по проблематиці дисертаційної роботи, сформульовано мету і завдання дослідження. Автор особисто брав участь в отримані основної частини представлених в дисертації експериментальних результатів, їх аналізу, науковій інтерпретації, узагальненні і підготовці до публікації. Написання текстів статей і їх обговорення проводилось в тісній співпраці з іншими співавторами роботи.

Деякі експерименти були виконані разом зі співавторами опублікованих робіт, зокрема співробітниками Інституту молекулярної біології і генетики НАН України к.б.н. Будкевич Т.В., к.б.н. Петрушенко З.М., к.б.н. Яремчук А.Д., к.б.н. Бондарчук Т.В., Ложко Д.М., Власенко Д.О.

Експерименти по малокутовому розсіюванню нейтронів (SANS) проводили на базі інституту Пола Шререра, Швейцарія (Paul Scherrer Institute, Switzerland), керівники роботи д-р Колбрехер (Dr. J. Kohlbrecher) і проф. Сердюк І.Н. (Prof. I.N. Serdyuk).

Кристалізацію і рентген-структурний аналіз eEF1A2 проводили на базі Університету Гренобль Альпи, Франція (University of Grenoble Alpes, France) і Європейського синхротрону (European Synchrotron Radiation Facility), відповідальний за роботу д-р Т. Крепан (Dr. T. Crepin).

Дослідження взаємодії фактора елонгації трансляції eEF1A1 з метіоніл-тРНК синтетазою, TCTP, а також цикл робіт по функціональній ролі білка p43 високомолекулярного комплексу аміноацил-тРНК синтетаз проводились на базі Лабораторії ензимології і структурної біохімії, Франція (Laboratoire d'Enzymologie et Biochimie Structurales, CNRS, Gif-sur-Yvette, France), керівник групи д-р М. Міранд, члени групи, які брали участь у дослідженні і з якими автор має спільні публікації М. Камінська (M. Kaminska), Л. Гігу (L. Guigou), д-р К. Канс (Dr. C. Cans).

Дослідження воднево-дейтерієвого обміну білків з наступним мас-спектрометричним аналізом проводили на базі Інституту біохімії і біофізики Польської академії наук (Institute of Biochemistry and Biophysics, PAN, Poland), керівник лабораторії проф. М. Дадлез (Prof. M. Dadlez) за участі А. Фатальської (A. Fatalska).

Автор висловлює щиру подяку співробітникам Інституту молекулярної біології і генетики НАН України М. Вівчарик і Р. Ніколаєву за допомогу у вимірюванні спектрів кругового дихроїзму і флюоресценції білків.

Автор висловлює щиру подяку д-ру Р. Щепановському з Міжнародного Інституту молекулярної і клітинної біології, Польща (R. Szczepanowski, International Institute of Molecular and Cell Biology, Poland), за допомогу в проведені експериментів з аналітичного центрифугування.

Автор вдячний д-ру Марі-Поль Вот'є, Франція (Dr. Marie-Paule Wautier, Universite Paris 7/Institut National de la Transfusion Sanguine, France) за допомогу в проведенні тесту з активації ендотеліальних клітин (HUVEC).

Автор вдячний д-ру Риті Мітнах-Краус і проф. Матіасу Клаусу (Dr. Rita Mitnacht-Kraus and Prof. Matthias Clauss, Max-Planck-Institut, Germany) за проведення експерименту з активації моноцитів.

Автор щиро вдячний проф. Єльській Г.В. за постійну підтримку і слушні поради під час виконання цієї дисертаційної роботи.

Автор висловлює щиру подяку науковому консультанту проф. Негруцькому Б.С. за допомогу в обговоренні та підготовці матеріалів дисертаційної роботи.

Апробація результатів дисертації. Основні положення роботи доповідались на міжнародних і вітчизняних конференціях, зокрема 18th International tRNA Workshop - "tRNA 2000" (2000, Cambridge, UK), Asilomar Conference on Aminoacyl-tRNA synthetases in Biology, Medicine & Evolution (2002, Pacific Grove, USA), 19th International tRNA Workshop (2002, Shanghai, China); 20th International tRNA Workshop (2003, Banz, Germany), 5éme Rencontre sifrARN "ARN, le nouveau monde" (2004, Arcachon, France), 5th Parnas Conference "Molecular mechanisms of Cellular Signaling" (2005, Kyiv, Ukraine), aaRS2008. International conference on aminoacyl-tRNA synthetase: from basic mechanisms to systems biology.

(2008, Veyrier du Lac, France), International life sciences' students' conference (2009. Kyiv, Ukraine), X, XI і XII Українських біохімічних конгресах (2010, м. Одеса, 2014, м. Київ, 2019, м. Тернопіль, Україна), VII and VIII conferences of Young Scientists of the Institute of Molecular Biology and Genetics NAS of Ukraine (2013, 2014, Kyiv, Ukraine), COMBIOM in research of translation elongation factors. Combiom Final Scientific Meeting (2015, Kyiv, Ukraine), International Conference for the Young Scientists (CYS-2015) (2015, Kyiv, Ukraine), 41st FEBS congress "Molecular and systems biology for a better life" (2016, Ephesus/Kusadasi, Turkey), XII Відкритій конференцій молодих вчених ІМБГ НАН України (2018, м. Київ).

Публікації. Результати дисертації викладено у 12 статтях які входять до першого і другого квартилів **(Q1** і **Q2)** відповідно до класифікації SCImago Journal and Country Rank або Journal Citation Reports та 18 тезах міжнародних і вітчизняних конференцій та з'їздів.

Структура та обсяг дисертації. Дисертація складається з анотації, вступу, основної частини, яка має три розділи, висновків і додатку. Обсяг дисертації становить 169 сторінок.

РОЗДІЛ 1

СТРУКТУРНА ОРГАНІЗАЦІЯ eEF1A1 та eEF1A2 – ВИСОКОГОМОЛОГІЧНИХ ПАРАЛОГІВ ФАКТОРА ЕЛОНГАЦІЇ ТРАНСЛЯЦІЇ ССАВЦІВ. НЕКАНОНІЧНІ ВЗАЄМОДІЇ eEF1A1

1.1. Некомпактна просторова організація фактора елонгації трансляції eEF1A1 в розчині

15342 *Biochemistry* **2002,** *41,* 15342−15349

Extended Conformation of Mammalian Translation Elongation Factor 1A in Solution†

T. V. Budkevich,‡ A. A. Timchenko,§ E. I. Tiktopulo,§ B. S. Negrutskii,‡ V. F. Shalak,‡ Z. M. Petrushenko,‡ V. L. Aksenov,|| R. Willumeit,⊥ J. Kohlbrecher,# I. N. Serdyuk,§ and A. V. El'skaya*,‡

Institute of Molecular Biology and Genetics, National Academy of Sciences, 150 Zabolotnogo Street, Kiev, 03143 Ukraine, Institute of Protein Research, Russian Academy of Sciences, Pushchino, Russia, Neutron Physics Laboratory, JINR, Dubna, Russia, GKSS Research Center, Geesthacht, Germany, and Paul Scherrer Institute, Villingen, Switzerland

Received July 23, 2002; Revised Manuscript Received October 22, 2002

ABSTRACT: The conformation of mammalian elongation factor eEF1A in solution was examined by the small angle neutron scattering and scanning microcalorimetry. We have found that in contrast to the bacterial analogue the eEF1A molecule has no fixed rigid structure in solution. The radius of gyration of the eEF1A molecule (5.2 nm) is much greater than that of prokaryotic EF1A. The specific heat of denaturation is considerably lower for eEF1A than for EF1A, suggesting that the eEF1A conformation is significantly more disordered. Despite its flexible conformation, eEF1A is found to be highly active in different functional tests. According to the neutron scattering data, eEF1A becomes much more compact in the complex with uncharged tRNA. The absence of a rigid structure and the possibility of large conformational change upon interaction with a partner molecule could be important for eEF1A functioning in channeled protein synthesis and/or for the well-known capability of the protein to interact with different ligands besides the translational components.

The eukaryotic translation elongation factor eEF1A[1] (formerly EF-1α) is a functional analogue of bacterial factor EF1A (formerly EF-Tu). The function of EF1A in prokaryotic cells is well studied. EF1A·GTP delivers the elongator aminoacyl-tRNA to the ribosome and promotes the accurate interaction of the tRNA anticodon with the codon of mRNA located at the ribosomal A-site. Following the codon−anticodon recognition, hydrolysis of GTP in the complex with EF1A takes place. As a result, the factor affinity for aminoacyl-tRNA and ribosome is lost. EF1A·GDP leaves the ribosome, and after the GDP/GTP exchange catalyzed by special factor EF1B (formerly EF-Ts), the protein can participate in the next elongation cycle.

Though the basic principles of the eEF1A functioning are similar to those of EF1A, there are some differences in the action of prokaryotic and eukaryotic proteins (*1*). One of the reasons may be the compartmentalization of the translation apparatus (*2*) serving as a structural basis for tRNA/aminoacyl-tRNA channeling during protein synthesis in mammalian cells (*3*). No indication of compartmentalization and channeling was observed in prokaryotic protein synthesis.

The channeling or vectorial transfer of tRNA/aminoacyl-tRNA means its transportation from the site of synthesis (aminoacyl-tRNA synthetase) to the site of utilization (ribosome) in such a way that aminoacyl-tRNA is never free and always remains bound to some protein(s) or ribosome (*4*). One of the noncanonical complexes thought to mediate the channeling of tRNA in mammalian cells is the [eEF1A·GDP·deacylated tRNA] complex (*5*). This complex was assumed to appear due to the acceptance of deacylated tRNA from the E-site of 80S ribosome by eEF1A·GDP (*1*). The putative function of this complex is to deliver tRNA from the ribosomal exit site to the aminoacyl-tRNA synthetase for subsequent recharging (*1*). The nonrandom, specific character of [eEF1A·GDP·tRNA] complex formation demonstrated by nuclease and chemical modification footprinting assay revealed a similarity of tRNA and aminoacyl-tRNA sites involved into the interaction with eEF1A·GDP and EF1A·GDPPNP, respectively (*5*, *6*).

Structural studies on EF1A involved in the various complexes with GDP or GTP/GDPPNP, aminoacyl-tRNA, and the exchange factor EF1B have provided an almost complete understanding of the molecular details of the EF1A functioning beyond the ribosome (*6*−*11*). Factor EF1A from *Escherichia coli* has the molecular mass of 43.15 kDa (*12*). The crystal structure of the protein complexed with GDP is known for trypsin-modified and native EF1A. The trypsin-modified EF1A molecule (*13*) consists of three distinct globular domains, connected by flexible interconnecting peptides, like beads on a string. The three domains form a flattened triangular shape of 7.5 nm by 5.0 nm by 3.0 nm. The theoretical radius of gyration calculated for such three-axis ellipsoid is 2.124 nm. The native EF1A·GDP molecule (*11*) has overall dimensions of 5.7 nm by 5.1 nm by 7.8 nm.

† This work was supported by International Association for the Promotion of Cooperation with Scientists from the New Independent States of the Former Soviet Union (INTAS) Grant 96-1594 and by Ministry for Science and Technologies of Ukraine Grant 5.7/0003.

* Corresponding author. E-mail: elskaya@biosensor.kiev.ua.
‡ Institute of Molecular Biology and Genetics.
§ Institute of Protein Research.
|| JINR.
⊥ GKSS Research Center.
Paul Scherrer Institute.

[1] Abbreviations: eEF1A, eukaryotic translation elongation factor 1A (formerly EF-1α); EF1A, prokaryotic translation elongation factor 1A (formerly EF-Tu); DTT, dithiothreitol.

10.1021/bi026495h CCC: $22.00 © 2002 American Chemical Society
Published on Web 11/28/2002

The theoretical radius of gyration calculated for such three-axis ellipsoid is 2.347 nm; the theoretical radius of gyration calculated with the CRYSOL program is 2.354 nm (*14*). According to the crystallographic data domain I (nucleotide-binding domain) is connected with domain II by a 1.6 nm long peptide. Domain III is connected with domain I by a short extended stretch of the polypeptide (*11*).

The solution structure of EF1A from *E. coli* was studied by small-angle neutron scattering using the procedure of triple isotopic substitution, and the radius of gyration was found equal to 2.39 nm (*15*). It should be mentioned that in the absence of GDP EF1A from *E. coli* is not stable; it is inactivated at 40 °C, but the thermal stability is strongly increased upon the addition of GDP (*16*). The rate of hydrogen/deuterium exchange for the free EF1A from *E. coli* at all pH values and temperatures used is higher than that for the GTP-bound or GDP-bound EF1A (*16*).

The crystal structures are also known for EF1A·GTP from *Thermus aquaticus* (*7*) and *Thermus thermophilus* (*8*). Molecular masses are 45.3 kDa (*17*) and 44.8 kDa (*18*), respectively. The polypeptide chain is folded into three domains, the overall structure of which is very close to that of EF1A·GDP from *E. coli.* The theoretical radius of gyration calculated with the CRYSOL program for EF1A·GTP from *T. aquaticus* is 2.165 nm. Contrary to EF1A from *E. coli*, the thermal stability of EF1A from *T. thermophilus* only slightly depends on the presence of GDP in the molecule. The free EF1A and EF1A·GDP from *T. thermophilus* have an almost equal rate of hydrogen/deuterium exchange (*16*).

GDP/GTP exchange changes mutual positions of the domains toward a more compact state, demonstrating the high plasticity of EF1A (*7*, *8*). The two parts of the molecule, one of them corresponding to domain I and another comprising domains II and III, move toward each other as rigid bodies. Domain II moves along with domain III and forms a largely polar interface with domain I. It was shown that binding of the aminoacyl-tRNA occurs in a cleft formed between the parts of EF1A·GTP (*6*). The ternary complex consisting of yeast phenylalanyl-tRNA, *T. aquaticus* elongation factor EF1A, and GDPPNP is elongated (11.5 nm by 4.0 nm by 6.4 nm) and has an overall shape resembling a corkscrew. The theoretical radius of gyration calculated from such three-axis ellipsoid is 3.075 nm. It is assumed that interaction of EF1A·GTP with the aminoacyl-tRNA slightly compresses the protein molecule (*6*, *19*).

The structure of eEF1A unlike its prokaryotic counterpart is poorly understood. The X-ray structure of the eEF1A-like elongation factor in complex with GDP from the archaeon *Sulfolobus solfataricus* (molecular mass 48.5 kDa) has been described (*20*). The structure of the complex exhibits a triangular shape with a peculiar large hole, located at one side of the molecule. The polypeptide chain (nine amino acid residues) joins domain I and domain II. This connecting peptide adopts a rather rigid structure, despite the absence of stabilizing interactions with the rest of the protein. The theoretical radius of gyration of the protein calculated with the CRYSOL program is 2.549 nm.

Recently (*21*), X-ray data have been published for the yeast eEF1A (molecular mass 50 kDa) crystallized in a complex with a fragment of the nucleotide-exchanging subunit eEF1Bα (molecular mass 11 kDa). As expected, eEF1A contains three structural domains similar to EF1A. The complex has overall dimensions of 7.6 nm by 6.7 nm by 5.2 nm. The theoretical radius of gyration calculated for this spheroid is 2.546 nm.

At present there is no information on the crystal or solution structure of mammalian eEF1A. It is not known how the conformation of eEF1A is affected by its interaction with tRNA either. To address the issues, we have analyzed here the structure of both rabbit liver eEF1A·GDP and its complex with tRNA in solution by the neutron scattering and microcalorimetry methods. We have found that rabbit liver eEF1A has a considerably more disordered conformation than its prokaryotic analogue. The conformation of eEF1A becomes significantly more compact during the interaction with tRNA. The eEF1A molecule is hypothesized to adopt an extended conformation due to the loss of the association between domains I and III. The interaction is renewed upon addition of the biological ligand (tRNA) leading to significant compactization of the protein.

EXPERIMENTAL PROCEDURES

Isolation and Characterization of eEF1A. eEF1A was purified from rabbit liver using a combination of gel filtration, ion-exchange, and hydroxyapatite chromatographies in the presence of 25% glycerol and 20 μM GDP as described previously (*22*). GDP/[^{3}H]GDP exchange in the eEF1A molecule was carried out as in ref *23*. The eEF1A ability to support the poly(U)-dependent translation in the mammalian cell-free system assembled from individual components was investigated as described (*24*).

The effect of eEF1A·GTP on the spontaneous deacylation of aminoacyl-tRNA was studied at 25 °C in 110 μL of 70 mM imidazole, pH 7.0, 50 mM NH_4Cl, 10 mM $MgCl_2$, 2 mM DTT, 10% glycerol, 0.2 mM GTP, and 2.7 μM [^{14}C]-Leu-tRNA^{Leu} (from beef liver). At definite time points (0, 0.5, 1, 2 and 3 h) the 20 μL aliquots were immersed into 1 mL of ice-cold 10% TCA. The mixtures were filtered through GF/C (Whatman) and washed twice with 5% cold TCA. The radioactivity of dried filters was counted using toluene-based scintillation fluid.

The concentration of eEF1A was measured by the conventional procedure (*25*) using bovine serum albumin as a standard.

Isolation of tRNA. Total tRNA was isolated from rabbit liver as described (*26*). The tRNA preparation enriched with tRNA^{Val} was purified by HPLC chromatography using an ion-exchange DEAE column (Phenomenex). tRNA^{Val} constituted about 45% of the tRNA preparation.

Isolation and Characterization of EF1A from T. thermophilus. The elongation factor EF1A purification from *T. thermophilus* was carried out as described (*27*). The crude cell-free extract was a kind gift of Dr. M. Garber (Institute of Protein Research, RAS, Pushchino). EF1A free from nucleotide was prepared as in ref *28*. The EF1A concentration was measured using a molar extinction coefficient $\epsilon_{280} = 32900\ M^{-1}\ cm^{-1}$.

Scanning Microcalorimetry. Calorimetric measurements were done on a precision scanning microcalorimeter SCAL-1 (Scal Co. Ltd., Pushchino, Russia) with glass cells (volume 0.3 mL) at scanning rate of 1.0 K/min (*29*). Degassing during the calorimetric experiments was prevented by maintaining an additional constant pressure of 3.0 atm in the cells.

Before the measurements all samples were dialyzed overnight against the corresponding buffer. The concentration of protein used in the calorimetric experiments was in the range of 0.7−1.0 mg/mL. A typical value of 0.74 cm^3/g for the partial specific volume for globular proteins was accepted. The analyses of the heat capacity curves were undertaken using the fitting routine based on the two-state transition (*30*).

Neutron Scattering. Two neutron scattering methods were applied during this study: small angle neutron scattering (SANS) in a H_2O−solvent and polarization-dependent neutron scattering in a solvent containing 39% *h*-glycerol, 15% *d*-glycerol, and 0.8% Cr(V)-EHBA [sodium bis(2-ethyl-2-hydroxybutyrato)oxochromate(V) monohydrate {Na[Cr-$(C_6H_{10}O_3)_2$]·H_2O}] diluted in the deuterated D_2O−sample solution.

The small angle neutron scattering experiments were carried out on the SANS camera of Paul Scherrer Institute (Switzerland) at the wavelength of 0.6 nm. The quartz cuvette of 1 mm thickness was thermostated at 4 °C. The range of scattered vectors was 0.1−2.5 nm^{-1}. The raw data were corrected on the detector sensitivity and normalized to the absolute scale by using the scattering of light water at the same experimental conditions.

The stoichiometry of the [eEF1A·GDP·tRNA] complex was determined from the value of the initial ordinate $I(0)/C$ on a Guinier plot. It is known that

$$I(0)/C \sim \sum C_i M_i (v_i \Delta\rho_i)^2 / \sum C_i \qquad (1)$$

where C_i is the weight concentration of *i*th component, M_i is the molecular mass, v_i is the partial specific volume, and $\Delta\rho_i$ is the excess of scattering density.

For eEF1A and tRNA $v = 0.74$ cm^3/g and $v = 0.55$ cm^3/g and $\Delta\rho = 2.0 \times 10^{-14}$ cm/Å^3 and $\Delta\rho = 3.8 \times 10^{-14}$ cm/Å^3, respectively. Taking into account the high affinity of eEF1A·GDP for deacylated tRNA (*31*) and using $M_{eEF1A}/M_{tRNA} \sim 2$, one can estimate the value of $I(0)/C$ for a mixture of eEF1A and tRNA.

The polarization-dependent neutron scattering experiments were performed using the SANS-1 beam line of the GKSS Research Center as described earlier (*32*). The idea was to create contrast variation only by changing the polarization of the hydrogen atoms (spin contrast variation). This has the great advantage that systematic errors from different samples can be neglected since only one sample is needed. In principle, it should even be possible to find a matching polarization for either protein or RNA contributions of the scattering.

For the polarization-dependent measurements the sample plate was cooled to approximately 120 mK in a $^3He/^4He$ dilution refrigerator. Following the procedure of dynamic nuclear polarization the hydrogen (=proton) spins in the sample were aligned with respect to the external magnetic field of 2.5 T up to a maximum negative polarization, and polarization-dependent neutron scattering data were taken.

The sample with eEF1A (10 mg/mL) was measured at proton polarization $P_H = \pm 60\%, \pm 50\%, \pm 30\%$ and in the unpolarized case giving data for seven different contrast conditions. The sample containing tRNA (2 mg/mL) was measured only at zero polarization. In the case of the [eEF1A·GDP·tRNA] complex five different contrast conditions were obtained: $P_H = 0\%, \pm 40\%$, and $\pm 28\%$. In all cases the data were taken at three different distances with 0.85 nm neutrons.

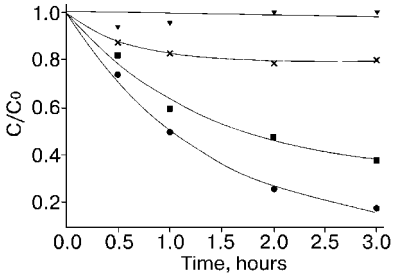

FIGURE 1: Influence of eEF1A·GTP on spontaneous hydrolysis of [^{14}C]Leu-tRNA^{Leu}. 2.7 μM [^{14}C]Leu-tRNA^{Leu} was incubated alone (●) and in the presence of 2 μM (■), 4.5 μM (×), and 6 μM (▼) eEF1A·GTP. Incubation was carried out at 25 °C in the buffer containing 0.2 mM GTP and 10% glycerol. C/C_0 is the fraction of unhydrolyzed [^{14}C]Leu-tRNA^{Leu}.

RESULTS

Functional Tests of Mammalian eEF1A. To make sure that the eEF1A preparation was fully active and could be adequately used for physical studies, different functional characteristics of the protein were investigated.

Practically all molecules of eEF1A after purification contained endogenous GDP as determined by HPLC chromatography (*22*). In the GDP/[^{3}H]GDP exchange test more than 95% of eEF1A·GDP molecules were capable to exchange endogenous GDP for [^{3}H]GDP. Importantly, GDP-exchanging properties of eEF1A were similar before and after the neutron scattering experiments.

The ability of rabbit eEF1A used in this study to interact with aminoacyl-tRNA and GTP resulting in a ternary complex formation was demonstrated in the experiment where aminoacyl-tRNA was protected from spontaneous deacylation in the presence of eEF1A·GTP (Figure 1). Total protection during 3 h was achieved at the aminoacyl-tRNA:eEF1A ratio of 1:2, suggesting a rather high ability of eEF1A to interact with aminoacyl-tRNA. High functional activity of eEF1A was also demonstrated in the experiments on the stimulation of aminoacyl-tRNA binding to the ribosomal A-site and poly(U) translation in a cell-free protein synthesizing system assembled from individual components [40S and 60S ribosomal subunits, [^{14}C]Phe-tRNA, eEF2, poly(U) (Figure 2)].

Thus, we concluded that the eEF1A preparation was functionally active.

Scanning Microcalorimetry of eEF1A. Figure 3 shows the temperature dependence of the excess heat capacity of eEF1A (a) and EF1A (b) measured in the absence of GDP (see Experimental Procedures). The heat absorption curves for both proteins reveal a complex shape which correlates with recently published thermodynamic data for EF1A obtained under somewhat different buffer conditions (*33*). The excess heat capacity curves were deconvoluted into three peaks using the best fit program (*30*) with each peak corresponding to two-state transition; i.e., the denaturation enthalpy calculated from the calorimetric curve (ΔH_{cal}) coincided with the effective van't Hoff enthalpy (ΔH_{eff}). It implies that each of proteins consists of three cooperative thermodynamic domains with the appropriate transition temperatures. The thermodynamic parameters characterizing these transitions

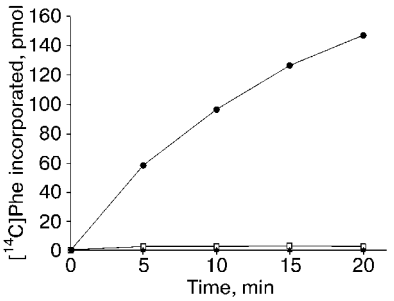

FIGURE 2: Dependence of the poly(U)-directed poly(Phe) synthesis on factor addition: (▲) factor-free translation; (□) translation in the presence of eEF2 only; (●) translation in the presence of eEF1A and eEF2. The reaction was carried out in 100 μL of reaction mixture containing 5 mM $MgCl_2$, 100 mM NH_4Cl, 3.5 mM spermidine, 0.4 mM GTP, 1 mM ATP, 18 pmol of 80S ribosomes, 15 μg of poly(U), 20 pmol of eEF2, and 50 pmol of eEF1A. No aminoacyl-tRNA was added, but instead 700 pmol of $tRNA^{Phe}$ was preincubated with 30 ng of PheRS, 3 mM ATP, and 60 μM [^{14}C]Phe for 10 min at 37 °C.

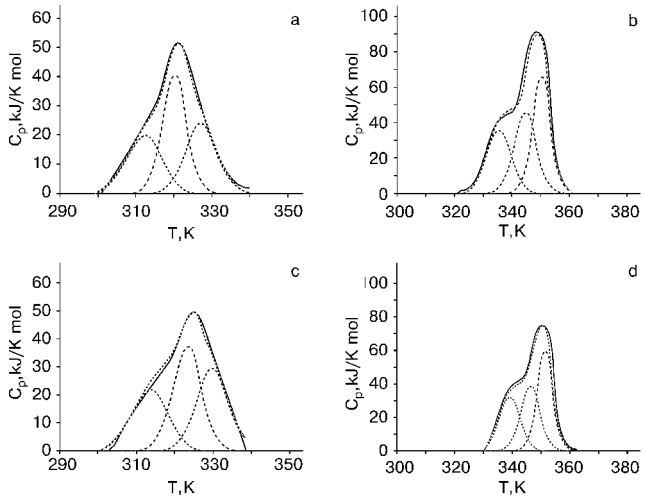

FIGURE 3: Temperature dependence of the excess heat capacity of eEF1A (a) and EF1A (b) in 20 mM Tris-HCl, pH 7.9, 10 mM magnesium acetate, and 5 mM 2-mercaptoethanol; eEF1A (c) and EF1A (d) in the same buffer with 20 μM GDP. Solid line: experimental curve. Dotted line: calculated heat capacity function.

are given in Table 1. It should be noted that the presence of three thermodynamic domains in the mammalian protein molecule correlates with the fact that both prokaryotic and lower eukaryotic proteins have three structural domains revealed by X-ray analysis (see the introduction).

In the buffer containing 20 μM GDP (Figure 3c,d), the heat absorption curves for each protein can also be deconvoluted into three heat absorption peaks. The melting of all three domains occurs at the higher temperatures (see Table 1). Noteworthy, the principal character of the protein melting is not changed within the GDP concentration range from 20 to 200 μM (Tiktopulo et al., unpublished).

The heat effect (heat absorption during the denaturation process) differs considerably for the two proteins. While for the prokaryotic protein the transition enthalpy of all three domains corresponds to the melting of small compact globular proteins with a specific heat of denaturation of 7 cal/g, this value for the eukaryotic protein is much lower (about 4 cal/g). Strictly speaking, these values should be compared at the same temperature. According to Kirchhoff's equation the temperature dependence of the denaturation enthalpy can be described as

$$\Delta H_t = \Delta H_d - \Delta C_p(T_d - T_t) \quad (2)$$

where ΔH_d is the enthalpy of denaturation at temperature T_d, ΔH_t is the enthalpy of denaturation at temperature T_t, and ΔC_p is the heat capacity jump during the heat transition.

In our experiments the heat capacity jump for the eukaryotic protein was very small. Hence, the enthalpy of denaturation only slightly depends on temperature, at least at the first approximation. Thus, the difference in specific enthalpy values for the two proteins does exist, and the eEF1A molecule (or its part) has a far more disordered conformation than its prokaryotic analogue. The GDP effect on the melting curves of EF1A and eEF1A is different. In the case of EF1A the addition of 20 μM GDP causes the significant increase of the enthalpy values of the first two peaks whereas for eEF1A one can observe the preferable increase of the third peak stability (see Table 1).

Neutron Scattering of eEF1A. Figure 4 shows the dependence of the neutron scattering intensity I on the scattering vector Q ($Q = 4\pi \sin(\Theta)/\lambda$, where λ is the wavelength of incident neutrons and 2Θ is the scattering angle) in Guinier coordinates ($\log I$ vs Q^2) extrapolated to the zero concentration of eEF1A·GDP.

The protein molecular mass calculated from the scattering intensity value extrapolated to the zero scattering angle [$I(0)/C$] is 48.6 ± 2.0 kDa, which is close to 50.34 kDa calculated from the primary sequence (*34*). The correspondence of the slope obtained to the correct molecular mass indicates that there is no aggregation of eEF1A·GDP molecules despite the high concentrations (40−120 μM) of the protein in these experiments. The partial specific volume calculated from amino acid composition (*35*) is equal to 0.74 cm^3/g. The values of gyration radii calculated from the Guinier graph do not depend on the concentration. The average value of a gyration radius was 5.2 ± 0.2 nm, evidencing an extremely extended conformation of protein eEF1A in solution at 20 μM GDP.

eEF1A·GDP was studied independently by spin-dependent neutron scattering in the presence of 10 μM GDP. The scattering intensity of negative hydrogen polarization decreased linearly with the decrease of spin polarization to zero polarization. The curves were very similar; only very close to the matching polarization the shape changed. From all curves (negative or zero polarization values) the radius of gyration found was 6.1 ± 0.5 nm. Since the statistical errors for positive polarization were very high, we did not take correspondent data into account. An extrapolation to zero contrast was not made in this case but will be of interest for further exploitation of the method of spin contrast variation. A direct comparison of the scattering curves at low temperatures with measurements at room temperature was not made since it is well established for ribosome (*36*, *37*, *38*) and chaperone (R. Willumeit, personal communications) samples that the freezing process does not influence the shape of the molecules.

Neutron Scattering of the [eEF1A·GDP·tRNA] Complex. The formation of the [eEF1A·GDP·tRNA] complex was studied by small angle neutron scattering at different molar eEF1A:tRNA ratios (1:2, 1:3, 2:1, 3:1). Figure 5 shows

Table 1: Thermodynamic Parameters Describing the Melting of eEF1A and EF1A

protein	q,[a] cal/g	ΔH_{cal},[a] kJ/mol	ΔH_1,[a] kJ/mol	ΔH_2,[a] kJ/mol	ΔH_3,[a] kJ/mol	T_{d1},[a] K	T_{d2},[a] K	T_{d3},[a] K
eEF1A	4.30	905.0	256.0	361.0	288.0	311.7	320.1	326.9
eEF1A + 20 μM GDP	4.40	931.0	238.0	363.0	330.0	312.9	322.0	330.1
EF1A	6.60	1192.0	340.5	370.0	481.5	335.8	344.3	350.1
EF1A + 20 μM GDP	6.95	1252.0	361.0	398.0	493.2	339.1	347.4	352.0

[a] q is the specific heat of denaturation; calorimetric enthalpy $\Delta H_{cal} = Mq$, where M is the molecular mass; ΔH_i and T_{di} are the calorimetric enthalpy and midpoint temperature of each heat transition peak, correspondingly.

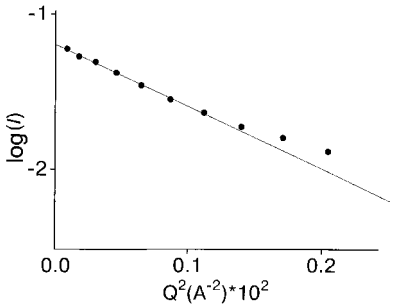

FIGURE 4: Dependence of neutron scattering intensity I on scattering vector Q in Guinier coordinates (log I vs Q^2) extrapolated to the zero concentration of eEF1A at 20 μM GDP.

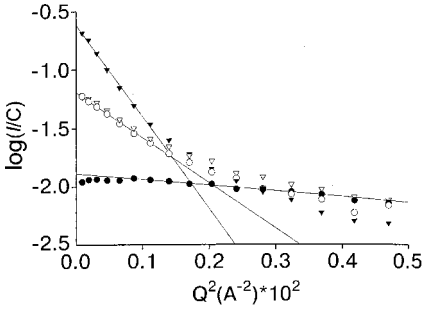

FIGURE 5: Dependence of neutron scattering intensity I on scattering vector Q in Guinier coordinates to tRNA (●), eEF1A (○), eEF1A:tRNA = 1:3 (▽), and eEF1A:tRNA=3:1 (▼).

Guinier dependencies of the neutron scattering intensity normalized for the concentration at the molar eEF1A:tRNA ratios of 1:3 and 3:1. The essential changes of $I(0)/C$ were observed at the excess of protein over tRNA. From the intercept value $I(0)/C$ the approximate stoichiometry of the complex was estimated as described in Experimental Procedures. Preliminary interpretation of the data could be that the complex consists of two protein molecules and one tRNA molecule. However, further investigations with another methodical approach may be useful to clarify the point more definitely.

In Figure 6 the scattering curves obtained in a wide range of scattering vectors (from 0.1 to 1.5 nm^{-1}) are plotted in Kratky coordinates (IQ^2 vs Q). In that case the scattering curve for eEF1A is typical for nonglobular disordered structures (*39*). Such shape of curves was observed also for the protein:tRNA mixtures at ratios of 1:3 and 1:2 (data are not shown for the sake of clarity of the picture). On the contrary, the scattering curves became much closer to those typical for globular structures (*39*) when eEF1A:tRNA ratios were 3:1 and 2:1 (Figure 6; data at 2:1 ratio are not shown for the sake of clarity of the picture). Thus, the formation of the [eEF1A·GDP·tRNA] complex led to the essential compactization of the eEF1A molecule.

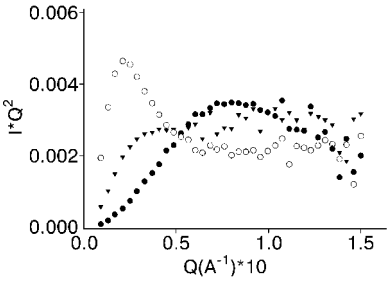

FIGURE 6: Dependence of neutron scattering intensity I on scattering vector Q in Kratky coordinates for tRNA (●), eEF1A (▼), and eEF1A:tRNA = 3:1 (○).

DISCUSSION

The Mammalian Translation Factor Has Significantly More Extended Conformation in Solution than the Prokaryotic Analogue. According to the neutron scattering measurements the rabbit liver eEF1A in the presence of 20 μM GDP has a radius of gyration of 5.2 ± 0.2 nm, which is 2-fold more than the calculated radius of gyration of its bacterial analogue EF1A (2.6 nm, taking into account the molecular mass difference; see the introduction). Thus, eEF1A is more extended in solution than EF1A. According to the scanning microcalorimetry the eEF1A molecule contains elements of tertiary structure (three thermodynamic domains), melting of which is reflected by the curves of heat absorption. The positions of the peaks are affected by GDP. The characteristic feature of the eEF1A melting was that the heat effect is much lower than that expected for globular proteins with inflexible three-dimensional structure. Such a behavior was observed in a limited set of proteins containing unstructured regions (histones, ribosomal protein L7) (*40*).

Thus, both the neutron scattering and microcalorimetry data evidence the existence of a significantly disordered structure of the mammalian eEF1A in solution. The following possible structure of the mammalian eEF1A in solution could be proposed. The eEF1A molecule consists of three distinct globular domains, connected by rigid interconnecting peptides, like prokaryotic EF1A. For *S. solfataricus* eEF1A (*20*) a large interface between domains I and III is shown to be responsible for the protein heat stability. Therefore, domains I and III of the mammalian protein are hypothesized to be disconnected in solution, resulting in the decreased heat stability of eEF1A in comparison with the bacterial analogue. Taking the length of the polypeptide chain joining domain I and domain II equal to 1.5 nm, the length of polypeptide chain joining domain II and domain III equal to 1.0 nm (*13*), and approximating each domain by sphere with radius of 2.1 nm, one can calculate the radius of gyration of such a trumbell model. This value is about 5.0 nm, which is close to our experimental data obtained by the neutron scattering.

Such an "open" conformation of eEF1A may explain why high glycerol concentration is absolutely required for isolation and preservation of activity of the mammalian protein contrary to the bacterial EF1A (*23*, *41*). Glycerol seems to stabilize the conformation of the mammalian elongation factor.

Peculiarities of Formation of the Noncanonical [eEF1A·GDP·tRNA] Complex. eEF1A·GDP is known to bind uncharged tRNA (*5*). This binding is thought to be rather specific since the regions of tRNA protected by eEF1A·GDP from nuclease hydrolysis and chemical modifications in footprinting assay closely resemble those of aminoacyl-tRNA involved in the interaction with EF1A·GTP according to the X-ray studies (*6*). The [eEF1A·GDP·tRNA] complex is thermodynamically stable [K_d is 20 nM as determined by the fluorescence polarization studies (*31*)].

The neutron scattering data presented on the Kratky plot (Figure 6) and the value of the eEF1A radius of gyration (about 3.2 nm) inside the [eEF1A·GDP·tRNA] complex measured by polarization-dependent neutron scattering (Willumeit et al., to be published) show essential compactization of the protein molecule upon complex formation. The stoichiometry of the [eEF1A·GDP·tRNA] complex appears to be two molecules of the protein per one molecule of tRNA. The stoichiometry of the regular ternary prokaryotic complex [EF1A·GTP·aminoacyl-tRNA] was not determined unambiguously. One set of data demonstrated that the complex might include one molecule of tRNA and two molecules of the protein, depending on the experimental conditions (*42*, *43*), while other experiments showed the stoichiometry of the protein and tRNA in the ternary complex being 1:1 (*19*, *44*). The crystallographic data describing the [EF1A·GDPPNP·aminoacyl-tRNA] complex favored the last point of view, though the crystallization conditions were far from the physiological conditions (*6*). The neutron scattering experiments presented in this paper suggest that in the higher eukaryotes the stoichiometry of 2:1 for the factor−tRNA binding might be also found at least in the [eEF1A·GDP·tRNA] complex. The biological importance of the presence of two protein molecules and one tRNA molecule in the complex remains unclear though such a stoichiometry in the classical ternary complex is suggested to support the translation accuracy under some conditions (*43*).

Functioning of the Elongation Factors 1A in the Prokaryotic and Eukaryotic Protein Synthesis. What could be the biological sense of the partially unfolded conformation of the mammalian eEF1A in solution? Structural aspects of the functioning of the translation machinery in prokaryotes and higher eukaryotes do not appear to be identical. The mammalian protein synthesizing apparatus is highly compartmentalized, which is proven now both in vitro (*2*), and in vivo (*45*, *46*). The prokaryotic factor EF1A·GTP has in solution the compact conformation which is not changed much upon interaction with aminoacyl-tRNA (*19*). On the contrary, mammalian eEF1A has in solution a significantly extended conformation, which undergoes dramatic changes during its interaction with tRNA. That might be a reason for observed significant difficulties in the crystallization of the isolated higher eukaryotic factor 1A (unpublished observation).

Thus, the idea of the absolute similarity of the functioning of the elongation factors 1A in prokaryotic and eukaryotic translation may be reconsidered with more critical view. The concept of the "conformational switch" between functional GTP and nonfunctional GDP conformations of the prokaryotic EF1A which sharply alter the protein affinity for such partners as tRNA and ribosome might not be plainly applicable for the mammalian protein because of a possibly less pronounced difference between GDP and GTP solution conformations of eEF1A (*1*). However, significant conformational changes in the eEF1A molecule do occur depending on whether the factor is alone or interacting with some of its biological partners. Such way of functioning may be optimal under the conditions of compartmentalized and channeled mammalian protein synthesis. Therefore, the comparison of the eEF1A conformations during the interaction with deacylated and aminoacyl-tRNA, with aminoacyl-tRNA synthetase and 80S ribosome, will be of special interest for future investigations.

The Mammalian Translation Elongation Factor 1A as a Possible Member of the Family of Unstructured Proteins. It has long been axiomatic that the majority of the biological functions in the cell (such as enzymatic catalysis, immunological and receptor recognition) are performed by proteins with unique three-dimensional structure. However, there is an increasing set of data concerning proteins that are totally or partially unstructured under physiological conditions and yet are functional. Intrinsically disordered proteins adopt folded structures upon binding to their biological ligands. The characteristic features of those proteins are the high positive charge of a molecule and participation in the most important regulatory functions in the cell (*47*). Some translational components belong to this family. For example, the 98 amino acid long domain of the eukaryotic translation initiation factor eIF4G is disordered but becomes structured upon the interaction with initiation factor eIF4E (*48*).

The experimental data presented here give the basis to conclude that eEF1A, which is highly positively charged (p*I* 9.1), may be partially unstructured in solution and, thus, can be a member of the family of unstructured proteins. The chaperone properties of eEF1A (those are also characteristic for such polypeptides) have been recently found as well (*49*; Turkovskaya et al., in press). We believe that the partially unstructured solution conformation of eEF1A might explain the well-known ability of the protein to form a complex with very different ligands such as actin (*50*), tubulin (*51*), calmodulin (*52*), calmodulin-dependent protein kinase (*53*), some regulatory proteins (*54*, *55*), the components of the ubiquitin-dependent proteolytic system (*56*), and viral RNA (*57*). Taking into account the abundant quantity of eEF1A in the cell, the eEF1A−ligand interaction in cytoplasm may be called "net-casting" by analogy with the recently proposed "fly-casting" (*58*) mechanism for the interaction of unstructured regulatory proteins and their targets present in cells at low concentrations.

ACKNOWLEDGMENT

We thank Yuliya Yudina for technical assistance.

REFERENCES

1. Negrutskii, B. S., and El'skaya, A. V. (1998) Eukaryotic translation elongation factor 1α: Structure, expression, functions, and possible role in aminoacyl-tRNA channeling, *Prog. Nucleic Acids Res. Mol. Biol. 60*, 47−78.

2. Ryazanov, A. G., Ovchinnikov, L. P., and Spirin, A. S. (1987) Development of structural organization of protein-synthesizing machinery from prokaryotes to eukaryotes, *Biosystems 20*, 275−288.
3. Negrutskii, B. S., Stapulionis, R., and Deutscher, M. P. (1994) Supramolecular organization of the mammalian translation system, *Proc. Natl. Acad. Sci. U.S.A. 91*, 964−968.
4. Negrutskii, B. S., and Deutscher, M. P. (1991) Channeling of aminoacyl-tRNA for protein synthesis *in vivo*, *Proc. Natl. Acad. Sci. U.S.A. 88*, 4991−4995.
5. Petrushenko, Z. M., Negrutskii, B. S., Ladokhin, A. S., Budkevich, T. V., Shalak, V. F., and El'skaya, A. V. (1997) Evidence for the formation of an unusual ternary complex of rabbit liver tRNA with GDP and deacylated tRNA, *FEBS Lett. 407*, 13−17.
6. Nissen, P., Kjeldgaard, M., Thirup, S., Polekhina, G., Reshetnikova, L., Clark, B. F. C., and Nyborg, J. (1995) Crystal structure of the ternary complex of Phe-tRNA^{Phe}, EF-Tu, and a GTP analog, *Science 270*, 1464−1472.
7. Kjeldgaard, M., Nissen, P., Thirup, S., and Nyborg, J. (1993) The crystal structure of elongation factor EF-Tu from *Thermus aquaticus* in the GTP conformation, *Structure 1*, 35−50.
8. Berchtold, H., Reshetnikova, L., Reiser, C. O., Schirmer, N. K., Sprinzl, M., and Hilgenfeld, R. (1993) Crystal structure of active elongation factor Tu reveals major domain rearrangements, *Nature 365*, 126−132.
9. Kawashima, G., Berthet-Colominas, C., Wulff, M., Cussack, S., and Leberman, R. (1996) The structure of the *Echerichia coli* EF-Tu:EF-Ts complex at 2.5 Å resolution, *Nature 379*, 579−518.
10. Polekhina, G., Thirup, S., Kjeldgaard, M., Nissen, P., Lippman, C., and Nyborg, J. (1996) Helix unwinding in the effector region of elongation factor EF-Tu·GDP, *Structure 4*, 1141−1151.
11. Song, H., Parsons, M. R., Rowsell, S., Leonard, G., and Phillips, S. E. (1999) Crystal structure of intact elongation factor EF-Tu from *Escherichia coli* in GDP conformation at 2.05 Å resolution, *J. Mol. Biol. 285*, 1245−1256.
12. Cavallius, J., and Merrick, W. C. (1992) Nucleotide sequence of rabbit elongation factor 1α cDNA, *Nucleic Acids Res. 20*, 1422−1445.
13. Kjeldgaard, M., and Nyborg, J. (1992) Refined structure of elongation factor EF-Tu from *Escherichia coli*, *J. Mol. Biol. 223*, 721−742.
14. Svergun, D., Barberato, C., and Koch, M. H. J. (1995) CRYSOL−a program to evaluate X-ray solution scattering of biological macromolecules from atomic coordinates, *J. Appl. Crystallogr. 28*, 768−773.
15. Serdyuk, I. N., Pavlov, M. Yu., Rublevskaya, I. N., Zaccai, G., and Leberman, R. (1994) The triple isotopic substitution method in small angle neutron scattering. Application to the study of the ternary complex EF-Tu·GTP·aminoacyl-tRNA, *Biophys. Chem. 53*, 123−130.
16. Ohta, S., Nakanishi, M., Tsuboi, M., Arai, K., and Kaziro, Y. (1977) Structural fluctuation of the polypeptide-chain elongation factor Tu, *Eur. J. Biochem. 78*, 599−608.
17. Kushiro, M., Shimizu, M., and Tomita, K. (1987) Molecular cloning and sequence determination of the tuf gene coding for the elongation factor Tu of *Thermus thermophilus* HB8, *Eur. J. Biochem. 170*, 93−98.
18. Voss, R. H., Hartmann, R. K., Lippmann, C., Alexander, C., Jahn, O., and Erdmann, V. (1992) Sequence of the tufA gene encoding elongation factor EF-Tu from *Thermus aquaticus* and overproduction of the protein in *Escherichia coli*, *Eur. J. Biochem. 207*, 839−846.
19. Bilgin, N., Ehrenberg, M., Ebel, C., Zaccai, G., Sayers, Z., Koch, M. H. J., Svergun, D. I., Barberato, C., Volkov, V., Nissen, P., and Nyborg, J. (1998) Solution structure of the ternary complex between aminoacyl-tRNA, elongation factor Tu and guanosine triphosphate, *Biochemistry 37*, 8163−8172.
20. Vitagliano, L., Masullo, M., Sica, F., Zagari, A., and Bocchini, V. (2001) The crystal structure of *Sulfolobus solfataricus* elongation factor 1α in complex with GDP reveals novel feature in nucleotide binding and exchange, *EMBO J. 20*, 5305−5311.
21. Andersen, G. R., Pedersen, L., Valente, L., Chatterjee, I., Kinzy, T. G., Kjeldgaard, M., and Nyborg, J. (2000) Structural basis for nucleotide exchange and competition with tRNA in the yeast elongation factor complex eEF1A:eEF1Bα, *Mol. Cell 6*, 1261−1266.
22. Shalak, V. F., Budkevich, T. V., Negrutskii, B. S., and El'skaya, A. V. (1997) A fast and effective method for purification of elongation factor 1α from rabbit liver, *Ukr. Biokhim. Zh. 69*, 104−109.
23. Carvalho, M. D., Carvalho, J. F., and Merrick, W. C. (1984) Biological characterization of various forms of elongation factor 1 from rabbit reticulocytes, *Arch. Biochem. Biophys. 234*, 603−611.
24. El'skaya, A. V., Ovcharenko, G. V., Pal'chevskii, S. S., Petrushenko, Z. M., Triana-Alonso, F. J., and Nierhaus, K. H. (1997) Three tRNA binding sites in rabbit liver ribosomes and role of the intrinsic ATPase in 80S ribosomes from higher eukaryotes, *Biochemistry 36*, 10492−10497.
25. Bradford, M. M. (1976) A rapid and sensitive method for the quantitation of microgram quantities of protein utilizing the principle of protein-dye binding, *Anal. Biochem. 72*, 248−254.
26. El'skaya, A. V., and Negrutskii, B. S. (1987) The interaction between biologically inactive tRNA conformers and leucyl-tRNA synthetase from rabbit liver, *Eur. J. Biochem. 164*, 65−69.
27. Arai, O., Ota, Y., Arai, N., Nakamura, S., Henneke, C., Oshima, T., and Kaziro, Y. (1978) Studies on polypeptide-chain-elongation factors from an extreme thermophile, *Thermus thermophilus* HB8, *Eur. J. Biochem. 92*, 509−519.
28. Limmer, S., Reiser, C. O. A., Schirmer, N. K., Grillenbeck, N. W., and Sprinzl, M. (1992) Nucleotide binding and GTP hydrolysis by elongation factor Tu from *Thermus thermophilus* as monitored by proton NMR, *Biochemistry 31*, 2970−2977.
29. Senin, A. A., Potekhin, S. A., Tiktopulo, E. I., and Filimonov, V. V. (2000) Differential scanning microcalorimeter Scal-1, *J. Therm. Anal. Calorim. 62*, 153−160.
30. Privalov, P. L., and Potekhin, S. A. (1986) Scanning microcalorimetry in studying temperature-induced changes in proteins, *Methods Enzymol. 131*, 1−51.
31. Petrushenko, Z. M., Budkevich, T. V., Shalak, V. F., Negrutskii, B. S., and El'skaya A. V. (2002) Novel complexes of mammalian translation elongation factor eEF1A·GDP with uncharged tRNA and aminoacyl-tRNA synthetase. Implications for tRNA channeling, *Eur. J. Biochem. 269*, 4811−4818.
32. Zhao, J., and Stuhrmann, H. B. (1993) The in situ structure of the L3 and L4 proteins of the large subunit of *E. coli* ribosomes as determined by nuclear-spin contrast variation, *J. Phys. 3*, 233−236.
33. Seldak, E., Sprinzl, M., Grillenbeck, N., and Antalik M. (2002) Microcalorimetric study of elongation factor Tu from *Thermus thermophilus* in nucleotide-free, GDP and GTP forms and in the presence of elongation factor Ts, *Biochim. Biophys. Acta 1596*, 357−365.
34. Rosenberry, T. L., Krall, J. A., Dever, T. E., Haas, R., Louvard, D., and Merrick, W. C. (1989) Biosynthetic incorporation of [^{3}H]-ethanolamine into protein synthesis elongation factor 1α reveals a new posttranslational protein modification, *J. Biol. Chem. 264*, 7096−7099.
35. Zamyatnin, A. A. (1984) Amino acid, peptide and protein volume in solution, *Annu. Rev. Biophys. Bioeng. 13*, 145−165.
36. Burkhardt, N., Diedrich, G., Nierhaus, K. H., Meerwinck, W., Stuhrmann, H. B., Pedersen, J. S., Koch, M. H. J., Volkov, V. V., Kozin, M. B., and Svergun, D. I. (1997) Architecture of the *E. coli* 70S ribosomes, *Phys. B 234*, 199−201.
37. Svergun, D. I., Burkhardt, N., Pedersen, J. S., Koch, M. H. J., Volkov, V. V., Kozin, M. B., Meerwinck, W., Stuhrmann, H. B., Diedrich, G., and Nierhaus, K. H. (1997a) Solution scattering structural analysis of the 70S *Escherichia coli* ribosome by contrast variation. I. Invariants and validation of electron microscopy models, *J. Mol. Biol. 271*, 588−601.
38. Svergun, D. I., Burkhardt, N., Pedersen, J. S., Koch, M. H. J., Volkov, V. V., Kozin, M. B., Meerwinck, W., Stuhrmann, H. B., Diedrich, G., and Nierhaus, K. H. (1997b) Solution scattering structural analysis of the 70S *Escherichia coli* ribosome by contrast variation. II. A model of the ribosome and its RNA at 3.5 nm resolution, *J. Mol. Biol. 271*, 602−618.
39. Glatter, O., and Kratky, O. (1982) in *Small-angle X-ray scattering*, pp 167−196, Academic Press, London.
40. Gudkov, A. T., and Khechinashvili, N. N. (1978) Studies on the structure of protein L7/L12 from *Escherichia coli* ribosomes, *Eur. J. Biochem. 90*, 313−318.
41. Nagata, S., Iwasaki, K., and Kaziro, Y. (1976) Interaction of the low molecular weight form of elongation factor 1 with guanine nucleotides and aminoacyl-tRNA, *Arch. Biochem. Biophys. 172*, 168−177.

42. Ehrenberg, M., Rojas, A. M., Weiser, J., and Kurland, C. G. (1990) How many EF-Tu molecules participate in aminoacyl-tRNA binding and peptide bond formation in *Escherichia coli* translation?, *J. Mol. Biol. 211*, 739−749.
43. Rodnina, M. V., and Wintermeyer, W. (1995) GTP consumption of elongation factor Tu during translation of heteropolymeric mRNAs, *Proc. Natl. Acad. Sci. U.S.A. 92*, 1945−1949.
44. Bensch, K., Pieper, U., Ott, G., Schirmer, N., Sprinzl, M., and Pingoud, A. (1991) How many EF-Tu molecules participate in aminoacyl-tRNA binding?, *Biochimie 73*, 1045−1050.
45. Stapulionis, R., and Deutscher, M. P. (1995) A channeled tRNA cycle during mammalian protein synthesis, *Proc. Natl. Acad. Sci. U.S.A. 92*, 7158−7161.
46. Job, C., and Eberwine, J. (2001) Identification of sites for exponential translation in living dendrites, *Proc. Natl. Acad. Sci. U.S.A. 98*, 13037−13042.
47. Wright, P. E., and Dyson, H. J. (1999) Intrinsically unstructured proteins: reassessing the protein structure−function paradigm, *J. Mol. Biol. 293*, 321−331.
48. Hershey, P. E., McWhirter, S. M., Gross, J. D., Wagner, G., Alber, T., and Sachs, A. B. (1999) The Cap-binding protein eIF4E promotes folding of a functional domain of yeast translation initiation factor eIF4G1, *J. Biol. Chem. 274*, 21297−21304.
49. Hotokezaka, Y., Tobben, U., Hotokezaka, H., Van Leyen, K., Beatrix, B., Smith, D. H., Nakamura, T., and Wiedmann, M. (2002) Interaction of the eukaryotic elongation factor 1A with newly synthesized polypeptides, *J. Biol. Chem. 277*, 18545−18551.
50. Liu, G., Tang, J., Edmonds, B. T., Murray, J., Levin, S., and Condeelis, J. (1996) F-actin sequesters elongation factor 1α from interaction with aminoacyl-tRNA in a pH-dependent reaction, *J. Cell Biol. 135*, 953−963.
51. Moore, R. C., and Cyr, R. J. (2000) Association between elongation factor-1α and microtubules in vivo is domain dependent and conditional, *Cell Motil. Cytoskeleton 45*, 279−292.
52. Kaur, K. J., and Ruben, L. (1994) Protein translation elongation factor-1α from *Trypanosoma brucei* binds calmodulin, *J. Biol. Chem. 269*, 23045−23050.
53. Wang, W., and Poovaiah, B. W. (1999) Interaction of plant chimeric calcium/calmodulin-dependent protein kinase with a homolog of eukaryotic elongation factor-1α,. *J. Biol. Chem. 274*, 12001−12008.
54. Gangwani, L., Mikrut, M., Galcheva-Gargova, Z., and Davis, R. J. (1998) Interaction of ZPR1 with translation elongation factor-1α in proliferating cells, *J. Cell Biol. 143*, 1471−1484.
55. Kim, M. J., Si, F., Kim, S. J., Hong, S. B., Hwang, J. I., Lee, H. J., Lee, S. J., Chang, J. S., Lee, Y. H., Ryu, S. H., and Suh, P. G. (1999) The SH2-SH2-SH3 domain of phospholipase C-γ1 directly binds to translational elongation factor-1α, *Mol. Cells 9*, 631−637.
56. Gonen, H., Smith, C. E., Siegel, N. R., Kahana, C., Merrick, W. C., Chakraburetty, K., Schwartz, A. L., and Ciechanover, A. (1994) Protein synthesis elongation factor EF-1α is essential for ubiquitin-dependent degradation of certain N^{α}-acetylated proteins and may be substituted for by the bacterial elongation factor EF-Tu, *Proc. Natl. Acad. Sci. U.S.A. 91*, 7648−7652.
57. Blackwell, J. L., and Brinton, M. A. (1997) Translation elongation factor-1α interacts with the 3′ stem-loop region of West Nile virus genomic RNA, *J. Virol. 71*, 6433−6444.
58. Dyson, H. J., and Wright, P. E. (2002) Coupling of folding and binding for unstructured proteins, *Curr. Opin. Struct. Biol. 12*, 54−60.

BI026495H

1.2. Кристалографічна структура фактора елонгації трансляції eEF1A2 і особливості реакції обміну гуанінового нуклеотиду на цьому білку

Nucleic Acids Research

Nucleic Acids Research, 2014 **1**
doi: 10.1093/nar/gku974

Mammalian translation elongation factor eEF1A2: X-ray structure and new features of GDP/GTP exchange mechanism in higher eukaryotes

Thibaut Crepin[1,2,3,†], Vyacheslav F. Shalak[4,†], Anna D. Yaremchuk[4,5,†], Dmytro O. Vlasenko[4], Andrew McCarthy[3,5], Boris S. Negrutskii[4,*], Michail A. Tukalo[4] and Anna V. El'skaya[4,*]

[1]University of Grenoble Alpes, UVHCI, F-38000 Grenoble, France, [2]CNRS, UVHCI, F-38000 Grenoble, France, [3]Unit for Virus Host-Cell Interactions, University of Grenoble Alpes-EMBL-CNRS, 71 avenue des Martyrs, 38042 France, [4]State Key laboratory of Molecular and Cellular Biology, Institute of Molecular Biology and Genetics, 150 Zabolotnogo str., Kiev 03680, Ukraine and [5]European Molecular Biology Laboratory, Grenoble Outstation, 71 avenue des Martyrs, 38042 France

Received February 12, 2014; Revised September 29, 2014; Accepted October 2, 2014

ABSTRACT

Eukaryotic elongation factor eEF1A transits between the GTP- and GDP-bound conformations during the ribosomal polypeptide chain elongation. eEF1A*GTP establishes a complex with the aminoacyl-tRNA in the A site of the 80S ribosome. Correct codon– anticodon recognition triggers GTP hydrolysis, with subsequent dissociation of eEF1A*GDP from the ribosome. The structures of both the 'GTP'- and 'GDP'-bound conformations of eEF1A are unknown. Thus, the eEF1A-related ribosomal mechanisms were anticipated only by analogy with the bacterial homolog EF-Tu. Here, we report the first crystal structure of the mammalian eEF1A2*GDP complex which indicates major differences in the organization of the nucleotidebinding domain and intramolecular movements of eEF1A compared to EF-Tu. Our results explain the nucleotide exchange mechanism in the mammalian eEF1A and suggest that the first step of eEF1A*GDP dissociation from the 80S ribosome is the rotation of the nucleotide-binding domain observed after GTP hydrolysis.

INTRODUCTION

A number of eukaryotic translation factors demonstrate RNA-binding properties; however, quite a few of them directly interact with both tRNA and ribosomes. eEF1A initiates the ribosomal peptide elongation process by the formation of the eEF1A*GTP*aminoacyl-tRNA complex and the timely arrival of the aminoacyl-tRNA to the A site facil itates the selection of the correct anticodon by the mRNA-programmed ribosome. GTP hydrolysis on eEF1A leads to the steady positioning of the aminoacyl-tRNA in the A site, which subsequently triggers the transpeptidation reaction. After adopting the GDP conformation, eEF1A is thought to leave the ribosome for the eEF1Bαβγ complex, which catalyzes the exchange of GDP for GTP. This sequence of events has only been established for the bacterial elongation factor EF-Tu (1), although this is also commonly believed to be valid for the eukaryotic elongation factors (2,3). However, peculiarities of the eukaryotic eEF1A function during translation have been described (4–9).

High-resolution crystal structures of the eubacterial homolog of eEF1A, EF-Tu, were obtained for the GTP- (or, more precisely, GDPNP), GDP- and (GDPNP+aminoacyltRNA)-bound forms (10–12). Archaeal elongation factors 1A (aEF1A) were crystallized in both the GDP- (13) and GTP-form complexed with Pelota (14) or termination factor RF1 (15). The only studies to date on the crystal structure of eukaryotic eEF1A have described the cocrystallization of the yeast elongation factor 1A ($eEF1A_y$) with the truncated guanine exchange factor (GEF) (16,17).
Subsequently, this structure served as a universal model to explain molecular features of any eukaryotic homolog in any nucleotide-bound conformation. Numerous attempts to crystallize the higher eukaryotic eEF1A in a GTP or GDP form were unsuccessful, and a precise understanding of the eEF1A function was not possible.

Here, we report the X-ray crystal structure of a natively folded and a post-translationally modified rabbit isoform 2 of eEF1A (eEF1A2) in a complex with GDP. The results suggest the dissociation of eEF1A*GDP from 80S ribosome is a multistage process, the first step of which is a GTP

*To whom correspondence should be addressed. Tel: +380 442000337; Fax: +380 445260759; Email: negrutskii@imbg.org.ua
Correspondence may also be addressed to Anna El'skaya. Tel: +380 445260749; Fax: +380 445260759; Email: anna.elskaya@yahoo.com
†The authors wish it to be known that, in their opinion, the first three authors should be regarded as Joint First Authors.

Downloaded from http://nar.oxfordjournals.org/ by guest on October 20, 2014

hydrolysis-induced rotation of the nucleotide-binding domain from the ribosome. Notably, the data obtained are inconsistent with the currently accepted concept of the Mg^{2+}-dependent nucleotide exchange in eEF1A (16–18). The absence of Mg^{2+} contribution to the binding and dissociation of GDP explains the similar eEF1A affinity for GDP and GTP, contrary to the bacterial homolog EF-Tu. The current model refines a mechanism of the guanine exchange process in eEF1A, which is important for understanding the ribosomal polypeptide elongation in mammalian cells and contributes to the concept of mechanics of G proteins functioning.

MATERIALS AND METHODS

Purification and crystallization of the rabbit eEF1A isoform 2 was performed as described (19). Recombinant eEF1Bα (*Homo Sapiens*) was produced essentially as described previously (20). Briefly, eEF1Bα was cloned into the pGEX-6P-1 vector (GE Healthcare, Buckinghamshire, UK). The expression of GST-fusion protein was induced by the addition of 1 mM isopropyl β-D-1-thiogalactopyranoside (IPTG) for 3 h at 37°C in BL21(DE3)pLysE bacteria strain (Stratagene, La Jolla, CA, USA). Cells were harvested and disrupted by sonication followed by centrifugation. GST-eEF1Bα protein was purified from clear lysate on glutathione-agarose beads (Sigma-Aldrich, St. Louis, MO, USA). The beads were extensively washed and GST-eEF1Bα was eluted stepwise using a glutathione containing buffer solution. The GST moiety was removed by incubation with a Prescission protease according to the manufacturer's instructions (GE Healthcare). eEF1Bα was further purified using a Q-sepharose column and a 150–400 mM NaCl linear gradient. Pure eEF1Bα, as judged by sodium dodecyl sulphate-polyacrylamide gel electrophoresis, was dialyzed against 50% glycerol solution containing 30 mM Tris-HCl, pH 7.5, 50 mM NaCl, 1 mM DTT and stored at –20°C.

Crystals of the eEF1A2*GDP complex were obtained as previously described (19). For structure determination, crystals of the eEF1A2*GDP complex were soaked in the mother liquor solution containing 0.5 mM $GdCl_2$ before freezing in liquid nitrogen. The diffraction data were collected on ID14–4 (ESRF) and processed using the XDS package (21). The phasing procedure was performed using SHARP (22). The model was built and refined using CCP4i suite program for crystallography (REFMAC, COOT) (23). The final model was checked with MolProbity (24). The structure files and coordinates of the eEF1A2*GDP complex were deposited in the Protein Data Bank. All the figures were drawn using PyMOL (the PyMOL MolecularGraphics System, Version 1.5.0.4 Schrödinger, LLC) or Chimera (25).

The guanine nucleotide exchange rate of eEF1A2 was determined by a filter binding assay mainly as in (6). For kinetic measurements eEF1A2*[^{3}H]GDP was prepared by incubation of 8 μM eEF1A2 with 8 μM [^{3}H]GDP (GE Healthcare, 1500 Ci/mol) in 135 μl of 45 mM Tris-HCl, pH 7.5, containing 0.5 mM DTT, 10 mM magnesium chloride, 100 mM NH_4Cl, 1 mg/ml bovine serum albumin (BSA) and 25% glycerol for 10 min at 37°C. The reaction mixture was placed at 25°C and was diluted into 1110 μl of exchange buffer (20 mM Tris-HCl, pH 7.5, 10 mM magnesium chloride, 50 mM NH_4Cl and 10% glycerol). The reaction mixture was then divided into two parts of 622 μl each. The exchange reaction was performed at 25°C and was initiated by the addition of 155.5 μl of exchange buffer containing 750 μM GDP in the presence or absence of eEF1Bα. Aliquots of 100 μl were withdrawn at different times and immediately filtered through nitrocellulose filters (Millipore, Billerica, MA, USA, pore size 0.45 μm). The filters were washed three times with 1 ml of ice-cold washing buffer (20 mM Tris-HCl, pH 7.5, 10 mM magnesium chloride, 100 mM NH_4Cl and 0.1 mg/ml BSA), dried and then were counted in a liquid scintillator. To evaluate the effect of ethylenediaminetetraacetic acid (EDTA) on the exchange reaction, 10 mM magnesium chloride in all buffer solutions was substituted with 10 mM EDTA. The time courses depicted in the figure were obtained by averaging four independent kinetics experiments; the error bars represent standard deviations. The data were evaluated by fitting to a single exponential function ($y = A1*\exp(-x/t1) + y_0$) using OriginPro 8 software (OriginLab, Northampton, MA, USA).

RESULTS

Overview of the structure

The crystal structure of the eEF1A2*GDP complex has been solved and refined at 2.7 Å resolution (19) (Table 1). The asymmetric unit contains two copies (molecules A and B) arranged in a 'head to tail' dimer configuration (Figure 1A). The physiological relevance of the dimer is uncertain although evidence for the presence of eEF1A dimers in a cellular context has recently been obtained which suggests a role in actin bundling (26) and control of eEF1A via phosphorylation (27).

Molecule A, in comparison with molecule B, displays a weaker electron density around Gly50 and contains 10 additional residues in the C-terminal region. The weak electron density around Gly50 of molecule A is consistent with the significantly increased mobility of helix A* in the eEF1A2 structure as determined from the high B-factor value and subsequent molecular dynamics simulation studies (data not shown). The local conformations of some sections of the molecules A and B fluctuate (root-mean-square (rms) deviation 0.068 Å for all C_α atoms), and results in a minor (<1 Å) shift of the GDP position. The synchronous fluctuations of Mg^{2+} and GDP are observed to favor the contribution of GDP to the stabilization of Mg^{2+} in the eEF1A2*GDP complex. Three structural domains are present in eEF1A2, domain I (4–234), domain II (241–328) and domain III (337–445) connected by linker sequences (Figure 1A). The nomenclature and location of α-helices and β-strands in the tertiary structure is depicted in Figure 1B. Studies on the native eEF1A2 structure allowed for the detection of phosphorylated Thr239 and Ser163 residues (Figure 1C). To the best of our knowledge, Thr239 phosphorylation in eEF1A2 has never been reported and has not been described by numerous phosphorylation prediction programs. The phosphorylation of Ser163 in eEF1A2 has been predicted by several programs, but has not been shown experimentally.

Downloaded from http://nar.oxfordjournals.org/ by guest on October 20, 2014

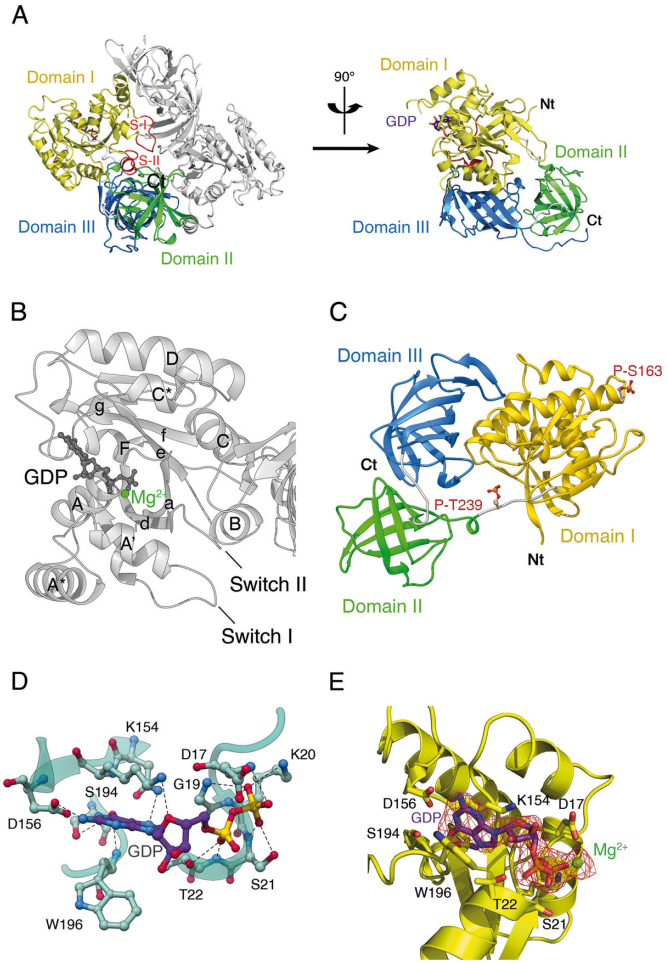

Figure 1. Overall structure of *Oryctolagus cuniculus* eEF1A2*GDP. (A) eEF1A2 is crystallized as a dimer. Three domains of eEF1A2 are colored as follows: domain I in yellow, domain II in green and domain III in blue. The Switch I and II regions are designated as S-I and S-II. The GDP is shown as a ball-and-stick representation. The N-terminus and the C-terminus are marked as Nt and Ct, respectively. (B) Presentation of the helices and beta-folds in domain I of eEF1A2*GDP. The α-helices are labeled by upper case letters, and β-strands are labeled by lower case letters. (C) Location of phosphorylated Thr239 and Ser163 in eEF1A2. (D) Network of interactions in the nucleotide-binding pocket of the GDP-bound eEF1A2. Magnesium ion is not shown for sake of clarity. (E) Electron density map corresponding to the molecule of GDP bound to eEF1A. Magnesium ion is colored in green.

Table 1. Data collection and refinement statistics

	eEF1A2
Data collection	
X-ray source	ESRF ID14-EH4
Wavelength (Å)	0.979
Space group	$P6_122$
Cell dimensions	
a (Å)	135.4
b (Å)	135.4
c (Å)	304.6
[a]Resolution range (Å)	25–2.7 (2.82–2.7)
[a]Completeness (%)	98.6 (95.7)
[a,b]Rsym I (%)	8.8 (86.6)
I/σI	18.5 (2.8)
[a]Total reflections	341,059 (34,459)
[a]Unique reflections	45,528 (4,452)
[a]Multiplicity	7.5 (7.7)
Phasing statistics	
[c]FOM (centric/acentric)	0.065/0.378
Phasing power (iso/ano)	-/1.68
Refinement statistics	
R-factor (%)	20.2
R_{free} (%)	25.5
Bond length (Å)	0.015
Bond angle (°)	1.51
Mean *B*-factor	
Protein	62.4
Ligand	44.1
Ion	51.5
Water	46.5
No. atoms	
Residues	6 884
Ligand	56
Ion	2
water	9
Ramachandran plot	
Allowed regions (%)	97.4
Disallowed regions (%)	2.6

[a]Values in parentheses are for the highest resolution shell.
[b]$R_{sym}\ (I) = [\sum_{hkl}\sum_i|<I_{hkl}> - I_{hkl,i}|]/[\sum_{hkl}\sum_i|I_{hkl}|]$, where *i* is the number of reflection *hkl*.
[c]Figure Of Merit $= \left|\sum P(\alpha)e^{i\alpha}/\sum P(\alpha)\right|$, where $P(\alpha)$ is the phase probability distribution and α is the phase.

The main contacts between GDP and eEF1A2 are depicted in Figure 1D. Two oxygen atoms of the Asp156 side chain form H-bonds with N1 and N2 atoms of the guanine ring, respectively. Nitrogen from a peptide bond of Trp196 and the Ser194 side chain form H-bond with O6 atom of the guanine base. Asn153 forms H-bonds with N7 atom of GDP. Lys154 is linked to the ribose ring. Gly19 and Lys20 interact with O1 atom of the β-phosphate moiety. Peptide groups of Asp17 and Ser21 form H-bond with O3 and O2 atoms of the β-phosphate, correspondingly. Thr22, a part of the Walker motif, binds O2 atom of the α-phosphate. Electron density map corresponding to the molecule of GDP bound to eEF1A is shown in Figure 1E. In the mammalian eEF1A2 the GDP binding site is similar to that of the yeast and archaeal homologs.

There are no contacts between domains I and II of eEF1A2. Domain III has an eight stranded β-barrel-type structure, which interacts with domain I through a large interface including helices B and C. Interestingly, the unstructured C-terminal tail observed in molecule A is not free but linked to the 'Domain II–linker-Domain III' surface.

A, A* and A' helices of eEF1A2 in nucleotide exchange

A comparative analysis of eEF1A2*GDP with the aEF1A*GTP (3AGJ), aEF1A*GDP (1SKQ) and $eEF1A_y$*eEF1Bα (1IJF) structures reveals a unique orientation for the A′ and A* helices in eEF1A2*GDP. While the N-terminal end of the helix A* is situated in a similar position in all molecules, the C-terminus is rotated approximately 50° in eEF1A2*GDP compared to aEF1A*GDP or $eEF1A_y$, and is only rotated ∼23°

Downloaded from http://nar.oxfordjournals.org/ by guest on October 20, 2014

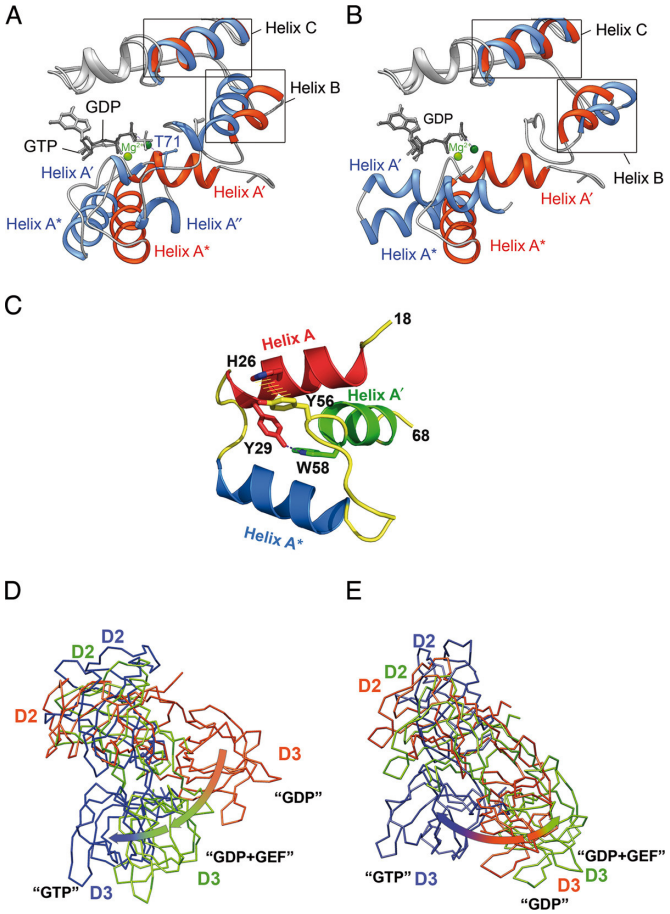

Figure 2. Main conformational rearrangements upon GTP hydrolysis. (A and B) A′ and A* helical arrangement in the mammalian and archaeal elongation factors. eEF1A2*GDP is superimposed with aEF1A*GTP (A) and aEF1A*GDP (B). The structure of eEF1A2 is colored in red with GDP in dark gray, aFF1A*GDP and aEF1A*GTP are colored blue with GDP or GTP in light gray. Mg^{2+} ions are colored light green in eEF1A2*GDP and dark green in aEF1A*GDP or aEF1A*GTP. Note the unwinding of helix A′ in aEF1A*GTP and similar orientation of helices A* in eEF1A2*GDP and aEF1A*GTP. (C) Tyr56 and Trp58 are responsible for an interaction of the A′ and A helices. Mutation of Tyr56 or Trp58 impairs the A′- A interaction during GTP binding and hydrolysis. (D) Superimposition of the domain II+III units of eEF1A2*GDP (pink), $eEF1A_y$ (green) in the complex with eEF1Bα (not shown for sake of clarity) and aEF1A*GTP (blue) after alignment of domain I (not shown for sake of clarity) of all complexes. (E) Superimposition of the domain II+III units of bacterial EF-Tu in GDP (pink), GEF-induced (green) and GTP (blue) conformations after alignment of domain I (not shown for sake of clarity) of all complexes.

relative to aEF1A*GTP (Figure 2A and B). Helix A′ of eEF1A2*GDP is shifted right compared to both aEF1A*GDP and $eEF1A_y$.

Thus, the positions of the A* and A′ helices are significantly different from the 'intermediate' state observed in the eukaryotic elongation factor complex with GEF (16).

A possible mechanism of the GDP-/GTP-dependent reversible changes in the A′-A* region may encompass the subdivision of A′ into two smaller helixes in the GTP form of aEF1A (14) (Figure 2A). Assuming the 'GTP-conformations' of eEF1A and aEF1A are similar, a comparison of the eEF1A2*GDP and aEF1A*GTP structures suggests the following mechanism. During the transition from the GDP to GTP conformation, the Tyr56-Trp58 segment of the helix A′ remains unchanged, whereas A″ approaches the GTP-binding pocket, permitting Thr71 (Thr72 in eEF1A2) from the Switch I region to bind the γ-phosphate of GTP via Mg^{2+} (Figure 2A).

The role of conformational changes in the helix A′ is supported by recent findings that demonstrated the absolute importance of Tyr56 and Trp58 in $eEF1A_y$ for yeast growth (28). There was no obvious reason for the lethality from the currently available data. However, the crystal structure of eEF1A2*GDP illustrates the importance of these residues in the interaction of the A′ and A helices. The aromatic ring of Tyr56 situated in the helix A′ forms a π-stacking interaction with the His26 imidazole ring, whereas the Nε1 atom of Trp58 forms a hydrogen bond with the hydroxyl group of Tyr29 in the helix A (Figure 2C). These interactions are probably needed to keep A′ and A helices together, leaving A″ mobile and capable of promoting the Thr71/Thr72 interaction with GTP in aEF1A/eEF1A. Upon GTP hydrolysis, Thr71/Thr72 loses the Mg^{2+}-mediated contact with the γ-phosphate, so the A″ helix can move back and restore the integrity of the A′ helix. Thus, the strong fixation of A′ by the A helix may provide a basis for the correct positioning of the A′ helix in eEF1A2*GDP. The A-A′ contacts are obviously absent in the 'intermediate state' conformation of $eEF1A_y$ observed in the complex with eEF1Bα (16). Consequently, eEF1Bα is supposedly able to interact with aY56A W58A mutated eEF1A. However, it is unlikely that the mutated protein would achieve the correct 'GTP conformation' after dissociation of eEF1Bα. Interestingly, the prokaryotic EF-Tu*GDP shows a different secondary structure of the effector region. Instead of A″ in eEF1A2, an unstructured region in the *Thermus aquaticus* or β-hairpin in *Escherichia coli* EF-Tu*GDP is present (29).

Rotation of the domains (II+III) structural unit relative to domain I is different in eEF1A2*GDP and $eEF1A_y$ bound to eEF1Bα

A comparison of the domain organization in eEF1A2*GDP, $eEF1A_y$ bound to eEF1Bα and aEF1A*GTP illustrates the domain (II+III) unit movements relative to domain I during GDP/GTP exchange. Domains II and III of the factors were reported to move as a single body in molecular dynamic simulations (30). Evidently, eEF1Bα binding induces a 56° switch in position of the domain (II+III) unit relative to domain I (Figure 2D). The rearrangements of the nucleotide binding site and subsequent GTP binding lead to an increased angle of the domain II+III unit rotation (Figure 2D). A backward movement of the domain (II+III) unit is permitted only after GTP hydrolysis and produced the GDP-bound conformation. Notably, the bacterial and eukaryotic GEFs induce rotations of domain II+III of counterparts in opposite directions whereas subsequent GTP binding produces unidirectional rotation of aEF1A, and, possibly, eEF1A and EF-Tu domains (II+III) relative to domain I (Figure 2D and E).

The rotation of the domain (II+III) unit is accompanied by conformational changes in other regions connected with

Downloaded from http://nar.oxfordjournals.org/ by guest on October 20, 2014

domain III. The interaction of GEF with domain II induces a change in the linker connecting domains II and III. Domain III is bound to domain I and cannot easily follow the domain II movement without rearrangement of the H-bond network. Indeed, in the eEF1A$_y$ bound to eEF1Bα complex, the B and C helices acquire some novel contacts as compared to eEF1A2*GDP. Specifically, helix B binds to residues 422 and 430 instead of Arg381 and Arg382; and Thr142 of helix C contacts Ile343 and Val435 (Val433 in eEF1A$_y$) instead of Lys439 and Val437. Additionally, the Glu135–Lys386 salt bridge and the His136–Ser383 contact in eEF1A2*GDP are not observed in eEF1A$_y$ because the conformational change induced by eEF1Bα enables Glu135 and His136 to contact the Switch II region.

Role of Mg^{2+} in GDP/GTP exchange in EF1A from evolutionary distinct organisms

The addition of homologous eEF1Bα to eEF1A$_y$ or *Artemia salina* eEF1A accelerated the nucleotide exchange process *in vitro* (31,32). In eEF1A$_y$, the acceleration was hypothesized to be induced mainly by the forced exit of Mg^{2+} from the nucleotide binding site by GEF. In particular, Mg^{2+} displacement by Lys205 from eEF1Bα was suggested to destabilize and facilitate the dissociation of GDP from eEF1A$_y$ (16–18).

Conversely, although Mg^{2+} was visible and functionally important for GTP hydrolysis in aEF1A*GTP (14), it was observed only under highly artificial conditions in aEF1A*GDP (33). Consequently, an alternative hypothesis was that the GDP/GTP exchange in aEF1A and eEF1A may occur solely due to the protein structure rearrangements, which are not necessarily coupled with the presence of Mg^{2+} (33).

Mg^{2+} had only a marginal effect on both spontaneous (Figure 3A) and GEF-dependent (Figure 3B) nucleotide exchanges in eEF1A2. The values of k_{off} for spontaneous GDP/GDP exchange in eEF1A2 were $5.6 \pm 0.3 \cdot 10^{-4}$ s^{-1} and $4.4 \pm 0.5 \cdot 10^{-4}$ s^{-1}, whereas the first-order rate constants for the GDP/GDP exchange catalyzed by eEF1Bα were $6.3 \pm 0.3 \cdot 10^{-3}$ s^{-1} and $10.0 \pm 0.5 \cdot 10^{-3}$ s^{-1} in the presence of 10 mM Mg^{2+} or EDTA, respectively. The spontaneous GDP/GDP exchange was observed to be independent of Mg^{2+} in eEF1A$_y$; however, the same study reported the importance of Mg^{2+} for the eEF1Bα-catalyzed nucleotide exchange process (18).

In the eEF1A2*GDP structure Mg^{2+} is in contact with the α- and β-phosphates of GDP. In molecule A the distance from the Mg^{2+} ion to the Asp17 side chain is 2.7 Å, in molecule B it rises to 3.5 Å. Because molecule A is crystallized in more flexible conformation as evidenced by the unresolved electron density of Gly50 situated in the effector region we believe that approaching the Mg^{2+} ion by Asp17 occurs due to local intramolecular fluctuations and does not play any role in stabilization of the metal ion by eEF1A2. To our knowledge, the aspartate residue at the fourth position of a Walker A motif (GxxXxGKS/T) has never been described as a ligand in GTPases.

The affinity of eEF1A for GDP is much less than that of EF-Tu (reviewed in (34)). In EF-Tu*GDP (pdb–1EFC), Mg^{2+} is in contact with the β-phosphate and α-phosphate

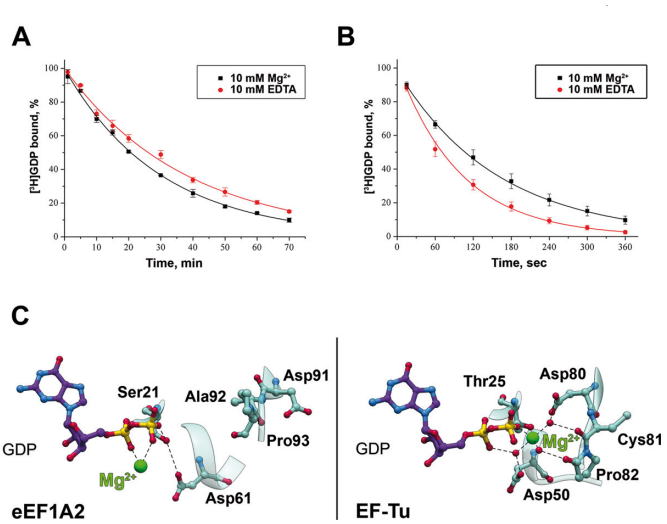

Figure 3. Mg^{2+} does not influence nucleotide exchange in eEF1A2. Mg^{2+} (black) and EDTA (red) do not have an impact on spontaneous (A) and eEF1Bα-catalyzed (B) nucleotide exchange process. The eEF1A2 concentration in the incubation mixture was 692 nM and eEF1Bα - 4 nM. The concentration of either Mg^{2+} or EDTA was 10 mM. Goodness (R^2) of single exponential fits was calculated to be >0.999 for nucleotide exchange in the presence of both Mg^{2+} and EDTA. (C) Mg^{2+} contributes to GDP binding in EF-Tu rather than in eEF1A2.

(12). However, Mg^{2+} is also linked to EF-Tu*GDP via direct contact with Thr25 and via water-mediated bonds with Asp51 and Asp81, whereas the corresponding residues in eEF1A2 (Asp61 and Asp91) are situated far from the magnesium binding site. There is also a direct Mg^{2+} contact with Thr25 which is conserved in all available EF-Tu*GDP structures. The side chain of corresponding Ser21 from the P-loop in eEF1A2 forms an H-bond with Asp61 instead. Thus, in eEF1A2*GDP the contacts of Mg^{2+} are limited by the α- and β-phosphates (Figure 3C). This finding, along with the kinetic data, favors the assumption that the presence of the magnesium ion cannot add any strength to the GDP stabilization in eEF1A2.

Molecular mechanism of the nucleotide exchange factor eEF1Bα function

Using the structures of both eEF1A2*GDP and eEF1A$_y$*GDP*eEF1Bα, we can deduce the GEF-mediated nucleotide exchange mechanism in eEF1A.

In order to destabilize GDP in eEF1A, the Switch I region has to be displaced, with a subsequent disruption of the (Glu68–His95, Arg69-Asp97, Glu68-Asp97) interaction network between Switch I and Switch II in the eEF1A2*GDP structure (Figure 4A and B). Such a rearrangement causes the loop 90–97 to move upwards and rotate. A key new observation is the orientation of Asp91, which is stabilized in eEF1A2*GDP by the interaction with His95, Asn101 and Ser107. In the presence of eEF1Bα, this residue makes a 180° flip to form a salt bridge with Lys20 and an H-bond with Ser21, which binds and stabilizes the β-phosphate in eEF1A2*GDP (Figure 4C and D). Ser21 also forms an H-bond with Lys205 of eEF1Bα (18). All of these events cause a destabilization of the β-phosphate position,

Downloaded from http://nar.oxfordjournals.org/ by guest on October 20, 2014

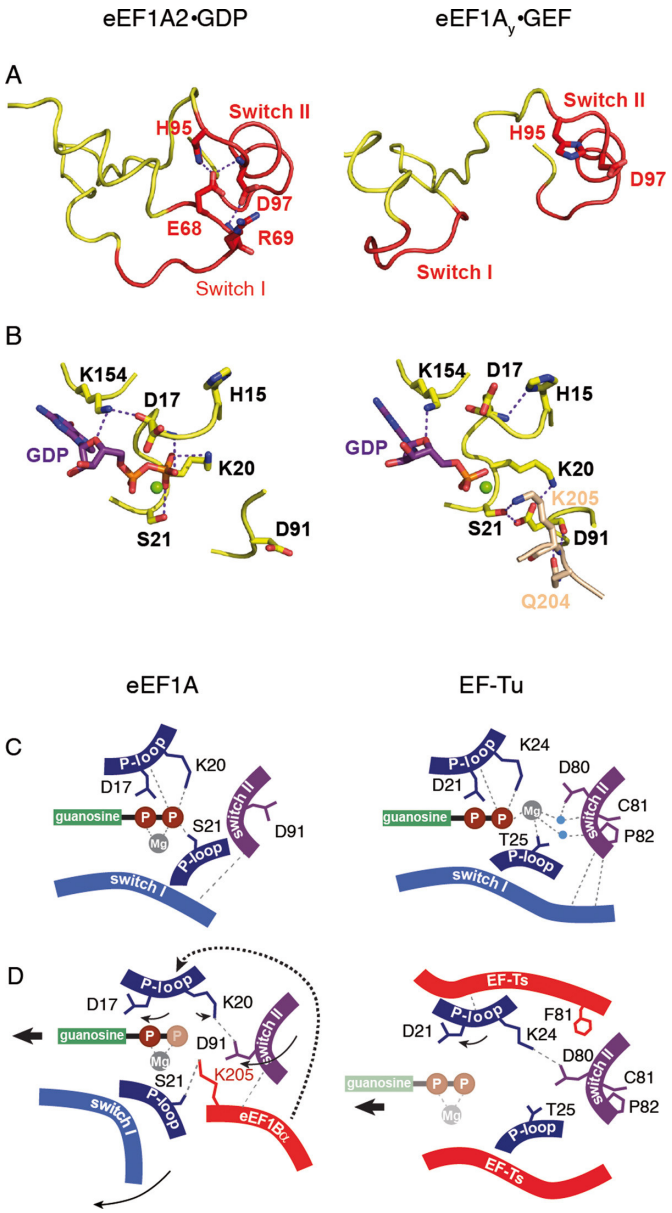

Figure 4. Mechanism of GEF-induced nucleotide exchange in eEF1A. (A) Conformation of the Switch I–Switch II region in eEF1A*GDP and in eEF1A$_y$-GEF. (B) Conformation of the GDP binding site in the absence and in the presence of GEF. Note the 180° rotation of Asp91. K205 and Q204 of eEF1Bα (numeration of yeast eEF1Bα) are shown in light brown. (C) Arrangement of the GDP-bound structures of eEF1A and EF-Tu. (D) Changes introduced in the GDP-bound structures of eEF1A and EF-Tu by corresponding GEFs. Eukaryotic GEF eEF1Bα directly disrupts contact of Ser21 with the β-phosphate, induces the conformational switch in P-loop leading to the disruption of Asp17 contact and prompts the conformational change in Switch II inducing 180° rotation of Asp91, with subsequent disruption of the Lys20 contact with the β-phosphate. Note the non-involvement of Mg^{2+} and GEF-induced rotation of Asp91 by 180°. Prokaryotic GEF EF-Ts causes conformational change in P loop, precluding contacts of Trp25 with Mg^{2+} linked to the β-phosphate, inducing rotation of Asp21 away from the β-phosphate and switch of Lys24 toward Asp81. Note the direct role of Mg^{2+} in the GDP stabilization, as well as similar positions of Asp81 in the GDP- and GEF-bound conformations. Water molecules are shown in blue. Magnesium ion is shown in gray. Compounds which are invisible in the structure, depicted as semi-transparent.

which probably reflects its disorder in the eEF1A$_y$*eEF1Bα crystal structure (16). eEF1Bα clearly induces a rotamer change of His95 in eEF1A and permits the formation of H-bonds with Asp97 (eEF1A, helix B) and Val179 (eEF1Bα).

In the presence of eEF1Bα, the rotation of the domain (II+III) unit and the subsequent restoration of its interaction with helix B are observed. Such domain rearrangements decrease the distance between helices B and C. Consequently, the Arg96 side chain can reposition upwards and interact with Gln132 and Glu135 of helix C that disrupts the Gln132-His15 interaction. This results in His15 forming an H-bond with Asp17, which prevents it from interacting with the β-phosphate group and causes the peptide bond 16–17 to flip and reorient.

Upon interaction with eEF1Bα the H-bond between Asp17 and Lys154 is broken and amino group of the Lys154 residue flipped by about 70° when compared to eEF1A2*GDP alone (Figure 4C and D). Despite this rotation, Lys154 retains the H-bond with the oxygen atom of the ribose ring, but not Glu122. This leads to an alteration of the ribose and guanine ring orientation, whereas the α-phosphate remains in a similar position in the presence or absence of eEF1Bα.

DISCUSSION

Two models for the nucleotide exchange process in eEF1A exist. One implicates Lys205 from eEF1Bα inducing the Mg^{2+} removal and peptide flip in the P-loop of eEF1A for the dissociation of GDP and prevention of its re-binding (16,17). Another hypothesis suggests that Mg^{2+} is dispensable for GDP binding and dissociation, and instead emphasizes that the significant domain rotation destabilizes the interaction of the P-loop and the β-phosphate of GDP (33). The first model was based on the EF-Tu-GDP and eEF1A$_y$-eEF1Bα structures, and assumed that the GDP exchange mechanism is similar in pro- and eukaryotic elongation factors. The second model accounts for the structure of aEF1A*GDP and expands the available data from archaeal to eukaryotic elongation factors.

The structure of eEF1A2*GDP demonstrates no direct Mg^{2+}-protein interactions. A spherical electron density observed between the α- and β-phosphates of GDP and the side chain of Asp17 was interpreted as the electrostatic interaction of the magnesium ion with the oxygen atoms of the phosphate groups situated ~2.5 Å away. The distance from Mg^{2+} to the Asp17 side chain in the molecule A is about 2.7 Å, however, in the molecule B this distance increases to 3.5 Å which makes the formation of a bond between Asp17 and Mg^{2+} less probable. No interaction of Mg^{2+} with the corresponding Asp is found in all known X-ray structures of the translational GTPases. Furthermore, the fluctuations of Mg^{2+} and GDP in molecules A and B of the dimer coincide, which favors the notion that Mg^{2+} is stabilized in eEF1A2 via the GDP molecule. The coordination geometry for Mg^{2} was not determined, however, the water-mediated contacts, which are not visible at 2.7 Å resolution, are still possible. The kinetic experiments do not show any substantial Mg^{2+} effect on the nucleotide exchange rate in the presence or absence of eEF1Bα, which is consistent with the non-involvement of Mg^{2+} in the mechanism of

Downloaded from http://nar.oxfordjournals.org/ by guest on October 20, 2014

GDP stabilization. The exclusion of Mg^{2+} resulted in the 3.6-fold acceleration of the eEF1Bα-catalyzed GDP dissociation from $eEF1A_y$ (18) and in small 1.6-fold increase of k_{off} for eEF1A2 (Figure 3B). Though one cannot entirely exclude some impact of Mg^{2+} upon the GDP release from eEF1A, the Mg^{2+} effect appears rather indirect and probably results from either subtle rearrangements of the GDP-binding site (35) induced by eEF1Bα or the increased stability of eEF1A*eEF1Bα complex in the presence of magnesium ions. Mg^{2+}-induced constriction has been observed for other protein–protein complexes (36,37).

The insertion of the Gln-204 side chain from eEF1Bα between two antiparallel β-strands linking the Switch I and Switch II regions was previously claimed to force Asp91 away from Ser21 and a water molecule, contributing to GDP dissociation (16). This is inconsistent with our observations because the Asp91 of eEF1A2*GDP undergoes a 180° rotation away from the nucleotide binding site, and forms H-bonds with His95 and Asn101 from helix B of the Switch II region. However, in the GTP form of aEF1A (14) and in the GEF-complexed form of $eEF1A_y$ (16) Asp91 is situated near the β-phosphate. Thus, eEF1Bα forces Asp91 back into the nucleotide-binding site rather than moving it out as was previously suggested (16) which may contribute to the dissociation of GDP as described in the Results section.

The 180° turn of Asp91 away from the GDP-binding site is detected also in aEF1A*GDP (13) and appears to be exclusive for non-bacterial elongation factors 1A. Interestingly, in the yeast termination factor eRF3, the corresponding Asp322 adopts the same as Asp91/90 in eEF1A2*GDP/aEF1A*GDP flipped position comparing to Asp81/Asp90 in EF-Tu*GTP/aEF1A*GTP correspondingly. However, contrary to the elongation factors, no nucleotide-dependent change in position of Asp322 was found in eRF3 (38).

The eEF1A2*GDP structure presented here contributes to the evolutionary understanding of the elongation factor 1 family. It is known that the structures of GDP-bound proteins display a large difference, while the GTP-bound forms of the G domain are mostly similar (39). The functional GTP form has the same configuration in EF-Tu and aEF1A and, possibly, in eEF1A, considering the principal common translation function of the factors. GTP forms of the elongation factors are very likely to preserve a universal mechanism of interaction with ribosomes in pro- and eukaryotes. However, the GDP-bound conformations of EF-Tu, aEF1A and eEF1A2 demonstrate essential differences. Thus, EF-Tu*GDP and aEF1A*GDP/eEF1A2*GDP represent various starting points toward achieving a universal GTP-bound conformation via different GEF-mediated mechanisms in bacterial and archaeal or eukaryotic cells. The bacterial and non-bacterial nucleotide exchange factors catalyze GDP/GTP exchange via distinct conformational changes, which results in similar GTP-bound conformations. Molecular details of the different mechanisms in prokaryotes and eukaryotes depicted as in (40) are summarized in Figure 4C and D.

The role for the domains' rotation during the transition of ribosome-bound eEF1A from the GTP- to GDP-bound conformation has been assessed. The structure of the eEF1A*GTP*aminoacyl-tRNA complex in the 80S ribosome was modeled by superimposing the X-ray structures of the yeast 80S ribosomes (41) and the bacterial 70S ribosome with the aminoacyl-tRNA and EF-Tu*GDPCP (12). We observed that substitution of the GTP form of eEF1A with eEF1A*GDP, assuming that an interaction of eEF1A*GDP with tRNA persists for some time after GTP hydrolysis (8,9), caused domain I to rotate out of the ribosome while domains II and III remained in place (Supplementary Figure S1). This result means that after GTP hydrolysis, there is a disruption in the interaction between domain I of eEF1A and the ribosome. Consequently, eEF1A*GDP is retained on the ribosome mainly due to some domain (II+III) contacts and can dissociate easier. Thus, the domain rotation in eEF1A*GDP upon GTP hydrolysis is a first step of releasing the protein from the 80S ribosome, which resembles dissociation of EF-Tu from the 70S ribosome (reviewed in (1)).

The link between the A and A′ helices provided by the Tyr56-His26 and Trp58-Tyr29 interactions is suggested to play a vital role for adopting a specific GDP-bound conformation of eEF1A2. Otherwise the α-helical A*-A′ region would shift away from the nucleotide as seen in the *Sulfolobus solfataricus* aEF1A*GDP (13). As compared to eEF1A2, the archaeal protein has two Phe residues substituted for Tyr56 and Trp58 correspondingly, lacks the aromatic ring, equivalent to His26 and contains Met28 instead of Tyr29. Also, the A-A′ interaction may be important for the correct positioning of Thr71/Thr72 into the GTP nucleotide binding site of eEF1A. The mutation of either Trp58 or Tyr56 is lethal (28); therefore, the stabilization strength of each residue is probably not sufficient to maintain the interaction of the helix A and A′ during the unwinding of the helix A′ and shift of A″ to the GTP-binding site. Moreover, we speculate that the link between A and A′, which forces these helices to move as a single unit, may be important for the GEF binding and dissociation mechanism. To reach the GDP binding site in eEF1A*GDP, GEF must separate the Switch I and Switch II regions. In eEF1A*GTP, the A-A′ unit apparently moves back into place and provides a mechanic force to dissociate GEF. This mechanism may be specific for the eukaryotic nucleotide exchange because the A-A′ link apparently cannot be formed in archaeal factors.

In higher vertebrates, there are two isoforms of eEF1A, which are 97% similar and are encoded by different genes. The expression of the isoforms is mutually exclusive: eEF1A2 appears in skeletal myocytes, cardiomyocytes and neurons; eEF1A1 is present in all remaining cells of the organism (42). Therefore, the role of isoforms during translation should be principally the same, whereas their tissue-specific localization suggests they may have different additional functions. Importantly, eEF1A2 is overexpressed in a number of human cancers (43,44) and was shown to have oncogene-like properties in some cases (45,46). The phosphorylation of Tyr29 has been reported in global phospho-proteomic cancer studies (47,48). This modification would prevent the Tyr29–Trp58 interaction in eEF1A2 (Figure 2C), which may affect the stability of the A-A′ helices linkage and result in an impairment of translation. The

Downloaded from http://nar.oxfordjournals.org/ by guest on October 20, 2014

Tyr29-phosphorylated cellular pool could fulfill some other functional duty, such as signaling or actin bundling (49,50).

Phosphorylated Ser163 and Thr239 are highly conserved in both eEF1A1 and eEF1A2 of higher eukaryotes. Bioinformatics predicts that the phosphorylation of Ser163 in eEF1A1 and eEF1A2 (92% identical) is probably performed by different protein kinases, ataxia telangiectasia mutated or casein kinase 1, respectively, due to a local difference in the primary structures of the isoforms. Identification of a kinase for Thr239 is an intriguing task for the future. The local landscape near the phosphorylated Thr239 residue includes Lys146 and Lys244 which can be acetylated *in vivo* (51,52). Phosphorylated Ser163 is situated near Lys165 which is dimethylated in the A1 isoform (53) and trimethylated in the A2 isoform (6). Cross-talk between the modifications may provide a unique isoform-specific local landscape for eEF1A, which can be utilized, in particular, to differentially distribute and/or functionally modify the 97% similar isoforms.

A segment of the unstructured C-terminus was observed in molecule A of the eEF1A2 dimer. The C-terminal tail was previously proposed to participate in aminoacyl-tRNA binding by EF-Tu (54). However, the C-terminal tail of eEF1A2 adopts a somewhat different form compared to the EF-Tu conformation and is situated far from the putative tRNA-binding region. This region of eEF1A2 contains a number of lysine residues which may serve as a platform for binding other kinds of RNA (55,56).

eEF1A belongs to a family of G-proteins, which function as GTP hydrolysis-dependent molecular switches and are pivotal for cell life. Typically, the activity of G-proteins is regulated by GEF that stimulate dissociation of tightly bound GDP produced by GTP hydrolysis (57). Mechanism of GDP/GTP exchange usually involves Mg^{2+}. The affinity of eEF1A for GDP and GTP is similar, contrary to its prokaryotic homolog EF-Tu. The data on X-ray structure of eEF1A2 explain the mechanics behind this, suggesting that a drop in the affinity for GDP is caused by exclusion of the magnesium ion role in the stabilization of GDP in eEF1A (Figure 3C). The independence from Mg^{2+}, with consequent decrease in the GDP binding strength, seems to ensure the reliability of eEF1A functioning in case of GEF deficiency. In addition, eEF1A plays a number of non-orthodox roles and, therefore, is distributed evenly throughout the cell while the function and localization of its GEFs is mostly limited to the protein synthesis compartments (58). Similar affinity of eEF1A for GDP and GTP may help to maintain spontaneous GDP/GTP exchange in the GEF-deficient regions of cells where the eEF1A functions are not related to the protein synthesis. That is possible because the intracellular concentration of GTP is much higher than GDP.

The overall strategy of the eukaryotic ribosomal chain elongation is to ensure a high accuracy of the protein synthesis along with a reasonable rate. The change of the rate-limiting step from GDP dissociation in EF-Tu to GTP hydrolysis in eEF1A (32), which is a consequence of decreased affinity of the eukaryotic protein for GDP, apparently contributes to this function as the hydrolysis of GTP is directly triggered by the correct codon–anticodon recognition. We believe that the understanding of difference in the molecular mechanisms of nucleotide exchange in pro- and eukaryotic elongation factors will be helpful for the development of anti-bacterial drugs specifically targeted to EF-Tu.

The analysis of the crystal structure of eEF1A2*GDP together with the structures of $eEF1A_y$*eEF1Bα and aEF1A*GDP provides the important information on the conformational changes essential for the eEF1A function, refines existing and describes novel aspects of the mechanics of the nucleotide exchange process in the translation factors. The results provide background for comprehensive knowledge of the mechanism and evolution of the polypeptide chain elongation by the ribosome.

ACCESSION NUMBERS

Coordinates and structure factors have been deposited at the Protein Data Bank (pdb–4C0S).

SUPPLEMENTARY DATA

Supplementary Data are available at NAR Online.

ACKNOWLEDGEMENTS

We thank Dr. Stephen Cusack (EMBL Grenoble Outstation, France) for continued interest and support of this work. The contribution of Oleksandra Novosylna and Nikolay Pydiura into the preparatory part of the work is greatly appreciated. We thank the staff of ESRF and of EMBL-Grenoble for their assistance and support in using beamlines ID14–4.

FUNDING

France-Ukraine PICS.
Conflict of interest statement. None declared.

REFERENCES

1. Voorhees,R.M. and Ramakrishnan,V. (2013) Structural basis of the translational elongation cycle. *Annu. Rev. Biochem.*, **82**, 203–236.
2. Dever,T.E. and Green,R. (2012) The elongation, termination, and recycling phases of translation in eukaryotes. *Cold Spring Harb. Perspect Biol.*, **4**, a013706.
3. Rodnina,M.V. and Wintermeyer,W. (2009) Recent mechanistic insights into eukaryotic ribosomes. *Curr. Opin. Cell. Biol.*, **21**, 435–443.
4. Budkevich,T.V., Timchenko,A.A., Tiktopulo,E.I., Negrutskii,B.S., Shalak,V.F., Petrushenko,Z.M., Aksenov,V.L., Willumeit,R., Kohlbrecher,J., Serdyuk,I.N. *et al.* (2002) Extended conformation of mammalian translation elongation factor 1A in solution. *Biochemistry*, **41**, 15342–15349.
5. Guzzo,C.M. and Yang,D.C. (2008) Lysyl-tRNA synthetase interacts with EF1alpha, aspartyl-tRNA synthetase and p38 in vitro. *Biochem. Biophys. Res. Commun.*, **365**, 718–723.
6. Kahns,S., Lund,A., Kristensen,P., Knudsen,C.R., Clark,B.F., Cavallius,J. and Merrick,W.C. (1998) The elongation factor 1 A-2 isoform from rabbit: cloning of the cDNA and characterization of the protein. *Nucleic Acids Res.*, **26**, 1884–1890.
7. Negrutskii,B.S., Shalak,V.F., Kerjan,P., El'skaya,A.V. and Mirande,M. (1999) Functional interaction of mammalian valyl-tRNA synthetase with elongation factor EF-1alpha in the complex with EF-1H. *J. Biol. Chem.*, **274**, 4545–4550.
8. Petrushenko,Z.M., Budkevich,T.V., Shalak,V.F., Negrutskii,B.S. and El'skaya,A.V. (2002) Novel complexes of mammalian translation elongation factor eEF1A.GDP with uncharged tRNA and aminoacyl-tRNA synthetase. Implications for tRNA channeling. *Eur. J. Biochem.*, **269**, 4811–4818.

Downloaded from http://nar.oxfordjournals.org/ by guest on October 20, 2014

9. Petrushenko,Z.M., Negrutskii,B.S., Ladokhin,A.S., Budkevich,T.V., Shalak,V.F. and El'skaya,A.V. (1997) Evidence for the formation of an unusual ternary complex of rabbit liver EF-1alpha with GDP and deacylated tRNA. *FEBS Lett.*, **407**, 13–17.
10. Kjeldgaard,M., Nissen,P., Thirup,S. and Nyborg,J. (1993) The crystal structure of elongation factor EF-Tu from Thermus aquaticus in the GTP conformation. *Structure*, **1**, 35–50.
11. Nissen,P., Thirup,S., Kjeldgaard,M. and Nyborg,J. (1999) The crystal structure of Cys-tRNACys-EF-Tu-GDPNP reveals general and specific features in the ternary complex and in tRNA. *Structure*, **7**, 143–156.
12. Song,H., Parsons,M.R., Rowsell,S., Leonard,G. and Phillips,S.E. (1999) Crystal structure of intact elongation factor EF-Tu from Escherichia coli in GDP conformation at 2.05 A resolution. *J. Mol. Biol.*, **285**, 1245–1256.
13. Vitagliano,L., Masullo,M., Sica,F., Zagari,A. and Bocchini,V. (2001) The crystal structure of Sulfolobus solfataricus elongation factor 1alpha in complex with GDP reveals novel features in nucleotide binding and exchange. *EMBO J.*, **20**, 5305–5311.
14. Kobayashi,K., Kikuno,I., Kuroha,K., Saito,K., Ito,K., Ishitani,R., Inada,T. and Nureki,O. (2010) Structural basis for mRNA surveillance by archaeal Pelota and GTP-bound EF1alpha complex. *Proc. Natl. Acad. Sci. U.S.A.*, **107**, 17575–17579.
15. Kobayashi,K., Saito,K., Ishitani,R., Ito,K. and Nureki,O. (2012) Structural basis for translation termination by archaeal RF1 and GTP-bound EF1alpha complex. *Nucleic Acids Res.*, **40**, 9319–9328.
16. Andersen,G.R., Pedersen,L., Valente,L., Chatterjee,I., Kinzy,T.G., Kjeldgaard,M. and Nyborg,J. (2000) Structural basis for nucleotide exchange and competition with tRNA in the yeast elongation factor complex eEF1A:eEF1Balpha. *Mol. Cell*, **6**, 1261–1266.
17. Andersen,G.R., Valente,L., Pedersen,L., Kinzy,T.G. and Nyborg,J. (2001) Crystal structures of nucleotide exchange intermediates in the eEF1A-eEF1Balpha complex. *Nat. Struct. Biol.*, **8**, 531–534.
18. Pittman,Y.R., Valente,L., Jeppesen,M.G., Andersen,G.R., Patel,S. and Kinzy,T.G. (2006) Mg2+ and a key lysine modulate exchange activity of eukaryotic translation elongation factor 1B alpha. *J. Biol. Chem.*, **281**, 19457–19468.
19. Yaremchuk,A., Shalak,V.F., Novosylna,O.V., Negrutskii,B.S., Crepin,T., El'skaya,A.V. and Tukalo,M. (2012) Purification, crystallization and preliminary X-ray crystallographic analysis of mammalian translation elongation factor eEF1A2. *Acta Crystallogr. F Struct .Biol. Cryst. Com.***68**, 295–297.
20. Cans,C., Passer,B.J., Shalak,V., Nancy-Portebois,V., Crible,V., Amzallag,N., Allanic,D., Tufino,R., Argentini,M., Moras,D. *et al.* (2003) Translationally controlled tumor protein acts as a guanine nucleotide dissociation inhibitor on the translation elongation factor eEF1A. *Proc. Natl. Acad. Sci. U.S.A.*, **100**, 13892–13897.
21. Kabsch,W. (2010) Integration, scaling, space-group assignment and post-refinement. *Acta Crystallogr. D Biol. Crystallogr.*, **66**, 133–144.
22. Vonrhein,C., Blanc,E., Roversi,P. and Bricogne,G. (2007) Automated structure solution with autoSHARP. *Methods Mol. Biol.*, **364**, 215–230.
23. Collaborative Computational Project, N. (1994) The CCP4 suite: programs for protein crystallography. *Acta Crystallogr. D Biol. Crystallogr.*, **50**, 760–763.
24. Chen,V.B., Arendall,W.B. 3rd, Headd,J.J., Keedy,D.A., Immormino,R.M., Kapral,G.J., Murray,L.W., Richardson,J.S. and Richardson,D.C. (2010) MolProbity: all-atom structure validation for macromolecular crystallography. *Acta Crystallogr. D Biol. Crystallogr.*, **66**, 12–21.
25. Yang,Z., Lasker,K., Schneidman-Duhovny,D., Webb,B., Huang,C.C., Pettersen,E.F., Goddard,T.D., Meng,E.C., Sali,A. and Ferrin,T.E. (2012) UCSF Chimera, MODELLER, and IMP: an integrated modeling system. *J. Struct. Biol.*, **179**, 269–278.
26. Bunai,F., Ando,K., Ueno,H. and Numata,O. (2006) Tetrahymena eukaryotic translation elongation factor 1A (eEF1A) bundles filamentous actin through dimer formation. *J. Biochem.*, **140**, 393–399.
27. Sanges,C., Scheuermann,C., Zahedi,R.P., Sickmann,A., Lamberti,A., Migliaccio,N., Baljuls,A., Marra,M., Zappavigna,S., Reinders,J. *et al.* (2012) Raf kinases mediate the phosphorylation of eukaryotic translation elongation factor 1A and regulate its stability in eukaryotic cells. *Cell Death Dis.*, **3**, e276.
28. Belyi,Y., Tartakovskaya,D., Tais,A., Fitzke,E., Tzivelekidis,T., Jank,T., Rospert,S. and Aktories,K. (2012) Elongation factor 1A is the target of growth inhibition in yeast caused by Legionella pneumophila glucosyltransferase Lgt1. *J. Biol. Chem.*, **287**, 26029–26037.
29. Polekhina,G., Thirup,S., Kjeldgaard,M., Nissen,P., Lippmann,C. and Nyborg,J. (1996) Helix unwinding in the effector region of elongation factor EF-Tu-GDP. *Structure*, **4**, 1141–1151.
30. Kanibolotsky,D.S., Novosyl'na,O.V., Abbott,C.M., Negrutskii,B.S. and El'skaya,A.V. (2008) Multiple molecular dynamics simulation of the isoforms of human translation elongation factor 1A reveals reversible fluctuations between 'open' and 'closed' conformations and suggests specific for eEF1A1 affinity for Ca2+-calmodulin. *BMC Struct. Biol.*, **8**, e4.
31. Gromadski,K.B., Schummer,T., Stromgaard,A., Knudsen,C.R., Kinzy,T.G. and Rodnina,M.V. (2007) Kinetics of the interactions between yeast elongation factors 1A and 1Balpha, guanine nucleotides, and aminoacyl-tRNA. *J. Biol. Chem.*, **282**, 35629–35637.
32. Janssen,G.M. and Moller,W. (1988) Kinetic studies on the role of elongation factors 1 beta and 1 gamma in protein synthesis. *J. Biol. Chem.*, **263**, 1773–1778.
33. Vitagliano,L., Ruggiero,A., Masullo,M., Cantiello,P., Arcari,P. and Zagari,A. (2004) The crystal structure of Sulfolobus solfataricus elongation factor 1alpha in complex with magnesium and GDP. *Biochemistry*, **43**, 6630–6636.
34. Negrutskii,B.S. and El'skaya,A.V. (1998) Eukaryotic translation elongation factor 1 alpha: structure, expression, functions, and possible role in aminoacyl-tRNA channeling. *Prog. Nucleic Acid Res. Mol. Biol.*, **60**, 47–78.
35. Schummer,T., Gromadski,K.B. and Rodnina,M.V. (2007) Mechanism of EF-Ts-catalyzed guanine nucleotide exchange in EF-Tu: contribution of interactions mediated by helix B of EF-Tu. *Biochemistry*, **46**, 4977–4984.
36. Yamazoe,M., Onogi,T., Sunako,Y., Niki,H., Yamanaka,K., Ichimura,T. and Hiraga,S. (1999) Complex formation of MukB, MukE and MukF proteins involved in chromosome partitioning in Escherichia coli. *EMBO J.*, **18**, 5873–5884.
37. Oliveira,L., Cuervo,A. and Tavares,P. (2010) Direct interaction of the bacteriophage SPP1 packaging ATPase with the portal protein. *J. Biol. Chem.*, **285**, 7366–7373.
38. Kong,C., Ito,K., Walsh,M.A., Wada,M., Liu,Y., Kumar,S., Barford,D., Nakamura,Y. and Song,H. (2004) Crystal structure and functional analysis of the eukaryotic class II release factor eRF3 from S. pombe. *Mol. Cell*, **14**, 233–245.
39. Vetter,I.R. and Wittinghofer,A. (2001) The guanine nucleotide-binding switch in three dimensions. *Science*, **294**, 1299–1304.
40. Yang,J., Zhang,Z., Roe,S.M., Marshall,C.J. and Barford,D. (2009) Activation of Rho GTPases by DOCK exchange factors is mediated by a nucleotide sensor. *Science*, **325**, 1398–1402.
41. Ben-Shem,A., Garreau de Loubresse,N., Melnikov,S., Jenner,L., Yusupova,G. and Yusupov,M. (2011) The structure of the eukaryotic ribosome at 3.0 A resolution. *Science*, **334**, 1524–1529.
42. Abbott,C.M., Newbery,H.J., Squires,C.E., Brownstein,D., Griffiths,L.A. and Soares,D.C. (2009) eEF1A2 and neuronal degeneration. *Biochem. Soc. Trans.*, **37**, 1293–1297.
43. Pinke,D.E., Kalloger,S.E., Francetic,T., Huntsman,D.G. and Lee,J.M. (2008) The prognostic significance of elongation factor eEF1A2 in ovarian cancer. *Gynecol. Oncol.*, **108**, 561–568.
44. Scaggiante,B., Dapas,B., Bonin,S., Grassi,M., Zennaro,C., Farra,R., Cristiano,L., Siracusano,S., Zanconati,F., Giansante,C. *et al.* (2012) Dissecting the expression of EEF1A1/2 genes in human prostate cancer cells: the potential of EEF1A2 as a hallmark for prostate transformation and progression. *Br. J. Cancer*, **106**, 166–173.
45. Anand,N., Murthy,S., Amann,G., Wernick,M., Porter,L.A., Cukier,I.H., Collins,C., Gray,J.W., Diebold,J., Demetrick,D.J. *et al.* (2002) Protein elongation factor EEF1A2 is a putative oncogene in ovarian cancer. *Nat. Genet.*, **31**, 301–305.
46. Tomlinson,V.A., Newbery,H.J., Wray,N.R., Jackson,J., Larionov,A., Miller,W.R., Dixon,J.M. and Abbott,C.M. (2005) Translation elongation factor eEF1A2 is a potential oncoprotein that is overexpressed in two-thirds of breast tumours. *BMC Cancer*, **5**, e113.
47. Rikova,K., Guo,A., Zeng,Q., Possemato,A., Yu,J., Haack,H., Nardone,J., Lee,K., Reeves,C., Li,Y. *et al.* (2007) Global survey of

Downloaded from http://nar.oxfordjournals.org/ by guest on October 20, 2014

phosphotyrosine signaling identifies oncogenic kinases in lung cancer. *Cell*, **131**, 1190–1203.
48. Rush,J., Moritz,A., Lee,K.A., Guo,A., Goss,V.L., Spek,E.J., Zhang,H., Zha,X.M., Polakiewicz,R.D. and Comb,M.J. (2005) Immunoaffinity profiling of tyrosine phosphorylation in cancer cells. *Nat. Biotechnol.*, **23**, 94–101.
49. Mateyak,M.K. and Kinzy,T.G. (2010) eEF1A: thinking outside the ribosome. *J. Biol. Chem.*, **285**, 21209–21213.
50. Negrutskii,B., Vlasenko,D. and El'skaya,A. (2012) From global phosphoproteomics to individual proteins: the case of translation elongation factor eEF1A. *Expert Rev. Proteom.*, **9**, 71–83.
51. Choudhary,C., Kumar,C., Gnad,F., Nielsen,M.L., Rehman,M., Walther,T.C., Olsen,J.V. and Mann,M. (2009) Lysine acetylation targets protein complexes and co-regulates major cellular functions. *Science*, **325**, 834–840.
52. Wu,X., Oh,M.H., Schwarz,E.M., Larue,C.T., Sivaguru,M., Imai,B.S., Yau,P.M., Ort,D.R. and Huber,S.C. (2011) Lysine acetylation is a widespread protein modification for diverse proteins in Arabidopsis. *Plant Physiol.*, **155**, 1769–1778.
53. Dever,T.E., Costello,C.E., Owens,C.L., Rosenberry,T.L. and Merrick,W.C. (1989) Location of seven post-translational modifications in rabbit elongation factor 1 alpha including dimethyllysine, trimethyllysine, and glycerylphosphorylethanolamine. *J. Biol. Chem.*, **264**, 20518–20525.
54. Andersen,G.R., Thirup,S., Spremulli,L.L. and Nyborg,J. (2000) High resolution crystal structure of bovine mitochondrial EF-Tu in complex with GDP. *J. Mol. Biol.*, **297**, 421–436.
55. Miura,P., Coriati,A., Belanger,G., De Repentigny,Y., Lee,J., Kothary,R., Holcik,M. and Jasmin,B.J. (2010) The utrophin A 5′-UTR drives cap-independent translation exclusively in skeletal muscles of transgenic mice and interacts with eEF1A2. *Hum. Mol. Genet.*, **19**, 1211–1220.
56. Sikora,D., Greco-Stewart,V.S., Miron,P. and Pelchat,M. (2009) The hepatitis delta virus RNA genome interacts with eEF1A1, p54(nrb), hnRNP-L, GAPDH and ASF/SF2. *Virology*, **390**, 71–78.
57. Wittinghofer,A. and Vetter,I.R. (2011) Structure-function relationships of the G domain, a canonical switch motif. *Annu. Rev. Biochem.*, **80**, 943–971.
58. Sanders,J., Brandsma,M., Janssen,G.M., Dijk,J. and Moller,W. (1996) Immunofluorescence studies of human fibroblasts demonstrate the presence of the complex of elongation factor-1 beta gamma delta in the endoplasmic reticulum. *J. Cell Sci.*, **109**, 1113–1117.

Downloaded from http://nar.oxfordjournals.org/ by guest on October 20, 2014

1.3. Взаємодія eEF1A1 у ГДФ-зв'язаній формі з деацильованою тРНК і фенілаланіл-тРНК синтетазою

Eur. J. Biochem. **269**, 4811–4818 (2002) © FEBS 2002 doi:10.1046/j.1432-1033.2002.03178.x

Novel complexes of mammalian translation elongation factor eEF1A·GDP with uncharged tRNA and aminoacyl-tRNA synthetase

Implications for tRNA channeling

Zoya M. Petrushenko, Tatyana V. Budkevich, Vyacheslav F. Shalak, Boris S. Negrutskii and Anna V. El'skaya

Institute of Molecular Biology and Genetics, National Academy of Sciences of Ukraine, Kiev, Ukraine

Multimolecular complexes involving the eukaryotic elongation factor 1A (eEF1A) have been suggested to play an important role in the channeling (vectorial transfer) of tRNA during protein synthesis [Negrutskii, B.S. & El'skaya, A.V. (1998) *Prog. Nucleic Acids Res. Mol. Biol.* **60,** 47–78]. Recently we have demonstrated that besides performing its canonical function of forming a ternary complex with GTP and aminoacyl-tRNA, the mammalian eEF1A can produce a noncanonical ternary complex with GDP and uncharged tRNA [Petrushenko, Z.M., Negrutskii, B.S., Ladokhin, A.S., Budkevich, T.V., Shalak, V.F. & El'skaya, A.V. (1997) *FEBS Lett.* **407,** 13–17]. The [eEF1A·GDP·tRNA] complex has been hypothesized to interact with aminoacyl-tRNA synthetase (ARS) resulting in a quaternary complex where uncharged tRNA is transferred to the enzyme for amino acylation. Here we present the data on association of the [eEF1A·GDP·tRNA] complex with phenylalanyl-tRNA synthetase (PheRS), e.g. the formation of the above quaternary complex detected by the gel-retardation and surface plasmon resonance techniques. To estimate the stability of the novel ternary and quaternary complexes of eEF1A the fluorescence method and BIAcore analysis were used. The dissociation constants for the [eEF1A·GDP·tRNA] and [eEF1A·GDP·$tRNA^{Phe}$·PheRS] complexes were found to be 20 nM and 9 nM, respectively. We also revealed a direct interaction of PheRS with eEF1A in the absence of $tRNA^{Phe}$ (K_d = 21 nM). However, the addition of $tRNA^{Phe}$ accelerated eEF1A·GDP binding to the enzyme. A possible role of these stable novel ternary and quaternary complexes of eEF1A·GDP with tRNA and ARS in the channeled elongation cycle is discussed.

Keywords: translation elongation factor; macromolecular complexes; tRNA channeling; eukaryotic protein synthesis; BIAcore analysis.

Aminoacyl-tRNA synthetase (ARS) and eEF1A are the proteins that advance the translation elongation cycle. ARS binds ATP, an amino acid and tRNA to produce aminoacyl-tRNA. The molecules of eEF1A bind GTP and aminoacyl-tRNA, and deliver the latter to the A site of a translating ribosome. The main steps of protein biosynthesis are similar in all living organisms. However, some peculiarities of the higher eukaryotic translation have been revealed, among which a compartmentalization of the translation apparatus is of particular importance. There is an increasing body of evidence for special structural organization of the protein synthesis machinery in the higher eukaryotic cells. The existence of multimolecular complexes of ARS [1], initiation factors [2] and eEF1 [3,4], ribosome–ARS interactions [5–7], and the association of translation components with cytoskeletal framework [8] are among the important signs of the protein synthesis compartmentalization. Moreover, detailed fluorescence-based measurements of translation in living dendrites have visualized the mammalian protein synthesis compartments *in situ* [9].

An important mechanism to put into effect the potential advantages of the compartmentalization is thought to be a channeling (vectorial transfer) of aminoacyl-tRNA/tRNA from ARS to the elongation factor, ribosome and back to ARS without dissociation into the surrounding medium [10,11]. The channeling influences positively the translational efficiency because the number of nonspecific searches is diminished, the effective concentrations of translational components are increased and the leakage of important compounds to another metabolic processes is hampered [12]. The channeling is a mechanism operating by the formation of intermediate complexes between subsequent participants of the metabolic pathway. Deutscher and coauthors revealed that aminoacyl-tRNA and tRNA were never free in the cytoplasm of the eukaryotic cell [10–12]. ARS and eEF1A are supposed to play a main role in the tRNA sequestering during the mammalian translation [13].

Several examples of the functional interaction of eEF1A with ARS resulting in the activation of the latter have been described [4,14,15]. While the stimulation of the valyl-tRNA

Correspondence to A. V. El'skaya, Department of Translation Mechanisms, Institute of Molecular Biology and Genetics, 150, Zabolotnogo Str., Kiev 03143 Ukraine.
Fax: +38 044 2660759, Tel.: +38 044 2660749,
E-mail: elskaya@biosensor.kiev.ua

Abbreviations: ARS, aminoacyl-tRNA synthetase; eEF1A, eukaryotic translation elongation factor 1A (formerly EF-1α); EF1A, prokaryotic translation elongation factor 1A (formerly EF-Tu); FITC, fluorescein isothiocyanate isomer I; GMP-PNP, guanosine-5′-(β,γ-imido)triphosphate; PheRS, phenylalanyl-tRNA synthetase; RU, resonance unit.

(Received 10 May 2002, revised 11 July 2002, accepted 13 August 2002)

49

14321033, 2002, 19, Downloaded from https://febs.onlinelibrary.wiley.com/doi/10.1046/j.1432-1033.2002.03178.x by Ukraine - Cochrane, Wiley Online Library on [17/01/2025]. See the Terms and Conditions (https://onlinelibrary.wiley.com/terms-and-conditions) on Wiley Online Library for rules of use; OA articles are governed by the applicable Creative Commons License

synthetase activity by eEF1A·GTP fits well for the customary channeling scheme, representing transfer of aminoacyl-tRNA from the enzyme to eEF1A·GTP [4], the explanation of the eEF1A·GDP stimulating effect [14] is not so obvious. We have hypothesized the activation of ARS by eEF1A·GDP could be a consequence of the interaction of ARS with the [eEF1A·GDP·tRNA] complex [13]. A functional meaning of the latter is supposed to accept deacylated tRNA directly from the E site of 80S ribosome. We postulated the following order of the interactions during vectorial transfer of tRNA/aminoacyl-tRNA in the eukaryotic elongation cycle [13]: [ribosomal E site·tRNA] (**1**) → [eEF1A·GDP·tRNA] (**2**) → [eEF1A·GDP·tRNA]·ARS (**3**) → [eEF1A·GTP·aminoacyl-tRNA] (**4**) → [ribosomal A site·aminoacyl-tRNA] (**5**) → [ribosomal P site·peptidyl-tRNA] (**6**) → [ribosomal E site·tRNA] (**1**).

The existence of complexes **1**, **4**, **5** and **6** was well documented and considered in all textbook schemes of protein synthesis. The formation of noncanonical complex **2** has been demonstrated recently [16] but its thermodynamic stability has not been determined. The idea of noncanonical quaternary complex **3** assembling was based on the stimulatory effect of eEF1A·GDP on the activity of several ARS [14], however, it remains to be shown directly.

In this work, the formation of a specific complex of [eEF1A·GDP·tRNA] with PheRS was shown by the gel-shift assay and surface plasmon resonance technique. High stability of both novel ternary and quaternary complexes of eEF1A·GDP, [eEF1A·GDP·tRNA] and [eEF1A·GDP·tRNA^{Phe}·PheRS], was observed, the dissociation constants being determined as 20 nM and 9 nM, respectively. The BIAcore analysis revealed a direct protein–protein interaction within the quaternary complex **3**. The sequence of events in the channeled elongation cycle of protein synthesis is discussed considering a putative supercomplex of ARS and GDP/GTP exchanging subunits of eEF1.

MATERIALS AND METHODS

Materials

Q-Sepharose, SP-Sepharose and Sephacryl S-400 were purchased from Pharmacia. Bio-Gel HTP hydroxylapatite was from Bio-Rad. [α-^{32}P]ATP, [^{14}C]phenylalanine and [^{3}H]GDP were purchased from Amersham. CTP, GDP, phospho*enol*pyruvate and phospho*enol*pyruvate kinase were from Sigma. tRNA nucleotidyltransferase was isolated from yeast as described [17]. Bovine catalase was from Serva, rabbit glyceraldehyde-3′-phosphate dehydrogenase (GADPH) was from Boehringer Mannheim. Bacterial EF1A was a gift from Dr I. Rublevskaya (this Department). BIAcore 2000 apparatus, sensor chip CM-5 and reagents for the surface plasmon resonance assay (Surfactant P20, amine coupling reagents, *N*′-ethyl-*N*′-(dimethylaminopropyl)carbodiimide, *N*-hydroxysuccinimide, ethanolamine hydrochloride) were obtained from Pharmacia Biosensor. Other chemicals were obtained from Sigma and Fluka.

Purification of rabbit liver PheRS and eEF1A

PheRS was isolated as described in [18], except that heparin-sepharose was used instead of tRNA-sepharose. The activity of PheRS in [^{14}C]phenylalanyl-tRNA formation was determined according to [14]. eEF1A·GDP was purified using the combination of gel-filtration and ion-exchange chromatography as previously described [19]. GDP/[^{3}H]GDP exchange on the eEF1A molecule was performed as described [19]. The purity of the enzymes was more than 95% according to the SDS/PAGE.

Preparation of bacterial EF1A·GTP

To obtain the GTP form of bacterial EF1A, the factor was incubated with 100 μM GTP in the incubation mixture containing 25 mM Tris/HCl, pH 7.5, 50 mM NH_4Cl, 10 mM $MgCl_2$, 1 mM dithiothreitol, 0.5 mM EDTA in the presence of 30 μg·mL^{-1} phospho*enol*pyruvate kinase and 2 mM phospho*enol*pyruvate to remove traces of GDP. Incubation was carried out at 30 °C for 15 min, and the EF1A·GTP preparation was used immediately.

tRNA^{Phe} purification

Enriched tRNA^{Phe} preparation was obtained from crude rabbit liver tRNA by BD-cellulose chromatography. Individual tRNA^{Phe} was purified using Hypersil 5C4 column (HPLC Gold system, Beckman). 3′-^{32}P-labeling of tRNA^{Phe} was performed with tRNA nucleotidyltransferase according to [20]. The labeled tRNA was purified in 8% polyacrylamide gel containing 8 M urea.

Fluorescence measurements

The fluorescein isothiocyanate isomer I (FITC)-labeled eEF1A was prepared according to [21] with some modifications. The protein (300 μg) was dialyzed for 2 h in 100 mM $NaHCO_3$, pH 8.1, 2 mM $MgCl_2$, 25 mM KCl, 20% glycerol, 10 μM phenylmethanesulfonyl fluoride and 2 mM dithiothreitol at 4 °C. The stock solution of FITC was added to the final concentration of 0.05 mg·mL^{-1} and the incubation was continued for 40 min at 28 °C. The reaction was quenched by addition of 2 M NH_4Cl (final concentration 50 mM) and the protein was separated from the dye by gel-filtration on Sephadex G-25.

To obtain eEF1A·GMP-PNP, the factor was incubated with 200 μM GMP-PNP in the incubation mixture containing 25 mM Tris/HCl, pH 7.5, 5 mM $MgCl_2$, 50 mM KCl, 13% glycerol and 2 mM dithiothreitol. Incubation was carried out at 37 °C for 5 min directly before start of the experiment.

Steady-state fluorescence measurements were made with spectrofluorimeter Hitachi F-4000, Japan. Excitation monochromator was set at 495 nm, emission wavelength was 525 nm.

Measurements were made in 1-mL quartz cuvettes containing 800 μL of 25 mM Tris/HCl, pH 7.5, 5 mM $MgCl_2$, 50 mM KCl, 13% glycerol, 2 mM dithiothreitol, 200 μM GDP (GMP-PNP) and 0.2 μM FITC-eEF1A·GDP (FITC-eEF1A·GMP-PNP) at +24 °C. FITC-eEF1A·GDP or FITC-eEF1A·GMP-PNP were titrated by increasing concentrations of tRNA to measure K_d of the [eEF1A·GDP/GMP-PNP·tRNA] complex. An increase in the mixture volume after tRNA addition did not exceed 3–5%. The data were corrected for the background fluorescence and dilution.

To confirm complex formation, the polarization value was determined after each tRNA addition. When plane

50
14321033, 2002, 19, Downloaded from https://febs.onlinelibrary.wiley.com/doi/10.1046/j.1432-1033.2002.03178.x by Ukraine - Cochrane, Wiley Online Library on [17/01/2025]. See the Terms and Conditions (https://onlinelibrary.wiley.com/terms-and-conditions) on Wiley Online Library for rules of use; OA articles are governed by the applicable Creative Commons License

polarized light is used to excite a fluorophore, molecules in which the absorption oscillators are orientated parallel to the direction of polarization will excite preferentially. The polarized components of the emission can be used to calculate a polarization value $P = I_{||} - I_{\perp}/I_{||} + I_{\perp}$ (where $I_{\perp}$ is the perpendicular component of fluorescence intensity and $I_{||}$ is the parallel component of fluorescence intensity) which is dependent on the rotational mobility of the fluorophores, which in turn relates directly to its size; therefore, larger fluorophores (with lower rotational mobility) exhibit higher polarization value under constant buffer conditions.

Because the polarization change is a nonlinear function [22], the effect of tRNA on a value of the perpendicular component of fluorescence intensity ($I_{\perp}$) was measured to estimate the K_d of the complex. The intensity was normalized according to Eqn. (1):

$$I_{\perp}\text{norm} = I_{\perp}^{0} - I_{\perp}^{\text{tRNA}}/I_{\perp}^{0} - 1 \quad (1)$$

where $I_{\perp}$norm is the normalized intensity, $I_{\perp}^{0}$ is the fluorescence intensity before tRNA addition, $I_{\perp}^{\text{tRNA}}$ is the intensity at given tRNA concentration. Data were curve-fitted by nonlinear least squares to a bimolecular binding isotherm according to the expression:

$$I_{\perp}\text{norm} = I_{\perp}^{\text{fin}} \times C/K_d + C \quad (2)$$

where $I_{\perp}^{\text{fin}}$ is the normalized intensity at final point of the titration curve, C is the tRNA concentration, K_d is the dissociation constant.

Gel mobility shift assay

A possibility of eEF1A·GDP in forming the complex with deacylated tRNA was studied by nondenaturing PAGE. The samples containing 10 μM eEF1A·GDP were incubated for 10 min at 37 °C in the presence of different concentrations of tRNA in buffer containing 25 mM Tris/HCl pH 7.5, 5 mM $MgCl_2$, 50 mM KCl, 10% glycerol, 6 mM 2-mercaptoethanol and 200 μM GDP. After the addition of 0.1 volume of 80% glycerol (containing traces of bromophenol blue) the samples were applied to 5% polyacrylamide gel (19 : 1). PAGE was performed for 6 h at 4 °C (40 mA, 100 V) in a buffer containing 100 mM Bes, pH 6.8, 10% glycerol, 10 μM GDP, 0.5 mM EDTA and 1 mM dithiothreitol. Protein bands were stained with Coomassie brilliant blue.

The formation of the complex of [^{32}P]tRNA^{Phe} with eEF1A and/or PheRS was studied on 0.7% agarose gel. Three picomoles of tRNA were incubated with 10 pmol of protein (eEF1A, PheRS or their mixture) at 37 °C for 10 min in 15 μL of 25 mM Hepes/KOH, pH 7.6, 5 mM $MgCl_2$, 100 mM KCl, 10% glycerol, 2 mM dithiothreitol and 100 μM GDP. The electrophoresis was run at 20 V·cm^{-1} (50 mM Tris/borate, pH 7.5, containing 1 mM EDTA) at 4 °C for 2 h. The radioactivity retained in the gel was visualized by autoradiography with Kodak BioMax film. Protein bands were stained with Coomassie brilliant blue.

Surface plasmon resonance analysis

The PheRS (250 000 Da) immobilization to the sensor chip was carried out in a buffer containing 10 mM Hepes/KOH, pH 7.4, 150 mM NaCl, 3.4 mM EDTA, 0.005% P20-surfactant at a flow rate of 5 μL·min^{-1} at 25 °C. The carboxymethyl dextran matrix of the sensor chip was activated by a 30-μL injection of the mixture of 0.2 M 1-ethyl-3-[(3-dimethylamino)propyl]carbodiimide and 0.05 M *N*-hydroxysuccinimide in water. PheRS coupling was performed in 10 mM Hepes/KOH, pH 7.4 by a 20-μL injection of the protein (50 μg·mL^{-1}). Unreacted *N*-hydroxysuccinimide ester groups were quenched by a 30-μL injection of 1 M ethanolamine/HCl, pH 8.0. The final level of PheRS immobilization was about 2500 resonance units (RU). Bovine catalase (2500 RU) was immobilized to the sensor chip in the same way. While studying the binding kinetics by BIAcore technique there is a danger of deviations from the real data in case of high surface density of an immobilized ligand. The mass transport effect was hypothesized to reduce the effective binding affinity for a soluble analyte [23]. However, a comparative analysis [24] of the binding data for immobilized influenza virus N9 neuraminidase (3000 RU surface density) with molecular mass 190 000 Da (close to PheRS) and the Fab fragment of monoclonal antibody of 50 000 Da (equal to eEF1A) with and without the mass transport correction term at a flow rate of 50 μL·min^{-1} showed that there was no significant difference in the fits indicating, in turn, that the values measured at such a high flow rate did not contain significant contribution from the mass transport.

To produce so-called 'blank' chip for the assessment of nonspecific adsorption of the analyte onto the sensing surface the sensor chip was activated as described above with the subsequent quenching of the active groups of *N*-hydroxysuccinimide ester by 1 M ethanolamine/HCl, pH 8.0. Association and dissociation of eEF1A·GDP or [eEF1A·GDP·tRNA^{Phe}] with PheRS immobilized surface were measured in the running buffer containing 25 mM Hepes/KOH, pH 7.6, 5 mM $MgCl_2$, 100 mM KCl, 10% glycerol, 2 mM dithiothreitol, 100 μM GDP and 0.005% P20-surfactant at the flow rate of 50 μL·min^{-1} at 25 °C. The solutions of eEF1A·GDP or [eEF1A·GDP·tRNA^{Phe}] (30–500 nM) were injected for 200 s followed by dissociation in the same buffer flow for 10 min. KCl (0.5 M) was used to regenerate a sensor chip after each binding event. The concentration of the ternary complex was set by eEF1A concentration.

BIAcore evaluation

The kinetic parameters were calculated using the kinetics evaluation software package BIAEVALUATION 3.0 (Pharmacia Biosensor). The theory of BIAcore measurement technique and calculations has been extensively described [25]. The formation of a surface-bound quaternary complex [eEF1A·GDP·tRNA·PheRS] was treated using Eqn (3):

$$A + B \xrightarrow{k_a} AB \xrightarrow{k_d} A + B \quad (3)$$

where A corresponds to the immobilized ligand (PheRS), B corresponds to analyte (eEF1A·GDP or [eEF1A·GDP·tRNA]), k_a is the association rate constant ($M^{-1}\cdot s^{-1}$), k_d is the dissociation rate constant (s^{-1}).

RESULTS AND DISCUSSION

Stability of the [eEF1A·GDP/GMP-PNP·tRNA] complexes

The stability of the noncanonical [eEF1A·GDP/GMP-PNP·tRNA] complexes was studied by the fluorescence method. The eEF1A preparation, containing approximately one molecule of the fluorescence reagent (FITC) per one protein molecule was obtained using an optimized labeling procedure. The functional activity of the FITC-modified eEF1A was verified by two independent techniques: the GDP/[^{3}H]GDP exchange and stimulation of poly(Phe) synthesis on poly(U)-programmed 80S ribosomes in reconstituted cell-free translation system [26]. The FITC-eEF1A activity was found to be 85–95% of the native protein activity in both tests (data not shown). The proportion of active molecules in the eEF1A·GDP preparation, i.e. amount of the protein molecules capable to form the complex with tRNA, was estimated as in [27] by gel-shift assay. Constant amounts of eEF1A were mixed with different tRNA concentrations and run in nondenaturing 5% PAGE (Fig. 1). Under the conditions described in detail in Materials and methods, eEF1A·GDP moves rather slowly (Fig. 1, lane 1) due to its high positive charge. It did not fully enter the gel even after 6 h of electrophoresis. As expected, the binding of negatively charged tRNA during complex formation accelerates the protein band movement (lanes 2–5). Lane 2 also shows that only at the ratio of factor to tRNA less than 2 : 1 a part of eEF1A·GDP remains on the start. Thus, practically all molecules of eEF1A·GDP were found in the complex and the amount of inactive eEF1A molecules being negligible.

The [eEF1A·GDP·tRNA] complex was shown earlier by several independent qualitative methods [16]. Here its formation during the factor titration with tRNA was confirmed by the fluorescence polarization technique (Fig. 2A). Indeed, gradual increase in the fluorescence polarization seen upon the addition of tRNA shows a change in the rotational mobility of the FITC-eEF1A·GDP in the free and tRNA-complexed state. The perpendicular component of fluorescence intensity ($I_\perp$) was normalized as described in Materials and methods. To determine K_d of the

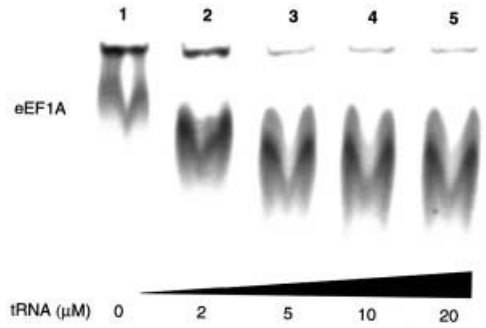

Fig. 1. Electrophoresis of eEF1A·GDP in nondenaturing conditions in the presence of different tRNA concentrations. eEF1A (10 μM) and indicated amounts of tRNA were incubated 10 min as described in Materials and methods and the mixture was applied to 5% polyacrylamide gel. Electrophoresis was performed for 6 h at 4 °C (40 mA, 100 V) in a buffer containing 100 mM Bes, pH 6.8, 10% glycerol, 10 μM GDP, 0.5 mM EDTA and 1 mM dithiothreitol. Protein bands were visualized by staining with Coomassie brilliant blue.

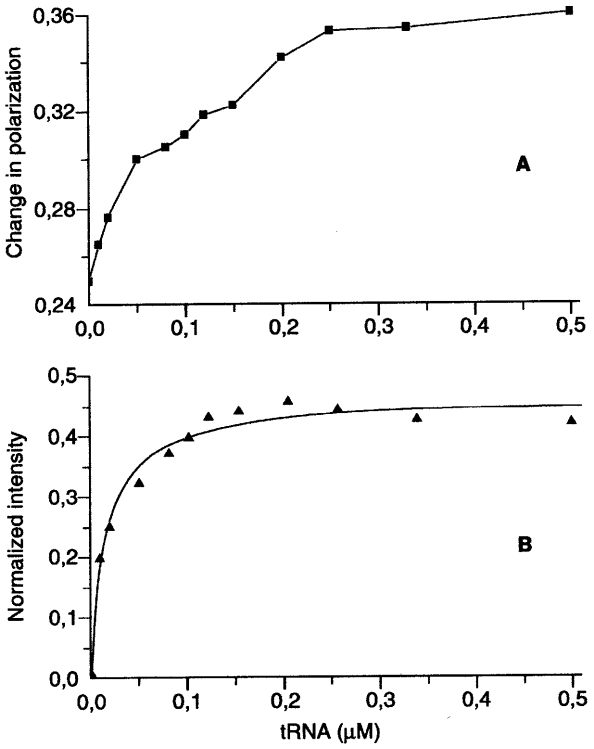

Fig. 2. Binding of tRNA to FITC-eEF1A·GDP. The protein fluorescence polarization (A) and perpendicular component of fluorescence intensity (B) of 0.2 μM FITC-eEF1A·GDP were recorded in the presence of indicated tRNA concentrations (0–0.5 μM final) as described in Materials and methods. Reactions were allowed to reach equilibrium and data were corrected for the background fluorescence and probe dilution.

[eEF1A·GDP·tRNA] complex the experimental points were fit to a bimolecular binding isotherm (Fig. 2B) according to Eqn (2). K_d for this complex was estimated to be 20 ± 3.1 nM. Substitution of GDP by a nonhydrolyzable GTP analog, GMP-PNP, diminished the affinity of the factor for uncharged tRNA causing a more than fourfold increase in the K_d value (91.7 ± 3.6 nM).

The high stability of the [eEF1A·GDP·tRNA] complex suggests a physiological meaning of its formation *in vivo* and is in accordance with the earlier obtained data concerning the specific sites of tRNA-factor interaction detected by various footprinting assays [16]. These sites of interaction of mammalian tRNA with eEF1A·GDP were shown to coincide with those of aminoacyl-tRNA in the complex with EF1A·GTP revealed by X-ray analysis [28].

Specific association of the [eEF1A·GDP·tRNA] complex with PheRS

Nondenaturing gel-retardation procedure was used to investigate a possibility of the formation of a stable complex between [eEF1A·GDP·tRNA] and PheRS. The usage of the polyacrylamide gel for the gel-shift experiments was ineffective because of the high positive charges of eEF1A and PheRS (pI are 9.1 and 8.2, respectively) and the high molecular mass of PheRS resulting in low electrophoretic mobility of the proteins and their complexes. Therefore, the

14321033, 2002, 19, Downloaded from https://febs.onlinelibrary.wiley.com/doi/10.1046/j.1432-1033.2002.03178.x by Ukraine - Cochrane, Wiley Online Library on [17/01/2025]. See the Terms and Conditions (https://onlinelibrary.wiley.com/terms-and-conditions) on Wiley Online Library for rules of use; OA articles are governed by the applicable Creative Commons License

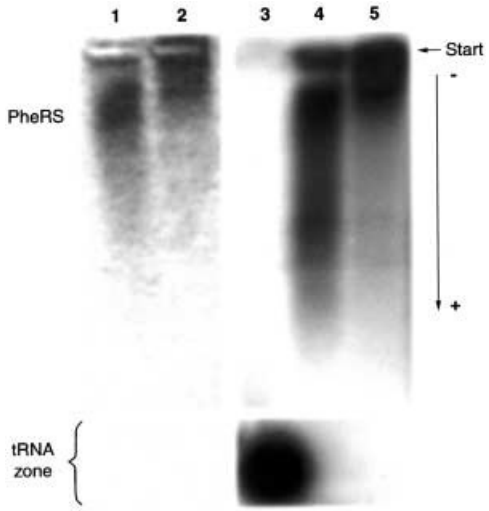

Fig. 3. Nondenaturing agarose electrophoresis assay of the [^{32}P]tRNA^{Phe} binding to PheRS and eEF1A·GDP. tRNA^{Phe} (3 pmol) was incubated with 10 pmol of PheRS (lanes 1, 4) or the mixture of 10 pmol of PheRS and 10 pmol of eEF1A (lanes 2, 5) at 37 °C for 10 min. The electrophoresis was run for 2 h at +4 °C in 0.7% agarose gel. Lane 3 shows [^{32}P]tRNA^{Phe} alone. The proteins were stained by Coomassie blue (lanes 1, 2). [^{32}P]tRNA^{Phe} was visualized by autoradiography (lanes 3, 4, 5). To save space, the tRNA^{Phe} radioactive signal is shown in a separate box below.

[eEF1A·GDP·tRNA·PheRS] complex formation was analyzed by the gel-retardation assay in 0.7% agarose (Fig. 3). Mixing all four components of the complex led to a marked delay of the [^{32}P]tRNA zone (lane 5) which coincided with the protein zone detected by Coomassie staining (lane 2).

To verify the specificity of the quaternary complex formation, [^{32}P]tRNA^{Phe} was incubated with rabbit GADPH or bovine catalase instead of PheRS (Fig. 4).

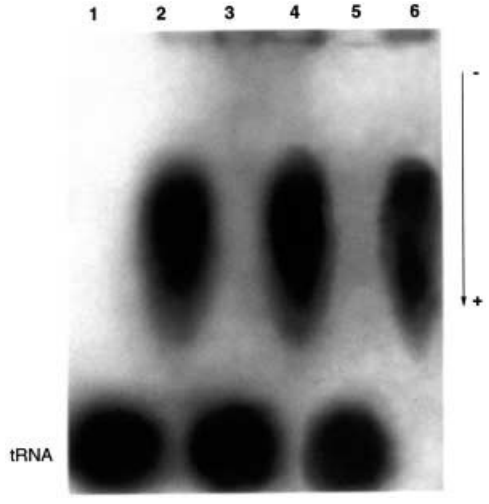

Fig. 4. Nondenaturing agarose electrophoresis of [^{32}P]tRNA^{Phe} in the presence of eEF1A·GDP and control proteins. tRNA was incubated with eEF1A (lane 2), GADPH (lane 3), eEF1A and GADPH (lane 4), bovine catalase (lane 5), bovine catalase and EF1A (lane 6) at 37 °C for 10 min. Lane 1 shows tRNA^{Phe} alone. Each lane contained 3 pmol of [^{32}P]tRNA^{Phe} and 10 pmol of protein.

These proteins were chosen as controls due to high positive charge of GADPH (pI 9.0) and molecular weight of catalase (240 000 Da) like PheRS. Moreover, GAPDH is known to possess nonspecific tRNA-binding properties [29]. Neither GAPDH (lane 3) nor catalase (lane 5) was found to interact with tRNA^{Phe} under the same conditions and no quaternary complexes were detected by the agarose gel electrophoresis.

The novel complexes found are specific for the mammalian eEF1A because the bacterial EF1A·GDP/GTP, like the above control proteins, does not form any complex when incubated with tRNA and PheRS (data not shown). It would be expected because the prokaryotic EF1A is known to possess a very low affinity for deacylated tRNA [30].

Stability of the quaternary [eEF1A·GDP·tRNA^{Phe}·PheRS] complex

The stability of the [eEF1A·GDP·tRNA^{Phe}·PheRS] complex was evaluated by the surface plasmon resonance technique. The BIAcore instrument detects changes in the surface plasmon resonance to monitor the interaction of an immobilized ligand with analyte molecules in flow solution [31]. PheRS was the immobilized ligand in all experiments because the immobilization of eEF1A led to a significant loss of its ability to bind tRNA. Therefore, the ternary [eEF1A·GDP·tRNA^{Phe}] complex was preformed for 4 min at 25 °C in the running buffer and injected as analyte. To estimate the contribution of nonspecific adsorption property of the sensor surface, control injections of the ternary complex over a blank chip (see Materials and methods) were performed. A background signal was automatically subtracted from the sensograms obtained with immobilized PheRS. The specificity of the ligand–analyte interaction was verified by the immobilization of bovine catalase instead of PheRS over the sensor chip with subsequent injection of eEF1A·GDP in flow buffer. It resulted in a signal equal to the control injection over a blank chip under the same experimental conditions (data not shown).

Figure 5 shows the increase in the chip response level upon addition of various concentrations of the [eEF1A·GDP·tRNA^{Phe}] complex. The kinetic and equilibrium constants determined in three separate runs with the injection of [eEF1A·GDP·tRNA^{Phe}] at six different concentrations are shown in Table 1.

It is noteworthy that the interaction of eEF1A·GDP with PheRS was observed in the absence of tRNA as well (Fig. 6). It means that tRNA binding is not critically important for the quaternary complex formation. However, tRNA^{Phe} accelerates the association phase of eEF1A·GDP binding to PheRS (see Table 1). In this case, the binding could be interpreted as biphasic and the apparent K_d value was calculated taking into account not only hyperbolic but also biphasic binding mode offered by the BIAEVALUATION 3.0 software package. Similar K_d values were obtained by both procedures. As complete dissociation of the [eEF1A·GDP·PheRS] and [eEF1A·GDP·tRNA^{Phe}·PheRS] complexes required significant period of time, the dissociation curves were extrapolated to zero by the software package. The apparent K_d for the [eEF1A·GDP·PheRS] complex formation was 21 nM. The high affinity of eEF1A for PheRS may be the reason of their co-purification from rabbit liver extract during several chromatographic steps

14321033, 2002, 19, Downloaded from https://febs.onlinelibrary.wiley.com/doi/10.1046/j.1432-1033.2002.03178.x by Ukraine - Cochrane, Wiley Online Library on [17/01/2025]. See the Terms and Conditions (https://onlinelibrary.wiley.com/terms-and-conditions) on Wiley Online Library for rules of use; OA articles are governed by the applicable Creative Commons License

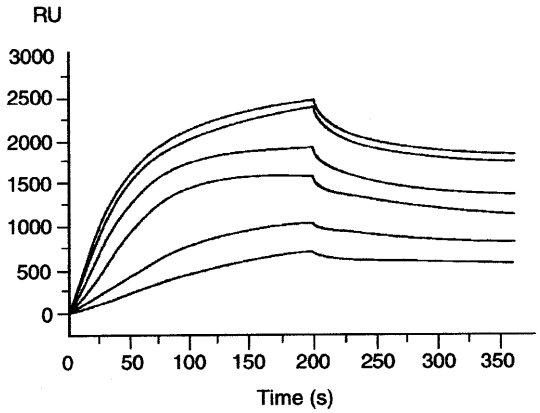

Fig. 5. Biosensor assay of the quaternary [eEF1A·GDP·tRNA^{Phe}·PheRS] complex formation. PheRS was immobilized on the chip as described in Materials and methods. Injections of the [eEF1A·GDP·tRNA^{Phe}] complex at concentrations of 60, 80, 125, 150, 250 and 500 nM (curves from bottom to top) were carried out for 200 s at flow rate of 50 μL·min^{-1} with the following dissociation of the quaternary complex for 10 min. The sensograms show the kinetics of the [eEF1A·GDP·tRNA^{Phe}] complex binding to immobilized PheRS and its subsequent dissociation from the immobilized enzyme.

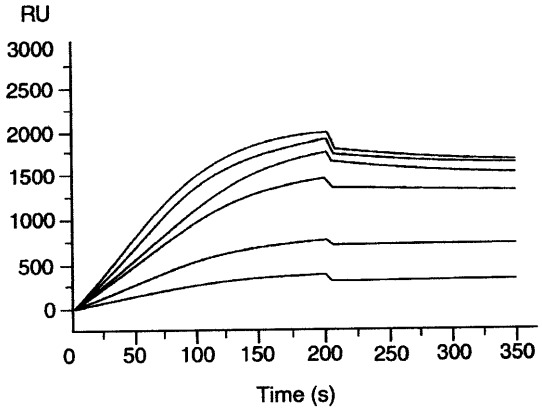

Fig. 6. Biosensor assay of the [eEF1A·GDP·PheRS] complex formation. PheRS was immobilized on the chip as described in Materials and methods. Injections of eEF1A·GDP were carried out for 200 s at flow rate of 50 μL·min^{-1} at concentrations of 40, 60, 100, 150, 250 and 500 nM (the curves from bottom to top) with the following dissociation of the [eEF1A·GDP·PheRS] complex for 10 min. The sensograms show the kinetics of the eEF1A·GDP binding to immobilized PheRS and its subsequent dissociation from the immobilized enzyme.

Table 1. Equilibrium and kinetic rate constants for [eEF1A·GDP·tRNA^{Phe}] and eEF1A·GDP binding to PheRS derived from the BIAcore measurements.

	k_a ($M^{-1}·s^{-1}$)	k_d (s^{-1})	K_d (M)
[eEF1A·GDP·tRNA^{Phe}]·PheRS	1.1×10^5	1.0×10^{-3}	9×10^{-9}
[eEF1A·GDP·PheRS]	3.8×10^5	0.8×10^{-3}	21×10^{-9}

(Turkovskaya, G.V. & El'skaya, A.V., unpublished observation). These data altogether seem to favor a possibility of the protein–protein association *in vivo*.

Vectorial transfer of tRNA/aminoacyl-tRNA during mammalian translation elongation cycle

Recently, the crystal structure of the [eEF1A·eEF1Bα] complex became available revealing a possibility of competition between tRNA/aminoacyl-tRNA and eEF1Bα for the same site on the eEF1A molecule [32]. The results presented here combined with these data, allowed us to propose the tRNA channeling scheme in detail (Fig. 7).

Taking into account rather low affinity of tRNA for the E site of 80S ribosomes (the apparent K_d is about 600 nM [33]), it is plausible to assume that the transfer of tRNA from the E site to eEF1A·GDP occurs due to the affinity gradient (K_d for [eEF1A·GDP·tRNA] is 20 nM, this study). Furthermore, the ARS affinity for [eEF1A·GDP·tRNA] (K_d is 9 nM, this study) is higher than that for free tRNA (K_d in the range of 100–200 nM [34,35]), which makes association of the enzyme with tRNA bound to eEF1A·GDP thermodynamically favorable. In this quaternary complex, a transfer of tRNA from the factor to ARS may occur. As the quaternary complex [eEF1A·GDP·tRNA·ARS] (B) is stabilized by the protein–protein and protein–tRNA interactions, eEF1A·GDP, being in the quaternary complex, may interact with eEF1Bα, the factor of GDP/GTP exchange. A possible association of ARS, eEF1A and

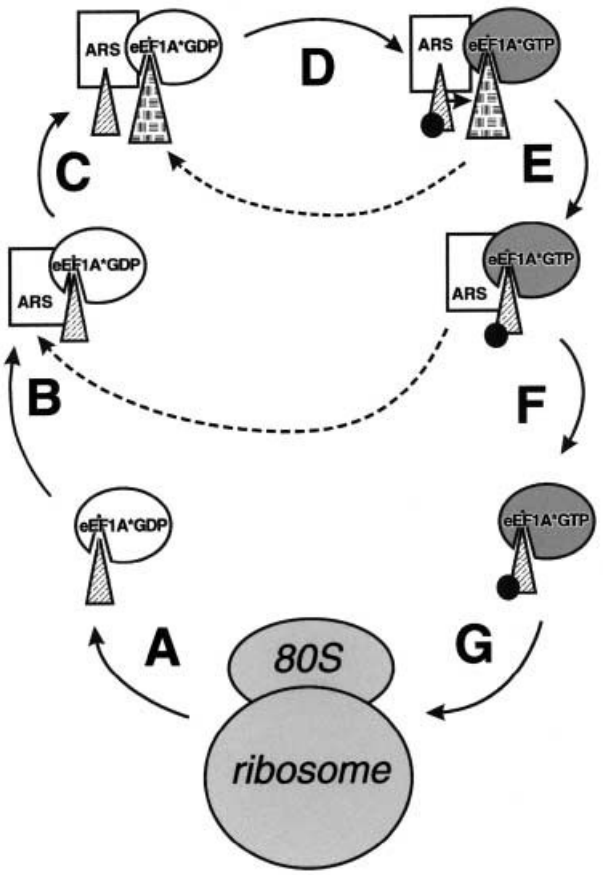

Fig. 7. Scheme showing the tRNA/aminoacyl-tRNA channeling in the translation elongation cycle. ●, amino acid; small and large triangles, tRNA and eEF1Bα, respectively.

14321033, 2002, 19, Downloaded from https://febs.onlinelibrary.wiley.com/doi/10.1046/j.1432-1033.2002.03178.x by Ukraine - Cochrane, Wiley Online Library on [17/01/2025]. See the Terms and Conditions (https://onlinelibrary.wiley.com/terms-and-conditions) on Wiley Online Library for rules of use; OA articles are governed by the applicable Creative Commons License

eEF1Bαβγ in a supercomplex is corroborated by the recent data on the ARS contacts with different subunits of eEF1 [36]. eEF1Bα, which possesses higher than tRNA affinity for eEF1A, displaces tRNA while the eEF1A·ARS and tRNA·ARS contacts remain intact (C). Thus, aminoacylation of tRNA and GDP/GTP exchange in the eEF1A molecule can occur at the same time (D). Then eEF1Bα departs from eEF1A being ousted by newly synthesized aminoacyl-tRNA (E) [32]. The finding that the complex of eEF1A, eEF1Bα and nonhydrolyzable analog of GTP could be dissociated by aminoacyl-tRNA rather than by deacylated tRNA [37] favors the decrease in affinity for eEF1A in the following order: [eEF1A·GDP·tRNA] < [eEF1A·eEF1Bα] < [eEF1A·GTP·aminoacyl-tRNA], supporting the sequence of interactions described above. The resulting quaternary complex [eEF1A·GTP·aminoacyl-tRNA·ARS] dissociates rapidly giving the canonical ternary complex [eEF1A·GTP·aminoacyl-tRNA] (F) and free ARS.

The scheme proposed and the results reported in this paper are in good agreement with the observation that tRNA in the eukaryotic cell is always bound to some protein [11], never being in a 'free' state. Further verification of the sequence of events during tRNA/aminoacyl-tRNA channeling involving the ARS molecule, as well as the elucidation of eEF1A·GDP action during dissociation of deacylated tRNA from the E site of 80S ribosome is presently underway.

ACKNOWLEDGMENT

We thank Ivan Gout (the Ludwig Institute for Cancer Research, London, UK) for permanent support in BIAcore experiments and Marc Mirande (Laboratoire d'Enzymologie et Biochimie Structurales, CNRS, Gif-sur-Yvette, France) for helpful comments on the manuscript. This work was supported by International Association for the Promotion of Cooperation with Scientists from the New Independent States of the Former Soviet Union (INTAS) Grant 96–1594 and by Ministry for Science and Technologies of Ukraine Grants 5.4/73 and 5.7/0003. Z.M.P. was supported in part by the Wellcome Trust Research Travel Grant and FEBS Short-term Fellowship.

REFERENCES

1. Mirande, M. (1991) Aminoacyl-tRNA synthetase family from prokaryotes and eukaryotes: structural domains and their implications. *Prog. Nucleic Acids Res. Mol. Biol.* **40**, 95–142.
2. Asano, K., Clayton, J., Shalev, A. & Hinnebusch, A.G. (2000) A multifactor complex of eukaryotic initiation factors, eIF1, eIF2, eIF3, eIF5, and initiator $tRNA^{Met}$ is an important translation initiation intermediate *in vivo*. *Genes Dev.* **14**, 2534–2546.
3. Janssen, G.M.C., van Damme, H.T.F., Kriek, J., Amons, R. & Möller, W. (1994) The subunit structure of elongation factor 1 from *Artemia*. Why two alpha-chains in this complex? *J. Biol. Chem.* **269**, 31410–31417.
4. Negrutskii, B.S., Shalak, V.F., Kerjan, P., El'skaya, A.V. & Mirande, M. (1999) Functional interaction of mammalian valyl-tRNA synthetase with elongation factor EF-1α in the complex with EF-1H. *J. Biol. Chem.* **274**, 4545–4550.
5. Irvin, J.D. & Hardesty, B. (1972) Binding of aminoacyl transfer ribonucleic acid synthetases to ribosomes from rabbit reticulocytes. *Biochemistry* **11**, 1915–1920.
6. Popenko, V.I., Cherny, N.E., Beresten, S.F., Zargarova, T.A. & Favorova, O.O. (1989) Immune electron microscope determination of the localization of tryptophanyl-tRNA synthetase in bacteria and higher eukaryotes. *Mol. Biol. (Moscow)* **23**, 1669–1681.
7. Turkovskaya, H.V., Belyanskaya, L.L., Kovalenko, M.I. & El'skaya, A.V. (1999) Renaturation of rabbit liver aminoacyl-tRNA synthetases by 80S ribosomes. *Int. J. Biochem. Cell Biol.* **31**, 759–768.
8. Stapulionis, R., Kolli, S. & Deutscher, M.P. (1997) Efficient mammalian protein synthesis requires an intact F-actin system. *J. Biol. Chem.* **272**, 24980–24986.
9. Job, C. & Eberwine, J. (2001) Identification of sites for exponential translation in living dendrites. *Proc. Natl Acad. Sci. USA* **98**, 13037–13042.
10. Negrutskii, B.S., Stapulionis, R. & Deutscher, M.P. (1994) Supramolecular organization of the mammalian translation system. *Proc. Natl Acad. Sci. USA* **91**, 964–968.
11. Stapulionis, R. & Deutscher, M.P. (1995) A channeled tRNA cycle during mammalian protein synthesis. *Proc. Natl Acad. Sci. USA* **92**, 7158–7161.
12. Negrutskii, B.S. & Deutscher, M.P. (1991) Channeling of aminoacyl-tRNA for protein synthesis *in vivo*. *Proc. Natl Acad. Sci. USA* **88**, 4991–4995.
13. Negrutskii, B.S. & El'skaya, A.V. (1998) Eukaryotic translation elongation factor 1α: structure, expression, functions, and possible role in aminoacyl-tRNA channeling. *Prog. Nucleic Acids Res. Mol. Biol.* **60**, 47–78.
14. Negrutskii, B.S., Budkevich, T.V., Shalak, V.F., Turkovskaya, G.V. & El'skaya, A.V. (1996) Rabbit translation elongation factor 1α stimulates the activity of homologous aminoacyl-tRNA synthetase. *FEBS Lett.* **382**, 18–20.
15. Reed, V.S., Wastney, M.E. & Yang, D.S.H. (1994) Mechanisms of the transfer of aminoacyl-tRNA from aminoacyl-tRNA synthetase to the elongation factor 1α. *J. Biol. Chem.* **269**, 3293–3296.
16. Petrushenko, Z.M., Negrutskii, B.S., Ladokhin, A.S., Budkevich, T.V., Shalak, V.F. & El'skaya, A.V. (1997) Evidence for the formation of an unusual ternary complex of rabbit liver EF-1α with GDP and deacylated tRNA. *FEBS Lett.* **407**, 13–17.
17. Rether, B., Bonnet, J. & Ebel, J.P. (1974) Studies on tRNA nucleotidyltransferase from baker's yeast. 1. Purification of the enzyme. Protection against thermal inactivation and inhibition by several substrates. *Eur. J. Biochem.* **50**, 281–288.
18. Pailliez, J.P. & Waller, J.P. (1984) Phenylalanyl-tRNA synthetases from sheep liver and yeast. Correlation between net charge and binding to ribosomes. *J. Biol. Chem.* **259**, 15491–15496.
19. Shalak, V.F., Budkevich, T.V., Negrutskii, B.S. & El'skaya, A.V. (1997) A fast and effective method for purification of elongation factor 1α from rabbit liver. *Ukr. Biochim. J.* **69**, 104–109.
20. Silberclang, M., Gillum, A.M. & RajBhandary, U.L. (1977) The use of nuclease P1 in sequence analysis of end group labeled RNA. *Nucleic Acids Res.* **4**, 4091–4108.
21. Weiel, J. & Hershey, J.W.B. (1981) Fluorescence polarization studies of the interaction of *Escherichia coli* protein synthesis initiation factor 3 with 30S ribosomal subunits. *Biochemistry* **20**, 5859–5865.
22. Ladokhin, A.S. (2000) Fluorescence spectroscopy in peptide and protein analysis. In *Encyclopedia of Analytical Chemistry: Instrumentation and Applications* (Meyers, R.A., ed.), pp. 5762–5779. John Wiley and Sons, New York.
23. Kortt, A.A., Oddie, G.W., Iliades, P., Gruen, L.C. & Hudson, P.J. (1997) Nonspecific amine immobilization of ligand can be a potential source of error in BIAcore binding experiments and may reduce binding affinities. *Anal. Biochem.* **253**, 103–111.
24. Kortt, A.A., Nice, E. & Gruen, L.C. (1999) Analysis of the binding of the Fab fragment of monoclonal antibody NC10 to influenza virus N9 neuraminidase from tern and whale using the BIAcore biosensor: effect of immobilization level and flow rate on kinetic analysis. *Anal. Biochem.* **273**, 133–141.

14321033, 2002, 19, Downloaded from https://febs.onlinelibrary.wiley.com/doi/10.1046/j.1432-1033.2002.03178.x by Ukraine - Cochrane, Wiley Online Library on [17/01/2025]. See the Terms and Conditions (https://onlinelibrary.wiley.com/terms-and-conditions) on Wiley Online Library for rules of use; OA articles are governed by the applicable Creative Commons License

25. Karlsson, R., Roos, H., Fagerstam, L. & Persson, B. (1994) Kinetic and concentration analysis using BIA technology. *Methods* **6**, 99–110.
26. El'skaya, A.V., Ovcharenko, G.V., Palchevskii, S.S., Petrushenko, Z.M., Triano-Alonso, F.J. & Nierhaus, K.H. (1997) Three tRNA binding sites in rabbit liver ribosomes and role of the intrinsic ATPase in 80S ribosomes from higher eukaryotes. *Biochemistry* **36**, 10492–10497.
27. Bilgin, N., Ehrenberg, M., Ebel, C., Zaccai, G., Sayers, Z., Koch, M.H., Svergun, D.I., Barberato, C., Volkov, V., Nissen, P. & Nyborg, J. (1998) Solution structure of the ternary complex between aminoacyl-tRNA, elongation factor Tu and guanosine triphosphate. *Biochemistry* **37**, 8163–8172.
28. Nissen, P., Kjeldgaard, M., Thirup, S., Polekhina, G., Reshetnikova, L., Clark, B.F.C. & Nyborg, J. (1995) Crystal structure of the ternary complex of Phe-tRNA^{Phe}, EF-Tu, and a GTP analog. *Science* **270**, 1464–1472.
29. Sioud, M. & Jespersen, L. (1996) Enhancement of hammerhead ribozyme catalysis by glyceraldehyde-3-phosphate dehydrogenase. *J. Mol. Biol.* **257**, 775–789.
30. Dell, V.A., Miller, D.L. & Johnson, A.E. (1990) Effects of nucleotide- and aurodox-induced changes in elongation factor Tu conformation upon its interactions with aminoacyl transfer RNA. A fluorescence study. *Biochemistry* **29**, 1757–1763.
31. Canziani, O., Zhang, W., Cines, D., Rux, A., Willis, B., Cohen, G., Eisenberg, R. & Chaiken, I. (1999) Exploring biomolecular recognition using optical biosensors. *Methods* **19**, 253–269.
32. Andersen, G.R., Pedersen, L., Valente, L., Chatterjee, I., Kinzy, T.G., Kjeldgaard, M. & Nyborg, J. (2000) Structural basis for nucleotide exchange and competition with tRNA in the yeast elongation factor complex eEF1A: eEF1Bα. *Mol. Cell* **6**, 1261–1266.
33. Graifer, D.M., Nekhai, S.Y., Mundus, D.M., Fedorova, O.F. & Karpova, G.G. (1992) Interaction of human and *Escherichia coli* tRNA^{Phe} with human 80S ribosomes in the presence of oligo- and polyuridylate templates. *Biochem. Biophys. Acta* **1171**, 56–67.
34. Kaminska, M., Shalak, V. & Mirande, M. (2001) The appended C-domain of human methionyl-tRNA synthetase has a tRNA-sequestering function. *Biochemistry* **40**, 14309–14316.
35. Merle, M., Trezeguet, V., Gandar, J.C. & Labouesse, B. (1988) Effects of the ligands of beef tryptophanyl-tRNA synthetase on the elementary steps of the tRNA^{Trp} aminoacylation. *Biochemistry* **27**, 2244–2252.
36. Sang, L.J., Gyu, P.S., Park, H., Seol, W., Lee, S. & Kim, S. (2002) Interaction network of human aminoacyl-tRNA synthetases and subunits of elongation factor 1 complex. *Biochem. Biophys. Res. Commun.* **291**, 158–164.
37. Janssen, G.M. & Möller, W. (1988) Kinetic studies on the role of elongation factors 1β and 1γ in protein synthesis. *J. Biol. Chem.* **263**, 1773–1778.

14321033, 2002, 19, Downloaded from https://febs.onlinelibrary.wiley.com/doi/10.1046/j.1432-1033.2002.03178.x by Ukraine - Cochrane, Wiley Online Library on [17/01/2025]. See the Terms and Conditions (https://onlinelibrary.wiley.com/terms-and-conditions) on Wiley Online Library for rules of use; OA articles are governed by the applicable Creative Commons License

1.4. Взаємодія eEF1A1 з метіоніл-тРНК синтетазою

The Appended C-Domain of Human Methionyl-tRNA Synthetase Has a tRNA-Sequestering Function†

Monika Kaminska,‡,§ Vyacheslav Shalak,‡,|| and Marc Mirande*,‡

Laboratoire d'Enzymologie et Biochimie Structurales, CNRS, 1 Avenue de la Terrasse, 91190 Gif-sur-Yvette, France, Institute of Bioorganic Chemistry, Polish Academy of Sciences, 60-704 Poznan, Poland, and Institute of Molecular Biology and Genetics, National Academy of Sciences of Ukraine, Kiev, Ukraine

Received August 10, 2001; Revised Manuscript Received September 7, 2001

ABSTRACT: An ancillary RNA-binding domain is appended to the C-terminus of human methionyl-tRNA synthetase. It comprises a helix−turn−helix (HTH) motif related to the repeated units of the linker region of bifunctional glutamyl-prolyl-tRNA synthetase, and a specific C-terminal KGKKKK lysine-rich cluster (LRC). Here we show by gel retardation and tRNA aminoacylation experiments that these two regions are important for tRNA binding. However, the two pieces of this bipartite RNA-binding domain are functionally distinct. Analysis of MetRS mutant enzymes revealed that the HTH motif is more specifically endowed with a tRNA-sequestering activity and confers on MetRS a rate-limiting dissociation of aminoacylated tRNA. Elongation factor EF-1α enhanced the turnover in the aminoacylation reaction. In contrast, the LRC region is most probably involved in accelerating the association step of deacylated tRNA. These two nonredundant RNA-binding motifs strengthen tRNA binding by the synthetase. The native form of MetRS, containing the C-terminal RNA-binding domain, behaves as a processive enzyme; release of the reaction product is not spontaneous, but may be synchronized with the subsequent step of the tRNA cycle through EF-1α-assisted dissociation of Met-tRNA^{Met}. Therefore, the eukaryotic-specific C-domain of human MetRS may have a dual function. It may ensure an efficient capture of tRNA^{Met} under conditions of suboptimal deacylated tRNA concentration prevailing in vivo, and may instigate direct transfer of aminoacylated tRNA from the synthetase to elongation factor EF-1α.

Aminoacyl-tRNA synthetases are RNA binding proteins that catalyze the esterification of amino acids to the 3 -end of tRNAs (*1*). With few exceptions, the proper orientation of the acceptor stem of tRNA in the active site of these enzymes involves conjunction of RNA−protein interactions with the catalytic domain (binding of the acceptor stem of the RNA molecule) and with the anticodon-binding domain of the synthetase. However, a productive positioning of the 3 -terminal adenosine of the RNA molecule can often be achieved with minihelix substrates mimicking the acceptor-TΨC domain of tRNA (*2*). Additional RNA-binding domains are primarily appended to eukaryotic enzymes and may serve as cis- or trans-acting cofactors. In yeast, the RNA-binding protein Arc1p is associated with MetRS and GluRS and functions as a cofactor (*3*, *4*). Plant MetRS possesses a C-terminal polypeptide chain extension related to Arc1p (*5*). A similar RNA-binding domain is also recovered in the mammalian multisynthetase complex (*6*). Its crystal structure revealed an OB-fold conformation characteristic of numerous RNA binding proteins (*7*, *8*). A large, functionally redundant, 228-amino acid N-terminally appended domain is associated with yeast GlnRS (*9*−*11*). In contrast, *Bombyx mori* GlyRS diplays a short 50-amino acid C-terminal RNA-binding domain corresponding to a single helix−turn−helix (HTH) motif (*12*−*14*). Finally, yeast LysRS and human AspRS and AsnRS share with class IIb aminoacyl-tRNA synthetases another type of RNA-binding module (*15*−*17*).

Methionyl-tRNA synthetase (MetRS) displays an especially variable structural organization throughout evolution. As compared with the minimal monomeric enzyme found in the eubacteria *Aquifex aeolicus* (GenBank accession number AE000731), N- and/or C-terminal polypeptide extensions are frequently appended to the core enzyme that associates a catalytic module organized around a Rossmann fold with an α-helical anticodon-binding domain (*18*, *19*). In eukaryotes, a supplementary, nonspecific RNA-binding domain built a C-terminal polypeptide extension associated in cis with plant MetRS (*5*) or is provided in trans to the yeast enzyme through protein−protein interaction (*3*, *4*). In the latter case, yeast MetRS possesses a large N-domain interacting with the N-domain of Arc1p, the RNA-binding cofactor.

In mammals, methionyl-tRNA synthetase is one of the components of a multisynthetase complex containing the nine synthetases specific for amino acids Glu, Pro, Ile, Leu, Met, Gln, Lys, Arg, and Asp, as well as three auxiliary proteins (*20*). Following controlled trypsin digestion of the purified complex, it has been shown that the 103 kDa polypeptide corresponding to MetRS is cleaved into 96, 77, and 68 kDa

† This work was supported by grants from the Association pour la Recherche sur le Cancer and La Ligue. M.K. was supported in part by grants from the Jumelage Franco-Polonais program from CNRS. V.S. was supported by INTAS and NATO fellowships.

* To whom correspondence should be addressed: LEBS-CNRS, 1 Avenue de la Terrasse, 91190 Gif-sur-Yvette, France. E-mail: mirande@lebs.cnrs-gif.fr.

‡ CNRS.

§ Polish Academy of Sciences.

|| National Academy of Sciences of Ukraine.

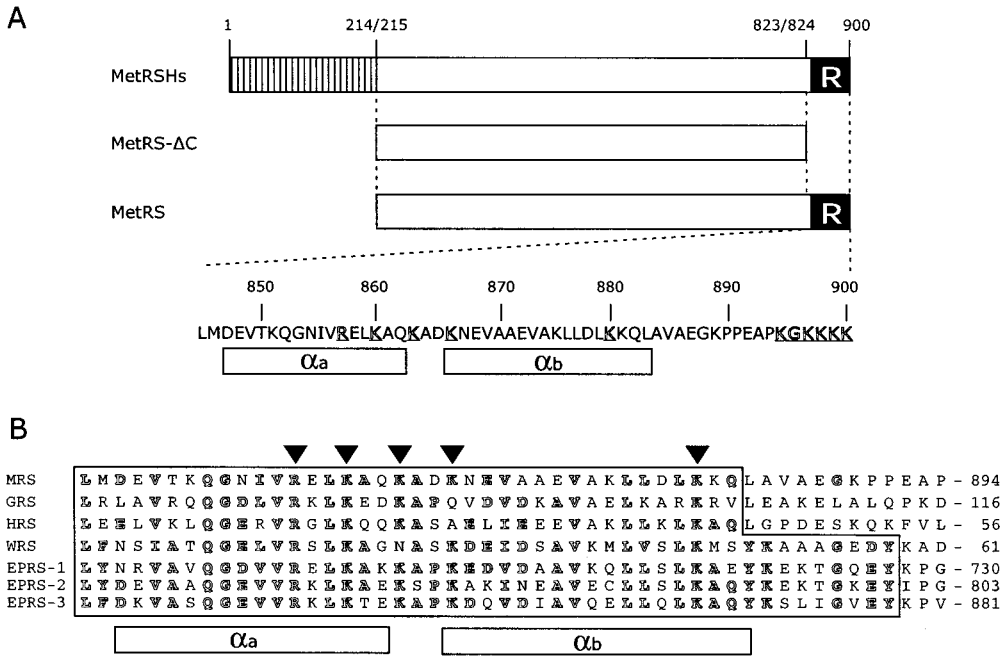

FIGURE 1: Structure of human MetRS. (A) The wild-type enzyme (MetRSHs) comprises a 214-amino acid N-terminal extension (hatched box), a core domain, and a 77-amino acid C-terminal region containing an RNA binding motif (R) initially described as repeated units in the multifunctional GluProRS (*24*). Two derivatives, with (MetRS) or without (MetRS-ΔC) this C-terminal domain, were expressed in *E. coli*. The amino acid sequence from the RNA binding motif is shown; conserved Arg857 and Lys860, -863, -866, and -880 residues that were changed into Ala are underlined. In addition, the four Lys residues from the very C-terminal LRC motif, removed in the MetRS-ΔK mutant, are marked. The two α-helices that build the HTH motif are indicated. (B) Alignment of the single motifs of human MetRS (MRS), GlyRS (GRS), HisRS (HRS), and TrpRS (WRS) and of the three repeated motifs of human GluProRS (EPRS). Residues conserved in at least four sequences are outlined.

polypeptides (*21*). The two 103 and 96 kDa species retained their ability to associate with the complex, in contrast with the 77 and 68 kDa polypeptides which were released as monomeric entities. The analysis of human MetRS cDNA (*22*; M. Lazard and M. Mirande, unpublished data) revealed a tripartite structural organization (see Figure 1A) and allowed us to rationalize the aforementioned biochemical data. A 214-amino acid N-terminal extension and a 77-amino acid C-terminal domain are appended to the main catalytic body of the enzyme, made of 609 amino acids that are 27% identical to the monomeric *Escherichia coli* enzyme. The native polypeptide was converted into a 93 or 77 kDa species by the removal of either the N- or C-terminal module. Deletion of both extensions led to the 68 kDa form. The free monomeric species of 77 and 68 kDa lack the large N-terminal appendage involved in complex assembly and differ by the presence of the C-terminal domain in the 77 kDa protein. The latter domain is a member of a family of general RNA-binding domains (*13*, *23*) initially found in the linker region of multifunctional glutamyl-prolyl-tRNA synthetase (*24*). The RNA-binding capacity of an isolated domain is weak [10 μM (*13*)].

We previously determined that the RNA-binding domain of plant MetRS acts as a cofactor for aminoacylation (*5*). Because plant and human MetRSs possess unrelated RNA-binding domains of different origins, we now analyzed the functional significance of the extra human domain. To unravel the role of this discrete RNA binding module, deletions and point mutations were introduced into the C-domain of human MetRS. This analysis revealed that the supplementary RNA-binding domain of MetRSs from higher eukaryotes contributes an unexpected tRNA-sequestering activity. These results have strong implications for the organization of translation in metazoan cells.

MATERIALS AND METHODS

Protein Overexpression and Purification. The cDNA fragment encoding the catalytic domain of human MetRS (MetRS-ΔC; from Ala215 to Lys823) was obtained by PCR with oligonucleotides MHs01 (5′-CCCCATATGGCTGT-CACCAATGAGCCT) and MHs02 (5′-AAAAAGCTTAG-GTCGACTTTGCCTGGCCCCCTCCAAA) and inserted into the *Nde*I−*Hin*dIII sites of the bacterial expression vector pET-28b (Novagen) to give pET/MHsΔC. The cDNA encoding the C-terminal extension was amplified with oligonucleotides MHs03 (5′-GGGGTCGACCCCGAAGC-CAGCAGTTGT) and MHs04 (5′-CCCCTCGAGTTACTTT-TTCTTCTTGCC) and inserted into the *Sal*I−*Xho*I sites of pET/MHsΔC to give pET/MHs. Deletion of the four C-terminal lysine residues of MetRS was performed by inserting into pET/MHsΔC a *Sal*I−*Xho*I fragment obtained by PCR with MHs03 and MHs05 (5′-CCCCTCGAGTTAGC-CTTTAGGGGCTTCAGGGGGT) to give pET/MHsΔK. Site-directed mutagenesis of Arg857, Lys860, Lys863, Lys866, and Lys880 into Ala was performed according to the method of Ho et al. (*25*). All constructs were verified by DNA sequencing.

The proteins encoded by the recombinant plasmids were expressed in *E. coli* BL21(DE3) grown in LB medium supplemented with kanamycin (50 μg/mL). Cultures (4.5 L) were grown at 37 °C to an A_{600} of 0.25 and transferred at 28 °C, and expression was induced at an A_{600} of 0.5 by addition of 1 mM IPTG for 4 h. Cells were washed with ice-cold buffer N1 [20 mM Tris-HCl (pH 8.0), 10 mM imidazole,

500 mM NaCl, and 10 mM 2-mercaptoethanol], resuspended in the same buffer (1.5 mL/g of cell pellet) containing 1 mM diisopropylfluorophosphate, and sonicated. After centrifugation at 45000*g* for 20 min, the lysate was incubated with 5 mL of Ni-NTA Superflow matrix (QIAGEN) at 4 °C. After it had been washed with buffer N1, MetRS was eluted stepwise with buffer N2 (buffer N1 containing 200 mM imidazole). After dialysis against buffer Q1 [20 mM Tris-HCl (pH 7.0), 10 mM NaCl, and 2 mM dithiothreitol], the solution was fractionated by anion-exchange chromatography with a Mono Q HR 5/5 column (Amersham Pharmacia Biotech) developed with a linear gradient of 10 to 300 mM NaCl. Fractions containing MetRS were dialyzed against 20 mM Tris-HCl (pH 7.0), 50 mM NaCl, 2 mM DTT, and 55% glycerol and stored at −20 °C. Protein concentrations were determined by using calculated absorption coefficients of 1.27 and 1.42 A_{280} units mg^{-1} cm^2 for MetRS and MetRS-ΔC, respectively.

Sedimentation Equilibrium. Ultracentrifugation experiments were conducted as described previously (*26*) in a Beckman Optima XL-A analytical ultracentrifuge, using an An 60 Ti rotor and a double-sector cell with a path length of 12 mm. Equilibrium was verified from the superimposition of duplicate scans recorded at 4 h intervals.

The experimental sedimentation equilibrium data were fitted to a model for a single homogeneous species following the equation

$$c(r) = c(r_{ref}) \exp\{[M_r(1 - \bar{\nu}\rho)\omega^2/2RT](r^2 - r_{ref}^2)\}$$

where $c(r)$ is the protein concentration at radial position r, $c(r_{ref})$ is the concentration of the protein at an arbitrary reference radial distance r_{ref}, M_r is the molecular mass, $\bar{\nu}$ is the partial specific volume (0.732 and 0.730 at 4 °C for MetRS and MetRS-ΔC, respectively) of the solute, ρ is the density of the solvant, ω is the angular velocity of the rotor, and R and T are the molar gas constant and the absolute temperature, respectively.

Gel Retardation Assay. ^{32}P-labeled tRNAs were obtained by in vitro transcription with T7 RNA polymerase and were purified on denaturing polyacrylamide gels. Protein−tRNA interactions were analyzed using a band shift assay as previously described (*5*). Free and bound tRNA species were quantified with a PhosphorImager.

The amino acid acceptor (Acc-tRNA^{Met}) and anticodon (Ant-tRNA^{Met}) RNA minihelices corresponding to rabbit liver elongator tRNA^{Met} were produced by in vitro transcription of *Bst*NI- and *Bcl*I-digested pUC118 derivatives constructed by insertion into their *Hin*dIII−*Bam*HI sites of oligonucleotides RS101 (5′-AGCTTAATACGACTCACT)/RS111 (5′-CTATAGTGAGTCGTATTA) and MR101 (5′-ATAGCCTCGTGTGAGTTCGATCCTCACACGGGGCACCAG)/MR111 (5′-GATCCTGGTGCCCCGTGTGAGGATCGAACTCACACGAGG), and RS101/RS111 and MR102 (5′-ATAGTCAGTCTCATAATCTGATCAG)/MR112 (5′-GATCCTGATCAGATTATGAGACTGA), respectively.

Aminoacylation Assay. Initial rates of tRNA aminoacylation were measured at 25 °C in 0.1 mL of 20 mM imidazole-HCl (pH 7.5), 150 mM KCl, 0.5 mM DTE, 5 mM $MgCl_2$ (except where stated otherwise), 3 mM ATP, 52 μM ^{14}C-labeled methionine (NEN; 58 Ci/mol), and saturating amounts of tRNA, as previously described (*27*). Total brewer's yeast tRNA (Roche, methionine acceptance of 9 pmol/A_{260}) or homogeneous rabbit elongator tRNA^{Met} purified from an *E. coli* overproducing strain as described in ref *28* (methionine acceptance of 1215 pmol/A_{260}) was used as the tRNA substrate. Total bovine tRNA was depleted of tRNA^{Met} by chromatography on a benzoyl-DEAE column. The incubation mixture contained catalytic amounts (1−15 nM) of enzymes appropriately diluted in 10 mM Tris-HCl (pH 7.5) and 10 mM 2-mercaptoethanol, containing 4 mg/mL bovine serum albumin. One unit of activity is the amount of enzyme producing 1 nmol of methionine-tRNA^{Met}/min at 25 °C. For the determination of K_M values for tRNA, tRNA^{Met} concentrations of 0.05−25 μM were used. Michaelian parameters were obtained by nonlinear regression of the theoretical Michaelis−Menten equation to the experimental curve using the KaleidaGraph 3.0.8 software (Abelbeck Software).

For measurement of the maximal rates of Met-tRNA^{Met} formation in the presence of EF-1α at the indicated concentrations, aminoacylation was conducted as described previously (*29*). Briefly, the incubation mixture was 20 mM imidazole-HCl (pH 7.5), 6 mM Tris-HCl (pH 7.5), 100 mM KCl, 11.5 mM NH_4Cl, 10% glycerol, 0.5 mM DTE, 5 mM $MgCl_2$, 3 mM ATP, 52 μM [^{14}C]methionine, 12 μM rabbit elongator tRNA^{Met}, and 0.6 mg/mL BSA. Where indicated, GTP and GDP were used at concentrations of 120 μM.

RESULTS

The Repeated Unit Provides Human MetRS with RNA Binding Properties. Human MetRS is a modular enzyme made of three distinct blocks (Figure 1A). The central domain, homologous to other known MetRSs, can aminoacylate tRNA in the absence of its eukaryotic-specific N- and C-terminal polypeptide extensions. To probe the function of the RNA-binding C-domain of MetRS, we expressed two derivatives of this enzyme in *E. coli* with an N-terminal His tag. Because the N-domain, involved in complex assembly, is dispensable for catalysis (ref *21*, and see below), we cloned into the pET28b expression vector the cDNA of human MetRS starting from residue 215. A derivative (MetRS-ΔC) with a deletion of residues 824−900, encompassing the RNA-binding unit, was also constructed. Purification over Ni-NTA and MonoQ columns led to homogeneous proteins that displayed the expected molecular masses (80 kDa for MetRS and 72 kDa for MetRS-ΔC) as assessed by SDS−PAGE. MetRS and MetRS-ΔC catalyzed the aminoacylation of tRNA^{Met} with similar efficiencies (specific activities of 262 and 300 units/mg of protein, respectively, when measured with saturating amounts of total yeast tRNA). The two enzyme species were subjected to equilibrium sedimentation analysis in 20 mM Tris-HCl (pH 7.5), 100 mM NaCl, 10% glycerol, and 1 mM DTT (Figure 2). Experimental data could be fitted to monodisperse solutes with M_rs of 82 345 and 77 528 for MetRS and MetRS-ΔC, respectively. Therefore, as opposed to the C-domain of *E. coli* MetRS (*30*), the C-domain of human MetRS is not a dimerization domain. The finding that human MetRS is a monomer in solution is consistent with the finding that the multisynthetase complex contains a single copy of the MetRS polypeptide (*21*).

We showed earlier that the repeated units from the linker region of GluProRS (EPRS repeats) display general RNA binding properties (*13*). However, its affinity for tRNA was

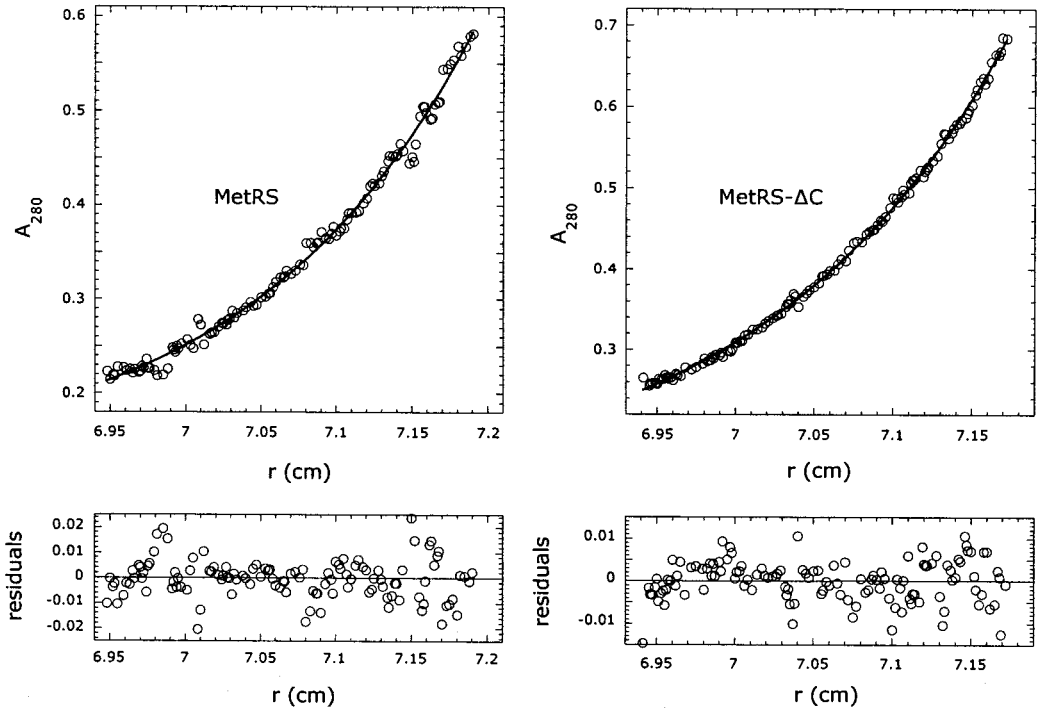

FIGURE 2: Human MetRS is a monomer in solution. MetRS and MetRS-ΔC (initial concentrations of 2.6 and 3.2 μM, respectively) were analyzed by equilibrium sedimentation at 10 000 rpm in 20 mM Tris-HCl (pH 7.5), 100 mM NaCl, 10% glycerol, and 1 mM DTT at 4 °C. Experimental values (○) were fitted (—) to monodisperse 82 345 and 77 528 Da solutes. The residuals are indicated.

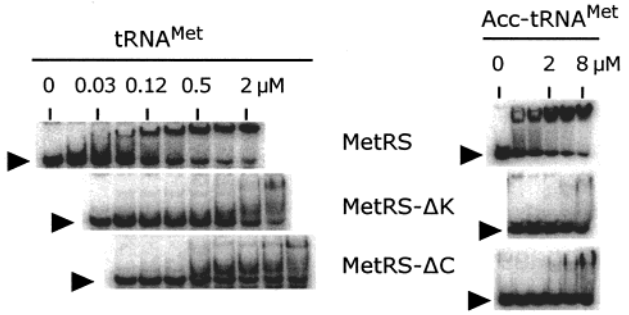

FIGURE 3: C-Domain conferring on human MetRS the ability to bind the acceptor domain of tRNA. Gel mobility shift assays of MetRS and deletion mutants to ^{32}P-labeled yeast initiator tRNA^{Met} (left) or the acceptor-TΨC domain of rabbit elongator tRNA^{Met} (right) are shown. The arrowheads point to free RNA species. Numbers refer to concentrations of MetRS and of its derivatives.

Table 1: Apparent Dissociation Constants of Wild-Type and Mutant Human MetRS for tRNA^{Met} and Acc-tRNA^{Met} Determined by a Gel Retardation Assay

	K_d for tRNA^{Met} (μM)	K_d for Acc-tRNA^{Met} (μM)
MetRS	0.1	0.5
MetRS-ΔK	1.5	~10.0
MetRS-ΔC	4.0	~10.0
MetRS-R857A	0.4	1.5
MetRS-K860A	1.5	8.0
MetRS-K863A	0.15	0.5
MetRS-K866A	0.15	0.5
MetRS-K880A	2.5	8.0

[a] Standard errors for K_d are in the range of 20−30% of the value.

weak ($K_d \sim 10\ \mu$M). Because the C-domain of human MetRS is extensively similar to these motifs (Figure 1B), we analyzed by a band shift assay the ability of MetRS and MetRS-ΔC to form stable complexes with tRNAs transcribed in vitro (Figure 3 and Table 1). Substrate (initiator yeast tRNA^{Met}) and nonsubstrate tRNAs (yeast tRNA^{Asp}, not shown) produced stable RNA−protein complexes with MetRS (apparent dissociation constants K_d of 100 and 150 nM, respectively). The C-terminally truncated protein, MetRS-ΔC, displayed a much weaker binding capacity for tRNA^{Met} (Figure 3; $K_d \sim 4\ \mu$M). These results exemplified the nonspecific general RNA binding capacity conferred on MetRS by its C-terminally appended unit. The stable association of MetRS with tRNA results from the synergy of two weak interactions between tRNA and (i) the body of MetRS (MetRS-ΔC) and (ii) its C-domain.

The EPRS repeats appended to various aaRSs have been classified into two groups according to the extent of conserved residues (*13*, *23*). The solution structure of the second repeated motif of GluProRS revealed a conserved helix−turn−helix fold followed by an Ω-loop (*13*). In the case of MetRS, only the helix−turn−helix motif is conserved (Figure 1B). The presence of a lysine-rich cluster (LRC) at its very C-terminal extremity (Figure 1) suggested that two regions of this extension could be involved in tRNA binding. We produced in *E. coli* a MetRS mutant with a deletion of the four C-terminal lysine residues, MetRS-ΔK. This mutant also displayed a severely reduced ability to bind tRNA^{Met} (Figure 3; $K_d \sim 1.5\ \mu$M). For MetRS-ΔC and MetRS-ΔK, a discrete band of the protein−tRNA complex was not easily detectable. The smear visible on the gel is most likely due to partial dissociation of the weak complex during electrophoretic separation of free and bound species of tRNAs.

To probe the region of tRNA involved in the interaction with MetRS, RNA minihelices mimicking the acceptor and anticodon stems of rabbit elongator tRNA^{Met} were produced by in vitro transcription with T7 RNA polymerase. The acceptor minihelix (Acc-tRNA^{Met}) (Figure 3), but not the anticodon minihelix (Ant-tRNA^{Met}) (not shown), formed a complex with MetRS. The apparent dissociation constant for

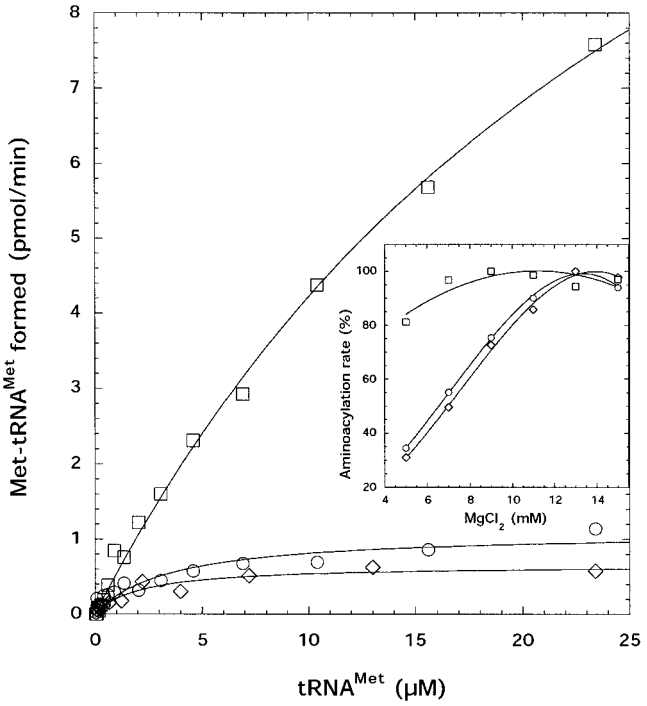

FIGURE 4: HTH motif of MetRS that severely restricts its turnover in the aminoacylation reaction. The tRNA saturation kinetics in the $tRNA^{Met}$ aminoacylation reaction were determined with nearly homogeneous rabbit elongator $tRNA^{Met}$ (methionine acceptance of 1215 pmol/A_{260} unit) in the presence of 5 nM MetRS (○), MetRS-ΔK (◇), or MetRS-ΔC (□). Experimental values (symbols) were fitted to the Michaelis−Menten equation (—). The inset shows the initial velocity ($V_{i,max}$) of MetRSs (symbols as above) measured as a function of $MgCl_2$ added to the aminoacylation mixture.

Acc-$tRNA^{Met}$ ($K_d \sim 0.5$ μM), identical with that observed for the acceptor domain of yeast $tRNA^{Asp}$ (not shown), a noncognate tRNA, was increased to ~10 μM with MetRS-ΔK and MetRS-ΔC (Figure 3 and Table 1). Therefore, the C-terminally appended domain of human MetRS is mainly involved in binding the acceptor region of tRNA.

Roles of the HTH and LRC Regions of the Bipartite RNA-Binding Domain on tRNA Aminoacylation. Homogeneous rabbit elongator $tRNA^{Met}$ (methionine acceptance of 1215 pmol/A_{260}) was used to determine the steady-state kinetic parameters in the aminoacylation reaction catalyzed by MetRS, MetRS-ΔK, and MetRS-ΔC (Figure 4 and Table 2). Although the specificity constants (k_{cat}/K_M) of the three MetRS species were similar, they resulted from large compensatory changes in the K_M and k_{cat} values. The truncated enzyme MetRS-ΔC exhibited a 9-fold increase in the K_M for $tRNA^{Met}$ but, unexpectedly, also displayed a 16-fold increase in the k_{cat} of Met-$tRNA^{Met}$ formation, as compared with those of the wild-type enzyme. As a control, we observed that the MetRS component of the multisynthetase complex displayed kinetic parameters essentially similar to those obtained with the native but ectopic MetRS used in this study (Table 2). Therefore, the presence of the C-domain significantly restricts the turnover number of the enzyme. In contrast, the removal of the four C-terminal lysine residues had no discernible effect on the k_{cat} and K_M values of MetRS-ΔK, as compared with those of the wild type. Because both mutants, MetRS-ΔC and MetRS-ΔK, had partially lost their ability to form stable complexes with tRNAs (Figure 3) but displayed radically different aminoacylation kinetics, the HTH and LRC motifs from the C-domain were quite likely to be nonredundant functional motifs.

Table 2: Apparent Kinetic Parameters[a] for the $tRNA^{Met}$ Aminoacylation Reaction[b] of Rabbit Elongator $tRNA^{Met}$ with Wild-Type and Mutant MetRS

	K_M (μM)	k_{cat} (s^{-1})
MetRS-Cx[c]	3.9 ± 1.3	0.46 ± 0.05
MetRS	3.5 ± 1.0	0.15 ± 0.04
MetRS-ΔK	2.2 ± 0.7	0.09 ± 0.02
MetRS-ΔC	32 ± 4	2.4 ± 0.5
MetRS-R857A	5.7 ± 1.1	0.47 ± 0.05
MetRS-K860A	17.2 ± 5.0	0.85 ± 0.15
MetRS-K863A	3.3 ± 0.8	0.22 ± 0.03
MetRS-K866A	3.9 ± 1.4	0.23 ± 0.04
MetRS-K880A	16.3 ± 5.7	1.03 ± 0.20

[a] Standard errors were determined from at least two independent data sets. [b] $tRNA^{Met}$ acceptance of 1215 pmol/A_{260}. [c] Multienzyme complex containing MetRS. The k_{cat} value is calculated taking into account that 1 mol of complex ($M_r \sim 1.5$ MDa) contains 1 mol of MetRS (101 kDa).

The C-domain of MetRS, including the HTH and LRC regions, is rich in basic residues (Figure 1). We surmised that positively charged compounds that may form complexes with tRNA molecules could modulate MetRS activity. The effect of Mg^{2+} and spermidine on tRNA aminoacylation by MetRS and its C-domain deletion mutants was investigated. We found that increasing the Mg^{2+} concentration from 5 to 13 mM was accompanied by an ~4-fold increase in the activity of MetRS and MetRS-ΔK, resulting from a 4-fold increase in k_{cat} without a noticeable change in the K_M value for tRNA, but had only a slight effect on MetRS-ΔC (inset of Figure 4). Likewise, addition of 6 mM spermidine in the aminoacylation mixture (in the presence of 5 mM $MgCl_2$) stimulated MetRS and MetRS-ΔK activity, but not MetRS-ΔC activity (not shown).

We previously observed that the presence of a large excess of noncognate tRNA in the aminoacylation assay may conceal kinetic effects contributed by the appended RNA-binding domains of eukaryotic enzymes (*5*). Similarly, the three enzymes MetRS, MetRS-ΔK, and MetRS-ΔC exhibited similar apparent K_M values for tRNA (0.5−0.9 μM) and identical k_{cat} values (1.2 ± 0.4 s^{-1}) when total yeast tRNA (methionine acceptance of 9 pmol/A_{260}) or partially purified beef tRNA (methionine acceptance of 80 pmol/A_{260}) was used.

To ascertain that noncognate tRNAs may affect the rate of $tRNA^{Met}$ aminoacylation by MetRS, the activity of MetRS was assayed using homogeneous rabbit $tRNA^{Met}$ as the RNA substrate (1215 pmol/A_{260}), with the addition of increasing amounts of total beef tRNA which had been depleted of $tRNA^{Met}$ (1:1, 1:3, and 1:6 mixtures of $tRNA^{Met}$ and depleted tRNA). At a low Mg^{2+} concentration (5 mM), addition of a 6-fold molar excess of noncognate tRNA led to a 4-fold increase in the activity of MetRS and MetRS-ΔK, but not in that of MetRS-ΔC. In the presence of 15 mM Mg^{2+} in the aminoacylation reaction mixture (resulting in a 4-fold increase in k_{cat}), no further stimulation of MetRS activity by noncognate tRNA was observed. Collectively, these results suggest that the rate-limiting step of Met-$tRNA^{Met}$ formation by human MetRS can be alleviated in vitro either by lowering the extent of the intrinsic tRNA−protein interaction (use of Mg^{2+} or spermidine, removal of the C-terminal RNA-binding domain) or by enhancing dissociation of Met-$tRNA^{Met}$ by

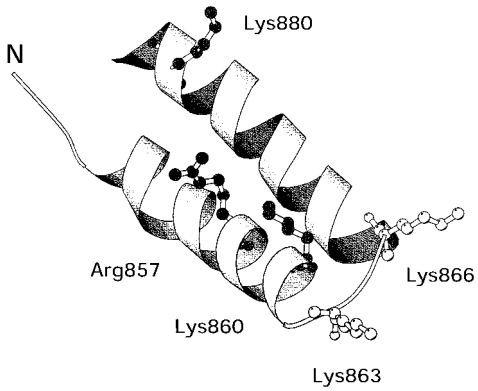

FIGURE 5: Model of tRNA binding to the HTH motif of the repeated unit of MetRS. The helix−turn−helix motif of MetRS of residues 845−883 is shown as a ribbon diagram, and the five conserved basic residues are depicted as ball-and-stick diagrams. The putative interaction region with the acceptor domain of tRNA is likely to involve residues Arg857, Lys860, and Lys880 (indicated in gray). This figure was generated using MOLSCRIPT (*43*).

competition (use of nonspecific tRNAs in excess that compete for interaction with the C-domain). The finding that noncognate tRNAs also formed stable complexes with native MetRS is consistent with their ability to displace Met-tRNA^{Met} from the synthetase.

Role of the Conserved Basic Residues from the HTH Motif. To probe the functional role of the HTH motif in a wild-type background, that is to say, independently of the removal of the LRC motif, we performed site-directed mutagenesis of its conserved, presumably functionally important residues. One arginine residue (Arg857) and four lysine residues (Lys860, -863, -866, and -880) (Figure 1B) are conserved in most of the HTH motifs reported to date (*23*). Because these residues have no structural role (*13*) and are clustered on one side of this domain (Figure 5), we tested for the impact of point mutations of these conserved basic residues on tRNA binding and on the steady-state kinetic parameters for the aminoacylation reaction. We substituted one by one these basic residues with Ala to give the R857A, K860A, K863A, K866A, and K880A mutants of human MetRS. Otherwise, all the mutant proteins contained the native LRC at their very C-termini. The five resultant mutants were expressed in *E. coli* and purified to homogeneity.

Using the gel-mobility shift assay described above, mutants K860A and K880A displayed a large decrease in their affinity for tRNA^{Met} and Acc-tRNA^{Met} (15−25-fold; Table 1). These single mutations induced a loss in affinity comparable to that observed for the deletion mutant MetRS-ΔC, which comprises a deletion of both the HTH and LRC motifs. MetRS-R857A also displayed a significant increase in K_d (3−4-fold). In contrast, mutations K863A and K866A did not alter the apparent affinity of MetRS for tRNA. It is worth mentioning that analysis of the sequences for 34 repeated units revealed that Arg857, Lys860, and Lys880 are invariant residues, as opposed to the more limiting conservation of Lys863 and Lys866 which are located in the loop of the HTH motif (27 and 26 occurrences, respectively) (*23*).

Measurement of the kinetic parameters of the aminoacylation reaction corroborated the relative tRNA binding properties of the mutants. The K_M and k_{cat} values determined for MetRS-K863A and -K866A were similar to those of the wild type (Table 2), and both values were significantly higher for mutants K860A and K880A. Basically, these two mutants recapitulated the properties of the deletion mutant MetRS-ΔC. Therefore, the HTH motif has a dominant effect over the LRC motif. The putative RNA binding site is likely to involve residues Arg857, Lys860, and Lys880 located on one side of the HTH structural motif, but not Lys863 and Lys866 located in the turn of this motif (Figure 5).

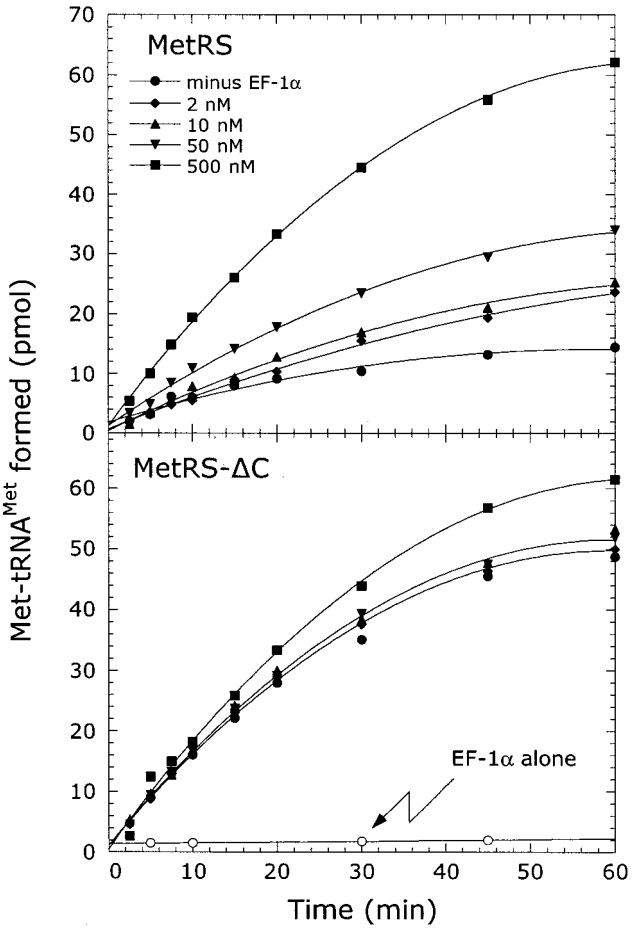

FIGURE 6: Elongation factor EF-1α stimulates MetRS activity. The time course of Met-tRNA^{Met} formation by wild-type MetRS or MetRS-ΔC was monitored in the absence or presence of increasing amounts (2−500 nM) of homogeneous EF-1α added to the aminoacylation mixture. The reaction mixtures contained 10 nM MetRS, 1 nM MetRS-ΔC, and 12 μM rabbit tRNA^{Met}. In the absence of MetRS, no detectable Met-tRNA^{Met} was formed in the presence of 500 nM EF-1α.

Are Protein Factors Needed for Optimal MetRS Activity? The above results suggested that product release could be the limiting step for Met-tRNA^{Met} formation in vivo. Since elongation factor 1α carries aminoacylated tRNA to the ribosome, we surmised that it could be involved in facilitating the dissociation of Met-tRNA^{Met} from the synthetase to ensure channeling of tRNA in the cycle of protein synthesis. Therefore, we examined the effect of EF-1α [the purified factor is in the GDP form (*31*)], in the presence or absence of saturating amounts of GDP or GTP, on the rate of aminoacylation catalyzed by MetRS or by the mutant enzymes described above. Addition of EF-1α to the reaction mixture, in the presence or absence of nucleotide, increased the rate of Met-tRNA^{Met} formation by the native enzyme (Figure 6). The enhancement of MetRS activity ($V_{i,max}$) was

maximal at an EF-1α concentration of 500 nM and followed a saturation kinetics with an apparent dissociation constant K_d of 180 ± 40 nM. The extent of stimulation was independent of the addition of nucleotides [in vitro, both EF-1α−GDP and EF-1α−GTP complexes have been shown to interact with aminoacyl-tRNAs with similar affinities (*32*, *33*)]. EF-1α also increased the rate of Met-tRNA^{Met} formation by MetRS-ΔK with a similar apparent affinity (not shown). Conversely, MetRS-ΔC did not show any significant stimulation by EF-1α (Figure 6).

DISCUSSION

The C-terminal polypeptide extension provides human methionyl-tRNA synthetase with general tRNA binding properties. This domain is related to the repeated motifs initially discovered in the linker region of the bifunctional glutamyl-prolyl-tRNA synthetase. The catalytic domain of MetRS ($K_d \sim 4\ \mu$M for tRNA) and its C-domain containing a single repeat [$K_d \sim 10\ \mu$M (*13*)] act synergistically to confer on the native enzyme the ability to bind tRNA with a much higher apparent affinity ($K_d \sim 0.1\ \mu$M). Both the HTH and LRC regions of this bipartite module are essential for tRNA binding and are not functionally redundant.

The requirement for an additional RNA-binding domain is a general feature of eukaryotic MetRSs. However, neither the type of RNA-binding module nor the mode of association is conserved among species. In plants and nematodes, MetRS displays a C-terminal polypeptide extension similar to the C-domain of p43, an RNA-binding protein arranged in an OB-fold conformation, associated within the mammalian multisynthetase complex (*6*, *8*). In yeast, MetRS associates with Arc1p, a protein that provides in trans a p43-like RNA-binding domain (*4*). In higher eukaryotic species, from *Drosophila* to mammals, corresponding to the coelomate branch of metazoan organisms, MetRS displays a strikingly different structural organization. First, this enzyme is associated with a macromolecular assembly containing eight other aminoacyl-tRNA synthetases (*20*). Second, it displays an original RNA-binding domain related to the repeated units of GluProRS (*13*, *23*). Among higher eukaryotes, apart from the human enzyme, only the preliminary genomic sequence of *Drosophila* MetRS can be retrieved from GenBank (AE003798; gene CG15100). In accordance with the analysis of the enzyme purified from *Drosophila* cells (*34*), the fly MetRS is larger than the human enzyme. Its C-terminal polypeptide extension is made of three HTH motifs, and it displays a KGKKKK C-terminal sequence identical to the LRC of the human enzyme. Thus, the two distinct blocks identified within the RNA-binding domain of human MetRS are likely to be conserved from fly to human.

MetRS is one of the rare examples of a sudden change of structural organization in evolution. Why do higher eukaryotic MetRSs need an RNA-binding domain distinct from that found in MetRSs from lower eukaryotes? We had previously shown that the p43-like domain of plant MetRS contributed a 10-fold decrease in K_M for tRNA in the aminoacylation reaction catalyzed by the native enzyme, as compared with the C-terminally truncated MetRS (*5*). No evidence for k_{cat} limitation was obtained. Because the free tRNA concentration is nonsaturating within the cell, we concluded that the C-terminally appended domain of plant MetRS is required for an efficient capture of tRNA by the synthetase. In contrast, the appended domain of human MetRS not only decreases the apparent affinity for tRNA but also causes a severe turnover limitation. Because removal of the LRC region did not relieve turnover restriction (Figure 4) but impaired tRNA association at equilibrium (Figure 3), we suggest that the HTH and LRC regions have distinct roles in sustaining tRNA aminoacylation. The LRC might be involved in tRNA capture via an increase in the association rate (k_{on}) of tRNA. The five exposed lysine residues would create a high positive electrostatic potential involved in long-distance interactions with these negatively charged molecules, thus leading to a higher local concentration in tRNA. In contrast, the HTH module is likely to contribute a rate-limiting product release. Stimulation of Met-tRNA^{Met} synthesis was observed upon deletion of the entire C-terminal domain, or in the presence of the LRC region when point mutations are introduced into the HTH segment.

Polyamines have long been known as modulators of protein biosynthesis efficiency both in vivo and in vitro (*35*). Our data show that Mg^{2+} or spermidine, and to a lesser extent KCl (not shown), partially releases the rate-limiting step of Met-tRNA^{Met} dissociation observed for the native enzyme. Magnesium and polyamines are known to interact with tRNA and to contribute important interactions in maintaining the tertiary structure of tRNA (*36*−*38*). Because Mg^{2+} or spermidine did not enhance the activity of MetRS-ΔC, stimulation of MetRS or MetRS-ΔK is not related to a structural change in the tRNA used in our study. As more polyamine is added, neutralization of phosphate charges may alter the interaction of tRNA with the basic patches from the C-domain of MetRS.

The acquisition of supplementary RNA-binding domains by mammalian aminoacyl-tRNA synthetases may be related to the emergence of tRNA channeling in translation (*39*). This is supported by the finding that EF-1α may mediate the release of Met-tRNA^{Met} (this study), of Val-tRNA^{Val} (*29*), of Phe-tRNA^{Phe} (*31*), and of Asp-tRNA^{Asp} (*40*) from their cognate synthetase. This would be a rational means of ensuring EF-1α-assisted vectorial transfert of tRNA from its aminoacylation site (the synthetase) to its utilization site (the ribosome). In the case of ValRS, the channeling is mediated by stable association of this synthetase with elongation factor EF-1H, the heavy form of elongation factor 1 that comprises the three subunits EF-1β, EF-1γ, and EF-1δ and contributes the guanine nucleotide exchange activity (*41*, *42*). The finding that Met-tRNA^{Met} is not spontaneously released from the synthetase suggests that mammalian synthetases work in vivo in a processive manner. Product dissociation awaits productive interaction between the synthetase and elongation factor EF-1α. The high cellular content in EF-1α may be essential for this process to occur.

ACKNOWLEDGMENT

We thank Y. Mechulam (Ecole Polytechnique, Palaiseau, France) for the gift of the pBSTNAV2 expression vector for rabbit liver elongator tRNA^{Met} and G. Batelier (Laboratoire d'Enzymologie et Biochimie Structurales, CNRS) for performing sedimentation equilibrium analyses. The excellent technical assistance of Françoise Triniolles is gratefully acknowledged.

REFERENCES

1. Ibba, M., and Söll, D. (2000) *Annu. Rev. Biochem. 69*, 617−650.
2. Beuning, P. J., and Musier-Forsyth, K. (1999) *Biopolymers 52*, 1−28.
3. Simos, G., Segref, A., Fasiolo, F., Hellmuth, K., Shevchenko, A., Mann, M., and Hurt, E. C. (1996) *EMBO J. 15*, 5437−5448.
4. Deinert, K., Fasiolo, F., Hurt, E. C., and Simos, G. (2001) *J. Biol. Chem. 276*, 6000−6008.
5. Kaminska, M., Deniziak, M., Kerjan, P., Barciszewski, J., and Mirande, M. (2000) *EMBO J. 19*, 6908−6917.
6. Shalak, V., Kaminska, M., Mitnacht-Kraus, R., Vandenabeele, P., Clauss, M., and Mirande, M. (2001) *J. Biol. Chem. 276*, 23769−23776.
7. Kim, Y., Shin, J., Li, R. B., Cheong, C., Kim, K., and Kim, S. (2000) *J. Biol. Chem. 275*, 27062−27068.
8. Renault, L., Kerjan, P., Pasqualato, S., Menetrey, J., Robinson, J. C., Kawaguchi, S., Vassylyev, D. G., Yokoyama, S., Mirande, M., and Cherfils, J. (2001) *EMBO J. 20*, 570−578.
9. Whelihan, E. F., and Schimmel, P. (1997) *EMBO J. 16*, 2968−2974.
10. Wang, C. C., and Schimmel, P. (1999) *J. Biol. Chem. 274*, 16508−16512.
11. Wang, C. C., Morales, A. J., and Schimmel, P. (2000) *J. Biol. Chem. 275*, 17180−17186.
12. Wu, H., Nada, S., and Dignam, J. D. (1995) *Biochemistry 34*, 16327−16336.
13. Cahuzac, B., Berthonneau, E., Birlirakis, N., Guittet, E., and Mirande, M. (2000) *EMBO J. 19*, 445−452.
14. Jeong, E. J., Hwang, G. S., Kim, K. H., Kim, M. J., Kim, S., and Kim, K. S. (2000) *Biochemistry 39*, 15775−15782.
15. Frugier, M., Moulinier, L., and Giegé, R. (2000) *EMBO J. 19*, 2371−2380.
16. Hammamieh, R., and Yang, D. C. H. (2001) *J. Biol. Chem. 276*, 428−433.
17. Beaulande, M., Kron, M., and Härtlein, M. (2001) *FEBS Lett. 494*, 170−174.
18. Mechulam, Y., Schmitt, E., Maveyraud, L., Zelwer, C., Nureki, O., Yokoyama, S., Konno, M., and Blanquet, S. (1999) *J. Mol. Biol. 294*, 1287−1297.
19. Sugiura, I., Nureki, O., Ugaji-Yoshikawa, Y., Kuwabara, S., Shimada, A., Tateno, M., Lorber, B., Giegé, R., Moras, D., Yokoyama, S., and Konno, M. (2000) *Structure 8*, 197−208.
20. Mirande, M. (1991) *Prog. Nucleic Acid Res. Mol. Biol. 40*, 95−142.
21. Mirande, M., Kellermann, O., and Waller, J. P. (1982) *J. Biol. Chem. 257*, 11049−11055.
22. Lage, H., and Dietel, M. (1996) *Gene 178*, 187−189.
23. Berthonneau, E., and Mirande, M. (2000) *FEBS Lett. 470*, 300−304.
24. Cerini, C., Kerjan, P., Astier, M., Gratecos, D., Mirande, M., and Semeriva, M. (1991) *EMBO J. 10*, 4267−4277.
25. Ho, S. N., Hunt, H. D., Horton, R. M., Pullen, J. K., and Pease, L. R. (1989) *Gene 77*, 51−59.
26. Agou, F., Waller, J. P., and Mirande, M. (1996) *J. Biol. Chem. 271*, 29295−29303.
27. Mirande, M., Cirakoglu, B., and Waller, J. P. (1983) *Eur. J. Biochem. 131*, 163−170.
28. Meinnel, T., Mechulam, Y., Fayat, G., and Blanquet, S. (1992) *Nucleic Acids Res. 20*, 4741−4746.
29. Negrutskii, B. S., Shalak, V. F., Kerjan, P., El'skaya, A. V., and Mirande, M. (1999) *J. Biol. Chem. 274*, 4545−4550.
30. Cassio, D., and Waller, J. P. (1971) *Eur. J. Biochem. 20*, 283−300.
31. Negrutskii, B. S., Budkevich, T. V., Shalak, V. F., Turkovskaya, G. V., and El'skaya, A. V. (1996) *FEBS Lett. 382*, 18−20.
32. Roobol, K., and Möller, W. (1978) *Eur. J. Biochem. 90*, 471−477.
33. Crechet, J. B., and Parmeggiani, A. (1986) *Eur. J. Biochem. 161*, 647−653.
34. Kerjan, P., Cerini, C., Semeriva, M., and Mirande, M. (1994) *Biochim. Biophys. Acta 1199*, 293−297.
35. Tabor, C. W., and Tabor, H. (1984) *Annu. Rev. Biochem. 53*, 749−790.
36. Quigley, G. J., Teeter, M. M., and Rich, A. (1978) *Proc. Natl. Acad. Sci. U.S.A. 75*, 64−68.
37. Sampson, J. R., and Uhlenbeck, O. C. (1988) *Proc. Natl. Acad. Sci. U.S.A. 85*, 1033−1037.
38. Frydman, L., Rossomando, P. C., Frydman, V., Fernandez, C. O., Frydman, B., and Samejima, K. (1992) *Proc. Natl. Acad. Sci. U.S.A. 89*, 9186−9190.
39. Stapulionis, R., and Deutscher, M. P. (1995) *Proc. Natl. Acad. Sci. U.S.A. 92*, 7158−7161.
40. Reed, V. S., Wastney, M. E., and Yang, D. C. H. (1994) *J. Biol. Chem. 269*, 32932−32936.
41. Motorin, Y. A., Wolfson, A. D., Löhr, D., Orlovsky, A. F., and Gladilin, K. L. (1991) *Eur. J. Biochem. 201*, 325−331.
42. Bec, G., Kerjan, P., and Waller, J. P. (1994) *J. Biol. Chem. 269*, 2086−2092.
43. Kraulis, P. J. (1991) *J. Appl. Crystallogr. 24*, 946−950.

BI015670B

Translationally controlled tumor protein acts as a guanine nucleotide dissociation inhibitor on the translation elongation factor eEF1A

Christophe Cans*†, Brent J. Passer*†, Vyacheslav Shalak‡, Vanessa Nancy-Portebois*, Virginie Crible*, Nathalie Amzallag*, David Allanic*, Rowena Tufino*, Manuela Argentini§, Dino Moras§, Giusy Fiucci*, Bruno Goud¶, Marc Mirande‡, Robert Amson*, and Adam Telerman*‖

*Molecular Engines Laboratories, 20 Rue Bouvier, 75011 Paris, France; ‡Laboratoire d'Enzymologie et Biochimie Structurales, Centre National de la Recherche Scientifique-Unité Propre de Recherche 9063, 1 Avenue de la Terrasse, 91990 Gif-sur-Yvette, France; §Institut de Genetique et de Biologie Moleculaire et Cellulaire, Centre National de la Recherche Scientifique/Institut National de la Santé et de la Recherche Médicale/Université Louis Pasteur, 1 Rue Laurent Fries, BP 163, 67404 Illkirch Cedex, France; and ¶Institut Curie, Centre National de la Recherche Scientifique-Unité Mixte de Recherche 144, 26 Rue d'Ulm, 75248 Paris Cedex 05, France

Communicated by Georges Charpak, European Organization for Nuclear Research, Geneva, Switzerland, September 16, 2003 (received for review August 1, 2003)

Recently, we demonstrated that the expression levels of the translationally controlled tumor protein (TCTP) were strongly down-regulated at the mRNA and protein levels during tumor reversion/suppression and by the activation of p53 and Siah-1. To better characterize the function of TCTP, a yeast two-hybrid hunt was performed. Subsequent analysis identified the translation elongation factor, eEF1A, and its guanine nucleotide exchange factor, eEF1Bβ, as TCTP-interacting partners. *In vitro* and *in vivo* studies confirmed that TCTP bound specifically eEF1Bβ and eEF1A. Additionally, MS analysis also identified eEF1A as a TCTP interactor. Because eEF1A is a GTPase, we investigated the role of TCTP on the nucleotide exchange reaction of eEF1A. Our results show that TCTP preferentially stabilized the GDP form of eEF1A, and, furthermore, impaired the GDP exchange reaction promoted by eEF1Bβ. These data suggest that TCTP has guanine nucleotide dissociation inhibitor activity, and, moreover, implicate TCTP in the elongation step of protein synthesis.

Translationally controlled tumor protein (TCTP), also termed p23, is ubiquitously expressed and is present in evolutionarily diverse organisms. TCTP was initially identified in Ehrlich ascites tumor cells, as a serum-inducible mRNA whose expression is regulated at both the transcriptional and translational levels (1–4). Biochemical and immunofluorescence studies demonstrated that TCTP is a tubulin-binding protein that associates with microtubules in a cell-cycle dependent fashion (5). Recently, the polo-like kinase was shown to directly interact with and phosphorylate TCTP and was shown to be required for the normal progression of cytokinesis (6). In addition, TCTP binds the myeloid cell leukemia 1 protein, which is involved in programmed cell death (7, 8). Importantly, TCTP has also been characterized as the histamine-releasing factor (9).

Recently, a series of biological models of tumor reversion have been developed that have aided in understanding some of the molecular events underlying tumor reversion (10). Comparing gene expression profiles from leukemia and breast cancer cell lines with their revertant counterparts, as well as Siah-1 and p53 transfectants, we identified *tpt1* transcripts of TCTP as being significantly down-modulated among series of 263 genes differentially expressed. Decreasing TCTP expression levels, either by antisense or siRNA, was shown to either promote apoptosis, or more strikingly, induce the reorganization of MCF7 and T47D breast cancer cells into ductal/acinar structures of the now suppressed malignant phenotype (10).

A breakthrough was recently achieved by J. Craven's group by solving the solution structure of TCTP from *Schizosaccharomyces pombe* (11). These studies revealed that TCTP is structurally similar to the mammalian suppressor of Sec4 (MSS4/DSS4). MSS4 has a weak guanine nucleotide exchange factor (GEF) activity for various Rab proteins, however, subsequent experiments demonstrated that MSS4 functions, instead, as a guanine nucleotide-free chaperone (12, 13). MSS4/DSS4 binds to the nucleotide-free form of a subset of Rabs, which are members of the Ras superfamily of small G proteins involved in regulating the secretory pathway (14, 15). Its interaction with the nucleotide-free form of Rab15 is essential for endocytic trafficking (14). Interestingly, these structural studies showed that the highest homology observed between TCTP and MSS4 coincides with the Rab-binding site on MSS4. Thus, these structural studies indicate that TCTP may associate with and regulate the activities of GTPases in a similar fashion.

The small monomeric G proteins transition between active and inactive forms, depends on whether GTP or GDP is bound, respectively. This process is regulated by accessory factors that either stimulate GTP hydrolysis (GTPase activating proteins) or promote GDP exchange (GEFs) (16, 17). Guanine nucleotide dissociation inhibitors (GDIs) represent another class of molecules that regulate small G protein activity. GDIs act by inhibiting the dissociation of GDP bound to the GTPase, thereby maintaining the GTPase in its inactive state (18). The structural analysis of the GDIs complexed to one of the members of the Rho family, for example, has provided insight on the mechanism by which GDIs are able to execute their function. The interaction of a Rho-GDI with Rac shows how the GDI influences the stabilization of the Mg^{2+} ions associated with the nucleotide binding pocket via a system of switches present in Rho, which determines the fate of the bound nucleotide. On the other hand, the presence of a hydrophobic pocket inside the Rho-GDI explains how Cdc42 is able to quit its membrane anchorage by its geranylgeranyl moiety that is displaced toward the Rho-GDI in this precise pocket composed of β-sheets. This mechanism is at the basis of the shuttle function of the Rho-GDI between cytoplasm and membrane (19–21).

In this article, the elongation factor eEF1A and its GEF, eEF1Bβ, were identified as TCTP-binding partners in a yeast two-hybrid hunt. The eukaryotic elongation machinery consists of the large G protein, eEF1A (1 or 2), which is homologous to the bacterial EF-Tu. In higher eukaryotes, GDP/GTP exchange

Abbreviations: GEF, guanine nucleotide exchange factor; GDI, guanine nucleotide dissociation inhibitor; MSS4, mammalian suppressor of Sec4; NKTR, NK tumor recognition protein; IVT, *in vitro*-transcribed/translated; AIP1, ALG-2-interacting protein 1.

†C.C. and B.J.P. contributed equally to this work.

‖To whom correspondence should be addressed. E-mail: atelerman@molecular-engines.com.

© 2003 by The National Academy of Sciences of the USA

is triggered by eEF1B, which consists of α, β, and γ. eEF1A recruits the aminoacyl-tRNA to the programmed ribosome, which requires the binding of GTP (aminoacyl-tRNA–eEF1A–GTP). On correct codon–anticodon interaction, GTP hydrolysis is triggered, and, in the resulting eEF1A–GDP complex, GDP is removed by two GEFs, eEF1Bα and eEF1Bβ, allowing for another cycle of elongation (22, 23). Interaction mapping studies indicate that eEF1A and the eEF1B subunits form a pentamer composed of two molecules of eEF1A, complexed with either eEF1Bα or eEF1Bβ, held together by eEF1Bγ (24).

Here, we show that TCTP is involved in the elongation step of translation. TCTP is shown to impair the GDP exchange reaction promoted by eEF1Bβ on eEF1A. Thus, by stabilizing eEF1A in its GDP-bound form, TCTP functions as a GDI.

Materials and Methods

Antibodies. Rabbit anti-eEF1Bβ and chicken anti-TCTP antibodies were generated against synthetic peptides corresponding to residues 14–30 of human eEF1Bβ or residues 55–65 of human TCTP, respectively (Agro-Bio, La Ferté St. Aubin, France). Rabbit anti-TCTP and mouse anti-eEF1A antibodies were purchased from Medical & Biological Laboratories (Nagoya, Japan) and Upstate Biotechnology, respectively.

Purification of Recombinant Proteins. Full-length TCTP, eEF1Bβ, and NK tumor recognition protein (NKTR) cDNAs were cloned in-frame into pGEX-6P (Amersham Biosciences). Production and purification of GST-fusion proteins are discussed in *Supporting Materials and Methods*, which is published as supporting information on the PNAS web site.

Yeast Two-Hybrid Hunt. Full-length or the first 84 amino acids of TCTP were fused in-frame with the LexA DNA-binding domain of pEG202. A cDNA library derived from human monocytic leukemia U937 cells was cloned into galactose-inducible pYESTrp2 vector. A yeast two-hybrid hunt was performed as described (25).

***In Vitro* and *in Vivo* Interaction.** *In vitro*-transcribed/translated (IVT) ^{35}S-methionine-labeled proteins were generated as described by the manufacturer (Promega). GST or GST-fusion proteins immobilized on beads were incubated with IVT radiolabeled products or purified rabbit eEF1A for 3 h at 4°C. Proteins bound to the GST-fusion proteins or GST alone, were washed and eluted directly in Laemmli buffer or in the presence of 10 mM reduced glutathione (ICN) (see *Supporting Materials and Methods*). For detection of endogenous interactions, 293T and HeLa cells were lysed for 1 h in 1% Nonidet P-40 lysis buffer containing 25 mM Tris·HCl, pH 7.5, 150 mM NaCl, 10% glycerol, plus the protease inhibitors 1 mM 4-(2-aminoethyl)benzenesulfonyl fluoride (AEBSF), 1% aprotinin, 1 mM leupeptin, and 2 mM pepstatin (all reagents from ICN) and cell lysates clarified by centrifugation (16,000 $\times$ *g*) for 20 min. Endogenous TCTP or eEF1Bβ were immunoprecipitated from lysates with either anti-TCTP, anti-eEF1Bβ, or an isotype-matched control antibody. The addition of G protein agarose beads (Amersham Biosciences) was followed for an additional 3 h at 4°C. Immune complexes were washed four times in the lysis buffer, eluted in Laemmli buffer, and analyzed by Western blot.

Immunofluorescence Analysis. Details of the immunofluorescence staining can be seen in *Supporting Materials and Methods*. Confocal imaging was performed on a Leica TCS SP1 confocal microscope.

Affinity Chromatography and MS Analysis. See *Supporting Materials and Methods* for further information.

Guanine Nucleotide Exchange Assay. Rabbit liver eEF1A was purified as described (26). The guanine nucleotide exchange on eEF1A was monitored essentially as described (27, 28). The eEF1A–[^{3}H]GDP complex was prepared after incubation of 4 μM eEF1A with 4 μM [^{3}H]GDP [Amersham Pharmacia Biosciences; 1,500 Ci/mol (1 Ci = 37 GBq)] in 80 μl of 45 mM Tris·HCl, pH 7.5, containing 0.5 mM DTT, 10 mM magnesium acetate, 100 mM NH_4Cl, 1 mg/ml BSA, and 25% glycerol for 5 min at 37°C. The reaction mixture was placed on ice and diluted by the addition of 640 μl of ice-cold exchange buffer (20 mM Tris·HCl, pH 7.5, 10 mM magnesium acetate, 50 mM NH_4Cl, and 10% glycerol). The exchange reaction was conducted at 0°C after the addition of 160 μl of exchange buffer containing nucleotide and specified exchange factors. Aliquots of 100 μl were taken at times indicated, and were immediately filtered through nitrocellulose filters (Millipore; pore size 0.45 μm). Filters were washed three times with 1 ml of ice-cold washing buffer (20 mM Tris·HCl, pH 7.5, 10 mM magnesium acetate, 100 mM NH_4Cl, and 0.1 mg/ml BSA), dried, and counted in a liquid scintillator.

Results

TCTP Interacts with the Elongation Factors eEF1Bβ and eEF1A. A yeast two-hybrid hunt was undertaken to identify proteins that interact with TCTP. Full-length or the first 84 amino acids of TCTP were used as baits to screen a cDNA library obtained from the human monocytic leukemia U937 cell line. Among the positive clones isolated were two proteins involved in the elongation step of protein synthesis, the GTPase eEF1A, and one of its GEFs, eEF1Bβ. Mating assays subsequently confirmed an interaction between LexA–TCTP and either B42–eEF1A or B42–eEF1Bβ (see Table 1, which is published as supporting information on the PNAS web site, and Fig. 1*A*). As defined by growth and β-gal activity, a robust interaction between LexA–TCTP and B42–eEF1Bβ was observed. A LexA–TCTP and B42–eEF1A interaction was also seen, although it was not as strong. Furthermore, the C-terminal GEF-containing region of eEF1Bβ (amino acids 153–281) was mapped as the TCTP-binding region (Fig. 1*A*). GST pull-down assays confirmed direct and reciprocal binding between TCTP and eEF1Bβ. IVT ^{35}S-labeled eEF1Bβ derived from reticulocyte lysates bound to GST-TCTP (Fig. 1*B Left*), but not to GST alone. Furthermore, GST-TCTP did not interact with the IVT-negative control protein, ALG-2-interacting protein 1 (AIP1) (29). A reciprocal interaction was also demonstrated for GST-eEF1Bβ and IVT-generated TCTP (Fig. 1*B Right*). Moreover, purified eEF1A derived from rabbit liver bound specifically to GST-TCTP, but not to the negative control, GST-NKTR (30) (Fig. 1*C*). Because the apparent K_d of TCTP–eEF1A interaction is high (see below; Fig. 4*C*), we could not quantitatively address the binding of TCTP to eEF1A in a nucleotide-dependent manner in an *in vitro* pull-down experiment. Kinetic studies described below showed that TCTP preferentially binds the GDP form of the factor.

To investigate the presence of endogenous interaction between TCTP and eEF1Bβ, antibodies directed against TCTP and eEF1Bβ were generated and initially tested on total cell lysates derived from 293T cells. Immunoblot analysis revealed that the anti-TCTP antibody detected a protein band of 23 kDa, corresponding to its expected molecular weight (see Fig. 6, which is published as supporting information on the PNAS web site). In addition, the anti-eEF1Bβ antibody recognized a single protein band of 36–38 kDa, which corresponded to the predicted size of eEF1Bβ. Finally, anti-TCTP and anti-eEF1Bβ antibodies immunoprecipitated their respective recombinant protein, indicating that both antibodies recognize native proteins (see Fig. 6).

Coimmunoprecipitation experiments were subsequently carried out on lysates derived from either 293T or HeLa cells to identify the presence of an endogenous association between TCTP with either eEF1Bβ or eEF1A. Rabbit anti-TCTP or

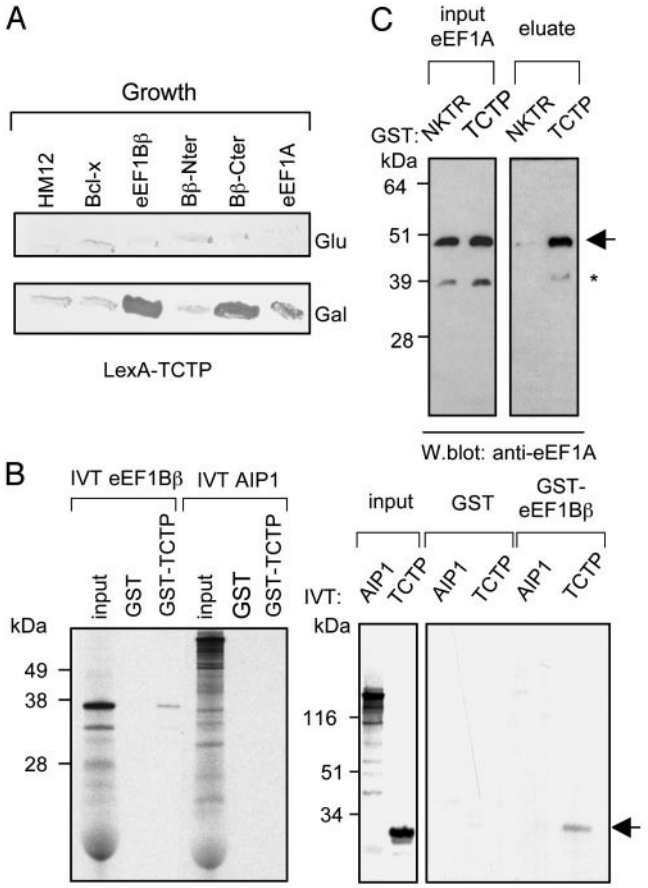

Fig. 1. Association of TCTP with either eEF1Bβ or eEF1A. (*A*) TCTP interacts with the C terminus of eEF1Bβ and eEF1A in yeast. Diploids carrying the constructs HM12, Bcl-x, eEF1A, eEF1Bβ, or truncated form of eEF1Bβ (Bβ-Nter residues 1–152 or Bβ-Cter residues 153–281) fused to B42 domain (activation domain) and LexA-TCTP were streaked onto either glucose (Glu) or galactose (Gal) plates and assayed for growth. (*B* and *C*) *In vitro* interaction of TCTP with either eEF1Bβ or eEF1A. (*B*) The indicated GST-fusion proteins immobilized on glutathione beads were incubated with AIP1, TCTP, or eEF1Bβ IVT. Radiolabeled proteins bound to the GST proteins were visualized by autoradiography. Inputs for each experiment are indicated. The negative controls, AIP1 and NKTR, are 120- and 150-kDa proteins, respectively. (*C*) GST-NKTR or GST-TCTP were incubated with eEF1A purified from rabbit liver. Eluted eEF1A was detected with the anti-eEF1A antibody. Arrow, full-length eEF1A. *, a degraded product of eEF1A.

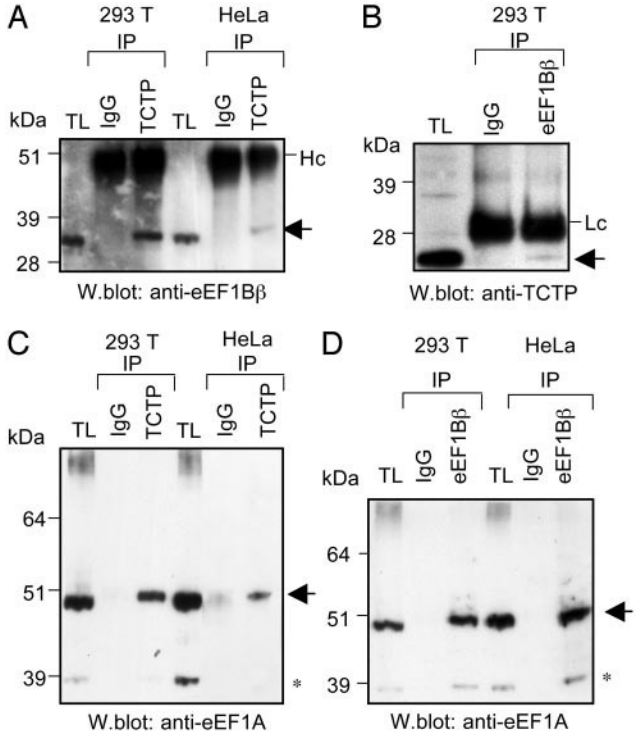

Fig. 2. Endogenous interaction of TCTP with either eEF1Bβ or eEF1A. TCTP was immunoprecipitated from either 293T or HeLa cell extracts with a rabbit anti-TCTP or an isotype-matched control antibody (IgG). Immunoprecipitates (IP) were analyzed by Western blot using anti-eEF1Bβ (*A*) or anti-eEF1A (*C*) antibodies. (*B*) Anti-eEF1Bβ antibodies or preimmune serum (IgG) were used to immunoprecipitate eEF1Bβ from 293T or HeLa cell extracts. Western blot analysis on the immune complexes using either anti-TCTP (*B*) or anti-eEF1A (*D*) antibodies revealed a specific association. Total cell lysates (TL) are indicated. Arrows highlight IP proteins. *, a degraded product of eEF1A; Hc and Lc, heavy and light chain of IgG, respectively.

isotype-matched IgG control antibodies were initially incubated with cell lysates. Immunoblot analysis with antibodies against either eEF1Bβ (Fig. 2*A*) or eEF1A (Fig. 2*C*) revealed that anti-TCTP, but not rabbit IgG, specifically coimmunoprecipitated protein bands of 36 and 51 kDa, respectively. In addition, immunoblotting with the chicken anti-TCTP antibody on immune complexes immunoprecipitated with anti-eEF1Bβ revealed a reciprocal association between TCTP and eEF1Bβ (Fig. 2*B*). In agreement with previous studies (24), Fig. 2*D* illustrates an association between eEF1Bβ and eEF1A. Finally, MS analysis of affinity-purified TCTP-binding partners confirmed that eEF1A interacts with TCTP. Interestingly, eEF2, a GTPase also involved in elongation, was identified as an additional TCTP-interacting partner in the same screening (see Tables 2–4, which are published as supporting information on the PNAS web site). Overall, the above data show that TCTP associates with eEF1Bβ and eEF1A, proteins involved in translation elongation.

TCTP Colocalizes with Either eEF1Bβ or eEF1A. Indirect immunofluorescence studies were also performed on HeLa cells to further investigate an endogenous association between TCTP and either eEF1Bβ or eEF1A. Fig. 3 shows that staining with the chicken anti-TCTP antibody appeared punctate and cytoplasmic and partially colocalized with the endoplasmic reticulum (ER) marker protein disulfide isomerase (PDI) (see Fig. 7, which is published as supporting information on the PNAS web site). Moreover, in agreement with previous reports (5), confocal imaging also showed a strong perinuclear staining with the anti-TCTP, partially overlapping with ER marker. Anti-eEF1Bβ staining was restricted primarily to the ER (Fig. 3*A Upper*), costaining with PDI (31) (see Fig. 7). The overlay of TCTP and eEF1Bβ staining indicates that these proteins partially colocalize to the perinuclear region of the cell. Finally, colocalization studies of eEF1A and TCTP were also performed. Immunofluorescence analysis using an anti-eEF1A antibody revealed staining around the nucleus and throughout the cytoplasm (31). Confocal analysis on HeLa cells stained with chicken anti-TCTP and anti-eEF1A antibodies revealed a partial colocalization around the nucleus (Fig. 3*B*).

TCTP Preferentially Stabilizes the GDP Form of eEF1A. The functional relevance of a TCTP and eEF1A association was further investigated by monitoring the effects of TCTP on the rate of dissociation of GDP from the eEF1A–[^{3}H]GDP complex. We sought to determine whether TCTP preferentially binds to the GDP-bound form of the factor (and pushes the equilibrium toward the formation of eEF1A-GDP) or associates with the nucleotide-free form of eEF1A (and displaces the exchange

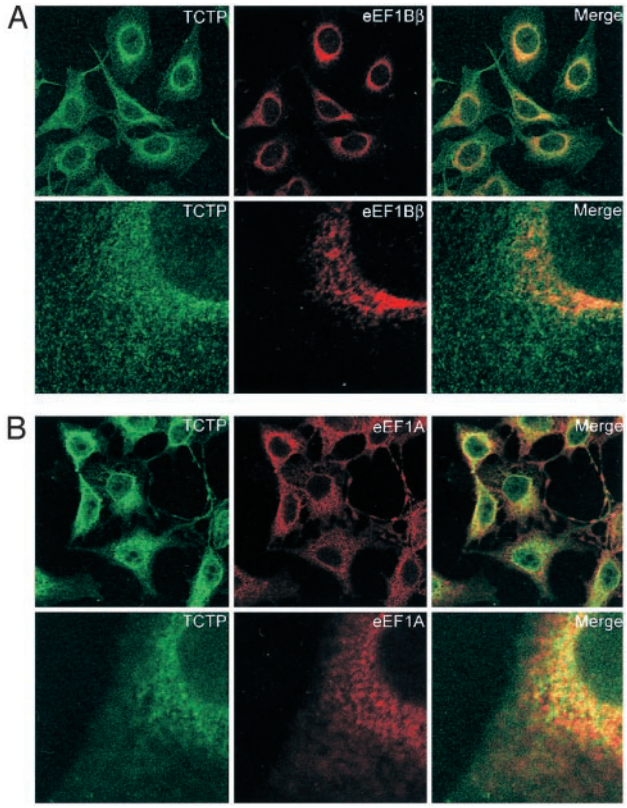

Fig. 3. Endogenous colocalization of TCTP with either eEF1Bβ or eEF1A in HeLa cells. (*A*) Immunofluorescence analysis of anti-TCTP (green) and anti-eEF1Bβ (red) staining. Merge shows a partial colocalization of TCTP and eEF1Bβ (yellow). A higher magnification of cell is shown in *Lower*. (*B*) Immunofluorescence analysis of anti-TCTP (green) and anti-eEF1A (red) staining. Merge indicates a partial colocalization of TCTP and eEF1A. A higher magnification of cell is shown in *Lower*. Note the enhanced colocalization of TCTP with either eEF1Bβ or eEF1A within the perinuclear region of the cell. Each confocal image represents a similar plane through the cell.

reaction toward the formation of eEF1A). When eEF1A was preloaded with [^{3}H]-GDP and incubated in the presence of saturating amounts of unlabeled GDP (150 μM), GDP dissociation followed monoexponential kinetics corresponding to a half-life of the complex of 12 min (Fig. 4*A*). This result corresponded to a rate of 0.082 ± 0.004 pmol GDP exchanged per min per pmol of eEF1A. In the absence of free GDP in the incubation mixture, the eEF1A–[^{3}H]GDP complex remained stable over a period of 40 min. Increasing amounts of TCTP (from 0.2 to 3.0 μM) were added in the exchange assay, and the rate of dissociation of the eEF1A–[^{3}H]GDP complex was monitored in the presence of 150 μM free GDP (Fig. 4*A*). TCTP by itself did not bind nucleotides (data not shown). When 3 μM of TCTP were added, the half-life of the eEF1A–[^{3}H]GDP complex increased to 39 min, corresponding to a rate of GDP dissociation of 0.026 ± 0.003 pmol GDP exchanged per min per pmol of eEF1A. Therefore, TCTP is devoid of exchange activity; its addition decreases the rate of GDP exchange on eEF1A. The inhibition of GDP exchange by TCTP was concentration dependent and followed a saturation kinetics with an apparent dissociation constant, K_d, of 1.2 ± 0.2 μM (Fig. 4*C*). The stabilization of the eEF1A–[^{3}H]GDP complex by TCTP suggests that TCTP preferentially binds the GDP form of eEF1A as compared with the nucleotide-free form of the factor.

The eukaryotic elongation factor, eEF1A, binds GDP and GTP with similar affinity (2–4 μM) (32). To determine whether TCTP preferentially binds the GDP or the GTP form of eEF1A, the effect of the addition of TCTP on the GDP–GTP exchange on eEF1A was monitored (Fig. 4*B*). When unlabeled free GTP (150 μM) was added in the exchange reaction instead of GDP, a similar protection of the eEF1A–[^{3}H]GDP complex was observed (rate of GDP dissociation decreasing from 0.078 ± 0.004 to 0.024 ± 0.003 pmol GDP exchanged per min per pmol of eEF1A), showing that TCTP does not displace the equilibrium toward the formation of an eEF1A–GTP complex. The apparent K_d of TCTP for the GDP form of eEF1A (1.6 ± 0.3 μM; Fig. 4*C*) was not significantly affected. These data show that TCTP preferentially binds the GDP form of eEF1A and impairs GDP dissociation.

TCTP Inhibits the eEF1Bβ-Mediated Exchange Reaction. Higher eukaryotes contain two GEFs, eEF1Bα (formerly EF-1β, 27 kDa), and eEF1Bβ (formerly EF-1δ, 35 kDa) (28, 33). The exchange activity of eEF1Bα is enhanced by its association with eEF1Bγ (formerly EF-1γ, 50 kDa). Because TCTP stabilizes the GDP form of eEF1A, we investigated its effect on eEF1Bα–eEF1Bγ complex or eEF1Bβ-mediated GDP exchange on eEF1A (only

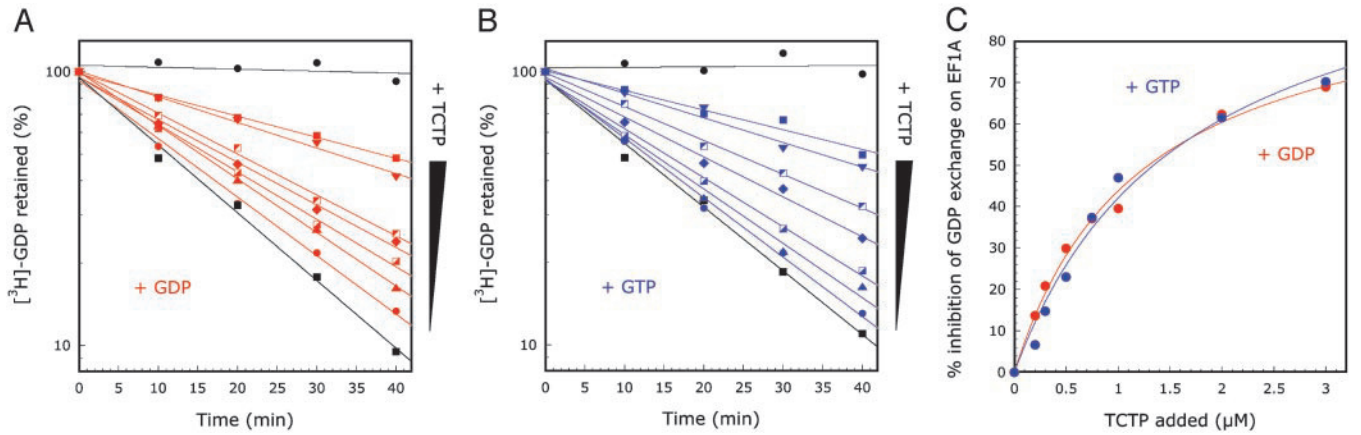

Fig. 4. TCTP preferentially stabilizes the GDP form of eEF1A. The time course of GDP exchange was assayed at 0°C in the presence of 350 nM eEF1A-[^{3}H]GDP without TCTP (■) or with increasing amounts of TCTP (final concentrations of 200, 300, 500, and 750 nM, and 1, 2, and 3 μM, which are indicated by red and blue symbols in *A* and *B*, respectively). The reaction was monitored in the presence of 150 μM unlabeled GDP (*A*) or 150 μM unlabeled GTP (*B*). In the absence of unlabeled nucleotide, the eEF1A–[^{3}H]GDP complex remained stable (●). All reactions were performed in triplicate. (*C*) The inhibition of GDP exchange on eEF1A observed in *A* and *B* in the presence of GDP or GTP is plotted as a function of TCTP added.

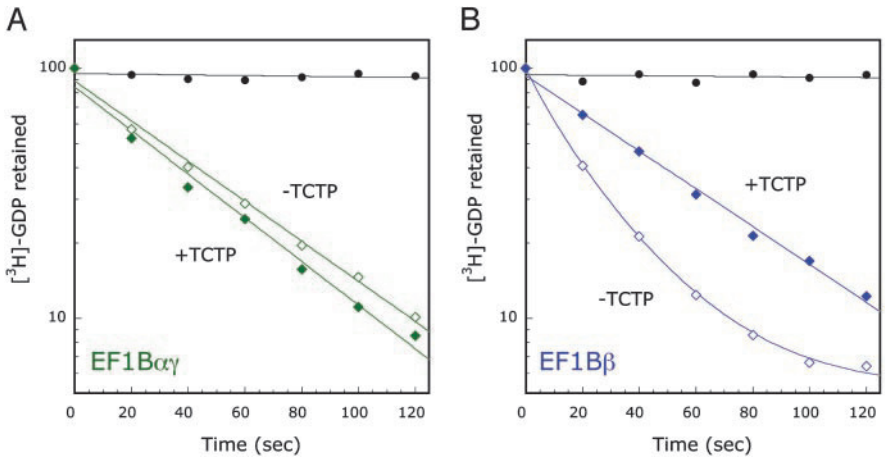

Fig. 5. TCTP inhibits the eEF1Bβ-mediated exchange reaction. Kinetics of GDP exchange promoted by 10 nM of the eEF1Bα–eEF1Bγ complex (EF1Bαγ) (*A*) or by 50 nM of eEF1Bβ (EF1Bβ) (*B*) were conducted in the presence (+TCTP) or in the absence (−TCTP) of 2 μM TCTP. In the absence of unlabeled nucleotide, the eEF1A–[^{3}H]GDP complex remained stable (●). The time course of GDP exchange was initiated by addition of 150 μM unlabeled GDP.

eEF1Bβ was found to interact with TCTP in the two-hybrid screen). As reported (28), in the presence of the eEF1Bαγ complex, GDP exchange followed first-order kinetics (initial rate of 0.84 min^{-1} per pmol of eEF1Bαγ; Fig. 5*A*) whereas eEF1Bβ-mediated exchange was biphasic (initial rates of 0.66 min^{-1} and 1.68 min^{-1} per pmol of eEF1Bβ; Fig. 5*B*) as reported (28). When TCTP was added in the exchange reaction at a final concentration of 2 μM, the kinetics of GDP exchange in the presence of eEF1Bαγ remained essentially unchanged (initial rate of 0.96 min^{-1}; Fig. 5*A*). By contrast, the initial rate of GDP exchange in the presence of eEF1Bβ and TCTP was no more biphasic and followed a simple first-order rate (0.294 min^{-1} per pmol of eEF1Bβ; Fig. 5*B*). From these data, we conclude that TCTP stabilizes the GDP form of eEF1A and specifically antagonizes the eEF1Bβ-mediated exchange reaction.

Discussion

TCTP has been proposed to be involved in growth-related activities (2). In this study, we found by yeast two-hybrid assay and confirmed by coimmunoprecipitation and immunofluorescence studies that TCTP associates with components of the translational machinery, the elongation factors, eEF1A and eEF1Bβ.

Elongation factors of translation have been implicated in tumor formation (34). For example, constitutive expression of eEF1A caused fibroblasts to become highly susceptible to transformation (35). In addition, a truncated form of eEF1A, encoded by the PTI-1 gene, was identified in prostatic cancers (36–38). Inhibiting PTI-1 expression with PTI-1 antisense resulted in the suppression of its tumorigenic potential. eEF1Bβ has also been implicated in cell transformation and tumorigenesis. Its overexpression resulted in anchorage-independent growth and in the formation of tumors in nude mice (39).

In agreement with the structural studies on the shared homology between MSS4 and TCTP, we show that TCTP interacts with the GTPase, eEF1A, preferentially in a GDP-bound form. We propose that TCTP acts as a GDI, based on the following observations: (*i*) TCTP inhibited the eEF1A–[^{3}H]GDP complex dissociation in the presence of cold GDP in excess, and (*ii*) TCTP preferentially stabilized eEF1A–[^{3}H]GDP in the presence of cold GTP in excess. Furthermore, we demonstrated that TCTP impaired the GDP exchange reaction promoted by eEF1Bβ on the eEF1A–[^{3}H]GDP complex.

Takai and coworkers (40) first identified GDIs, which inhibited the specific release of GDP, but not GTP from Rab3A. GDIs generally prevent the translocation of small G proteins to the membrane, thereby sequestering them in cytoplasm (18). In the case of Rabs, GDIs have the potential to regulate the availability of specific intracellular transport effectors (41). More recently, GDIs have been shown to regulate the large heterotrimeric G proteins. For example, the activator of G protein signaling 3 (AGS3) acts as a GDI on Galpha (i3). AGS3 prevents Galpha (i3) activation by keeping the GTPase in the cytoplasm in a GDP-bound state (42, 43).

The findings that GDIs are associated with both small and large G proteins implies that they could be implicated in regulation of GTPases involved in translation. In this regard, TCTP could selectively modulate the activity of eEF1A during the process of translation elongation. Our data show that TCTP specifically impaired the exchange reaction promoted by eEF1Bβ, and not eEF1Bαγ. The function and the existence of two exchange factors for eEF1A is largely not understood. However, kinetics studies indicate that they act differently on the elongation factor, eEF1A. The eEF1Bα–eEF1Bγ complex mediates GDP dissociation from eEF1A in a linear way according to the time. By contrast, eEF1Bβ mediates a biphasic exchange reaction. It has been hypothesized that the first step, a fast-exchange reaction, corresponds to the rate of exchange under single-turnover conditions (28). This initial, fast rate of GDP exchange in the presence of eEF1Bβ (1.68 min^{-1}) is believed to correspond to the intrinsic rate of exchange promoted by the formation of the eEF1A–eEF1Bβ complex. The second, slow-exchange reaction step (0.66 min^{-1}) only observed in the presence of eEF1Bβ, may be due to the slow dissociation of eEF1Bβ from the nucleotide-free form of eEF1A, which would be the rate-limiting step of the reaction. In the presence of TCTP, because the rate of GDP-exchange promoted by eEF1Bβ is significantly decreased (0.294 min^{-1}), and is slower than the rate of dissociation of the eEF1A–eEF1Bβ complex, monophasic kinetics are observed. The crystal structure of the eukaryotic elongation factor complex eEF1A–eEF1Bα from yeast revealed that the GEF interacts with domains 1 and 2 of eEF1A. On binding, eEF1Bα causes reorganization of the switch 2 region of eEF1A and inserts a lysine side chain in the Mg^{2+}-binding site, which promotes nucleotide release (44, 45). These two features are common to the nucleotide exchange mechanism for several G proteins. In this context, TCTP binding to eEF1A-GDP may either prevent the conformational rearrangement occurring in the switch 2 region of eEF1A on binding of eEF1Bβ or impair the formation of a productive eEF1A–eEF1Bβ complex. That

TCTP was found to impair the function of eEF1Bβ, but not of eEF1Bα–eEF1Bγ on eEF1A, indicates the specificity of the effect and suggests that TCTP interferes with the proper binding of eEF1Bβ. TCTP binds specifically the C-terminal GEF domain of eEF1Bβ, which is highly conserved with eEF1Bα, suggesting that the two exchange factors do not interact in the same region on eEF1A, or have somewhat different exchange mechanisms.

During protein synthesis, eEF1A forms a ternary complex with aminoacylated tRNA and GTP (eEF1A–GTP–aatRNA), and delivers aatRNA to the ribosome after GTP hydrolysis. Inactive eEF1A-GDP and deacylated tRNA are released from the ribosome and must be recycled. Maintaining eEF1A in a GDP-bound form by TCTP could represent an important step of tRNA channeling. The concept of tRNA channeling during translation assumes that tRNA is first vectorially transferred from its specific aminoacyl-tRNA synthetase (to be aminoacylated), next to eEF1A (to form the tRNA species competent for ribosomal translation), then to the ribosome, and finally back to the synthetase without mixing with the cellular fluid (27, 46, 47). In this context, the formation of a complex between TCTP and eEF1A-GDP may be involved in the channeling of tRNA. It has been shown that eEF1A-GDP can bind deacylated tRNA (48). The GDI activity of TCTP may prevent eEF1A activation into eEF1A-GTP before it is recruited by other components of the translation machinery to form a ternary complex with a *de novo*-aminoacylated tRNA. Thus, TCTP may play a prominent role in the elongation cycle of translation. Accordingly, decreasing the expression of TCTP in cancer cells might be a means to decrease the efficiency of protein synthesis, and to down-regulate cell proliferation.

We thank Jeremy Craven for helpful discussion and Philippe Fontanges, Institut Federatif de Recherche, Hopitâl Tenon for excellent confocal microscopy support.

1. Yenofsky, R., Cereghini, S., Krowczynska, A. & Brawerman, G. (1983) *Mol. Cell. Biol.* **3,** 1197–1203.
2. Bohm, H., Benndorf, R., Gaestel, M., Gross, B., Nurnberg, P., Kraft, R., Otto, A. & Bielka, H. (1989) *Biochem. Int.* **19,** 277–286.
3. Bohm, H., Gross, B., Gaestel, M., Bommer, U. A., Ryffel, G. & Bielka, H. (1991) *Biomed. Biochim. Acta* **50,** 1193–1203.
4. Xu, A., Bellamy, A. R. & Taylor, J. A. (1999) *Biochem. J.* **342,** 683–689.
5. Gachet, Y., Tournier, S., Lee, M., Lazaris-Karatzas, A., Poulton, T. & Bommer, U. A. (1999) *J. Cell Sci.* **112,** 1257–1271.
6. Yarm, F. R. (2002) *Mol. Cell. Biol.* **22,** 6209–6221.
7. Li, F., Zhang, D. & Fujise, K. (2001) *J. Biol. Chem.* **276,** 47542–47549.
8. Zhang, D., Li, F., Weidner, D., Mnjoyan, Z. H. & Fujise, K. (2002) *J. Biol. Chem.* **277,** 37430–37438.
9. MacDonald, S. M., Rafnar, T., Langdon, J. & Lichtenstein, L. M. (1995) *Science* **269,** 688–690.
10. Tuynder, M., Susini, L., Prieur, S., Besse, S., Fiucci, G., Amson, R. & Telerman, A. (2002) *Proc. Natl. Acad. Sci. USA* **99,** 14976–14981.
11. Thaw, P., Baxter, N. J., Hounslow, A. M., Price, C., Waltho, J. P. & Craven, C. J. (2001) *Nat. Struct. Biol.* **8,** 701–704.
12. Yu, H. & Schreiber, S. L. (1995) *Nature* **376,** 788–791.
13. Esters, H., Alexandrov, K., Iakovenko, A., Ivanova, T., Thoma, N., Rybin, V., Zerial, M., Scheidig, A. J. & Goody, R. S. (2001) *J. Mol. Biol.* **310,** 141–156.
14. Strick, D. J., Francescutti, D. M., Zhao, Y. & Elferink, L. A. (2002) *J. Biol. Chem.* **277,** 32722–32729.
15. Nuoffer, C., Wu, S. K., Dascher, C. & Balch, W. E. (1997) *Mol. Biol. Cell* **8,** 1305–1316.
16. Cherfils, J. & Chardin, P. (1999) *Trends Biochem. Sci.* **24,** 306–311.
17. Donovan, S., Shannon, K. M. & Bollag, G. (2002) *Biochim. Biophys. Acta* **1602,** 23–45.
18. Takai, Y., Sasaki, T. & Matozaki, T. (2001) *Physiol. Rev.* **81,** 153–208.
19. Scheffzek, K., Stephan, I., Jensen, O. N., Illenberger, D. & Gierschik, P. (2000) *Nat. Struct. Biol* **7,** 122–126.
20. An, Y., Shao, Y., Alory, C., Matteson, J., Sakisaka, T., Chen, W., Gibbs, R. A., Wilson, I. A. & Balch, W. E. (2003) *Structure (London)* **11,** 347–357.
21. Hoffman, G. R., Nassar, N. & Cerione, R. A. (2000) *Cell* **100,** 345–356.
22. Hershey, J. W. (1991) *Annu. Rev. Biochem.* **60,** 717–755.
23. Proud, C. G. (2000) in *Translational Control of Gene Expression*, eds. Sonenberg, N., Hershey, J. W. B. & Mathews, M. B. (Cold Spring Harbor Lab. Press, Plainview, NY), pp. 719–40.
24. Mansilla, F., Friis, I., Jadidi, M., Nielsen, K. M., Clark, B. F. & Knudsen, C. R. (2002) *Biochem. J.* **365,** 669–676.
25. Finley, R., Jr., & Brent, R. (1995) in *DNA Cloning, Expression Systems: A Practical Approach*/(Oxford University Press, New York), pp. 169–203.
26. Shalak, V. F., Budkevich, T. V., Negrutskil, B. S. & El'skaia, A. V. (1997) *Uk. Biokhim. Zh.* **69,** 104–109.
27. Negrutskii, B. S., Shalak, V. F., Kerjan, P., El'skaya, A. V. & Mirande, M. (1999) *J. Biol. Chem.* **274,** 4545–4550.
28. Bec, G., Kerjan, P. & Waller, J. P. (1994) *J. Biol. Chem.* **269,** 2086–2092.
29. Vito, P., Pellegrini, L., Guiet, C. & D'Adamio, L. (1999) *J. Biol. Chem.* **274,** 1533–1540.
30. Nestel, F. P., Colwill, K., Harper, S., Pawson, T. & Anderson, S. K. (1996) *Gene* **180,** 151–155.
31. Sanders, J., Brandsma, M., Janssen, G. M., Dijk, J. & Moller, W. (1996) *J. Cell Sci.* **109,** 1113–1117.
32. Crechet, J. B. & Parmeggiani, A. (1986) *Eur. J. Biochem.* **161,** 647–653.
33. Janssen, G. M., van Damme, H. T., Kriek, J., Amons, R. & Moller, W. (1994) *J. Biol. Chem.* **269,** 31410–31417.
34. Sonenberg, N. (1993) *Curr. Opin. Cell Biol.* **5,** 955–960.
35. Tatsuka, M., Mitsui, H., Wada, M., Nagata, A., Nojima, H. & Okayama, H. (1992) *Nature* **359,** 333–336.
36. Shen, R., Su, Z. Z., Olsson, C. A. & Fisher, P. B. (1995) *Proc. Natl. Acad. Sci. USA* **92,** 6778–6782.
37. Su, Z., Goldstein, N. I. & Fisher, P. B. (1998) *Proc. Natl. Acad. Sci. USA* **95,** 1764–1769.
38. Sun, Y., Lin, J., Katz, A. E. & Fisher, P. B. (1997) *Cancer Res.* **57,** 18–23.
39. Joseph, P., Lei, Y. X., Whong, W. Z. & Ong, T. M. (2002) *J. Biol. Chem.* **277,** 6131–6136.
40. Sasaki, T., Kikuchi, A., Araki, S., Hata, Y., Isomura, M., Kuroda, S. & Takai, Y. (1990) *J. Biol. Chem.* **265,** 2333–2337.
41. Soldati, T., Shapiro, A. D., Svejstrup, A. B. & Pfeffer, S. R. (1994) *Nature* **369,** 76–78.
42. De Vries, L., Fischer, T., Tronchere, H., Brothers, G. M., Strockbine, B., Siderovski, D. P. & Farquhar, M. G. (2000) *Proc. Natl. Acad. Sci. USA* **97,** 14364–14369.
43. Kimple, R. J., De Vries, L., Tronchere, H., Behe, C. I., Morris, R. A., Gist Farquhar, M. & Siderovski, D. P. (2001) *J. Biol. Chem.* **276,** 29275–29281.
44. Andersen, G. R., Pedersen, L., Valente, L., Chatterjee, I., Kinzy, T. G., Kjeldgaard, M. & Nyborg, J. (2000) *Mol. Cell* **6,** 1261–1266.
45. Andersen, G. R., Valente, L., Pedersen, L., Kinzy, T. G. & Nyborg, J. (2001) *Nat. Struct. Biol.* **8,** 531–534.
46. Negrutskii, B. S. & Deutscher, M. P. (1991) *Proc. Natl. Acad. Sci. USA* **88,** 4991–4995.
47. Stapulionis, R. & Deutscher, M. P. (1995) *Proc. Natl. Acad. Sci. USA* **92,** 7158–7161.
48. Petrushenko, Z. M., Budkevich, T. V., Shalak, V. F., Negrutskii, B. S. & El'skaya, A. V. (2002) *Eur. J. Biochem.* **269,** 4811–4818.

РОЗДІЛ 2

СТРУКТУРНА ОРГАНІЗАЦІЯ КОМПЛЕКСУ ФАКТОРІВ ЕЛОНГАЦІЇ ТРАНСЛЯЦІЇ eEF1B ЛЮДИНИ. СТРУКУТУРНО-ФУНКЦІОНАЛЬНА ХАРАКТЕРИСТИКА ЙОГО СУБОДИНИЦЬ

2.1. Особливості структурної організації і функціональної активності субодиниці eEF1Bα

The FEBS Journal

FEBS PRESS science publishing by scientists

A non-catalytic N-terminal domain negatively influences the nucleotide exchange activity of translation elongation factor 1Bα

Tetiana V. Trosiuk[1], Vyacheslav F. Shalak[1], Roman H. Szczepanowski[2], Boris S. Negrutskii[1] and Anna V. El'skaya[1]

1 State Key Laboratory of Molecular and Cell Biology, Institute of Molecular Biology and Genetics, National Academy of Sciences of Ukraine, Kyiv, Ukraine
2 International Institute of Molecular and Cell Biology, Warsaw, Poland

Keywords
eukaryotic translation: guanine nucleotide exchange; non-globular proteins; protein–protein interactions; translation elongation factor 1

Correspondence
A. El'skaya and V. Shalak, State Key Laboratory of Molecular and Cell Biology, Institute of Molecular Biology and Genetics, National Academy of Sciences of Ukraine, 150 Zabolotnogo Street, 03680 Kyiv, Ukraine
Fax: +380 445260759
Tel: +380 445260749; +380 442000337
E-mails: gannaelska@gmail.com; shalak@imbg.org.ua

(Received 25 August 2015, revised 15 October 2015, accepted 11 November 2015)

doi:10.1111/febs.13599

Eukaryotic translation elongation factor 1Bα (eEF1Bα) is a functional homolog of the bacterial factor EF-Ts, and is a component of the macromolecular eEF1B complex. eEF1Bα functions as a catalyst of guanine nucleotide exchange on translation elongation factor 1A (eEF1A). The C-terminal domain of eEF1Bα is necessary and sufficient for its catalytic activity, whereas the N-terminal domain interacts with eukaryotic translation elongation factor 1Bγ (eEF1Bγ) to form a tight complex. However, eEF1Bγ has been shown to enhance the catalytic activity of eEF1Bα attributed to the C-terminal domain of eEF1Bα. This suggests that the N-terminal domain of eEF1Bα may in some way influence the guanine nucleotide exchange process. We have shown that full-length recombinant eEF1Bα and its truncated forms are non-globular proteins with elongated shapes. Truncation of the N-terminal domain of eEF1Bα, which is dispensable for catalytic activity, resulted in acceleration of the rate of guanine nucleotide exchange on eEF1A compared to full-length eEF1Bα. A similar effect on the catalytic activity of eEF1Bα was observed after its interaction with eEF1Bγ. We suggest that the non-catalytic N-terminal domain of eEF1Bα may interfere with eEF1A binding to the C-terminal catalytic domain, resulting in a decrease in the overall rate of the guanine nucleotide exchange reaction. Formation of a tight complex between the eEF1Bγ and eEF1Bα N-terminal domains abolishes this inhibitory effect.

Introduction

The heavy form of eukaryotic translation elongation factor 1 (eEF1H) is a unique macromolecular assembly of translation elongation factors that exists only in higher eukaryotes. It comprises the transiently associating eEF1A protein and the stable eEF1B complex containing the α, β and γ subunits: the nomenclature used is that proposed by Merrick and Nyborg [1,2]. eEF1A in the GTP-bound form is responsible for delivery of aminoacylated tRNA to the ribosome. In turn, the eEF1B complex functions as a catalyst of guanine nucleotide exchange on eEF1A. Both the eEF1Bα and eEF1Bβ subunits possess guanine exchange activity, but the functional role of eEF1Bγ remains obscure [1,3].

In higher vertebrates, there are two isoforms of eEF1A (designated eEF1A1 and eEF1A2) that are

Abbreviations
eEF1A, eukaryotic translation elongation factor 1A; eEF1Bα, eukaryotic translation elongation factor 1Bα; eEF1Bβ, eukaryotic translation elongation factor 1Bβ; eEF1Bγ, eukaryotic translation elongation factor 1Bγ; GEF, guanine exchange factor; S_w, weight-average sedimentation coefficient.

97% similar and are encoded by different genes [4]. cDNAs of both isoforms of eEF1A and all three subunits of eEF1B have been expressed in yeast two-hybrid analyses to map the interaction patterns between the proteins [5]. It was reported that, in contrast with eEF1A1, eEF1A2 has weak affinity for both the eEF1Bα and eEF1Bβ exchange factors. This surprising finding suggests the existence of different guanine exchange factor (GEF) for eEF1A2 [5]. However, this proposal has not been experimentally confirmed. Moreover, recombinant eEF1Bα was shown to catalyze guanine nucleotide exchange on eEF1A2 *in vitro* [6]. In addition, eEF1Bα and eEF1A2 were recently shown to co-localize in mammalian cells and tissues [7]. Thus, the absence of interaction between eEF1Bα and eEF1A2 in yeast two-hybrid experiments was possibly a false-negative result.

eEF1Bα is the smallest subunit (24–28 kDa) of the eEF1B complex, and is the functional homolog of the bacterial translation elongation factor EF-Ts. The amino acid sequence of eEF1Bα is highly conservative among all eukaryotes, but the homology with EF-Ts is relatively low. The structure of yeast eEF1A complexed with the C-terminal catalytic fragment of eEF1Bα was the first reported crystal structure of a eukaryotic translation elongation factor [8]. Lys205, located at the C-terminal end of *Saccharomyces cerevisiae* eEF1Bα, has been proposed to play a pivotal role in the nucleotide exchange mechanism [8]. Despite the reported similarity of the tertiary structures of the eEF1Bα C-terminus and the EF-Ts catalytic domains [9], the proteins interact respectively with eEF1A and EF-Tu in different ways [8,10].

It has been demonstrated that the C-terminal domain of eEF1Bα is necessary and sufficient for the catalytic activity [11–13], while the N-terminal domain is involved in interaction with eEF1Bγ [11,12]. eEF1Bα is tightly associated with eEF1Bγ, such that the two proteins may only be separated under strong denaturing conditions [14,15]. Moreover, eEF1Bγ enhances the catalytic activity of eEF1Bα [14,16]. The mechanism of this effect is still not understood.

To obtain insight into the mechanism of eEF1Bγ-mediated enhancement of the eEF1Bα catalytic activity, we designed a set of eEF1Bα truncated forms, characterized them by various methods, and tested their activity in a guanine nucleotide exchange assay with two isoforms of mammalian eEF1A. We also assessed the interaction between eEF1Bα, its truncated forms and both eEF1A isoforms by native gel electrophoresis in order to estimate their relative affinity.

Results and Discussion

Domain structure of eEF1Bα

Two domains joined by a linker region are apparent in the eEF1Bα primary structure (Fig. 1). The highly conserved C-terminal domain (residues 98–225) is responsible for the catalytic activity, while the less conserved N-terminal domain (residues 1–62) is involved in interaction with the N-terminal part of eEF1Bγ [11–14]. The linker region contains a hydrophilic stretch of amino acids that includes a recognition site for casein kinase II [12,17]. The structure of the human eEF1Bα fragment (residues 135–225) has been solved by NMR [9].

To explore the significance of the eEF1Bα N-terminal domain for the catalytic activity of the protein, a set of deletion mutants lacking 18, 38, 65 and 90 amino acids from the N-terminus (Fig. 1A) were designed, based on multiple amino acid sequence alignments (Fig. 1B). The first three mutants represent a stepwise truncation of the N-terminal domain, whereas the last one also lacks the linker region. Shorter N-terminally truncated fragments of eEF1Bα were not used in this study as peptides 116–225 and 135–225 of eEF1Bα have been shown to possess considerably lower catalytic activity: ~ 65% and 50% of that of the full-length protein, respectively [13]. The N-terminal part of eEF1Bα (residues 1–92), encompassing the N-terminal domain and the linker region, was also used for the experiments (Fig. 1A).

Expression and purification of full-length eEF1Bα and its truncated forms

Full-length eEF1Bα, also referred to as eEF1Bα(FL), and its truncated forms, except for GST–eEF1Bα (91–225), were purified by a two-step chromatographic procedure. As a first step, chromatography on a glutathione agarose column was performed. The isolated GST-fused proteins were then subjected to PreScission protease treatment. PreScission protease was chosen as it efficiently cleaved the target sequence at 4 °C, which was important to preserve the catalytic activity of the exchange factors. Then the mixtures of GST and eEF1Bα(FL) or its truncated variants were separated on a HiTrap Q Sepharose column. GST does not bind the matrix at 200 mM NaCl in the buffer solution, whereas eEF1Bα(FL) and the three truncated forms eEF1Bα(19–225), eEF1Bα(39–225) and eEF1Bα(66–225) do. Finally, as determined by SDS/PAGE (Fig. 2), highly purified proteins were retrieved after elution from the column by a salt gradient. Approximately 2 mg of eEF1Bα(FL) was obtained from 1 L

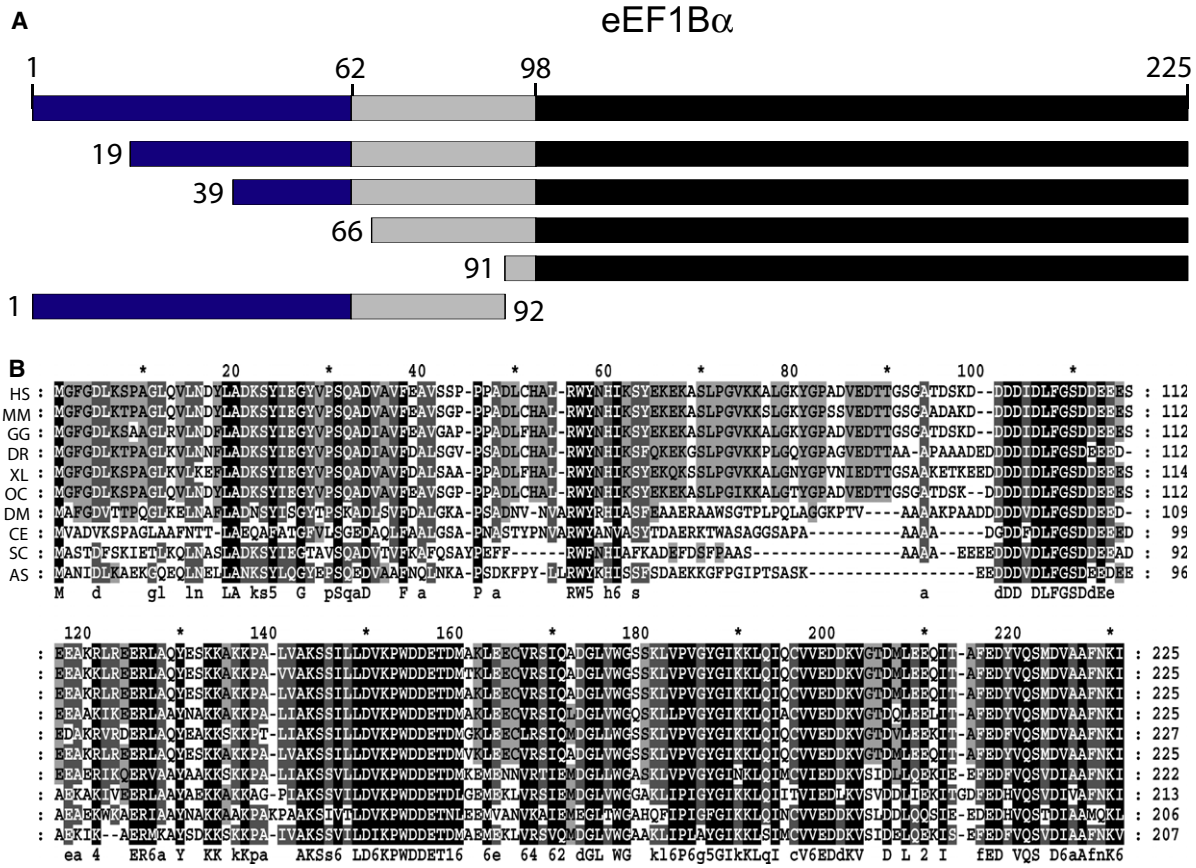

Fig. 1. Primary structure of eEF1Bα. (A) Schematic representation of the eEF1Bα truncated forms. (B) Multiple amino acid sequence alignment of eEF1Bα from various species. Abbreviations: HS, *Homo sapiens*; MM, *Mus musculus*; GG, *Gallus gallus*; DR, *Danio rerio*; XL, *Xenopus laevis*; OC, *Oryctolagus cuniculus*; DM, *Drosophila melanogaster*; CE, *Caenorhabditis elegans*; SC, *Saccharomyces cerevisiae*; AS, *Artemia salina*.

of BL21 (DE3) pLysE bacterial culture. The yield of the N-terminally truncated forms was similar to that of the full-length protein: ~ 2 mg each of purified eEF1Bα(19–225) and eEF1Bα(39–225), and 4 mg eEF1Bα(66–225), per 1 L of BL21 Gold culture.

GST–eEF1Bα(91–225) was purified on a glutathione agarose column only, because treatment with PreScission protease resulted in precipitation of the eEF1Bα fragment. Approximately 17 mg of the GST–eEF1Bα (91–225) deletion mutant was obtained per liter of culture, and its purity was more than 90% based on SDS/PAGE (Fig. 2).

The N-terminal part of eEF1Bα comprising residues 1–92 was also expressed as a GST fusion protein. After the first purification step and the PreScission protease treatment, eEF1Bα(1–92) was separated from GST and other contaminating proteins in a HiLoad 16/600 Superdex 200 per grade column. HiTrap Q sepharose could not be employed in this case since eEF1Bα(1–92) and GST possess a similar affinity for this resin. About 9 mg of more than 90% pure eEF1Bα(1–92) was obtained from 1 L of BL21Gold culture (Fig. 2).

Recombinant full-length eEF1Bα behaves as a non-globular monomer in solution

Recombinant eEF1Bα(FL) was eluted from a Superose 6 HR column as a 75 kDa protein (Fig. 3), i.e. three times larger than the theoretical value of the monomer (25.4 kDa), suggesting oligomerization of the protein. To address this issue, sedimentation velocity analysis of eEF1Bα(FL) was performed as described in Experimental procedures. The size distribution pattern obtained by continuous *c(s)* size distribution analysis is shown in Fig. 4A. The RMSD of the best fit was 0.0042. eEF1Bα(FL) sedimented as a single species at S_w = 0.932 S (weight-average sedimentation coefficient corrected to standard conditions of water at 20°C, $S_{20,w}$ = 1.910 S). Integration of

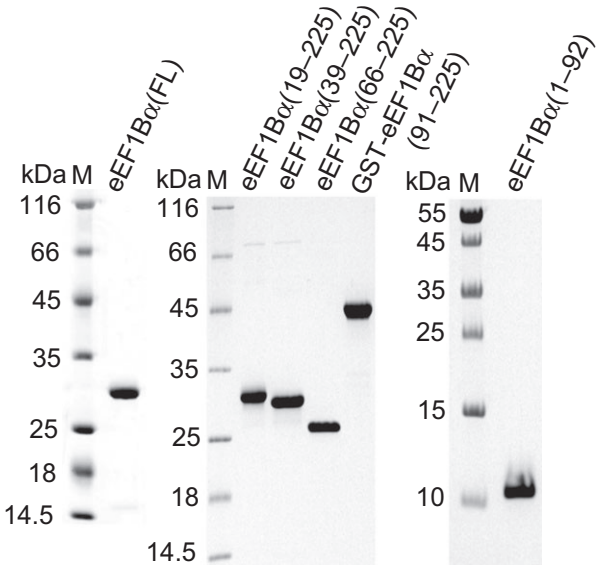

Fig. 2. SDS/PAGE of purified eEF1Bα(FL) and its truncated forms. Left and middle panels: the indicated proteins (3 μg each) were loaded onto a 12.5% polyacrylamide gel. Right panel: 4 μg of eEF1Bα(1-92) were loaded onto a 17% polyacrylamide gel.

the *c(s)* distribution showed that eEF1Bα(FL) peak represented 93.4% of the total absorbance signal. Using a best-fit frictional ratio (f/f_0) of 1.64, the molecular mass of eEF1Bα(FL) was estimated to be 25.5 kDa, in perfect agreement with the theoretical molecular mass of the monomer. The ratio S_{max}/S was calculated to be 1.6, as described in Experimental procedures. Importantly, the f/f_0 obtained and the calculated S_{max}/S values are characteristic of non-globular moderately elongated proteins [18].

This result was confirmed by sedimentation equilibrium analysis, which does not depend on the shape of the molecule. First, eEF1Bα(FL) at three initial concentrations was subjected to centrifugation at 17 000 rpm. After equilibrium was established, the speed was changed to 21 000 rpm (Fig. 4B). The experimental data obtained at different velocities were fitted to a single non-interacting species model using SEDPHAT, as described in Experimental procedures [19]. The molecular mass of eEF1Bα (FL) was estimated to be 26.3 ± 2.6 kDa after analysis of six single-speed scans (data not shown). Multi-speed analysis in SEDPHAT using the same model for the three protein concentrations was also applied [19]. In this case, the calculated molecular mass of eEF1Bα(FL) was 25.5 kDa (Fig. 4B), which coincides with the theoretical mass of its monomer (25.4 kDa).

Therefore, we conclude that full-length recombinant eEF1Bα behaves as a monomer in solution, and most probably belongs to the family of non-globular proteins with a moderately elongated shape.

The C-terminal domain and the linker region are the major contributors to the extended shape of eEF1Bα

Four N-terminally truncated forms of eEF1Bα and one C-terminally truncated form were purified to homogeneity (Fig. 2) and analyzed by size-exclusion chromatography on Superose 6 HR (Fig. 3). The apparent molecular mass of the eEF1Bα truncated mutant lacking the 18 N-terminal amino acids was estimated to be the same as that of the wild-type protein, whereas eEF1Bα lacking 38 amino acids and eEF1Bα(66–225), which lacks the entire N-terminal domain, eluted from the column in the same volume, corresponding to the apparent molecular mass of 60 kDa. The theoretical molecular masses of these truncated forms are approximately three times lower than the values assessed by gel filtration. The apparent molecular mass of the GST–eEF1Bα(91–225) fusion protein was estimated to be ~ 300 kDa, suggesting oligomerization of this protein. Similarly to the full-length eEF1Bα, the difference between the theoretical and experimental molecular masses of the N-terminally truncated mutants may be explained by the extended shapes of these mutants. However, truncation of the eEF1Bα N-terminal domain may destroy its hydrophobic core, and exposed hydrophobic residues may allow protein association.

To address this issue, sedimentation velocity analysis of all N-terminally truncated mutants of eEF1Bα was performed (Fig. 5). eEF1Bα(19-225) sediments as a single species at S_w = 0.740 S ($S_{20,w}$ = 1.434 S). Integration of the *c(s)* distribution showed that eEF1Bα(19–225) peak represented 92.4% of the total absorbance signal. The RMSD of the best fit was 0.0056. Using a best-fit friction ratio (f/f_0) of 1.86, the molecular mass of eEF1Bα(19-225) was estimated to be 20 kDa, close to the theoretical molecular mass of the monomer (22.7 kDa). The S_{max}/S value for eEF1Bα(19-225) was calculated as 2.02.

Continuous *c(s)* size distribution analysis of eEF1Bα (39-225) revealed three sedimenting species (Fig. 5). The first species sediments at S_w = 0.83 S ($S_{20,w}$ = 1.612 S), the second at S_w = 1.554 S ($S_{20,w}$ = 3.017 S), and the third at S_w = 2.217 S ($S_{20,w}$ = 4.3 S). Integration of the *c(s)* distribution showed that the peak of first species represented 49.3%, second species – 9.9% and third – 40.8% of the total absorbance signal. The RMSD of the best fit was 0.0061. Using a best-fit friction ratio (f/f_0) of 1.64, the molecular masses of the first, second and third species were estimated to be 19.8, 50 and 85 kDa, respectively. The S_{max}/S values for the first, second and third species were calculated to be 1.68, 1.43 and 1.59, respectively. The molecular mass

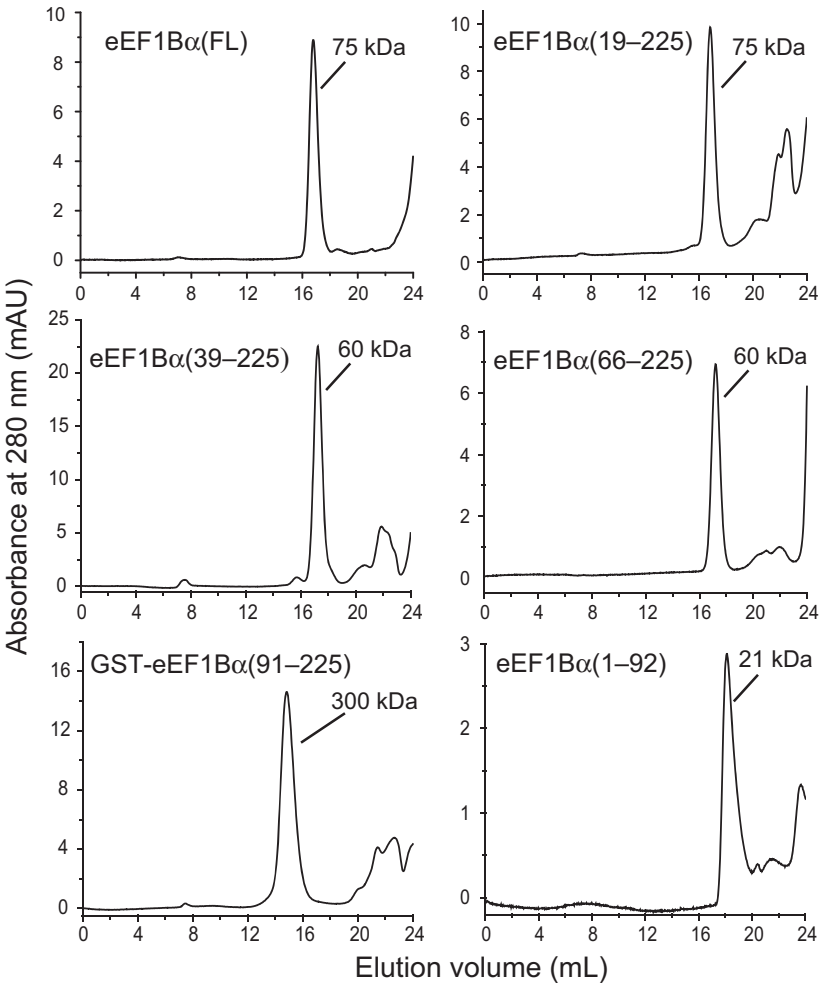

Fig. 3. Analysis of eEF1Bα(FL) and its truncated forms by size-exclusion chromatography: 100 μL of 10 μM eEF1Bα (FL), eEF1Bα(19–225), eEF1Bα(66–225) or GST–eEF1Bα(91–225), 20 μM eEF1Bα(39–225) or 30 μM eEF1Bα(1–92) were injected into a Superose 6 HR column.

of the first species is close to the theoretical molecular mass of the eEF1Bα(39-225) monomer (20.5 kDa). The second and third species most probably represent a dimer and a tetramer, respectively. Thus, sedimentation velocity analysis demonstrated that, under these conditions, 49.3% of eEF1Bα(39-225) is monomeric and 50.7% forms oligomers. This contradicts the gel filtration results (Fig. 3), showing very small amounts of oligomers. Moreover, when eEF1Bα(39-225) at the same initial concentration as used for the sedimentation velocity experiment was re-analyzed on a Superose 6 HR column, oligomers represented < 20% of total protein in the eluate (data not shown). This suggests that oligomerization of eEF1Bα(39-225) may be reversible, and that protein dilution during gel filtration may shift the equilibrium toward the monomeric form.

eEF1Bα(66-225) sediments as a single species at S_w = 0.766 S ($S_{20,w}$ = 1.485 S). Integration of the *c(s)* distribution showed that eEF1Bα(66–225) peak represented 98.7% of the total absorbance signal. The RMSD of the best fit was 0.0063. Using a best-fit friction ratio (f/f_0) of 1.69, the molecular mass of eEF1Bα (66-225) was estimated to be 18.3 kDa, close to the monomer theoretical mass (17.5 kDa). The S_{max}/S value for eEF1Bα(66-225) was calculated to be 1.63.

The GST–eEF1Bα(91-225) fusion protein sediments as a single species at S_w = 1.981 S ($S_{20,w}$ = 3.967 S). Integration of the *c(s)* distribution showed that GST-eEF1Bα(91–225) peak represented 91.2% of the total absorbance signal. The RMSD of the best fit was 0.0062. Using a best-fit friction ratio (f/f_0) of 1.73, the molecular mass of GST–eEF1Bα(91-225) was estimated to be 83 kDa, which is similar to the molecular mass of the dimer, as the theoretical molecular mass of the monomer is 42.2 kDa. The S_{max}/S value for the GST–eEF1Bα(91-225) dimer was calculated to be 1.75.

The N-terminal part of eEF1Bα, comprising residues 1-92, was also analyzed by size-exclusion chromatography (Fig. 3). Its molecular mass was estimated to be 21 kDa, which is twice the theoretical mass of the monomer (10.5 kDa). This suggests that, the eEF1Bα(1-92) truncated form may also possess a non-globular shape.

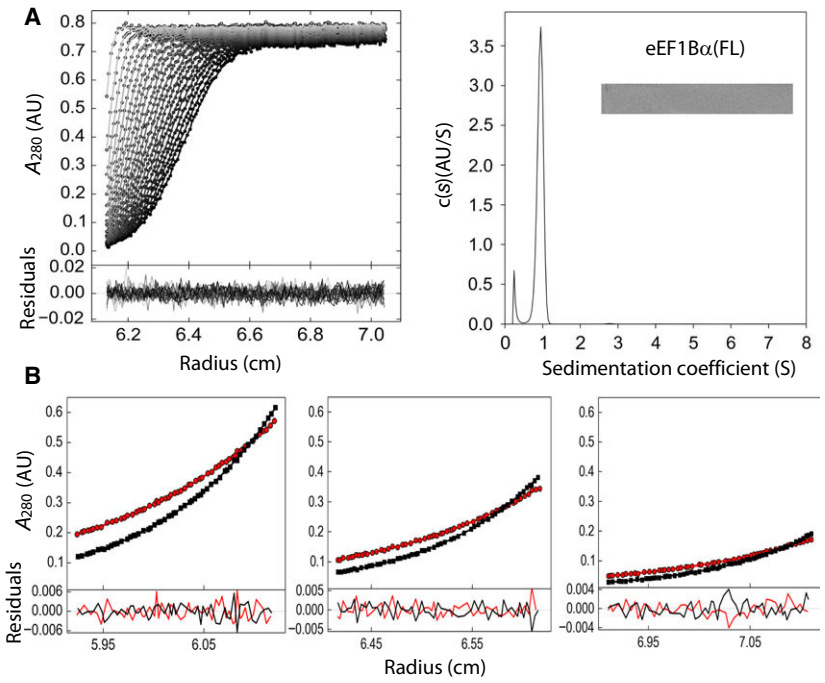

Fig. 4. Analytical ultracentrifugation analysis of the full-length recombinant eEF1Bα. (A) Left panel: absorbance scans of the sedimentation velocity data (only symbols for every third data point of every third scan are shown for clarity) and best-fit boundary model from the c(s) analysis (solid lines). Residuals are indicated. Right panel: continuous size distribution analysis, *c(s)*, plotted as a function of sedimentation coefficient. Inset: 2D grayscale 'bitmap' residual plot shows a high quality of fit. The initial concentration of eEF1Bα was 0.85 mg·mL^{-1}. (B) Absorbance scans of the sedimentation equilibrium data (only symbols for every second data point are shown for clarity) and best fits for the single-species model in the multi-speed analysis (solid lines). Red curves and symbols represent the equilibrium experiments performed at 17 000 rpm; black curves and symbols represent the equilibrium experiments performed at 21 000 rpm. Residuals are indicated. The initial concentrations of eEF1Bα were 0.2 mg·mL^{-1} (left), 0.12 mg·mL^{-1} (middle) and 0.06 mg·mL^{-1} (right). Graphs were prepared using GUSSI module (version 1.0.8d) in SEDFIT and SEDPHAT softwares.

Therefore, the N-terminally truncated variants of eEF1Bα used in this study are monomeric in solution, with the exception of eEF1Bα(39-225), which may partly form oligomers. The GST–eEF1Bα(91-225) fusion protein most probably exists as a stable dimer due to the presence of the GST moiety. It is worth noting that the truncated variants analyzed by sedimentation velocity have a frictional ratio in the range of 1.64–1.86 and S_{max}/S values in the range 1.68–2.02, which is typical of non-globular proteins that are moderately or highly elongated [18]. Altogether, the results obtained suggest that the linker region, together with the C-terminal domain, make the most significant contribution to the extended shape of eEF1Bα.

Our results are in agreement with observations made using the yeast eEF1Bα C-terminal fragment comprising residues 110–206. This 11 kDa tryptic fragment eluted from the gel filtration column as a 30 kDa protein [20]. Based on the crystal structure of the eEF1A*eEF1Bα complex [8], the authors attributed this threefold difference between apparent and theoretical molecular mass to the highly elongated shape of this domain [20].

Truncation of the N-terminal domain enhances the catalytic activity of eEF1Bα

The kinetics of the guanine nucleotide exchange reaction were measured as described previously [6]. As shown in Fig. 6A,B, deletion of 18 amino acids from the eEF1Bα N-terminal domain only slightly increases the rate of GDP/GDP exchange on eEF1A2, whereas deletion of 38 amino acids increases the rate by 50%. Complete deletion of the N-terminal domain (65 residues) results in more than 2.5-fold acceleration of the guanine nucleotide exchange rate on eEF1A2. The GST–eEF1Bα (91-225) mutant lacking the N-terminal domain and the linker region displayed the same catalytic activity as eEF1Bα(66-225). The eEF1Bγ subunit positively influences the catalytic activity of eEF1Bα(FL) (Fig. 6A). The apparent rate constant of GDP/GDP exchange on eEF1A2 in the presence of the eEF1Bαγ complex was estimated to be $17.2 \pm 0.4 \times 10^{-3}$ s^{-1}, which is more than 3.6 times higher than with eEF1Bα alone.

Unexpectedly, a weak stimulatory effect of eEF1Bα truncation was observed on the eEF1A1 isoform. The

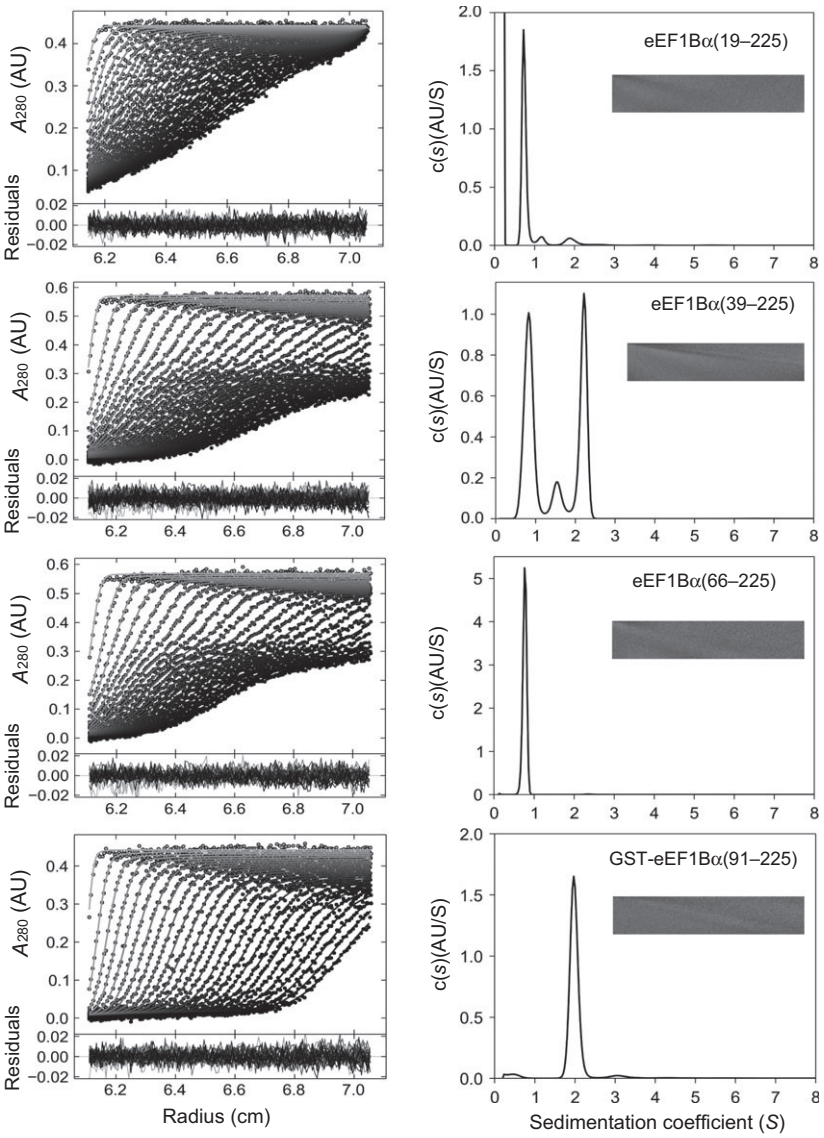

Fig. 5. Sedimentation velocity analysis of the eEF1Bα N-terminally truncated forms. (A) Left panel: absorbance scans of the sedimentation velocity data (only symbols for every third data point of every fifth scan are shown for clarity) and best-fit boundary model from the *c(s)* analysis (solid lines). Residuals are indicated. Right panel: continuous size distribution analysis, *c(s)*, plotted as a function of sedimentation coefficient. Inset: 2D grayscale 'bitmap' residual plot shows a high quality of fit. The initial concentration of eEF1Bα(19–225) was 0.3 mg·mL^{-1}, that of eEF1Bα (39–225) was 0.37 mg·mL^{-1}, that of eEF1Bα(66–225) was 0.47 mg·mL^{-1}, and that of GST–eEF1Bα(91–225) was 0.28 mg·mL^{-1}.

eEF1Bα truncated forms and the eEF1Bαγ complex enhance the rate of guanine nucleotide exchange on eEF1A1 to a significantly lesser extent than on eEF1A2 (Fig. 6C,D). A relatively small (~ 13%) increase of the exchange rate compared to eEF1Bα (FL) is observed only in the case of eEF1Bα(66-225). The effect of eEF1Bγ addition is also quite modest (~ 20%). However, the tendency is observed: deletion of the whole eEF1Bα N-terminal domain and its binding to eEF1Bγ result in enhancement of the guanine nucleotide exchange rate on eEF1A1. Importantly, the kinetic data obtained for eEF1A1 and eEF1A2 cannot be directly compared due to the different reaction temperatures and concentrations of the exchange factors. The rate of spontaneous GDP release from eEF1A1 is much higher even at 0 °C ($k_{-1} = 6.6 \times 10^{-3}$ s^{-1}) than that from eEF1A2 at 25 °C ($k_{-1} = 5.4 \times 10^{-4}$ s^{-1}). In addition, at least a fivefold higher concentration of eEF1Bα(FL) and its truncated variants was required for a substantial effect on the rate of GDP/GDP exchange on eEF1A1 compared to eEF1A2.

Our data on spontaneous GDP/GDP exchange on both eEF1A isoforms are in agreement with those reported previously [4]. It worth noting that, despite the differences in the guanine nucleotide exchange activity, eEF1A1 and eEF1A2 demonstrated similar specific translation elongation activity *in vitro* [4]. The residues of eEF1A2 involved in direct contact with GDP [6] and the corresponding residues of eEF1A1 are identical. Thus, there is no obvious explanation for

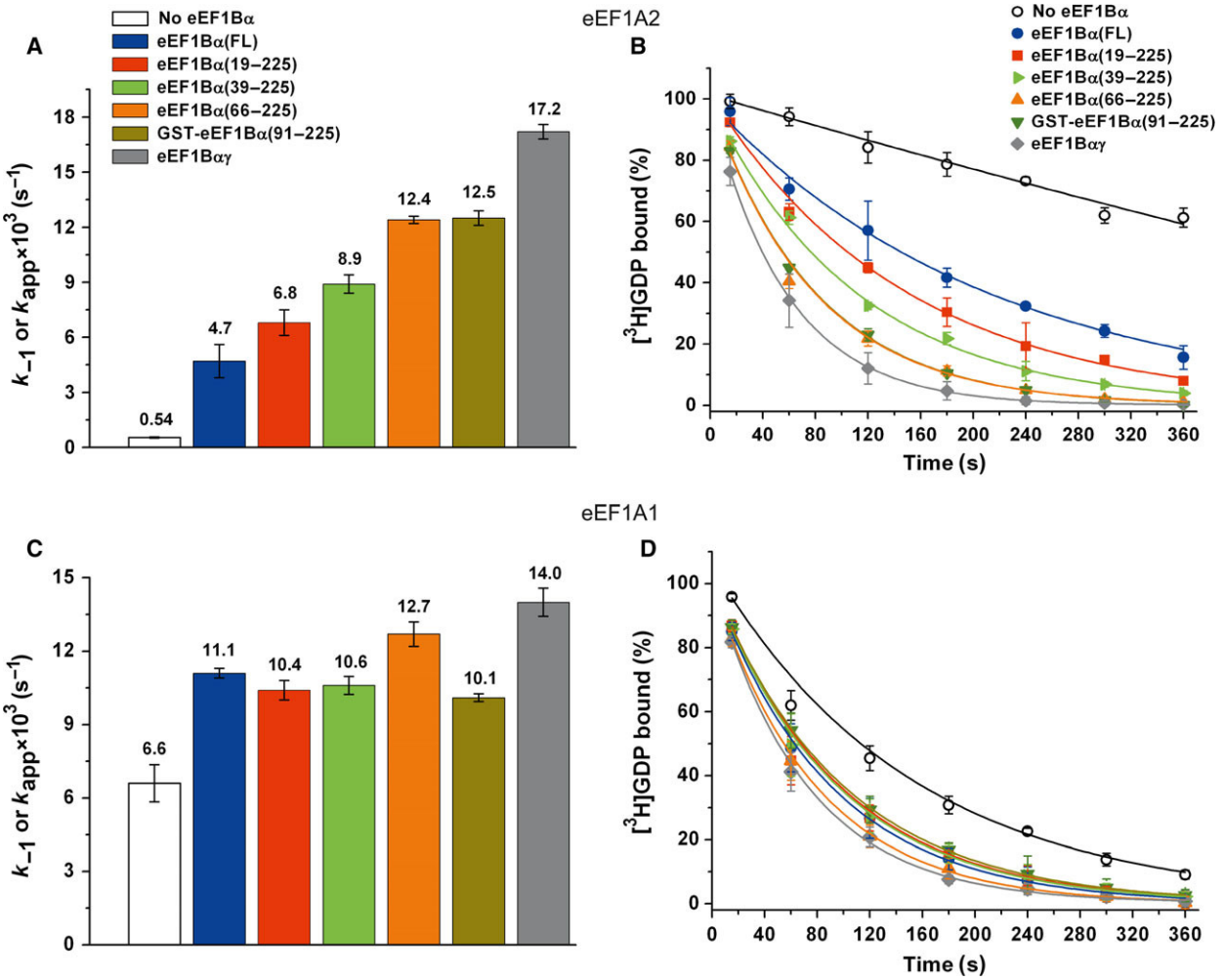

Fig. 6. Rates of guanine nucleotide exchange on eEF1A2 and eEF1A1 and in the absence or presence of full-length eEF1Bα, its truncated forms and the eEF1Bαγ complex. (A,C) First-order rate constants of the [^{3}H]GDP/GDP exchange reaction on eEF1A2 (A) and eEF1A1 (C) in the absence (k_{-1}) and the presence (k_{app}) of various exchange factors. The numbers above the bars indicate the mean values; the error bars represent standard errors. (B,D) Time course of the [^{3}H]GDP/GDP exchange reactions on eEF1A2 (B) and eEF1A1 (D) without or with eEF1Bα(FL), its truncated forms and the eEF1Bαγ complex. The time courses were obtained by averaging four independent kinetics experiments; the error bars represent standard deviations. Experimental data (symbols) were fitted to a single exponential function (curves). The first-order rate constant (k_{-1}) of spontaneous GDP/GDP exchange on eEF1A2 was calculated from the kinetic curve obtained for the time period of 40 min (not shown).

the difference in the affinity of the isoforms for GDP. Information about the structure of the eEF1A1*GDP complex is required to elucidate this issue.

eEF1A1 has been reported to be less resistant to heat and chemical denaturation, to possess a more extended shape in solution and to have a higher hydrophobicity compared with eEF1A2 [21,22]. Thus, the eEF1A isoforms appear to interact with eEF1Bα in a somewhat different manner. However, the nucleotide exchange in eEF1A1 was measured at a much lower temperature, which may weaken the protein–protein interactions and decrease the stimulatory effect of the eEF1Bα truncation. We believe that further examination of the eEF1A1 and eEF1A2 guanine nucleotide exchange activities by stop-flow kinetic experiments may provide additional information about the affinity of both proteins for guanine nucleotides and exchange factor(s).

Deletion of the N-terminal domain increases eEF1Bα affinity for eEF1A

Amino acid residues directly involved in the catalytic process were identified exclusively at the C-terminal extremity of eEF1Bα [8]. The *Artemia salina* eEF1Bα

(114-206) fragment and the *Saccharomyces cerevisiae* eEF1Bα(110-205) fragment form complexes with eEF1A, but the N-terminal parts of the protein do not [11,20]. Consequently, only the C-terminal part of eEF1Bα was suggested to be involved in the nucleotide exchange reaction [11–13]. In this context, the enhancement of the rate of [^{3}H]GDP/GDP exchange on eEF1A in the presence of the N-terminally truncated variants of eEF1Bα (Fig. 6) is rather surprising. One possible explanation for this phenomenon is that the N-terminal domain of eEF1Bα may somehow impair eEF1A binding to the catalytic domain. This may be due to either direct eEF1A binding to the eEF1Bα N-terminal domain or interaction between the eEF1Bα N-terminal and C-terminal domains themselves, which restrains eEF1A binding.

To clarify these points, we examined the interactions between the eEF1Bα N-terminal and C-terminal domains and eEF1A2 by native gel electrophoresis. As shown in Fig. 7, the eEF1Bα(1-92) fragment does not form a stable complex with either eEF1A2 or eEF1Bα (66-225). The absence of direct interaction between eEF1Bα(1-92) and eEF1A2 suggests that the N-terminal domain of eEF1Bα may be folded in a manner that restrains eEF1A binding to the catalytic C-terminal domain. In this case, the full-length eEF1Bα and the truncated form that lacks the N-terminal domain may be expected have a different affinity for eEF1A. To verify this possibility, we compared the stability of the eEF1Bα(66-225)*eEF1A(1/2) and eEF1Bα(FL) *eEF1A(1/2) complexes by native gel electrophoresis. Indeed, eEF1Bα(66-225) retains both eEF1A isoforms better in the complex compared to eEF1Bα(FL) [Fig. 8A, compare lanes 10 and 17.5 μM of eEF1Bα (66–225) with respective lanes 10 and 17.5 μM of eEF1Bα(FL), and Fig. 8B, compare lanes 5 and 10 μM of eEF1Bα(66–225) with respective lanes 5 and 10 μM of eEF1Bα(FL). This result demonstrates that eEF1Bα (66-225) may have a higher affinity for both isoforms of eEF1A compared to full-length eEF1Bα.

Conclusions

Hence, the following mechanism for eEF1Bγ-mediated stimulation of eEF1Bα activity can be proposed. The N-terminal domain of the free eEF1Bα molecule most probably possesses a conformation that partially restrains eEF1A binding to the GEF domain. The formation of a tight complex between eEF1Bγ and the eEF1Bα N-terminal domain leads to conformation changes in the latter that allow the eEF1Bα GEF domain to be fully accessible for eEF1A binding. As a result, the inhibitory effect of the eEF1Bα N-terminal domain is eliminated, and the eEF1Bαγ complex displays a higher rate of guanine nucleotide exchange compared to eEF1Bα alone.

Another important conclusion that may be drawn from native electrophoresis experiments is that eEF1Bα (FL) has a lower affinity for eEF1A1 compared to eEF1A2. As shown in Fig. 8A,B (lower parts), dissociation of the eEF1Bα(FL)*eEF1A1 complex occurs at a concentration of 10 μM of both proteins, whereas dissociation of the eEF1Bα(FL)*eEF1A2 complex occurs only at 17.5 μM eEF1Bα(FL). Thus, taking into account the low rate of spontaneous GDP release from eEF1A2 and its higher affinity for eEF1Bα, this isoform may be more dependent on the guanine nucleotide exchange factors than eEF1A1.

Our data favor the notion that full-length eEF1Bα and its truncated forms belong to the family of non-globular proteins with moderately or highly elongated shapes. Truncation of the non-catalytic N-terminal domain accelerates the rate of guanine nucleotide exchange on eEF1A compared to full-length eEF1Bα. Moreover, eEF1Bα lacking its N-terminal domain possesses higher affinity for eEF1A than full-length eEF1Bα. Therefore, the N-terminal domain of eEF1Bα may interfere with eEF1A binding to the GEF domain and thus decrease the rate of guanine nucleotide exchange. The formation of a tight complex between the eEF1Bγ and eEF1Bα N-terminal domains leads to

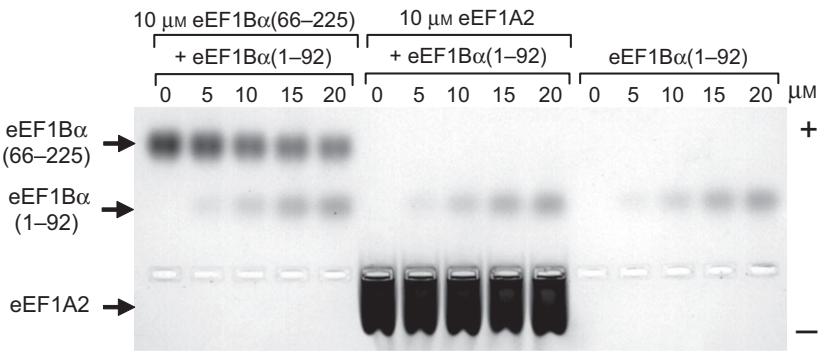

Fig. 7. The isolated eEF1Bα N-terminal fragment (residues 1-92) does not form a stable complex with eEF1A2 and eEF1Bα (66-225). eEF1A2 and eEF1Bα(66–225) (10 μM each) were incubated with increasing concentrations (0–20 μM) of eEF1Bα(1–92) and applied onto a 0.7% native agarose gel. Proteins were detected by Coomassie Brilliant Blue staining.

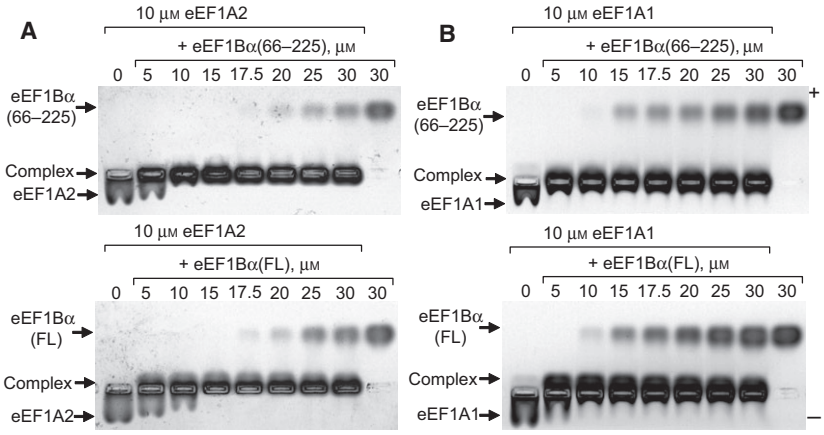

Fig. 8. Comparison of eEF1A*eEF1Bα(FL) and eEF1A*eEF1Bα(66–225) complexes by 0.7% native gel electrophoresis. (A) Simultaneous electrophoresis of 10 μM eEF1A2 alone and in a complex with increasing concentrations of eEF1Bα(66–225) (upper part) or eEF1Bα(FL) (lower part) in the same gel. (B) Simultaneous electrophoresis of 10 μM eEF1A1 alone and in a complex with increasing concentrations of eEF1Bα(66–225) (upper part) or eEF1Bα(FL) (lower part) in the same gel. Proteins were detected by Coomassie Brilliant Blue staining.

conformational changes in the latter and thus elimination of this inhibitory effect.

Experimental procedures

The conservative domains in the primary structure of eEF1Bα were defined by multiple sequences alignment using CLUSTAL W [23]. The following eEF1Bα amino acid sequences from the Genbank database were used: *Homo sapiens*, NCBI reference sequence NP_066944.1; *Mus musculus*, NCBI reference sequence NP_061266.2; *Gallus gallus*, NCBI reference sequence NP_990232.1; *Danio rerio*, NCBI reference sequence NP_956243.1; *Xenopus laevis*, NCBI reference sequence NP_001084134.1; *Oryctolagus cuniculus*, NCBI reference sequence NP_001075868.1; *Drosophila melanogaster*, GenBank accession number AAF57941.3; *Caenorhabditis elegans*, NCBI reference sequence NP_498737.1; *Saccharomyces cerevisiae*, GenBank accession number BAA03165.1; *Artemia salina*, GenBank accession number AAC83402.1.

Plasmid construction

The cDNA encoding the full-length human eEF1Bα was amplified from pGBKT7-eEF1Bα (kindly provided by Charlotte R. Knudsen, Institute of Molecular and Structural Biology, Aarhus University, Denmark) using Pwo polymerase (Roche Diagnostics, Mannheim, Germany) using 5′-TTTTGAATTCATGGGTTTCGGAGACCTGA-3′ as the forward primer and 5′-CCCCTCGAGTTAGATCTTGTTGAAAGCAGC-3′ as the reverse primer, containing *Eco*RI and *Xho*I restriction sites, respectively. The PCR fragment was inserted into the pGEX6P-1 expression vector (GE Healthcare, Buckinghamshire, UK) digested using the same enzymes. The resulting recombinant plasmid pGEX6P-1/eEF1Bα(FL) contained the cDNA of full-length human eEF1Bα in-frame with the GST sequence.

cDNA fragments encoding the N-terminally truncated forms of human eEF1Bα were produced by PCR using appropriate forward primers containing the *Eco*RI restriction site (as listed below) and the reverse primer 5′-TTCTCGAGTTAGATCTTGTTGAAAGCAGCCACATCCAT-3′, containing an *Xho*I restriction site. The forward primer for the eEF1Bα(19–225) fragment was 5′-AAGAATTCGCGGACAAGAGCTACATCGA-3′, that for eEF1Bα(39–225) was 5′-AAGAATTCGCCGTGTCCAGCCCACCGCCT-3′, that for eEF1Bα(66–225) was 5′-AAGAATTCGCCAGCCTGCCAGGAGTGAAGAAA-3′, and that for eEF1Bα(91–225) was 5′-AAAGAATTCGCTACAGATAGTAAAGATGATGATGAC-3′. The cDNA fragment encoding the N-terminal part of eEF1Bα comprising residues 1–92 was amplified using the forward primer 5′-AAAGAATTCATGGGTTTCGGAGACCTGAAAAGCCT-3′ and the reverse primer 5′-TTTCTCGAGTTATGTAGTGTCTTCCACAT-3′, containing an *Eco*RI and an *Xho*I restriction site, respectively. PCR was performed using DreamTaq or Pfu DNA polymerase (both from Thermo Fisher Scientific, Waltham, MA, USA) using the pGEX6P-1/eEF1Bα(FL) plasmid as template. The PCR products were purified and digested using *Xho*I and *Eco*RI, and ligated into the pGEX6P-1 vector digested by the same enzymes. The resulting recombinant plasmids encoded the truncated forms of eEF1Bα in-frame with the GST sequence. All constructs were confirmed by sequencing.

Expression and purification of recombinant proteins

The full-length human eEF1Bα encoded by pGEX6P-1/eEF1Bα(FL) was expressed in the *Escherichia coli* BL21 (DE3) pLysE strain (Stratagene, La Jolla, CA) grown on LB medium supplemented with 100 $\mu g \cdot mL^{-1}$ ampicillin and 2% glucose. The bacterial culture was grown at 37 °C until an attenuance at 600 nm of 0.5 was reached, and expression of the target protein was induced using 0.7 mM isopropyl-β-D-thiogalactopyranoside for 3 h. The cells were then harvested by centrifugation (3220 ***g*** for 10 min at 4 °C) and washed twice (10 min at 4 °C) with 40 mL of ice-cold

extraction buffer containing PBS (1.47 mM KH_2PO_4, 10 mM Na_2HPO_4, 137 mM NaCl, 2.7 mM KCl, pH 7.4), 10% glycerol and 5 mM 2-mercaptoethanol, followed by centrifugation (6000 ***g*** for 5 min at 4 °C). The cell pellet was dissolved in 8 mL extraction buffer per mg of cells and sonicated. All subsequent steps were performed at 4 °C. After centrifugation at 18 500 ***g*** for 30 min, the clear supernatant was recovered. This solution was mixed with 6–7 mL of a 50% slurry of glutathione agarose (Sigma-Aldrich, St Louis, MO, USA), pre-equilibrated with the same buffer, and incubated on an orbital shaker overnight. The resin was washed three times for 20 min in a tube with 40 mL of the extraction buffer, followed by centrifugation at 3000 ***g*** for 5 min. After the last wash, the glutathione agarose was packed into a column and washed extensively to remove unbound material. eEF1Bα(FL) was stepwise eluted using 20 mM glutathione, pH 8.0, in the extraction buffer. Fractions were collected and analyzed by SDS/PAGE. The purest fractions were combined and dialyzed against the cleavage buffer (30 mM Tris/HCl, pH 7.5, 150 mM NaCl, 10% glycerol, 5 mM 2-mercaptoethanol and 0.01% Tween-20). The GST tag was removed by incubation with PreScission protease (GE Healthcare) according to the manufacturer's instructions. The protein mixture was applied onto a HiTrap Q Sepharose (volume 1 mL) column (GE Healthcare), equilibrated with cleavage buffer. The column was extensively washed with 250 mM NaCl in buffer containing 30 mM Tris/HCl, pH 7.5, 150 mM NaCl, 10% glycerol, 5 mM 2-mercaptoethanol and 0.01% Tween-20. eEF1Bα(FL) was eluted from the column using a 250–450 mM NaCl gradient in the same buffer. Fractions were collected and analyzed by SDS/PAGE. The purest fractions were combined and dialyzed against the storage buffer (30 mM Tris/HCl, pH 7.5, 150 mM NaCl, 55% glycerol and 5 mM 2-mercaptoethanol). The protein was stored at −20 °C. The eEF1Bα concentration was determined using a calculated absorption coefficient of 1.18 A_{280} units mg^{-1} cm^2.

All N-terminally truncated forms of eEF1Bα were produced as GST fusion proteins in the *E. coli* BL21 Gold strain (Stratagene) grown on LB medium supplemented with 100 $\mu g \cdot mL^{-1}$ ampicillin. The expression and purification protocol was essentially the same as described for full-length eEF1Bα, except that the eEF1Bα(19–225), eEF1Bα (39–225) and eEF1Bα(66–225) deletion mutants were eluted from the HiTrap Q Sepharose (volume 1 mL) column using a 200–450 mM NaCl gradient. Unfortunately, the eEF1Bα (91–225) deletion mutant precipitated after incubation with PreScission protease, and therefore the GST fusion protein was used for the experiments.

The eEF1Bα(1-92) fragment was also produced as a GST fusion protein as described for the N-terminally truncated forms. After treatment with PreScission protease, the eEF1Bα(1-92) fragment was purified on a HiLoad 16/600 Superdex 200 per grade (diameter 16 mm × length 600 mm, volume 120 mL) column (GE Healthcare), equilibrated with buffer containing 25 mM Tris/HCl, pH 7.5, 150 mM NaCl, 5% glycerol and 5 mM 2-mercaptoethanol. The purest fractions were combined and dialyzed against the storage buffer described above and stored at −20 °C.

The protein concentrations were determined using the following calculated absorption coefficients (A_{280} units mg^{-1} cm^2): 1.25 for eEF1Bα(19–225), 1.24 for eEF1Bα (39–225), 0.97 for eEF1Bα(66–225), 1.4 for GST–eEF1Bα (91–225) and 1.37 for eEF1Bα(1-92).

Preparation of the eEF1Bαγ complex

Human recombinant eEF1Bγ was purified as described previously [24]. For formation of the eEF1Bαγ complex, purified eEF1Bγ and eEF1Bα were mixed in buffer containing 25 mM imidazole HCl, pH 7.5, 150 mM NaCl, 10% glycerol, 5 mM 2-mercaptoethanol, and incubated for 5 min at 37 °C. The final concentrations of eEF1Bγ and eEF1Bα were 8 and 10 μM, respectively. The eEF1Bαγ complex was then purified on a Superose 6 HR 10/30 (volume 24 mL) column (GE Healthcare), equilibrated in the same buffer, to eliminate excess eEF1Bα. The most concentrated fractions of the eEF1Bαγ complex was used to measure the rate of guanine nucleotide exchange on eEF1A1 and eEF1A2. The protein concentration of the eEF1Bαγ complex was determined using the calculated molar absorption coefficient 117 270 $M^{-1} \times cm^{-1}$, assuming that the stoichiometry of the subunits in the complex is 1 : 1.

Analytical gel filtration of proteins

The aggregation state of all the purified proteins was monitored by size-exclusion chromatography on a Superose 6 HR 10/30 column. The column was equilibrated with 25 mM imidazole HCl, pH 7.5, 150 mM NaCl, 10% glycerol and 5 mM 2-mercaptoethanol. The sample (0.1 mL) was loaded onto the column and eluted at a flow rate of 0.4 $mL \cdot min^{-1}$. The absorbance of the eluate was monitored at 280 nm. The column calibration and molecular mass determination of the protein of interest have been described previously [24].

Analytical ultracentrifugation

Analytical ultracentrifugation experiments were performed using a ProteomeLab XL-I analytical ultracentrifuge (Beckman-Coulter, Indianapolis, IN, USA), equipped with an An-60 Ti analytical rotor, at 2.3 °C for eEF1Bα(FL) and at 4 °C for the eEF1Bα N-terminally truncated forms, using absorbance optics at 280 nm.

In sedimentation velocity experiments, sample (400 μL) and reference (410 μL) solutions were loaded onto 12 mm double-sector Epon charcoal-filled centerpieces (Beckman-Coulter). The experiments were performed at a rotor speed of 50 000 rpm. Absorbance was monitored using a continu-

ous-mode time interval of 270 s and a step size of 0.003 cm. The multiple scans at various time points were fitted to a continuous size distribution model using SEDFIT [25–27]. All size distributions were solved and regularized at a confidence level of 0.95 by maximum entropy, using the best-fit mean anhydrous frictional ratio (f/f_0), and a resolution N of 300 sedimentation coefficients for the range between 0.2 and 12.0 S. Additionally, to assess the shape of the proteins analyzed, the ratio S_{max}/S was calculated, where S_{max} is the sedimentation coefficient if the protein was a smooth sphere without water, and S is the sedimentation coefficient $S_{20,w}$ estimated for the protein by size distribution analysis. S_{max} for the protein was calculated using the formula $S_{max} = 0.00361\ (M_r)^{2/3}$, where M_r is the molecular mass of the protein in Daltons [18].

The sedimentation equilibrium experiment was performed using six-channel Epon charcoal-filled centerpieces (Beckman-Coulter). Three samples (0.1 mL) were loaded into the sample channels, and 0.12 mL of buffer solution was loaded into the reference channels. The cells were then loaded into the rotor and run at 17 000 and 21 000 rpm. The approach to equilibrium was monitored using SEDFIT, and sedimentation equilibrium absorbance data were collected every 4 h. The eEF1Bα protein achieved equilibrium after 40.5 h at 17 000 rpm and 28 h after the speed change to 21 000 rpm. The scan obtained at a single rotor speed or scans obtained at various rotor speeds (multi-speed equilibrium data) were then fitted to a non-interacting discrete species model assuming a single species by using SEDPHAT [19]:

$$A_R = C_{r0}\,\varepsilon\,d\exp\left\{M(1-\overline{\nu}\rho)\frac{\omega^2}{2RT}(r^2-r_0^2)\right\} \qquad (1)$$

in which r indicates the distance from the center of rotation, r_0 is the arbitrary reference radius, ω is the angular velocity, T is the absolute temperature of the rotor, R is the gas constant, $\overline{\nu}$ is the partial specific volume, ρ is the solvent density, ε is the extinction coefficient, d is the optical path length, and c_{r0} is the concentration at the reference radius. For multi-speed data analysis at each channel, a single baseline parameter was included as a floating parameter that is common to all rotor speeds. The time invariant and radial invariant noise components were also fitted for better fitting quality.

The sedimentation velocity and equilibrium analysis were performed in buffer solution containing 25 mM Tris/HCl, pH 7.5, 150 mM NaCl, 5% v/v glycerol and 1 mM dithiothreitol. The solvent density of 1.0216 g·cm^{-3} and viscosity of 0.01962 Poise at 2.3 °C, and 1.02164 g·cm^{-3} and 0.01857 Poise at 4 °C, were calculated using SEDNTERP software (http://sednterp.unh.edu).

The partial specific volume (cm^3 g^{-1}) and extinction coefficient (M^{-1} cm^{-1}) for eEF1Bα(FL) were calculated using SEDNTERP software to be 0.72585 and 30 030, respectively; those for eEF1Bα(19–225) were 0.72472 and 28 545, those for eEF1Bα(39–225) were 0.72532 and 25 570, those for eEF1Bα(66–225) were 0.72499 and 17 085, and those for GST–eEF1Bα(91–225) were 0.73301 and 5870.

[^{3}H]GDP/GDP exchange

eEF1A2 and eEF1A1 were purified as described previously [28,29]. The kinetics of guanine nucleotide exchange on eEF1A2 were assessed as described in detail previously [6]. For eEF1A1, the same conditions were used except for the temperature of the reaction and the concentration of exchange factors. For the eEF1A2 guanine nucleotide exchange assay, a reaction mixture containing a final concentration of 4 nM eEF1Bα(FL), its truncated forms or the eEF1Bαγ complex, 692 nM of the eEF1A2*[^{3}H]GDP complex and 150 μM GDP were incubated at 25 °C. For the eEF1A1 guanine nucleotide exchange assay, a reaction mixture containing a final concentration of 20 nM eEF1Bα(FL), its truncated forms or the eEF1Bαγ complex, 692 nM of eEF1A1*[^{3}H]GDP complex and 150 μM GDP were incubated at 0 °C.

First-order rate constants of the GDP/GDP exchange reaction in the absence (k_{-1}) and in the presence (k_{app}) of various exchange factors were obtained by fitting to a single exponential function ($y = A_1 \exp(-x/t_1) + y_0$) using ORIGINPRO 8 software (OriginLab, Northampton, MA, USA).

Native gel electrophoresis of protein complexes

eEF1A1 and eEF1A2 complexes with respective exchange factors were prepared as follows: 10 μM eEF1A1 or eEF1A2 were mixed with increasing (5–30 μM) concentrations of eEF1Bα(FL) or eEF1Bα(66–225) and 150 μM GDP in buffer containing 10 mM Tris/HCl, pH 7.5, 150 mM NaCl, 10% glycerol and 5 mM 2-mercaptoethanol in a final volume of 20 μL, or 10 μM eEF1A2 or eEF1Bα(66–225) were mixed in a final volume of 20 μL with increasing (5–20 μM) concentrations of eEF1Bα(1-92) in buffer containing 10 mM Tris/HCl, pH 7.5, 150 mM NaCl, 10% glycerol and 5 mM 2-mercaptoethanol.

Protein mixtures were incubated for 5 min at 37 °C and directly loaded onto a 0.7% agarose gel containing 89 mM Tris/boric acid, pH 8.3. The gel was run at 50 V/22–24 mA for 2 h at room temperature. Then the gel was stained in standard Coomassie Brilliant Blue R250 solution for 1–2 min, and de-stained in solution containing 40% ethanol and 3% acetic acid with gentle shaking. The gel was photographed using a MiniBIS Pro imaging system (DNR Bio-Imaging Systems, Jerusalem, Israel).

Acknowledgements

This work was supported by the France/Ukraine Projet International de Coopération Scientifique (PICS),

and in part by the interdisciplinary scientific program of the National Academy of Sciences of Ukraine 'Fundamental basis for molecular and cell biotechnologies'. S.V.F. was supported by the Józef Mianowski Fund and Strengthening Cooperation in Molecular Biomedicine between EU and Ukraine (COMBIOM) project (FP7/2007–2013 under grant agreement number 294932) for performing the analytical ultracentrifugation experiments. Part of this work was performed using the infrastructure of the Centre for Preclinical Research and Technology (CePT; European Union POIG.02.02.00-14-024/08-00 project). The authors are grateful to Charlotte R. Knudsen (Institute of Molecular and Structural Biology, Aarhus University, Denmark) for providing the pGBKT7-eEF1Bα construct, and to D. Vlasenko for help with eEF1A1 preparation. We thank Anne-Lise Haenni (Institut Jacques Monod, Paris, France) for careful reading of the manuscript and for her useful comments.

Author contributions

TVT participated in the design of the study, performed the experiments, analyzed the data and helped draft the manuscript; VFS planed and performed the experiments, analyzed the data and wrote the paper; RHS performed the analytical ultracentrifugation experiments, analyzed the data, and contributed to preparation of the manuscript; BSN and AVE wrote the paper.

References

1 Merrick WC & Nyborg J (2000) The protein biosynthesis, elongation cycle. *Cold Spring Harbor Monograph Archive* **39**, 89–125.

2 Ad Hoc Nomenclature Subcommittee (1996) Prokaryotic and eukaryotic translation factors. *Biochimie* **78**, 1119–1122.

3 Le Sourd F, Boulben S, Le Bouffant R, Cormier P, Morales J, Belle R & Mulner-Lorillon O (2006) eEF1B: at the dawn of the 21st century. *Biochim Biophys Acta* **1759**, 13–31.

4 Kahns S, Lund A, Kristensen P, Knudsen CR, Clark BF, Cavallius J & Merrick WC (1998) The elongation factor 1 A-2 isoform from rabbit: cloning of the cDNA and characterization of the protein. *Nucleic Acids Res* **26**, 1884–1890.

5 Mansilla F, Friis I, Jadidi M, Nielsen KM, Clark BF & Knudsen CR (2002) Mapping the human translation elongation factor eEF1H complex using the yeast two-hybrid system. *Biochem J* **365**, 669–676.

6 Crepin T, Shalak VF, Yaremchuk AD, Vlasenko DO, McCarthy A, Negrutskii BS, Tukalo MA & El'skaya AV (2014) Mammalian translation elongation factor eEF1A2: X-ray structure and new features of GDP/GTP exchange mechanism in higher eukaryotes. *Nucleic Acids Res* **42**, 12939–12948.

7 Cao Y, Portela M, Janikiewicz J, Doig J & Abbott CM (2014) Characterisation of translation elongation factor eEF1B subunit expression in mammalian cells and tissues and co-localisation with eEF1A2. *PLoS One* **9**, e114117.

8 Andersen GR, Valente L, Pedersen L, Kinzy TG & Nyborg J (2001) Crystal structures of nucleotide exchange intermediates in the eEF1A–eEF1Bα complex. *Nat Struct Biol* **8**, 531–534.

9 Perez JM, Siegal G, Kriek J, Hard K, Dijk J, Canters GW & Moller W (1999) The solution structure of the guanine nucleotide exchange domain of human elongation factor 1β reveals a striking resemblance to that of EF-Ts from *Escherichia coli*. *Structure* **7**, 217–226.

10 Kawashima T, Berthet-Colominas C, Wulff M, Cusack S & Leberman R (1996) The structure of the *Escherichia coli* EF-Tu·EF-Ts complex at 2.5 Å resolution. *Nature* **379**, 511–518.

11 van Damme H, Amons R, Janssen G & Moller W (1991) Mapping the functional domains of the eukaryotic elongation factor 1βγ. *Eur J Biochem* **197**, 505–511.

12 van Damme HT, Amons R, Karssies R, Timmers CJ, Janssen GM & Moller W (1990) Elongation factor 1β of artemia: localization of functional sites and homology to elongation factor 1δ. *Biochim Biophys Acta* **1050**, 241–247.

13 Perez JM, Kriek J, Dijk J, Canters GW & Moller W (1998) Expression, purification, and spectroscopic studies of the guanine nucleotide exchange domain of human elongation factor, EF-1β. *Protein Expr Purif* **13**, 259–267.

14 Bec G, Kerjan P & Waller JP (1994) Reconstitution *in vitro* of the valyl-tRNA synthetase–elongation factor (EF) 1βγδ complex. Essential roles of the NH_2-terminal extension of valyl-tRNA synthetase and of the EF-1δ subunit in complex formation. *J Biol Chem* **269**, 2086–2092.

15 Janssen GM & Moller W (1988) Elongation factor 1βγ from *Artemia,* Purification and properties of its subunits. *Eur J Biochem* **171**, 119–129.

16 Janssen GM & Moller W (1988) Kinetic studies on the role of elongation factors 1β and 1γ in protein synthesis. *J Biol Chem* **263**, 1773–1778.

17 Janssen GM, Maessen GD, Amons R & Moller W (1988) Phosphorylation of elongation factor 1β by an endogenous kinase affects its catalytic nucleotide exchange activity. *J Biol Chem* **263**, 11063–11066.

18 Erickson HP (2009) Size and shape of protein molecules at the nanometer level determined by

sedimentation, gel filtration, and electron microscopy. *Biol Proced Online* **11**, 32–51.

19 Vistica J, Dam J, Balbo A, Yikilmaz E, Mariuzza RA, Rouault TA & Schuck P (2004) Sedimentation equilibrium analysis of protein interactions with global implicit mass conservation constraints and systematic noise decomposition. *Anal Biochem* **326**, 234–256.

20 Pedersen L, Andersen GR, Knudsen CR, Kinzy TG & Nyborg J (2001) Crystallization of the yeast elongation factor complex eEF1A–eEF1Bα. *Acta Crystallogr D* **57**, 159–161.

21 Timchenko AA, Novosylna OV, Prituzhalov EA, Kihara H, El'skaya AV, Negrutskii BS & Serdyuk IN (2013) Different oligomeric properties and stability of highly homologous A1 and proto-oncogenic A2 variants of mammalian translation elongation factor eEF1. *Biochemistry*, **52**, 5345–5353.

22 Novosylna AV, Timchenko AA, Tiktopulo EI, Serdyuk IN, Negrutskii BS & El'skaya AV (2007) Characterization of physical properties of two isoforms of translation elongation factor 1A. *Biopolym Cell* **23**, 386–390.

23 Thompson JD, Higgins DG & Gibson TJ (1994) CLUSTAL W: improving the sensitivity of progressive multiple sequence alignment through sequence weighting, position-specific gap penalties and weight matrix choice. *Nucleic Acids Res* **22**, 4673–4680.

24 Trosiuk TV, Liudkovska VV, Shalak VF, Negrutskii BS & El'skaya AV (2014) Structural dissection of human translation elongation factor 1Bγ (eEF1Bγ): expression of full-length protein and its truncated forms. *Biopolym Cell* **30**, 96–106.

25 Schuck P (2000) Size-distribution analysis of macromolecules by sedimentation velocity ultracentrifugation and lamm equation modeling. *Biophys J* **78**, 1606–1619.

26 Schuck P, Perugini MA, Gonzales NR, Howlett GJ & Schubert D (2002) Size-distribution analysis of proteins by analytical ultracentrifugation: strategies and application to model systems. *Biophys J* **82**, 1096–1111.

27 Schuck P (2003) On the analysis of protein self-association by sedimentation velocity analytical ultracentrifugation. *Anal Biochem* **320**, 104–124.

28 Yaremchuk A, Shalak VF, Novosylna OV, Negrutskii BS, Crepin T, El'skaya AV & Tukalo M (2012) Purification, crystallization and preliminary X-ray crystallographic analysis of mammalian translation elongation factor eEF1A2. *Acta Crystallogr F* **68**, 295–297.

29 Shalak VF, Budkevich TV, Negrutskil BS & El'skaia AV (1997) A fast and effective method for purification of elongation factor 1α from rabbit liver. *Ukr Biokhim Zh* **69**, 104–109.

2.2. Визначення структурної організації N-кінцевого домену субодиниці eEF1Bbeta

Contents lists available at ScienceDirect

International Journal of Biological Macromolecules

journal homepage: http://www.elsevier.com/locate/ijbiomac

The protein-binding N-terminal domain of human translation elongation factor 1Bβ possesses a dynamic α-helical structural organization

Tetiana V. Bondarchuk [a], Dmytro M. Lozhko [a], Vyacheslav F. Shalak [a,*], Agnieszka Fatalska [b], Roman H. Szczepanowski [c], Michał Dadlez [b], Boris S. Negrutskii [a], Anna V. El'skaya [a]

[a] Institute of Molecular Biology and Genetics, NAS of Ukraine, 150, Zabolotnogo St., 03680 Kyiv, Ukraine
[b] Institute of Biochemistry and Biophysics, PAN, Pawinskiego 5a, 02-109 Warsaw, Poland
[c] International Institute of Molecular and Cell Biology, Trojdena 4, 02-109 Warsaw, Poland

ARTICLE INFO

Article history:
Received 7 August 2018
Received in revised form 19 December 2018
Accepted 22 December 2018
Available online 24 December 2018

Keywords:
Translation elongation factor 1 complex
Analytical ultracentrifugation
Circular dichroism
Hydrogen-deuterium exchange
3D structure modeling

ABSTRACT

Translation elongation factor 1Bβ (eEF1Bβ) is a metazoan-specific protein involved into the macromolecular eEF1B complex, containing also eEF1Bα and eEF1Bγ subunits. Both eEF1Bα and eEF1Bβ ensure the guanine nucleotide exchange on eEF1A while eEF1Bγ is thought to have a structural role. The structures of the eEF1Bβ catalytic C-terminal domain and neighboring central acidic region are known while the structure of the protein-binding N-terminal domain remains unidentified which prevents clear understanding of architecture of the eEF1B complex.

Here we show that the N-terminal domain comprising initial 77 amino acids of eEF1Bβ, eEF1Bβ(1–77), is a monomer in solution with increased hydrodynamic volume. This domain binds eEF1Bγ in equimolar ratio. The CD spectra reveal that the secondary structure of eEF1Bβ(1–77) consists predominantly of α-helices and a portion of disordered region. Very rapid hydrogen/deuterium exchange for all eEF1Bβ(1–77) peptides favors a flexible tertiary organization of eEF1Bβ(1–77). Computational modeling of eEF1Bβ(1–77) suggests several conformation states each composed of three α-helices connected by flexible linkers.

Altogether, the data imply that the protein-binding domain of eEF1Bβ shows flexible spatial organization which may be needed for interaction with eEF1Bγ or other protein partners.

© 2018 Elsevier B.V. All rights reserved.

1. Introduction

Translation elongation factor eEF1Bβ is a metazoan-specific protein involved into macromolecular eEF1B complex, containing evolutionary conserved in eukaryotes translation elongation factors eEF1Bα and eEF1Bγ [1,2]. In turn, eEF1B is a part of a bigger complex containing translation elongation factor 1A (eEF1A) and valyl-tRNA synthetase (VRS) [3,4]. We use the nomenclature of translation elongation factors proposed by Merrick and Nyborg [5,6]. Similarly to eEF1Bα, eEF1Bβ catalyzes the guanine nucleotide exchange on eEF1A restoring its active GTP-bound conformation necessary for aminoacyl-tRNA binding and delivering to the ribosome [5,7]. The function of eEF1Bγ is believed to be a structural component of the eEF1B complex [7].

The domain structure of eEF1Bβ is shown in Fig. 1. C-terminal domain (CT, Fig. 1) is a catalytic domain, which is highly homologous to the C-terminal domain of eEF1Bα [8]. Recently, the structure of the human eEF1Bβ C-terminal fragment comprising the CT and CAR domains has been solved by NMR [9]. The CAR domain was shown to bind translationally controlled tumor protein (TCTP) [10], with unknown functional consequences.

The N-terminal region of eEF1Bβ (1–115) does not share a significant homology with any known protein and contains long leucine-zipper motif (LZ, 80–115) [11,12]. By using yeast two-hybrid system, it has been demonstrated that the large N-terminal fragment (residues 1–150) of eEF1Bβ interacts with the N-terminal domain of eEF1Bγ [13]. Recently, we have shown that LZ is responsible for the self-association of eEF1Bβ [14]. The role and structural organization of the very N-terminal fragment (eEF1Bβ (1–77)) preceding LZ motif, remained unknown despite several indications that it may provide a landing site for eEF1Bγ and/or VRS in the eEF1B complex [4,13].

Here, recombinant human eEF1Bβ(1–77) was expressed, purified to homogeneity and characterized by analytical gel filtration and ultracentrifugation techniques. The ability of eEF1Bβ(1–77) to bind eEF1Bγ was shown by size-exclusion chromatography. The characteristics of the

Abbreviations: eEF1Bα, eukaryotic translation elongation factor 1Bα; eEF1Bβ, eukaryotic translation elongation factor 1Bβ; eEF1Bγ, eukaryotic translation elongation factor 1Bγ; eEF1A, eukaryotic translation elongation factor 1A; GEF, guanine exchange factor; GST, glutathione S-transferase; VRS, valyl-tRNA synthetase.

* Corresponding author.
E-mail address: shalak@imbg.org.ua (V.F. Shalak).

https://doi.org/10.1016/j.ijbiomac.2018.12.220
0141-8130/© 2018 Elsevier B.V. All rights reserved.

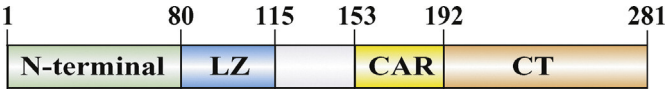

Fig. 1. Domain organization of human full-length eEF1Bβ. Abbreviations: eEF1Bβ(1–77) – N-terminal domain, LZ – leucine-zipper motif, CAR – central acidic region, CT – C-terminal catalytic domain.

secondary structure elements in eEF1Bβ(1–77) were obtained by the circular dichroism (CD) spectral analysis. Hydrogen-deuterium exchange coupled with mass spectrometry (HDX-MS) revealed no protection in the eEF1Bβ(1–77) peptides. The 3D model of eEF1Bβ(1–77) was built *in silico*. Integration of the experimental and computational data implies that the protein binding eEF1Bβ(1–77) domain shows dynamic tertiary structure which is predominantly composed of α-helical elements connected by flexible linkers. A functional importance of such organization is discussed.

2. Materials and methods

2.1. Plasmid construction

The cDNA encoding the N-terminal domain (residues 1–77) of human eEF1Bβ was PCR amplified using 5′-AAAGAATTCATGGCTACAA ACTTCCTAGC as the forward primer and 5′- TTTCTCGAGTCAGTG GTC TCC GCT GGT GCC as the reverse primer, containing *Eco*RI and *Xho*I restriction sites, respectively. The reaction was carried out using DreamTaq DNA Polymerase (Thermo Fisher Scientific, USA). pGEX6P-1/eEF1Bβ plasmid encoding full-length human eEF1Bβ was used as a template. The PCR product was purified and digested by *Xho*I and *Eco*RI (Thermo Fisher Scientific, USA), and inserted into pGEX6P-1 (GE Healthcare, UK) expression vector digested by the same enzymes. The obtained construct was verified by sequencing. The resulting recombinant plasmid encoded eEF1Bβ(1–77) in-frame with the glutathione-S transferase (GST) sequence.

2.2. Expression and purification of recombinant eEF1Bβ(1–77)

eEF1Bβ(1–77) containing an N-terminal GST tag was expressed in *Escherichia coli* BL21Gold (Stratagene, USA) grown on LB medium supplemented with 100 μg/ml ampicillin at 37 °C. The expression of the protein was induced for 3 h with 0.8 mM isopropyl-β-D-thiogalactopyranoside when the absorbance of culture at 600 nm reached 0.5. The extract preparation and affinity chromatography of the GST-eEF1Bβ(1–77) fusion protein on a Glutathione sepharose™ 4B (GE Healthcare) was done as previously described in details in [14]. The GST tag was removed by incubation with PreScission protease (GE Healthcare) according to the manufacturer's manual. Then eEF1Bβ(1–77) was isolated from GST and other contaminating proteins on a HiLoad 16/600 Superdex 200 per grade (diameter 16 mm × length 600 mm, volume 120 ml) column (GE Healthcare), equilibrated with the buffer containing 25 mM Tris-HCl, pH 7.5, 150 mM NaCl, 5% glycerol and 5 mM 2-mercaptoethanol. All purest fractions were combined and dialyzed against the storage buffer (25 mM Tris-HCl, pH 7.5, 150 mM NaCl, 55% glycerol and 5 mM 2-mercaptoethanol) and stored at −20 °C. eEF1Bβ(1–77) concentration was determined using calculated absorption coefficient (A_{280} units·mg^{-1}·cm^2) – 0.92. The purity of eEF1Bβ(1–77) was determined by SDS-PAGE.

2.3. Analytical gel filtration of proteins

The molecular masses of purified eEF1Bβ(1–77), eEF1Bγ, and the eEF1Bβ(1–77)-eEF1Bγ complex were determined by size-exclusion chromatography on a Superose 6 HR 10/30 (volume 24 ml) column (GE Healthcare). The column was equilibrated with 25 mM Tris-HCl, pH 7.5, 150 mM NaCl, 5% glycerol and 5 mM 2-mercaptoethanol. The sample (0.1 ml) was injected into the column and eluted at a flow rate of 0.4 ml·min^{-1}. The absorbance of the column eluate was monitored at 280 nm. The elution volume of the protein of interest was converted into a K_{av} value according to the formula: $K_{av} = (V_e - V_0)/(V_t - V_0)$, where V_e is the elution volume of a particular protein, V_0 is the void volume of the column, and V_t is the total bad volume. The column calibration and molecular mass determination of the protein of interest have been described in details previously [15]. The molecular mass (mean ± standard deviation) of the eEF1Bβ(1–77) protein and its complex with eEF1Bγ was estimated by size-exclusion chromatography in three replicates.

For formation of the eEF1Bβ(1–77)-eEF1Bγ complex, purified eEF1Bβ(1–77) and eEF1Bγ [15] were mixed in the buffer containing 25 mM Tris-HCl, pH 7.5, 150 mM NaCl, 5% glycerol and 5 mM 2-mercaptoethanol, and incubated for 10 min at 37 °C. The final concentration of both proteins was 15 μM. Then, the complex was injected onto a Superose 6 HR 10/30 column, equilibrated by the buffer solution indicated above. The main peak fractions were collected, concentrated on Amicon Ultra membrane (Cutt-Off 30 kDa, Merck Millipore, Darmstadt, Germany), and analyzed by SDS-PAGE.

2.4. Analytical ultracentrifugation

Analytical ultracentrifugation (AUC) experiment was performed using a ProteomeLab XL-I analytical ultracentrifuge (Beckman-Coulter, Indianapolis, USA), equipped with An-60 Ti analytical rotor at 4 °C as previously described [16].

Briefly, for the sedimentation equilibrium analysis two samples (0.1 ml) at eEF1Bβ(1–77) concentration of 0.14 mg/ml and 0.09 mg/ml were loaded into the sample channels of 6-channel centerpiece, and 0.11 ml of buffer solution was loaded as a reference. The cells were then loaded into the rotor and run at 20,000, 25,000, and 30,000 rpm. The approach to equilibrium was monitored using the SEDFIT "Test approach to equilibrium" procedure [17] and the sedimentation equilibrium absorbance data were collected every 4 h. The eEF1Bβ(1–77) protein achieved equilibrium after 18 h at 20,000 rpm and 14 and 12 h after subsequent speed change to 25,000 and 30,000 rpm, respectively. The scan obtained at a single rotor speed or the scans obtained at different rotor speeds (multispeed equilibrium data) were then fitted to a non-interacting discrete species model assuming a single species by using SEDPHAT [18] with Eq. (1):

$$A_R = c_{r0}\varepsilon d \exp\left\{\left[M(1-\bar{v}\rho)\omega^2/2RT\right](r^2-r_0{}^2)\right\} \quad (1)$$

in which r denotes the distance from the center of rotation; r_0 is the arbitrary reference radius; ω is the angular velocity; T is the absolute temperature of the rotor; R is the gas constant; $\bar{v}$ is the partial specific volume; ρ is the solvent density; ε is the extinction coefficient; d is the optical path length, and c_{r0} is the concentration at the reference radius. For a multispeed global data analysis at each channel, a single base-line parameter was included as a floating parameter common to all rotor speeds. The time invariant and radial invariant noise were also fitted for the better fitting quality.

The buffer solution used for the sedimentation equilibrium experiment contained 25 mM Tris-HCl, pH 7.5, 150 mM NaCl, 5% glycerol (v/v) and 1 mM dithiothreitol. Solvent density 1.02344 g/cm^3 at 4 °C were measured by Anton Paar DMA 5000 (Graz, Austria) densitometer.

Partial specific volume and extinction coefficient for eEF1Bβ(1–77) was calculated to be 0.70931 cm^3/g (4 °C) and 8480 M^{-1} cm^{-1}, respectively, using SEDNTERP software (https://www.spinanalytical.com/auc-software.php).

2.5. Circular dichroism (CD) measurements

The CD spectra of purified recombinant eEF1Bβ(1–77) were obtained at the temperature range of 25–55 °C and at a protein

concentration of 0.076 mg/ml (8.25 μM) in 5 mM Tris-HCl, pH 7.5 buffer using 0.5 cm pathlength quartz cuvette in JASCO-810 (JASCO Corporation, Tokyo, Japan) spectropolarimeter with a Peltier thermal-controlled cuvette holder. The spectra were recorded from 190 to 260 nm ("far" UV range) using a step size of 0.5 nm and a bandwidth of 1 nm with a speed of 50 nm/min. After subtraction of solvent background (buffer solution alone) the average of three spectra was taken to convert the CD signal to mean residue ellipticity [Θ] using the following equation [19]:

$$[\Theta] = \Theta_\lambda / cnl$$

where Θ_λ is the observed ellipticity (millidegrees) at wavelength λ, c – molar concentration of protein in solution, n – number of amino acid residues, and l – path length in millimeters.

Evaluation of the secondary structure content of recombinant eEF1Bβ(1–77) by means of its circular dichroism data was done using CDNN – a neural network program freely available for non-profit organizations (http://www.gerald-böhm.de/download/cdnn) [20], and CONTINLL program from the CDPro package [21]. A set of 33 (NNET 33) and 29 (SP29) reference proteins with known structure and known CD spectra was used by CDNN and CONTINLL, respectively, to calculate the fraction of each secondary structure motif (α-helix, β-sheet, turn and unordered structure) that contributes to the eEF1Bβ(1–77) spectrum. As the average error (%) of the secondary structure elements prediction in eEF1Bβ(1–77) made by CDNN, we report here the value of the minimum error made by this program on average and without further training. As a goodness-of-fit parameter for the CONTINLL algorithm, we used the normalized root mean square deviation (σ), defined as $\sigma = (\Sigma_\lambda(\Theta_{exp} - \Theta_{cal})^2 / \Sigma_\lambda(\Theta_{exp})^2)^{1/2}$ [22]. This parameter demonstrates how well the theoretical CD spectrum matches the experimental data over measured wavelength range. The value of $\sigma < 0.1$ corresponds to an accurate computations and the value of $\sigma = 0.05$ or lower may be considered as a perfect fit [22].

Besides, in order to determine the tertiary structure class for eEF1Bβ(1–77) we analyzed its CD spectra by the CLUSTER program included into the CDPro package [22].

2.6. Hydrogen-deuterium exchange (HDX) measurements

Initially, we created a peptide list of the non-deuterated eEF1Bβ(1–77) protein. 5 μl of the eEF1Bβ(1–77) protein stock solution (46 μM) was combined with 45 μL of H_2O reaction buffer containing 25 mM Tris-HCl, pH 7.5, 150 mM NaCl, 150 mM KSCN, and 5 mM 2-mercaptoethanole. The sample was acidified by mixing with 10 μl of 2 M glycine, pH 2.5, and added to 2 μl of protease from *Aspergillus saitoi* (Sigma-Aldrich) in 1% formic acid and offline digested with shaking for 30 s at 4 °C followed by online digestion in an immobilized pepsin resin column (Porozyme, ABI). The obtained peptides were loaded directly to a C18 trapping column (ACQUITY BEH C18 VanGuard pre-column) and eluted onto a reversed phase analytical column (Acquity UPLC BEH C18 column 2.1 × 100 mm, 1.7 μm resin, Waters, Milford, MA) using a 10–35% gradient of acetonitrile in 0.1% formic acid at a flow rate 90 μl/min, controlled by the nanoACQUITY Binary Solvent Manager. The total run time was 12 min. The fluidics, valves, and columns were maintained at 0.5 °C to minimize deuterium back-exchange, using the HDX Manager (Waters), but the pepsin digestion column was kept at 20 °C inside the temperature-controlled digestion compartment of the HDX Manager. The C18 column outlet was directly coupled to the ion source of SYNAPT G2 HDMS mass spectrometer (Waters) working in Ion Mobility mode. The spectrometer parameters were as follows: ESI positive mode, capillary voltage 3 kV, sampling cone voltage 35 V, extraction cone voltage 3 V, source temperature 80 °C, desolvation temperature 175 °C and desolvation gas flow 800 l h^{-1}.

HDX experiments were carried out in a similar way as described for the non-deuterated sample, with the reaction buffer prepared using D_2O (99.8% Cambridge Isotope Laboratories, Inc.). 5 μl of the eEF1Bb (1–77) protein stock (46 μM) was diluted 10-fold by adding 45 μl D_2O reaction buffer and incubated at 20 °C for 10 s, 1 min, 5 min, 25 min or 2.5 h before quenching. The samples were immediately frozen in the liquid nitrogen and stored at −80 °C until using.

Out-time point controls were performed by incubation of the protein in D_2O buffer for 24 h to obtain maximum exchange for each peptide and then, mixed with 10 μl of 2 M glycine, pH 2.5, and analyzed as described above. The deuteration level was calculated and denoted as 100% exchange.

The experiments were repeated three times, the results represent the mean of all replicates. Peptides were identified using ProteinLynx Global Server software (PLGS, Waters) and further filtered in the DynamX 3.0 program (Waters) with the following acceptance criteria: minimum intensity threshold of 3000, minimum products per amino acids of 0.3, minimum score of 7.5 and theoretical value for parent ions below 10 ppm. The values reflecting experimental mass of each peptide in all possible states, replicates, time points and charge states were exported from the DynamX 3.0 and further data analysis was carried out using in house written script.

2.7. Structure modeling

The 3D structure models were generated by the I-TASSER and Modeller programs. I-TASSER Suite, a stand-alone software package for protein structure and function modeling [23]. Further high-resolution protein structure refinement for the best predicted 3D model was done by ModRefiner [24]. The Modeller program (9.14 software) models three-dimensional structures of proteins by satisfaction of spatial restraints derived from related protein structures available in the Protein Data Bank [25]. Additionally, all structures were verified using the MolProbity web server (http://molprobity.biochem.duke.edu/) [26]. Visualization and analysis of the protein was performed using UCSF Chimera [27]. To predict unstructured regions in eEF1Bβ(1–77) we used a MetaDisorderMD2 meta-server [28].

3. Results

3.1. Purification and characterization of recombinant eEF1Bβ(1–77)

Since eEF1Bβ (1–77) was expressed in the *E. coli* strain as a GST fusion protein, the affinity chromatography on Glutathione sepharose™ 4B was used as a first purification step. Then, after the PreScission protease treatment, eEF1Bβ(1–77) was separated from GST in a HiLoad Superdex 200 column. About 2 mg of >90% pure eEF1Bβ(1–77) was obtained from 1 l of BL21Gold culture (Fig. 2A). Purified eEF1Bβ(1–77) migrates in the gel slower than the 10 kDa marker (Fig. 2A) that does not correlate well with the theoretical mass of the monomer (9.2 kDa). This indicates that eEF1Bβ(1–77) may bound more SDS than can be expected for the globular protein of this size [29]. The size-exclusion chromatography on a Superpose 6 HR column was performed to estimate the molecular mass of purified eEF1Bβ(1–77) in the native conditions. Surprisingly, the apparent molecular mass of eEF1Bβ(1–77) was found to be 19.7 ± 0.6 kDa (Fig. 2B) that was almost two times higher than the theoretical mass of the monomer, suggesting that a dimerization of the protein may occur.

To verify this assumption we performed the sedimentation equilibrium analysis of the recombinant eEF1Bβ(1–77) protein. First, eEF1Bβ(1–77) at two different initial concentrations was centrifuged at 20,000 rpm. After first equilibrium was established, the speed was changed to 25,000 rpm to attain the second equilibrium, and finally to 30,000 rpm to attain the third one (Fig. 2C). The experimental data obtained at different velocities were fitted to a single non-interacting species model using SEDPHAT [18] as described in the Section 2.4. The analysis of six single-speed scans showed the molecular mass of eEF1Bβ(1–77) equal to 9125 ± 379 Da (data not shown) that is close

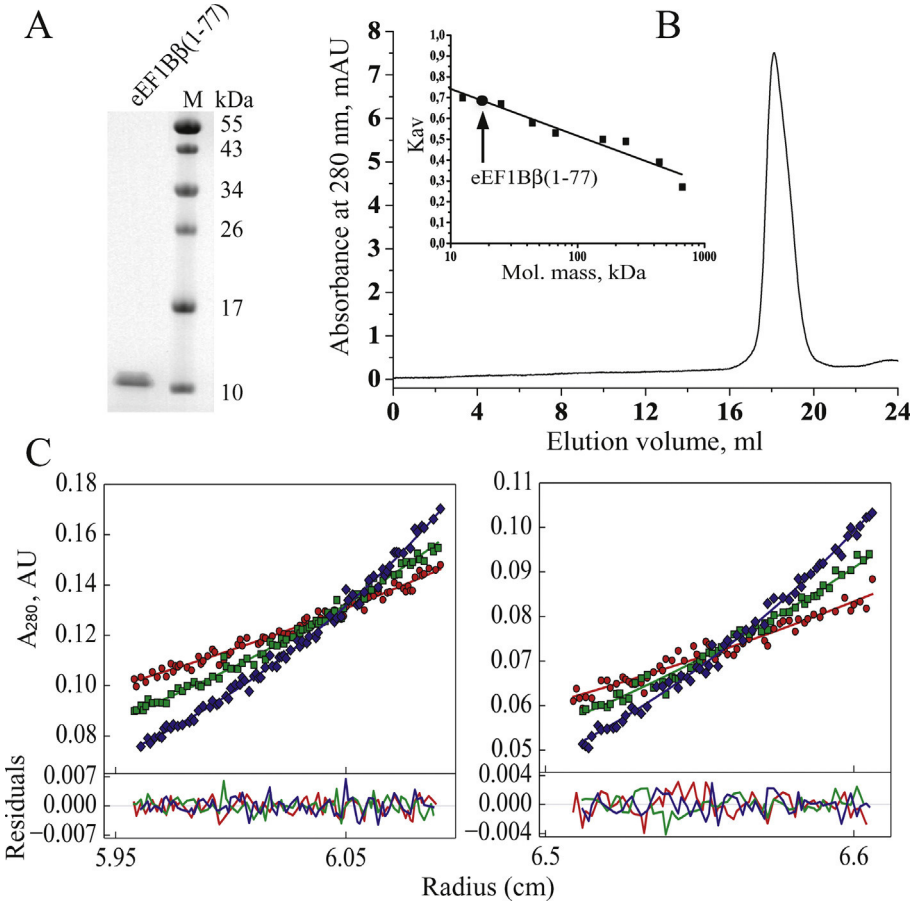

Fig. 2. Characterization of the recombinant eEF1Bβ(1–77) protein. A. SDS-PAGE of purified eEF1Bβ(1–77). 3 μg of eEF1Bβ(1–77) was loaded onto a 18% polyacrylamide gel. B. Analysis of eEF1Bβ(1–77) by size-exclusion chromatography. One hundred μl of 25 μM eEF1Bβ(1–77) was injected into a Superose 6 HR column. Inset. Calibration curve of a Superose 6 HR column was prepared using a set of standard proteins (solid squares): cytochrome C (12.4 kDa), chymotrypsinogen A (25 kDa), ovalbumin (44 kDa), bovine serum albumin (66 kDa), aldolase (160 kDa), catalase (240 kDa), ferritin (450 kDa), thyroglobulin (670 kDa). The position of eEF1Bβ(1–77) on the calibration line is indicated by the solid circle. C. Absorbance scans of the sedimentation equilibrium data (symbols) and best-fits for single species model in the multispeed analysis (solid lines). Red curves and symbols represent the equilibrium experiments performed at 20,000 rpm, green and blue curves and symbols – at 25,000 and 30,000 rpm, respectively. Residuals are indicated. Initial concentrations of eEF1Bβ(1–77) were 0.14 mg/ml (*left*), and 0.09 mg/ml (*right*). Graphs were prepared using GUSSI program (version 1.0.8d) (Chad Brautigam, UT Southwestern).

to the theoretical mass of the monomer. The multi-speed analysis by SEDPHAT [18] produced 8609 and 9485 Da values for the 0.14 mg/ml and 0,09 mg/ml concentrations of eEF1Bβ(1–77), respectively (Fig. 2C).

Therefore, we conclude that the purified recombinant eEF1Bβ(1–77) protein is a monomer in solution and most probably has either a moderately elongated or a globular shape with increased hydrodynamic volume.

3.2. Purified recombinant eEF1Bβ(1–77) forms a stable complex with eEF1Bγ

It has been demonstrated that the large N-terminal fragment (residues 1–150) of eEF1Bβ interacts with the N-terminal domain of eEF1Bγ [13]. This fragment encompasses the N-terminal domain, the LZ motif and the linker region (Fig. 1). Earlier we have reported that the LZ motif is involved in oligomerization of eEF1Bβ [14] while the function of the N-terminal domain remained unassigned. To verify whether the N-terminal domain, eEF1Bβ(1–77), may bind eEF1Bγ by itself we performed analytical gel filtration analysis. Co-incubation of eEF1Bβ(1–77) and eEF1Bγ in equimolar quantities led to the formation of a stable complex (Fig. 3). SDS-PAGE confirmed that eEF1Bβ(1–77) is present in the fractions of complex (Fig. 3, inset). The molecular mass of the eEF1Bβ(1–77)-eEF1Bγ complex was estimated to be 185 ± 5 kDa, that is close to the sum of the eEF1Bβ(1–77) (19.7 ± 0.6 kDa) and the eEF1Bγ (160 ± 5 kDa) molecular masses determined by the same

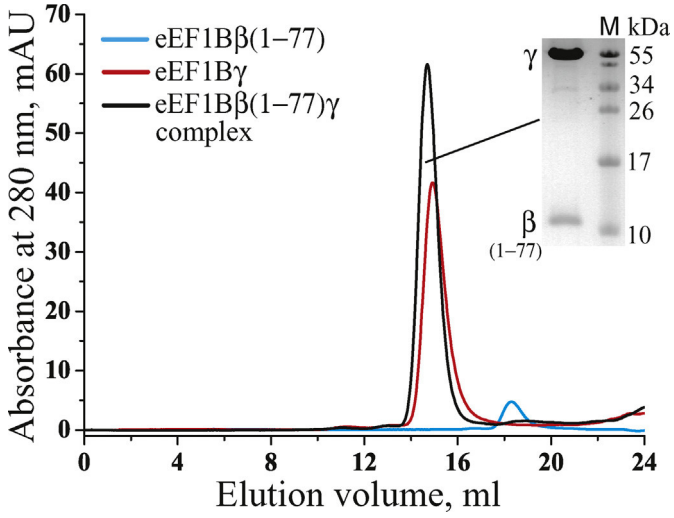

Fig. 3. Analysis of eEF1Bβ(1–77) and eEF1Bγ interaction by size-exclusion chromatography. One hundred μl of 15 μM eEF1Bβ(1–77)-eEF1Bγ complex was injected into a Superose 6 HR column. Inset. SDS-PAGE of the main peak fractions of the eEF1Bβ(1–77)γ complex. 4 μg of eEF1Bβ(1–77)γ was loaded onto a 18% polyacrylamide gel.

method. As the LZ motif and linker region of eEF1Bβ were unable to bind eEF1Bγ (data not shown) we can conclude that eEF1Bγ binds to eEF1Bβ via 1–77 fragment of the latter.

3.3. Determination of the secondary structure of eEF1Bβ(1–77)

We used the CD spectroscopy in far-UV region (190–260 nm) to determine the content of the eEF1Bβ(1–77) secondary structure elements. To estimate stability of the secondary structure elements the measurements were done at several increasing temperatures.

The recombinant eEF1Bβ(1–77) protein showed the CD spectra (Fig. 4) typical for the α-helix-reach structure with the minima at 208 and 222 nm and a positive band with a strong maximum close to 195 nm. Indeed, the spectral analysis using the CDNN program indicates that 78.4% of the eEF1Bβ(1–77) protein populate the α-helix conformation at 24 °C and the remaining part is an unstructured region (Table 1).

Gradual increase of the protein solution temperature does not change the shape of the CD spectra (Fig. 4) suggesting that a considerable α-helical content remains in the eEF1Bβ(1–77) structure during heating. Indeed, the analysis of six CD spectra obtained at the temperature range from 30 to 55 °C by the CDNN program demonstrated rather small gradual decrease of α-helical conformation (Table 1). At 55 °C the structure of eEF1Bβ(1–77) still had considerable α-helical content close to 70% (Table 1), so the only about 10% of the α-helix elements of eEF1Bβ(1–77) was lost compared to its secondary structure at 24 °C (Table 1). These data suggest that eEF1Bβ(1–77) mainly preserves the secondary structure organization in this range of temperatures.

Similar results were obtained when the CD spectra of eEF1Bβ(1–77) were analyzed by the CONTILL program from the CDPro package (Table 2).

The total content of α-helices in the eEF1Bβ(1–77) structure at 24 °C was calculated to be 78%, while the unordered region comprises 22%. Increasing temperature caused about 13% decrease of α-helical content from 78% at 24 °C to 65.5% at 55 °C. At the same time, the content of unordered structures, turns and β-sheets rises from 22%, 0% and 0% (at 24 °C) to 25.6%, 3.1% and 5.9% (at 55 °C), respectively (Table 2). A normalized rmsd value, ranged from 0.048 to 0.072 for different CD curves, confirmed an accurate calculation of the secondary structure

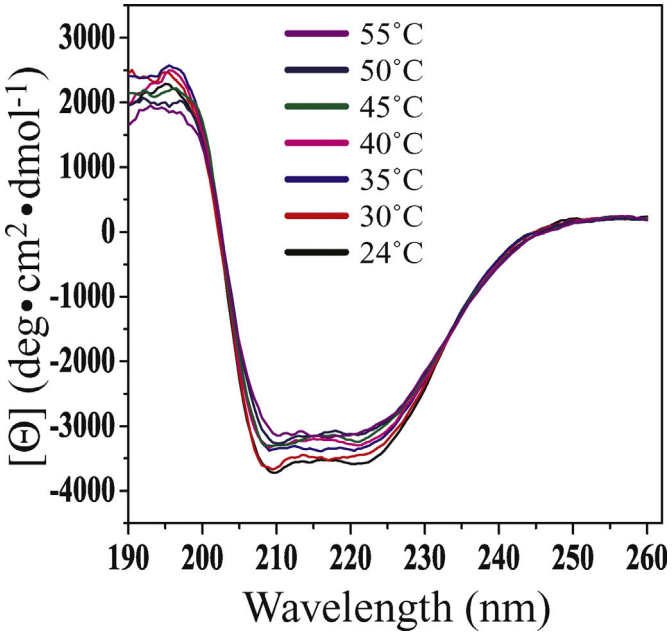

Fig. 4. The secondary structure elements of eEF1Bβ(1–77) studied by circular dichroism spectroscopy. Far-UV circular dichroic spectra of eEF1Bβ(1–77) obtained at different temperatures in 5 mM Tris-HCl, pH 7.5 buffer solution and represented as mean residue ellipticity [Θ] vs. wavelength.

Table 1
The secondary structure estimation made by the CDNN program from the CD spectra of eEF1Bβ(1–77) recorded at different temperatures. The average error for the prediction is 5.57%.

t, °C	CDNN program		
	α-Helix, %	β-Turn, %	Random coil, %
24	78.4	9.6	23.7
30	79.2	9.1	19.8
35	77.8	8.7	20.4
40	76.3	9.4	22.9
45	73.8	9.4	24.7
50	70.5	10.0	29.0
55	68.5	10.6	33.1

(Table 2). Additionally, the CD spectra of eEF1Bβ(1–77) obtained at different temperatures were analyzed by the CLUSTER program from the CDPro package [22]. This program allows estimating a tertiary structure class of the eEF1Bβ(1–77). Again, the best-fit result generated by CLUSTER after analyzing each CD spectrum was "All alpha" (Table 2). Altogether, the data obtained by two different algorithms permitted to conclude that the secondary structure of eEF1Bβ(1–77) consists predominantly of α-helices (78%), with a portion of unordered region (22%). Importantly, eEF1Bβ(1–77) retains the significant amount (65.5–68.5%) of its α-helical content when heating up to 55 °C (Tables1 and 2).

CD spectroscopy in the near-UV range (250–350 nm) is an approach that reflects the environment of aromatic amino acid residues and thus gives information about the tertiary structure of the protein [30]. When the spectra of eEF1Bβ(1–77) were measured in the near-UV range at 56 μM protein concentration the nearly zero signals were obtained (data not shown). This is consistent with the absence of the stable tertiary structure interactions in eEF1Bβ(1–77), since the proteins without rigid tertiary structure usually display dramatically reduced near-UV CD spectra in comparison with tightly packed molecules [31].

3.4. Hydrogen-deuterium exchange mass spectrometry shows rapid exchange for all eEF1Bβ(1–77) peptides

To get a deeper insight into the eEF1Bβ(1–77) tertiary structure organization we used the method of hydrogen-deuterium exchange coupled with mass-spectrometry (HDX-MS). This technique reveals the information about the stability of hydrogen bonds network in the protein, indicating the flexible and rigid regions and providing the insight into the structural dynamics of the protein. The optimized peptide map of this protein was generated (Fig. 5) and composed of 21 peptides covering 88.5% of the eEF1Bβ(1–77) sequence with the redundancy of 2.86.

The HDX-MS procedure was conducted at several time points. Initially, a short pulse of deuterium (10 s at 20 °C) was done. Normally, 10 s interval is sufficient for the H/D exchange in the unstructured regions and highly dynamic secondary structure elements but not for the peptides involved into tertiary interactions [32]. The exchange profile (Fig. 6) showed that after 10 s interval the maximum level of deuterium incorporation (about 100%) was achieved for all peptides, indicating the highly dynamic structure of eEF1Bβ(1–77).

Thus, no protection in eEF1Bβ(1–77) was found by HDX analysis. It is noteworthy that this region showed no protection in the full-sized eEF1Bβ as well (data not shown), while various level of exchange was found by HDX in other regions of the protein (manuscript in preparation).

3.5. eEF1Bβ(1–77) tertiary structure prediction and validation

Thus, regardless of 78% α-helical content, no protected peptides of eEF1Bβ(1–77) were found by HDX-MS. Apparently, all α-helices are

Table 2
The secondary structure estimation made by the CONTILL program from the CD spectra of eEF1Bβ(1–77) recorded at different temperatures. Symbols "r" and "d" in the parentheses refer to regular and distorted structures, respectively. σ – normalized root mean square deviation.

t, °C	CONTILL program								CLUSTER program prediction
	α-Helices			β-Sheets		Turns	Unordered	σ	
	α(r), %	α(d),%	α(total),%	β(r), %	β(d), %	%	%		
24	53.8	24.2	78.0	0.0	0.0	0.0	22.0	0.048	"All alpha"
30	52.3	24.1	76.4	0.0	0.0	6.0	22.9	0.054	"All alpha"
35	50.6	23.0	73.6	0.0	0.0	2.4	24.0	0.064	"All alpha"
40	46.4	23.3	67.7	0.0	0.0	4.2	26.2	0.061	"All alpha"
45	50.6	23.4	74.0	0.0	3.0	4.8	20.8	0.072	"All alpha"
50	46.5	22.3	68.8	0.0	1.9	4.3	24.9	0.065	"All alpha"
55	42.0	23.5	65.5	0.0	3.1	5.9	25.6	0.064	"All alpha"

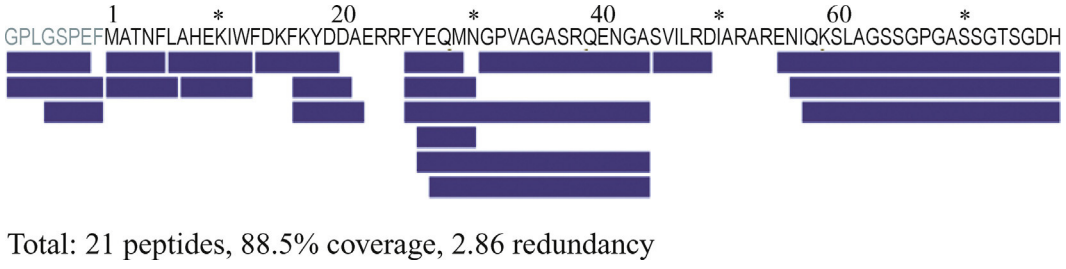

Fig. 5. The optimized peptide map of eEF1Bβ(1–77). The peptides generated after proteolytic digestion and identified by mass-spectrometry are shown on the eEF1Bβ(1–77) sequence. The rest of the linker region sequence before the starting Met residue is indicated in gray.

not tightly packed and all hydrophobic amino acids are accessible to solvent. Altogether, the obtained results suggest that the eEF1Bβ(1–77) secondary structure elements form a dynamic spatial structure.

The 3D structure of eEF1Bβ(1–77) was predicted using the I-TASSER Suite software package that implements I-TASSER based algorithms for protein structure and function predictions [23]. The 5 top models are shown in Fig.7A. Additionally, the Modeller program was used for the eEF1Bβ(1–77) structure modeling. In general terms, the models generated by Modeller were similar to those generated by I-TASSER: eEF1Bβ(1–77) was composed of three α-helices connected by the flexible linkers (data not shown). However, as the models of I-TASSER fitted better to the CD data (Tables 1 and 2), we proceeded further with the models generated by this algorithm.

The best-ranked model according to the C-score is Model 1 (C-score − 2.55, TM score 0.42 ± 0.14, and RMSD 8.9 ± 4.6 Å). C-score is a confidence score for quality estimation of the predicted models. C-score is typically in the range of −5 to 2.The higher value signifies a model with a high confidence. TM-score is a scale for measuring the structural similarity between two structures. TM-score > 0.5 indicates a model of correct topology and <0.17 means a random similarity (https://zhanglab.ccmb.med.umich.edu/I-TASSER/example/cscore.txt). The other four models have lower C-scores (from −3.38 to −3.83) compared to the Model 1. In general, all models differ in spatial orientation of α-helices (Fig. 7A). A moderate confidence of the scores reflects the absence of the highly homologous templates for eEF1Bβ(1–77) in the Protein Data Bank archive to date. All predicted models were additionally refined by ModRefiner, an algorithm for the atomic-level, high-resolution protein structure refinement [24]. After refinement the secondary structure content in the eEF1Bβ(1–77) models was estimated to be: 72.7% of α-helices, 0.0% of β-strands, 10.4% of β-turns, and 16.9% of unstructured regions (Model 1); 54.5% of α-helices, 0.0% of β-strands, 26.0% of β-turns, 19.5% of unstructured regions (Model 2); 55.8% of α-helices, 2.6% of β-strands, 13.0% of β-turns, 28.6% of unstructured regions (Model 3); 45.5% of α-helices, 0.0% of β-strands, 10.4% of β-turns, 44.2% of unstructured regions (Model 4); 55.9% of α-helices, 0.0% of β-strands, 20.8% of β-turns, 23.4% of unstructured regions (Model 5). Of note, α-helices, the only ordered structure elements in eEF1Bβ(1–77) correspond to the evolutionary conserved amino acid sequences (Fig. 7B). Further, the conformation of all eEF1Bβ(1–77) 3D models was validated by the MolProbity server [26]. The MolProbity Ramachandran plot for all refined models showed 75 amino acid residues in allowed (>99.8%) regions.

Three α-helices (α1, α2 and α3) represent all ordered secondary structure elements in the optimized eEF1Bβ(1–77) spatial models. There are also one short linker and two longer unstructured regions in this protein (Fig. 7A). To verify this result we used a MetaDisorderMD2 meta-server [28] as additional approach for unstructured region prediction. High disorder tendency (>50%) is predicted for two regions N30-G42 and E55-H77 (Fig. 7C). The obtained result is in a good agreement with the prediction of two long unstructured regions made by I-TASSER (Fig. 7A).

In total, the refined 3D model structures of eEF1Bβ(1–77) are consistent with the estimations of the secondary structure elements content made by the CONTILL and CDD programs based on the CD spectra

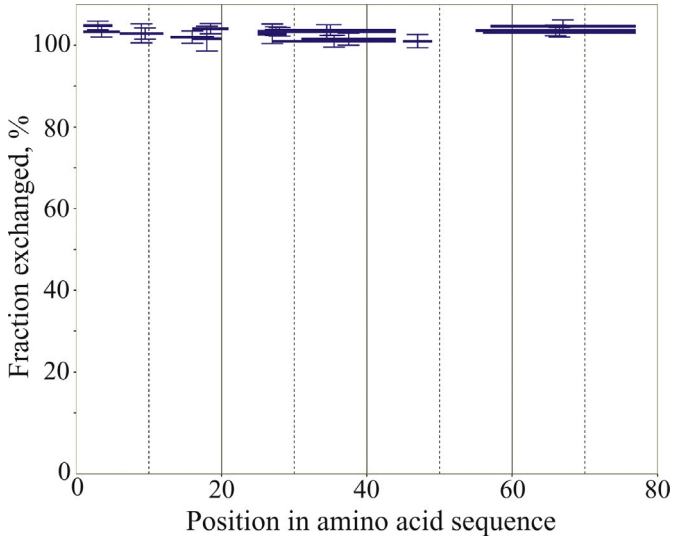

Fig. 6. The levels of hydrogen deuterium exchange of the eEF1Bβ(1–77) peptides after 10-s of deuterium exposure at 20 °C. Error bars represent standard deviation of three independent measurements.

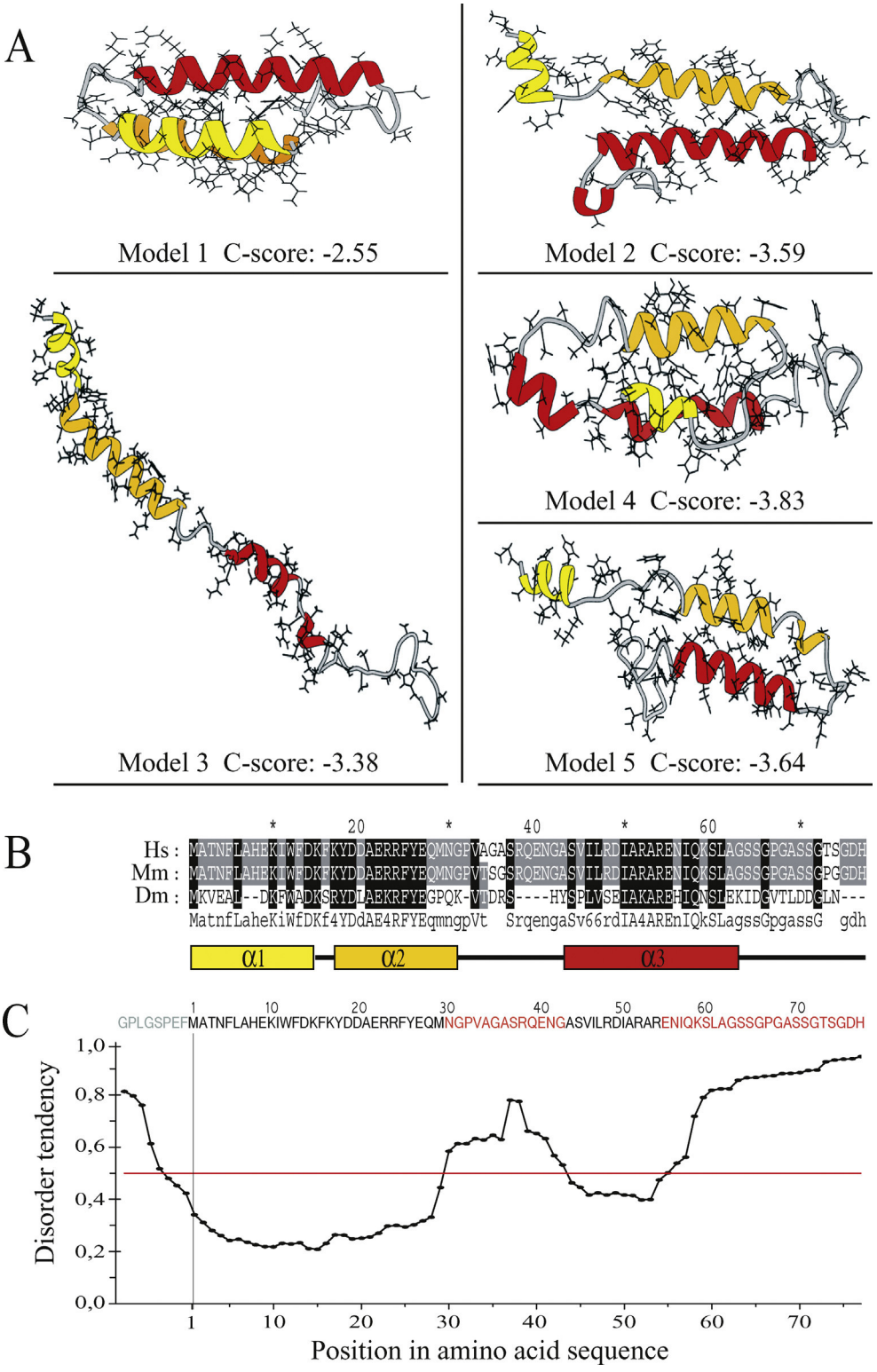

Fig. 7. eEF1Bβ(1–77) structural organization. A. Ribbon representation of the predicted by I-TASSER and refined by ModRefiner models of eEF1Bβ(1–77). Amino acid side chains are shown in sticks. I-TASSER's confidence score (C-score) is indicated for each model. B. Multiple amino acid sequence alignment of eEF1Bβ(1–77) from different species. Abbreviations: Hs, *Hommo sapience*; Mm, *Mus musculus*; Dm, *Drosophila melanogaster*. Secondary structure elements, α-helices and unordered regions, are mapped on the amino acid sequence alignment accordingly to I-TASSER (Model 1). α-helices have the same colors as indicated in (A). C. Prediction of the disordered regions in eEF1Bβ(1–77) by a MetaDisorderMD2 meta-server. The disorder tendency parameter is mapped on the eEF1Bβ(1–77) sequence (top of the figure). All residues whose disorder probability is over 0.5 (red line) are considered as disordered. Vertical bar depicts the position of starting methionine on the plot. Residues belonging to the ordered and disordered regions are in black and in red colors, respectively. The part of the linker region before the starting methionine is in gray.

(Tables 1 and 2). In addition, the fluorescence measurements of a single tryptophan residue present in eEF1Bβ(1–77) showed that the emission spectra had the maximum at 349 nm (data not shown) indicating that this residue is highly exposed to solvent [33]. This is also consistent with the 3D models of eEF1Bβ(1–77) in which the tryptophan residue is not hidden (Fig. 7A). Besides, we checked whether the solvent

exposed hydrophobic residues form a hydrophobic cluster in the eEF1Bβ(1–77) molecule. For that, we used extrinsic fluorescent dye 8-anilino-1-naphthalene sulfonic acid (ANS) that specifically binds to the structured hydrophobic regions of proteins. Generally, upon binding of ANS to the hydrophobic pocket, its fluorescence quantum yield increases with a simultaneous blue shift in the emission maximum wavelength from 510 nm (free ANS in a polar environment) to 480 nm depending on the polarity of the binding site [34,35]. The ANS emission spectra obtained in the presence of the different concentration of eEF1Bβ(1–77) demonstrated the emission maximum wavelength similar to ANS alone (data not shown). Thus, eEF1Bβ(1–77) does not seem to possess a hydrophobic site for ANS binding. Altogether, the fluorescence experiments favor the notion about a dynamic organization of the eEF1Bβ(1–77) tertiary structure.

The agreement of the results obtained by the experimental and computational approaches allows us to conclude that eEF1Bβ(1–77) possesses a flexible tertiary structure made by α-helixes and disordered regions.

4. Discussion and conclusions

As mentioned above, eEF1Bβ(1–77) does not share any significant homology with other proteins while its secondary and tertiary structures are not known. We optimized the procedure of the expression and purification of eEF1Bβ(1–77) and characterized the recombinant protein. By means of gel filtration and analytical ultracentrifugation we found that eEF1Bβ(1–77) is a monomer in solution and has either a moderately elongated shape or a globular shape with increased hydrodynamic volume (Fig. 2). The CD spectra analysis revealed that the secondary structure of eEF1Bβ(1–77) consists of α-helices (about 78%) and a portion of non-ordered region (about 22%) (Tables 1 and 2). Importantly, α-helical content of eEF1Bβ(1–77) was reduced slightly (about 10%) and gradually during heating up to 55 °C (Fig. 4, Tables 1 and 2), indicating that the secondary structure organization of eEF1Bβ(1–77) was mostly retained under these conditions. The high speed of the deuterium incorporation in eEF1Bβ(1–77) suggests that this protein lacks a rigid tertiary structure, i.e. it does not have either hydrophobic core or network of stable hydrogen bonds (Fig. 6). Interestingly, anomalous SDS gel mobility (Fig. 2A) of purified eEF1Bβ(1–77) indicates that it may bind more detergent than could be expected for the globular protein of this size [29]. Such aberrant migration on SDS-PAGE is common for membrane proteins or more precisely for transmembrane domains of the membrane proteins that have helix-loop-helix tertiary structure [36]. These transmembrane domains bound different detergent amounts depending on their secondary structure content and spatial conformation. The transmembrane domains with increased helical content and increased hydrodynamic volume bound more detergent and migrated slower on SDS-PAGE than their expected theoretical molecular masses [36]. Such behavior correlates with that of eEF1Bβ(1–77) which has also high content of α-helices (Tables 1 and 2), increased hydrodynamic volume, and electrophoretic gel shifting (Fig. 2A).

A very broad class of proteins lacking rigid 3D structure under physiological conditions was discovered up to date [37]. These naturally flexible proteins do not have a unique conformation and have to be represented by a number of different conformations that are rapidly interconverting to each other [31,37]. One of the predicted roles of intrinsic structural plasticity of a protein is to provide interaction with a variety of partners in cell [38]. The N-terminal domain of eEF1Bβ is a new example of such spatial organization. This protein most probably exists in solution as dynamic conformational ensembles in which its secondary structure elements, α-helices, may adopt different spatial orientation, for instance, such as those represented by five predicted models (Fig. 7A).

Previously, it has been demonstrated that the eEF1Bβ N-terminal fragment (residues 1–150), including LZ and eEF1Bβ(1–77), interacts with the N-terminal domain of eEF1Bγ [13]. As the LZ role was found to provide a self-association of eEF1Bβ [14] one may suggest that the eEF1Bβ(1–77) domain can be responsible for the interaction with eEF1Bγ. Indeed, eEF1Bβ(1–77) forms a stable complex with eEF1Bγ (Fig. 3). Thus, it is reasonable to suggest that in the eEF1B complex eEF1Bγ is linked to eEF1Bβ via very N-terminal domain of the latter. An important evidence supporting the involvement of this fragment into the interaction with eEF1Bγ is the presence in the RCSB Protein Data Bank the X-ray structure of the 1–30 amino acid peptide of eEF1Bβ complexed with the N-terminal domains of eEF1Bγ (PDB ID: 5JPO). Of note, despite being present in the databank, this structure is not published yet which limits its discussion in detail. One may indicate, however, that in the 5JPO structure the 1–30 amino acid fragment of eEF1Bβ is α-helical that is consistent with our predicted eEF1Bβ(1–77) models (Fig. 7A).

We believe that the functional importance of a flexible conformation of the eEF1Bβ N-terminal domain is to provide a structural plasticity, which may permit it to interact with different protein partners, in particular, eEF1Bγ and VRS. Moreover, eEF1Bβ reveals oncogenic properties participating in Cd^{2+}-induced oncogenesis [39]. In cancer tissues, a part of eEF1Bβ pool may leave the eEF1B complex and function individually [40,41]. In this case, a structural plasticity of the eEF1Bβ N-terminal domain may be important for arranging a set of interactions with different cancer-related partners such as ILF2, ILF3, HNRNPU, CELF1 and USP39 [42].

Here, we provided evidence that the 1–77 domain of eEF1Bβ links this protein to eEF1Bγ. Moreover, we described α-helical secondary and flexible tertiary structural organization of this domain and built its 3D models *in silico*. Such a conformational flexibility may provide a strong structural support for the specific interaction of eEF1Bβ with the protein-partner(s) within the eEF1B and VRS-eEF1B complexes and outside of them.

Declarations of interest

None.

Funding

This work was partially supported by the Program of Joint Ukraine-Poland R&D Projects by Ministry of Education and Science of Ukraine and Ministry of Science and Higher Education, Republic of Poland (grant M/139-2018), and the Interdisciplinary Program of Scientific research of NAS of Ukraine "Molecular and cell biotechnologies for medicine, industry and agriculture". To perform the HDX experiments B.T.V. was supported by the short-term FEBS fellowship "Collaborative and Experimental Scholarship for Central & Eastern Europe". To perform the analytical ultracentrifugation experiments B.T.V. was supported by "The Grant for visits of young scientists of the NAS of Ukraine to Poland for the purpose of training in research institutions of the Polish Academy of Sciences". None of the funding body listed above participated in the design of the study, data collection, analysis, and interpretation or manuscript writing.

Authors' contributions

BTV participated in the design of the study, performed expression and purification of the protein, participated in CD and HDX measurements, analyzed the data and helped draft the manuscript; DML analyzed the CD data and performed protein structure modeling; VFS designed the study and analyzed the data, performed analytical ultracentrifugation experiments and wrote the paper; AF performed HDX measurements, analyzed the data and contributed to the preparation of the manuscript; RHS performed the analytical ultracentrifugation experiments, analyzed the data and contributed to the preparation of the manuscript, MD analyzed the HDX data and contributed in writing the

manuscript; BSN and AVE wrote the paper. All authors read and approved the final manuscript.

Acknowledgments

Authors are also grateful to Dr. Z.Yu. Tkachuk for the CD facility, M. Vivcharyk for the help with CD measurements, and R. Nikolaev for the help with fluorescence measurements.

References

[1] G.M. Janssen, H.T. van Damme, J. Kriek, R. Amons, W. Moller, The subunit structure of elongation factor 1 from Artemia. Why two alpha-chains in this complex? J. Biol. Chem. 269 (1994) 31410–31417.
[2] J.F. Carvalho, M.D. Carvalho, W.C. Merrick, Purification of various forms of elongation factor 1 from rabbit reticulocytes, Arch. Biochem. Biophys. 234 (1984) 591–602.
[3] Y.A. Motorin, A.D. Wolfson, D. Lohr, A.F. Orlovsky, K.L. Gladilin, Purification and properties of a high-molecular-mass complex between Val-tRNA synthetase and the heavy form of elongation factor 1 from mammalian cells, Eur. J. Biochem./FEBS 201 (1991) 325–331.
[4] G. Bec, P. Kerjan, J.P. Waller, Reconstitution in vitro of the valyl-tRNA synthetase-elongation factor (EF) 1 beta gamma delta complex. Essential roles of the NH2-terminal extension of valyl-tRNA synthetase and of the EF-1 delta subunit in complex formation, J. Biol. Chem. 269 (1994) 2086–2092.
[5] W.C. Merrick, J. Nyborg, 3 the Protein Biosynthesis, Elongation Cycle, Cold Spring Harbor Monograph Archive, 39, 2000 89–125.
[6] Prokaryotic and eukaryotic translation factors. Ad hoc nomenclature subcommittee report, Biochimie 78 (1996) 1119–1122.
[7] F. Le Sourd, S. Boulben, R. Le Bouffant, P. Cormier, J. Morales, R. Belle, O. Mulner-Lorillon, eEF1B: at the dawn of the 21st century, Biochim. Biophys. Acta 1759 (2006) 13–31, https://doi.org/10.1016/j.bbaexp.2006.02.003.
[8] H.T. van Damme, R. Amons, R. Karssies, C.J. Timmers, G.M. Janssen, W. Moller, Elongation factor 1 beta of artemia: localization of functional sites and homology to elongation factor 1 delta, Biochim. Biophys. Acta 1050 (1990) 241–247.
[9] H. Wu, C. Wang, W. Gong, J. Wang, J. Xuan, S. Perrett, Y. Feng, The C-terminal region of human eukaryotic elongation factor 1Bdelta, J. Biomol. NMR 64 (2016) 181–187, https://doi.org/10.1007/s10858-016-0012-6.
[10] H. Wu, W. Gong, X. Yao, J. Wang, S. Perrett, Y. Feng, Evolutionarily conserved binding of translationally controlled tumor protein to eukaryotic elongation factor 1B, J. Biol. Chem. 290 (2015) 8694–8710, https://doi.org/10.1074/jbc.M114.628594.
[11] M.A. Guerrucci, A. Monnier, C. Delalande, R. Belle, The elongation factor-1delta (EF-1delta) originates from gene duplication of an EF-1beta ancestor and fusion with a protein-binding domain, Gene 233 (1999) 83–87.
[12] R. Amons, M.A. Guerrucci, R.H. Karssies, J. Morales, P. Cormier, W. Moller, R. Belle, The leucine-zipper in elongation factor EF-1 delta, a guanine-nucleotide exchange protein, is conserved in Artemia and Xenopus, Biochim. Biophys. Acta 1218 (1994) 346–350.
[13] F. Mansilla, I. Friis, M. Jadidi, K.M. Nielsen, B.F. Clark, C.R. Knudsen, Mapping the human translation elongation factor eEF1H complex using the yeast two-hybrid system, Biochem. J. 365 (2002) 669–676, https://doi.org/10.1042/BJ20011681.
[14] T.V. Bondarchuk, V.F. Shalak, B.S. Negrutskii, A.V. El'skaya, Leucine-zipper motif is responsible for self-association of translation elongation factor 1Bβ, Biopolym. Cell 32 (2016) 11, https://doi.org/10.7124/bc.000907.
[15] T.V. Trosiuk, V.V. Liudkovska, V.F. Shalak, B.S. Negrutskii, A.V. El'skaya, Structural dissection of human translation elongation factor 1Bγ (eEF1Bγ): expression of full-length protein and its truncated forms, Biopolym. Cell 30 (2014) 96–106, https://doi.org/10.7124/bc.000887.
[16] T.V. Trosiuk, V.F. Shalak, R.H. Szczepanowski, B.S. Negrutskii, A.V. El'skaya, A non-catalytic N-terminal domain negatively influences the nucleotide exchange activity of translation elongation factor 1Balpha, FEBS J. 283 (2016) 484–497, https://doi.org/10.1111/febs.13599.
[17] P. Schuck, On the analysis of protein self-association by sedimentation velocity analytical ultracentrifugation, Anal. Biochem. 320 (2003) 104–124.
[18] J. Vistica, J. Dam, A. Balbo, E. Yikilmaz, R.A. Mariuzza, T.A. Rouault, P. Schuck, Sedimentation equilibrium analysis of protein interactions with global implicit mass conservation constraints and systematic noise decomposition, Anal. Biochem. 326 (2004) 234–256, https://doi.org/10.1016/j.ab.2003.12.014.
[19] N.J. Greenfield, Using circular dichroism spectra to estimate protein secondary structure, Nat. Protoc. 1 (2006) 2876–2890, https://doi.org/10.1038/nprot.2006.202.
[20] G. Bohm, R. Muhr, R. Jaenicke, Quantitative analysis of protein far UV circular dichroism spectra by neural networks, Protein Eng. 5 (1992) 191–195.
[21] N. Sreerama, R.W. Woody, Estimation of protein secondary structure from circular dichroism spectra: comparison of CONTIN, SELCON, and CDSSTR methods with an expanded reference set, Anal. Biochem. 287 (2000) 252–260, https://doi.org/10.1006/abio.2000.4880.
[22] L. Whitmore, B.A. Wallace, DICHROWEB, an online server for protein secondary structure analyses from circular dichroism spectroscopic data, Nucleic Acids Res. 32 (2004) W668–W673, https://doi.org/10.1093/nar/gkh371.
[23] J. Yang, R. Yan, A. Roy, D. Xu, J. Poisson, Y. Zhang, The I-TASSER Suite: protein structure and function prediction, Nat. Methods 12 (2015) 7–8, https://doi.org/10.1038/nmeth.3213.
[24] D. Xu, Y. Zhang, Improving the physical realism and structural accuracy of protein models by a two-step atomic-level energy minimization, Biophys. J. 101 (2011) 2525–2534, https://doi.org/10.1016/j.bpj.2011.10.024.
[25] B. Webb, A. Sali, Comparative protein structure modeling using MODELLER, Curr. Protoc. Bioinformatics 47 (56) (2014) 1–32, https://doi.org/10.1002/0471250953.bi0506s47.
[26] V.B. Chen, W.B. Arendall 3rd, J.J. Headd, D.A. Keedy, R.M. Immormino, G.J. Kapral, L.W. Murray, J.S. Richardson, D.C. Richardson, MolProbity: all-atom structure validation for macromolecular crystallography, Acta Crystallogr. D Biol. Crystallogr. 66 (2010) 12–21, https://doi.org/10.1107/S0907444909042073.
[27] E.F. Pettersen, T.D. Goddard, C.C. Huang, G.S. Couch, D.M. Greenblatt, E.C. Meng, T.E. Ferrin, UCSF Chimera–a visualization system for exploratory research and analysis, J. Comput. Chem. 25 (2004) 1605–1612, https://doi.org/10.1002/jcc.20084.
[28] L.P. Kozlowski, J.M. Bujnicki, MetaDisorder: a meta-server for the prediction of intrinsic disorder in proteins, BMC Bioinformatics 13 (2012) https://doi.org/10.1186/1471-2105-13-111.
[29] J. Miyake, S. Ochiai-Yanagi, T. Kasumi, T. Takagi, Isolation of a membrane protein from R rubrum chromatophores and its abnormal behavior in SDS-polyacrylamide gel electrophoresis due to a high binding capacity for SDS, J. Biochem. 83 (1978) 1679–1686.
[30] S.M. Kelly, N.C. Price, The use of circular dichroism in the investigation of protein structure and function, Curr. Protein Pept. Sci. 1 (2000) 349–384.
[31] M. Arai, K. Kuwajima, Role of the molten globule state in protein folding, Adv. Protein Chem. 53 (2000) 209–282.
[32] D. Balasubramaniam, E.A. Komives, Hydrogen-exchange mass spectrometry for the study of intrinsic disorder in proteins, Biochim. Biophys. Acta 1834 (2013) 1202–1209, https://doi.org/10.1016/j.bbapap.2012.10.009.
[33] Y.K. Reshetnyak, Y. Koshevnik, E.A. Burstein, Decomposition of protein tryptophan fluorescence spectra into log-normal components. III. Correlation between fluorescence and microenvironment parameters of individual tryptophan residues, Biophys. J. 81 (2001) 1735–1758, https://doi.org/10.1016/S0006-3495(01)75825-0.
[34] D. Sheluho, S.H. Ackerman, An accessible hydrophobic surface is a key element of the molecular chaperone action of Atp11p, J. Biol. Chem. 276 (2001) 39945–39949, https://doi.org/10.1074/jbc.M107252200.
[35] A.P. Chaudhary, N.H. Vispute, V.K. Shukla, B. Ahmad, A comparative study of fibrillation kinetics of two homologous proteins under identical solution condition, Biochimie 132 (2017) 75–84, https://doi.org/10.1016/j.biochi.2016.11.002.
[36] A. Rath, M. Glibowicka, V.G. Nadeau, G. Chen, C.M. Deber, Detergent binding explains anomalous SDS-PAGE migration of membrane proteins, Proc. Natl. Acad. Sci. U. S. A. 106 (2009) 1760–1765, https://doi.org/10.1073/pnas.0813167106.
[37] V.N. Uversky, A.K. Dunker, Understanding protein non-folding, Biochim. Biophys. Acta 1804 (2010) 1231–1264, https://doi.org/10.1016/j.bbapap.2010.01.017.
[38] R. Sajo, O. Toke, I. Hajdu, H. Jankovics, A. Micsonai, J. Dobo, J. Kardos, F. Vonderviszt, Structural plasticity of the Salmonella FliS flagellar export chaperone, FEBS Lett. 590 (2016) 1103–1113, https://doi.org/10.1002/1873-3468.12149.
[39] P. Joseph, Y.X. Lei, T.M. Ong, Up-regulation of expression of translation factors–a novel molecular mechanism for cadmium carcinogenesis, Mol. Cell. Biochem. 255 (2004) 93–101.
[40] M. Veremieva, A. Khoruzhenko, S. Zaicev, B. Negrutskii, A. El'skaya, Unbalanced expression of the translation complex eEF1 subunits in human cardioesophageal carcinoma, Eur. J. Clin. Investig. 41 (2011) 269–276, https://doi.org/10.1111/j.1365-2362.2010.02404.x.
[41] M. Veremieva, L. Kapustian, A. Khoruzhenko, V. Zakharychev, B. Negrutskii, A. El'skaya, Independent overexpression of the subunits of translation elongation factor complex eEF1H in human lung cancer, BMC Cancer 14 (2014) 913, https://doi.org/10.1186/1471-2407-14-913.
[42] L.M. Kapustian, M. Dadlez, B. Negrutskii, Protein partners of the eEF1Bβ subunit of the translation elongation complex eEF1B in the nuclear fraction of human lung carcinoma cells, Biopolym. Cell. 33 (2017), 12. https://doi.org/10.7124/bc.00095D.

9490–9504 *Nucleic Acids Research, 2022, Vol. 50, No. 16* *https://doi.org/10.1093/nar/gkac685*

Quaternary organization of the human eEF1B complex reveals unique multi-GEF domain assembly

Tetiana V. Bondarchuk[1], Vyacheslav F. Shalak[1,*], Dmytro M. Lozhko[1], Agnieszka Fatalska[2,5], Roman H. Szczepanowski[3], Vladyslava Liudkovska[1,3], Oleksandr Yu. Tsuvariev[4], Michal Dadlez[2], Anna V. El'skaya[1] and Boris S. Negrutskii[1]

[1]Institute of Molecular Biology and Genetics, NAS of Ukraine, 150 Zabolotnogo St., 03143 Kyiv, Ukraine, [2]Institute of Biochemistry and Biophysics, PAN, Pawinskiego 5a, 02-109 Warsaw, Poland, [3]International Institute of Molecular and Cell Biology, Trojdena 4, 02-109 Warsaw, Poland, [4]Institute of High Technologies, Taras Shevchenko National University of Kyiv, Akademik Glushkov Ave. 4-g, 03022 Kyiv, Ukraine and [5]Department of Genetics, University of Cambridge, Cambridge CB2 3EH, UK

Received February 25, 2022; Revised July 12, 2022; Editorial Decision July 13, 2022; Accepted July 31, 2022

ABSTRACT

Protein synthesis in eukaryotic cell is spatially and structurally compartmentalized that ensures high efficiency of this process. One of the distinctive features of higher eukaryotes is the existence of stable multi-protein complexes of aminoacyl-tRNA synthetases and translation elongation factors. Here, we report a quaternary organization of the human guanine-nucleotide exchange factor (GEF) complex, eEF1B, comprising α, β and γ subunits that specifically associate into a heterotrimeric form eEF1B(αβγ)$_3$. As both the eEF1Bα and eEF1Bβ proteins have structurally conserved GEF domains, their total number within the complex is equal to six. Such, so far, unique structural assembly of the guanine-nucleotide exchange factors within a stable complex may be considered as a 'GEF hub' that ensures efficient maintenance of the translationally active GTP-bound conformation of eEF1A in higher eukaryotes.

INTRODUCTION

Polypeptide synthesis on the ribosome requires aminoacylated tRNAs (aa-tRNAs) and a number of protein factors (1). To provide the substrate for polypeptide synthesis, translation elongation factor 1A (eEF1A) in a GTP-dependent manner binds aa-tRNA and delivers it to the ribosomal A-site. If the correct codon-anticodon interaction occurs, the ribosome induces GTP cleavage on eEF1A and promotes the release of GDP-bound eEF1A from the A-site (1). In higher eukaryotes, the translation elongation factor complex, eEF1B, mediates the GDP/GTP exchange on eEF1A, thus, restoring its active conformation. This complex consists of the eEF1Bα, eEF1Bβ and eEF1Bγ subunits (2). Herein we use the nomenclature for translation elongation factors proposed by Merrick and Nyborg (3). In the UniProtKB database, eEF1Bα is described as Elongation factor 1-beta (EF1B human, accession number P24534), eEF1Bβ—as Elongation factor 1-delta (EF1D human, accession number P29692), and eEF1Bγ—as Elongation factor 1-gamma (EF1G human, accession number P26641). Both eEF1Bα and eEF1Bβ have guanine-nucleotide exchange (GEF) activity, whereas eEF1Bγ is thought to be a structural component of the complex (2). To accomplish the guanine-nucleotide exchange reaction, eEF1B assembles with eEF1A into a 'heavy' complex known as eEF1H (4). Besides, eEE1B forms a stable complex with valyl-tRNA synthetase (VRS-eEF1B) (5,6). The presence of this enzyme in the GEF complex facilitates the direct transfer (channeling) of valyl-tRNA from the enzyme to eEF1A*GTP (7).

Although the subunits composing eEE1B are known, their number and how they combine within this complex remains unclear. Up to date, several models of eEE1B structural organization have been proposed, however, there are significant inconsistencies among them (8). According to the simplest model, eEF1Bα and eEF1Bβ bind to the same eEF1Bγ subunit via their N-terminal domains to form the eEF1Bαβγ complex (9). Another model assumes that eEF1Bγ creates a dimeric core, and eEF1Bα and eEF1Bβ bind to the separate eEF1Bγ subunits to form the eEF1Bαβγ$_2$ complex (10). The structural role for the catalytic eEF1Bα and eEF1Bβ subunits was also suggested. The protomer eEF1Bαβγ complex was proposed to dimerize (6) or even trimerize (11) in a larger entity via the leucine-zipper motif of the eEF1Bβ subunit. In turn, the protomer eEF1Bαβγ$_2$ complex was proposed to dimerize via the eEF1Bα subunit (10). Thus, neither the reconstitution experiments nor analysis of the natively purified complexes resulted in the unambiguous determination of the eEF1B quaternary organization (6,10–13). It seems that due to high

*To whom correspondence should be addressed. Tel: +380 442000337; Fax: +380 445260759; Email: shalak@imbg.org.ua

© The Author(s) 2022. Published by Oxford University Press on behalf of Nucleic Acids Research.
This is an Open Access article distributed under the terms of the Creative Commons Attribution-NonCommercial License (http://creativecommons.org/licenses/by-nc/4.0/), which permits non-commercial re-use, distribution, and reproduction in any medium, provided the original work is properly cited. For commercial re-use, please contact journals.permissions@oup.com

Downloaded from https://academic.oup.com/nar/article/50/16/9490/6667655 by guest on 17 January 2025

aggregation propensity of this complex, its structural characterization appeared to be a difficult task.

In this study, we decipher a quaternary architecture of the human eEF1B complex containing α, β and γ subunits. We show that eEF1Bβ self-associates in a stable trimer and its leucine-zipper motif is responsible for trimerization. eEF1Bγ carries distinct binding sites for the eEF1Bα and eEF1Bβ subunits and interacts with them in equimolar stoichiometry. Hence, eEF1Bα, eEF1Bβ and eEF1Bγ specifically associate into a heterotrimeric complex, eEF1B$(\alpha\beta\gamma)_3$, which encompasses six highly conserved GEF domains. We suggest that such multi-GEF assembly may ensure the efficient restoration of the GTP-bound eEF1A conformation for the translating ribosomes in higher eukaryotes.

MATERIALS AND METHODS

Protein expression and purification

The recombinant plasmid expressing N-terminally His-tagged full-length human eEF1Bα was prepared as follows: eEF1Bα ORF was excised from the pGEX6P-1/eEF1Bα construct (14) and cloned into the pET28α(+) vector (Novagene, Madison, WI, USA). The recombinant protein was purified to homogeneity by a two-step chromatographic procedure: affinity chromatography on a Ni-NTA column (Qiagen, Valencia, CA, USA) and anion-exchange chromatography on a HighTrapQ column (GE Healthcare, Buchinghamshire, UK) using linear NaCl gradient from 250 to 450 mM. The expression and purification procedures for eEF1Bα(19–225) (14); for full-length human eEF1Bγ and its truncated form eEF1Bγ(229–437) (15); for full-length eEF1Bβ and its truncated forms eEF1Bβ(43–281) and GST-eEF1Bβ(78–118) (16) were previously published.

Analytical gel filtration of proteins and protein complexes

The interaction between different proteins partners was studied by size-exclusion chromatography on a Superose 6 HR 10/30 column (24 ml, GE Healthcare) as previously described in (14,16). For the formation of binary eEF1Bαγ and eEF1Bβγ, and ternary eEF1Bαβγ complexes, the respective purified full-length proteins were mixed in buffer containing 25 mM Tris–HCl, pH 7.5, 150 mM NaCl, 10% glycerol, 5 mM 2-mercaptoethanol in the final volume 0.12 ml and incubated for 5 min at 37°C. Then the protein mixture was centrifuged at 16 000 g for 15 min (RT) and loaded onto a Superose 6 HR 10/30 column. The final concentration of subunits in the binary complexes incubation mixtures was 10 μM and in the ternary complex incubation mixture was 8 μM. The interaction of full-length eEF1Bγ with the N-terminally truncated forms of eEF1Bα and eEF1Bβ, as well as the interaction of full-length eEF1Bα and eEF1Bβ with the C-terminal domain of eEF1Bγ were examined in the same way as described for the full-length proteins.

Analytical ultracentrifugation

Analytical ultracentrifugation (AUC) experiment was performed using a ProteomeLab XL-I analytical ultracentrifuge (Beckman-Coulter, Indianapolis, USA), equipped with An-60 Ti analytical rotor, using absorbance optics at 280 nm as described previously (14). Briefly, in the sedimentation velocity experiments, protein sample (400 μl) and buffer reference (410 μl) solutions were loaded onto 12 mm double-sector Epon charcoal-filled centerpieces (Beckman-Coulter). For each experiment, the rotor speed and temperature are indicated in the figure legends. The sedimentation velocity multiple scans at various time-points were fitted to a continuous size distribution model using Sedfit (17). All size distributions were solved and regularized at a confidence level of 0.95 by maximum entropy, using the best-fit mean anhydrous frictional ratio (f/f_0). We calculated also a hydrodynamic parameter S_{max}/S that allows evaluating the shape of the proteins and the protein complexes. In this ratio, S_{max} is the maximum possible sedimentation coefficient for a protein of the given mass, corresponding to a sphere of the minimum diameter to contain this mass without water, and S is the sedimentation coefficient $S_{20,w}$ for the individual protein or protein complex estimated by size-distribution analysis. S_{max} was calculated using the formula $S_{max} = 0.00361(M_r)^{2/3}$, where M_r is the molecular mass of the protein or protein complex in Daltons. S_{max}/S is in the range from 1.5 to 1.9 for moderately elongated proteins and from two to three for highly elongated proteins (18).

The sedimentation equilibrium experiments were done as described previously (14). Briefly, the protein samples (0.1 ml) were loaded into the sample channels, and a buffer solution (0.11 ml) was loaded into reference channels of six-channel Epon charcoal-filled centerpieces (Beckman–Coulter). For each experiment, the rotor speed and temperature are indicated in the figure legends. The sedimentation equilibrium absorbance data were collected every four hours. The scan obtained at a single rotor speed or the scans obtained at different rotor speeds (multispeed equilibrium data) were then fitted to a non-interacting discrete species model assuming a single species by using SEDPHAT (19) with Equation (1):

$$A_R = c_{r0}\varepsilon d \exp\{[M(1-\bar{\upsilon}\rho)\omega^2/2RT](r^2 - r_0^2)\} \quad (1)$$

in which r denotes the distance from the center of rotation; r_0 is the arbitrary reference radius; ω is the angular velocity; T is the absolute temperature of the rotor; R is the gas constant; $\bar{\upsilon}$ is the partial specific volume; ρ is the solvent density; ε is the extinction coefficient; d is the optical path length, and c_{r0} is the concentration at the reference radius. For a multispeed global data analysis at each channel, a single base-line parameter was included as a floating parameter common to all rotor speeds. The time-invariant and radial-invariant noise was also fitted for better fitting quality.

If the experimental data could not be fitted to the single species model, the monomer–dimer equilibrium model in SEDPHAT corresponding to Equation (2) was applied:

$$A_R = c_{r0}\varepsilon d \exp\{[M(1-\bar{\upsilon}\rho)\omega^2/2RT](r^2 - r_0^2)\} + K_a c_{r0}^2 \varepsilon d \exp\{[2M(1-\bar{\upsilon}\rho)\omega^2/2RT](r^2 - r_0^2)\} \quad (2)$$

in which K_a denotes the association constant of the dimer.

The buffer solution used for the sedimentation velocity and equilibrium experiments contained 25 mM Tris–HCl, pH 7.5, 150 mM NaCl, 5% glycerol (v/v)

Downloaded from https://academic.oup.com/nar/article/50/16/9490/6667655 by guest on 17 January 2025

and 1 mM dithiothreitol. The solvent density of 1.0216 g/cm^3 and viscosity of 0.01962 Poise at 2.3°C, and 1.02164 g/cm^3 and 0.01857 Poise at 4°C were calculated using Sednterp software (https://www.spinanalytical.com/auc-software.php). Before analytical ultracentrifugation, the individual eEF1Bα, eEF1Bβ, eEF1Bγ proteins and eEF1Bαγ, eEF1Bβγ, eEF1Bαβγ complexes were additionally purified on a Superose 6 HR 10/30 column (GE Healthcare) equilibrated in the buffer solution specified above.

Partial specific volume (cm^3/g) and extinction coefficient (M^{-1}cm^{-1}) for full-length eEF1Bβ were calculated using SEDNTERP software to be 0.72259 and 22 590, respectively; those for GST-eEF1Bβ(7–118) were 0.73865 and 43 110; those for eEF1Bβ(117–281) were 0.72446 and 14 110; those for eEF1Bγ were 72 288 and 87 230; those for the eEF1Bαγ complex (1:1) were 0.72225 and 117 300; those for the eEF1Bβγ complex (1:1) were 0.72274 and 109 820; those for the eEF1Bαβγ complex (1:1:1) were 0.72330 and 139 855. All sedimentation velocity and equilibrium graphs were prepared in GUSSI program (version 1.0.8d, Chad Brautigam, UT Southwestern).

Hydrogen–deuterium exchange coupled to mass spectrometry (HDX-MS)

The HDX-MS experiments were carried out as previously described in (20). Briefly, freshly prepared individual eEF1Bα, eEF1Bβ and eEF1Bγ proteins were additionally purified on a Superose 6 HR 10/30 column (GE Healthcare), dialyzed (25 mM Tris–HCl, pH 7.5, 150 mM NaCl, 55% glycerol and 5 mM 2-mercaptoethanol) and kept at –20°C. The respective protein complexes were prepared as follows: 10 μM of each subunit were mixed and incubated for 5 min at 37°C, then concentrated on the AmiconUltra-4 (50 kDa, Merck) membrane to the volume of 200 μl and injected onto a Superose 6 HR 10/30 column. The most concentrated fractions of each complex were combined and dialyzed against the same buffer indicated above. The initial concentrations of samples used for the HDX-MS experiments: eEF1Bα – 56.6 μM, eEF1Bβ – 36.4 μM, eEF1Bγ – 46 μM, eEF1Bαγ – 39.2 μM, eEF1Bβγ – 35 μM, eEF1Bαβγ – 53.6 μM.

A 5 μl aliquot of the individual protein or the protein complex stock solution was combined with 45 μl of D_2O (99.8% Cambridge Isotope Laboratories) reaction buffer containing 25 mM Tris–HCl pH 7.5, 150 mM NaCl, 150 mM KSCN, and 5 mM 2-mercaptoethanol and incubated at 20°C for 10 s, 1 min, 5 min, 25 min or 2.5 h before quenching by addition 10 μL of 2 M glycine pH 2.5 in D_2O. The samples were immediately frozen in the liquid nitrogen and stored at –80°C until use. Out-time point controls were performed by incubation of the protein in D_2O buffer for 24 h to obtain maximum exchange for each peptide and then, quenched with 10 μl of 2 M glycine. The deuteration level was calculated and denoted as 100% exchange. Mass spectrometry measurements and data analysis were done as described in (21). The experiments were repeated three times, the results represent the mean of all replicates. The peptides were identified using ProteinLynx Global Server software (PLGS, Waters) and further filtered in the DynamX 3.0 program (Waters) with the following acceptance criteria: minimum intensity threshold of 3000, minimum products per amino acids of 0.3, minimum score of 7.5 and theoretical value for parent ions below 10 ppm. The values reflecting experimental mass of each peptide in all possible states, replicates, time points and charge states were exported from the DynamX 3.0 and further data analysis was carried out using in house written script (21).

To depict the kinetic of exchange for each peptide, we built a plot with an experimentally measured level of H/D exchange (in %) at 10 s, 1, 5, 25 and 150 min. The obtained curve dissects the kinetic plot into two parts. The area above the kinetic curve was integrated overall incubation time and divided by the whole area of the kinetic plot. The obtained value we call 'aggregated protection' of the peptide, which may be within the range from 0 (no protection) to 1 (full protection). We distinguish three categories of peptides with respect to their aggregated protection value: <0.05—the absence of aggregated protection; >0.05 and <0.15—weak aggregated protection; >0.15—high aggregated protection. The peptides with no and weak aggregated protection belong to dynamically structured regions while the peptides with high aggregated protection—to rigidly structured regions. 'Differential aggregated protection' graph shows the difference between the values of aggregated protection measured for the same peptide in different states, namely free and bound to a partner. A positive value of the differential aggregated protection indicates that the peptide becomes more protected in the complex with a partner, while a negative value means a decrease of protection.

Native gel electrophoresis of protein complexes

The eEF1Bαγ complex was prepared as follows: 5 μM eEF1Bα was mixed with increasing (2–7 μM) concentrations of eEF1Bγ and vice versa 5 μM eEF1Bγ was mixed with increasing (2–7 μM) concentrations of eEF1Bα in buffer containing 25 mM Tris–HCl, pH 7.5, 150 mM NaCl, 10% glycerol, 5 mM 2-mercaptoethanol in a final volume 20 μl. The eEF1Bβγ complex was prepared in the same way.

The complexes between eEF1Bβ and eEF1A2 were prepared as follows: 10 μM eEF1A2 was mixed with increasing (0.36–21 μM) concentrations of eEF1Bβ and 150 μM GDP in buffer containing 25 mM Tris–HCl, pH 7.5, 150 mM NaCl, 10% glycerol, 5 mM 2-mercaptoethanol in a final volume 25 μl.

The eEF1Bαβγ complex was prepared by mixing three individual subunits at 6 μM concentrations in buffer containing 25 mM Tris–HCl, pH 7.5, 150 mM NaCl, 10% glycerol, 5 mM 2-mercaptoethanol and incubated for 5 min at 37°C. Titration of the eEF1Bαβγ complex by eEF1A2 was performed as follows: 3 μM eEF1Bαβγ complex was mixed with increasing (3–30 μM) concentrations of eEF1A2 and 150 μM GDP in buffer indicated above in a final volume 20 μl.

The protein mixtures were incubated for 5 min at 37°C and loaded onto a 1.5% agarose gel (for eEF1B and eEF1Bβγ complexes) and 1% agarose gel (for the eEF1A2-eEF1Bβ and eEF1A2-eEF1Bαβγ complexes) containing 89 mM Tris-borate, pH 8.3. The gel was run at 100 V/31–34

Downloaded from https://academic.oup.com/nar/article/50/16/9490/6667655 by guest on 17 January 2025

mA for 2–3 h at room temperature, then stained and photographed as described previously (14).

Dynamic light scattering

To measure a hydrodynamic radius of eEF1Bα we used the Dynamic Light Scattering technique (DLS) and the Adaptive Correlation approach described in (22). DLS experiments were performed using a Zetasizer Nano ZS (Malvern Panalytical Ltd, UK) at 25°C with a scattering angle of 173° in air. All samples (1 ml) were measured in a 1 cm glass cuvette. Briefly, three measurements for each eEF1Bα concentration were done. Each measurement included 30 sub-measurements with duration time of 1, 2 and 3 s. The steady-state sub-measurements were analyzed using cumulants analysis. The correlation functions of the steady-state sub-measurements were averaged to report the hydrodynamic radius (Z_{ave}) and polydispersity index (PdI) values. Z_{ave} values were obtained for four different eEF1Bα concentrations. R_{H0} – a hydrodynamic radius of eEF1Bα at the infinite dilution was calculated from the plot of Z_{ave} versus eEF1Bα concentration by extrapolation to zero concentration.

Prior to the DLS measurements, eEF1Bα was subjected to gel filtration on a Sephacryl S200 column (GE Healthcare) equilibrated in buffer, containing 25 mM Tris–HCl, pH 7.5, 150 mM NaCl, 5% glycerol (v/v) and 1 mM dithiothreitol. Fractions with the highest eEF1Bα concentration were centrifuged at 16 000 g for 2.5 hours at 10°C. Buffer was prepared using ultrapure deionized water, filtered (pore size 0.2 μm) and degassed.

Homology structure modeling and molecular docking

The unstructured regions in proteins we predicted by a MetaDisorderMD2 meta-server (23). The 3D structure models of eEF1Bα, eEF1Bβ (monomer) and eEF1Bγ were generated by Modeller (version 9.14) (24). The unstructured regions in the proteins were modeled using the loops reconstruction option in this program (25). Further high-resolution protein structure refinement for the best predicted 3D model was done by ModRefiner (26). Additionally, all structures were verified using the MolProbity web server (http://molprobity.biochem.duke.edu) (27) and refined by YASARA Energy Minimization Server (28). Visualization and analysis of the protein were done using UCSF Chimera (29).

To model full-length eEF1Bα we used the available structures of its isolated GEF domain (PDB ID: 1B64), its N-terminal domain complexed with the GST-like domain of eEF1Bγ (PDB ID: 5DQS) and highly homologous C-terminal region of eEF1Bβ (PDB ID: 2N51) as templates. From the ensemble of eEF1Bα conformations created by Modeller, we selected a model with the hydrodynamic radius that matches the experimentally measured R_{H0} value.

eEF1Bβ monomer was modeled using the available structure of its C-terminal region (PDB ID: 2N51) and reported model of its N-terminal domain possessing a dynamic α-helical organization (20). Five structural ensembles with 40 structures in each were generated by Modeller. The best five structures were selected from each ensemble using the Discrete Optimized Protein Energy (DOPE) and Modeller Objective Function (MOF) scores (30) (Supplementary, Table S1). The model 1, which has the best DOPE score (Supplementary Table S1), was chosen for further computing of the eEF1Bβ trimer. Symmetric docking of the eEF1Bβ monomers was done by the SymmDock webserver (31) taking into account that the LZ-motif is responsible for trimerization. The best model of eEF1Bβ trimer was chosen according to the geometric shape complementarity score and then refined by the YASARA Energy Minimization Server (the energy value – 500 712 kJ/mol and energy score – 0.21).

Homology modeling of eEF1Bγ was performed using a structure of its C-terminal domain (PDB ID: 1PBU), structures of its GST-like N-terminal domain complexed with the N-terminal domain of eEF1Bα (PDB ID: 5DQS) and with the short N-terminal peptide of eEF1Bβ (PDB ID: 5JPO) as templates. From the ensemble of eEF1Bγ conformations created by Modeller, we selected one model with the extended conformation taking into account a moderately elongated shape of eEF1Bγ in solution.

In silico docking between the eEF1Bβ and eEF1Bγ proteins was performed using PatchDock web server (32). The N-terminal domain (residues 1–77) of eEF1Bβ was set as ligand and the N-terminal domain (residues 1–210) of eEF1Bγ was set as receptor. The coordinates for eEF1Bβ(1–77) and eEF1Bγ(1–210) were from the respective atomistic models mentioned above. Docking results were individually inspected and compared with HDX-MS data for the eEF1Bβγ complex. The best high scoring model was used for the refinement and re-scoring step with FireDock (33). Analysis and visualization of the molecular interfaces between proteins were performed by Cocomaps web server (34,35). The docking procedure between the full-length eEF1Bβ and eEF1Bγ proteins was done in the same way.

RESULTS

Structural organization of eEF1Bα

eEF1Bα is a monomeric non-globular protein with a moderately elongated shape (14). Two conserved regions can be delineated in its primary structure: the non-catalytic N-terminal domain (residues 1–62) and the catalytic C-terminal region (residues 97–225). Both parts are connected by a non-conserved linker (Figure 1A). The structure of the C-terminally located GEF domain (residues 135–225) of human eEF1Bα was solved by NMR (36). The presence of the structurally independent α-helical central acidic region (CAR) upstream the GEF domain in human eEF1Bα was suggested based on the structure of a long eEF1Bβ C-terminal fragment, which amino acid sequence is highly homologous to eEF1Bα (37). Besides, the crystallographic data on the eEF1Bα N-terminal domain (residues 1–90) complexed with the GST-like domain of eEF1Bγ are present in the PDB database (PDB ID: 5DQS). However, the complete three-dimensional structure of full-length eEF1Bα has never been reported.

MetaDisorderMD2 meta-server predicts high disorder probability for fragment 64–139 that includes the linker region and the CAR domain (Figure 1A and B). To confirm this prediction, we characterized the structural dynam-

Downloaded from https://academic.oup.com/nar/article/50/16/9490/6667655 by guest on 17 January 2025

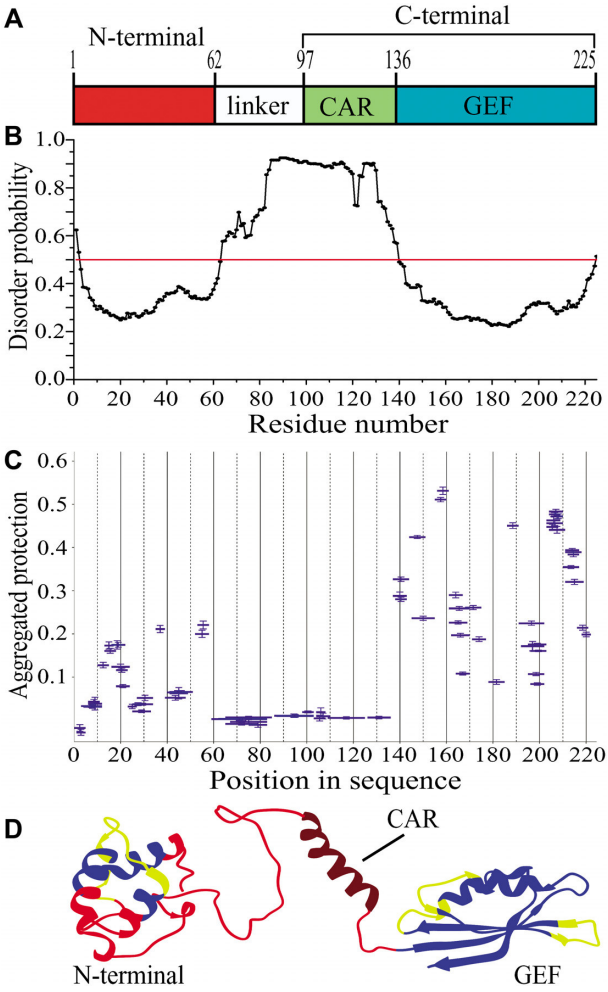

Figure 1. Structural organization of full-length eEF1Bα. (**A**) Schematic representation of the eEF1Bα domain structure. Abbreviations: CAR – the central acidic region, GEF – the guanine-nucleotide exchange factor domain. (**B**) Prediction of the disordered regions in eEF1Bα. All residues whose disorder probability is over 0.5 (red line) are considered as disordered. (**C**) The aggregated protection plot of the eEF1Bα peptides. The aggregated protection values for peptides (mean ± SD, $n = 3$ measurements) are plotted versus their position in the protein sequence. (**D**) The 3D model of eEF1Bα colored according to the HDX-MS data. Red color indicates unprotected and unstructured regions (<0.05), dark red – the CAR domain that displays no protection, but is predicted to have α-helical organization, yellow – weakly protected dynamic segments (0.05–0.15), blue – highly protected rigidly structured regions (>0.15).

ics of eEF1Bα by the method of hydrogen-deuterium exchange coupled to mass spectrometry (HDX-MS) (38). The unstructured and highly dynamic regions exchange with D_2O very rapidly (39). In the aggregated protection plot of eEF1Bα, the peptides covering the linker region and the CAR domain show near zero protection against H/D exchange (Figure 1C). The majority of peptides from the GEF domain display high protection except few weakly protected segments. In turn, unprotected, weakly and highly protected peptides are present in the N-terminal domain (Figure 1C). Thus, the linker region and the CAR domain are highly dynamic that is consistent with the predicted disorder probability profile for this protein (Figure 1B and C).

We created a 3D model of eEF1Bα (Figure 1D) that matches the experimentally measured hydrodynamic radius, $R_{H0} = 3.35 \pm 0.24$ nm, for this protein (Supplementary Figure S1) and agrees well with the HDX-MS data. The peptides comprising the core of the N-terminal three-helix bundle are protected against H/D exchange (Figure 1D, colored in blue), while the loop regions with the adjacent parts of α-helices show weak or no protection suggesting their dynamic conformation (Figure 1D, colored in yellow and red, respectively). The linker region is disordered that is consistent with the absence of protection against H/D exchange (Figure 1C and D, colored in red). Notably, no protection was detected for the peptides composing the CAR domain – an isolated α-helical element in eEF1Bα (Figure 1C and D). This α-helix is located between structurally dynamic linkers and may undergo local fluctuations that result in H-bonds breaking and exposure of the amide hydrogens to attack by deuterium (40). The conventional HDX method used in this study most probably is not sensitive enough to detect weakly structured (weak hydrogen bonding) and/or rapidly fluctuating secondary elements (41). We colored the unprotected α-helical CAR domain in dark red in order to distinguish it from the unstructured regions (Figure 1D). The GEF-domain represents a compact and tightly packed two-layer α/β sandwich in which most of peptides have substantial protection (Figure 1D, colored in blue) excluding few loop regions, which probably are conformationally flexible (Figure 1D, colored in yellow).

Hence, we established that eEF1Bα consists of two rigidly structured domains connected by a long dynamic linker region.

Structural organization of eEF1Bβ

It has been shown that eEF1Bβ forms oligomers in solution (12,16). To elucidate the exact number of monomers in the oligomeric eEF1Bβ structure, we performed analytical ultracentrifugation experiments. eEF1Bβ sedimented as one major species with a molecular mass of 92 ± 4 kDa calculated for the best-fit frictional ratio $f/f_0 = 1.97 \pm 0.07$ (Supplementary Figure S2A). The hydrodynamic parameter S_{max}/S was estimated to be 2.02 ± 0.04 that is characteristic of highly elongated proteins (18). Analysis of the sedimentation equilibrium data (Supplementary Figure S2B) gave the molecular mass value of 97.6 ± 2.4 kDa that corresponds to the theoretical mass of the eEF1Bβ trimer (95.7 kDa). Therefore, we conclude that recombinant eEF1Bβ self-associates in a stable trimer with a highly elongated shape.

Four conserved regions can be delineated in the primary structure of eEF1Bβ (Figure 2A): the N-terminal domain, leucine-zipper (LZ) motif, CAR domain, and GEF domain. The isolated N-terminal domain is a monomer with a dynamic α-helical organization (20). The structure of the C-terminal fragment (residues 153–281) including CAR and GEF domains was solved by NMR (37). This fragment is also monomeric in solution. Thus, it leaves a trimer-forming role to the middle part of the eEF1Bβ molecule that comprises the LZ motif and the linker region (Figure 2A). Previously, we have reported that the chimeric GST-eEF1Bβ(78–118) protein, which consists of the LZ-motif and GST,

Downloaded from https://academic.oup.com/nar/article/50/16/9490/6667655 by guest on 17 January 2025

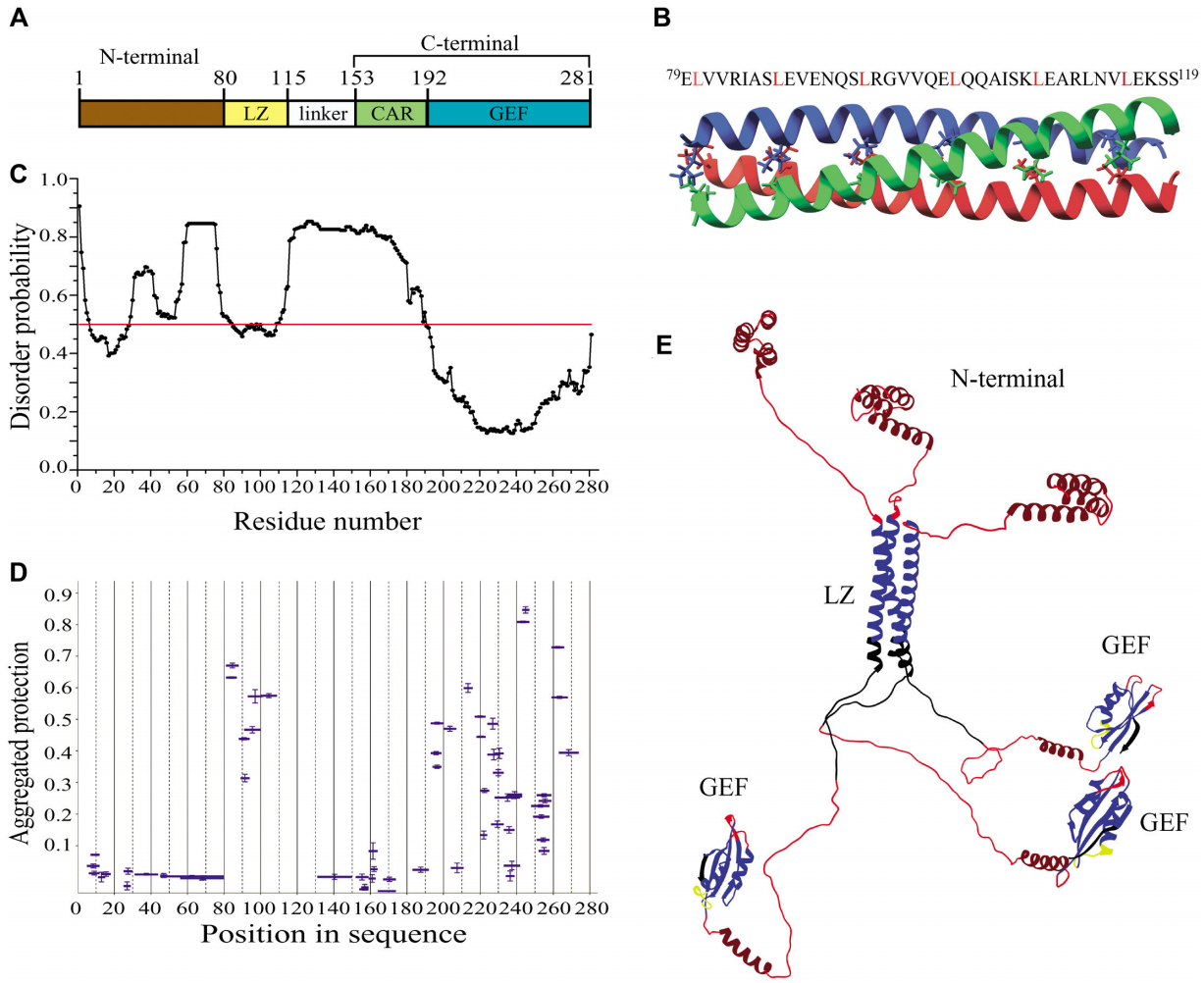

Figure 2. Structural organization of full-length eEF1Bβ. (**A**) Domain organization of eEF1Bβ. Abbreviations: LZ – the leucine-zipper motif, CAR – the central acidic region, GEF – the guanine-nucleotide exchange factor domain. (**B**) Structural model of the LZ-motif built by CCBuilder 2.0. Three α-helices twist around each other to form a bundle with following parameters: radius – 5.6 Å, interface angle – 19º, pitch – 61.8 Å, number of residues per turn – 3.62. The model has the lowest (–425.6 kJ/mol) BUDE score (the interaction energy between the helices). All leucine residues involved onto assembly of the α-helical coiled-coils are shown by colored sticks. The amino acid sequence of the LZ-motif is shown on the top of the figure. (**C**) Prediction of the disordered regions in eEF1Bβ. All residues whose disorder probability is over 0.5 (red line) are considered as disordered. (**D**) The aggregated protection plot of eEF1Bβ peptides. The aggregated protection values for peptides (mean ± SD, n = 3 measurements) are plotted versus they position in the protein sequence. (**E**) The 3D-model of eEF1Bβ colored according to the HDX-MS data. Red color indicates unprotected and unstructured regions (<0.05), dark red – the CAR domain and the N-terminal α-helixes that display no protection, but are predicted to have α-helical organization, yellow – weakly protected dynamic segments (0.05-0.15), blue – highly protected rigidly structured regions (>0.15), black – the regions with missing peptides.

forms oligomers *in vitro* (16). Here, using sedimentation velocity and equilibrium approaches we established that GST-eEF1Bβ(78–118) forms trimers and hexamers in solution (Supplementary Figure S3) confirming the intrinsic trimerization capacity of LZ-motif. Additionally, the possible contribution of the linker region into eEF1Bβ self-association was tested by using its truncated form, eEF1Bβ(117–281), that comprises the linker region, CAR and GEF domains, but not LZ-motif (Figure 2A). Sedimentation equilibrium analysis proved that eEF1Bβ(117–281) is a monomeric protein (Supplementary Figure S3C). Hence, we conclude that the linker region does not mediate eEF1Bβ self-association. Altogether, the obtained results clearly indicate that the LZ-motif is responsible for eEF1Bβ trimerization.

Typical LZ-motif consists of a periodic repetition of a leucine residue at every seventh position known as a heptad repeat and forms a continuous α-helix, which mediates dimerization and in some cases oligomerization of proteins (42,43). In the eEF1Bβ primary structure, a heptad repeat contains six leucine residues that occupy every seventh position and create a hydrophobic stripe along the helix (Figure 2B, upper part). This heptad repeat self-associates in the trimeric coiled-coil conformation (Figure 2B) according to CCBuilder software (44).

The LZ-motif, the GEF domain and a part of the N-terminal domain were predicted by MetaDisorderMD2 meta-server to be ordered, whereas the long linker region between the LZ-motif and the GEF domain, and two short regions within the N-terminal domain—disordered (Figure 2C). This prediction was further supported by the HDX-MS analysis of eEF1Bβ (Figure 2D). All peptides that constitute the LZ-motif display substantial protection against

Downloaded from https://academic.oup.com/nar/article/50/16/9490/6667655 by guest on 17 January 2025

H/D exchange indicating a rigidly structured region. The most of the GEF domain peptides are highly protected except few weakly protected and unprotected segments (Figure 2D). The N-terminal domain, linker region and CAR domain display near zero protection indicating highly dynamic structures (Figure 2D). It has been shown that the CAR domain is an independent and structurally dynamic element of eEF1Bβ (37). The absence of protection for the N-terminal domain is also in agreement with the previous result obtained on the isolated eEF1Bβ(1–77) confirming its rapidly fluctuating tertiary structure (20). As mentioned above, the sensitivity of the conventional HDX method may be not sufficient to detect weakly structured and/or rapidly fluctuating secondary elements. Using homology modeling, we built an atomistic model of full-sized eEF1Bβ (Figure 2E) that correlate with the HDX-MS (Figure 2D) and analytical ultracentrifugation data (Supplementary Figure S2A). In Figure 2E, the elements of the CAR and N-terminal domain, which are highly dynamic according to HDX-MS but predicted to possess α-helical organization, are colored in dark red in order to differentiate them from the factual unstructured regions (colored in red). The tightly packed LZ-motif and GEF-domain are colored in blue except for weakly protected and unprotected loop regions of the latter, which most probably are conformationally flexible (Figure 2E, colored in yellow and red, respectively).

Thus, we conclude that eEF1Bβ is an elongated trimeric molecule, in which the monomers are kept together by the α-helical coil-coiled bundle. The C-terminal fragment of each monomer comprising highly dynamic linker and CAR, and rigidly structured GEF domain extends from one side of this bundle. Three α-helical N-terminal fragments are located at the opposite side.

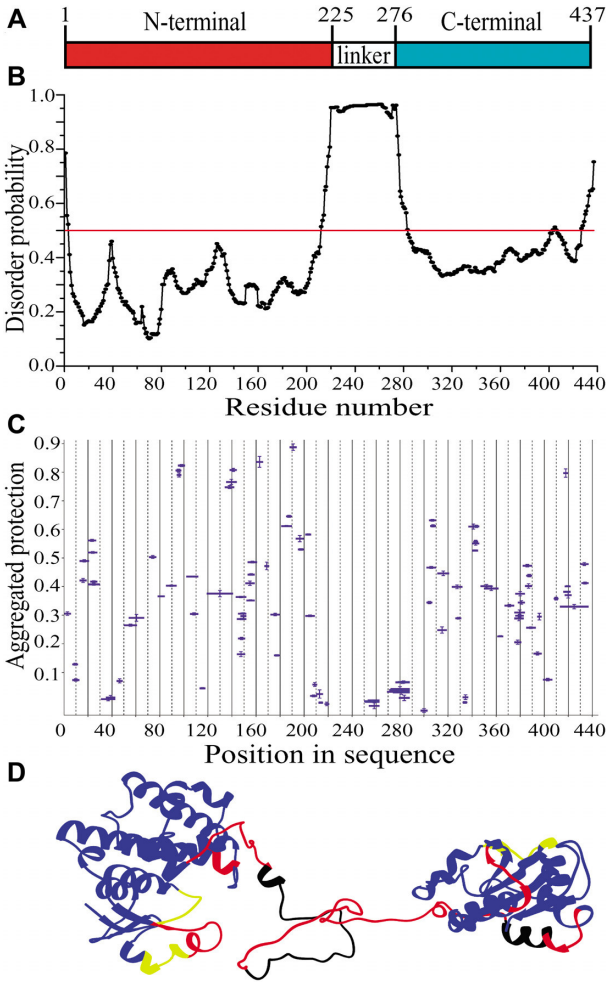

Figure 3. Structural organization of full-length eEF1Bγ. (**A**) Domain organization of eEF1Bγ. (**B**) Prediction of the disordered region in eEF1Bγ. All residues whose disorder probability is over 0.5 (red line) are considered as disordered. (**C**) The aggregated protection plot of the eEF1Bγ peptides. The aggregated protection values for peptides (mean ± SD, $n = 3$ measurements) are plotted versus their position in the protein sequence. (**D**) A 3D model of eEF1Bγ colored according to the HDX-MS data. Red color indicates unprotected and unstructured regions (<0.05), yellow – weakly protected dynamic segments (0.05–0.15), blue – highly protected rigidly structured regions (>0.15), black – the regions with missing peptides.

Structural organization of eEF1Bγ

Purified recombinant eEF1Bγ has strong self-aggregation propensities. Its apparent molecular mass varies from 100 to 1000 kDa according to analytical size-exclusion chromatography (12,15,45). Here, we used the analytical ultracentrifugation analysis to describe the oligomeric state of full-length eEF1Bγ in more detail. The sedimentation velocity experiment revealed minor and major eEF1Bγ sedimentating species of 50 and 91 kDa, calculated for the best-fit frictional ratio $f/f_0 = 1.65$, respectively (Supplementary Figure S4A). These values are close to those of monomer (52.6 kDa) and dimer (105.2 kDa). The calculated hydrodynamic parameter S_{max}/S of 1.74 for the monomer and 1.84 for the dimer indicates a moderately elongated shape of both species (18). The sedimentation equilibrium experiment showed that depending on protein concentration eEF1Bγ may form a mixture of dimeric and tetrameric forms, stable dimers, and a mixture of monomeric and dimeric forms (Supplementary Figure S4B). Different values of the apparent dissociation constant obtained at different protein concentrations and different centrifugation velocities indicate that self-association of eEF1Bγ is irreversible (Supplementary Figure S4B).

eEF1Bγ consists of two conserved domains connected by a lysine-rich linker (46) (Figure 3A). Importantly, MetaDisorderMD2 meta-server predicts with the highest probability for this inter-domain linker region (residues 215–280) to be disordered (Figure 3B). The HDX-MS analysis also showed the absence of protection against H/D exchange for this region (Figure 3C) confirming its high structural dynamics. In contrast, most peptides from the N- and C-terminal domains are substantially protected with few exceptions (Figure 3C).

Until now, the 3D structure of full-length eEF1Bγ has not been reported. However, the structure of its isolated C-terminal domain (PDB ID: 1PBU) has been published (46) and the structures of its GST-like N-terminal domain in the complex with both the N-terminal domain of eEF1Bα (PDB ID: 5DQS) and short N-terminal peptide of eEF1Bβ (PDB ID: 5JPO) have been deposited in the PDB database. Using homology modeling we built an atomistic model of

Downloaded from https://academic.oup.com/nar/article/50/16/9490/6667655 by guest on 17 January 2025

full-sized eEF1Bγ (Figure 3D) that is consistent with the HDX-MS data. Indeed, the majority of peptides from both folded domains display significant protection against H/D exchange (Figure 3C and D, colored in blue). Only few loop segments in both domains display weak or no protection probably due to their local conformational fluctuations (Figure 3D, colored in yellow and red, respectively). The long inter-domain linker region is disordered that also correlates with the absence of protection (Figure 3D, colored in red). Thus, we conclude that eEF1Bγ is a non-globular protein with a moderately elongated shape, which consists of two rigidly structured domains connected by a long highly dynamic linker region.

Reconstitution of the eEF1B complex

Several techniques were employed to estimate the stoichiometry of the subunits in the binary eEF1Bαγ and eEF1Bβγ, and ternary eEF1Bαβγ complexes. First, the native gel electrophoresis showed the formation of both the eEF1Bαγ and eEF1Bβγ complexes at equimolar concentrations of subunits (Supplementary Figure S5). Then, the molecular masses of the complexes were estimated by analytical size-exclusion chromatography, sedimentation velocity and equilibrium analysis (Figure 4, Supplementary Figures S6 and 7).

The eEF1Bαγ complex (1:1 subunit ratio) demonstrated the apparent molecular mass of about 400 kDa in the gel filtration experiment (Figure 4A) that is five times higher than its theoretical value (79.9 kDa). Sedimentation velocity analysis of the same complex showed the presence of two protein species sedimenting with S_w = 1.973 S ($S_{(20,w)}$ = 3.998 S), and S_w = 2.716 S ($S_{(20,w)}$ = 5.503 S) that correspond to the molecular masses of 80 and 130 kDa, respectively, calculated with the best-fit friction ratio f/f_0 = 1.68. These values are close to those of the heteromeric eEF1Bαγ and heterodimeric eEF1B$(\alpha\gamma)_2$ forms of this complex (Figure 4B, Supplementary Figure S6A). The sedimentation equilibrium analysis revealed the presence of the stable eEF1B$(\alpha\gamma)_2$ complex and eEF1Bαγ-eEF1B$(\alpha\gamma)_2$ mixture (Supplementary Figure S6B).

The eEF1Bβγ complex (1:1 subunit ratio) showed the apparent molecular mass of about 1000 kDa in analytical gel filtration (Figure 4C) that is almost twelve times higher than its theoretical value (84.4 kDa). Sedimentation velocity analysis of the same complex revealed the presence of two major protein species sedimenting at S_w = 4.30 S ($S_{(20,w)}$ = 8.729 S), and S_w = 7.66 S ($S_{(20,w)}$ = 15.551 S) that correspond to the molecular masses of 250 and 590 kDa, respectively (Figure 4D, Supplementary Figure S6C), calculated with the best-fit friction ratio f/f_0 = 1.64. The molecular mass of the first species is close to the value of a heterotrimer eEF1B$(\beta\gamma)_3$, whereas the second species represents supposedly a heterohexamer eEF1B$(\beta\gamma)_6$. Sedimentation equilibrium analysis of eEF1Bβγ confirmed the presence of the heterotrimer-heterohexamer mixture in solution (Supplementary Figure S6D). However, the presence of some admixtures of self-associated single subunits and/or species with other eEF1Bβγ stoichiometry cannot be excluded.

The ternary eEF1Bαβγ complex (1:1:1 subunit ratio) migrated as a single peak of more than 1 MDa during analytical gel filtration on a Superose 6HR (Figure 4E). Sedimentation velocity analysis of the same complex showed the presence of three protein species sedimenting at S_w = 3.588 S ($S_{(20,w)}$ = 6.965 S), S_w = 5.021 S ($S_{(20,w)}$ = 9.746 S), and S_w = 6.297 S ($S_{(20,w)}$ = 12.224 S) that correspond to the molecular masses of 200, 340 and 480 kDa, respectively (Figure 4F, Supplementary Figure S7A), calculated with the best-fit friction ratio f/f_0 = 1.85. Considering that the theoretical molecular mass of the heteromeric eEF1Bαβγ complex (1:1:1 ratio) is 111.8 kDa, the molecular mass of the major species (340 kDa) corresponds to a heterotrimer eEF1B$(\alpha\beta\gamma)_3$. The first and third sedimenting species remain undefined. Sedimentation equilibrium analysis of eEF1Bαβγ showed the presence of the heterotrimer-heterohexamer mixture in solution (Supplementary Figure S7B). Hence, the α, β and γ subunits of eEF1B preferably associate in a stable heterotrimeric complex as revealed by analytical ultracentrifugation. This is consistent with the observed 1:1 stoichiometric complex formation between the α and γ as well as β and γ subunits (Supplementary Figure S5). However, the higher order oligomers are also present in the *in vitro* preparation of this complex. Like in the case of eEF1B$(\beta\gamma)_3$, further oligomerization of eEF1B$(\alpha\beta\gamma)_3$ most probably is mediated by the eEF1Bγ subunit. We cannot exclude that some species with other eEF1Bαβγ stoichiometry may be present among higher order oligomers while the slowest sedimenting protein fraction may also contain self-associated single subunits. Of note, all complexes possess the moderately elongated shapes (18) (S_{max}/S = 1.68 for eEF1Bαγ, S_{max}/S = 1.73 for eEF1Bβγ, and S_{max}/S = 1.79 for eEF1Bαβγ) that also contributes to the overestimation of their molecular masses by the analytical gel filtration technique (Figure 4A-E).

Macromolecular architecture of the eEF1B complex

In order to map the interaction sites on the subunits involved in the eEF1B complex, we applied two approaches: the site-directed mutagenesis and HDX-MS. Deletion of the first 19 amino acids in eEF1Bα and the first 43 amino acids in eEF1Bβ completely abolished their interaction with full-length eEF1Bγ (Supplementary Figure S8A and B). As expected, eEF1Bγ(228–437), comprising the linker region and the C-terminal domain, interacts with neither full-length eEF1Bα nor eEF1Bβ (Supplementary Figure S8C and D), thus confirming the exclusive role of the eEF1Bγ N-terminal domain in eEF1B complex formation (9).

Next, the regions of the eEF1Bα, eEF1Bβ and eEF1Bγ subunits that contribute to the protein-protein binding sites was determined by HDX-MS. Usually, the interacting proteins create the binding interfaces with increased structural rigidity and/or decreased solvent accessibility that results in reducing of H/D exchange. To map the eEF1Bγ binding site on eEF1Bα and eEF1Bβ, we compared the peptide protection patterns of the isolated eEF1Bα and eEF1Bβ proteins and their complex with eEF1Bγ (Figure 5A and B). The 'differential aggregated protection' plots display the peptides that changed their protection. The majority of peptides composing the N-terminal domain, except the first

Downloaded from https://academic.oup.com/nar/article/50/16/9490/6667655 by guest on 17 January 2025

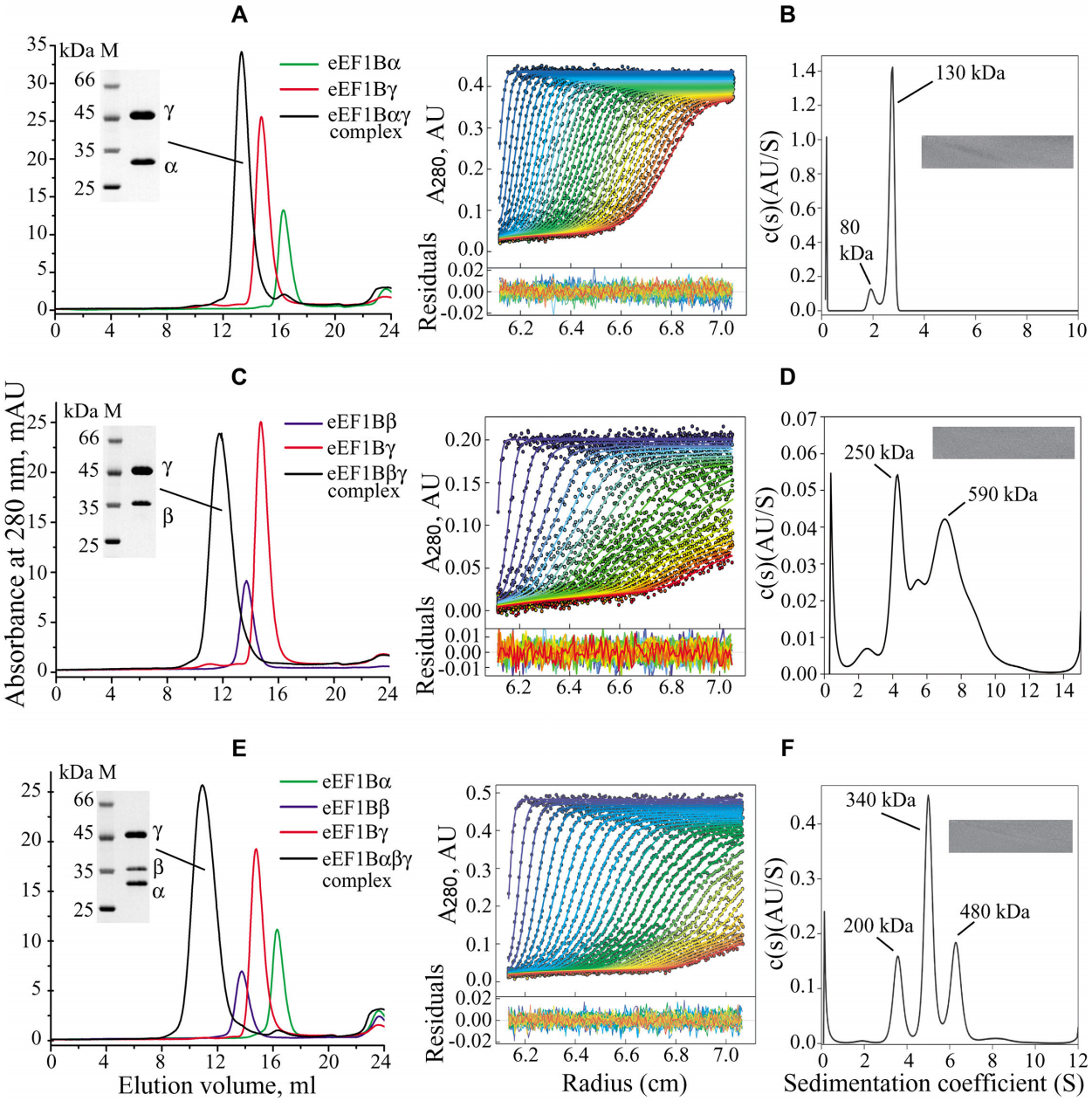

Figure 4. Size-exclusion chromatography and sedimentation velocity analysis of the eEF1Bαγ, eEF1Bβγ and eEF1Bαβγ complexes. (Plots **A, C** and **E**) 100 μl of 10 μM indicated binary and ternary complexes or individual subunits were injected into a Superose 6 HR column. Inset: SDS-PAGE of the binary and ternary complexes. The central fractions of each protein complex peak were combined, concentrated and loaded (5 μg) onto 12% polyacrylamide gels. (Plots **B, D** and **F**) Left: absorbance scans of the sedimentation velocity data (symbols show only every third data point of every third scan for clarity) and best-fit boundary model from the c(s) analysis (solid lines). Residuals are indicated. Right: continuous size distribution analysis, c(s), plotted as a function of sedimentation coefficient. Inset: 2D grayscale 'bitmap' residual plot shows a high quality of fit. The initial concentration of the complexes was: eEF1Bαγ – 0.3 mg/ml (3.8 μM), eEF1Bβγ – 0.15 mg/ml (1.9 μM), eEF1Bαβγ – 0.36 mg/ml (3 μM).

five amino acids, increase their protection against H/D exchange, while the other part of eEF1Bα remains unaffected (Figure 5C). This suggests that the entire N-terminal domain of eEF1Bα undergoes a global decrease in dynamics upon binding to eEF1Bγ (Figure 5E). In contrast, only the peptides encompassing a narrow region, residues 11–29, of eEF1Bβ increase their protection within eEF1Bβγ complex (Figure 5D and F). According to the biochemical data, eEF1Bγ binds the eEF1Bα and eEF1Bβ simultaneously (Figure 4E). Upon binding to eEF1Bα, the eEF1Bγ peptides covering the regions 144–161 and 170-190 became more protected (Figure 6A and C) that indicates their involvement in the formation of the eEF1Bα binding interface (Figure 6E). No significant difference of protection was observed for the C-terminal domain and the linker region (Figure 6C). Binding of eEF1Bβ to eEF1Bγ results in a dramatic increase of protection for the majority of peptides covering the N-terminal domain of the latter, indi-

Downloaded from https://academic.oup.com/nar/article/50/16/9490/6667655 by guest on 17 January 2025

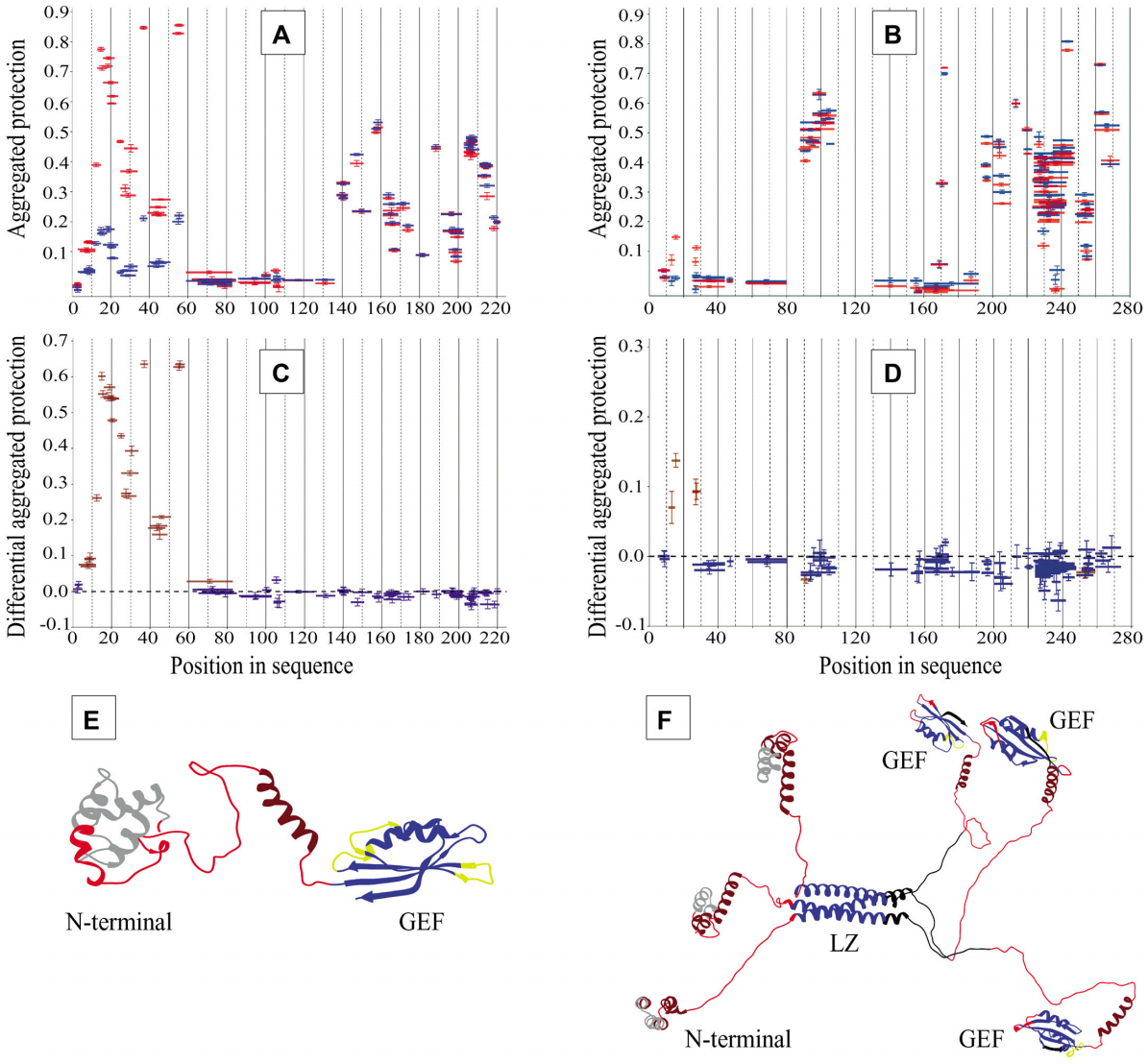

Figure 5. Mapping the protein-protein interactive surfaces on the eEF1Bα and eEF1Bβ subunits by HDX-MS. The aggregated protection of peptides derived from eEF1Bα (**A**) and eEF1Bβ (**B**) in a free state (blue color) and involved into the eEF1Bαγ and eEF1Bβγ complexes (red color) is depicted. The differential aggregated protection plots show the eEF1Bα (**C**) and eEF1Bβ (**D**) peptides that change their protection (brown color) against H/D exchange in the complex with eEF1Bγ (the difference is statistically significant for at least three or more incubation time-points). The peptides indicated in blue in the plots (**C**) and (**D**) do not change their protection. The regions of eEF1Bα (**E**) and eEF1Bβ (**F**) that change their aggregated protection values upon interaction with eEF1Bγ are painted in gray.

cating that upon interaction with eEF1Bβ the whole N-terminal domain of eEF1Bγ experiences the global increase of structural rigidity excluding the short region involved in the interaction with eEF1Bα (Figure 6B, D and F). The C-terminal domain and the linker region of eEF1Bγ remain unaffected (Figure 6D).

We also compared the HDX protection patterns of the binary eEF1Bαγ and eEF1Bβγ, and ternary eEF1Bαβγ complexes. The eEF1Bα and eEF1Bβ protection patterns in the eEF1Bαβγ complex do not significantly differ from those observed in the eEF1Bαγ and eEF1Bβγ complexes, respectively, as jugged by the differential aggregation protection plots of the ternary and binary complexes (Supplementary Figure S9A and B). However, a region comprising the residues 137–154 in the GEF domain of eEF1Bα display higher protection in the ternary complex as compared to the binary one (Supplementary Figure S9A). This fragment corresponding to the first β-strand of the GEF domain is not involved into direct interaction between eEF1Bα and eEF1Bγ. The observed decrease of deuterium uptake in this case may be attributed to the local conformational change in this region of eEF1Bα. In the case of eEF1Bβ, two regions slightly altered their protection in the ternary complex as compared to the binary one (Supplementary Figure S9B). A region comprising the residues 80–120 that corresponds to the LZ-motif increases its protection indicating a greater stabilization of the α-helical coil-coiled bundle in the ternary complex. Unlike eEF1Bα, a small region of eEF1Bβ (residues 192–200) that belongs to the first β-strand of the GEF domain displays lower protection in the

Downloaded from https://academic.oup.com/nar/article/50/16/9490/6667655 by guest on 17 January 2025

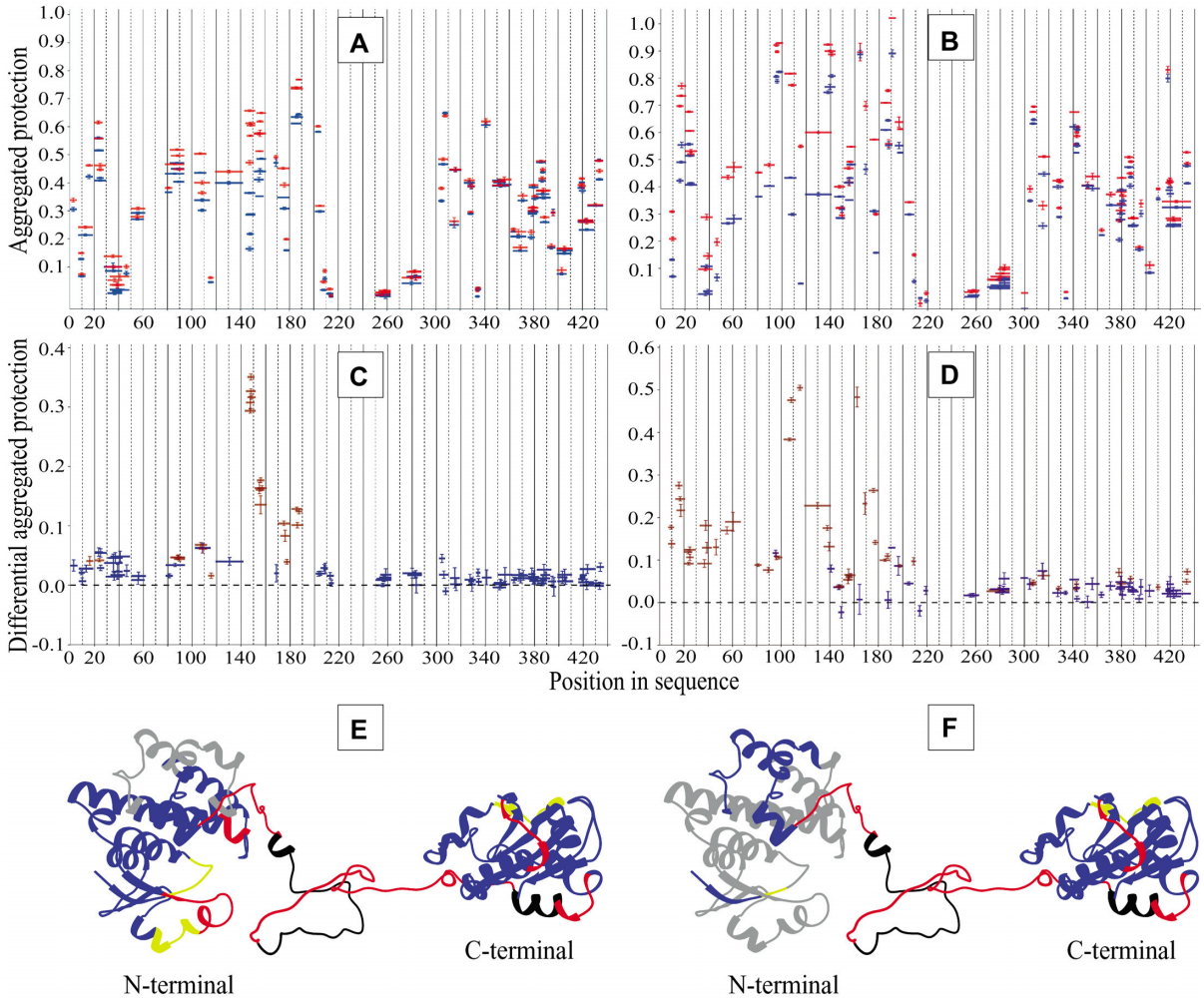

Figure 6. Mapping the protein-protein interactive surfaces on the eEF1Bγ subunits by HDX-MS. The aggregated protection of peptides derived from eEF1Bγ (blue color) and involved into the eEF1Bαγ (**A**) and eEF1Bβγ (**B**) complexes (red color) are depicted. The differential aggregated protection plots (**C**) and (**D**) show the eEF1Bγ peptides that change their protection (brown color) in the complexes with eEF1Bα and eEF1Bβ, respectively (the difference is statistically significant for at least three or more incubation time-points). The peptides indicated in blue in the plots (**C**) and (**D**) do not change their protection. The regions of eEF1Bγ that change their aggregated protection values upon interaction with eEF1Bα (**E**) and eEF1Bβ (**F**) are painted in gray.

eEF1Bαβγ complex compared to eEF1Bβγ, probably due to local conformational fluctuations.

The N-terminal domain of eEF1Bγ interacts simultaneously with both eEF1Bα and eEF1Bβ. The HDX protection patterns of eEF1Bγ in the eEF1Bαβγ complex strongly resemble those obtained for the eEF1Bαγ and eEF1Bβγ complexes, respectively, (Supplementary Figure S9C-F) confirming an independent binding mode of eEF1Bα and eEF1Bβ to eEF1Bγ (47).

Importantly, the HDX-MS data obtained for eEF1Bαγ are in agreement with the crystal structure of their N-terminal domains complex (PDB ID: 5DQS). However, there is no crystal structure for eEF1Bβγ with 1:1 stoichiometry. Using the molecular docking algorithm (32,48) we successfully modeled such complex, in which the first two α-helices of eEF1Bβ insert into a cleft inside the eEF1Bγ N-terminal domain (Supplementary Figure S10A). A superposition of the crystal structure of the eEF1Bαγ N-terminal domains (PDB ID: 5DQS) with the atomistic model of the eEF1Bβγ N-terminal domains using the N-terminal domain of eEF1Bγ as a common part resulted in the ternary complex model that agrees well with the HDX-MS data (Supplementary Figure S10B). The same docking procedure applied for the full-length subunits resulted in the reconstruction of the eEF1B$(\alpha\beta\gamma)_3$ complex (Figure 7, Supplementary video). The modeled complex has an extended overall shape and contains six structurally conserved GEF domains.

We have previously reported that eEF1A forms a complex in equimolar stoichiometry with eEF1Bα through its GEF domain (14). In the case of eEF1Bβ, one molecule of this trimeric protein is expected to bind minimum one and maximum three molecules of eEF1A. To verify this assumption, we incubated eEF1A2 with increasing concentrations of eEF1Bβ and resolved the samples by native gel electrophoresis. Indeed, three discrete eEF1Bβ-eEF1A2 complexes with different electrophoretic mobility were detected in the gel (Figure 8A) demonstrating the ability of all eEF1Bβ GEF domains to concurrently bind eEF1A. Consequently, there are as many as six GEF domains within the

Downloaded from https://academic.oup.com/nar/article/50/16/9490/6667655 by guest on 17 January 2025

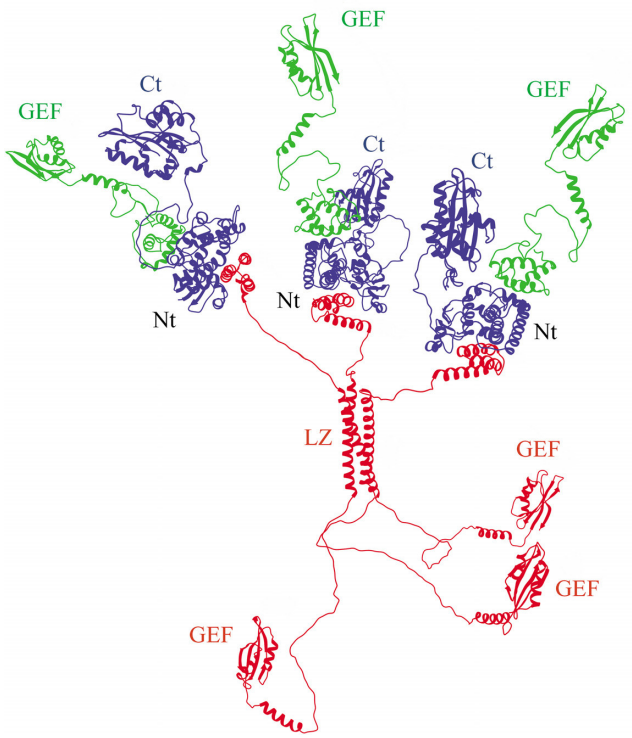

Figure 7. The quaternary organization of the eEF1B($\alpha\beta\gamma$)$_3$ complex. eEF1Bα is in green, eEF1Bβ – in red, and eEF1Bγ – in blue. Abbreviations: GEF – the GEF domain of eEF1Bα and eEF1Bβ, Nt – the complex of eEF1Bα, eEF1Bβ and eEF1Bγ N-terminal domains, Ct – the C-terminal domain of eEF1Bγ, LZ – the LZ-motif of eEF1Bβ.

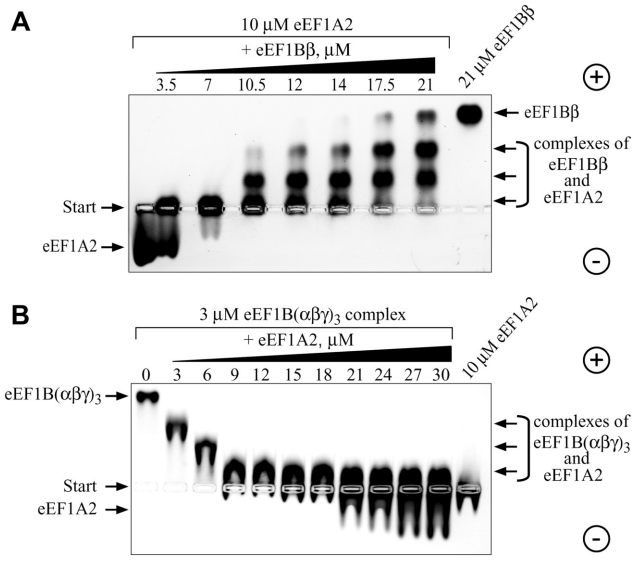

Figure 8. Interaction of eEF1A2 with eEF1Bβ and the eEF1B($\alpha\beta\gamma$)$_3$ complex. eEF1A2 was incubated with increasing amounts of eEF1Bβ (**A**) and the eEF1B($\alpha\beta\gamma$)$_3$ complex was incubated with increasing amounts of eEF1A2 (**B**) The protein mixtures were resolved by 1% native agarose gel electrophoresis and the proteins were visualized by Coomassie Brilliant Blue staining.

eEF1B($\alpha\beta\gamma$)$_3$ complex located at the C-terminal extremities of the α and β subunits (Figure 7). The titration experiment with the whole eEF1B complex revealed that 3 μM eEF1B($\alpha\beta\gamma$)$_3$ was saturated by 18 μM eEF1A2 that corresponds to a ratio 1:6 (Figure 8B). Thus, one molecule of the eEF1B complex is indeed capable of binding up to six molecules of eEF1A2.

DISCUSSION

In this work, we presented the structural models of the eEF1Bα, eEF1Bβ and eEF1Bγ subunits and reconstruction of the whole eEF1B complex. Two proteins play a structural role within eEF1B: eEF1Bβ that is a stable homotrimer (Figure 2E and Supplementary Figure S2) and eEF1Bγ that binds eEF1Bβ and eEF1Bα (Figure 4E).

With the aid of site-directed mutagenesis and HDX-MS analysis, we outlined the protein interactive surfaces on eEF1Bα, eEF1Bβ and eEF1Bγ (Figures 5 and 6 and Supplementary Figure S8). As mentioned above, the HDX-MS data obtained for the eEF1Bαγ complex correlate well with the crystal structure of the eEF1Bαγ N-terminal domain complex (PDB ID: 5DQS). In this structure, eEF1Bα domain contacts eEF1Bγ via the loop region (D21-V29) and third α-helix (C50-I59). Indeed, the peptides composing these two regions significantly increase their protection against H/D exchange upon binding to eEF1Bγ (Figure 5C). Besides, an increase of protection is also observed for the peptides from the first (S8-Y18) and second (N32-S42) α-helices and the loop region (S43-A47) that do not interact with eEF1Bγ directly but may contribute to the appropriate conformation of the binding surface (Figure 5E). This holds true at least for the first α-helix (S8-Y18) of eEF1Bα since its deletion prevents the interaction with eEF1Bγ (Supplementary Figure S8A). According to the 5DQS structure, loop K147-E155 and α-helix N186-N196 of eEF1Bγ directly interact with eEF1Bα in the complex. The HDX-MS data reveal the same regions of eEF1Bγ that become significantly more protected upon interaction with eEF1Bα (Figure 6C and E).

According to the crystal structure of the eEF1Bβ N-terminal fragment (residues 1-32) complexed with the eEF1Bγ N-terminal domain (PDB ID: 5JPO), two α-helices of the eEF1Bβ fragment in a straight conformation form a complex with the eEF1Bγ N-terminal domain tetramer. The first α-helix is squeezed between two N-terminal domains and the second one is bound to the cleft of the third domain. Importantly, an increase of protection against H/D exchange was observed for the same region of eEF1Bβ in the complex with eEF1Bγ (Figure 5D). It worth noting that our data indicate the equimolar stoichiometry of eEF1Bβ and eEF1Bγ in the complex (Figure 4C and Supplementary Figure S5) that contradicts to the 5JPO crystal structure. This may be due to a short size of the eEF1Bβ fragment used for crystallization and a tendency of the eEF1Bγ N-terminal domain to form oligomers at a high protein concentration (Supplementary Figure S4B).

As both eEF1Bα and eEF1Bβ have similar guanine nucleotide exchange activity *in vitro* (14,16) a reason of the existence of two different nucleotide exchanging proteins in one complex as well as their functional equivalence remain

Downloaded from https://academic.oup.com/nar/article/50/16/9490/6667655 by guest on 17 January 2025

unknown. Binding eEF1Bγ enhances the catalytic activity of eEF1Bα (6,49) due to elimination of the self-inhibitory action of the eEF1Bα N-terminal domain (14) while no effect of eEF1Bγ on the eEF1Bβ activity was observed (6,16). The functional activity of the eEF1Bαβγ complex has been also compared with eEF1Bα and eEF1Bβ by polyphenylalanine synthesis *in vitro*, eEF1Bαβγ was found to be several times more active than eEF1Bα or eEF1Bβ alone (12). It suggests that association of these nucleotide exchanging subunits within the ternary complex allows them to execute their activity more efficiently as compared to the individual proteins.

eEF1Bα and eEF1Bβ may perform a different role within the eEF1B complex containing valyl-tRNA synthetase. It has been shown that the N-terminal domain of VRS interacts with the eEF1Bβ subunit, however the enzyme interaction site on eEF1Bβ has not been mapped (6). Taking into account that eEF1Bβ is a homotrimer (Figure 3), one may expect the binding of up to three molecules of valyl-tRNA synthetase to eEF1Bβ. Although, two parallel reactions take place in the VRS-eEF1B complex, namely the GDP/GTP exchange on eEF1A that catalyzes the GEF subunit and valylation of tRNA on VRS, a ternary complex valyl-tRNA*eEF1A*GTP is finally formed as a common product of both reactions (7). This ternary complex is a result of the 'hand to hand' transfer from the enzyme to eEF1A and such transfer can be realized when eEF1A bound to the GEF domain is located in a close vicinity to the valyl-tRNA synthetase catalytic site. Thus, if three molecules of VRS are attached to the eEF1B complex, they may act in concert with three of six available GEF domains. The remaining GEF domains most probably function independently to provide eEF1A*GTP for other aa-tRNAs. Regarding the functional significance of VRS-eEF1B complex, an important question arises why the only valyl-tRNA synthetase is exclusively associated with eEF1B? One of the possible explanations is that valyl-tRNA has a lowest affinity to eEF1A among other aa-tRNAs. In the bacterial system, the lowest valyl-tRNA affinity to EF-Tu is compensated by its higher amount in cell as compared to the other aminoacylated tRNAs (50,51). In turn, in higher eukaryotes poor affinity of valyl-tRNA to the elongation factor 1A may be compensated by its 'hand-to-hand' transfer within the VRS-eEF1B complex. In such a way valyl-tRNA may avoid competition with other aa-tRNAs that have stronger affinity for eEF1A.

Importantly, at least two cases of a disease-causing loss of function variants in the human gene *EEF1B2* that encodes eEF1Bα have been reported to date (52,53). In both cases, the pathogen variants in *EEF1B2* led to moderate intellectual disability in patients. Of note, the complete loss of function of the eEF1Bα protein could not be compensated by the presence of eEF1Bβ. To explain the pathologic neurological consequences in the case of *EEF1B2* mutation, it has been hypothesized that neurons are more susceptible to perturbation of the translation than other types of cells (54). Taking into account that a neuron-specific isoform eEF1A2 is more dependent on GDP/GTP exchange than eEF1A1 (14,55), one may suggest that proper functioning of the eEF1B complex could be critical for efficient translation in neurons.

It has been reported that the subunits involved into eEF1B can interact with several protein partners in human cancer cells (56). However, only translationally controlled tumor protein (TCTP) was shown to bind the CAR domain of eEF1Bβ (57) that resulted in inhibition of its guanine-nucleotide exchange activity (58). Further studies are required to establish the interaction sites of other identified protein partners of eEF1B in order to understand structural and functional consequences of these interactions.

Apparently, the multi-GEF eEF1B complex appeared lately in evolution, as the leucine-zipper-containing eEF1Bβ sequence is present in all metazoans from cnidarians to mammals while it is not found in the available sequences from fungi and plants (2). Its appearance could become favorable because voluminous metazoan cell requires some sort of compartmentalization or increase in local concentration of the metabolic components in particular places of the cytoplasm. Consequently, one obvious explanation of the existence of the multi-GEF complex might be the necessity to maintain high efficiency of eEF1A conversion into active GTP-bound conformation in the translational compartment. Besides, a part of the eEF1B complex associated with VRS functions as an exclusive valyl-tRNA*eEF1A*GTP supplier to the translating ribosome.

DATA AVAILABILITY

The mass spectrometry proteomics data have been deposited to the ProteomeXchange Consortium via the PRIDE (59) partner repository with the dataset identifier PXD031783.

SUPPLEMENTARY DATA

Supplementary Data are available at NAR Online.

ACKNOWLEDGEMENTS

Authors are grateful to Dr A. N. Zaderko for the help with DLS measurements, Drs O.V. Novosylna, and D.S. Gurianov for the help with protein expressions and purifications. The technical assistance of N. Kolodka and D. Futorny is gratefully acknowledged.

FUNDING

National Research Foundation of Ukraine [2020.02/0028 'Study on the structural features of human translation elongation complex eEF1B']; A.F., R.H.S., M.D. acknowledge support by the National Science Centre: MAESTRO [UMO-2014/14/A/NZ1/00306]; Centre of Preclinical Research and Technology [POIG.02.02.00-14-024/08-00]; National Multidisciplinary Laboratory of Functional Nanomaterials [POIGT.02.02.00-00-025/09-00]; Foundation of Polish Science: TEAM-Tech Core Facility grant [TEAM TECH CORE FACILITY/2016-2/2]; T.V.B. was a recipient of short-term FEBS fellowship 'Collaborative and Experimental Scholarship for Central & Eastern Europe'. Funding for open access charge: We have no source of funding for the publication charges.

Downloaded from https://academic.oup.com/nar/article/50/16/9490/6667655 by guest on 17 January 2025

Conflict of interest statement. None declared.

REFERENCES

1. Dever,T.E. and Green,R. (2012) The elongation, termination, and recycling phases of translation in eukaryotes. *CSH Perspect. Biol.*, **4**, a013706.
2. Le Sourd,F., Boulben,S., Le Bouffant,R., Cormier,P., Morales,J., Belle,R. and Mulner-Lorillon,O. (2006) eEF1B: At the dawn of the 21st century. *Biochim. Biophys. Acta*, **1759**, 13–31.
3. Clark,B.F.C., Grunberg-Manago,M., Gupta,N.K., Hershey,J.W.B., Hinnebusch,A.G., Jackson,R.J., Maitra,U., Mathews,M.B., Merrick,W.C., Rhoads,R.E., Sonenberg,N., Spremulli,L.L., Trachsel,H. and Voorma,H.O. (1996) Prokaryotic and eukaryotic translation factors: International Union of Biochemistry and Molecular Biology (IUBMB). *Biochimie.*, **78**, 1119–1122.
4. Carvalho,J.F., Carvalho,M.D. and Merrick,W.C. (1984) Purification of various forms of elongation factor 1 from rabbit reticulocytes. *Arch. Biochem. Biophys.*, **234**, 591–602.
5. Motorin,Y.A., Wolfson,A.D., Lohr,D., Orlovsky,A.F. and Gladilin,K.L. (1991) Purification and properties of a high-molecular-mass complex between Val-tRNA synthetase and the heavy form of elongation factor 1 from mammalian cells. *Eur. J. Biochem./FEBS*, **201**, 325–331.
6. Bec,G., Kerjan,P. and Waller,J.P. (1994) Reconstitution in vitro of the valyl-tRNA synthetase-elongation factor (EF) 1 beta gamma delta complex. Essential roles of the NH2-terminal extension of valyl-tRNA synthetase and of the EF-1 delta subunit in complex formation. *J. Biol. Chem.*, **269**, 2086–2092.
7. Negrutskii,B.S., Shalak,V.F., Kerjan,P., El'skaya,A.V. and Mirande,M. (1999) Functional interaction of mammalian valyl-tRNA synthetase with elongation factor EF-1alpha in the complex with EF-1H. *The J. Biol. Chem.*, **274**, 4545–4550.
8. Sasikumar,A.N., Perez,W.B. and Kinzy,T.G. (2012) The many roles of the eukaryotic elongation factor 1 complex. *Wiley Interdiscipl. Rev. RNA*, **3**, 543–555.
9. Janssen,G.M., van Damme,H.T., Kriek,J., Amons,R. and Moller,W. (1994) The subunit structure of elongation factor 1 from Artemia. Why two alpha-chains in this complex?*The J. Biol. Chem.*, **269**, 31410–31417.
10. Sheu,G.T. and Traugh,J.A. (1999) A structural model for elongation factor 1 (EF-1) and phosphorylation by protein kinase CKII. *Mol. Cell. Biochem.*, **191**, 181–186.
11. Minella,O., Mulner-Lorillon,O., Bec,G., Cormier,P. and Belle,R. (1998) Multiple phosphorylation sites and quaternary organization of guanine-nucleotide exchange complex of elongation factor-1 (EF-1betagammadelta/ValRS) control the various functions of EF-1alpha. *Biosci. Rep.*, **18**, 119–127.
12. Sheu,G.T. and Traugh,J.A. (1997) Recombinant subunits of mammalian elongation factor 1 expressed in Escherichia coli. Subunit interactions, elongation activity, and phosphorylation by protein kinase CKII. *J. Biol. Chem.*, **272**, 33290–33297.
13. Janssen,G.M. and Moller,W. (1988) Elongation factor 1 beta gamma from Artemia. Purification and properties of its subunits. *Eur. J. Biochem./FEBS*, **171**, 119–129.
14. Trosiuk,T.V., Shalak,V.F., Szczepanowski,R.H., Negrutskii,B.S. and El'skaya,A.V. (2016) A non-catalytic N-terminal domain negatively influences the nucleotide exchange activity of translation elongation factor 1Balpha. *FEBS J.*, **283**, 484–497.
15. Trosiuk,T.V., Liudkovska,V.V., Shalak,V.F., Negrutskii,B.S. and El'skaya,A.V. (2014) Structural dissection of human translation elongation factor 1Bγ (eEF1Bγ): expression of full-length protein and its truncated forms. *Biopolym. Cell.*, **30**, 10.
16. Bondarchuk,T.V., Shalak,V.F., Negrutskii,B.S. and El'skaya,A.V. (2016) Leucine-zipper motif is responsible for self-association of translation elongation factor 1Bβ. *Biopolym. Cell.*, **32**, 11.
17. Schuck,P. (2000) Size-distribution analysis of macromolecules by sedimentation velocity ultracentrifugation and lamm equation modeling. *Biophysical. J.*, **78**, 1606–1619.
18. Erickson,H.P. (2009) Size and shape of protein molecules at the nanometer level determined by sedimentation, gel filtration, and electron microscopy. *Biol. Proced. Online*, **11**, 32–51.
19. Vistica,J., Dam,J., Balbo,A., Yikilmaz,E., Mariuzza,R.A., Rouault,T.A. and Schuck,P. (2004) Sedimentation equilibrium analysis of protein interactions with global implicit mass conservation constraints and systematic noise decomposition. *Anal. Biochem.*, **326**, 234–256.
20. Bondarchuk,T.V., Lozhko,D.M., Shalak,V.F., Fatalska,A., Szczepanowski,R.H., Dadlez,M., Negrutskii,B.S. and El'skaya,A.V. (2019) The protein-binding N-terminal domain of human translation elongation factor 1Bbeta possesses a dynamic alpha-helical structural organization. *Int. J. Biol. Macromol.*, **126**, 899–907.
21. Fatalska,A., Dzhindzhev,N.S., Dadlez,M. and Glover,D.M. (2020) Interaction interface in the C-terminal parts of centriole proteins Sas6 and Ana2. *Open Biol.*, **10**, 200221.
22. Malm,A.V. and Corbett,J.C.W. (2019) Improved Dynamic Light Scattering using an adaptive and statistically driven time resolved treatment of correlation data. *Sci. Rep.*, **9**, 13519.
23. Kozlowski,L.P. and Bujnicki,J.M. (2012) MetaDisorder: a meta-server for the prediction of intrinsic disorder in proteins. *BMC Bioinformatics*, **13**, 111.
24. Webb,B. and Sali,A. (2014) Comparative Protein Structure Modeling Using MODELLER. *Curr. Protoc. Bioinformatics*, **47**, 5.6.1–5.6.37.
25. Fiser,A., Do,R.K. and Sali,A. (2000) Modeling of loops in protein structures. *Protein Sci.*, **9**, 1753–1773.
26. Xu,D. and Zhang,Y. (2011) Improving the physical realism and structural accuracy of protein models by a two-step atomic-level energy minimization. *Biophys. J.*, **101**, 2525–2534.
27. Chen,V.B., Arendall,W.B. 3rd, Headd,J.J., Keedy,D.A., Immormino,R.M., Kapral,G.J., Murray,L.W., Richardson,J.S. and Richardson,D.C. (2010) MolProbity: all-atom structure validation for macromolecular crystallography. *Acta Crystallogr. D Biol. Crystallogr.*, **66**, 12–21.
28. Krieger,E., Joo,K., Lee,J., Raman,S., Thompson,J., Tyka,M., Baker,D. and Karplus,K. (2009) Improving physical realism, stereochemistry, and side-chain accuracy in homology modeling: Four approaches that performed well in CASP8. *Proteins*, **77**, 114–122.
29. Pettersen,E.F., Goddard,T.D., Huang,C.C., Couch,G.S., Greenblatt,D.M., Meng,E.C. and Ferrin,T.E. (2004) UCSF Chimera–a visualization system for exploratory research and analysis. *J. Comput. Chem.*, **25**, 1605–1612.
30. Shen,M.Y. and Sali,A. (2006) Statistical potential for assessment and prediction of protein structures. *Protein Sci.*, **15**, 2507–2524.
31. Schneidman-Duhovny,D., Inbar,Y., Nussinov,R. and Wolfson,H.J. (2005) PatchDock and SymmDock: servers for rigid and symmetric docking. *Nucleic Acids Res.*, **33**, W363–367.
32. Duhovny,D.N.R. and Wolfson,H.J. (2002) In: *International Workshop on Algorithms in Bioinformatics*. Lecture Notes in Computer Science, Vol. **2452**, pp. 185–200.
33. Mashiach,E., Schneidman-Duhovny,D., Andrusier,N., Nussinov,R. and Wolfson,H.J. (2008) FireDock: a web server for fast interaction refinement in molecular docking. *Nucleic Acids Res.*, **36**, W229–W232.
34. Vangone,A., Spinelli,R., Scarano,V., Cavallo,L. and Oliva,R. (2011) COCOMAPS: a web application to analyze and visualize contacts at the interface of biomolecular complexes. *Bioinformatics*, **27**, 2915–2916.
35. Zhu,X. and Mitchell,J.C. (2011) KFC2: a knowledge-based hot spot prediction method based on interface solvation, atomic density, and plasticity features. *Proteins*, **79**, 2671–2683.
36. Perez,J.M., Siegal,G., Kriek,J., Hard,K., Dijk,J., Canters,G.W. and Moller,W. (1999) The solution structure of the guanine nucleotide exchange domain of human elongation factor 1beta reveals a striking resemblance to that of EF-Ts from *Escherichia coli*. *Structure*, **7**, 217–226.
37. Wu,H., Wang,C., Gong,W., Wang,J., Xuan,J., Perrett,S. and Feng,Y. (2016) The C-terminal region of human eukaryotic elongation factor 1Bdelta. *J. Biomol. NMR*, **64**, 181–187.
38. Engen,J.R. (2009) Analysis of protein conformation and dynamics by hydrogen/deuterium exchange MS. *Anal. Chem.*, **81**, 7870–7875.
39. Balasubramaniam,D. and Komives,E.A. (2013) Hydrogen-exchange mass spectrometry for the study of intrinsic disorder in proteins. *Biochim. Biophys. Acta*, **1834**, 1202–1209.
40. Skinner,J.J., Lim,W.K., Bedard,S., Black,B.E. and Englander,S.W. (2012) Protein dynamics viewed by hydrogen exchange. *Protein Sci.*, **21**, 996–1005.

Downloaded from https://academic.oup.com/nar/article/50/16/9490/6667655 by guest on 17 January 2025

41. Zhu,S., Shala,A., Bezginov,A., Sljoka,A., Audette,G. and Wilson,D.J. (2015) Hyperphosphorylation of intrinsically disordered tau protein induces an amyloidogenic shift in its conformational ensemble. *PloS One*, **10**, e0120416.
42. Landschulz,W.H., Johnson,P.F. and McKnight,S.L. (1988) The leucine zipper: a hypothetical structure common to a new class of DNA binding proteins. *Science*, **240**, 1759–1764.
43. Lupas,A.N. and Bassler,J. (2017) Coiled coils - a model system for the 21st century. *Trends Biochem. Sci.*, **42**, 130–140.
44. Wood,C.W. and Woolfson,D.N. (2018) CCBuilder 2.0: powerful and accessible coiled-coil modeling. *Protein Sci.*, **27**, 103–111.
45. Achilonu,I., Siganunu,T.P. and Dirr,H.W. (2014) Purification and characterisation of recombinant human eukaryotic elongation factor 1 gamma. *Protein Express. Purif.*, **99**, 70–77.
46. Vanwetswinkel,S., Kriek,J., Andersen,G.R., Guntert,P., Dijk,J., Canters,G.W. and Siegal,G. (2003) Solution structure of the 162 residue C-terminal domain of human elongation factor 1Bgamma. *The J. Biol. Chem.*, **278**, 43443–43451.
47. Mansilla,F., Friis,I., Jadidi,M., Nielsen,K.M., Clark,B.F. and Knudsen,C.R. (2002) Mapping the human translation elongation factor eEF1H complex using the yeast two-hybrid system. *The Biochem. J.*, **365**, 669–676.
48. Guigo,R. and Gusfield,D. eds. (2002) In: *Second International Workshop, WABI 2002, Rome, Italy, September 17-21, 2002, Proceedings*. Springer-Verlag Berlin Heidelberg, Vol. **2452**, pp. 554.
49. Janssen,G.M. and Moller,W. (1988) Kinetic studies on the role of elongation factors 1 beta and 1 gamma in protein synthesis. *J. Biol. Chem.*, **263**, 1773–1778.
50. Louie,A., Ribeiro,N.S., Reid,B.R. and Jurnak,F. (1984) Relative affinities of all Escherichia coli aminoacyl-tRNAs for elongation factor Tu-GTP. *J. Biol. Chem.*, **259**, 5010–5016.
51. Jakubowski,H. (1988) Negative correlation between the abundance of Escherichia coli aminoacyl-tRNA families and their affinities for elongation factor Tu-GTP. *J. Theor. Biol.*, **133**, 363–370.
52. Najmabadi,H., Hu,H., Garshasbi,M., Zemojtel,T., Abedini,S.S., Chen,W., Hosseini,M., Behjati,F., Haas,S., Jamali,P. *et al.* (2011) Deep sequencing reveals 50 novel genes for recessive cognitive disorders. *Nature*, **478**, 57–63.
53. Larcher,L., Buratti,J., Heron-Longe,B., Benzacken,B., Pipiras,E., Keren,B. and Delahaye-Duriez,A. (2020) New evidence that biallelic loss of function in EEF1B2 gene leads to intellectual disability. *Clin. Genet.*, **97**, 639–643.
54. McLachlan,F., Sires,A.M. and Abbott,C.M. (2019) The role of translation elongation factor eEF1 subunits in neurodevelopmental disorders. *Hum. Mutat.*, **40**, 131–141.
55. Kahns,S., Lund,A., Kristensen,P., Knudsen,C.R., Clark,B.F., Cavallius,J. and Merrick,W.C. (1998) The elongation factor 1 A-2 isoform from rabbit: cloning of the cDNA and characterization of the protein. *Nucleic Acids Res.*, **26**, 1884–1890.
56. Negrutskii,B. (2020) Non-translational connections of eEF1B in the cytoplasm and nucleus of cancer cells. *Front. Mol. Biosci.*, **7**, 56.
57. Wu,H., Gong,W., Yao,X., Wang,J., Perrett,S. and Feng,Y. (2015) Evolutionarily conserved binding of translationally controlled tumor protein to eukaryotic elongation factor 1B. *J. Biol. Chem.*, **290**, 8694–8710.
58. Cans,C., Passer,B.J., Shalak,V., Nancy-Portebois,V., Crible,V., Amzallag,N., Allanic,D., Tufino,R., Argentini,M., Moras,D. *et al.* (2003) Translationally controlled tumor protein acts as a guanine nucleotide dissociation inhibitor on the translation elongation factor eEF1A. *Proc. Natl. Acad. Sci. U.S.A.*, **100**, 13892–13897.
59. Perez-Riverol,Y., Bai,J., Bandla,C., Garcia-Seisdedos,D., Hewapathirana,S., Kamatchinathan,S., Kundu,D.J., Prakash,A., Frericks-Zipper,A., Eisenacher,M. *et al.* (2022) The PRIDE database resources in 2022: a hub for mass spectrometry-based proteomics evidences. *Nucleic Acids Res.*, **50**, D543–D552.

Downloaded from https://academic.oup.com/nar/article/50/16/9490/6667655 by guest on 17 January 2025

Supplementary information.

Table S1.

Characteristics of the eEF1Bβ monomer models created by Modeller.

Selected models	Objective Function Value	DOPE score	Radius of gyration, Å
1	-13884.143	-19321.953	88.168
2	-13752.726	-19923.576	87.865
3	-13827.81	-19314.553	89.162
4	-13636.722	-19099.238	87.085
5	-13945.419	-19253.365	95.940

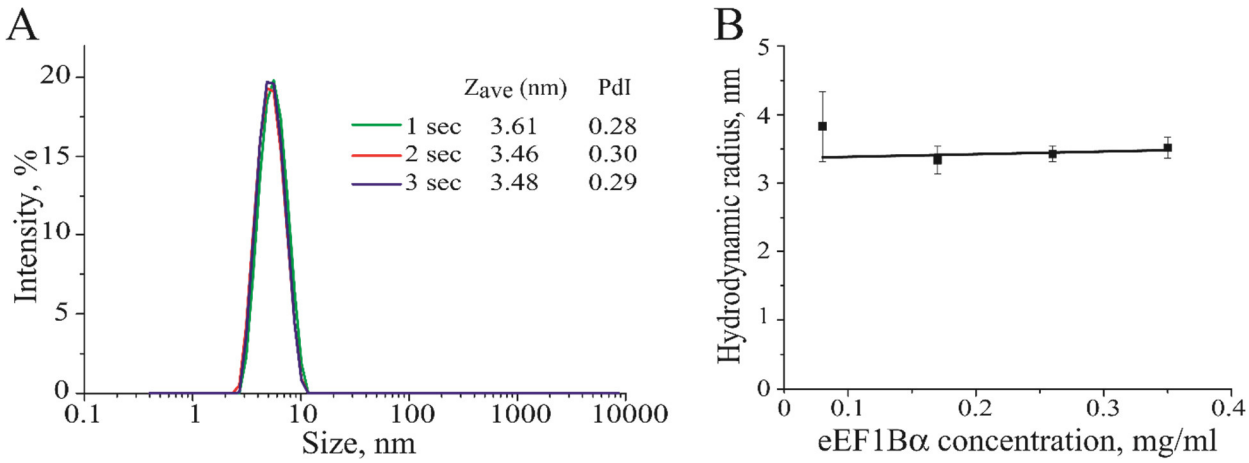

Fig. S1. Determination of the eEF1Bα hydrodynamic radius.

A. Intensity weighted particle size distributions for a 0.35 mg/ml solution of eEF1Bα obtained using the Adaptive Correlation technique. Each distribution represents 30 averaged sub-measurements of 1, 2 and 3 sec duration. Calculated Z_{ave} and PdI values are indicated. **B.** Dependence of the mean hydrodynamic radius of eEF1Bα upon its concentration. The mean Z_{ave} value ± SD for the different eEF1Bα concentrations was calculated from three scattered light intensity measurements with the sub-measurement time of 1, 2 and 3 sec. Extrapolation to zero concentration gives the hydrodynamic radius R_{H0} = 3.35±0.24 nm of freely diffusing eEF1Bα molecule in an infinitely diluted solution.

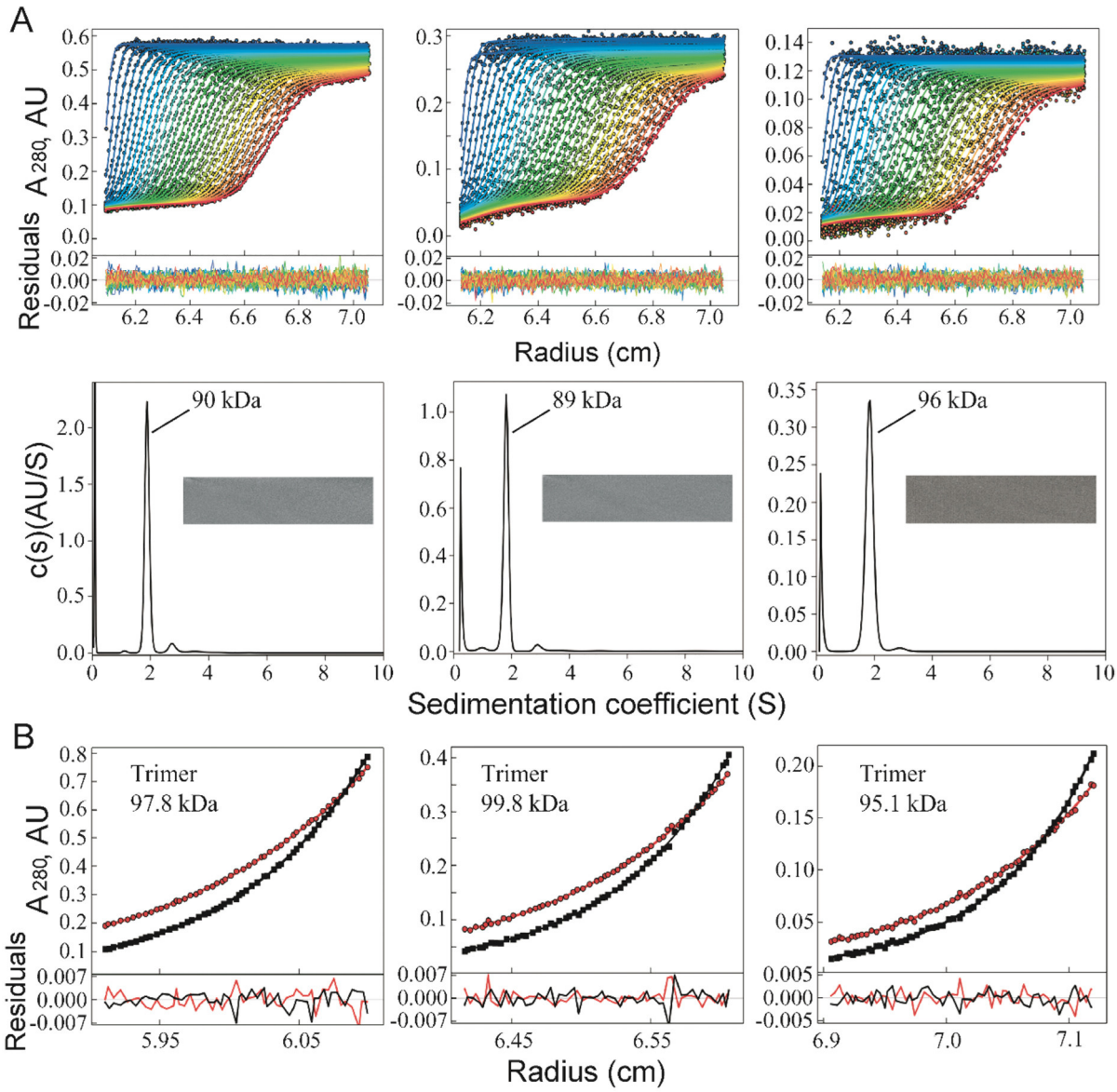

Fig. S2. Sedimentation velocity and equilibrium analysis of full-length recombinant eEF1Bβ. For both experiments, the initial protein concentration was: left – 0.7 mg/ml (21.9 μM), middle – 0.35 mg/ml (11 μM) and right – 0.17 mg/ml (5.3 μM).

(**A**) eEF1Bβ was subjected to sedimentation velocity run at 45,000 rpm at 2.3ºC. **Upper panel**: Absorbance scans of the sedimentation velocity data (symbols show only every third data point of every third scan for clarity) and best-fit boundary model from the c(s) analysis (solid lines) are depicted. Residuals are indicated. **Lower panel**: continuous size distribution analysis, c(s), plotted as a function of sedimentation coefficient. Inset: 2D grayscale "bitmap" residual plot shows a high quality of fit. eEF1Bβ sediments at S_w = 1.84±0.04 S (weight-average sedimentation coefficient corrected to standard conditions of water at 20ºC, $S_{(20,w)}$ = 3.74±0.07 S). (**B**) eEF1Bβ was

subjected to sedimentation equilibrium run at 10,000 rpm (red curves and symbols) and 12,000 rpm (black curves and symbols) at 2.3ºC, and multispeed data analysis was performed. Absorbance scans of the sedimentation equilibrium data (symbols show only every second data point for clarity) and best-fits for a single species model (solid lines) are depicted. Residuals are indicated. Independent data fitting to a single species model for the depicted six scans gave the molecular mass value of 101.2±3.9 kDa.

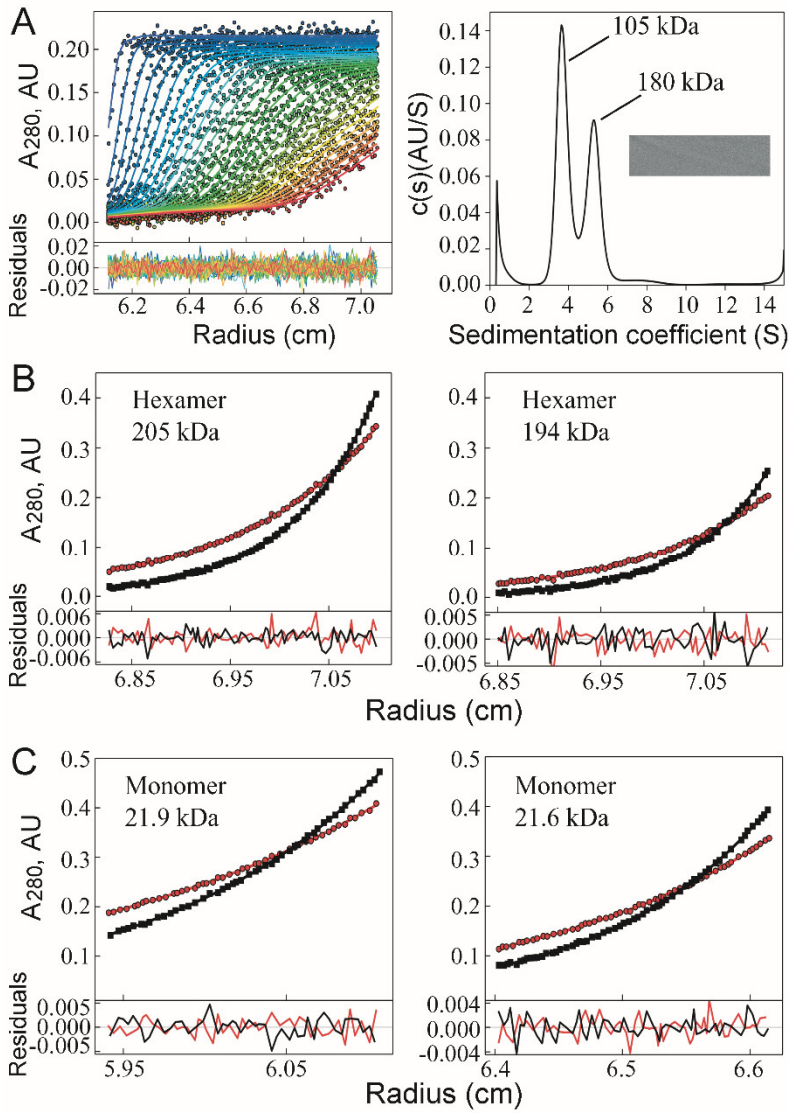

Fig. S3. Sedimentation velocity and equilibrium analysis of the chimeric GST-eEF1Bβ(78-118) protein, and sedimentation equilibrium analysis of eEF1Bβ(117-281).

(**A**) GST-eEF1Bβ(78-118) at the initial 0.15 mg/ml (5 μM) concentration was subjected to sedimentation velocity run at 38,000 rpm at 4ºC. **Left plot**: absorbance scans of the sedimentation velocity data (symbols show only every third data point of every third scan for clarity) and best-fit boundary model from the c(s) analysis (solid lines). Residuals are indicated. **Right plot**: continuous size distribution analysis, c(s), plotted as a function of sedimentation coefficient. Inset: 2D grayscale "bitmap" residual plot shows a high quality of fit. The sedimentation coefficients of the major and minor species were estimated to be 3.728 S ($S_{(20,w)}$ = 7.638 S) and 5.316 S ($S_{(20,w)}$ = 10.893 S), respectively. Using the best-fit friction ratio (f/f_0) of 1.1, their molecular masses were estimated to be 105 and 180 kDa that corresponds to the trimeric (95.2 kDa) and hexameric (190.4

kDa) forms of this protein, respectively. **(B)** GST-eEF1Bβ(78-118) at the initial concentration of 0.15 mg/ml or 5 μM (left) and 0.1 mg/ml or 3.3 μM (right) was subjected to sedimentation equilibrium run at 7,000 rpm (red curves and symbols) and 9,000 rpm (black curves and symbols) at 4ºC, and multispeed data analysis was performed. Both plots represent the absorbance scans of the sedimentation equilibrium data (symbols show only every second data point for clarity) and best-fits for a single species model (solid lines). Residuals are indicated. Independent analysis of four single speed scans gave the molecular mass value of 194.5±4.8 kDa. Fitting the multispeed sedimentation equilibrium data to a single species model, resulted in the molecular mass value of 205.2±0.1 kDa. (**C**) Multispeed sedimentation equilibrium analysis of eEF1Bβ(117-281) was done at the initial protein concentration of 0.35 mg/ml or 18.2 μM (left) and 0.23 mg/ml or 12 μM (right). Absorbance scans of the sedimentation equilibrium data (symbols show only every second data point for clarity) and best-fits for a single species model (solid lines) are depicted. Red curves and symbols denote the equilibrium experiments performed at 17,000 rpm, black curves and symbols – at 21,000 rpm. Residuals are indicated. The calculated molecular mass values are shown in the plots. Independent analysis of four single speed scans gave the molecular mass value of 21.6±1.1 kDa.

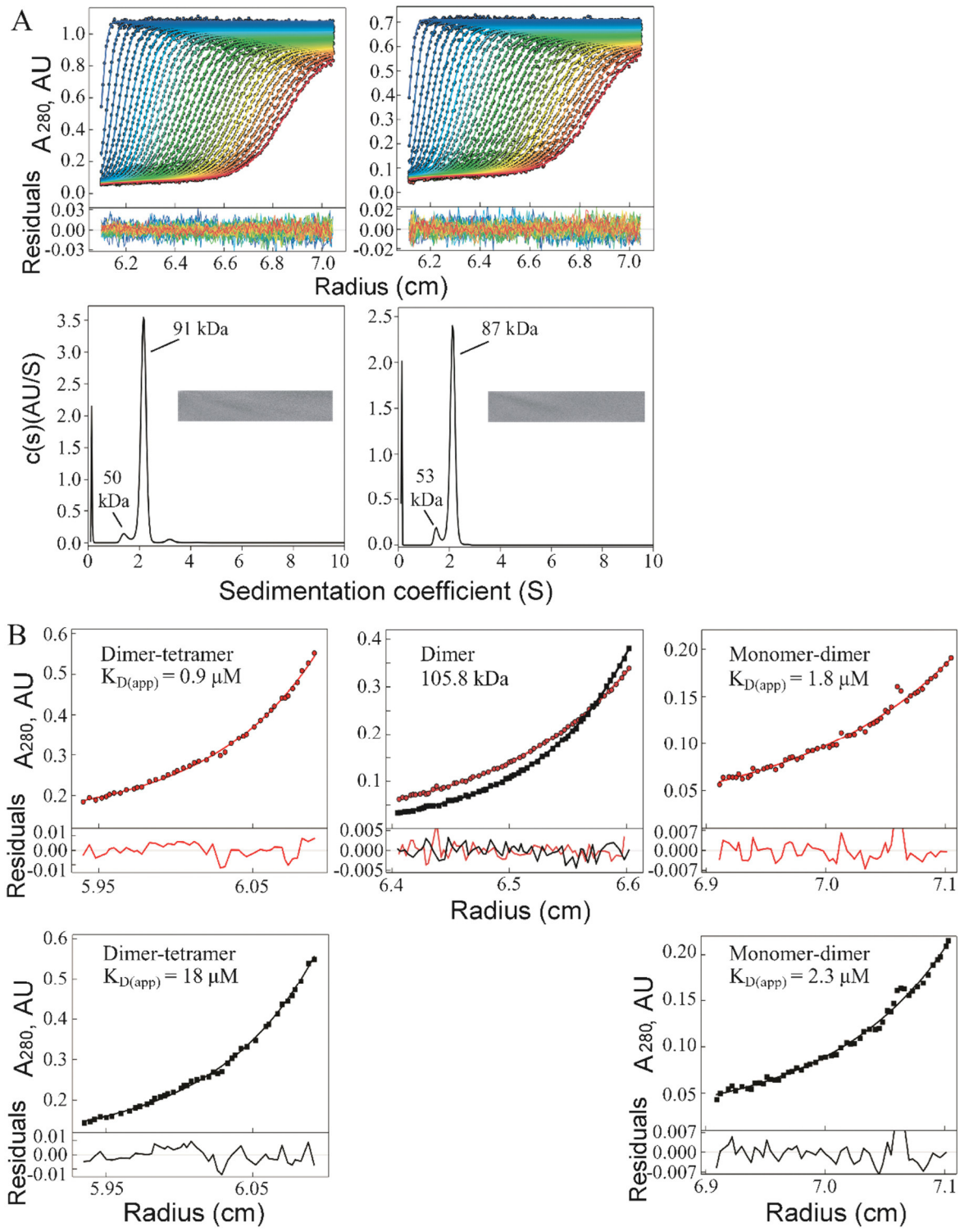

Fig. S4. Sedimentation velocity and equilibrium analysis of full-length eEF1Bγ.

(**A**) eEF1Bγ was subjected to sedimentation velocity run at 45,000 rpm at 2.3ºC. **Upper panel:** Absorbance scans of the sedimentation velocity data (symbols show only every third data point of every third scan for clarity) and best-fit boundary model from the c(s) analysis (solid lines). Residuals are indicated. **Lower panel:** continuous size distribution analysis, c(s), plotted as a

function of sedimentation coefficient. Inset: 2D grayscale “bitmap” residual plot shows a high quality of fit. For the eEF1Bγ initial concentration of 0.57 mg/ml (10.8 μM), the sedimentation coefficient of the minor species was estimated to be 1.435 S ($S_{(20,w)}$ = 2.915 S) and the major – 2.151 S ($S_{(20,w)}$ = 4.369 S) (left plot). For the initial concentration of 0.34 mg/ml (6.46 μM), the sedimentation coefficients of the minor and major species were estimated to be 1.52 S, ($S_{(20,w)}$ = 3.087 S) and 2.123 S, S ($S_{(20,w)}$ = 4.313 S), respectively (right plot). (**B**) eEF1Bγ was subjected to sedimentation equilibrium run at 10,000 rpm (red curves and symbols) and 12,000 rpm (black curves and symbols) at 2.3ºC. The initial protein concentration was: 0.27 mg/ml or 5.1 μM (left plots), 0.18 mg/ml or 3.4 μM (middle plot) and 0.09 mg/ml or 1.7 μM (right plots). Absorbance scans of the sedimentation equilibrium data (symbols show only every second data point for clarity) and best-fits (solid lines) for a monomer-dimer equilibrium model (left and right plots) and a single species model (middle plot, a multispeed analysis) are depicted. Residuals are indicated. To describe the dimer-tetramer equilibrium state of we used a monomer-dimer model and assumed the monomer value to be 105.2 kDa. As a self-association state of eEF1Bγ is concentration dependent, the estimated dissociation constant represents an apparent value. This value varies also at different centrifugation velocities additionally pointing out the irreversible self-association process.

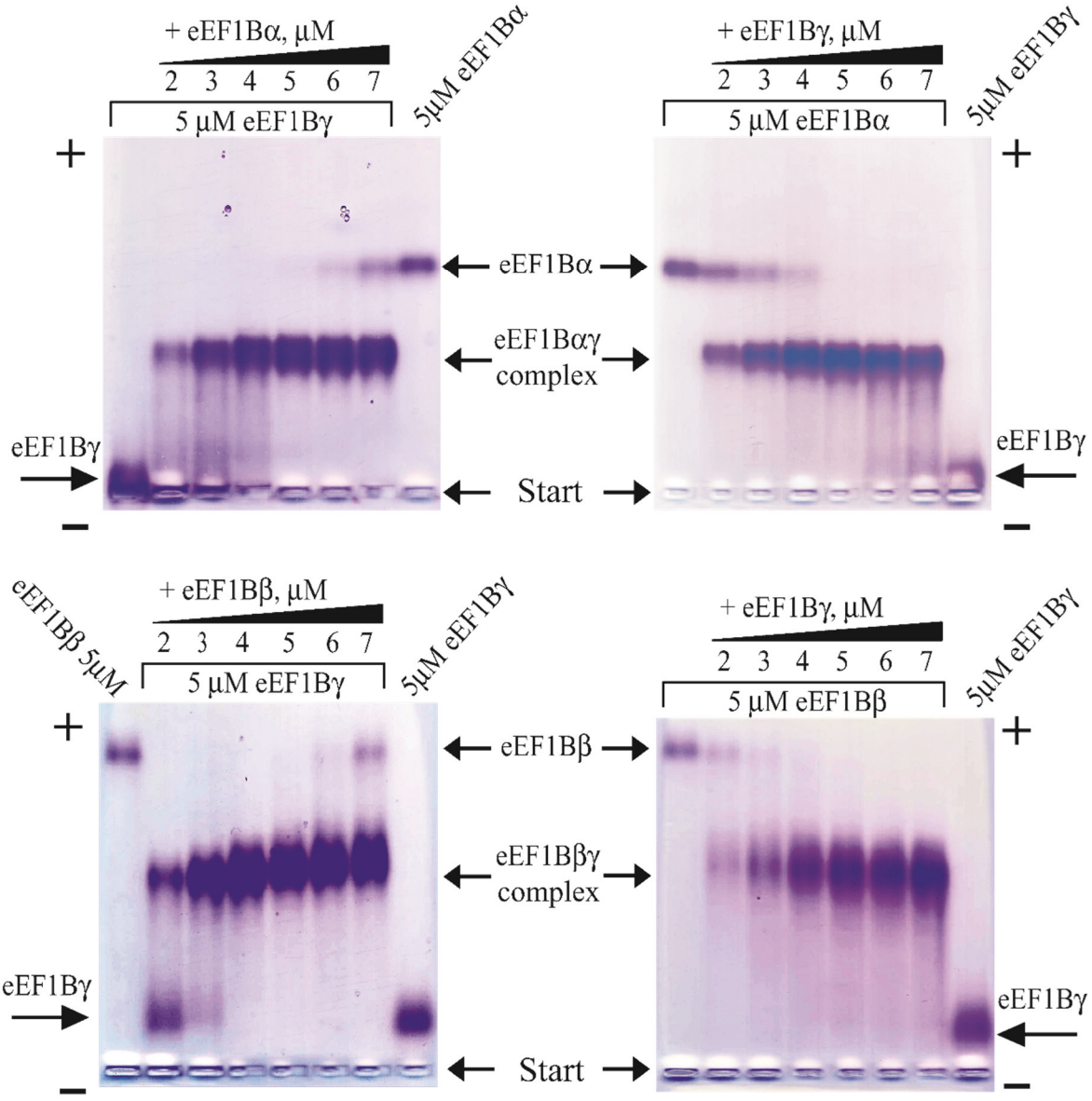

Fig. S5. Formation of the stoichiometric complexes between the eEF1Bα and eEF1Bγ, and the eEF1Bβ and eEF1Bγ proteins monitored by 1% native agarose gel electrophoresis. Proteins were detected by Coomassie Brilliant Blue staining.

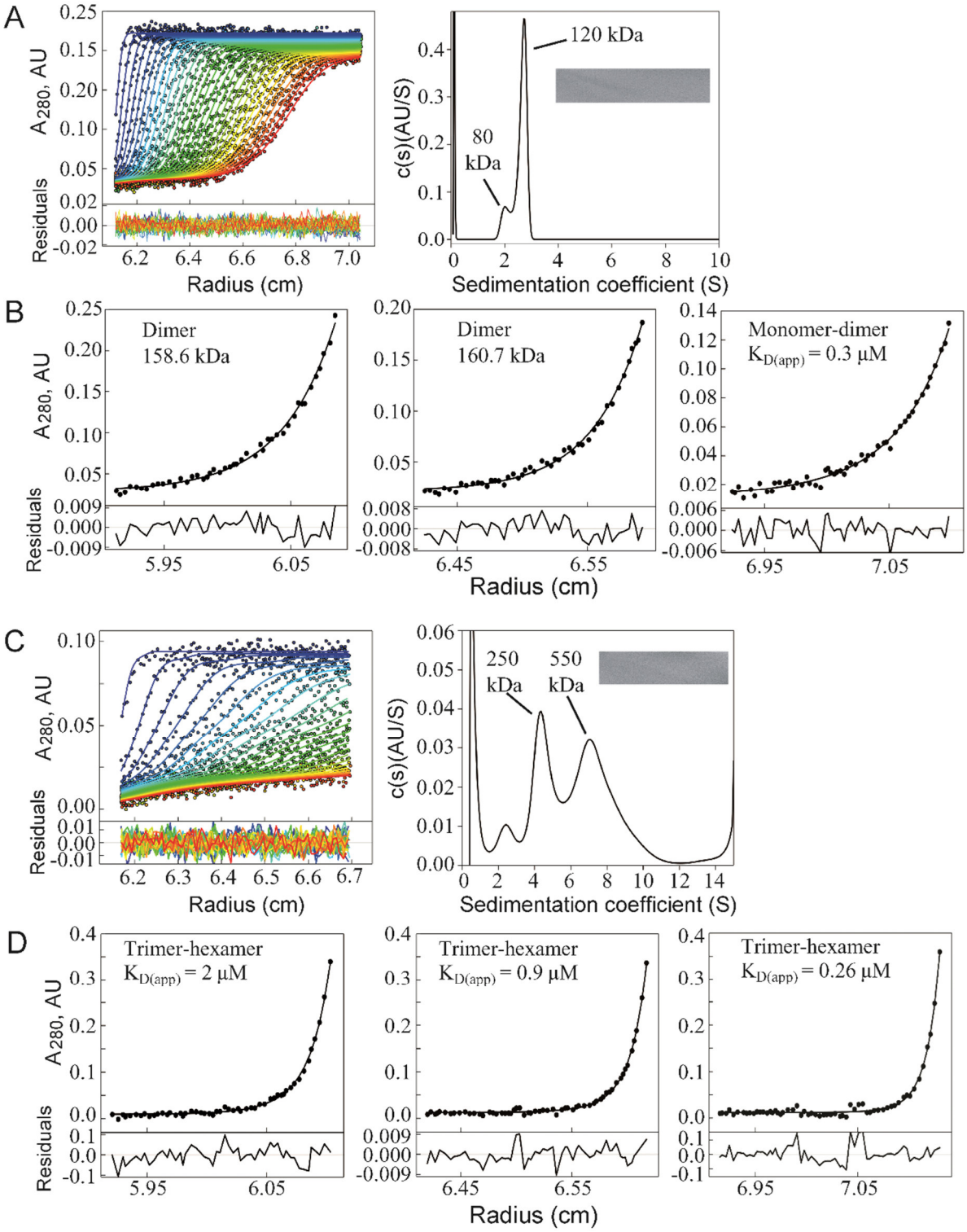

Fig. S6. Sedimentation velocity and equilibrium analysis of the eEF1Bαγ and eEF1Bβγ complexes.

A. The eEF1Bαγ complex at the initial concentration of 0.15 mg/ml (1.9 µM) was subjected to sedimentation velocity run at 42,000 rpm at 2.3ºC. **Left:** absorbance scans of the sedimentation velocity data (symbols show only every third data point of every third scan for clarity) and best-

fit boundary model from the c(s) analysis (solid lines). Residuals are indicated. **Right:** continuous size distribution analysis, c(s), plotted as a function of sedimentation coefficient. Inset: 2D grayscale "bitmap" residual plot shows a high quality of fit. With the best-fit friction ratio (f/f_0) of 1.66, the molecular masses of the minor and major species were estimated to be about 80 and 120 kDa, respectively. **B.** The eEF1Bαγ complex was subjected to sedimentation equilibrium run at 14,000 rpm, at 2.3ºC. The initial concentration of the complex was: left - 0.24 mg/ml (3 μM), middle - 0.12 mg/ml (1.5 μM) and right - 0.06 mg/ml (0.75 μM). Absorbance scans of the sedimentation equilibrium data (symbols show only every second data point for clarity) and best-fits (solid lines) for a single species model (left and middle plots) and a monomer-dimer model (right plot) are depicted. Residuals are indicated. For the highest and middle concentrations of the eEF1Bαγ complex, the molecular mass was calculated to be 158.6 and 160.7 kDa, respectively, that indicates the presence of stable heterodimers in solution. For the lowest concentration, the data were fitted to a monomer-dimer equilibrium model with the monomer molecular mass of 80 kDa and apparent dimer dissociation constant of 0.3 μM. **C.** The eEF1Bβγ complex at the initial concentration of 0.06 mg/ml (0.7 μM) was subjected to sedimentation velocity run at 42,000 rpm at 2.3ºC. **Left:** absorbance scans of the sedimentation velocity data (symbols show only every third data point of every third scan for clarity) and best-fit boundary model from the c(s) analysis (solid lines). Residuals are indicated. **Right:** continuous size distribution analysis, c(s), plotted as a function of sedimentation coefficient. Inset: 2D grayscale "bitmap" residual plot shows a high quality of fit. With the best-fit friction ratio (f/f_0) of 1.59, the molecular masses of the minor and major species were estimated to be about 250 and 550 kDa, respectively. **D.** The eEF1Bβγ complex was subjected to sedimentation equilibrium run at 14,000 rpm at 2.3ºC. The initial concentration of the complex was: left - 0.24 mg/ml (2.8 μM), middle - 0.12 mg/ml (1.4 μM) and right - 0.06 mg/ml (0.7 μM). Absorbance scans of the sedimentation equilibrium data (symbols show only every second data point for clarity) and best-fits (solid lines) are depicted. Residuals are indicated. The data were fitted to a monomer-dimer equilibrium model with the monomer molecular mass of

253.2 kDa and the apparent dissociation constant of 2 μM (left), 0.9 μM (middle) and 0.26 μM (right). Since the estimated trimer-hexamer dissociation constant depends on the protein concentration, it is labeled as “apparent”. A decrease of the apparent dissociation constant with decreasing protein concentration indicates the irreversible oligomerization process.

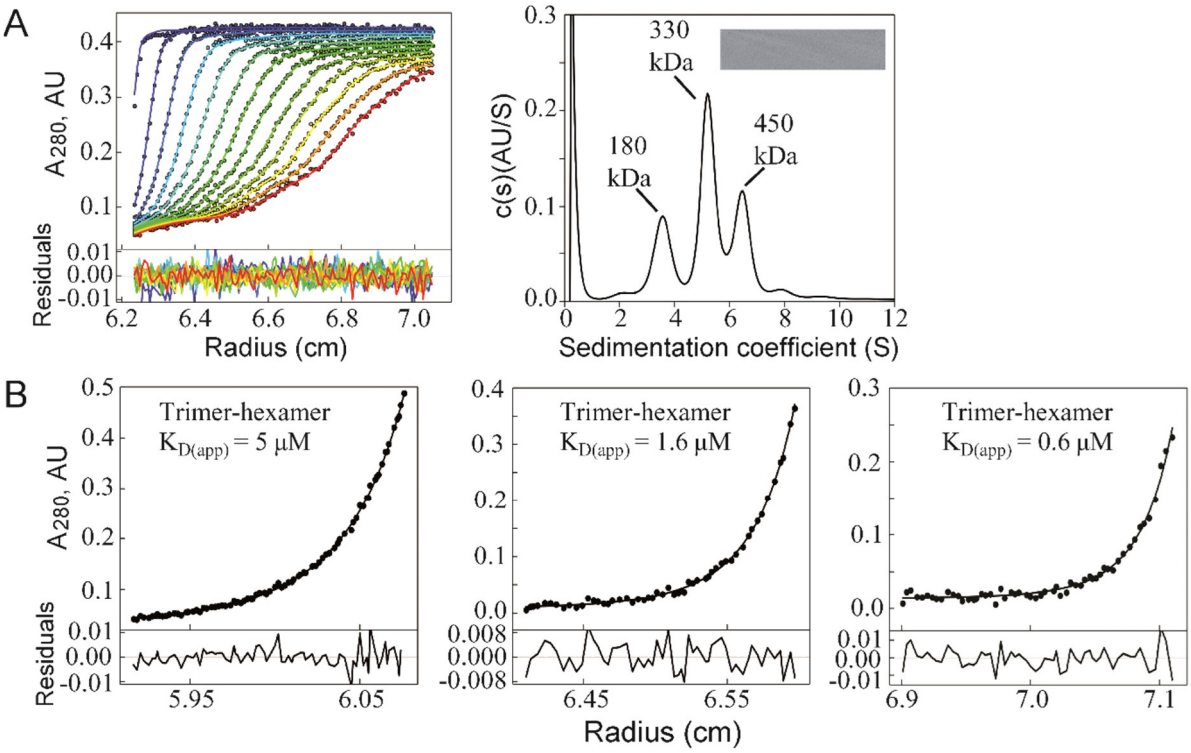

Fig. S7. Sedimentation velocity and equilibrium analysis of the eEF1Bαβγ complex.

A. The eEF1Bαβγ complex at the initial concentration of 0.28 mg/ml (2.5 µM) was subjected to sedimentation velocity run at 42,000 rpm at 2.3ºC. **Left:** absorbance scans of the sedimentation velocity data (symbols show only every third data point of every third scan for clarity) and best-fit boundary model from the c(s) analysis (solid lines). Residuals are indicated. **Right:** continuous size distribution analysis, c(s), plotted as a function of sedimentation coefficient. Inset: 2D grayscale "bitmap" residual plot shows a high quality of fit. With the best-fit friction ratio (f/f_0) of 1.61, the molecular masses of the sedimenting species were estimated to be about 180, 330 and 450 kDa. **B**. The eEF1Bαβγ complex was subjected to sedimentation equilibrium run at 9,000 rpm at 2.3ºC. The initial concentration of the complex was: left - 0.24 mg/ml (2.8 µM), middle - 0.12 mg/ml (1.4 µM) and right - 0.06 mg/ml (0.7 µM). Absorbance scans of the sedimentation equilibrium data (symbols show only every second data point for clarity) and best-fits (solid lines) are depicted. Residuals are indicated. The data were fitted to a monomer-dimer equilibrium model with the monomer molecular mass of 335.6 kDa and the apparent equilibrium dissociation constant of 5 µM (left), 1.6 µM (middle) and 0.6 µM (right). Since the estimated trimer-hexamer dissociation constant depends on the protein concentration, it is labeled as "apparent". A decrease

of the apparent dissociation constant with decreasing protein concentration indicates the irreversible oligomerization process.

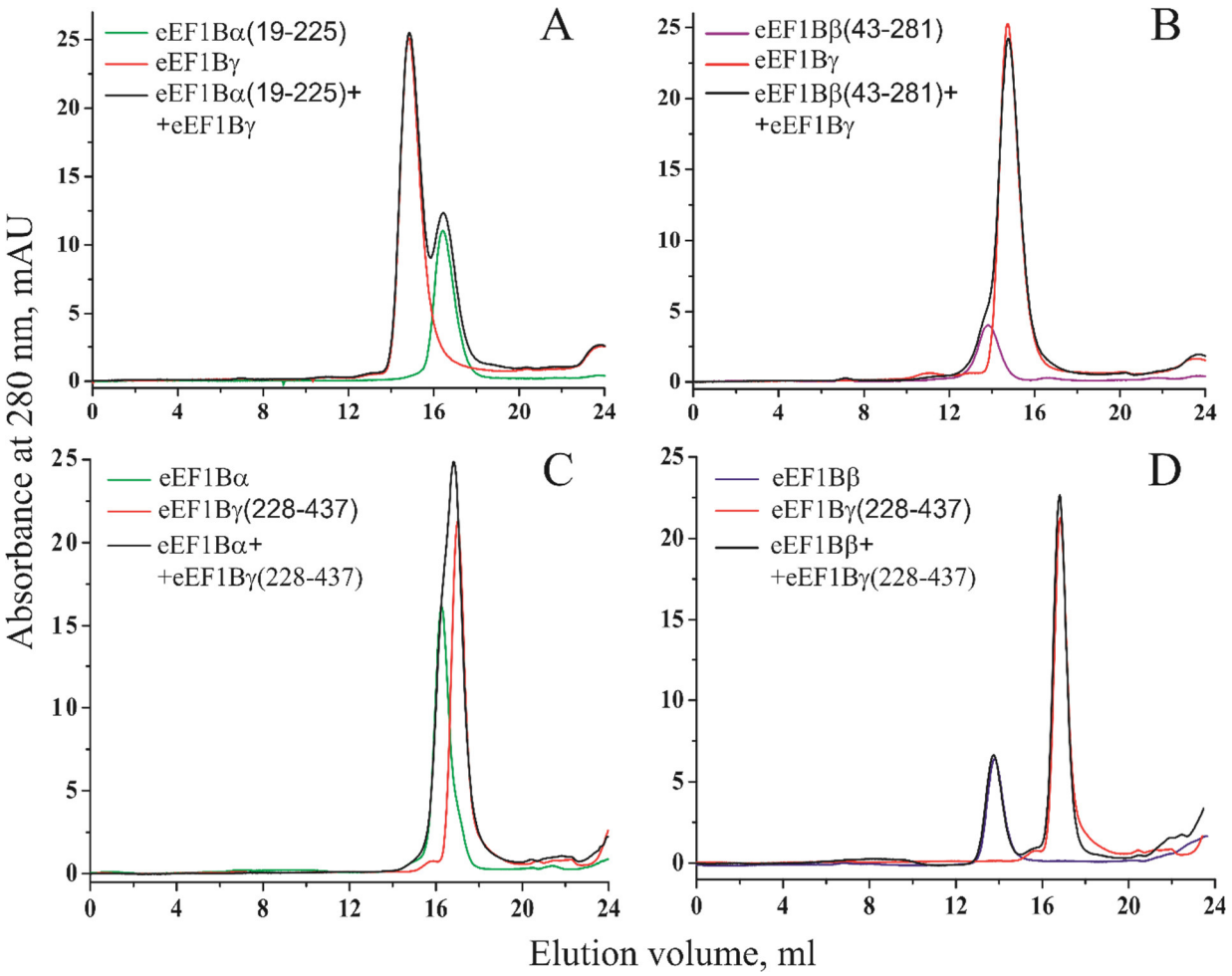

Fig. S8. The N-terminally truncated forms of eEF1Bα and eEF1Bβ do not interact with full-length eEF1Bγ as well as the C-terminal fragment of eEF1Bγ does not bind full-length eEF1Bα and eEF1Bβ.

One hundred µl of the mixture containing 10 µM of each protein was injected into a Superose 6 HR column. **(A)** eEF1Bα(19-225) and **(B)** eEF1Bβ(43-281) were mixed with eEF1Bγ**.** eEF1Bγ(228-437) was mixed with eEF1Bα **(C)** and eEF1Bβ **(D)**. The individual full-length proteins and the respective N-terminally truncated forms were run separately.

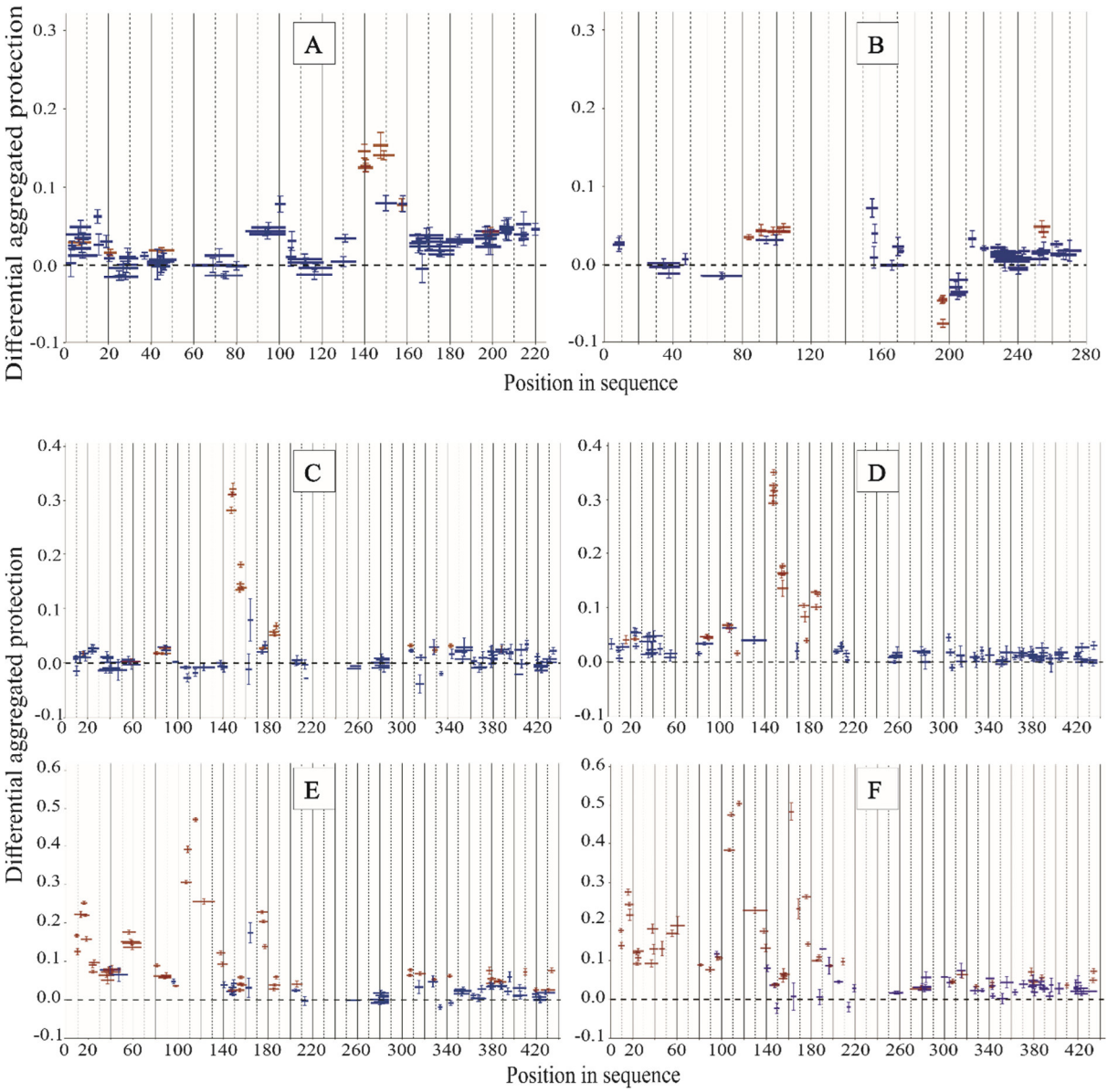

Fig. S9. Comparison of the eEF1Bα, eEF1Bβ and eEF1Bγ aggregated protection between binary eEF1Bαγ, eEF1Bβγ and ternary eEF1Bαβγ complexes.

The differential aggregated protection plots show the eEF1Bα (**A**) and eEF1Bβ **(B)** peptides that change their protection (brown color) against H/D exchange in the eEF1Bαβγ complex compared to the eEF1Bαγ (**A**) and eEF1Bβγ **(B)** complexes (the difference is statistically significant for at least three or more incubation time-points).

The differential aggregated protection plots (**C**) and **(D)** show the eEF1Bγ peptides that change their protection (brown color) in the eEF1Bαβγ and eEF1Bαγ complexes, respectively. The differential aggregated protection plots (**E**) and **(F)** show the eEF1Bγ peptides that change their protection (brown color) in the eEF1Bαβγ and eEF1Bβγ complexes, respectively. The difference

is statistically significant for at least three or more incubation time-points. The peptides indicated in blue in all plots do not change their protection.

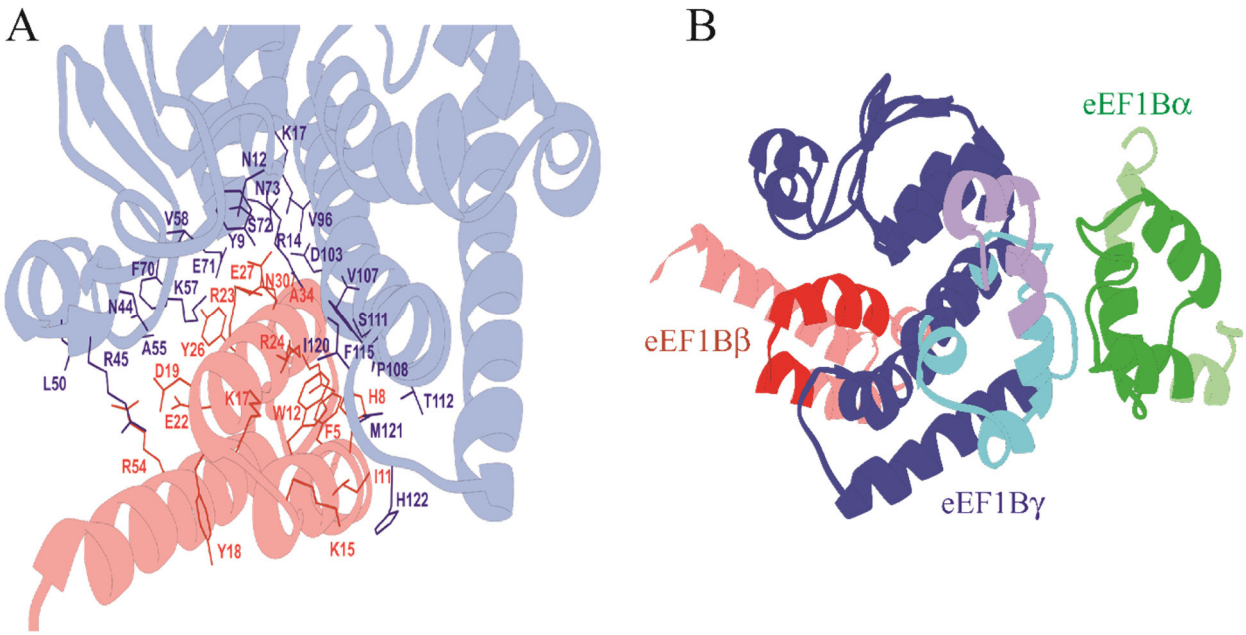

Fig. S10. The atomistic models of the eEF1Bβγ and eEF1Bαβγ N-terminal domain complexes.

A. The complex between the eEF1Bβ and eEF1Bγ N-terminal domains obtained by the docking procedure. The amino acid side chains of eEF1Bβ (red color) and eEF1Bγ (blue color) involved in the interaction between proteins are indicated. Distance cut-off is 5Å.

B. An atomistic model of the eEF1Bα, eEF1Bβ and eEF1Bγ N-terminal domains ternary complex colored according to the HDX-MS data. The regions of the eEF1Bα N-terminal domain and the eEF1Bβ N-terminal domain protected against H/D exchange within this complex are indicated in green and in red, respectively. The regions of the same domains that do not change their protection in the complex are indicated in light green and light red, respectively. The regions of the eEF1Bγ N-terminal domain that become more protected upon interaction with eEF1Bα and eEF1Bβ are indicated in light blue and in dark blue, respectively. A short fragment of the eEF1Bγ N-terminal domain that does not change its protection in the ternary complex is in light violet.

РОЗДІЛ 3

ДУАЛІЗМ p43: тРНК-ЗВ'ЯЗУВАЛЬНИЙ БІЛОК АМІНОАЦИЛ-тРНК СИНТЕТАЗНОГО КОМПЛЕКСУ І ПРЕКУРСОР ЦИТОКІН-ПОДІБНИХ БІЛКІВ. МІТОХОНДРІАЛЬНА ЛОКАЛІЗАЦІЯ ДОВГОЇ ІЗОФОРМИ БІЛКА p43

3.1. p43 – тРНК-зв'язувальний білок аміноацил-тРНК синтетазного комплексу, який взаємодіє з аргініл-тРНК синтетазою, однак не впливає на її каталітичну активність

4592 *Biochemistry* **2004,** *43,* 4592−4600

The tRNA-Interacting Factor p43 Associates with Mammalian Arginyl-tRNA Synthetase but Does Not Modify Its tRNA Aminoacylation Properties†

Ludovic Guigou, Vyacheslav Shalak, and Marc Mirande*

Laboratoire d'Enzymologie et Biochimie Structurales, C.N.R.S., 1 Avenue de la Terrasse, 91190 Gif-sur-Yvette, France

Received December 1, 2003; Revised Manuscript Received February 9, 2004

ABSTRACT: Arginyl-tRNA synthetase (ArgRS) is one of the nine synthetase components of a multienzyme complex containing three auxiliary proteins as well. We previously established that the N-terminal moiety of the auxiliary protein p43 associates with the N-terminal, eukaryotic-specific polypeptide extension of ArgRS. Because p43 is homologous to Arc1p, a yeast general RNA-binding protein that associates with MetRS and GluRS and plays the role of tRNA-binding cofactor in the aminoacylation reaction, we analyzed the functional significance of p43−ArgRS association. We had previously showed that full-length ArgRS, corresponding to the ArgRS species associated within the multisynthetase complex, and ArgRS with a deletion of 73 N-terminal amino acid residues, corresponding to a free species of ArgRS, both produced in yeast, have similar catalytic parameters (Lazard, M., Kerjan, P., Agou, F., and Mirande, M. (2000) *J. Mol. Biol. 302*, 991−1004). However, a recent study had suggested that association of p43 to ArgRS reduces the apparent K_M of ArgRS to tRNA (Park, S. G., Jung, K. H., Lee, J. S., Jo, Y. J., Motegi, H., Kim, S., and Shiba, K. (1999) *J. Biol. Chem. 274*, 16673−16676). In this study, we analyzed in detail, by gel retardation assays and enzyme kinetics, the putative role of p43 as a tRNA-binding cofactor of ArgRS. The association of p43 with ArgRS neither strengthened tRNA-binding nor changed kinetic parameters in the amino acid activation or in the tRNA aminoacylation reaction. Furthermore, selective removal of the C-terminal RNA-binding domain of p43 from the multisynthetase complex did not affect kinetic parameters for ArgRS. Therefore, p43 has a dual function. It promotes association of ArgRS to the complex via its N-terminal domain, but its C-terminal RNA-binding domain may act as a tRNA-interacting factor for an as yet unidentified component of the complex.

Aminoacyl-tRNA synthetases specifically bind their cognate tRNA isoacceptors and transfer the corresponding activated amino acid to the 3′-end of the tRNA molecule (*1*). A set of specific interactions between amino acid side chains of the synthetase and tRNA bases and of nonspecific interactions with the phosphate−sugar backbone of tRNA contribute to the accurate positioning of the 3′-end of tRNA into the active site crevice of the enzyme. Most synthetases exclusively interact with the inner, concave side of the L-shaped tRNA molecule (*2*−*7*). Although the mode of tRNA binding seems to be well conserved from prokaryotes to eukaryotes, one of the major differences that characterizes aminoacyl-tRNA synthetases from higher eukaryotes (from Drosophila to human), is the presence of polypeptide chain extensions that may serve as auxiliary tRNA-interacting factors (tIFs).[1]

Several types of tIFs have been described so far. They either are added to the polypeptide chain of the synthetases as N- or C-terminal extensions (association in cis) or may be appended in trans via protein−protein interaction. In mammals, MetRS, GlyRS, HisRS, TrpRS, and bifunctional GluProRS (*8*) (where XxxRS indicates the aminoacyl-tRNA synthetase and Xxx is the amino acid abbreviation) share a coiled-coil motif of ∼50 amino acid residues (*9*, *10*). It constitutes an N-terminal extension in GlyRS, HisRS, TrpRS, and ProRS and a C-terminal extension in GluRS and MetRS. In the case of human MetRS (*11*) and HisRS (*12*) or of *Bombyx mori* GlyRS (*13*), its involvement as a cis-acting tIF for aminoacylation has been established. The C-terminally appended tIF of MetRS confers on the native enzyme the ability to bind tRNA with a much higher apparent affinity ($K_d \approx 0.1$ μM) as compared with a MetRS mutant lacking this domain ($K_d \approx 4$ μM). Another type of cis-acting tIF has been identified in mammalian LysRS (*14*) and AspRS (*15*−*17*). This lysine-rich N-terminal polypeptide extension of LysRS, made of ∼70 amino acid residues, may form an α-helix-based tRNA binding motif (*18*). The cis-acting tIFs appended to eukaryotic aminoacyl-tRNA synthetases decrease dissociation constants for their cognate tRNAs. Because the concentration of non-acylated tRNA in the cytoplasm of higher eukaryotic cells is believed to be 1 order of magnitude lower than the K_m value for the cognate synthetase (discussed in ref *14*), tIFs are thought to be required for tRNA cycling during translation (*19*).

A second family of tIF concerns trans-acting general tRNA binding modules that were first described in yeast (*20*−*22*). In the yeast *Saccharomyces cerevisiae*, the protein Arc1p is associated in trans with MetRS and GluRS and increases

† This work was supported by grants from the CNRS (UPR9063), the Agence Nationale de Recherche sur le SIDA, the Association pour la Recherche sur le Cancer and La Ligue.

* To whom correspondence should be addressed. Tel: (+33)-169823505. Fax: (+33)-169823129. E-mail: mirande@lebs.cnrs-gif.fr.

[1] Abbreviations: tIF, tRNA-interacting factor.

10.1021/bi036150e CCC: $27.50 © 2004 American Chemical Society
Published on Web 03/25/2004

their aminoacylation efficiency. A human homologue of Arc1p has been described. The p43 protein, one of the nine polypeptide components of the mammalian multisynthetase complex, has the potential to bind tRNA nonspecifically (*23*) and may play the role of a trans-acting tIF for one of the synthetase components of the complex. A homologous domain is appended in cis to the C-terminus of human TyrRS, but its involvement in tRNA binding has not yet been established (*24*, *25*). The crystal structure of the C-terminal moiety of p43 identified a putative OB-fold-based tRNA-binding site (*26*). This trans-acting tIF is also the precursor of the EMAPII cytokine generated during apoptosis (*27*−*29*). The cytokine activity has been assigned to the fragment encompassing residues 92−256 of p43 (*30*). The involvement of p43 in angiogenesis has also been proposed (*31*). Immunoelectron microscopy suggested that p43 occupies a central position within the complex and thus may serve as a donor of tRNA for several aminoacyl-tRNA synthetases (*32*). Because p43 and ArgRS are interacting proteins (*33*, *34*), the involvement of p43 in modulating the activity of ArgRS has been proposed (*35*).

In this work, we investigated the role of p43 as a factor involved in the assembly of ArgRS within the multisynthetase complex and as a tIF promoting the aminoacylation activity of ArgRS. Our results stress the dual role of p43. Its N-terminal domain is responsible for association of ArgRS within the complex and its C-terminal moiety binds tRNA but does not serve as a tIF for ArgRS.

EXPERIMENTAL PROCEDURES

Protein Overexpression and Purification. Hamster arginyl-tRNA synthetase and an N-terminally truncated derivative with a deletion of the 73 terminal amino acid residues were expressed in yeast and purified as described (*36*). The auxiliary p43 subunit of the multisynthetase complex, as well as its N-terminal (p43-N) or C-terminal (p43-C) moieties, was expressed in *Escherichia coli* with a C-terminal His-tag (*23*). Plasmid for expression of *Aquifex aeolicus* Trbp111 was a gift from Paul Schimmel (The Skaggs Institute for Chemical Biology, La Jolla, CA). Trbp111 was expressed and purified as described (*37*).

Protein concentrations were determined by using calculated absorption coefficients of 0.728, 0.803, 0.257, 0.068, and 0.408 A_{280} units·mg^{-1}·cm^2, respectively, for ArgRS, ArgRS-ΔN, p43, p43-N, and p43-C.

Immunoprecipitation. His-tagged p43, p43-N, or p43-C (2 μM each) were incubated 30 min at 4 °C with ArgRS or ArgRS-ΔN (5 μM) in buffer A50 [buffer A (8 mM Na_2HPO_4, 1.5 mM KH_2PO_4, 2.7 mM KCl, pH 7.5) including 50 mM NaCl] containing 0.1% Triton X-100 and 0.2% BSA. A preadsorption step was conducted. After a 15-min incubation with a polyclonal goat anti-rabbit-IgG antibody (1 μg), 20 μl of a 1:1 slurry of Protein-A Sepharose in buffer A50 containing 0.1% Triton X-100 was added. Incubation was continued at 4 °C for 30 min. After centrifugation, the supernatant was recovered and incubated at 4 °C for 1 h with 1 μg of Penta-His antibody (QIAGEN). After addition of 25 μl of a 1:1 slurry of Protein-A Sepharose and incubation at 4 °C for 30 min, the immunoprecipitate was washed five times with 1 mL of buffer A100 (buffer A including 100 mM NaCl) containing 0.1% Triton X-100 and once with 100 mM Tris-HCl, pH 7.5, and the pellet was recovered in 25 μl of SDS−PAGE loading buffer, boiled for 2 min, and loaded on a 12% SDS−polyacrylamide gel. Immunoprecipitates were analyzed by Western blotting with antibodies raised in rabbit against ArgRS-ΔN.

Gel Retardation Assay. Protein−tRNA interactions were assayed using a band shift assay as previously described (*28*). Plasmid carrying the beef $tRNA_2^{Arg}$ gene under control of the T7 polymerase promoter was constructed by simultaneous ligation of 10 oligonucleotides into pUC18 (5′-agcttaatacgactcact, 5′-ctatagtgagtcgtatta, 5′-atagccccagtggcctaatg, 5′-ttatccattaggccactgggg, 5′-gataaggcattggcctccta, 5′-tggcttaggaggccaatgcc, 5′-agccagggattgtgggttcg, 5′-ggactcgaacccacaatccc, 5′-agtcccatctggggtcccaggatccaaacatcc, 5′-gatcggatgtttggatcctgggaccccagatg). Plasmid $ptRNA_2^{Arg}$ was linearized with *Fok*I and subjected to in vitro transcription. The amino acid acceptor minihelix (Acc_2^{Arg}) and anticodon microhelix (Ant_2^{Arg}) of beef $tRNA_2^{Arg}$ were produced from *Fok*I-digested pUC18 derivatives. T7 RNA polymerase was purified from the strain BL21/pAR1219 generously provided by Prof. W. Studier (Brookhaven National Laboratory). ^{32}P-labeled tRNAs were synthesized in a reaction mixture (50 μl) containing 1 μg of template DNA, 40 mM Tris-HCl (pH 8.0), 6 mM $MgCl_2$, 1 mM spermidine, 5 mM dithiothreitol, 0.01% Triton X-100, 1 mM each CTP, UTP, and GTP, 10 μM [α-^{32}P]ATP (200 Ci/mmol), and 1000 U/ml T7 RNA polymerase. After incubation at 37 °C for 1 h, the transcripts were purified by electrophoresis on a denaturing 12% polyacrylamide gel (mono/bis, 19:1), recovered from the gel by soaking in H_2O, precipitated with ethanol, and resuspended in 5 mM $MgCl_2$. Transcripts were renatured by heating at 90 °C and slow cooling (90−30 °C in 2 h).

Homogeneous proteins were incubated at increasing concentrations with radiolabeled-tRNA (50 000 cpm per point) in an 11 μl volume containing 20 mM Tris-HCl (pH 7.5), 150 mM NaCl, 10 mM $MgCl_2$, 10 mM 2-mercaptoethanol (2-ME), 10% glycerol, and BSA at 0.1 mg/mL. After incubation at 25 °C for 30 min, the mixture was placed on ice and loaded on a 6% polyacrylamide gel (mono/bis, 29:1) containing 5% glycerol in 0.5× TBE (45 mM Tris, 45 mM boric acid, 1.25 mM EDTA, pH 8.3) at 4 °C. After electrophoresis, the gel was fixed, dried, and subjected to autoradiography. Free and bound tRNA was quantified by densitometry analysis. Because the amount of labeled transcripts added in the assays is negligible as compared with the amount of protein added, concentration of protein at which half of the tRNA forms a complex corresponds to the apparent K_d value of the complex.

Aminoacylation Assay. Initial rates of tRNA aminoacylation were measured at 25 °C in 0.1 mL of 20 mM imidazole-HCl buffer (pH 7.5), 150 mM KCl, 0.5 mM DTT, 5 mM $MgCl_2$, 3 mM ATP, 20 μM ^{14}C-labeled arginine (PerkinElmer Life Sciences; 50 Ci/mol), and saturating amounts of tRNA, as previously described (*38*). Partially purified beef tRNA (arginine acceptance of 43 pmol/A_{260}) or homogeneous beef $tRNA_2^{Arg}$ obtained by in vitro transcription (arginine acceptance of 500 pmol/A_{260}) were used as tRNA substrate. The incubation mixture contained catalytic amounts (1−10 nM) of enzymes appropriately diluted in 10 mM Tris-HCl (pH 7.5) and 10 mM 2-mercaptoethanol containing bovine serum albumin at 4 mg/mL. One unit of activity is the amount of enzyme producing 1 nmol/min of arginine−

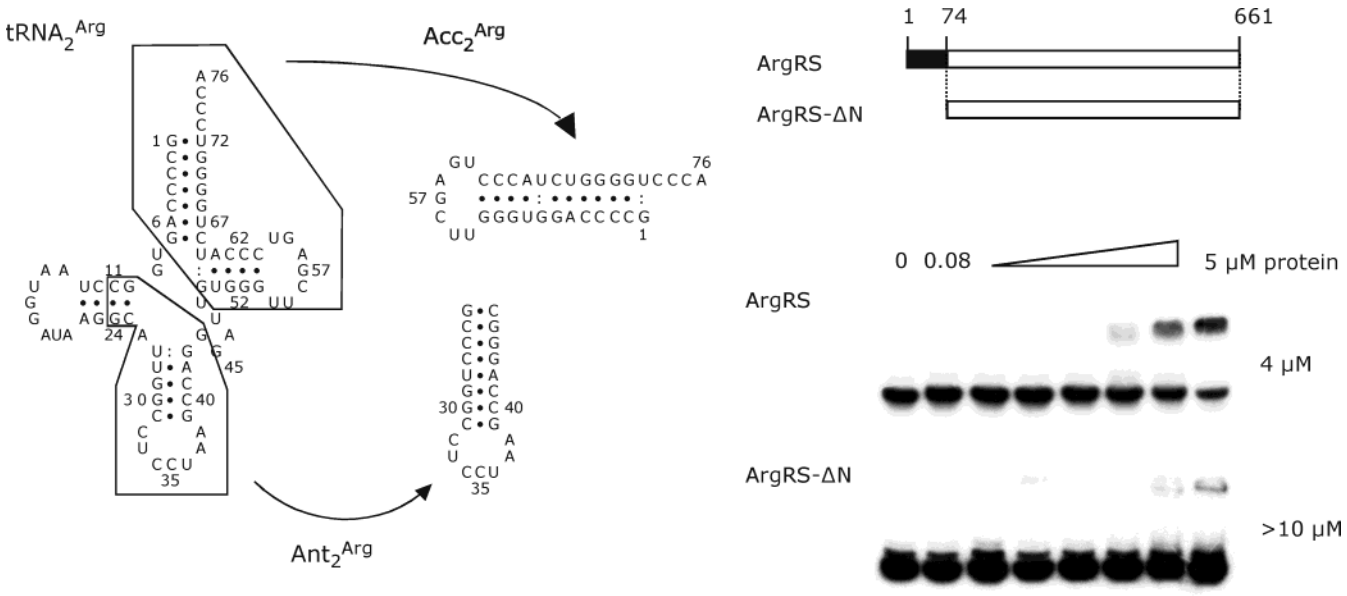

FIGURE 1: Binding of ArgRS to $tRNA^{Arg}$. The sequence and cloverleaf structure of $tRNA_2^{Arg}$ and sequence and hairpin structures of acceptor minihelix (Acc_2^{Arg}) and anticodon microhelix (Ant_2^{Arg}) used in this study are shown on the left. Full-length ArgRS (1−661) and the N-terminally truncated naturally occurring ArgRS derivative (ArgRS-ΔN; 74−661) were used. In vitro transcribed, ^{32}P-labeled $tRNA_2^{Arg}$ was incubated with hamster ArgRS or ArgRS-ΔN at different concentrations (0.08−5 μM). After electrophoresis at 4 °C on a 6% native polyacrylamide gel, the mobility shift of tRNA was visualized by autoradiography. In each assay, the bottom band corresponds to the free tRNA species. Apparent K_d values are indicated at right.

$tRNA^{Arg}$ at 25 °C. For the determination of K_M values for tRNA, $tRNA^{Arg}$ concentrations of 0.02−5 μM were used. Michaelian parameters were obtained by nonlinear regression of the theoretical Michaelis−Menten equation to the experimental curve using the KaleidaGraph 3.6 software (Abelbeck Software).

For large scale synthesis of RNA substrates, in vitro transcription was conducted on 0.5 mg of linearized template DNA in a final volume of 5 mL containing 40 mM Tris-HCl (pH 8.0), 22 mM $MgCl_2$, 1 mM spermidine, 5 mM dithiothreitol, 0.01% Triton X-100, 4 mM each CTP, UTP, GTP, and ATP, 16 mM GMP, and 500 U/ml T7 RNA polymerase. After a 1 h incubation at 37 °C, 100 units of inorganic pyrophosphatase (BioLabs) were added, and synthesis was resumed for a 4 h period. After phenol−chloroform extraction, transcripts were purified on a 1.6 mm thick 12% polyacrylamide urea-gel, electroeluted with a Bio-Trap apparatus (Schleicher & Schuell), ethanol-precipitated, and resuspended in 5 mM $MgCl_2$. Transcripts were renatured by heating at 90 °C and slow cooling (90−30 °C in 2 h).

Arginine Activation Assay. The isotopic [^{32}P]PP_i-ATP exchange reaction was conducted as described previously (*36*). The assay mixture contained, in a final volume of 0.1 mL, 20 mM imidazole-HCl (pH 7.5), 10 mM $MgCl_2$, 0.1 mM EDTA, and 2 mM each of ATP, [^{32}P]pyrophosphate (2.5 Ci/mol), and arginine. The reaction was started by the addition of limiting amounts of enzymes (10−20 nM) appropriately diluted in 10 mM Tris-HCl, pH 7.5, containing 10 mM 2-ME and BSA at 4 mg/mL. After 10 min at 25 °C, the reaction was stopped by the addition of 2.5 mL of a solution containing 100 mM pyrophosphate, 50 mM sodium acetate (pH 4.5), 0.35% perchloric acid, and 0.4% Norit to absorb ATP. Samples were filtered through Whatmann no. 1 filters and washed extensively with a solution of 100 mM PP_i. [^{32}P]-labeled ATP absorbed on Norit was quantified by liquid scintillation counting. A unit of enzyme activity is defined as the amount of enzyme required to form 1 nmol/min of [^{32}P]ATP.

For the determination of kinetic parameters in the PP_i−ATP exchange reaction, the concentration of tRNA in the assay was varied from 1 nM to 1 μM. Michaelian parameters were deduced as described above.

RESULTS

tRNA-Binding Capacity of Mammalian ArgRS. The native form of mammalian arginyl-tRNA synthetase (ArgRS) is a monomer of 75.6 kDa that makes protein−protein interactions with the p43 RNA-binding protein and associates with the multisynthetase complex (the ArgRS component of the complex is referred to as ArgRS-Cx) (*33*, *39*). A free form of that enzyme (ArgRS-ΔN), starting at the Met74 residue (Figure 1) is also encountered in the cytoplasm of mammalian cells (*40*, *41*). We previously reported that the two enzyme species ArgRS and ArgRS-ΔN, expressed in yeast and purified to homogeneity, display very similar kinetic parameters for arginine activation and tRNA arginylation (*36*). This result left open the possibility that association of ArgRS with p43 within the multisynthetase complex might influence the activity of ArgRS. However, comparison of their specific activities (*36*) and other initial investigations suggested that ArgRS and ArgRS-Cx have similar kinetic parameters. Because there is some disagreement on this point (*35*), we reanalyzed in detail the putative role of the RNA-binding protein p43 on the ability of ArgRS to bind and aminoacylate its tRNA.

We first asked whether the 73 additional residues found in ArgRS as compared with ArgRS-ΔN provide the full-length enzyme with tRNA-binding properties. Indeed, we recently reported that the eukaryotic-specific C-terminal or N-terminal polypeptide extensions of MetRS and LysRS,

Table 1: Kinetic Constants of ArgRS and ArgRS-ΔN in ATP−PP_i Exchange and tRNA Aminoacylation[a]

	ATP−PPi exchange[d]	tRNA arginylation	
	$tRNA_2^{Arg}$ [b]	$tRNA_2^{Arg}$ [b]	global tRNA[c]
	ArgRS		
K_m (μM)	0.023 ± 0.007	0.16 ± 0.03	0.32[e] ± 0.04
k_{cat} (s^{-1})	3.9 ± 0.4	0.40 ± 0.08	1.8[e] ± 0.2
k_{cat}/K_m (s^{-1} μM^{-1})	170	2.5	5.6
	ArgRS-ΔN		
K_m (μM)	0.024 ± 0.006	0.085 ± 0.005	0.39[e] ± 0.04
k_{cat} (s^{-1})	4.0 ± 0.5	0.17 ± 0.03	2.6[e] ± 0.3
k_{cat}/K_m (s^{-1} μM^{-1})	167	2.0	6.7

[a] Standard errors were determined from at least two independent data sets. [b] In vitro transcribed beef $tRNA_2^{Arg}$; acceptance of 500 pmol/A_{260}. [c] Partially purified native $tRNA^{Arg}$ from beef liver; acceptance of 43 pmol/A_{260}. [d] K_m values correspond to apparent K_{act} (activation constant) values for tRNAs. [e] Values from ref *36*.

repectively, two other components of this multienzyme complex, are tRNA-interacting factors (*11*, *14*). To assess the role of the N-terminal extension of ArgRS on tRNA binding, the two enzyme species ArgRS and ArgRS-ΔN were subjected to a band shift assay. Radiolabeled in vitro transcribed $tRNA_2^{Arg}$ was incubated with increasing amounts of ArgRS and ArgRS-ΔN (80 nM to 5 μM), and free and bound tRNA species were separated by electrophoresis on a native gel (Figure 1). The apparent K_d value of ArgRS-ΔN for $tRNA_2^{Arg}$ was higher than 10 μM, and ArgRS interacted with $tRNA_2^{Arg}$ with an apparent dissociation constant of 4 ± 1 μM. This K_d value determined for the full-length form of ArgRS is about 2 orders of magnitude higher than that obtained with MetRS (100 nM, ref *11*) and LysRS (60 nM, ref *14*) toward their cognate tRNAs but is in the range of the K_d's determined for these two enzymes after removal of their tRNA-interacting factors (4 and 6 μM, respectively, for MetRS-ΔC and LysRS-ΔN). Therefore, its eukaryotic-specific N-terminal polypeptide extension does not provide ArgRS with potent RNA binding properties.

ArgRS and ArgRS-ΔN Display Similar Catalytic Constants. We have shown previously that the two monomeric forms of ArgRS produced in yeast, ArgRS and ArgRS-ΔN, display the same kinetic parameters for tRNA in the $tRNA^{Arg}$ aminoacylation reaction when a partially purified beef liver tRNA is used as a substrate (ref *36* and Table 1). Because we observed that the presence of a large excess of noncognate tRNAs in the aminoacylation reaction may conceal kinetic effects contributed by the eukaryotic-specific, general tRNA-binding domains of two other eukaryotic aminoacyl-tRNA synthetases, namely, MetRS and LysRS (*11*, *14*, *42*), possibly via neutralization of the nonspecific RNA binding sites, we reinvestigated kinetic parameters of the various ArgRS species using a homogeneous $tRNA^{Arg}$ substrate. In vitro transcribed $tRNA_2^{Arg}$ proved to be an efficient substrate of ArgRS in the aminoacylation reaction, with a k_{cat}/K_m only 2 to 3-fold lower as compared with partially purified native beef $tRNA^{Arg}$, resulting essentially from a lower k_{cat} (Table 1).

The kinetic constants for $tRNA_2^{Arg}$ were determined in the tRNA aminoacylation reaction (Table 1). The K_m of the two recombinant free forms, ArgRS and ArgRS-ΔN, for $tRNA_2^{Arg}$ and the corresponding k_{cat} values were similar. In addition, because arginine activation by mammalian ArgRS is strictly tRNA-dependent (*36*), K_m and k_{cat} values for $tRNA_2^{Arg}$ in the ATP−PPi exchange reaction were also determined. The N-terminal domain did not improve the catalytic efficiency (k_{cat}/K_m) of ArgRS (Table 1). The turnover number of ArgRS and ArgRS-ΔN was about 10-fold higher in the ATP−PP_i exchange step as compared with the tRNA aminoacylation step. Thus, tRNA esterification or the release of aminoacylated tRNA may be the limiting step of the global reaction catalyzed by ArgRS or ArgRS-ΔN. These results, together with the tRNA binding assays described above, confirm that the eukaryotic-specific N-terminal extension of ArgRS is not a functional tRNA-interacting factor.

p43 and ArgRS Associate through Their N-Termini. The p43 component of the mammalian multisynthetase complex is a dimer of two 35.4 kDa subunits (*28*). Its C-terminal domain, from residues 147−312, is released from the complex after cleavage with caspase 7, a protease specifically activated during apoptosis, whereas its N-terminal domain remains associated with the synthetase components (*23*). A protein interaction map of the complex determined by a two-hybrid analysis revealed that p43 and ArgRS are interacting proteins (*33*). Surface plasmon resonance analysis established that ArgRS binds p43 with a dissociation constant of 93 nM whereas ArgRS-ΔN does not (*34*). The interaction of ArgRS and p43 was further addressed by in vitro pull-down experiments.

His-tagged p43 was incubated with ArgRS or ArgRS-ΔN and immunoprecipitated with anti-His antibodies. The presence of ArgRS in the immunoprecipitate was detected by Western blotting with antibodies directed to the ArgRS-ΔN moiety (Figure 2A). ArgRS but not ArgRS-ΔN was recovered in the immunoprecipitate obtained in the presence of p43. p43-N and p43-C represent the N-terminal (amino acid residues 1−146) or C-terminal (147−312) domain of p43, respectively. p43-N also co-immunoprecipitated ArgRS (Figure 2B), whereas p43-C did not (Figure 2C). These results clearly established that the N-terminal domains of p43 and ArgRS are involved in protein−protein interaction.

Association with ArgRS Does Not Impair the tRNA-Binding Capacity of p43. The 312-amino acid p43 protein has a potent general tRNA binding capacity (K_d = 0.2 μM) (*23*). In vitro transcribed $tRNA_2^{Arg}$ is also a good ligand for p43 with a K_d of 0.5 μM (Figure 3A). p43 was preincubated with ArgRS or ArgRS-ΔN at a 1:1 ratio to allow formation of a complex between ArgRS and p43; afterward, $tRNA_2^{Arg}$ was added to determine the tRNA binding capacity of the mixture by gel shift analysis. As shown in Figure 3A, addition of ArgRS, which associates with p43, or ArgRS-ΔN, which does not bind to p43, neither impaired nor significantly improved the tRNA binding capacity observed with p43 alone. This result suggested that the tRNA binding site of p43 is not sterically hindered after interaction of p43 with ArgRS. The supershift of tRNA induced by additional association of ArgRS to the tRNA−p43 complex is barely discernible (possibly because the two complexes have similar net charges) and could be best observed after longer electrophoresis in a less cross-linked gel (see below).

To ascertain that the gel shift of tRNA observed in the presence of ArgRS and p43 (Figure 3A) did correspond to a ternary complex, we performed a control experiment in which unlabeled $tRNA_2^{Arg}$ was mixed with ArgRS, p43, or both, and the gel shift of ArgRS and p43 was followed by

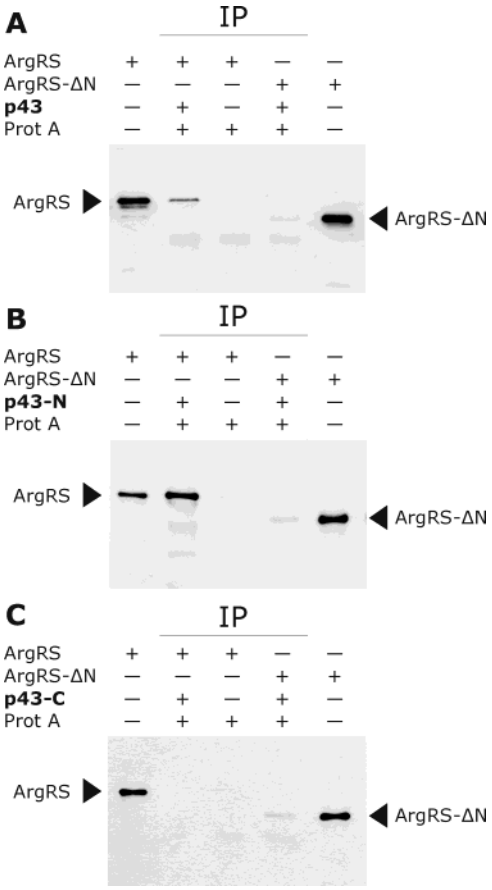

FIGURE 2: ArgRS associates with p43. His-tagged p43 (A), p43-N (B), or p43-C (C) was incubated with ArgRS (or ArgRS-ΔN) and subjected to immunoprecipitation (IP) using anti-His antibodies and Protein-A Sepharose. Immunoprecipitates were analyzed by Western blotting using antibodies directed to the conserved catalytic domain of ArgRS (ArgRS-ΔN). ArgRS (left lane) and ArgRS-ΔN (right lane) were analyzed in parallel (25 ng of homogeneous protein).

Western blotting with specific antibodies (Figure 3B). When p43 or ArgRS were added separately to $tRNA_2^{Arg}$, the electrophoretic mobility of p43, but not of ArgRS, was altered and corresponded to the single shift of tRNA. By contrast, when the two proteins were added together, ArgRS and p43 were both shifted and comigrated within the same complex, corresponding to a supershift of tRNA (Figure 3B).

We also verified that ArgRS and p43 remained associated in solution in the presence of tRNA. When His-tagged p43 was incubated with ArgRS in the presence of $tRNA_2^{Arg}$ at molar ratios of p43/tRNA of 1:1, 1:5, or 1:20, the immunoprecipitates obtained with anti-His antibodies also contained an invariable amount of ArgRS (Figure 1S, Supporting Information). Addition of tRNA did not antagonize p43−ArgRS interaction. Thus, the tRNA- and ArgRS-binding sites of p43 are not overlapping. Therefore, association of p43, a potent tRNA-interacting factor, might provide ArgRS with enhanced catalytic properties provided that p43-bound $tRNA^{Arg}$ is suitably presented to the catalytic center of ArgRS.

p43 Preferentially Binds the Acceptor-Stem, T-Stem−Loop Structure of tRNA. To further address the RNA binding properties of p43, the mode of binding of tRNA to p43 was investigated. To probe the interaction of tRNA with p43, the acceptor-TΨC stem−loop (Acc_2^{Arg}) and anticodon stem−loop (Ant_2^{Arg}) structures of $tRNA_2^{Arg}$ were synthesized in vitro (Figure 1) and used in a gel mobility shift assay to analyze their association with ArgRS, p43, and ArgRS−p43 complexes (Figure 4). Neither Acc_2^{Arg} nor Ant_2^{Arg} showed significant binding to ArgRS. The acceptor minihelix formed a stable complex with p43 with an apparent K_d value of about 0.5 μM, similar to the binding capacity of p43 for full-length

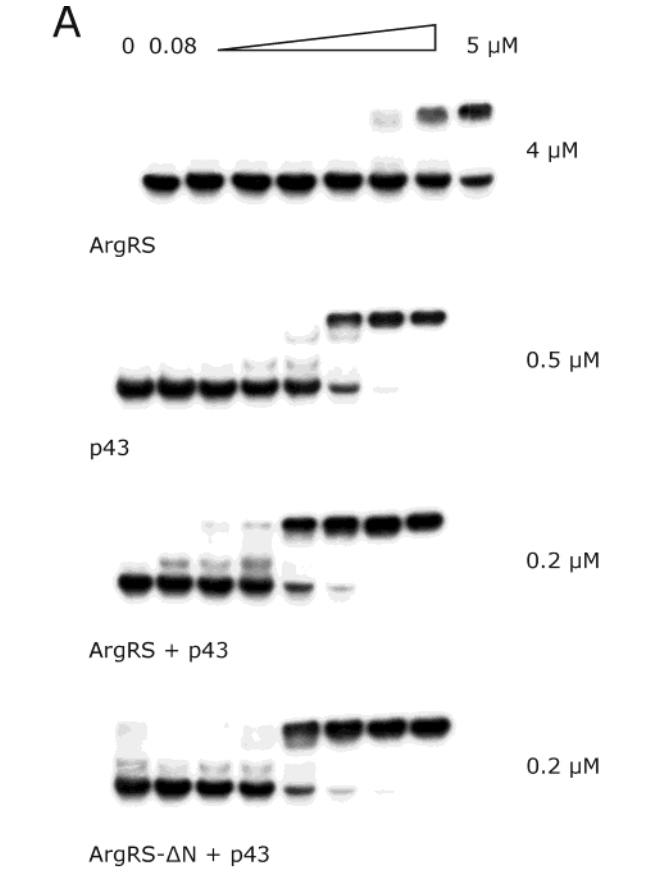

FIGURE 3: Binding of $tRNA^{Arg}$ by the ArgRS−p43 complex. In panel A, ^{32}P-labeled $tRNA_2^{Arg}$ was incubated with ArgRS (0.08−5 μM), p43 (0.04−2.5 μM; monomer concentration), or a mixture of ArgRS and p43 or ArgRS-ΔN and p43 (0.04−2.5 μM of each protein). After electrophoresis (30 min, 100 V) at 4 °C on a 6% native polyacrylamide gel, the mobility shift of tRNA was visualized by autoradiography. Apparent K_d values are indicated at right. In panel B, ArgRS, p43, or a mixture of both (0.5 μM each, monomer concentration) was incubated with or without in vitro transcribed $tRNA_2^{Arg}$ (0.3 μM). The mixture was subjected to electrophoresis (2 h; 100 V) at 4 °C on a 4% native polyacrylamide gel. The mobilities of ArgRS and p43 were identified by Western blotting (WB) with specific antibodies. The white and black arrows indicate the single mobility shift of tRNA in the presence of p43 or the supershift of tRNA in the presence of ArgRS and p43, respectively.

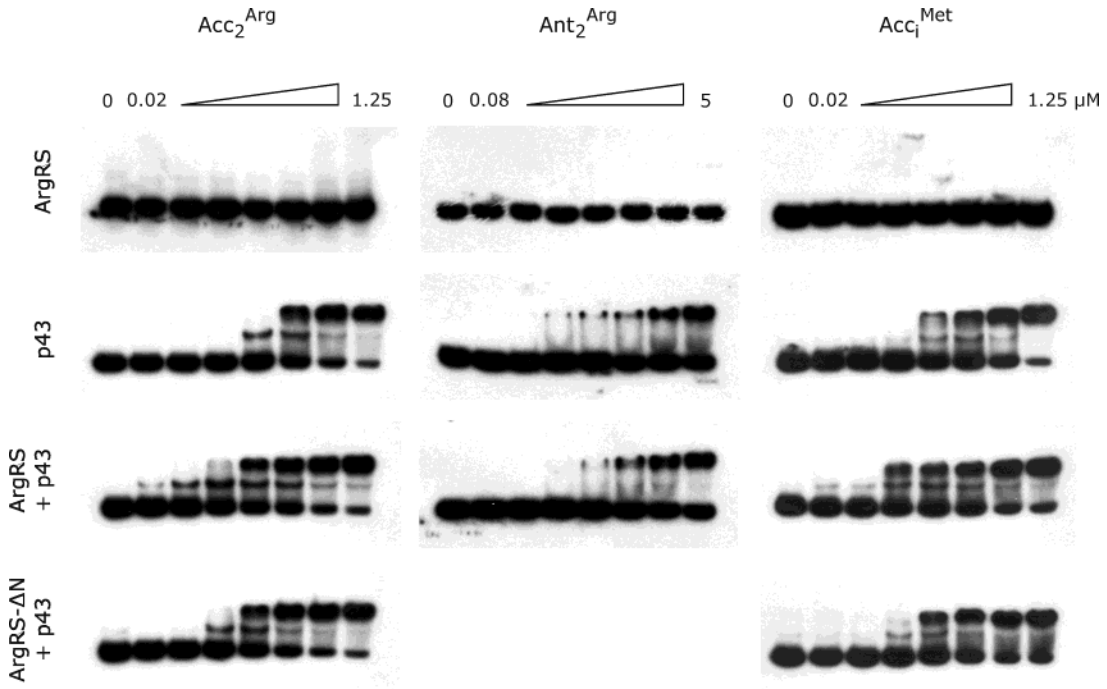

FIGURE 4: The mode of tRNA binding by p43 is not altered following its association with ArgRS. Binding of the acceptor-TΨC stem−loop (Acc_2^{Arg}) and anticodon stem−loop (Ant_2^{Arg}) minihelices of beef $tRNA_2^{Arg}$ by ArgRS, p43, and p43 in the presence of equimolar amounts of ArgRS or ArgRS-ΔN is shown. The mobility shift of the ^{32}P-labeled RNA minihelices was analyzed as described in the legend of Figure 1. A similar analysis was conducted in parallel using a ^{32}P-labeled minihelix corresponding to the acceptor-TΨC domain of yeast initiator $tRNA^{Met}$.

tRNA. By contrast, p43 displayed a much weaker affinity for the anticodon domain of $tRNA_2^{Arg}$ ($K_d \approx 5$ μM). We concluded that p43 preferentially binds the acceptor-TΨC stem−loop of $tRNA_2^{Arg}$. As observed above for the binding of full-length $tRNA_2^{Arg}$, the tRNA binding capacity of p43 for Acc_2^{Arg} or Ant_2^{Arg} was not significantly improved in the presence of ArgRS (K_d's of about 0.3 and 5.0 μM, respectively). The slight increase in binding of Acc_2^{Arg} (but not of Ant_2^{Arg}) observed after incubation of p43 with ArgRS is also detectable after incubation of p43 with ArgRS-ΔN, a derivative of ArgRS that does not associate with p43. These results suggest that association of p43 with ArgRS neither alters the tRNA-binding capacity of p43 nor modifies the mode of tRNA−p43 interaction.

p43 in solution is a nonspecific tRNA-interacting factor (*23*). We sought to check whether its association with ArgRS rendered p43 specific for $tRNA^{Arg}$. When full-length yeast $tRNA_i^{Met}$ (not shown) or Acc_i^{Met} (Figure 4) and Ant_i^{Met} (not shown) minihelices were used in the band shift assay in place of $tRNA_2^{Arg}$, the tRNA binding potential of p43 was not impaired after incubation with ArgRS or ArgRS-ΔN.

p43 Is Not a Trans-Acting tRNA-Interacting Factor for ArgRS. The possibility that p43 might act as a tRNA-presenting protein for ArgRS was investigated. ArgRS and p43 were mixed together at molar ratios ranging from 1:0.25 to 1:20 000 to allow protein−protein interaction, and the mixture was directly used in the tRNA aminoacylation assay. Because we sought to determine the putative effect of p43−ArgRS association on the efficiency of the aminoacylation reaction independent of any potential effect that might be attributed to the binding of p43 to tRNA, we used the bacterial tRNA-binding protein Trbp111 as a control. Trbp111 is a dimeric protein that binds tRNA without specificity of sequence (*37*) and can form a ternary complex with tRNA and tRNA synthetase without impairing the aminoacylation activity of the synthetase (*43*). When increasing concentrations of p43 or Trbp111 were added to ArgRS, the $tRNA^{Arg}$ aminoacylation capacity of the enzyme was not significantly affected (Figure 2S, Supporting Information). In particular, the aminoacylation activity of ArgRS was not enhanced in the presence of a 2-fold molar excess of p43, as previously reported by others (*35*).

Activity of ArgRS from the Multienzyme Complex Is p43-Independent. ArgRS and p43 are two components of the mammalian multisynthetase complex. The results obtained with free recombinant species of ArgRS and of p43, two ectopic proteins, strongly suggested that p43 is not a trans-acting tIF of ArgRS in the $tRNA^{Arg}$ aminoacylation reaction. To investigate whether p43 may be a tIF of ArgRS under native conditions, when the two proteins are associated within the multisynthetase complex, kinetic parameters for tRNA in the $tRNA^{Arg}$ aminoacylation reaction were determined for ArgRS-Cx, the ArgRS component of the complex. To assess the role of p43 on ArgRS activity, we used the multisynthetase complex treated with caspase 7. The p43 component of the mammalian multisynthetase complex is a substrate for caspase 7, a protease activated upon onset of apoptosis on mammalian cells (*23*). After treatment with caspase 7, the complex retains native ArgRS but is completely deprived of the EMAPII C-terminal domain of p43 (*23*). Thus, the potential tIF activity of p43 is lost. The kinetic parameters for $tRNA_2^{Arg}$ determined for ArgRS-Cx in the ATP−PP_i exchange and in the tRNA aminoacylation reactions were not affected by proteolytic subtraction of the tRNA-binding domain of p43 (Table 2).

Table 2: Kinetic Constants of ArgRS-Cx in ATP−PP_i Exchange and tRNA Aminoacylation[a]

	$tRNA_2^{Arg}$ [b]	
	ATP−PPi exchange[c]	tRNA arginylation
	ArgRS-Cx	
K_m (μM)	0.006 ± 0.001	0.20 ± 0.02
k_{cat} (s^{-1})	1.1 ± 0.2	0.16 ± 0.03
k_{cat}/K_m (s^{-1} μM^{-1})	183	0.8
	ArgRS-Cx/Casp7	
K_m (μM)	0.008 ± 0.002	0.20 ± 0.02
k_{cat} (s^{-1})	1.4 ± 0.2	0.13 ± 0.03
k_{cat}/K_m (s^{-1} μM^{-1})	175	0.65

[a] Standard errors were determined from at least two independent data sets. [b] In vitro transcribed beef $tRNA_2^{Arg}$; acceptance of 500 pmol/A_{260}. [c] K_m values correspond to apparent K_{act} values for tRNA.

DISCUSSION

The work reported here showed that p43 forms a binary complex with ArgRS (Figure 2) and that this association neither modulates the tRNA binding capacity of p43 (Figures 3 and 4) nor modifies the amino acid activation and tRNA aminoacylation activities of ArgRS (Tables 1 and 2; Figure 2S, Supporting Information). These results contrast with an earlier report showing that addition of p43 to ArgRS led to a 2.5-fold increase in ArgRS activity (*35*). They described that a 2-fold molar excess of p43 to ArgRS reduces the apparent K_m of ArgRS for tRNA, whereas the k_{cat} value is not affected. Surprisingly, when p43 was added in excess the enhancement of ArgRS activity was no longer observed. Whether these apparent discrepancies arise from differences in experimental procedure could not be assessed because detailed experimental procedures were not given in this study (*35*). Surprisingly, no quantitative data on enzyme activity (specific activity of the purified enzyme, k_{cat}, and K_m parameters) are furnished, and all the results are indicated as relative values. Nevertheless, the reported experiments provide some indications of possible sources of the discrepancies. Perhaps critically, the enzyme preparation used by Park et al. (*35*) was obtained after expression in *E. coli*. Indeed, we previously reported that expression of ArgRS in *E. coli* cells produces inclusion bodies and that the fraction of soluble enzyme has a reduced (100-fold) specific activity as compared with the enzyme used here, produced in yeast (*36*). Therefore, the enhancement of ArgRS activity observed by Park et al. (*35*) in the presence of stoichiometric amounts of p43 could be due to a chaperone effect of the binding of p43 on an ArgRS species that would not be properly folded.

ArgRS and p43 are the first example in which the association of an eukaryotic aminoacyl-tRNA synthetase with a tRNA-interacting factor does not provide kinetic advantages to the synthetase. The yeast homologue of p43, Arc1p, forms a ternary complex with MetRS and GluRS and stimulates the activity of MetRS mainly by reducing the K_m for $tRNA^{Met}$ by about 100-fold (*21*, *22*). When Arc1p in solution forms a complex with several yeast tRNAs, only elongator and initiator $tRNA^{Met}$ associated with the Arc1p−MetRS complex (*22*). Thus, in the yeast system, MetRS determines the specificity of the interaction and Arc1p strengthens association. By contrast, we observed that $tRNA^{Arg}$ but also $tRNA^{Met}$ are able to associate with p43 or with the p43−ArgRS complex with similar affinities. These data also support the conclusion that p43 is not a functional tIF for ArgRS and therefore does not provide catalytic advantages for the synthetase. Because the N-terminal domain of p43 is essential for association of ArgRS with the complex, our results support the proposal that this auxiliary component of the complex has a dual function: its N-terminal domain is a structural determinant for the assembly of this macromolecular structure and its C-terminal moiety is a tIF for another component of the complex.

Our results also provide some clues for understanding the mode of binding of tRNA by p43 and Trbp111. The crystal structure of the complex between *S. cerevisiae* ArgRS and $tRNA^{Arg}$ was reported at high resolution (*44*). The contact areas between the synthetase and its tRNA include the end of the acceptor stem of the tRNA with the catalytic center of the protein, the anticodon loop with the C-terminal α-helical domain, and the D-loop with the N-terminal α/β globular domain. The latter contact that involves the outer corner of the L-shaped tRNA molecule is rather unusual among aminoacyl-tRNA synthetases but should be conserved in hamster ArgRS, which displays a primary sequence and hence a structural organization similar to yeast ArgRS. In the present study, we showed that $tRNA_2^{Arg}$ or a minihelix corresponding to the acceptor-TΨC stem−loop bind to p43 with similar affinities. We also reported earlier that the C-terminal appended domain of plant MetRS, homologuous to the C-terminal tRNA-binding domain of p43, preferentially binds the acceptor stem of tRNA (*42*). This is in contrast to Trbp111, which is believed to bind to the convex side of the tRNA structure (*45*). Convincing evidence for the simultaneous binding of Trbp111 and IleRS to a single tRNA molecule was presented (*43*). However, the docking model proposed for the Trbp111−tRNA complex is not compatible with the simultaneous binding of Trbp111 and ArgRS to the same tRNA molecule. Indeed, according to this model, the N-terminal α/β globular domain of ArgRS should compete with Trbp111 for binding to the D-loop region of tRNA. The finding that saturating amounts of Trbp111 or of p43 do not inhibit aminoacylation of $tRNA^{Arg}$ by ArgRS suggests that the two proteins bind tRNA without steric hindrance.

In view of the finding in this paper that p43 is not a functional tIF of the ArgRS component of the mammalian complex, the functional partner of p43 within the multisynthetase complex must now be searched out. The intricate structural organization of this particle could reveal that two nonphysically interacting proteins may be close in the 3D-structure and so may be functionally connected.

SUPPORTING INFORMATION AVAILABLE

Results of His-tag immunoprecipitations of ArgRS and His-tagged p43 in the presence of tRNA and of aminoacylation assays of p43−ArgRS and Trbp111−ArgRS mixtures. This material is available free of charge via the Internet at http://pubs.acs.org.

REFERENCES

1. Ibba, M., and Söll, D. (2000) Aminoacyl-tRNA synthesis, *Annu. Rev. Biochem. 69*, 617−650.
2. Rould, M. A., Perona, J. J., Söll, D., and Steitz, T. A. (1989) Structure of *E. coli* glutaminyl-tRNA synthetase complexed with $tRNA^{Gln}$ and ATP at 2.8 Å resolution, *Science 246*, 1135−1142.

3. Ruff, M., Krishnaswamy, S., Boeglin, M., Poterszman, A., Mitschler, A., Podjarny, A., Rees, B., Thierry, J. C., and Moras, D. (1991) Class II aminoacyl tRNA synthetases: crystal structure of yeast aspartyl-tRNA synthetase complexed with $tRNA^{Asp}$, *Science 252*, 1682−1689.
4. Cusack, S., Yaremchuk, A., and Tukalo, M. (1996) The crystal structures of *T. thermophilus* lysyl-tRNA synthetase complexed with *E. coli* $tRNA^{Lys}$ and a *T. thermophilus* $tRNA^{Lys}$ transcript: Anticodon recognition and conformational changes upon binding of a lysyl-adenylate analogue, *EMBO J. 15*, 6321−6334.
5. Sankaranarayanan, R., Dock-Bregeon, A. C., Romby, P., Caillet, J., Springer, M., Rees, B., Ehresmann, C., Ehresmann, B., and Moras, D. (1999) The structure of threonyl-tRNA synthetase-$tRNA^{Thr}$ complex enlightens its repressor activity and reveals an essential zinc ion in the active site, *Cell 97*, 371−381.
6. Yaremchuk, A., Cusack, S., and Tukalo, M. (2000) Crystal structure of a eukaryote/archaeon-like prolyl-tRNA synthetase and its complex with $tRNA^{Pro}$(CGG), *EMBO J. 19*, 4745−4758.
7. Sekine, S., Nureki, O., Shimada, A., Vassylyev, D. G., and Yokoyama, S. (2001) Structural basis for anticodon recognition by discriminating glutamyl-tRNA synthetase, *Nat. Struct. Biol. 8*, 203−206.
8. Berthonneau, E., and Mirande, M. (2000) A gene fusion event in the evolution of aminoacyl-tRNA synthetases, *FEBS Lett. 470*, 300−304.
9. Cahuzac, B., Berthonneau, E., Birlirakis, N., Guittet, E., and Mirande, M. (2000) A recurrent RNA-binding domain is appended to eukaryotic aminoacyl-tRNA synthetases, *EMBO J. 19*, 445−452.
10. Jeong, E. J., Hwang, G. S., Kim, K. H., Kim, M. J., Kim, S., and Kim, K. S. (2000) Structural analysis of multifunctional peptide motifs in human bifunctional tRNA synthetase: Identification of RNA-binding residues and functional implications for tandem repeats, *Biochemistry 39*, 15775−15782.
11. Kaminska, M., Shalak, V., and Mirande, M. (2001) The appended C-domain of human methionyl-tRNA synthetase has a tRNA-sequestering function, *Biochemistry 40*, 14309−14316.
12. Raben, N., Nichols, R., Dohlman, J., McPhie, P., Sridhar, V., Hyde, C., Leff, R., and Plotz, P. (1994) A motif in human histidyl-tRNA synthetase which is shared among several aminoacyl-tRNA synthetases is a coiled-coil that is essential for enzymatic activity and contains the major autoantigenic epitope, *J. Biol. Chem. 269*, 24277−24283.
13. Wu, H., Nada, S., and Dignam, J. D. (1995) Analysis of truncated forms of *Bombyx mori* glycyl-tRNA synthetase: function of an N-terminal structure in RNA binding, *Biochemistry 34*, 16327−16336.
14. Francin, M., Kaminska, M., Kerjan, P., and Mirande, M. (2002) The N-terminal domain of mammalian lysyl-tRNA synthetase is a functional tRNA-binding domain, *J. Biol. Chem. 277*, 1762−1769.
15. Reed, V. S., Wastney, M. E., and Yang, D. C. H. (1994) Mechanisms of the transfer of aminoacyl-tRNA from aminoacyl-tRNA synthetase to the elongation factor 1α, *J. Biol. Chem. 269*, 32932−32936.
16. Reed, V. S., and Yang, D. C. H. (1994) Characterization of a novel N-terminal peptide in human aspartyl-tRNA synthetase − Roles in the transfer of aminoacyl-tRNA from aminoacyl-tRNA synthetase to the elongation factor 1α, *J. Biol. Chem. 269*, 32937−32941.
17. Hammamieh, R., and Yang, D. C. H. (2001) Magnesium ion-mediated binding to tRNA by an amino-terminal peptide of a class II tRNA synthetase, *J. Biol. Chem. 276*, 428−433.
18. Francin, M., and Mirande, M. (2003) Functional dissection of the eukaryotic-specific tRNA-interacting factor of lysyl-tRNA synthetase, *J. Biol. Chem. 278*, 1472−1479.
19. Negrutskii, B. S., and Deutscher, M. P. (1991) Channeling of aminoacyl-tRNA for protein synthesis in vivo, *Proc. Natl. Acad. Sci. U.S.A. 88*, 4991−4995.
20. Simos, G., Segref, A., Fasiolo, F., Hellmuth, K., Shevchenko, A., Mann, M., and Hurt, E. C. (1996) The yeast protein Arc1p binds to tRNA and functions as a cofactor for the methionyl- and glutamyl-tRNA synthetases, *EMBO J. 15*, 5437−5448.
21. Simos, G., Sauer, A., Fasiolo, F., and Hurt, E. C. (1998) A conserved domain within Arc1p delivers tRNA to aminoacyl-tRNA synthetases, *Mol. Cell 1*, 235−242.
22. Deinert, K., Fasiolo, F., Hurt, E. C., and Simos, G. (2001) Arc1p organizes the yeast aminoacyl-tRNA synthetase complex and stabilizes its interaction with the cognate tRNAs, *J. Biol. Chem. 276*, 6000−6008.
23. Shalak, V., Kaminska, M., Mitnacht-Kraus, R., Vandenabeele, P., Clauss, M., and Mirande, M. (2001) The EMAPII cytokine is released from the mammalian multisynthetase complex after cleavage of its p43/proEMAPII component, *J. Biol. Chem. 276*, 23769−23776.
24. Kleeman, T. A., Wei, D. B., Simpson, K. L., and First, E. A. (1997) Human tyrosyl tRNA synthetase shares amino acid sequence homology with a putative cytokine, *J. Biol. Chem. 272*, 14420−14425.
25. Wakasugi, K., and Schimmel, P. (1999) Two distinct cytokines released from a human aminoacyl-tRNA synthetase, *Science 284*, 147−151.
26. Renault, L., Kerjan, P., Pasqualato, S., Menetrey, J., Robinson, J. C., Kawaguchi, S., Vassylyev, D. G., Yokoyama, S., Mirande, M., and Cherfils, J. (2001) Structure of the EMAPII domain of human aminoacyl-tRNA synthetase complex reveals evolutionary dimer mimicry, *EMBO J. 20*, 570−578.
27. Kao, J., Ryan, J., Brett, G., Chen, J., Shen, H., Fan, Y. G., Godman, G., Familletti, P. C., Wang, F., Pan, Y. C., Stern, D., and Clauss, M. (1992) Endothelial monocyte-activating polypeptide II. A novel tumor-derived polypeptide that activates host-response mechanisms, *J. Biol. Chem. 267*, 20239−20247.
28. Quevillon, S., Agou, F., Robinson, J. C., and Mirande, M. (1997) The p43 component of the mammalian multi-synthetase complex is likely to be the precursor of the endothelial monocyte-activating polypeptide II cytokine, *J. Biol. Chem. 272*, 32573−32579.
29. Knies, U. E., Behrensdorf, H. A., Mitchell, C. A., Deutsch, U., Risau, W., Drexler, H. C., and Clauss, M. (1998) Regulation of endothelial monocyte-activating polypeptide II release by apoptosis, *Proc. Natl. Acad. Sci. U.S.A. 95*, 12322−12327.
30. Ko, Y. G., Park, H., Kim, T., Lee, J. W., Park, S. G., Seol, W., Kim, J. E., Lee, W. H., Kim, S. H., Park, J. E., and Kim, S. (2001) A cofactor of tRNA synthetase, p43, is secreted to up-regulate proinflammatory genes, *J. Biol. Chem. 276*, 23028−23033.
31. Park, S. G., Kang, Y. S., Ahn, Y. H., Lee, S. H., Kim, K. R., Kim, K. W., Koh, G. Y., Ko, Y. G., and Kim, S. (2002) Dose-dependent biphasic activity of tRNA synthetase-associating factor, p43, in angiogenesis, *J. Biol. Chem. 277*, 45243−45248.
32. Norcum, M. T., and Warrington, J. A. (2000) The cytokine portion of p43 occupies a central position within the eukaryotic multi-synthetase complex, *J. Biol. Chem. 275*, 17921−17924.
33. Quevillon, S., Robinson, J. C., Berthonneau, E., Siatecka, M., and Mirande, M. (1999) Macromolecular assemblage of aminoacyl-tRNA synthetases: Identification of protein−protein interactions and characterization of a core protein, *J. Mol. Biol. 285*, 183−195.
34. Robinson, J. C., Kerjan, P., and Mirande, M. (2000) Macromolecular assemblage of aminoacyl-tRNA synthetases: Quantitative analysis of protein−protein interactions and mechanism of complex assembly, *J. Mol. Biol. 304*, 983−994.
35. Park, S. G., Jung, K. H., Lee, J. S., Jo, Y. J., Motegi, H., Kim, S., and Shiba, K. (1999) Precursor of pro-apoptotic cytokine modulates aminoacylation activity of tRNA synthetase, *J. Biol. Chem. 274*, 16673−16676.
36. Lazard, M., Kerjan, P., Agou, F., and Mirande, M. (2000) The tRNA-dependent activation of arginine by arginyl-tRNA synthetase requires inter-domain communication, *J. Mol. Biol. 302*, 991−1004.
37. Morales, A. J., Swairjo, M. A., and Schimmel, P. (1999) Structure-specific tRNA-binding protein from the extreme thermophile *Aquifex aeolicus*, *EMBO J. 18*, 3475−3483.
38. Mirande, M., Cirakoglu, B., and Waller, J. P. (1983) Seven mammalian aminoacyl-tRNA synthetases associated within the same complex are functionally independent, *Eur. J. Biochem. 131*, 163−170.
39. Rho, S. B., Kim, M. J., Lee, J. S., Seol, W. G., Motegi, H., Kim, S., and Shiba, K. (1999) Genetic dissection of protein−protein interactions in multi-tRNA synthetase complex, *Proc. Natl. Acad. Sci. U.S.A. 96*, 4488−4493.
40. Cirakoglu, B., and Waller, J. P. (1985) Multiple forms of arginyl- and lysyl-tRNA synthetases in rat liver: a reevaluation, *Biochim. Biophys. Acta 829*, 173−179.
41. Sivaram, P., and Deutscher, M. P. (1990) Existence of two forms of rat liver arginyl-tRNA synthetase suggests channeling of aminoacyl-tRNA for protein synthesis, *Proc. Natl. Acad. Sci. U.S.A. 87*, 3665−3669.

42. Kaminska, M., Deniziak, M., Kerjan, P., Barciszewski, J., and Mirande, M. (2000) A recurrent general RNA binding domain appended to plant methionyl-tRNA synthetase acts as a *cis*-acting cofactor for aminoacylation, *EMBO J. 19*, 6908−6917.
43. Nomanbhoy, T., Morales, A. J., Abraham, A. T., Vortler, C. S., Giegé, R., and Schimmel, P. (2001) Simultaneous binding of two proteins to opposite sides of a single transfer RNA, *Nat. Struct. Biol. 8*, 344−348.
44. Delagoutte, B., Moras, D., and Cavarelli, J. (2000) tRNA aminoacylation by arginyl-tRNA synthetase: induced conformations during substrates binding, *EMBO J. 19*, 5599−5610.
45. Swairjo, M. A., Morales, A. J., Wang, C. C., Ortiz, A. R., and Schimmel, P. (2000) Crystal structure of Trbp111: a structure-specific tRNA-binding protein, *EMBO J. 19*, 6287−6298.

BI036150E

3.2. С-кінцевий домен білка p43 вивільняється із макромолекулярного комплексу аміноацил-тРНК синтетаз під дією каспази 7 і є ідентичним до EMAPII

THE JOURNAL OF BIOLOGICAL CHEMISTRY Vol. 276, No. 26, Issue of June 29, pp. 23769–23776, 2001
© 2001 by The American Society for Biochemistry and Molecular Biology, Inc.
Printed in U.S.A.

The EMAPII Cytokine Is Released from the Mammalian Multisynthetase Complex after Cleavage of Its p43/proEMAPII Component*

Received for publication, January 18, 2001, and in revised form, March 28, 2001
Published, JBC Papers in Press, April 16, 2001, DOI 10.1074/jbc.M100489200

Vyacheslav Shalak‡, Monika Kaminska‡§, Rita Mitnacht-Kraus¶, Peter Vandenabeele‖, Matthias Clauss¶, and Marc Mirande‡**

From the ‡Laboratoire d'Enzymologie et Biochimie Structurales, CNRS, 1 Avenue de la Terrasse, 91190 Gif-sur-Yvette, France, ¶Department of Molecular Cell Biology, Max-Planck-Institut für Physiologische und Klinische Forschung, 61231 Bad Nauheim, Germany, and ‖Molecular Signalling and Cell Death Unit, Department of Molecular Biology, Flanders Interuniversity Institute for Biotechnology (VIB), University of Gent, B-9000 Gent, Belgium

Endothelial-monocyte-activating polypeptide II (EMAPII) is an inflammatory cytokine released under apoptotic conditions. Its proEMAPII precursor proved to be identical to the auxiliary p43 component of the aminoacyl-tRNA synthetase complex. We show here that the EMAPII domain of p43 is released readily from the complex after *in vitro* digestion with caspase 7 and is able to induce migration of human mononuclear phagocytes. The N terminus of *in vitro*-processed EMAPII coincides exactly with that of the mature cytokine isolated from conditioned medium of fibrosarcoma cells. We also show that p43/proEMAPII has a strong tRNA binding capacity (K_D = 0.2 μM) as compared with its isolated N or C domains (7.5 μM and 40 μM, respectively). The potent general RNA binding capacity ascribed to p43/proEMAPII is lost upon the release of the EMAPII domain. This suggests that after onset of apoptosis, the first consequence of the cleavage of p43 is to limit the availability of tRNA for aminoacyl-tRNA synthetases associated within the complex. Translation arrest is accompanied by the release of the EMAPII cytokine that plays a role in the engulfment of apoptotic cells by attracting phagocytes. As a consequence, p43 compares well with a molecular fuse that triggers the irreversible cell growth/cell death transition induced under apoptotic conditions.

In higher eukaryotic organisms, from *Drosophila* to mammals, the nine aminoacyl-tRNA synthetases specific for amino acids Glu, Pro, Ile, Leu, Met, Gln, Lys, Arg, and Asp are associated within a multienzyme complex containing three auxiliary proteins, as well (1). The p38 auxiliary component contributes a scaffold protein for the assembly of the complex (2, 3). The p18 subunit of the complex might be an anchor for transient association of elongation factor EF-1H (4). The p43 subunit is an RNA-binding protein (5) based on a classical oligonucleotide-oligosaccharide binding fold (6, 7) that might play a role of a cofactor for aminoacylation (8). Whereas the p18 and p38 proteins are always recovered as components of the multisynthetase complex, p43 or p43-like domains are widespread in evolution and distributed in the three kingdoms of the tree of life. They have been described as polypeptide appendices of MetRS[1] (8), PheRS, or TyrRS (9) or as discrete proteins interacting with aminoacyl-tRNA synthetases and/or tRNAs, Trbp in bacteria (10, 11), Arc1p in yeast (12), or p43 in ciliated protozoan (13) or in metazoan species (5, 7).

Unexpectedly, a human protein homologous to the C-terminal moiety of hamster p43 was reported to have cytokine activities (14, 15). The endothelial-monocyte-activating polypeptide II (EMAPII) has been isolated from methylcholanthrene A-induced fibrosarcoma cells. EMAPII is a proinflammatory cytokine that stimulates chemotactic migration of polymorphonuclear granulocytes and mononuclear phagocytes and induces tissue factor activity on endothelial cells. The C-terminal domain of human or bovine TyrRS, which is related to EMAPII, displays identical cytokine activities (16, 17). EMAPII is expressed constitutively in all cell types as a ~35-kDa precursor and is further processed to an ~18-kDa mature form upon onset of apoptosis (18, 19). Consistent with its maturation under apoptotic conditions, the precursor polypeptide obtained by *in vitro* transcription was shown to be a substrate for apoptotic proteases of the caspase family (20).

Because the p43 component of the multisynthetase complex is identical to proEMAPII, we wondered whether EMAPII could be processed from its complex-associated precursor. To address the consequences of p43 cleavage, we equally considered its involvement as a general RNA binding domain or as a cytokine. The results provide strong evidence for a dual role of p43 that can be identified with a molecular fuse. The function of p43 as a cofactor of aminoacyl-tRNA synthetases is lost upon cleavage and release of EMAPII, its C-domain with cytokine activity. Because proEMAPII is p43, a protein involved in translation and therefore ubiquitous to all cell types and tissues, previous reports dealing with the relative abundance of EMAPII mRNA or protein should be considered cautiously. They address, as well, the level of p43 in those tissues where active protein synthesis is required for tissue remodeling.

* This work was supported in part by grants from the Program Physique et Chimie du Vivant from CNRS, the Association pour la Recherche sur le Cancer, and La Ligue. V. S. was supported by INTAS (YSF 99-208) and NATO fellowships. M. K. was supported in part by grants from the Jumelage Franco-Polonais program from CNRS. The costs of publication of this article were defrayed in part by the payment of page charges. This article must therefore be hereby marked "*advertisement*" in accordance with 18 U.S.C. Section 1734 solely to indicate this fact.

§ Present address: Inst. of Bioorganic Chemistry, Polish Academy of Sciences, 60-704 Poznan, Poland.

** To whom correspondence should be addressed. Tel.: 33-1-69-82-35-05; Fax: 33-1-69-82-31-29; E-mail: marc.mirande@lebs.cnrs-gif.fr.

[1] The abbreviations used are: RS, tRNA synthetase; EMAPII, endothelial-monocyte-activating polypeptide II; DTT, dithiothreitol; h, human; N, N-terminal domain; C, C-terminal domain; m, murine; PAGE, polyacrylamide gel electrophoresis; Z-DEVD-CMK, benzyloxycarbonyl-Asp-Glu-Val-Asp-chloromethyl ketone; MP, mononuclear phagocyte.

MATERIALS AND METHODS

Purification of the Multisynthetase Complex from Mouse Liver—Livers (160 g) from 120 mice were homogenized in a Waring Blendor (2 × 15 s) after addition (1 ml per g) of extraction buffer (50 mM Tris-HCl, pH 7.5, 5 mM $MgCl_2$, 0.1 mM EDTA, 1 mM DTT, and 10% glycerol) containing protease inhibitors (1 mM diisopropyl fluorophosphate, 2 mM phenylmethylsulfonyl fluoride). Extract was cleared by centrifugation at 30,000 × *g* for 30 min and subjected further to high speed centrifugation at 260,000 × *g* for 2 h. The supernatant was applied on a 1,700-ml (5 × 85 cm) Sephacryl S-400 HR column (Amersham Pharmacia Biotech) equilibrated in Buffer A (75 mM potassium phosphate buffer, pH 7.5, 10 mM 2-mercaptoethanol, and 10% glycerol) and developed at a flow rate of 4 ml/min. Fractions with LysRS activity were combined and applied on a 30-ml (1.6 × 15 cm) tRNA-Sepharose column (21) developed at a flow rate of 1 ml/min. The complex was eluted with a linear gradient of potassium phosphate buffer (75 to 350 mM). After a 4-fold dilution with a solution containing 2 mM DTT and 10% glycerol, fractions were applied on a 1-ml Resource Q column (Amersham Pharmacia Biotech) equilibrated in Buffer B (25 mM Tris-HCl, pH 7.5, 50 mM KCl, 1 mM DTT, 10% glycerol) and developed at 1 ml/min with a linear gradient of KCl from 50 to 500 mM. Fractions were dialyzed against 25 mM potassium phosphate, pH 7.5, 2 mM DTT, and 55% glycerol and stored at −20 °C.

Expression and Purification of p43 and of Derivatives Thereof—Human p43 (h-p43), as well as its N-terminal (h-p43N) or C-terminal domains (h-p43C; EMAPII), were expressed in *Escherichia coli* with the pET-28b expression system (Novagen). The h-p43 cDNA was produced by polymerase chain reaction between the two oligonucleotides p43–3 (5′-ccccc**atgg**caaataatgatgctgttctgaagagac) and p43–2 (5′-ccc**ctcgag**tttgattccactgttgctca), which introduced an *Nco*I site with the ATG initiation codon and an *Xho*I site in frame with the vector sequences encoding the His tail, respectively. The cDNA encoding the equivalent region of murine p43 (m-p43) was also introduced into the pET28b vector after amplification between oligonucleotides p43-m1 (5′-ccccc**atgg**caacgaatgatgctgt) and p43-m2 (5′-ccc**ctcgag**tttaattccactattggccat). The h-p43N cDNA was amplified between oligonucleotides p43–3 and p43–160 (5′-ccc**ctcgaggt**cggcacttccagctattga). The h-p43C construct has been described previously (5). A derivative without a His tail at the C terminus was constructed after amplification between p43–1 (5′-ccccc**atgg**ccaagccaatagatgtttccc) and p43–20 (5′-ccc**ctcgagtta**tttgattccactgttgctca), which introduced a stop codon. The nucleotide sequence of the constructs was checked by DNA sequencing.

Expression and purification of p43 variants bearing a His tag was conducted essentially as described previously (5), following two chromatographic steps on a nickel-nitrilotriacetic acid Superflow matrix (Qiagen) and on a SOURCE 15S column (Amersham Pharmacia Biotech.). Purified proteins were stored at −20 °C after dialysis against 20 mM Tris-HCl, pH 7.0, 50 mM NaCl, 2 mM DTT, 55% glycerol.

For purification of h-p43C without His tag, cell extract obtained as described above in 20 ml of 30 mM Tris-HCl, pH 7.0, 30 mM KCl, 0.1 mM EDTA, 2 mM DTT, 10% glycerol was applied to a 1.6 × 13-cm column of S-Sepharose Fast Flow (Amersham Pharmacia Biotech) equilibrated in 20 mM Tris-HCl, pH 7.0, 30 mM NaCl, 1 mM DTT. The protein was eluted (at 300 mM) by a linear gradient of NaCl (30 to 500 mM) in the same buffer. To remove contaminating nucleic acids, fractions were dialyzed against 20 mM Tris-HCl, pH 7.0, 15 mM NaCl, 1 mM DTT and applied to a 2.0 × 9.5-cm SOURCE 15Q column equilibrated in the same buffer. The material recovered in the flow-through fraction was concentrated on a 1-ml Resource 15S column, eluted stepwise with 500 mM NaCl, and stored at −20 °C in 25 mM potassium phosphate buffer, pH 7.5, 2 mM DTT, and 55% glycerol. Protein concentrations were determined by using calculated absorption coefficients of 0.257, 0.260, 0.068, and 0.432 A_{280} units/mg^{-1}/cm^2, respectively, for h-p43, m-p43, h-p43N, and h-p43C.

Controlled Proteolysis with Caspase—The purified murine multienzyme complex or homogeneous murine or human p43 were incubated in the presence of various homogeneous murine caspases (caspase 3, 7, or 8; see Ref. 22) or with human caspase 7 (PharMingen) at 37 °C in CFS buffer (10 mM HEPES-NaOH, pH 7.4, 2.5 mM KH_2PO_4, 2 mM NaCl, 2 mM $MgCl_2$, 0.5 mM EGTA, 5 mM pyruvate, 68 mM sucrose, 220 mM mannitol, and 10 mM DTT). At the time intervals indicated, aliquots were treated with SDS for analysis by SDS-PAGE and Western blotting. Where indicated, 0.1 μM of the caspase inhibitor benzyloxycarbonyl-Asp-Glu-Val-Asp-chloromethyl ketone (Z-DEVD-CMK) was added.

Purification of Mouse EMAPII after Caspase 7 Digestion of the Complex—Mouse complex (500 μg) was digested with caspase 7 (10,250 units; 247,600 units/mg (22)) in 6 ml of CFS buffer containing 0.01% Tween 20. After 90 min of incubation at 37 °C, the mixture was placed on ice, diluted with 6 ml of 2-fold concentrated Buffer A (Buffer A is 20 mM Tris-HCl, pH 7.5, 15 mM NaCl, 1 mM DTT, 0.01% Tween 20, 10% glycerol), and applied on a 1-ml Resource Q column equilibrated in Buffer A. The flow-through fraction was applied to a 0.8-ml Mini-S column equilibrated in Buffer B (20 mM Tris-HCl, pH 7.5, 2 mM DTT, 0.01% Tween 20) and developed with a linear gradient of NaCl from 0 to 350 mM. EMAPII, eluted at an NaCl concentration of 120 mM, was concentrated by ultrafiltration on MICROSEP (Pall Filtron; 3-kDa molecular mass cutoff). The N-terminal sequence of EMAPII was determined by automated Edman degradation using an Applied Biosystems 473 sequencer.

Preparation of Antibodies and Western Blotting—Polyclonal antibodies were raised in rabbit against purified h-p43N and h-p43C following repeated injections at 2-week intervals of 0.5 mg of homogeneous protein emulsified with complete (first injection) or incomplete Freund's adjuvant. Other antibodies directed to murine EMAPII (18) or to components of the multisynthetase complex (23) were as described. After SDS-PAGE (24), Western blotting was conducted essentially as described (25), using polyvinylidene difluoride transfer membranes (Hybond-P; Amersham Pharmacia Biotech), goat anti-rabbit IgG conjugated with peroxidase, and the ECL detection reagents.

Monocyte Chemotactic Assay—Monocytes were isolated from buffy coats of healthy donors in a two-step procedure by density-gradient centrifugation and elutriation. Peripheral blood mononuclear cells were obtained from citrated venous blood (buffy coats) from healthy donors according to the method of Boyum (26). Blood was diluted 1:3 in Hanks' buffered saline, and 25 ml of this cell suspension was layered over 15 ml of Ficoll-Paque (Amersham Pharmacia Biotech). After centrifugation at 600 × *g* for 20 min cells at the interphase containing peripheral blood mononuclear cells were collected, and cell suspension was washed twice with Hanks' buffered saline to remove platelets. For further monocyte isolation cells were resuspended in 15 ml of Hanks' buffered saline and placed into the sample tube of a JE-6B elutriator rotor (Beckman). At a constant rotor speed of 2300 rpm flow rate was increased successively from 7 ml/min to 18 ml/min. Monocytes were reproducibly eluted in fractions 5 to 9, containing more than 90% monocytes ($CD14^+$ cells) as determined by fluorescence-activated cell sorter analysis with an anti-CD14 monoclonal antibody. After isolation cells were centrifuged (1000 rpm; 5 min), and monocytes were cultivated not longer than 24 h in serum-free macrophage medium, 2 mM L-glutamine, 100 units/ml penicillin, and 100 μg/ml streptomycin, at a concentration of 2 × 10^6 cells/ml. To avoid cell adhesion to the plastic surface hydrophobic culture plates (In Vitro Systems) were used.

Chemotaxis of monocytes was investigated using the method of Quinn *et al*. (27) as modified recently (14). Briefly, isolated monocytes were placed in the upper chamber, and the test substances were placed in the lower chamber. Chemotactic assays were performed for 1 h of incubation, unmigrated cells on the filter surface were removed, and migrated cells were stained with Giemsa stain. Cells in at least six power fields were counted for each condition assessed.

Sedimentation Equilibrium—Ultracentrifugation experiments were conducted and analyzed as described previously (8, 28). Sedimentation equilibrium data were fitted to theoretical models taking into account molecular weights of 35,418, 17,218, and 19,398, respectively, for the monomers of p43, p43N, and p43C and $\bar{v}$ values of 0.735, 0.734, and 0.733 at 4 °C.

Gel Retardation Assay—Protein-tRNA interactions were assayed using a band shift assay as described previously (5, 8). ^{32}P-Labeled tRNAs were synthesized in a reaction mixture (50 μl) containing 1 μg of template DNA, 40 mM Tris-HCl, pH 8.0, 6 mM $MgCl_2$, 1 mM spermidine, 5 mM DTT, 0.01% Triton X-100, 1 mM each of CTP, UTP, and GTP, 10 μM [α-^{32}P]ATP (200 Ci/mmol), 1000 units/ml T7 RNA polymerase. After incubation at 37 °C for 1 h, the transcripts were purified by electrophoresis on a denaturing 12% polyacrylamide gel (mono:bis, 19:1), recovered from the gel by electroelution, precipitated with ethanol, resuspended in 20 mM Tris-HCl, pH 7.5, 10 mM $MgCl_2$, heated at 65 °C for 5 min, and renaturated by slow cooling at 25 °C.

Homogeneous p43 and p43 derivatives were incubated at increasing concentrations with radiolabeled tRNA (100,000 cpm (Cerenkov) per point) in an 11-μl volume containing 20 mM Tris-HCl, pH 7.5, 150 mM NaCl, 10 mM $MgCl_2$, 10 mM 2-mercaptoethanol, 10% glycerol, and bovine serum albumin at 0.1 mg/ml. After incubation at 25 °C for 20 min, the mixture was placed on ice and loaded on a 6% polyacrylamide gel (mono:bis, 29:1) containing 5% glycerol in 0.5 × Tris borate-EDTA, pH 9.5, at 4 °C. After electrophoresis, the gel was fixed, dried, and subjected to autoradiography. Free and bound tRNA were quantified using a PhosphorImager (Molecular Dynamics).

Aminoacylation Assay—Initial rates of tRNA aminoacylation were measured at 25 °C in 0.1 ml of 20 mM imidazole-HCl buffer, pH 7.5, 150 mM KCl, 0.5 mM DTT, 5 mM $MgCl_2$, 3 mM ATP, 60 μM ^{14}C-labeled amino acid (50 Ci/mol; PerkinElmer Life Sciences), and saturating amounts of tRNA, as previously described (29). Total brewers' yeast tRNA (Roche Molecular Biochemicals) or partially purified beef tRNA were used as tRNA substrates. The incubation mixture contained catalytic amounts (1 to 10 nM) of enzymes appropriately diluted in 10 mM Tris-HCl, pH 7.5, 10 mM 2-mercaptoethanol containing bovine serum albumin at 4 mg/ml. One unit of activity is the amount of enzyme producing 1 nmol of aminoacyl-tRNA/min at 25 °C.

RESULTS

The p43 Component of the Multisynthetase Complex Is a Substrate of Caspase 7—The p43 component of the multisynthetase complex is the homolog of proEMAPII, the precursor of the EMAPII cytokine (5). Previous studies showed that [^{35}S]-labeled mouse proEMAPII produced in an *in vitro* transcription/translation system is a substrate of caspase 7 and, to a lesser extent, of caspase 3 (20). Because the only known cellular species of p43 is that associated within the multisynthetase complex (5), we surmised that if p43 is proEMAPII, the precursor of the cytokine, the caspase-7 cleavage site on p43 should be readily accessible in the complex. On the contrary, if the p43 component of the complex would be protected against caspase digestion, it could not be the direct precursor of EMAPII.

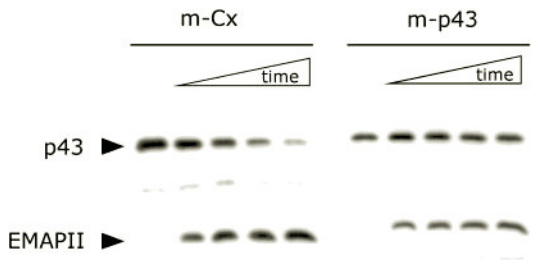

FIG. 1. **Time course of p43 digestion with caspase 7.** The purified murine multienzyme complex (*m-Cx*; 1.5 μg) or the recombinant murine p43 expressed in *E. coli* with a His tag (*m-p43*; 0.06 μg) was incubated at 37 °C in the absence or in the presence of murine caspase 7 (25 units). At different time intervals (0, 15, 30, 60, and 90 min), the incubation mixture was analyzed by SDS-PAGE and Western blotting using antibodies directed to the C-terminal domain of p43 (*EMAPII*).

Homogeneous mouse multisynthetase complex was incubated in the presence of mouse caspase 7, and time course of p43 digestion was monitored by Western blotting with anti-EMAPII antibodies directed to the C-terminal moiety of p43 (Fig. 1). After 90 min of incubation, the p43 polypeptide (80 ng of protein taking into account that 2 molecules of p43 (2 × 40 kDa) are associated per molecule of complex (1.5 MDa)) was almost entirely converted into EMAPII, an 18-kDa polypeptide. In contrast, after a 90-min digestion with caspase 7 of recombinant mouse p43 (60 ng of the dimeric protein) expressed in *E. coli* (see below), only ~50% of the p43 polypeptide was converted into EMAPII. We concluded that the p43 component of the complex is a substrate of caspase 7 and that its association within the complex facilitates its cleavage. Caspase 3 or caspase 8 did not efficiently cleave the complex-associated form of p43 or the isolated subunit (not shown).

To test the behavior of the other components of the complex toward caspase 7 treatment, the multisynthetase complex subjected to controlled proteolysis was analyzed by SDS-PAGE followed by Coomassie staining (Fig. 2) and Western blotting (see Fig. 2 and below) using antibodies directed to individual components. Complete analysis revealed that IleRS, LeuRS, MetRS, ArgRS, p38, and probably GlnRS were not affected by the addition of caspase 7. In contrast, GluProRS (163 kDa), LysRS (68 kDa), and AspRS (57 kDa), in addition to p43, were cleaved by caspase 7 and converted to polypeptides of 105 + 60 kDa for GluProRS, 66 and 61 kDa for LysRS, and 55 kDa for AspRS. As shown in Fig. 2, when Z-DEVD-CMK, a potent and specific inhibitor of caspase 7, was added in the incubation mixture, cleavage of p43, GluProRS, LysRS, and AspRS was completely abolished.

Caspase 7 Treatment Releases EMAPII from the Complex—If EMAPII is a cleavage product of the complex-associated form of p43, then it should be readily released from the complex after caspase 7 treatment. The mouse complex was incubated with caspase 7 as described above and subjected to size fractionation on a Superose 12 column (Fig. 3). A major peak was eluted with an apparent mass corresponding to the native complex (fraction B). Two additional minor peaks were observed corresponding to the elution volumes of proteins of ~100 kDa (fraction C) and of small proteins eluting near the inclusion volume of the column (fraction E). Fraction F corresponded to the elution of components of the incubation buffer in the total bed volume of

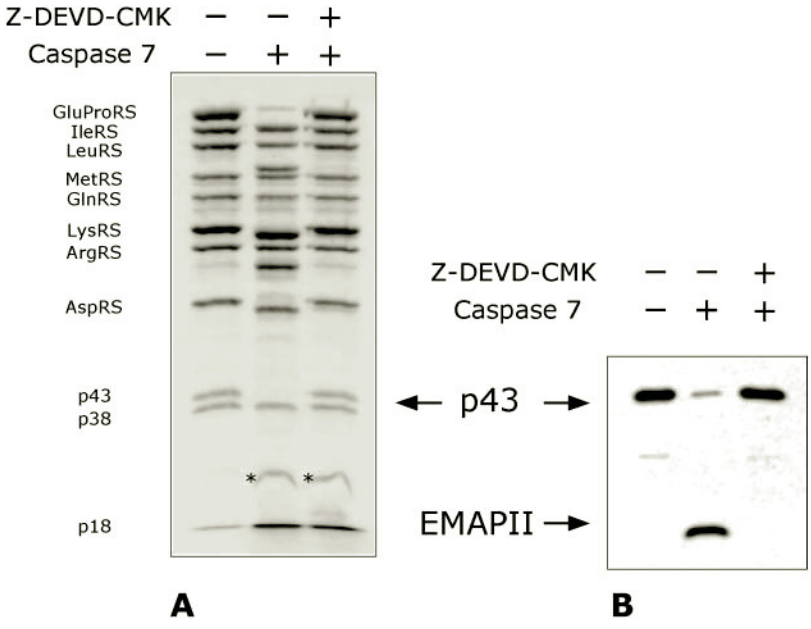

FIG. 2. **Search for components of the complex cleaved by caspase 7.** Murine multisynthetase complex (1.5 μg) was incubated with caspase 7 (50 units) and Z-DEVD-CMK (0.1 μM), as indicated. After 90 min of incubation at 37 °C, samples were analyzed by SDS-PAGE and Coomassie staining (*A*) or by Western blotting using antibodies directed to the C-terminal EMAPII domain of p43 (*B*). The polypeptide marked with an *asterisk* corresponded to the p20 polypeptide of caspase 7.

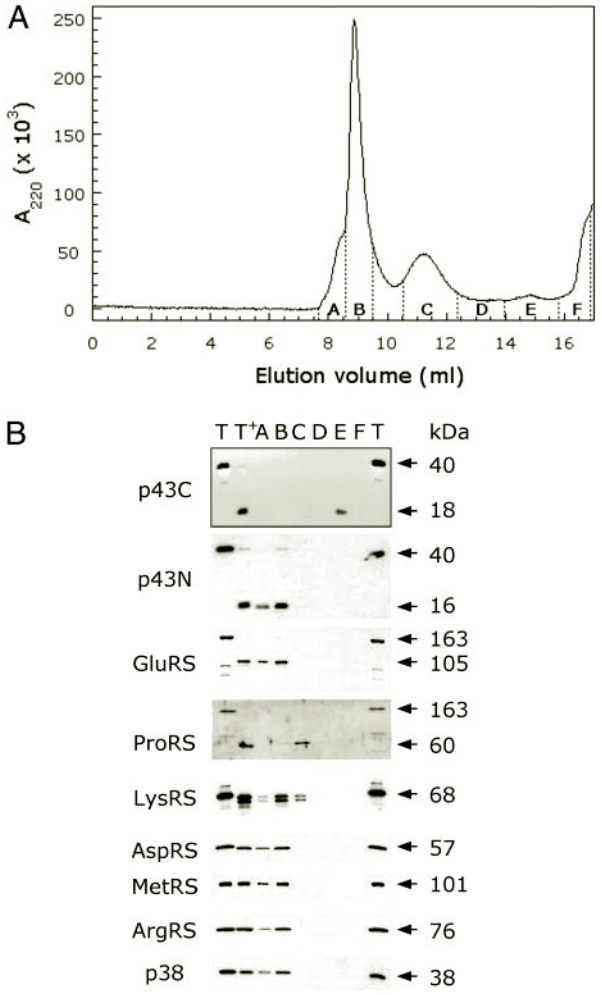

FIG. 3. **Probing the behavior of individual components of the complex after cleavage by caspase 7.** *A*, purified multienzyme complex from mouse (75 μg) was subjected to caspase 7 treatment (2200 units) followed by size fractionation on a Superose 12 HR 10/30 column equilibrated in 25 mM Tris-HCl, pH 7.5, 150 mM NaCl, 10% glycerol, 1 mM DTT. Elution was monitored at 220 nm. According to the elution profile, fractions were combined to give samples *A* and *B*, corresponding to complex-associated proteins, and *C–F*, corresponding to free species. *B*, samples *A–F* were concentrated by ultrafiltration on Centrisart-C4 (10,000 molecular weight cutoff; Sartorius) and analyzed by Western blotting using antibodies directed to the p43C or p43N region of p43, to the repeated units (*GluRS*) or ProRS domain (*ProRS*) of GluProRS, and to LysRS, AspRS, MetRS, ArgRS, or p38. Lanes *T* and T^+ corresponded to control samples of the multisynthetase complex before (*T*) or after (T^+) caspase treatment, recovered before size exclusion chromatography.

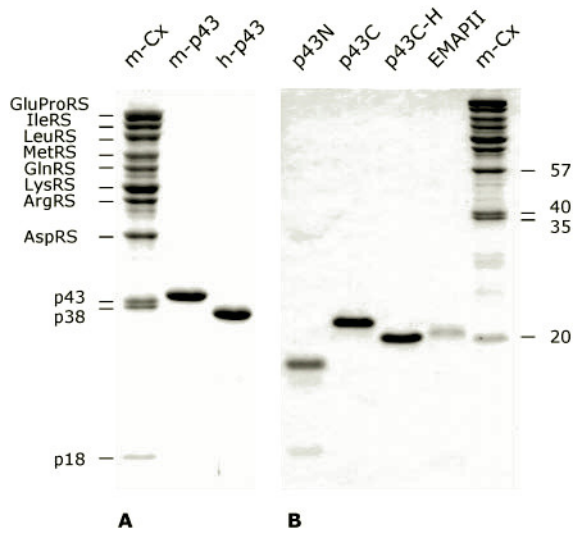

FIG. 4. **Expression of p43 and p43-related polypeptides.** *A*, the murine multisynthetase complex (*m-Cx*), corresponding to the natural form of p43/proEMAPII, the recombinant murine (*m-p43*) or human (*h-p43*) p43 polypeptides produced in *E. coli* with a C-terminal His tag, the (*B*) p43N and p43C and p43C-H segments of human p43 produced in *E. coli* with (p43N and p43C) or without (p43C-H) a C-terminal His tag, and the EMAPII polypeptide isolated after *in vitro* caspase treatment of the mouse multisynthetase complex (*EMAPII*) were analyzed by SDS-PAGE on a 12 (*A*) or 15% (*B*) polyacrylamide gel and visualized by Coomassie staining.

the column. Column fractions were analyzed by Western blotting to investigate the association state of the native and truncated components of the complex after caspase treatment. By using antibodies directed to the N-terminal or C-terminal domain of p43, we identified a ~16- or 18-kDa polypeptide, respectively, in fractions B or E. Therefore, caspase 7 digestion of p43 led to two discrete polypeptides. The N-terminal polypeptide behaves as a complex-associated entity, and EMAPII is released as a soluble monomeric protein.

Concerning the other components of the complex, only ProRS is released from the complex after caspase treatment. It is recovered in fraction C (Fig. 3*B*) as a dimeric protein with an apparent mass of ~100 kDa (Fig. 3*A*). The N-terminal moiety of bifunctional GluProRS, including GluRS and the linker region made of three repeated units (as assessed by Western blotting with antibodies directed to the GluRS domain or to the repeated units), remained associated with the complex. Similarly, the removal of a small polypeptide from LysRS and AspRS did not impair their association with the other components of the complex.

The consequences of caspase 7 treatment of the complex on the activity of its enzymatic components were appraised by measuring their tRNA aminoacylation capacity in the presence of saturating amounts of crude yeast or beef tRNA. Using these assay conditions, only ProRS activity was shown to be affected, with a 40% reduced initial velocity. This partial loss of activity could be related to the instability of the dimeric enzyme, which proved to readily dissociate into inactive monomers when released from the bifunctional GluProRS (30).

The EMAPII Domain Released by Caspase 7 Has Cytokine Activities—To establish that the EMAPII polypeptide initially isolated by Stern and co-workers (14) from conditioned medium of murine methylcholanthrene A fibrosarcoma cells does indeed correspond to the C-terminal domain of p43, substantial amounts of this polypeptide were isolated to perform its structural and functional characterization. Preparative digestion of the murine multisynthetase complex (500 μg of complex) was conducted with 10,000 units of caspase 7. Because two monomers of EMAPII (mass of the monomer = 18 kDa) could be isolated by molecules of complex (1500 kDa), a maximum of 12 μg of EMAPII were expected. To prevent absorption of this polypeptide on glassware, 0.01% Tween 20 was included in all buffers. EMAPII was isolated to homogeneity following two chromatographic steps on Resource Q and Mini-S columns and concentrated by ultrafiltration. Analysis by SDS-PAGE revealed a single polypeptide of 18 kDa (Fig. 4*B*), and a single N-terminal amino acid sequence was obtained by Edman degradation, *X*KPIDA . . . (the identity of the first amino acid residue was not determined). It precisely matches the sequence of the mouse p43 protein starting from residue 145, following the Asp^{144} residue from the ASTD sequence, corresponding to the caspase 7 cleavage site. It also coincides with the N-terminal sequence of the EMAPII cytokine initially isolated from medium of fibrosarcoma cells (14).

EMAPII has been shown to induce the migration of mononuclear phagocytes (MPs) and polymorphonuclear leukocytes

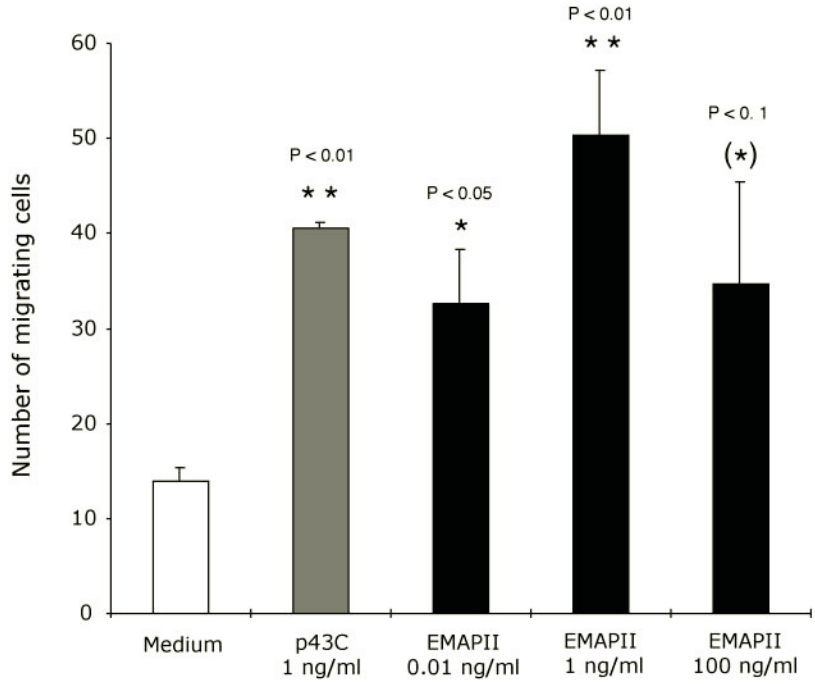

FIG. 5. **EMAPII derived from the multisynthetase complex induces chemotactic migration of monocytes.** Peripheral blood monocytes were added to the upper compartment of a modified Boyden chamber. Samples of EMAPII derived from the complex after cleavage with caspase 7 (*EMAPII*), of recombinant EMAPII (*p43C*), and of medium alone were added to the lower compartments at the indicated concentrations in ng/ml. The chambers were incubated for 1 h at 37 °C and then migrated cells were stained and counted. Results show mean ± S.E. of migrated cells from at least three independent experiments. In each experiment cells were counted in at least six representative high power fields. The statistical significance of the observed values was evaluated on the basis of the number of cells in the individual experiments as calculated from an unpaired *t* test using the InStat 2.01 program.

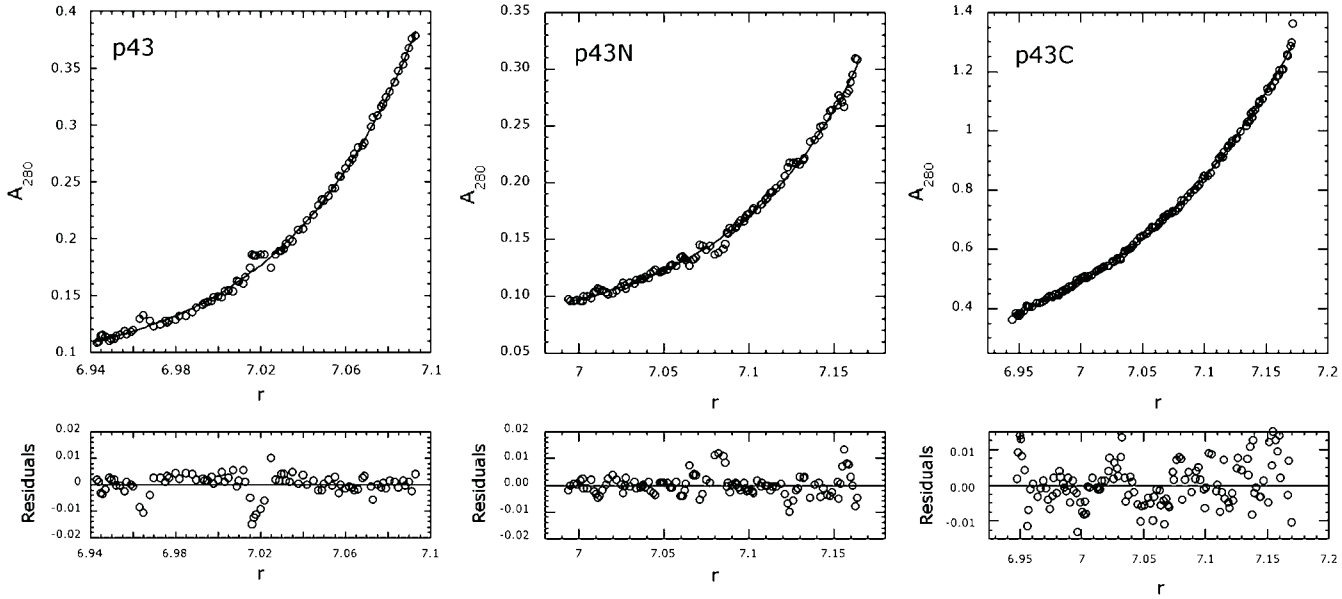

FIG. 6. **Quaternary structure of p43 and of its isolated N- and C-terminal domains.** The purified full-length human p43 (p43) and its isolated p43N or p43C moieties were analyzed by equilibrium sedimentation at 17,000 (p43 and p43N) or 20,000 rpm (p43C), at 4 °C, in 20 mM Tris-HCl, pH 7.5, 150 mM NaCl, 1 mM DTT, 10% glycerol, and 0.01% Tween 20 (p43 and p43N) or in 25 mM potassium phosphate, pH 7.5, 1 mM DTT (p43C). Initial protein concentrations were 38 μM for p43, 150 μM for p43N, and 60 μM for p43C. Experimental values (*open circles*) were fitted (*curves*) to monodisperse solutes of 70,912 Da for p43 and 18,843 Da for p43C or to a dimer-tetramer equilibrium with the mass of the monomer equal to 17,218 Da, and K_D = 20 ± 10 μM for p43N. The residuals are indicated.

and to stimulate the production of tissue factor by MPs and the release of myeloperoxidase from polymorphonuclear leukocytes. The cytokine activity of the EMAPII product derived from the multisynthetase complex by *in vitro* processing was assessed by its capacity to induce migration of human MPs (Fig. 5). EMAPII derived from the multisynthetase complex induced migration of MPs in a biphasic dose-response manner typical for chemokines. The chemotactic response was already significant at a concentration as low as 10 pg/ml, reached a maximum at about 1 ng/ml, and decreased to less significant values at an EMAPII concentration of 100 ng/ml. This dose response is very similar to that originally observed with EMAPII purified from tumor cell supernatants (14). When used at a protein concentration of 1 ng/ml, the recombinant cytokine (p43Ct) displayed a similar chemotactic activity (Fig. 5). The recombinant native human proEMAPII produced in *E. coli* (h-p43) also induced migration of MPs (results not shown).

The N and C Domains of p43 Contribute a Bipartite tRNA Binding Site—We previously reported that the C-terminal domain of p43 is a monomer and displays a weak nonspecific tRNA binding capacity (K_D = ~40 μM; see Ref. 5). To determine whether cleavage of p43 into EMAPII could modify the tRNA binding property of p43, we expressed and purified to homogeneity different forms of p43 from different origins. Murine and human p43 (m-p43 and h-p43) (Fig. 4*A*), as well as the human p43N and p43C moieties corresponding to the two polypeptides

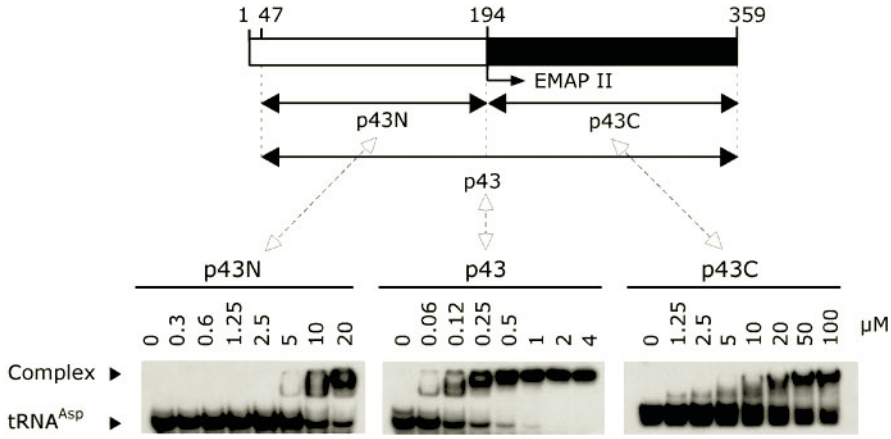

FIG. 7. **Synergistic binding of tRNA by the N and C regions of p43.** ^{32}P-Labeled *in vitro*-transcribed tRNA^{Asp} was incubated with human p43 or with its isolated p43N or p43C polypeptides at the concentrations indicated. After electrophoresis at 4 °C on a 6% native polyacrylamide gel, the mobility shift of tRNA was visualized by autoradiography.

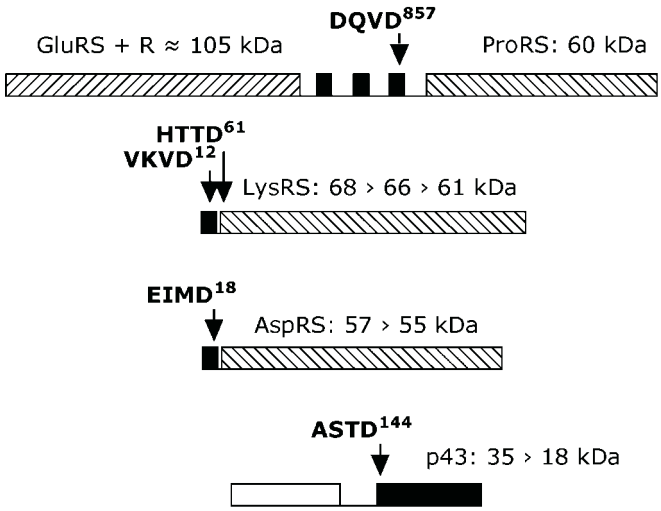

FIG. 8. **Deduced cleavage sites for caspase 7 on GluProRS, LysRS, AspRS, and p43 polypeptides.** Putative cleavage sites located within the third repeat of human GluProRS or between the polypeptide extension and the catalytic domain of human LysRS or human AspRS or within mouse proEMAPII are indicated.

generated by caspase 7 treatment (Fig. 4*B*), were expressed in *E. coli* with a C-terminal His tag. A C-terminal fragment deprived of a His tag was also isolated (p43C-H).

A double-hybrid screen of interactions between components of the complex showed that p43 associated with itself (2). In addition, multisynthetase complexes purified to homogeneity contain two copies of the p43 polypeptide per molecule of complex. These results suggested that p43 could be a dimer, even though p43C is a monomer when analyzed by gel filtration (5). The oligomeric structure of p43 was determined by sedimentation equilibrium (Fig. 6). When p43 was subjected to centrifugation equilibrium at an initial protein concentration of 38 μM, experimental data could be fitted to a single species with a molecular mass of 70,912 Da. Taking into account a calculated molecular mass of 35,418 Da for the monomer, we concluded that p43 is a dimer in solution. The C-terminal moiety of p43, p43C, behaved exclusively as a monomer of 18,843 Da (theoretical mass of a monomer, 19, 398 Da). In contrast, the N-terminal moiety of p43, p43N, gave a more complex sedimentation pattern. When analyzed at an initial protein concentration of 150 μM, experimental data were fitted to a dimer-tetramer equilibrium, with $K_D = 20 \pm 10$ μM, taking into account the theoretical mass of 17,218 Da of the monomer. Therefore, the native species of p43 is likely to form a dimer through its N-terminal segment.

We analyzed the ability of p43 to form stable complexes with various tRNAs. Radiolabeled *in vitro*-transcribed tRNAs (yeast tRNA^{Asp} or tRNA$_i^{Met}$; human tRNA^{Lys} or tRNA^{Arg}) were incubated with increasing amounts of p43 (0.06–4 μM; monomer concentration), and free and bound tRNA species were analyzed by a gel retardation assay (Fig. 7). p43 formed a stable complex with tRNA with an apparent K_D of ~0.2 μM (expressed as monomer concentration). The finding that two band shifts were observed suggests that p43 can bind one or two tRNAs per dimer. The interaction with p43 does not require the L-shaped structure of tRNA. Indeed, we observed that a minihelix mimicking the acceptor-TΨC stem-loop region of tRNA produced a similar interaction pattern (result not shown). In contrast with the robust interaction displayed by full-length p43, its isolated p43N or p43C domains formed weak complexes with tRNAs, with apparent K_D of 7.5 and 40 μM, respectively. As a control, we observed that p43C and p43C-H (a derivative without His tag) have indistinguishable tRNA binding capacities. Therefore, the two domains of p43 are likely to synergistically contribute a potent tRNA binding site on p43.

DISCUSSION

Here we showed that the p43 component of the mammalian multisynthetase complex is a substrate for caspase 7, an apoptotic protease. The free recombinant, as well as the natural complex-associated p43 species, are substrates of caspase 7. However, we found that the p43 entity associated within the complex was more efficiently processed into EMAPII than its soluble form. This result suggests that the site of cleavage is made more accessible to the caspase when p43 is forced into a conformation suited for its association with the other components of the complex. Although the EEVD sequence at position 175 to 178 of murine p43 would be an ideal site for caspase 7 according to its known preferred peptide substrates (31) the ^{141}ASTD ↓ S^{145} sequence is used *in vitro* by caspase 7 (this study), and the N terminus of the *in vivo*-generated EMAPII product also starts at residue Ser^{145} (14). We recently reported the crystal structure of human EMAPII (7). Its two-domain architecture builds a pseudodimer. The 100-amino acid residue N-terminal domain forms an open β-barrel related to the 60-amino acid residue C-terminal domain by a degenerated 2-fold symmetry. The EEVD peptide belongs to strand β1 that forms the first strand of the oligonucleotide-oligosaccharide binding fold β-barrel domain. This tetrapeptide appears to be buried in the protein core and is therefore not accessible for recognition by caspase. In contrast, the released Ser^{145} at the N terminus is protruding from the compact structure.

Following cleavage at the ^{141}ASTD ↓ S^{145} site, the EMAPII cytokine lost its propensity to associate with the complex and is released as a monomer. The N terminus of p43 remains bound to the complex. These results are in full agreement with our

previous analysis of protein-protein interactions involved in the assembly of the complex. We showed by a two-hybrid analysis that p43 is able to interact with p38, the scaffold component of the complex, but also with GlnRS and ArgRS (2). Furthermore, *in vitro* studies revealed that the isolated N-terminal moiety of p43 associates with ArgRS, but its C-terminal region corresponding to EMAPII does not (3). Similarly, p43 binds to p38 via its N-terminal domain.[2] Thus, we anticipated that the release of EMAPII would not destabilize the quaternary structure of the complex.

Examination of each of the components of the complex after caspase treatment revealed that, with the exception of ProRS, aminoacyl-tRNA synthetases remain associated. ProRS is carried by a multifunctional polypeptide (32) containing an N-terminal domain corresponding to GluRS, a linker region made of repeated units with nonspecific RNA binding properties (33), and a C-terminal ProRS domain. Cleavage of the GluProRS polypeptide by uncontrolled proteolysis led to the release of ProRS from the complex (30). Because of the size of the GluRS (105 kDa) and ProRS (60 kDa) polypeptides observed after cleavage by caspase, the finding that antibodies raised against the repeated units selectively recognized the N-terminal GluRS polypeptide of 105 kDa, and the known consensus sequence for caspase 7, the aspartate residue at position 857 from the sequence ^{854}DQVD^{857} of human GluProRS is likely to correspond to the cleavage site (Fig. 8). AspRS and LysRS are also subjected to proteolysis, but their activities are not affected. The short polypeptides removed after cleavage by caspase 7 are therefore likely to be located at the N terminus of the two proteins, position corresponding to the eukaryotic-specific sequences that characterize the mammalian enzymes. According to the crystal structure of yeast AspRS (34) and of *E. coli* LysRS (35), the removal of a short polypeptide at the C-terminal extremity of the two proteins should result in their inactivation. Indeed, the conserved motif 3 of class IIb aminoacyl-tRNA synthetases is located at the very C terminus of these proteins. The potential cleavage sites for caspase 7 are indicated in Fig. 8.

Of particular interest is the finding that the immediate consequence of the cleavage of p43 into two equal moieties is the loss of its tRNA binding ability. The isolated domains have a weak RNA binding capacity (K_D = ~7.5–40 μM), even though the N-terminal domain is very rich in basic residues and displays a calculated pI > 9. EMAPII-like polypeptides are recurrent domains associated with various proteins. In yeast, the Arc1p protein associates with MetRS and GluRS and acts as a cofactor for tRNA delivery to the synthetase (12). A polybasic sequence from the N-terminal region appended to the EMAPII-like domain of Arc1p is also required for efficient RNA binding. In plants, an EMAPII-like domain is appended at the C terminus of MetRS and synergizes with the MetRS domain for binding tRNA (8). Thus, EMAPII domains always require additional sequences to potentiate their interaction with tRNA molecules.

It is worth noting that besides p43, the other targets of caspase 7 in the complex also concern peptide appendices that are eukaryote-specific and/or that are known to contribute RNA binding domains. The DQVD sequence that might be the caspase 7 recognition site in GluProRS is located in the third of the repeated units that form the linker polypeptide between the GluRS and ProRS domains. We recently determined that in human MetRS, an enzyme that possesses a single of these repeats, this polypeptide extension provides the MetRS core domain with a higher catalytic efficiency for tRNA aminoacylation.[3] Similarly, the N-terminal polypeptide extension of human LysRS contributes an RNA binding domain that facilitates tRNA aminoacylation.[4] Consequently, *in vivo* processing of components of the multisynthetase complex by caspase 7 would have as an immediate consequence to restrict the availability of aminoacylated tRNAs and should result in the inhibition of protein synthesis. Following onset of apoptosis, cleavage of p43 and of other components of the complex would be a means to arrest translation in cells engaged in programmed cell death. Although other factors of the translation machinery, including eIF2α (36) and eIF4G (37), are cleaved by caspase 3 during inhibition of translation in apoptotic cells, their proteolytic products do not possess cytokine activity. Secretion of EMAPII, the C-terminal domain of p43, results in the recruitment of macrophages (14, 18, 38) that engulf apoptotic cells, thus preventing inflammation caused by the release of their cellular content because of secondary necrosis of apoptotic cells. In this regard, p43 may compare with a molecular fuse. In its native pro-EMAPII form, it is an important cofactor for aminoacylation. After the fuse has blown, translation is irreversibly switched off, and EMAPII enters the cell death signaling pathway. *In vitro* assays showed that full-length recombinant p43 is also a potent cytokine (17, 19).[5] This suggests that association of p43 within the multisynthetase complex inhibits its cytokine activity and/or sequesters proEMAPII in a cellular compartment and prevents its entry into apoptotic pathways until it is cleaved off the complex. Only a processed form of p43 is recovered in the supernatant of apoptotic cells.[6] The pathway of EMAPII secretion remains to be deciphered.

Acknowledgments—We thank M. Deniziak, J. C. Robinson, and S. Berranger for involvement in early parts of this work and D. Lê and G. Batelier (Laboratoire d'Enzymologie et Biochimie Structurales, CNRS) for performing amino acid sequence and sedimentation equilibrium analyses. The excellent technical assistance of Françoise Triniolles is gratefully acknowledged.

REFERENCES

1. Mirande, M. (1991) *Prog. Nucleic Acids Res. Mol. Biol.* **40,** 95–142
2. Quevillon, S., Robinson, J. C., Berthonneau, E., Siatecka, M., and Mirande, M. (1999) *J. Mol. Biol.* **285,** 183–195
3. Robinson, J. C., Kerjan, P., and Mirande, M. (2000) *J. Mol. Biol.* **304,** 983–994
4. Quevillon, S., and Mirande, M. (1996) *FEBS Lett.* **395,** 63–67
5. Quevillon, S., Agou, F., Robinson, J. C., and Mirande, M. (1997) *J. Biol. Chem.* **272,** 32573–32579
6. Kim, Y., Shin, J., Li, R., Cheong, C., Kim, K., and Kim, S. (2000) *J. Biol. Chem.* **275,** 27062–27068
7. Renault, L., Kerjan, P., Pasqualato, S., Menetrey, J., Robinson, J. C., Kawaguchi, S., Vassylyev, D. G., Yokoyama, S., Mirande, M., and Cherfils, J. (2001) *EMBO J.* **20,** 570–578
8. Kaminska, M., Deniziak, M., Kerjan, P., Barciszewski, J., and Mirande, M. (2000) *EMBO J.* **19,** 6908–6917
9. Kleeman, T. A., Wei, D. B., Simpson, K. L., and First, E. A. (1997) *J. Biol. Chem.* **272,** 14420–14425
10. Morales, A. J., Swairjo, M. A., and Schimmel, P. (1999) *EMBO J.* **18,** 3475–3483
11. Swairjo, M. A., Morales, A. J., Wang, C. C., Ortiz, A. R., and Schimmel, P. (2000) *EMBO J.* **19,** 6287–6298
12. Simos, G., Sauer, A., Fasiolo, F., and Hurt, E. C. (1998) *Mol. Cell* **1,** 235–242
13. Tan, M., Heckmann, K., and Brunen-Nieweler, C. (1999) *Gene* **233,** 131–140
14. Kao, J., Ryan, J., Brett, G., Chen, J., Shen, H., Fan, Y. G., Godman, G., Familletti, P. C., Wang, F., Pan, Y. C., Stern, D., and Clauss, M. (1992) *J. Biol. Chem.* **267,** 20239–20247
15. Kao, J., Houck, K., Fan, Y., Haehnel, I., Libutti, S. K., Kayton, M. L., Grikscheit, T., Chabot, J., Nowygrod, R., Greenberg, S., Kuang, W.-J., Leung, D. W., Hayward, J. R., Kisiel, W., Heath, M., Brett, J., and Stern, D. M. (1994) *J. Biol. Chem.* **269,** 25106–25119
16. Wakasugi, K., and Schimmel, P. (1999) *Science* **284,** 147–151
17. Kornelyuk, A., Tas, M. P. R., Dubrovsky, A., and Murray, J. C. (1999) *Biopolym. Cell* **15,** 168–172
18. Knies, U. E., Behrensdorf, H. A., Mitchell, C. A., Deutsch, U., Risau, W., Drexler, H. C., and Clauss, M. (1998) *Proc. Natl. Acad. Sci. U. S. A.* **95,** 12322–12327
19. Barnett, G., Jakobsen, A. M., Tas, M., Rice, K., Carmichael, J., and Murray,

[2] J. C. Robinson and M. Mirande, unpublished results.

[3] M. Kaminska and M. Mirande, submitted for publication.

[4] M. Francin and M. Mirande, unpublished results.

[5] Unpublished results.

[6] V. Shalak and M. Mirande, unpublished results.

J. C. (2000) *Cancer Res.* **60,** 2850–2857
20. Behrensdorf, H. A., van de Craen, M., Knies, U. E., Vandenabeele, P., and Clauss, M. (2000) *FEBS Lett.* **466,** 143–147
21. Kellermann, O., Viel, C., and Waller, J. P. (1978) *Eur. J. Biochem.* **88,** 197–204
22. Van de Craen, M., Declercq, W., Van den Brande, I., Fiers, W., and Vandenabeele, P. (1999) *Cell Death Differ.* **6,** 1117–1124
23. Mirande, M., Cirakoglu, B., and Waller, J. P. (1982) *J. Biol. Chem.* **257,** 11056–11063
24. Laemmli, U. K. (1970) *Nature* **227,** 680–685
25. Dunn, S. D. (1986) *Anal. Biochem.* **157,** 144–153
26. Boyum, A. (1983) *Scand. J. Immunol.* **17,** 429–436
27. Quinn, M. T., Parthasarathy, S., and Steinberg, D. (1988) *Proc. Natl. Acad. Sci. U. S. A.* **85,** 2805–2809
28. Agou, F., Waller, J. P., and Mirande, M. (1996) *J. Biol. Chem.* **271,** 29295–29303
29. Mirande, M., Le Corre, D., and Waller, J. P. (1985) *Eur. J. Biochem.* **147,** 281–289
30. Kerjan, P., Triconnet, M., and Waller, J. P. (1992) *Biochimie* (*Paris*) **74,** 195–205
31. Earnshaw, W. C., Martins, L. M., and Kaufmann, S. H. (1999) *Annu. Rev. Biochem.* **68,** 383–424
32. Cerini, C., Kerjan, P., Astier, M., Gratecos, D., Mirande, M., and Semeriva, M. (1991) *EMBO J.* **10,** 4267–4277
33. Cahuzac, B., Berthonneau, E., Birlirakis, N., Guittet, E., and Mirande, M. (2000) *EMBO J.* **19,** 445–452
34. Cavarelli, J., Eriani, G., Rees, B., Ruff, M., Boeglin, M., Mitschler, A., Martin, F., Gangloff, J., Thierry, J. C., and Moras, D. (1994) *EMBO J.* **13,** 327–337
35. Onesti, S., Miller, A. D., and Brick, P. (1995) *Structure* **3,** 163–176
36. Marissen, W. E., Guo, Y., Thomas, A. A., Matts, R. L., and Lloyd, R. E. (2000) *J. Biol. Chem.* **275,** 9314–9323
37. Marissen, W. E., and Lloyd, R. E. (1998) *Mol. Cell. Biol.* **18,** 7565–7574
38. Schluesener, H. J., Seid, K., Zhao, Y. H., and Meyermann, R. (1997) *GLIA* **20,** 365–372

THE JOURNAL OF BIOLOGICAL CHEMISTRY VOL. 282, NO. 15, pp. 10935–10943, April 13, 2007 © 2007 by The American Society for Biochemistry and Molecular Biology, Inc. Printed in the U.S.A.

Characterization of p43(ARF), a Derivative of the p43 Component of Multiaminoacyl-tRNA Synthetase Complex Released during Apoptosis*[S]

Received for publication, December 21, 2006, and in revised form, February 12, 2007 Published, JBC Papers in Press, February 15, 2007, DOI 10.1074/jbc.M611737200

Vyacheslav Shalak[‡1], Ludovic Guigou[‡2], Monika Kaminska[‡3], Marie-Paule Wautier[§], Jean-Luc Wautier[§], and Marc Mirande[‡4]

From the [‡]Laboratoire d'Enzymologie et Biochimie Structurales, CNRS, 1 Avenue de la Terrasse, 91190 Gif-sur-Yvette, France and [§]Université Paris 7/Institut National de la Transfusion Sanguine, 75015 Paris, France

In human, nine aminoacyl tRNA synthetases are associated with the three auxiliary proteins, p18, p38, and p43, to form a stable multiprotein complex. The p43 component, which has a potent tRNA binding capacity, is associated to the complex via its N-terminal moiety. This protein is also the precursor of the endothelial monocyte-activating polypeptide II (p43(EMAPII), corresponding to the C-terminal moiety of p43), a cytokine generated during apoptosis. Here we examined the cellular pathway that, starting from the p43 subunit of the complex, leads to this extracellular cytokine. We identified a new intermediate in this pathway, named p43(ARF) for Apoptosis-released Factor. This intermediate is produced *in cellulo* by proteolytic cleavage of endogenous p43 and is rapidly recovered in the culture medium. This p43 derivative was purified from the medium of human U937 cells subjected to serum starvation. It contains 40 additional N-terminal amino acid residues as compared with the cytokine p43(EMAPII) and may be generated by a member of the matrix metalloproteinase family. Recombinant p43(ARF) is a monomer in solution and binds tRNA with a K_d of ~6 nM, 30-fold lower than that of p43. Highly purified p43(ARF) or p43(EMAPII) do not stimulate the expression of E-selectin by human umbilical vein endothelial cells. Our results suggest that the cleavage of p43 and its cellular delocalization, and thus the release of this tRNA binding subunit from the complex, is one of the molecular mechanisms leading to the shut down of protein synthesis in apoptosis.

Protein synthesis is essential for cell growth. In cells undergoing apoptosis, the translation process is rapidly inhibited and correlates with caspase-dependent cleavage of the eukaryotic translation initiation factors eIF3, eIF4B, and eIF4G (1) and with phosphorylation of eIF2α (2). Inhibition of protein synthesis by addition of cycloheximide to culture cells also promotes apoptosis. Translation is not completely inhibited at early stages of apoptosis. For instance, the mRNA encoding antiapoptotic proteins XIAP or c-Myc may be produced, allowing cell recovery during the process of programmed cell death. By contrast, translation is not inhibited during the process of necrotic cell death (3). Although modification of translation initiation factors seems to be one of the primary steps of regulation of translation in apoptotic cells, other components of the protein synthesis machinery, including aminoacyl-tRNA synthetases, are also the target of apoptotic proteases (4, 5).

In higher eukaryotic organisms, from *Drosophila* to mammals, the nine aminoacyl-tRNA synthetases specific for amino acids Glu, Pro, Ile, Leu, Met, Gln, Lys, Arg, and Asp form a Multiaminoacyl-tRNA Synthetase complex (MARS)[5] with the three auxiliary proteins p18, p38, and p43 (6). The p43 subunit is an RNA-binding protein (5) organized around a pseudo-dimeric OB-fold-based domain (7). It occupies a central position within the multisynthetase complex (8). It has been proposed that p43 might play a role of a cofactor for aminoacylation (9), but this function remains a subject of controversy (10). The presence of p43, or of p43-related proteins, in the cytoplasm but also in the nucleus of rabbit kidney cells has been observed by immunoelectron microscopy (11).

The p43 component of MARS is also the precursor of the Endothelial-monocyte-activating polypeptide II (p43(EMAPII)) isolated from methylcholanthrene A-induced fibrosarcoma cells, a cytokine generated during apoptosis (12–14). The mature p43(EMAPII) has been ascribed to a proinflammatory cytokine that stimulates chemotactic migration of polymorphonuclear granulocytes and mononuclear phagocytes and induces tissue factor activity on endothelial cells. Whether p43(EMAPII) or its precursor, the p43 component of MARS, is the real cytokine remains controversial (13, 15). p43 as well as p43(EMAPII) have also been reported to have antiangiogenic properties that

* This work was supported by grants from the Centre National de la Recherche Scientifique, the Association pour la Recherche sur le Cancer, and La Ligue. The costs of publication of this article were defrayed in part by the payment of page charges. This article must therefore be hereby marked "*advertisement*" in accordance with 18 U.S.C. Section 1734 solely to indicate this fact.

[S] The on-line version of this article (available at http://www.jbc.org) contains supplemental Fig. S1.

[1] Recipient of a postdoctoral fellowship from the North Atlantic Treaty Organization. Present address: Inst. of Molecular Biology and Genetics, 150 Acad. Zabolotnogo St., 03143 Kiev, Ukraine.

[2] Recipient of a postdoctoral fellowship from Ministère de la Recherche et de la Technologie.

[3] Recipient of a postdoctoral fellowship from Fondation pour la Recherche Medicale. Present address: Institut Pasteur, Unité de Régulation Enzymatique des Activités Cellulaires, 25 Rue du Docteur Roux, 75015 Paris, France.

[4] To whom correspondence should be addressed. Tel.: 33-1-69-82-35-05; Fax: 33-1-69-82-31-29; E-mail: Marc.Mirande@lebs.cnrs-gif.fr.

This is an open access article under the CC BY license.

[5] The abbreviations used are: MARS, multiaminoacyl-tRNA synthetase; EMAPII, endothelial monocyte-activating polypeptide II; ARF, apoptosis-released factor; FCS, fetal calf serum; HUVEC, human umbilical vein endothelial cell; GFP, green fluorescent protein; DTT, dithiothreitol; 7-AAD, 7-amino-actinomycin D; FACS, fluorescence-activated cell sorter; IL-3, interleukin 3.

would limit establishment of neovasculature and thus would suppress tumor growth (16, 17).

We previously reported that the p43 component of MARS is a substrate for caspase 7 (5), but other data also indicated that p43 may not be primarily cleaved by this apoptotic protease (18), suggesting that the maturation of p43 into p43(EMAPII) may involve intermediate maturation stages. In this report, we investigated the pathway of p43 cleavage during apoptosis, we identified and characterized a new intermediate referred to as p43(ARF) for Apoptosis-released Factor, and analyzed the subcellular localization and the putative functions of p43, p43(ARF), and p43(EMAPII) during development of apoptosis.

EXPERIMENTAL PROCEDURES

Cell Culture and Induction of Apoptosis—The 32D murine myeloid precursor cell line (gift from Matthias Clauss, Max-Planck-Institut, Bad Nauheim, Germany) is dependent on an exogenous supply of IL-3 for growth (19). 32D cells were grown in RPMI medium (Invitrogen) supplemented with 10% fetal calf serum (FCS), 2 mM glutamine, 100 μg/ml of penicillin and streptomycin, and 10% conditioned medium derived from the IL-3-producing cell line WEHI. To induce apoptosis, cells were washed three times in the same medium lacking conditioned medium and incubated in the same medium for the times indicated. The human promonocytic cell line U937 (American Type Culture Collection) was grown in RPMI medium supplemented with 10% FCS and 2 mM glutamine, 100 μg/ml of penicillin and streptomycin, and induced to undergo apoptosis by serum withdrawal. Development of apoptosis was assessed by DNA fragmentation analysis (20), and poly(ADP-ribose) polymerase cleavage. Cell survival was determined by the 3-(4,5-dimethylthiazol-2-yl)-2,5-diphenyltetrazolium bromide MTT assay (Sigma) and cell death by the trypan blue (0.05%) exclusion assay. Cell extracts and culture media were analyzed by Western blotting. Human umbilical vein endothelial cells (HUVEC) were grown as previously described (21). After digestion by collagenase, HUVEC were cultured in M199 containing human AB serum (15% v/v) until confluence.

Antibodies and Western Blot Analysis—Monoclonal antibodies directed to poly(ADP-ribose) polymerase and to GFP were from BD Biosciences. Polyclonal anti-p43(EMAPII) antibodies have been described previously (5). Western blot analyses were conducted with goat anti-rabbit or goat anti-mouse secondary antibodies conjugated with peroxidase (Chemicon) and the ECL detection reagents (Amersham Biosciences).

Determination of E-selectin Expression—Endothelial cell E-selectin expression was measured as described previously (22). Briefly, confluent HUVEC grown in 96-well microtiter plates until confluence were incubated for 4 h at 37 °C in M199 medium containing 20% FCS and tumor necrosis factor α (5 ng/ml; 0.3 nM) or p43, p43(ARF), and p43(EMAPII) appropriately diluted in 20 mM Tris-HCl, pH 7.0, 50 mM NaCl, 1 mM DTT, and 0.01% Tween 20. Cells were washed once with M199 medium supplemented with 10% FCS, incubated with monoclonal antibodies directed to E-selectin (R&D Systems) in RPMI medium supplemented with 10% FCS for 1 h on ice, washed four times in the same medium, incubated for 1 h on ice in the same medium containing ^{125}I-labeled anti-mouse IgG (Amersham Biosciences), and washed four times before measuring the radioactivity.

Inducible Expression of p43 in U937 Cells—The cDNAs encoding p43, p43(ARF), or p43(EMAPII) were introduced between the BamHI and XbaI sites of the pTRE2hyg vector under the control of the tetracycline-response element (BD Biosciences). U937 Tet-Off (U937TO) cells grown in RPMI medium supplemented with 10% FCS and G418 at 0.3 mg/ml were transfected with Effectene (Qiagen). Stable transformants were isolated by selection with hygromycin, in the presence of tetracycline (transcription from the Tet-responsive element is turned off). Expression of the recombinant proteins was turned on by removal of tetracycline from the culture medium. Stably transfected cells were cultured in the absence of FCS to induce apoptosis and stained with the vital dye 7-amino-actinomycin D (7-AAD) and with Annexin V-PE (BD Biosciences) and subjected to FACS analysis (PAS-III; Partec) to identify early apoptotic cells (Annexin V-PE-positive and 7-AAD-negative).

Purification of p43(ARF) from the Supernatant of U937 Apoptotic Cells—U937 cells (10^9 cells) growing in RPMI medium containing 10% FCS were washed three times in RPMI without FCS and incubated in serum-free RPMI medium for 5 days at 37 °C. Cell culture medium was centrifuged at 40,000 × *g* for 20 min at 4 °C, diluted 1.5-fold by addition of 60 mM Tris-HCl, pH 7.0, and 0.03% Tween 20, and directly applied to a Mono S HR 5/5 column. Elution was achieved by a linear gradient (60-column volume) of NaCl from 0 to 300 mM in 20 mM Tris-HCl, pH 7.0, 2 mM DTT, and 0.01% Tween 20. Fractions containing p43(ARF), detected by Western blotting, were dialyzed (20 mM Tris-HCl, pH 8.5, 2 mM DTT, and 0.01% Tween 20), applied to a Mono Q HR 5/5 column equilibrated in the same buffer, and eluted by a linear gradient (40-column volume) of NaCl from 0 to 250 mM. Fractions containing p43(ARF) were dialyzed (20 mM Tris-HCl, pH 7.0, 2 mM DTT, and 0.01% Tween 20), applied to a Mini S PE 4.6/50 column equilibrated in the same buffer, and eluted by a linear gradient (50-column volume) of NaCl from 0 to 300 mM. Fractions containing p43(ARF) were concentrated by ultrafiltration (Vivaspin 500, 5000 MWCO) and subjected to N-terminal amino acid sequence analysis by automated Edman degradation.

Protein Overexpression and Purification—The cDNA fragment encoding p43(ARF) was produced by PCR with oligonucleotides 5′-cccccatggctggtaccaaagaacagataa and 5′-cccctcgagttatttgattccactgttgctca and inserted into the NcoI-XhoI sites of the bacterial expression vector pET-28b (Novagen) to give pET/p43(ARF). The construct was verified by DNA sequencing.

The protein encoded by pET/p43(ARF) was expressed in *Escherichia coli* BL21(DE3) grown in Luria Bertani medium supplemented with kanamycin (50 μg/ml). Culture (1.5 liters) was grown at 37 °C to an A_{600} = 0.5, transferred at 28 °C, and expression was induced by addition of 1 mM isopropyl 1-thio-β-D-galactopyranoside for 4 h. Cells were washed twice with ice-cold extraction buffer (30 mM Tris-HCl, pH 7.0, 30 mM KCl, 0.1 mM EDTA, 10% glycerol, 2 mM DTT), resuspended in 23 ml of the same buffer containing 1 mM diisopropyl-fluorophosphate, and sonicated. All subsequent steps were conducted at 4 °C. After centrifugation at 18,000 × *g* for 30 min, the clear

supernatant was applied to a 33-ml S-Sepharose FF column (Amersham Biosciences). p43(ARF) was eluted by a linear gradient (25-column volume) of NaCl from 50 to 350 mM in 20 mM Tris-HCl, pH 7.0, containing 1 mM DTT. After extensive dialysis against 20 mM Tris-HCl, pH 7.0, and 1 mM DTT, fractions were applied to a 25-ml Q-Sepharose FF column (Amersham Biosciences) equilibrated in the same buffer. The flowthrough fraction was recovered and immediately applied to a 30-ml Source 15S column equilibrated in 20 mM Tris-HCl, pH 7.0, 50 mM NaCl, 1 mM DTT and eluted by a linear gradient (23-column volume) of NaCl from 50 to 300 mM. Fractions containing p43(ARF) were concentrated by ultrafiltration, dialyzed against 25 mM potassium phosphate, pH 7.5, 2 mM DTT, 55% glycerol, and stored at −20 °C at a protein concentration of ~30 mg/ml. Protein concentration was determined by using a calculated absorption coefficient of 0.35 A_{280} units·mg^{-1}·cm^2.

Sedimentation Equilibrium—Ultra-centrifugation experiments were conducted as described previously (23) in a Beckman Optima XL-A analytical ultracentrifuge, using a 60 Ti rotor and a double sector cell of 12-mm path length. Equilibrium was verified from the superimposition of duplicate scans recorded at 4-h intervals. The experimental sedimentation equilibrium data were fitted to a model for a single homogeneous species following Equation 1

$$c(r) = c(r_{ref})\exp\{[M_r(1 - \bar{v}\rho)\omega^2/2RT](r^2 - r_{ref}^2)\} \quad \text{(Eq. 1)}$$

where $c(r)$ is the protein concentration at radial position r, $c(r_{ref})$ is the concentration of the protein at an arbitrary reference radial distance r_{ref}, M_r is the molecular mass, and $\bar{v}$ the partial specific volume (0.733 at 4 °C for p43(ARF)) of the solute, ρ is the density of the solvent, ω is the angular velocity of the rotor, and R and T are the molar gas constant and the absolute temperature, respectively.

Gel Retardation Assay—Protein-tRNA interactions were assayed using a band shift assay as previously described (5). The genes for human $tRNA_2^{Arg}$, for rabbit elongator $tRNA^{Met}$, or for minihelices corresponding to the acceptor-TΨC stem-loop domain of these two tRNAs, placed under the control of the T7 polymerase promoter, were subjected to *in vitro* transcription as described (10, 24). Briefly, ^{32}P-labeled tRNAs were synthesized in a reaction mixture (50 μl) containing 1 μg of linearized template DNA, 40 mM Tris-HCl, pH 8.0, 6 mM $MgCl_2$, 1 mM spermidine, 5 mM dithiothreitol, 0.01% Triton X-100, 1 mM each CTP, UTP, and GTP, 10 μM [α-^{32}P]ATP (200 Ci/mmol), 1000 units/ml T7 RNA polymerase. After incubation at 37 °C for 1 h, the transcripts were purified by electrophoresis on a denaturing 12% polyacrylamide gel (mono:bis, 19:1), recovered from the gel by soaking in H_2O, precipitated with ethanol, and resuspended in 5 mM $MgCl_2$. Transcripts were renatured by heating at 90 °C and slow cooling (90 to 30 °C in 2 h).

Homogeneous protein was incubated at increasing concentrations with radiolabeled tRNA in an 11-μl volume containing 20 mM Tris-HCl, pH 7.5, 150 mM NaCl, 10 mM $MgCl_2$, 10 mM 2-mercaptoethanol, 10% glycerol, and bovine serum albumin at 0.1 mg/ml. After incubation at 25 °C for 30 min, the mixture was placed on ice and loaded on a 6% polyacrylamide gel (mono:bis, 29:1) containing 5% glycerol in 0.5× Tris borate-EDTA at 4 °C. After electrophoresis, the gel was fixed, dried, and subjected to autoradiography. Free and bound tRNA were quantified by densitometry analysis. Because the amount of labeled transcripts added in the assays was negligible compared with the amount of protein added, concentration of protein at which half of the tRNA formed a complex corresponded to the apparent K_d value of the complex.

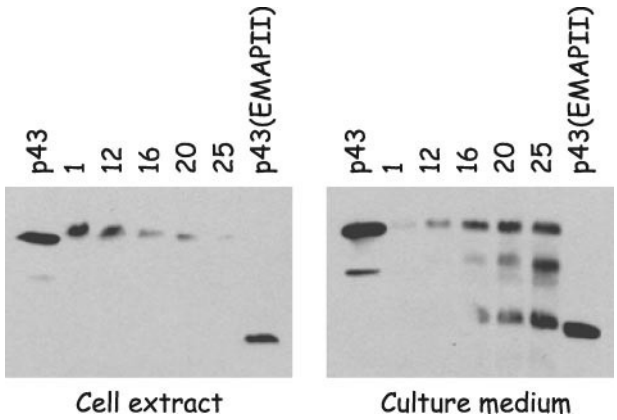

FIGURE 1. **IL-3 deprivation of murine 32D cells.** Western blot analysis of the total cell extract and of the culture medium reveals the cleavage of the p43 component of MARS and its release from the cell during apoptosis of 32D cells. The presence of p43-related polypeptides was detected with anti-p43(EMAPII) antibodies after 1, 12, 16, 20, and 25 h of IL-3 deprivation. Recombinant p43 and p43(EMAPII) were used as markers. Note the presence of unprocessed p43 in the culture medium.

Confocal Imaging—The cDNAs encoding human p43 and its derivatives were introduced between the EcoRI and BamHI sites of pEGFP-N1 (BD Biosciences). HeLa-ST cells were grown in F12 medium supplemented with 10% FCS. Cells were transfected with Effectene (Qiagen). Cells were grown in 8-well Lab-Tek II chambers (Nalge Nunc International) and observed by confocal laser scanning microscopy using a Leica TCS SP2 confocal microscope.

RESULTS

Release of p43(ARF) during Apoptosis—When murine 32D cells were subjected to apoptosis by IL-3 deprivation, p43(EMAPII) was recovered in the culture medium (Fig. 1) as reported previously (4). The release of mature p43(EMAPII) is observed after 16–20 h of IL-3 withdrawal. However, several other p43-related polypeptides, the native p43 polypeptide and a proteolytic intermediate of ~26–28 kDa, were also observed in the culture medium (Fig. 1). We also detected the presence of other proteins in the culture medium, including the 76-kDa species of ArgRS, an integral component of MARS, 12 h after onset of apoptosis (results not shown). The finding that the matured form of p43, p43(EMAPII), but also the p43 and ArgRS proteins that are integral components of the MARS complex, were found in the culture medium but were not subjected to proteolysis suggested that cytolysis also occurred in the population of apoptotic 32D cells. Accordingly, ~30–40% of the cells were permeable to trypan blue after 12 h of IL-3 starvation, as observed previously (19). Thus, the presence of p43(EMAPII) in the culture medium could be attributed either to secretion from apoptotic cells or to leakage from permeable necrotic cells. Therefore, we looked for a cell type where cytolysis would not rapidly occur after onset of apoptosis.

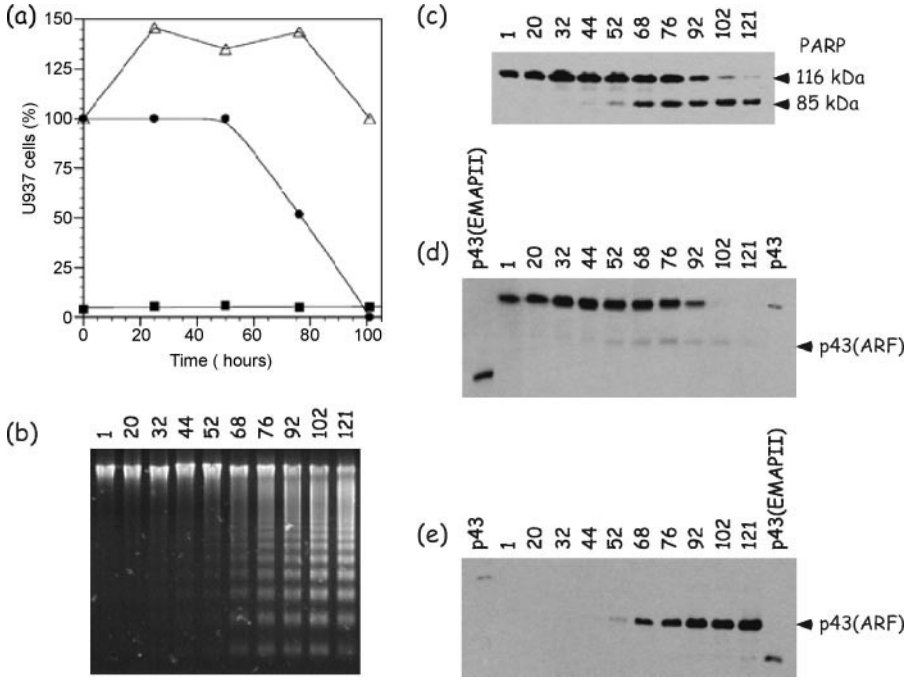

FIGURE 2. **Serum starvation of human U937 cells.** *a*, after serum withdrawal and at the times indicated, cells were counted (△) and stained with the vital dye trypan blue (■), and cell survival was estimated by the 3-(4,5-dimethylthiazol-2-yl)-2,5-diphenyltetrazolium bromide assay (●). *b*, DNA fragmentation was analyzed by electrophoresis on a 1.5% agarose gel. *c–e*, Western blot analyses with anti-poly(ADP-ribose) polymerase (*c*) and anti-p43(EMAPII) (*d*, *e*) antibodies of the cell extract (*c*, *d*) or the culture medium (*e*) obtained after different times of serum deprivation. Recombinant p43 and p43(EMAPII) were used as markers.

The human promonocytic U937 cell line undergoes apoptosis before cytolysis occurs (25). When U937 cells were subjected to serum starvation, DNA fragmentation and cleavage of poly(ADP-ribose) polymerase, two landmarks of apoptosis, occurred after 52–68 h of serum withdrawal (Fig. 2). The viability of the cells, measured by the 3-(4,5-dimethylthiazol-2-yl)-2,5-diphenyltetrazolium bromide assay, decreased after 52 h of starvation but the extent of dead cells that did not exclude trypan blue remained constant after more than 100 h of incubation (Fig. 2). In the meantime, antibodies directed to p43(EMAPII) were used to monitor the level of p43 in cell extracts prepared at different times of starvation. The p43 content of U937 cells drastically decreased after 92 h of serum deprivation, and a single polypeptide of ~26 kDa could be detected in the culture medium after 52–68 h of onset of apoptosis (Fig. 2). This polypeptide was distinct from p43(EMAPII) used as a marker. Only trace amounts of this polypeptide could be observed in the cellular fraction. By contrast with 32D cells, no polypeptide related to ArgRS, a marker of MARS, was detected in the culture medium fraction (results not shown). These results clearly showed that the p43 component of MARS is subjected to proteolysis during progression of apoptosis and that a degradation product is released in the culture supernatant. This degradation product of p43 was named p43(ARF), for Apoptosis-released Factor. No p43(EMAPII) degradation product could be detected in the culture medium of U937 cells subjected to apoptosis.

Purification and Structural Characterization of p43(ARF)—To characterize the p43 derivative generated during apoptosis, a 800-ml culture containing 10^9 U937 cells was subjected to serum withdrawal for 5 days and p43(ARF) was purified from the cell culture supernatant following three chromatographic steps on MonoS, MonoQ, and MiniS PE columns. The elution of p43(ARF) was monitored by Western blotting with antibodies directed to p43(EMAPII). About 0.2 μg of p43(ARF) was isolated and its N-terminal sequence was determined by automatic Edman degradation. The sequence SGTKEQIKGG was obtained and exactly matched the sequence of human p43 from residues 107 to 116. The calculated molecular mass of p43(ARF) is 22.5 kDa, in reasonably good agreement with the apparent mass of 26 kDa estimated by SDS-PAGE. The recombinant p43(ARF) protein produced in *E. coli* displayed an electrophoretic mobility similar to p43(ARF) isolated from the supernatant of U937 cells. The discrepancy between the observed and calculated masses is certainly related to the aberrant migration of p43, which also displays an apparent molecular mass of 43 kDa for a calculated mass of 34 kDa.

We showed previously that caspase 7, an apoptotic protease, is able to convert *in vitro* p43 into p43(EMAPII) (5). The sequence of cleavage of p43 into p43(ARF) (103TTVS ↓ SGTK110) does not correspond to any consensus cleavage site for a protease of the caspase family. Matrix metalloproteinases, including macrophage elastase, correspond to a family of proteases that possess a broad capacity to cleave components of the extracellular matrix but also non-matrix proteins that regulate *in cellulo* a variety of biological processes (26). Recombinant p43 and the MARS complex were subjected to controlled proteolytic digestion by elastase (Fig. 3). In both cases, the free and MARS-associated forms of p43 were cleaved by elastase to give a polypeptide of ~26 kDa, comigrating with recombinant p43(ARF), which was resistant to further proteolysis. The N-terminal amino acid sequence, S*X*GTKE, of the polypeptide recovered after elastase digestion of recombinant p43 was determined by Edman degradation. It is located 1 amino acid residue upstream of the N-terminal sequence of p43(ARF) isolated from apoptotic U937 cells. This suggests that, *in vivo*, elastase could be involved in processing p43 into p43(ARF), with the additional release of the N-terminal Ser residue by an aminopeptidase. Alternatively, another member of the large matrix metalloproteinase family with a slightly different specificity might be involved in the processing of p43 into p43(ARF). Whatever the protease involved in the cleavage, our data show that this segment of p43 is freely accessible.

Recombinant p43(ARF) was expressed in *E. coli* from the pET28b plasmid but without a His tag. Indeed, because the

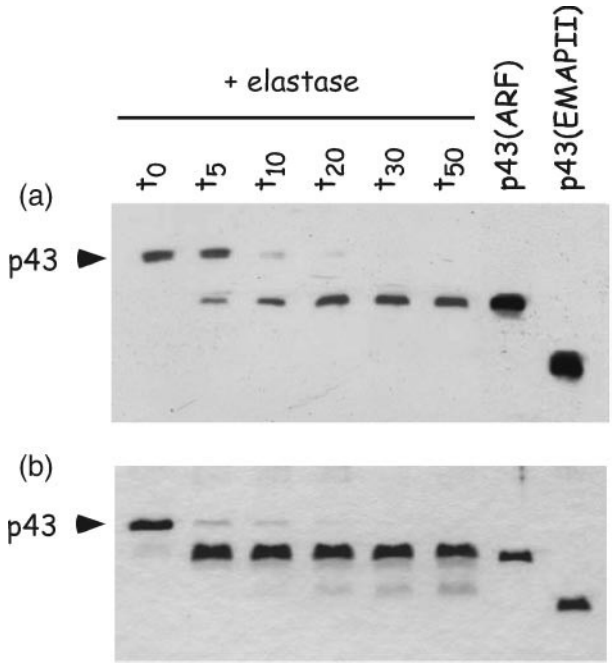

FIGURE 3. **Cleavage of p43 by elastase.** The rabbit MARS complex (*a*) or recombinant human p43 (*b*) were subjected to controlled elastase digestion at a protein:elastase ratio of 1:1000 or 1:10, respectively. At the times indicated, proteolysis was stopped by heating with SDS. The samples were analyzed by SDS-PAGE, and p43-related polypeptides were visualized by Western blotting with anti-p43(EMAPII) antibodies (*a*) or by Coomassie blue staining (*b*). Recombinant p43(ARF) and p43(EMAPII) were used as markers.

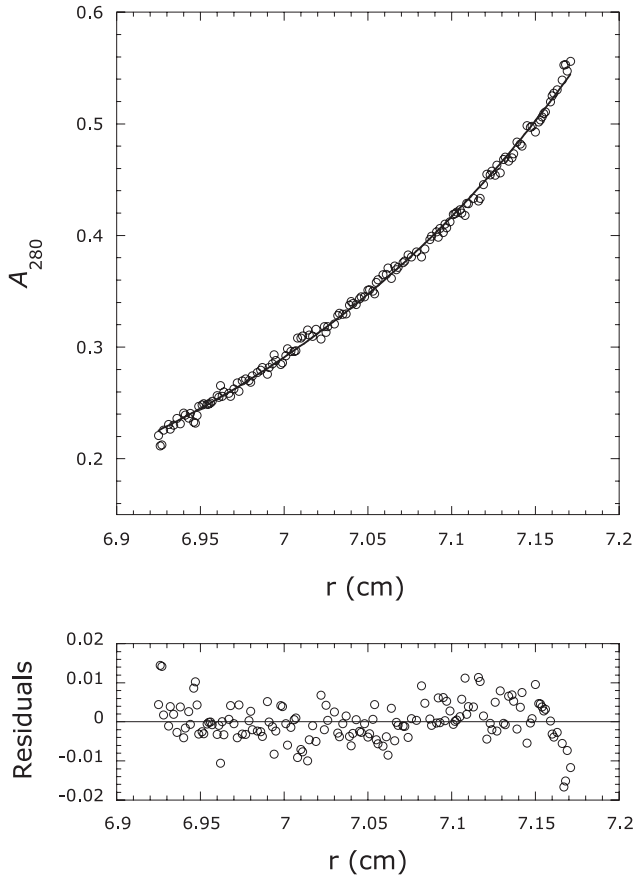

FIGURE 4. **Human p43(ARF) is a monomer in solution.** Recombinant p43(ARF) (initial concentration of 33 μM) was analyzed by equilibrium sedimentation at 15,000 rpm in 20 mM Tris-HCl, pH 7.5, 100 mM NaCl, 10% glycerol, and 1 mM DTT at 4 °C. Experimental values (*open circles*) were fitted (*curves*) to a monodisperse solute of 22,641 ± 812 Da. The residuals are indicated.

calculated isoelectric point of p43(ARF) is very basic (pI of 8.72), the protein eluted from the sulfopropyl cation exchanger at a NaCl concentration of 260 mM was already more than 80% homogeneous. The purified recombinant p43(ARF) is readily soluble at a protein concentration up to 30 mg/ml. It displayed an apparent molecular mass of 26 kDa by SDS-PAGE (Fig. 3).

The oligomeric structure of p43(ARF) was determined by sedimentation equilibrium (Fig. 4). We previously determined that p43 is a dimer in solution, whereas p43(EMAPII) is a monomer (5). The p43 derivative p43(EMAPII) is a compact domain based on an OB-fold structure (7). When p43(ARF) was subjected to centrifugation equilibrium at an initial protein concentration of 33 μM, experimental data could be fitted to a single species with a molecular mass of 22,641 ± 812 Da. The monodispersity of p43(ARF) in solution, bearing a 40-amino acid residue extension as compared with p43(EMAPII), containing 12 Lys residues, suggests that p43(ARF) is a discrete entity with a well defined structural organization. Taking into account a calculated molecular mass of 22,504 Da for the monomer, we concluded that p43(ARF) is a monomer in solution. Thus, the site of dimerization of p43 is comprised within the first 106 amino acid residues of the protein.

The tRNA Binding Potential of p43(ARF)—Recombinant p43, the precursor of p43(ARF), has the capacity to bind tRNA with a dissociation constant K_d of ~0.2 μM, as determined by a gel retardation assay (5). By contrast, p43(EMAPII) displayed a very weak tRNA binding capacity, with a K_d of ~40 μM. To evaluate the RNA binding ability of p43(ARF), the recombinant monomeric protein was incubated with *in vitro* transcribed tRNAs, and free and bound tRNAs were analyzed after separation on a native gel (Fig. 5). The apparent K_d determined for rabbit elongator $tRNA^{Met}$ or for human $tRNA^{Arg}$ was ~6 nM. Using the same tRNA substrates, K_ds of ~40 and ~0.2 μM were observed for p43(EMAPII) and p43, respectively (not shown). Stable complexes were also observed with p43(ARF) in the presence of minihelices representing the acceptor-TΨC stem-loop domains of these two tRNAs, with K_d of ~11 nM (Fig. 5). Thus, the strong interaction observed between p43(ARF) and these RNA substrates did not require the L-shaped structure of the tRNA molecules.

Test of the Cytokine Properties of p43(ARF)—The matured form of p43, p43(EMAPII), is thought to be an active cytokine that activates endothelial cells (13), causing a rise in Ca^{2+} concentration, the release of von Willebrand factor antigen, cell surface expression of P-selectin, the induction of tissue factor activity, and an enhanced expression of E-selectin. However, other reports have suggested that p43 itself, the precursor of p43(EMAPII), could be a real cytokine (15). To analyze the cytokine function of p43, p43(ARF), and p43(EMAPII), we examined the expression of E-selectin, one of the major landmarks of vascular inflammation induced by various cytokines such as IL-1β and tumor necrosis factor α (27) by HUVEC cells subjected to various stimuli. Addition of p43 at high concentration produced an increase in E-selectin expression (Fig. 6). When p43 was heat-treated (100 °C, 10 min) prior to incuba-

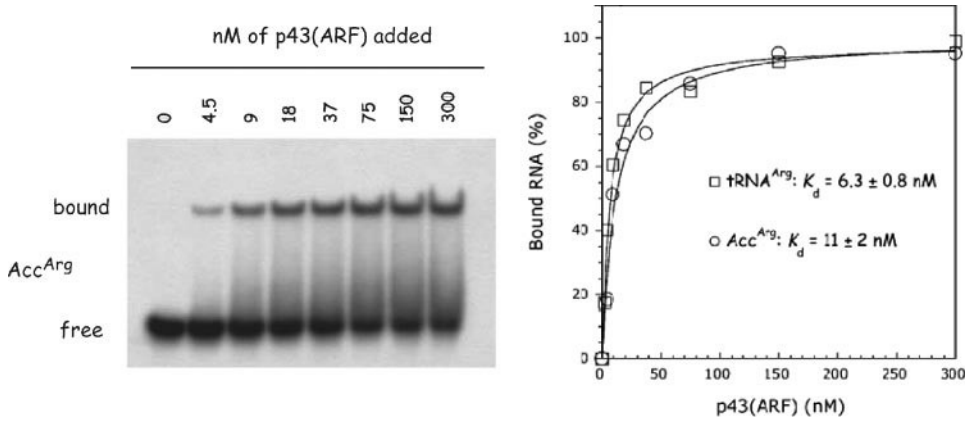

FIGURE 5. **Binding of tRNA by p43(ARF).** After incubation of p43(ARF) (4.5–300 nM) with ^{32}P-labeled $tRNA_2^{Arg}$ or a minihelix mimicking the acceptor-TΨC stem-loop domain of this tRNA (Acc^{Arg}), the mixture was analyzed on a native polyacrylamide gel and the mobility shift of RNA was visualized by autoradiography. The apparent K_d values are deduced from the plot of bound tRNA *versus* p43(ARF) concentration.

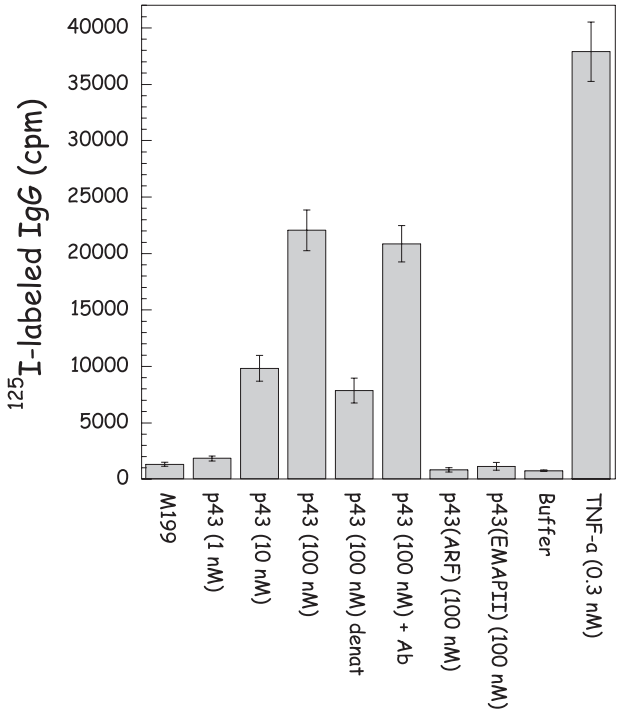

FIGURE 6. **Induction of E-selectin expression by p43 and its derivatives.** Expression of E-selectin by HUVEC was monitored in a two-step radioimmunoassay. After incubation with various amounts of p43, p43(ARF), or p43(EMAPII), or with p43 denatured by heating at 100 °C for 10 min, or with p43 preincubated for 1 h at 25 °C with anti-p43 antibodies, the extent of E-selectin expression was determined. As negative controls, HUVEC were also incubated in the medium without additives (*M199*) or in the medium containing the buffer used for dilution of p43 and its derivatives (*buffer*). As a positive control, cells were also incubated in the presence of tumor necrosis factor α. Each experiment was performed in quintuplicate; results are indicated as means ± S.E.

tion, the stimulation was decreased. Preincubation of p43 with anti-p43 antibodies had only a limited effect. By contrast, incubation of HUVEC with p43(ARF) or p43(EMAPII) at high concentration did not stimulate E-selectin expression.

To further understand the possible role of p43, p43(ARF), and p43(EMAPII) during the development of programmed cell death, these three proteins were expressed in human cells under the control of an inducible promoter. In a tetracycline-free medium, the three recombinant proteins were expressed to a level close to that of endogenous p43, as assessed by Western blot analysis with anti-p43(EMAPII) antibodies (results not shown). The aim of this experiment was to determine whether expression of p43 or of the matured products p43(ARF) or p43(EMAPII) may trigger apoptosis or may modify its time course of appearance and development. Alternatively, because all p43 is processed into p43(ARF) under apoptotic growth conditions (Fig. 2*d*), inactivation of this RNA binding cofactor associated with the nine aminoacyl-tRNA synthetases of MARS could be the main defect generated by the cleavage of the p43 component of MARS. The time course of apoptosis development was assessed by FACS after staining cells with 7-AAD, a nucleic acid dye excluded from viable cells, and with Annexin V-PE, which binds to phosphatidylserine that is translocated to the outer side of the plasma membrane at the early stages of apoptosis (Fig. 7). Expression of plasmid-borne p43, p43(ARF), or p43(EMAPII) in addition to endogenous p43 was not lethal for the cells and did not cause any noticeable phenotype. In particular, expression of p43 in excess neither accelerated nor impaired the cellular program of apoptosis (Fig. 7). Expression of p43(ARF) or of p43(EMAPII), the two p43 derivatives produced during apoptosis, did not induce the cells to enter apoptosis in the absence of other stimuli. When apoptosis was induced by serum starvation, expression of p43(ARF) had only a moderate effect on the time course of apoptosis development (Fig. 7). The percentage of apoptotic cells (annexin V-positive and 7-AAD-negative) was slightly increased in the presence of p43(ARF): 9.8, 14.7, 31.3, and 49.4% of apoptotic cells after 72, 80, 96, and 104 h of serum starvation, as compared with 7.2, 7.3, 16.7, and 28.8% in the absence of plasmid-borne p43(ARF). These results do not support the idea that the release of p43(ARF) or of p43(EMAPII) from MARS would be sufficient to induce apoptosis but leave open the possibility that the main cellular consequence of the cleavage of p43 might be related to the general breakdown of protein synthesis in apoptotic cells.

Subcellular Localization of p43 and of p43 Derivatives—To investigate the consequence of p43 cleavage on its subcellular localization, p43, p43(ARF), and p43(EMAPII) were fused with the green fluorescent protein (GFP) appended to their C-terminal ends. The fusion proteins were expressed in human cells for transient expression studies, and their stability and *in vivo* localization were analyzed 24 h after transfection. The various p43-GFP fusion proteins were not degraded *in vivo* as assessed by Western blot analysis with anti-GFP antibodies (results not shown). Their subcellular localization was analyzed by confocal microscopy on living cells. The recombinant p43 component of MARS was only found in the cytoplasmic compartment (Fig. 8). It should be noticed that the p43 protein, even when overexpressed after transient transfection in human cells, was com-

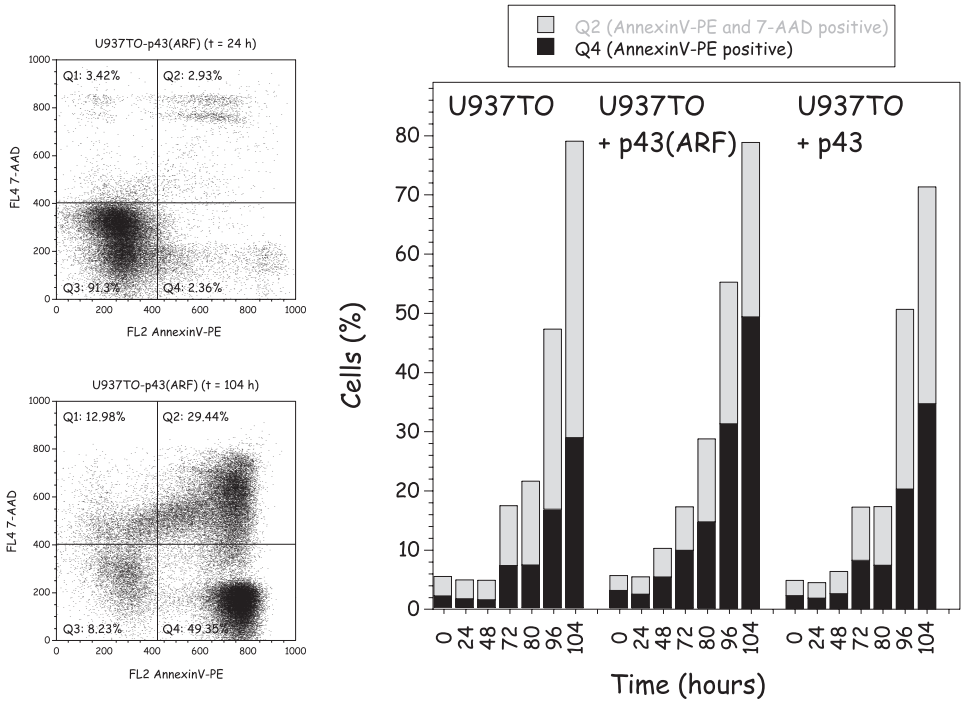

FIGURE 7. **Test of proapoptotic effect of p43 and p43(ARF).** Human U937TO cells and derivatives that expressed p43(ARF) or p43 were subjected to serum starvation. At the times indicated, cells were stained with the vital dye 7-AAD and with Annexin V-PE, a marker of early apoptosis, and analyzed by FACS. On the *left*, two examples of the FACS analysis are shown for U937TO cells that expressed p43(ARF) after 24 or 104 h of FCS deprivation. On the *right*, the frequency of early apoptotic cells (*Annexin V-PE-positive*; *Q4 quadrant*) and of cells in late stage of apoptosis (*Annexin V-PE- and 7-AAD-positive*, *Q2 quadrant*) are shown. Data are the mean values from three independent experiments.

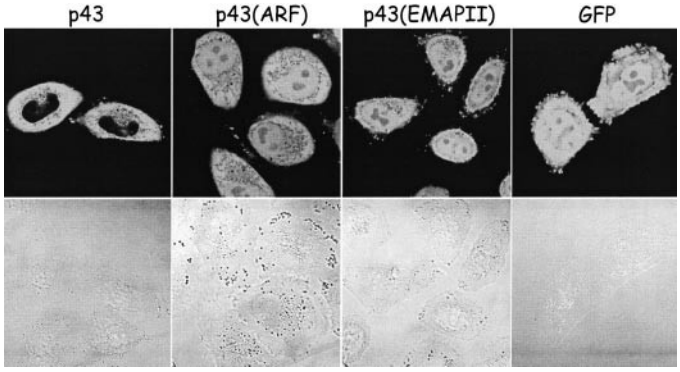

FIGURE 8. **Subcellular localization of p43 and of p43 derivatives.** HeLa cells were transiently transfected with pEGFP-N1 plasmids that expressed fusion proteins with p43, p43(ARF), or p43(EMAPII). The cellular localization of GFP alone or of the fusion proteins was analyzed by confocal laser scanning microscopy. GFP fluorescence (*top*) and differential interference contrast (*bottom*) imaging are shown.

pletely excluded from the nuclear compartment. As a control, GFP alone showed a diffuse pattern throughout the cell, with the exception of the nucleoli that displayed a limited GFP fluorescence. By contrast with p43-GFP, the p43(ARF)-GFP and p43(EMAPII)-GFP fusion proteins were found to be present in the cell cytoplasm but also in the nucleus (with the exception of the nucleoli). Thus, the release of the C-terminal domain of p43 upon apoptosis is accompanied by a delocalization of p43(ARF) or p43(EMAPII) into the whole cell and the OB-folded RNA-binding domain of p43(ARF) is no more excluded from the nuclear compartment. A GFP fusion protein containing the N-terminal domain of p43 upstream from the cleavage site of p43(ARF), from residues 1 to 106, was exclusively found in the cytoplasm (results not shown).

DISCUSSION

The p43 subunit of MARS, a 312-amino acid polypeptide, is involved in apoptosis. It was initially isolated as p43(EMAPII), a cytokine generated in apoptosis (13). This derivative of p43 corresponds to its C-terminal domain starting from residue Ser^{147}. It can be generated by cleavage with caspase 7, an apoptotic protease, both *in cellulo* (4) and *in vitro* (5). Recombinant p43 is also the substrate of other proteases, but they generate proteolytic products distinct from p43(EMAPII) (18). Whether the precursor (p43) or its maturation product (p43(EMAPII)) is secreted from apoptotic cells is not well established (4, 15). Here we characterized a new maturation product of p43 in human U937 cells induced in apoptosis.

As compared with other cell types used in previous studies, this promonocytic cell line can be induced in apoptosis independently of cytolysis. Induction of apoptosis in murine 32D cells or in human adenocarcinoma cell lines resulted in the recovery of p43, p43(EMAPII), and of uncharacterized intermediates in the culture medium (4, 15, 28). The appearance of a maturation product of p43 in the cytoplasm of U937 cells induced to undergo apoptosis is concomitant with DNA fragmentation, but it does not accumulate within the cell. Indeed, it is rapidly and specifically released from apoptotic cells and was therefore referred to as an Apoptosis-released Factor, p43(ARF). Neither its precursor (p43 from MARS) nor any other component of MARS was detected in the culture medium of apoptotic cells.

Concerning the putative function of p43 as a cytokine, the following observations are puzzling. Native recombinant p43, the precursor of p43(ARF), and p43(EMAPII) have been reported to have the capacity of inducing migration of the endothelial cells (17). The full-length recombinant p43 showed the highest activity (17), but the p43 subunit of MARS was exclusively found associated within the complex in extracts of exponentially growing human cells (14). This suggests that association of p43 within the MARS complex is a means to regulate the balance between the two functions of p43 and to sequester this protein in the cytoplasm of growing cells, as shown by the subcellular localization of a p43-GFP fusion protein. Although p43 could be *per se* a *bona fide* cytokine, its association with the synthetases would withdraw it from this cellular process. Thus, complex formation would be a means to regulate the spatio-temporal activity of p43. It has also been

reported that the cytokine activity of p43(EMAPII) could be mimicked by a synthetic peptide, RIGRIVT^{164} (29), but the crystal structure of p43(EMAPII) showed that only the side chains of Val^{163} and Thr^{164} are accessible to protein interactions (7), suggesting that the effects of the peptide are serendipitous. We also show in this work that highly purified preparations of p43, p43(ARF), or p43(EMAPII) do not induce the expression of E-selectin, a marker of the induction of endothelial cells, when used at concentrations similar to well known cytokines. This suggests that at least some of the effects previously ascribed to p43 or to some of its derivatives should be carefully reexamined. The finding that p43(ARF) is produced intracellularly in U937 but does not accumulate within the cell suggests that it is secreted and fulfills another function, as p43(ARF) or as a polypeptide subjected to an additional maturation step, p43(EMAPII).

Even if the amount of p43(ARF) recovered within the cell is low, a small but significant amount may localize to the nucleus, as exemplified by the finding that a p43(ARF)-GFP fusion protein could be translocated to the nucleus. This observation may explain some of the findings previously reported. For instance, p43-related polypeptides were identified within the nucleus by immunogold labeling on ultrathin sections of kidney cells, suggesting that p43 may also play a role in this cellular compartment (11). However, we show here that the p43-GFP fusion is efficiently excluded from the nucleus, whereas the p43(ARF)-GFP and p43(EMAPII)-GFP fusion proteins are no more excluded from the nuclear compartment. Thus, p43(ARF) may have in the nucleus a non-canonical function in addition to the role of its precursor in cytoplasmic protein synthesis. This function may be related to its high propensity to associate with nucleic acids.

Interestingly, monomeric p43(ARF) binds nucleic acids with a more than three orders of magnitude increase in affinity as compared with p43(EMAPII). The N-terminal polypeptide sequence of p43(ARF), made of 40 additional amino acid residues as compared with p43(EMAPII), is very rich in charged residues (2 Asp, 6 Glu, and 12 Lys) and displays a calculated isoelectric point of 9.79. This highly charged polypeptide may be responsible for the aberrant mobility of p43(ARF) observed by SDS-PAGE. The consensus sequence EKK*X*KEK*X*EKKGEKKEKK, containing four EKK motifs, is extensively conserved from *Xenopus* to human (supplemental Fig. S1). The precursor p43 also contains this signature sequence but binds nucleic acids with a 30-fold lower affinity. Thus, the conversion of p43 into p43(ARF) is accompanied by the exposure of this RNA binding site or by a conformational change of this domain that builds a high affinity binding site for nucleic acids. The possibility that the domain carrying this consensus sequence is not freely accessible in the native p43 protein is also supported by the observation that complete elastase digestion of the p43 component of MARS requires 100-fold higher protease concentrations than that required for the cleavage of recombinant p43. The accessibility of the highly charged segment of p43, also carrying the cleavage sites leading to p43(ARF) and p43(EMAPII), depends on the structural state of the protein.

The involvement of the components of MARS in pathways other than tRNA aminoacylation is not unusual. For instance, the bifunctional GluProRS of MARS is able to translocate to another complex that causes translational silencing of specific mRNAs (30), and LysRS may form an alternative complex with MITF and Hint and play a role in the activation of the microphthalmia transcription factor (31). In both cases, these are full-length components of MARS that are recruited in alternative complexes, which should cause profound structural rearrangement of MARS and may impair its activity in global translation. Concerning p43, after proteolytic cleavage, p43(ARF) loses its ability to associate with other components of MARS and is released in the intracellular space, but the N terminus polypeptide of p43, from residues 1 to 106, retains the capacity to associate within MARS and the structural integrity of the particle is not affected.[6] In contrast to necrotic cells that retain the capacity to synthesize proteins (3), translation inhibition occurs in apoptosis (1). Modification of initiation factors by phosphorylation or caspase-dependent cleavage is one of the major control points of translation regulation in apoptosis. The cleavage of p43 that supports translation when associated within MARS could be an additional control to regulate translation at the elongation step. An efficient shut down of protein synthesis at early stages of apoptosis may contribute to avoidance of production of abnormal or inflammatory proteins that would trigger an inflammatory response that is generally not observed in apoptosis.

The two cleavage sites on p43, after Ser^{106} and after Asp^{146}, are well conserved among species. The two consensus sequences TTøS^{106} ↓, where ø is an hydrophobic amino acid residue, and SAD^{146} ↓ SK, for a putative matrix metalloproteinase and for caspase 7, respectively, are conserved from hen to human (supplemental Fig. S1). This suggests that the same series of events leads to the release of the p43 component of MARS in these cell types. However, MARS is ubiquitous to all metazoan species, from Drosophila to human, studied so far (32). Thus, because the two consensus cleavage sites are not recovered from the p43 component of MARS from fish or Xenope (supplemental Fig. S1), the possibility that p43 may have a role as a switch in translation and as a putative cytokine seems to be a recent advance in evolution.

Acknowledgments—We thank Diep Lê (Laboratoire d'Enzymologie et Biochimie Structurales (LEBS), Gif-sur-Yvette) and Paulette Decottignies (Institut de Biochimie et Biophysique Moleculaire et Cellulaire, Orsay) for performing amino acid sequence analyses and Fatima El Khadali (LEBS, Gif-sur-Yvette) for sedimentation equilibrium experiments. We thank Spencer Brown and Susanne Bolte for access to the confocal microscope facility (Institut des Sciences du Véqétal, Gif-sur-Yvette).

REFERENCES

1. Morley, S. J., Coldwell, M. J., and Clemens, M. J. (2005) *Cell Death Differ.* **12,** 571–584
2. Saelens, X., Kalai, M., and Vandenabeele, P. (2001) *J. Biol. Chem.* **276,** 41620–41628
3. Saelens, X., Festjens, N., Parthoens, E., Vanoverberghe, I., Kalai, M., van Kuppeveld, F., and Vandenabeele, P. (2005) *J. Cell Biol.* **168,** 545–551

[6] M. Kaminska and M. Mirande, unpublished results.

4. Knies, U. E., Behrensdorf, H. A., Mitchell, C. A., Deutsch, U., Risau, W., Drexler, H. C., and Clauss, M. (1998) *Proc. Natl. Acad. Sci. U. S. A.* **95,** 12322–12327
5. Shalak, V., Kaminska, M., Mitnacht-Kraus, R., Vandenabeele, P., Clauss, M., and Mirande, M. (2001) *J. Biol. Chem.* **276,** 23769–23776
6. Mirande, M. (2003) in *The Aminoacyl-tRNA Synthetases* (Ibba, M., Francklyn, C., and Cusack, S., eds), pp. 298–308, Landes Bioscience, Georgetown, TX
7. Renault, L., Kerjan, P., Pasqualato, S., Menetrey, J., Robinson, J. C., Kawaguchi, S., Vassylyev, D. G., Yokoyama, S., Mirande, M., and Cherfils, J. (2001) *EMBO J.* **20,** 570–578
8. Norcum, M. T., and Warrington, J. A. (2000) *J. Biol. Chem.* **275,** 17921–17924
9. Park, S. G., Jung, K. H., Lee, J. S., Jo, Y. J., Motegi, H., Kim, S., and Shiba, K. (1999) *J. Biol. Chem.* **274,** 16673–16676
10. Guigou, L., Shalak, V., and Mirande, M. (2004) *Biochemistry* **43,** 4592–4600
11. Popenko, V. I., Ivanova, J. L., Cherny, N. E., Filonenko, V. V., Beresten, S. F., Wolfson, A. D., and Kisselev, L. L. (1994) *Eur. J. Cell Biol.* **65,** 60–69
12. Kao, J., Ryan, J., Brett, G., Chen, J., Shen, H., Fan, Y. G., Godman, G., Familletti, P. C., Wang, F., Pan, Y. C., Stern, D., and Clauss, M. (1992) *J. Biol. Chem.* **267,** 20239–20247
13. Kao, J., Houck, K., Fan, Y., Haehnel, I., Libutti, S. K., Kayton, M. L., Grikscheit, T., Chabot, J., Nowygrod, R., Greenberg, S., Kuang, W.-J., Leung, D. W., Hayward, J. R., Kisiel, W., Heath, M., Brett, J., and Stern, D. M. (1994) *J. Biol. Chem.* **269,** 25106–25119
14. Quevillon, S., Agou, F., Robinson, J. C., and Mirande, M. (1997) *J. Biol. Chem.* **272,** 32573–32579
15. Ko, Y. G., Park, H., Kim, T., Lee, J. W., Park, S. G., Seol, W., Kim, J. E., Lee, W. H., Kim, S. H., Park, J. E., and Kim, S. (2001) *J. Biol. Chem.* **276,** 23028–23033
16. Schwarz, M. A., Kandel, J., Brett, J., Li, J., Hayward, J., Schwarz, R. E., Chappey, O., Wautier, J. L., Chabot, J., Lo Gerfo, P., and Stern, D. (1999) *J. Exp. Med.* **190,** 341–354
17. Park, S. G., Kang, Y. S., Ahn, Y. H., Lee, S. H., Kim, K. R., Kim, K. W., Koh, G. Y., Ko, Y. G., and Kim, S. (2002) *J. Biol. Chem.* **277,** 45243–45248
18. Liu, J., and Schwarz, M. A. (2006) *Exp. Cell Res.* **312,** 2231–2237
19. Baffy, G., Miyashita, T., Williamson, J. R., and Reed, J. C. (1993) *J. Biol. Chem.* **268,** 6511–6519
20. Herr, I., Wilhelm, D., Bohler, T., Angel, P., and Debatin, K. M. (1997) *EMBO J.* **16,** 6200–6208
21. Wautier, J. L., Paton, R. C., Wautier, M. P., Pintigny, D., Abadie, E., Passa, P., and Caen, J. P. (1981) *N. Engl. J. Med.* **305,** 237–242
22. Wautier, M. P., Chappey, O., Vicart, P., Paulin, D., and Wautier, J. L. (1999) *Cell Biol. Toxicol.* **15,** 153–161
23. Agou, F., Waller, J. P., and Mirande, M. (1996) *J. Biol. Chem.* **271,** 29295–29303
24. Kaminska, M., Shalak, V., and Mirande, M. (2001) *Biochemistry* **40,** 14309–14316
25. Wright, S. C., Kumar, P., Tam, A. W., Shen, N., Varma, M., and Larrick, J. W. (1992) *J. Cell. Biochem.* **48,** 344–355
26. Nagase, H., Visse, R., and Murphy, G. (2006) *Cardiovasc. Res.* **69,** 562–573
27. Delomenie, C., Wautier-Pepin, M. P., Chappey, O., and Wautier, J. L. (1993) *Exp. Cell Res.* **207,** 122–130
28. Barnett, G., Jakobsen, A. M., Tas, M., Rice, K., Carmichael, J., and Murray, J. C. (2000) *Cancer Res.* **60,** 2850–2857
29. Kao, J., Fan, Y. G., Haehnel, I., Brett, J., Greenberg, S., Clauss, M., Kayton, M., Houck, K., Kisiel, W., Seljelid, R., Burnier, J., and Stern, D. (1994) *J. Biol. Chem.* **269,** 9774–9782
30. Sampath, P., Mazumder, B., Seshadri, V., Gerber, C. A., Chavatte, L., Kinter, M., Ting, S. M., Dignam, J. D., Kim, S., Driscoll, D. M., and Fox, P. L. (2004) *Cell* **119,** 195–208
31. Lee, Y. N., Nechushtan, H., Figov, N., and Razin, E. (2004) *Immunity* **20,** 145–151
32. Kerjan, P., Cérini, C., Semeriva, M., and Mirande, M. (1994) *Biochim. Biophys. Acta* **1199,** 293–297

BIOCHEMISTRY
including biophysical chemistry & molecular biology
Article

Biochemistry **2009,** *48,* 9959–9968 9959
DOI: 10.1021/bi901236g

Translation Initiation from Two In-Frame AUGs Generates Mitochondrial and Cytoplasmic Forms of the p43 Component of the Multisynthetase Complex†

Vyacheslav Shalak,‡ Monika Kaminska,§ and Marc Mirande*

Laboratoire d'Enzymologie et Biochimie Structurales, CNRS, 1 Avenue de la Terrasse, 91190 Gif-sur-Yvette, France. ‡*Present address: Institute of Molecular Biology and Genetics, 150 Acad. Zabolotnogo St., 03143 Kiev, Ukraine.* §*Present address: Institut Pasteur, Unité de Biochimie Structurale et Cellulaire, 25 Rue du Docteur Roux, 75015 Paris, France.*

Received July 20, 2009; Revised Manuscript Received September 7, 2009

ABSTRACT: In humans, nine aminoacyl-tRNA synthetases form a stable multiprotein complex with the three auxiliary proteins p18, p38, and p43. The N-terminal moiety of p43 is involved in its anchoring to the complex, and its C-terminal moiety has a potent tRNA binding capacity. The p43 component of the complex is also the precursor of p43(ARF), an apoptosis-released factor, and of p43(EMAPII), the endothelial-monocyte activating polypeptide II. Here we identified a new translation product of the gene of p43, which contains nine additional N-terminal amino acid residues. This gene product is targeted to the mitochondria and accounts for 2% of p43 expressed in human cells. The cytoplasmic and mitochondrial species of p43 are produced from the same mRNA by a mechanism of leaky scanning of the AUG codon at position −27, which is in an unfavorable sequence context for translation initiation. The finding that a mitochondrial species of p43 exists in human cells further exemplifies the multifaceted implications of p43 and opens new perspectives for the understanding of the role of p43 in the apoptotic cell.

In higher eukaryotic organisms belonging to the metazoan species of coelomates, from *Drosophila* to mammals, the nine aminoacyl-tRNA synthetases specific for amino acids Glu, Pro, Ile, Leu, Met, Gln, Lys, Arg, and Asp form a multi-aminoacyl-tRNA synthetase complex (MARS)[1] with the three auxiliary proteins p18, p38, and p43 (*1*). The p43 subunit of MARS is a structurally important building block of the complex. This dimeric protein of 312 amino acid residues interacts with GlnRS and ArgRS to form a subcomplex of MARS, and this subcomplex is anchored to MARS via p43−p38 interaction (*2*, *3*). The N-terminal moiety of p43 can replace full-length p43 for this function. It associates with the leucine zipper motif of p38 (*4*). The p43 subunit is also a RNA-binding protein (*5*, *6*) organized around a pseudodimeric OB fold-based domain (*7*). It occupies a central position within the multisynthetase complex (*8*). It has been proposed that p43 might play a role of a cofactor for aminoacylation (*9*), but this function remains a subject of controversy (*10*). The presence of p43, or of p43-related proteins, in the cytoplasm but also in the nucleus of rabbit kidney cells has been observed by immunoelectron microscopy (*11*). It has been shown that an N-terminally truncated form of p43, but not the full-length species, can localize to the nucleus (*5*).

The p43 protein is certainly among the most ancient proteins of the translation apparatus. Homologues of p43 have been described in all living kingdoms, suggesting that it fulfills an essential function in translation, in relation to its tRNA binding capacity, a property common to all p43-related proteins. The C-terminal moiety of p43 is recovered in a bacterial tRNA binding protein, Trbp111, that may form a ternary complex with a tRNA and an aminoacyl-tRNA synthetase (*12*). A similar domain is also associated in cis with other aminoacyl-tRNA synthetases: with bacterial and plant MetRS where it acts as a cofactor for aminoacylation (*13*), with human TyrRS where it may direct tRNA to the active site of the enzyme (*14*), or with bacterial PheRS where it contributes to the editing of noncognate aminoacyl-tRNA (*15*). In the yeast *Saccharomyces cerevisiae*, Arc1p, a p43-like protein, associates with MetRS and GluRS (*16*), acts as a cofactor of these enzymes for aminoacylation (*17*, *18*), and sequesters tRNA and aminoacyl-tRNA synthetases in the cytoplasm (*19*, *20*). However, more recent data showed that in mammals this protein is also involved in cellular mechanisms beyond translation, suggesting that p43 may have evolved additional functions.

The p43 component of MARS is also the precursor of the endothelial-monocyte activating polypeptide II isolated from methylcholanthrene A-induced fibrosarcoma cells, a cytokine generated during apoptosis (*21*−*23*). The mature p43(EMAPII) has been ascribed to a proinflammatory cytokine, which stimulates chemotactic migration of polymorphonuclear granulocytes and mononuclear phagocytes and induces tissue factor activity on endothelial cells. The C-terminal, p43-like domain of human TyrRS was also shown to have cytokine activities similar to that of p43(EMAPII) (*24*). Whether p43(EMAPII) or its precursor, the p43 component of MARS, is the real cytokine remains controversial (*21*, *23*, *25*). Stable overexpression of p43, of

†This work was supported by grants from the Centre National de la Recherche Scientifique (CNRS) and the Association pour la Recherche sur le Cancer (ARC). V.S. was the recipient of postdoctoral fellowship from the Agence Nationale de Recherches sur le SIDA, and M.K. was the recipient of postdoctoral fellowships from the Fondation pour la Recherche Médicale and Association pour la Recherche sur le Cancer.

*To whom correspondence should be addressed: Laboratoire d'Enzymologie et Biochimie Structurales, CNRS, 1 Avenue de la Terrasse, 91190 Gif-sur-Yvette, France. Telephone: +33 1 69 82 35 05. Fax: +33 1 69 82 31 29. E-mail: mirande@lebs.cnrs-gif.fr.

[1]Abbreviations: MARS, multi-aminoacyl-tRNA synthetase complex; ARF, apoptosis-released factor; EMAPII, endothelial-monocyte activating polypeptide II.

© 2009 American Chemical Society
Published on Web 09/23/2009

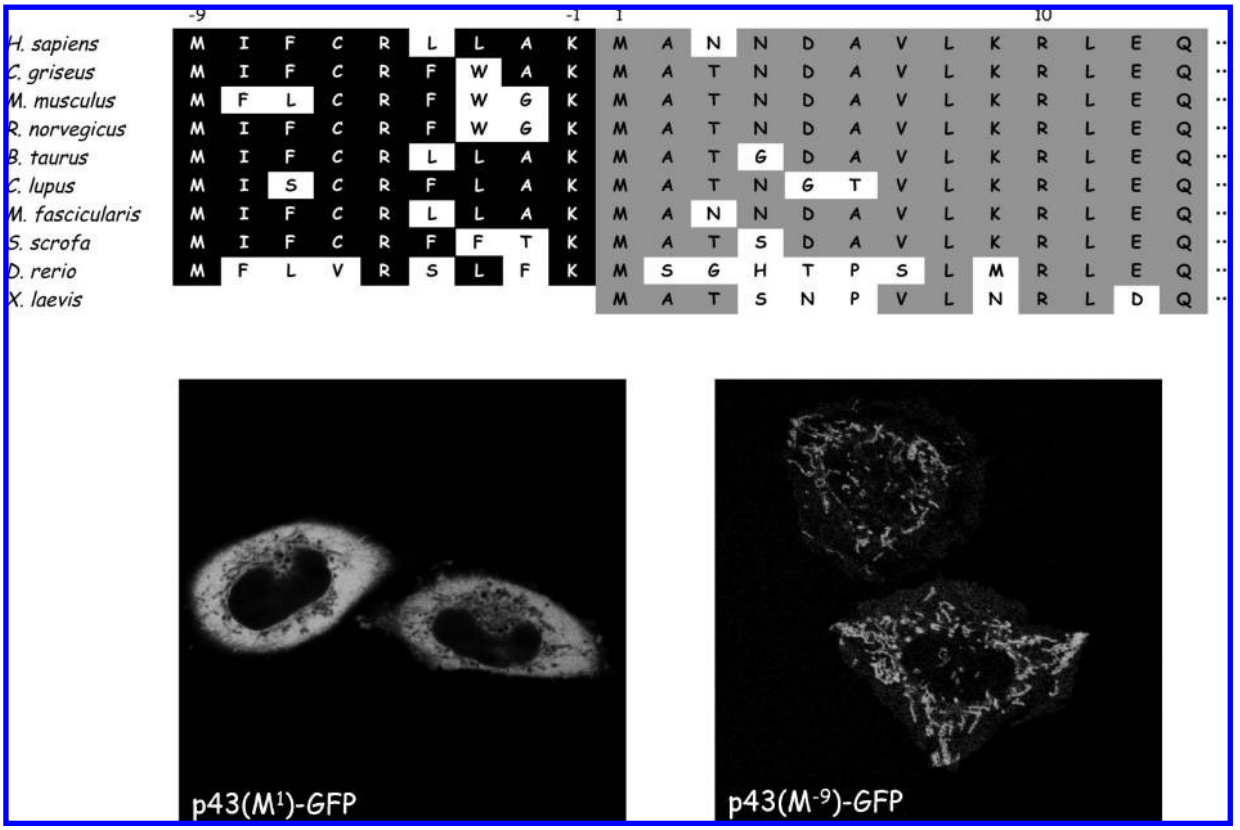

FIGURE 1: Differential subcellular localization of the two forms of p43 in human cells. The putative N-terminal amino acid sequences of the p43 proteins from various species were deduced from the most 5′-upstream sequences of the known cDNA. The sequences of p43 from human (*Homo sapiens*, NP_001135888), hamster (*Cricetulus griseus*, AAB95207), mouse (*Mus musculus*, NP_031952), rat (*Rattus norvegicus*, NP_446209), cattle (*Bos taurus*, NP_001030190), dog (*Canis lupus*, XP_545016), macaque (*M. fascicularis*, BAE90551), pig (*Sus scrofa*, NP_001107755), zebrafish (*Danio rerio*, NP_001039316), and frog (*X. laevis*, NP_001080110) are aligned. HeLa cells were transiently transfected with pEGFP-N1 plasmids that expressed fusion proteins with p43 starting at Met^{1} or at Met^{-9}. The cellular localization of the GFP fusion proteins was analyzed by confocal laser scanning microscopy.

p43(EMAPII), or of p43(ARF) in human HeLa of U937 cells was not lethal for the cells, which did not enter apoptosis in the absence of other stimuli (*2*, *5*). When p43(ARF) or p43(EMAPII) was overexpressed in U937 cells induced in apoptosis by serum starvation, the time course of apoptosis development was not significantly modified (*5*). p43 as well as p43(EMAPII) has also been reported to have anti-angiogenic properties that would limit establishment of neovasculature and thus would suppress tumor growth (*26*, *27*). This cytokine is believed to be involved in many other physiological processes and pathological disorders (see ref *28* for a review). However, in most of these studies, the real cytokine associated with these pathologies is not well-identified. Indeed, using immunohistology, antibodies directed to p43-(EMAPII) cannot discriminate between the full-length precursor protein, the p43 component of MARS ubiquitous to all cell types, and the mature p43(EMAPII) or p43(ARF) molecules (*6*, *29*). We now show that the diversity of p43 proteins is even more puzzling than previously thought.

EXPERIMENTAL PROCEDURES

Construction of Plasmids Expressing GFP Fusion Proteins. The complete cDNAs encoding human p43 starting from Met^{1} or Met^{-9} to Lys^{312} were amplified by PCR and introduced between the *Eco*RI and *Bam*HI sites of pEGFP-N1 (BD Biosciences) to express p43(M^{1})−GFP or p43(M^{-9})−GFP fusion protein, respectively. The cDNAs encoding p43 from Met^{-9} to Ser^{147}, from Met^{-9} to Phe^{80}, from Met^{-9} to Lys^{312} with a mutation of Met^{1} to Ile (AUG to AUU mutation), or from Met^{-9} to Lys^{312} with a mutation of Ile^{-8} to Ala (AUU to GCG mutation) were produced by PCR and introduced between the *Eco*RI and *Bam*HI sites of pEGFP-N1, to express p43(M^{-9}:S^{147})−GFP, p43(M^{-9}:F^{80})−GFP, p43(M^{-9}.M^{1}I)−GFP and p43(M^{-9}.I^{-8}A)−GFP proteins. To express p43(M^{-9}:K^{-1})−GFP (encoding p43 from Met^{-9} to Lys^{-1}), p43(M^{-9}:M^{1}I:D^{5})−GFP [encoding p43 from Met^{-9} to Asp^{5}, with a mutation of Met^{1} to Ile (AUG to AUU mutation)], p43(M^{-9}:M^{1}I:R^{10})−GFP (encoding p43 from Met^{-9} to Arg^{10}, with a mutation of Met^{1} to Ile), or p43(M^{-9}:I^{-8}A:K^{-1})−GFP [encoding p43 from Met^{-9} to Lys^{-1}, with a mutation of Ile^{-8} to Ala (AUU to GCG mutation)] protein, oligonucleotide duplexes were introduced between the *Eco*RI and *Bam*HI sites of pEGFP-N1. All constructs were verified by DNA sequencing.

Confocal Imaging. HeLa cells were grown in F12 medium (Invitrogen) supplemented with 10% fetal calf serum, 2 mM glutamine, and 100 μg/mL penicillin and streptomycin. Cells were transfected with Effectene (Qiagen). For localization experiments, cells were cotransfected with a pEGFP-N1 derivative and with pDsRed2-Mito (BD Biosciences). Cells were grown in eight-well Lab-Tek II chambers (Nalge Nunc International) and observed by confocal laser scanning microscopy using a Leica TCS SP2 confocal microscope equipped with a DD488/543 mirror. GFP was excited using a 488 nm laser line of an Ar laser and detected at 500−535 nm. DsRed was excited at 543 nm with a He−Ne laser and detected at 584−659 nm. Imaging of GFP and DsRed fluorescence was performed in a sequential manner. The expression and stability of the fusion proteins in HeLa cells

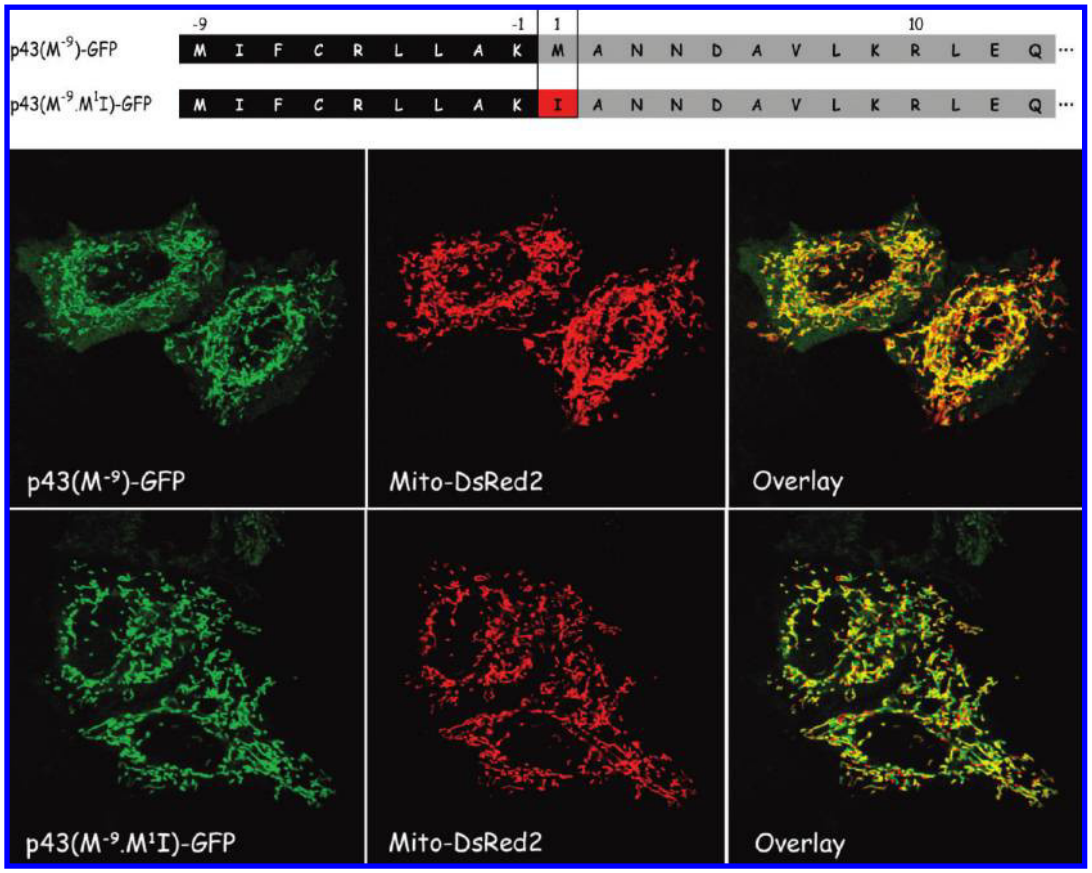

FIGURE 2: Colocalization of p43(M^{-9}) with mitochondria. HeLa cells were cotransfected with plasmids expressing the p43(M^{-9})−GFP or p43(M^{-9}.M^{1}I)−GFP fusion protein and with pDsRed2-Mito, a plasmid that expresses a mitochondrial protein marker. Cellular localization of the fusion proteins was analyzed by confocal microscopy. The overlay shows a perfect colocalization of the p43 proteins and of the mitochondrial marker, and a decreased green cytoplasmic background when Met^{1} is mutated to Ile.

were checked by Western blot analysis with anti-GFP and anti-DsRed antibodies.

Mapping the 5′-Ends of p43 Transcripts. Determination of the 5′-ends of the transcripts encoding p43 was conducted by rapid amplification of cDNA ends (5′-RACE, Roche). Poly(A^{+}) mRNA isolated from the U937 human cell line with Oligotex (Qiagen) was reverse transcribed into single-stranded cDNA using oligonucleotide 5′-GCTTAGAGTCGGCACTTCC-3′, complementary to nucleotides 445 to 427 of p43 mRNA (+1 corresponds to A of the AUG codon specifying the cytoplasmic protein). The first strand cDNA was dA-tailed and amplified by PCR between oligo d(T)-anchor primer (Roche) containing a *Cla*I site at the 5′-end and oligonucleotide 5′-GGGGGATCC-GGTATTTGCTTCACTCCATT-3′, complementary to nucleotides 236 to 217 of p43 mRNA and containing a *Bam*HI site at the 5′-end. PCR products were cloned and sequenced.

Antibodies and Western Blot Analysis. Monoclonal antibody directed to GFP or polyclonal antibody to DsRed was from BD Biosciences, and monoclonal antibody to human cytochrome *c* was from PharMingen. Polyclonal anti-p43, anti-LysRS, and anti-AspRS antibodies have been described previously (*30*). Western blot analyses were conducted with goat anti-rabbit or goat anti-mouse secondary antibodies conjugated with peroxidase (Chemicon) and the ECL detection reagents (Amersham Biosciences).

Isolation of Mitochondria. U937 cells were grown in suspension in RPMI medium (Invitrogen) supplemented with 10% FCS. Subcellular fractionation of U937 cell extracts was conducted essentially as described previously (*31*). U937 cells (100×10^{6} cells) were harvested by centrifugation at 600*g* for 10 min at 4 °C, washed once with 10 mL of ice-cold PBS, and resuspended in 2 mL of buffer MitoA [20 mM HEPES-KOH (pH 7.5), 10 mM KCl, 1.5 mM $MgCl_2$, 1 mM EDTA, 1 mM EGTA, 250 mM sucrose, and 1 mM DTT]. All subsequent steps were conducted at 4 °C. After incubation on ice for 10 min, cells were pelleted at 600*g*, resuspended in 550 μL of buffer MitoA, and incubated for 10 min. Cells were lysed with 30−50 strokes of a Teflon homogenizer (Kontes) and diluted with 1 volume of buffer MitoA. The lysate was centrifuged at 750*g* for 10 min and then at 900*g* for 10 min to remove cell debris and nuclei. After another centrifugation at 5500*g* for 10 min, the supernatant was recovered and centrifuged at 8000*g* for 10 min to remove residual mitochondria, and the resulting supernatant was termed the cytoplasmic fraction. The pellet from the centrifugation at 5500*g*, containing mitochondria, was resuspended with 0.5 mL of buffer MitoA, centrifuged at 5500*g* for 10 min, resuspended with 0.5 mL of buffer MitoA, and centrifuged at 8000*g* for 10 min. The resulting pellet was termed the mitochondrial fraction.

RESULTS

A Mitochondrial Species of p43 Is Encoded from an Upstream AUG Codon. The p43 protein is a ubiquitous component of all multi-aminoacyl-tRNA synthetase complexes isolated so far. Its N-terminal domain mediates its association with the arginyl- and glutaminyl-tRNA synthetase components of the complex, and with p38, the scaffold protein of MARS (*2*). Two human p43 species are registered on the NCBI Web site. Entry NP_004748.2, annotated "small inducible cytokine subfamily E,

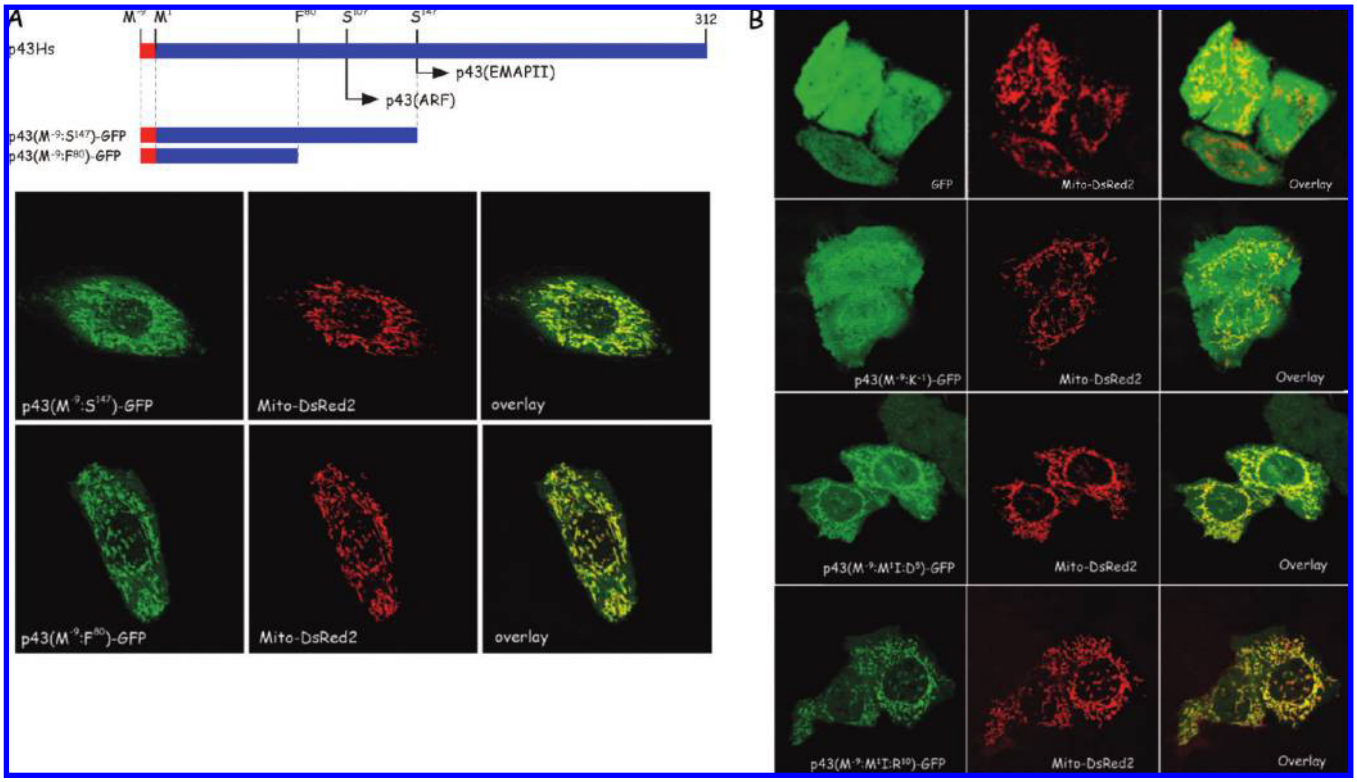

FIGURE 3: Identification of the minimal peptide required for mitochondrial targeting of p43(M^{-9}). (A) The mitochondrial p43 protein is composed of two conserved domains (from Met^1 to Phe^{80} and from Ser^{147} to Lys^{312}), a highly charged and more variable linker domain (from Phe^{80} to Ser^{147}), and a N-terminal sequence of nine amino acid residues specific for the mitochondrial protein. HeLa cells were transiently transfected with pDsRed2-Mito and with pEGFP-N1 plasmids that expressed GFP fusion proteins containing p43 sequences from Met^{-9} to Ser^{147} [p43(M^{-9}:S^{147})−GFP] or to Phe^{80} [p43(M^{-9}:F^{80})−GFP]. The colocalization of the GFP fusion proteins and of the mitochondrial marker was analyzed by confocal laser scanning microscopy. (B) The N-terminal nine-amino acid sequence specific to mitochondrial p43 was fused to GFP without [p43(M^{-9}:K^{-1})] or with 5 [p43(M^{-9}:M^1I:D^5)] or 10 [p43(M^{-9}:M^1I:R^{10})] additional amino acid residues of p43. The two last constructs also display a Met^1 to Ile mutation, to prevent translation initiation at the level of the Met codon specifying the cytoplasmic protein. As a control, localization of GFP alone is shown in the top panels. Localization of fluorescent proteins was analyzed by confocal laser scanning microscopy.

member 1 isoform a precursor", corresponds to the 312-amino acid protein that has been initially described as the precursor of the EMAPII-cytokine (*21*). It corresponds to the p43(M^1) species described below. When additional genomic sequences became available, a putative 336-amino acid p43 species was indexed as "small inducible cytokine subfamily E, member 1 isoform b precursor", described in entry NP_001135888.1. This p43 species would be encoded by a longer mRNA species containing two putative upstream AUG codons, but no experimental data have been provided to date to ascertain that these two upstream AUG codons are indeed functional.

Comparison of the amino acid sequences potentially encoded by the 5′-ends of p43 cDNA from different species revealed that a putative nine-amino acid polypeptide sequence is encoded upstream from the AUG codon specifying the cytoplasmic form of p43, p43(M^1). This peptide is highly conserved in p43(M^{-9}) forms from humans to fish (Figure 1). By contrast, the sequence data available for the p43 cDNA from *Xenopus laevis* suggest that it does not encode an additional N-terminal, nine-amino acid sequence. With regard to the most upstream AUG codon found on the longer mRNA, the finding that it is not recovered in p43 from other species of primates such as *Pan troglodytes* (chimpanzee), *Maccaca fascicularis* or *Maccaca mulatta*, and *Pongo abelii* (orangutan) indexed in the data libraries, proteins that are 96% identical with human p43, suggests that it might not be functional. Further analyses are required to validate this most upstream AUG codon as a functional one.

To gain some insight into the physiological significance of the p43(M^{-9}) species, the cellular localization of the two human p43 species, p43(M^1) and p43(M^{-9}), was determined by confocal microscopy of human cells transformed with GFP fusion proteins (Figure 1). The p43(M^1)−GFP fusion protein exhibited a diffuse fluorescence pattern extending throughout the cytoplasm, with a distinct exclusion of the nucleus (Figure 1), as reported previously (*5*). By contrast, the p43(M^{-9})−GFP fusion protein revealed a punctuate pattern within the cytoplasm, superimposed to a faint diffuse labeling of the whole cytoplasm.

The punctuate pattern displayed by the p43(M^{-9})−GFP fusion protein suggested that this protein could be localized into the mitochondria. To test this hypothesis, the p43(M^{-9})−GFP fusion protein was coexpressed in HeLa cells with a mitochondrial marker Mito-DsRed2, a DsRed fluorescent protein expressed with the mitochondrial targeting sequence of human cytochrome *c* oxidase. As shown in Figure 2, the green fluorescence labeling observed with the p43(M^{-9})−GFP fusion protein superimposed with the red fluorescence labeling observed with Mito-DsRed2. Thus, the nine additional amino-terminal residues found in p43(M^{-9}) are involved in mitochondrial targeting of p43. To ascertain that the AUG codon encoding methionine at position −9 was used as the initiation codon for the p43-(M^{-9})−GFP fusion protein, the second AUG codon encoding methionine at position 1 was mutated into an AUU codon (Ile). The p43(M^{-9}.M^1I)−GFP fusion protein was also directed to the mitochondria (Figure 2). It should be noticed that in the presence

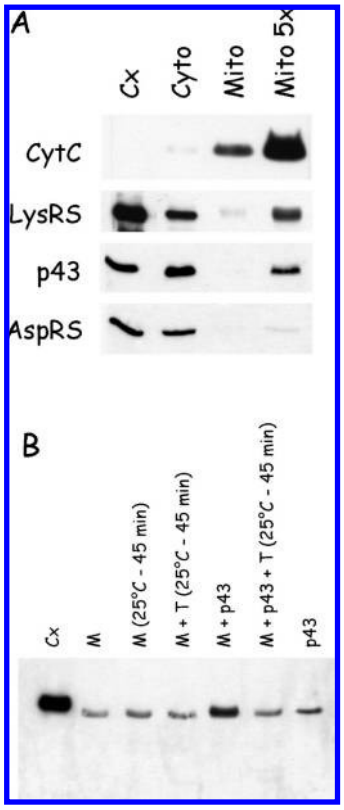

FIGURE 4: Detection of a p43-related polypeptide in isolated mitochondria. (A) The cytoplasmic (Cyto) or mitochondrial (Mito) fractions obtained after subcellular fractionation of a U937 cell extract were analyzed by Western blotting using antibodies directed to the LysRS, p43, or AspRS component of the multi-aminoacyl-tRNA synthetase complex (Cx) or to cytochrome *c* (CytC). Lanes Cyto and Mito contained equivalent amounts of the initial extract of U937 cells. Lane Mito 5× contained a 5-fold excess of the Mito fraction. (B) Mitochondria (M) purified from human U937 cells were incubated at 25 °C for 45 min in the absence or presence (M+T) of trypsin at a concentration of 0.1 mg/mL, and in the absence or presence (M+p43) of purified human cytoplasmic p43 added at a concentration of 1 μg/mL. Samples were heated for 5 min at 100 °C in 62.5 mM Tris-HCl (pH 7.5), 2% SDS, 5 M urea, 100 mM DTT, and 0.002% bromophenol blue and analyzed by Western blotting with anti-p43 antibody. The purified multi-aminoacyl-tRNA synthetase complex (Cx) and p43 protein (p43) were used as controls.

of the M^1I mutation, the green fluorescence cytoplasmic background observed with the p43(M^{-9})−GFP fusion protein is now virtually absent. Thus, the translation product starting at Met at position −9 is exclusively targeted to the mitochondria, and the AUG codon at position 1 is solely used for translation of the cytoplasmic form of p43.

The 19 N-Terminal Amino Acid Residues of p43 Specify the Mitochondrial Targeting Sequence. The mitochondrial targeting signals are generally located at the N-terminus of the imported proteins, but in some instances, mitochondrial precursors display internal or C-terminal targeting signals (*32*). When the C-terminal region of p43 was removed, from residue 148 to 312 or from residue 81 to 312, the polypeptides initiating at Met^{-9} were still directed to the mitochondria (Figure 3A), suggesting that the sequence elements responsible for mitochondrial targeting are localized only in the N-terminal region of p43(M^{-9}). To identify the minimal polypeptide that constitutes the mitochondrial targeting sequence of p43, N-terminal peptides of p43(M^{-9}) of different lengths were fused to GFP. When the cDNA sequences encoding the amino acid residues located upstream of Met^1, from Met^{-9} to Lys^{-1}, were fused to GFP to give the p43(M^{-9}:K^{-1})−GFP fusion protein, no labeling of mitochondria could be observed (Figure 3B). The labeling was very similar to that obtained with GFP alone (top of Figure 3B).

Thus, the additional sequences found in p43(M^{-9}) as compared to p43(M^1) are not sufficient to trigger mitochondrial localization of GFP. When five additional amino acid residues of p43 were fused to GFP, the p43(M^{-9}:M^1I:D^5)−GFP fusion protein, containing p43 sequences from Met^{-9} to Asp^5, including the M^1I mutation, revealed a clear mitochondrial labeling (Figure 3B). However, the cytoplasmic background was high, suggesting that these sequences contain most but not all the sequence information necessary for targeting. A nearly complete mitochondrial targeting of GFP was observed with the p43(M^{-9}:M^1I:R^{10})−GFP fusion protein (Figure 3B), suggesting that the 19 amino-terminal residues of p43(M^{-9}) are necessary and sufficient to trigger mitochondrial localization and account for its mitochondrial targeting signal.

p43(M^{-9}) Is Translocated into the Mitochondria. To ascertain that the p43(M^{-9}) polypeptide is not merely loosely interacting at the surface of the outer mitochondrial membrane but is translocated into the matrix of the mitochondria, we first isolated mitochondria from human cells in culture and checked for the presence of the p43-related polypeptide in an extract of purified mitochondria. The relative amount of the cytoplasmic and mitochondrial species of p43 was determined by Western blotting with an anti-p43 antibody directed to the common region of p43(M^1) and p43(M^{-9}). After subcellular fractionation of a U937 cell extract, antibodies to cytochrome *c* and to the cytoplasmic species of aspartyl-tRNA synthetase, representative of a mitochondrial and of a cytoplasmic protein, respectively, were used as markers of the subcellular fractions (Figure 4A). A trace amount of AspRS was observed in the mitochondrial fraction, showing a slight cytoplasmic contamination. By contrast, a clear signal was observed in the mitochondrial fraction when anti-p43 antibody was used (Figure 4A). Similarly, antibody directed to LysRS also showed the presence of LysRS in the mitochondrial fraction, as observed previously (*31*). The intensities of the signals obtained by Western blotting were quantified; the fractions of the mitochondrial species of p43 and LysRS were found to represent ~1−2% of the total. Interestingly, the amount of mitochondrial p43 is similar to that determined for mitochondrial LysRS, the only LysRS species that sustains mitochondrial translation. This observation is consistent with a functional role of mitochondrial p43.

If p43(M^{-9}) is translocated into the mitochondrial matrix, then it should not be accessible to proteases added to purified mitochondria. When isolated mitochondria were incubated at 25 °C, in the presence or absence of trypsin, the polypeptide corresponding to p43 was not degraded (Figure 4B). When an equal amount of purified, cytoplasmic p43 was added to purified mitochondria, the exogenously added p43 was completely degraded after incubation in the presence of trypsin (Figure 4B). These results are consistent with the import of p43(M^{-9}) into the mitochondrial matrix.

Mapping the 5′-Ends of p43 cDNA. The gene encoding the human, cytoplasmic, and mitochondrial species of p43 is located on chromosome 4, at position 4q24. It is made of seven exons that encompass 31898 nucleotides (Figure 5A). The first two exons are separated by a long intron of 8390 nucleotides. The AUG initiation codon for p43(M^1) is located within exon 2 (Figure 5A). The AUG initiation codon for p43(M^{-9}) is split by this large

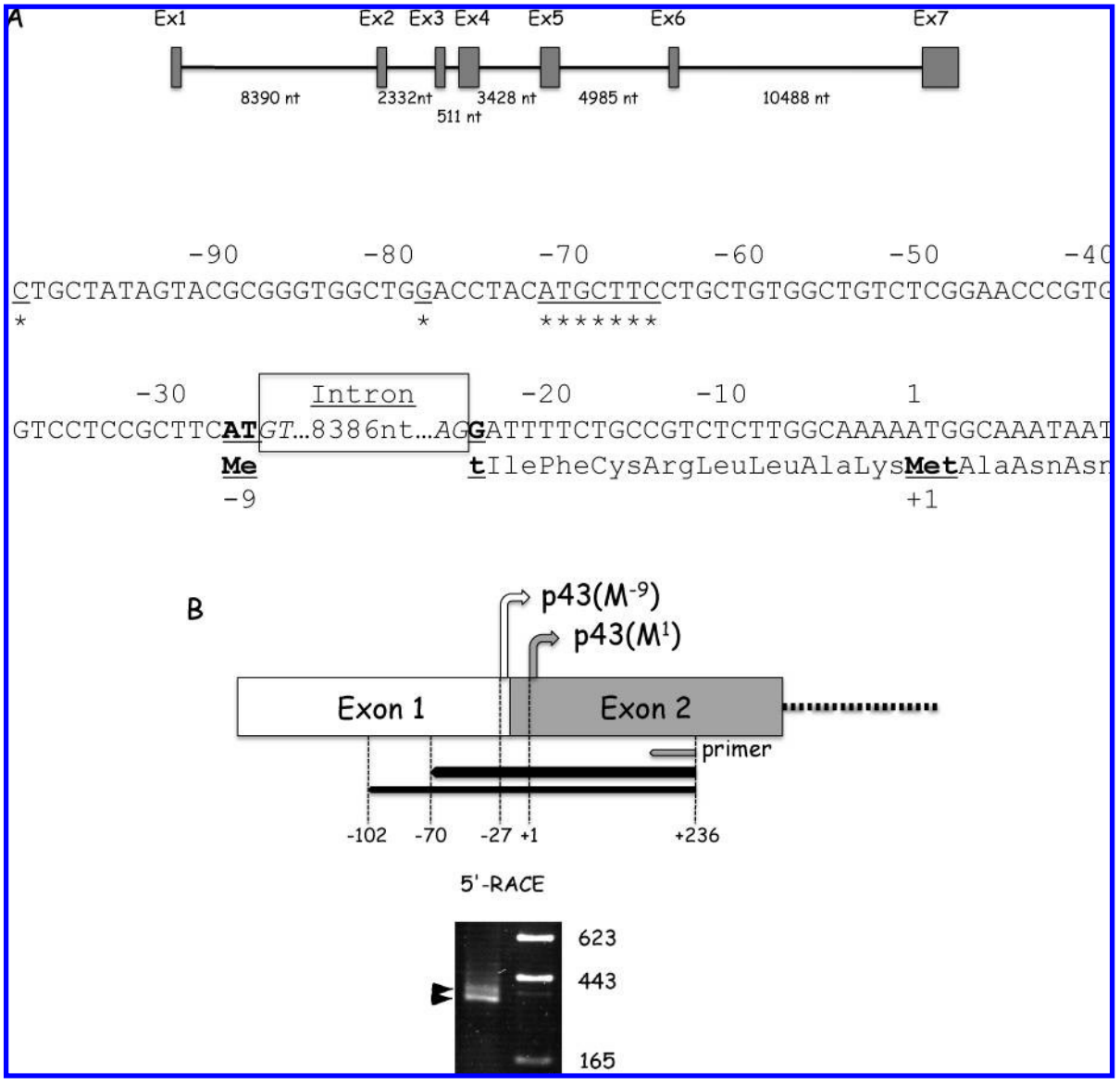

FIGURE 5: Mapping of the 5′-ends of p43 transcripts. (A) The top panel shows a schematic view of the gene encoding human p43, made of seven exons (boxes) linked by six introns (lines). The bottom panel shows the 5′-end DNA sequence of the gene. Sequences located at the 3′-end of exon 1 and at the 5′-end of exon 2 are indicated. Met residues at positions +1 and −9 correspond to the initiating methionine for the cytoplasmic and mitochondrial species of p43, respectively. The nucleotide at position 1 corresponds to the A residue of the ATG encoding cytoplasmic p43. The sequence of the ATG codon for Met^{-9} is interrupted by a long intron. The 5′-ends of the transcripts determined by 5′-RACE are denoted (asterisks). (B) The 5′-end of the spliced mRNA containing exons 1 and 2 is schematized. The two cDNA products obtained by 5′-RACE with the primer at position 236 (gray arrow) are indicated by arrowheads (left lane), and their sizes are compared with a DNA marker (right lane). The major cDNA extends up to nucleotides around position −70 (thick black arrow) and the minor one to position −102 (thin black arrow).

intron; the two first nucleotides are located at the 3′-end of exon 1, while the G of the AUG codon is provided by exon 2 after splicing of the intron. The formation of the AUG codon for $p43(M^{-9})$ requires that splicing occur at this position. Thus, we considered the possibility that two different mRNAs could be produced by this gene by a mechanism of alternative splicing.

To test this possibility, we performed a 5′-RACE experiment using a specific primer localized in exon 2 (Figure 5B). Two products of ∼300−350 nucleotides, corresponding to two putative mRNAs, were obtained. The smaller PCR product was the most abundant. Quantitative PCR experiments revealed that the longest mRNA is 4-fold less abundant than the short one (result not shown). To identify the 5′-ends of the PCR products, they were cloned and their nucleotide sequences determined. The 5′-ends of the smaller product fell in the region of nucleotides −66 to −72, as compared to the AUG codon for $p43(M^{1})$. Thus, the AUG codon at position −27, encoding $p43(M^{-9})$, is also carried by the shortest mRNA. The longer mRNA extended up to nucleotide −102 in exon 1 (Figure 5B). Thus, the two AUG codons at positions −27 and +1 are both present on the two mRNA species, and no evidence for a mechanism of alternative splicing of the first intron was observed.

Analysis of the Sequence Context of the AUGs. According to the proposed mechanism of ribosome scanning for translation initiation in mammals (*33*, *34*), the sequence context surrounding the AUG codons determines whether the putative initiation site is strong or weak. The optimal context corresponds to the sequence gcc(A/G)ccAUGG, where a purine at position −3 and a G at position +4 are the most important determinants for a strong context in mammals. The sequence context around the AUG at position −27, for initiation of translation of $p43(M^{-9})$, with a U at position −3 and an A at position +4,

	-3	+1	+4
Favorable context : g c c	A/G	c c A U G	G
p43(M[1]) : g c a	A	a a A U G	G
p43(M[-9]) : c g c	U	u c A U G	A

FIGURE 6: AUG contexts of p43(M^1) and p43(M^{-9}). The nucleotides surrounding the AUG codons specifying the cytoplasmic [p43(M^1)] or mitochondrial [p43(M^{-9})] species of p43 are aligned with the sequence of a canonical AUG codon in a favorable sequence context for translation initiation. The A of the AUG codons is numbered +1. Nucleotides at positions −3 and +4 are boxed.

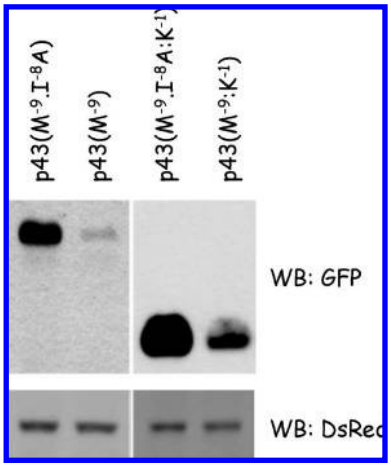

FIGURE 7: AUG codon specifying mitochondrial p43 in an unfavorable sequence context. The levels of expression of p43−GFP fusion proteins with an A [p43(M^{-9}) and p43(M^{-9}:K^{-1})] or a G [p43(M^{-9}.I^{-8}A) and p43(M^{-9}.I^{-8}A:K^{-1}] at position +4 were determined by Western blotting with anti-GFP antibody after cotransformation of HeLa cells with pEGFP-N1 plasmids expressing the p43-GFP fusion proteins and with pDsRed2-Mito. Expression of DsRed-Mito was monitored by Western blotting with an anti-DsRed antibody.

significantly deviates from the consensus for a favorable context (Figure 6). By contrast, the AUG codon for p43(M^1) displays a consensus context for a strong initiation site (A at position −3 and G at position +4). Thus, a mechanism of leaky scanning would allow the initiation complex to frequently bypass the AUG at position −27, to favor translation initiation at the level of the second AUG.

All the constructs used in this study were expressed from a plasmid carrying an ATA sequence upstream of the AUG initiation codon, thus with an A at position −3. To test the importance of the context of the AUG codon on the level of expression of the constructs, a derivative of the p43(M^{-9})−GFP fusion protein was expressed in HeLa cells after replacement of the AUU codon encoding Ile^{-8} by a GCG codon encoding Ala^{-8}. Thus, the AUG initiation codon of the p43(M^{-9}.I^{-8}A)−GFP fusion protein is placed into a favorable context, with a G at position +4 and an A at position −3. The level of expression of the p43(M^{-9}.I^{-8}A)−GFP fusion protein was found to be ~5-fold higher as compared to that of the p43-(M^{-9})−GFP fusion protein (Figure 7). The two fusion proteins were targeted to the mitochondria (not shown).

To further assess the role of the nucleotide at position +4 on the expression level of the protein, the level of expression of the cytoplasmic p43(M^{-9}:K^{-1})−GFP fusion protein (Figure 3B), containing p43 sequences from Met^{-9} to Lys^{-1}, was compared to that of the p43(M^{-9}.I^{-8}A:K^{-1})−GFP fusion protein, containing the AUU to GCG mutation at the second codon. The GFP fusion protein with the AUG codon in a favorable context, p43(M^{-9}.I^{-8}A:K^{-1})−GFP, was expressed much more efficiently than the p43(M^{-9}:K^{-1})−GFP fusion protein (Figure 7). Thus, a mitochondrial [p43(M^{-9})−GFP] or cytoplasmic [p43(M^{-9}:K^{-1})−GFP] fusion protein with an AUG initiation codon in a nonfavorable context, mimicking that of the endogenous p43-(M^{-9}) protein, is poorly expressed.

DISCUSSION

The low steady-state level of mitochondrial proteins involved in translation and in particular of the mitochondrial species of p43 precluded its identification when a crude extract of human cells was analyzed by molecular sieve chromatography (*23*), leading to the assumption that a single p43 species is present in the cell, as a component of the MARS complex. This protein has the capacity to bind tRNA via its C-terminal moiety (*5*) and to participate in the assembly of the MARS complex via its N-terminal moiety (*2*). The mitochondrial species of p43 identified in this study is identical to the p43 component of MARS but is expressed as a precursor possessing a short, nine-amino acid additional sequence at its N-terminus. Thus, the mitochondrial species of p43, mp43, should be able to bind tRNA as efficiently as its cytoplasmic counterpart, cp43. In addition, because mp43 and cp43 share the same N-terminal protein−protein interaction domain involved in the association of cp43 with GlnRS, ArgRS, and p38 (*2*), mp43 should also have the intrinsic capacity to bind to these components of MARS. However, all the components of MARS are confined to the cytoplasm (*35*). The only known exception is LysRS for which a cytoplasmic species and a mitochondrial species are encoded by the same gene by means of alternative splicing (*31*, *36*). Thus, mp43 certainly fulfills in the mitochondria a role distinct from its function in the cytoplasm.

Because the AUG codon specifying mp43 is interrupted by an intron, a possible mechanism to account for expression of mp43 and cp43 from the same gene was to consider that two distinct mRNA species were produced by a mechanism of alternative splicing of the single gene identified in the human genome. However, our data clearly show that mp43 and cp43 are two translation products of the same mRNA. Several examples of a single gene producing two translation products have been described for aminoacyl-tRNA synthetases, in yeast, plants, or humans, but different mechanisms could be involved. In the yeast *S. cerevisiae*, the cytoplasmic and mitochondrial HisRS and ValRS are encoded by two distinct mRNAs of different lengths transcribed from a single gene (*37*, *38*). The longer messages, translated from an upstream AUG codon, encode the mitochondrial enzymes. In yeast, a single gene also encodes the cytoplasmic and mitochondrial forms of AlaRS and GlyRS, which are produced from a single mRNA (*39*, *40*). The longer mitochondrial isoforms are translated from upstream non-AUG initiation codons. In the plant *Arabidopsis thaliana*, five aminoacyl-tRNA synthetases are shared between cytosol and mitochondria and 15 are shared between the two organelles, mitochondria and chloroplasts (*41*). In humans, the cytoplasmic and mitochondrial GlyRS and LysRS are encoded by a single gene. Whereas the two LysRS species are produced from two mRNAs arising by alternative splicing of the unique KARS gene (*31*, *36*), the two GlyRSs are believed to be translated from a single mRNA from two in-frame initiation codons (*42*). Similarly, two forms of human ArgRS are also translated from two in-frame initiation codons (*43*, *44*). The longest species corresponds to the cytoplasmic enzyme associated within MARS, but the function of the shortest

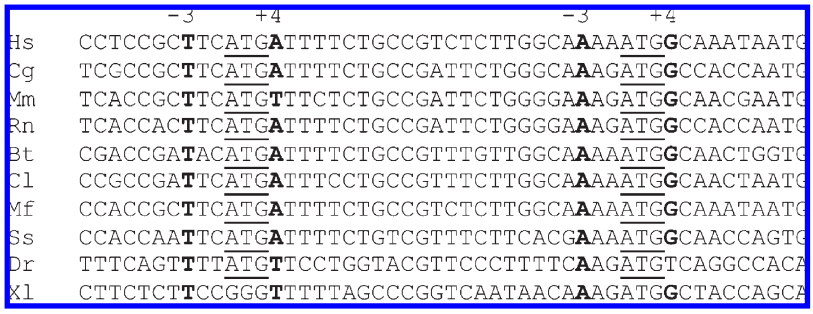

FIGURE 8: Sequence context of the AUG codon specifying the mitochondrial and cytoplasmic p43 from different species. The nucleotide sequences surrounding the AUG initiation codons for p43 starting at Met^{-9} or at Met^{1} are indicated for human (Hs), hamster (Cg), mouse (Mm), rat (Rn), cattle (Bt), dog (Cl), macaque (Mf), pig (Ss), zebrafish (Dr), and frog (Xl). Nucleotides at positions −3 and +4 of the two AUG are indicated in bold.

form remains hypothetical. The mitochondrial species of ArgRS is encoded by a separate gene (*45*).

The finding that the precursor of mp43 is produced from the upstream AUG codon found in an unfavorable sequence context, by a mechanism of leaky scanning of the mRNA, is in agreement with the lower expression level of the mitochondrial species of p43, which represents only 1−2% as compared to the cytoplasmic species. When comparing the sequence contexts of the AUG encoding the mitochondrial and cytoplasmic species of p43 from the different species listed in Figure 1, which display a mRNA with two putative translation initiation codons, similar to that of human p43 analyzed in this study, we find it appears that the first AUG codon is always located in an unfavorable sequence context (T at position −3 and, in most cases, A at position +4) as compared to the second AUG codon (A at position −3 and, in most cases, G at position +4) (Figure 8). The first AUG codon is always preceded by three pyrimidine nucleotides and the second by three purine nucleotides, positions that are the most relevant to determining the efficiency of an AUG codon. Thus, the expression pattern of p43 is certainly similar in many metazoan species. The putative role of the two mRNA species of different lengths on the expression of the two p43 translation products remains to be established.

The existence of a p43 protein within the mitochondria raises the question of its functional role in this organelle. Previous experiments have shown that the knock-down of p43 with a siRNA targeted to the sequences common to the cytoplasmic and mitochondrial p43 species is not lethal for human cells in culture (*2*). Thus, neither cp43 nor mp43 is essential in the context of cultured cells.

Several putative roles may be envisioned. In this regard, it should be recalled that truncated derivatives of p43, p43(ARF) and p43(EMAPII), have been identified in apoptotic cells. It was shown that overexpression or p43(ARF) or p43(EMAPII) in the cytoplasm of human cells did not stimulate apoptosis (*5*). It has been proposed that cleavage of the p43 component of MARS may have some negative effect on the efficiency of the translation process and, thus, may be one of the mechanisms leading to arrest of translation after the onset of apoptosis. However, because mitochondria are essential to many aspects of the apoptotic process, we examined the possibility that mp43 or one of its truncated derivatives identified in apoptotic cells may have a direct effect on apoptosis when targeted to the mitochondria. Overexpression of mp43 did not induce apoptosis on HeLa or U937 cells (unpublished results). Similarly, when p43(ARF) or p43(EMAPII) was overexpressed and targeted to the mitochondria after fusion to N-terminal sequence M^{-9}:M^{1}I:D^{5} or M^{-9}:M^{1}I:R^{10} of mp43, the two proteins were localized to the mitochondria but did not induce apoptosis (unpublished results). Thus, a putative link between mp43 and apoptosis remains to be established.

Whether mp43 itself is important for the biology of mitochondria or whether it mediates the mitochondrial import of other components essential for this organelle remains to be deciphered. The C-terminal domain of p43 is a classical OB fold (*7*), similar to that determined for the bacterial Trbp111 protein. This ancient tRNA-binding protein has been described as a tRNA-specific chaperone which may stabilize the L-shaped fold of the tRNA molecule (*46*). One possibility is that mp43 acts in the folding of some mitochondrial tRNAs which lack canonical elements important in assisting in the proper folding of the tRNA molecules (*47*). Alternatively, the tRNA binding capacity of mp43 could be used to target tRNA molecules to the mitochondria. Import of tRNA into mitochondria is a complex process that differs from one species to another (*48*). No unifying mechanism has emerged from the many studies performed in different organisms, but it is clear that cytosolic factors could be involved in this process. For instance, in yeast, both cytoplasmic and mitochondrial LysRS are involved in import of a cytoplasmic $tRNA^{Lys}$ in mitochondria (*49*).

Finally, mp43 might be used to trigger mitochondrial localization of cytoplasmic proteins. The N-terminal domain of mp43, from Met^{1} to Ser^{106}, is identical to the N-terminal domain of cp43 that is involved in the assembly of MARS via its interaction with GlnRS, ArgRS, and p38 (*2*). Recent studies showed the presence of nucleus-encoded $tRNA^{Gln}$ and of cytoplasmic GlnRS in the mitochondria of *S. cerevisiae* (*50*). Because no mitochondrial GlnRS could be identified in the yeast genome, it was suggested that Gln-$tRNA^{Gln}$ synthesis in mitochondria uses the components imported from the cytoplasm. If such a mechanism also prevails in humans, association of human, cytoplasmic GlnRS with mp43 may be a means of importing the glutaminylation pathway into human mitochondria. Alternatively, recent results also demonstrated that the transamidation pathway may be the pathway by which *S. cerevisiae* mitochondria synthesize its Gln-$tRNA^{Gln}$, using mitochondrial $tRNA^{Gln}$ first aminoacylated with Glu by a GluRS imported from the cytoplasm (*19*). Whether mp43 could be involved in the pathway of Gln-$tRNA^{Gln}$ formation in human mitochondria is an intriguing possibility.

The finding that a p43 species is targeted to human mitochondria opens new perspectives for the understanding of several physiological processes. It is also an interesting example of a protein that is targeted to a multienzyme complex in the cytoplasm and could fulfill additional functions when targeted

to the mitochondria. Future experiments should address this important issue.

ACKNOWLEDGMENT

We thank Spencer Brown, Susanne Bolte, and Marie-Noëlle Soler for access to the confocal microscope facility (ISV, Gif-sur-Yvette, France).

REFERENCES

1. Mirande, M. (2005) Multi-Aminoacyl-tRNA Synthetase Complexes. In The Aminoacyl-tRNA Synthetases (Ibba, M., Francklyn, C., and Cusack, S., Eds.) pp 298−308, Landes Bioscience, Georgetown, TX.
2. Kaminska, M., Havrylenko, S., Decottignies, P., Gillet, S., Le Marechal, P., Negrutskii, B., and Mirande, M. (2009) Dissection of the Structural Organization of the Aminoacyl-tRNA Synthetase Complex. *J. Biol. Chem. 284*, 6053–6060.
3. Robinson, J. C., Kerjan, P., and Mirande, M. (2000) Macromolecular assemblage of aminoacyl-tRNA synthetases: Quantitative analysis of protein-protein interactions and mechanism of complex assembly. *J. Mol. Biol. 304*, 983–994.
4. Ahn, H. C., Kim, S., and Lee, B. J. (2003) Solution structure and p43 binding of the p38 leucine zipper motif: Coiled-coil interactions mediate the association between p38 and p43. *FEBS Lett. 542*, 119–124.
5. Shalak, V., Guigou, L., Kaminska, M., Wautier, M. P., Wautier, J. L., and Mirande, M. (2007) Characterization of p43(ARF), a Derivative of the p43 Component of Multiaminoacyl-tRNA Synthetase Complex Released during Apoptosis. *J. Biol. Chem. 282*, 10935–10943.
6. Shalak, V., Kaminska, M., Mitnacht-Kraus, R., Vandenabeele, P., Clauss, M., and Mirande, M. (2001) The EMAPII cytokine is released from the mammalian multisynthetase complex after cleavage of its p43/proEMAPII component. *J. Biol. Chem. 276*, 23769–23776.
7. Renault, L., Kerjan, P., Pasqualato, S., Menetrey, J., Robinson, J. C., Kawaguchi, S., Vassylyev, D. G., Yokoyama, S., Mirande, M., and Cherfils, J. (2001) Structure of the EMAPII domain of human aminoacyl-tRNA synthetase complex reveals evolutionary dimer mimicry. *EMBO J. 20*, 570–578.
8. Norcum, M. T., and Warrington, J. A. (2000) The cytokine portion of p43 occupies a central position within the eukaryotic multisynthetase complex. *J. Biol. Chem. 275*, 17921–17924.
9. Park, S. G., Jung, K. H., Lee, J. S., Jo, Y. J., Motegi, H., Kim, S., and Shiba, K. (1999) Precursor of pro-apoptotic cytokine modulates aminoacylation activity of tRNA synthetase. *J. Biol. Chem. 274*, 16673–16676.
10. Guigou, L., Shalak, V., and Mirande, M. (2004) The tRNA-interacting factor p43 associates with mammalian arginyl-tRNA synthetase but does not modify its tRNA aminoacylation properties. *Biochemistry 43*, 4592–4600.
11. Popenko, V. I., Ivanova, J. L., Cherny, N. E., Filonenko, V. V., Beresten, S. F., Wolfson, A. D., and Kisselev, L. L. (1994) Compartmentalization of certain components of the protein synthesis apparatus in mammalian cells. *Eur. J. Cell Biol. 65*, 60–69.
12. Nomanbhoy, T., Morales, A. J., Abraham, A. T., Vortler, C. S., Giegé, R., and Schimmel, P. (2001) Simultaneous binding of two proteins to opposite sides of a single transfer RNA. *Nat. Struct. Biol. 8*, 344–348.
13. Kaminska, M., Deniziak, M., Kerjan, P., Barciszewski, J., and Mirande, M. (2000) A recurrent general RNA binding domain appended to plant methionyl-tRNA synthetase acts as a *cis*-acting cofactor for aminoacylation. *EMBO J. 19*, 6908–6917.
14. Kleeman, T. A., Wei, D. B., Simpson, K. L., and First, E. A. (1997) Human tyrosyl tRNA synthetase shares amino acid sequence homology with a putative cytokine. *J. Biol. Chem. 272*, 14420–14425.
15. Roy, H., and Ibba, M. (2006) Phenylalanyl-tRNA synthetase contains a dispensable RNA-binding domain that contributes to the editing of noncognate aminoacyl-tRNA. *Biochemistry 45*, 9156–9162.
16. Simader, H., Hothorn, M., Kohler, C., Basquin, J., Simos, G., and Suck, D. (2006) Structural basis of yeast aminoacyl-tRNA synthetase complex formation revealed by crystal structures of two binary subcomplexes. *Nucleic Acids Res. 34*, 3968–3979.
17. Graindorge, J. S., Senger, B., Tritch, D., Simos, G., and Fasiolo, F. (2005) Role of Arc1p in the modulation of yeast glutamyl-tRNA synthetase activity. *Biochemistry 44*, 1344–1352.
18. Simos, G., Segref, A., Fasiolo, F., Hellmuth, K., Shevchenko, A., Mann, M., and Hurt, E. C. (1996) The yeast protein Arc1p binds to tRNA and functions as a cofactor for the methionyl- and glutamyl-tRNA synthetases. *EMBO J. 15*, 5437–5448.
19. Frechin, M., Senger, B., Braye, M., Kern, D., Martin, R., and Becker, H. (2009) Yeast mitochondrial Gln-tRNA(Gln) is generated by a GatFAB-mediated transamidation pathway involving Arc1p-controlled subcellular sorting of cytosolic GluRS. *Genes Dev. 23*, 1119–1130.
20. Golinelli-Cohen, M. P., and Mirande, M. (2007) Arc1p is required for cytoplasmic confinement of synthetases and tRNA. *Mol. Cell. Biochem. 300*, 47–59.
21. Kao, J., Houck, K., Fan, Y., Haehnel, I., Libutti, S. K., Kayton, M. L., Grikscheit, T., Chabot, J., Nowygrod, R., Greenberg, S., Kuang, W.-J., Leung, D. W., Hayward, J. R., Kisiel, W., Heath, M., Brett, J., and Stern, D. M. (1994) Characterization of a novel tumor-derived cytokine. Endothelial monocyte activating polypeptide II. *J. Biol. Chem. 269*, 25106–25119.
22. Kao, J., Ryan, J., Brett, G., Chen, J., Shen, H., Fan, Y. G., Godman, G., Familletti, P. C., Wang, F., Pan, Y. C., Stern, D., and Clauss, M. (1992) Endothelial monocyte-activating polypeptide II. A novel tumor-derived polypeptide that activates host-response mechanisms. *J. Biol. Chem. 267*, 20239–20247.
23. Quevillon, S., Agou, F., Robinson, J. C., and Mirande, M. (1997) The p43 component of the mammalian multi-synthetase complex is likely to be the precursor of the endothelial monocyte-activating polypeptide II cytokine. *J. Biol. Chem. 272*, 32573–32579.
24. Wakasugi, K., and Schimmel, P. (1999) Two distinct cytokines released from a human aminoacyl-tRNA synthetase. *Science 284*, 147–151.
25. Ko, Y. G., Park, H., Kim, T., Lee, J. W., Park, S. G., Seol, W., Kim, J. E., Lee, W. H., Kim, S. H., Park, J. E., and Kim, S. (2001) A cofactor of tRNA synthetase, p43, is secreted to up-regulate proinflammatory genes. *J. Biol. Chem. 276*, 23028–23033.
26. Park, S. G., Kang, Y. S., Ahn, Y. H., Lee, S. H., Kim, K. R., Kim, K. W., Koh, G. Y., Ko, Y. G., and Kim, S. (2002) Dose-dependent biphasic activity of tRNA synthetase-associating factor, p43, in angiogenesis. *J. Biol. Chem. 277*, 45243–45248.
27. Schwarz, M. A., Kandel, J., Brett, J., Li, J., Hayward, J., Schwarz, R. E., Chappey, O., Wautier, J. L., Chabot, J., Lo Gerfo, P., and Stern, D. (1999) Endothelial-monocyte activating polypeptide II, a novel antitumor cytokine that suppresses primary and metastatic tumor growth and induces apoptosis in growing endothelial cells. *J. Exp. Med. 190*, 341–354.
28. van Horssen, R., Eggermont, A. M., and ten Hagen, T. L. (2006) Endothelial monocyte-activating polypeptide-II and its functions in (patho)physiological processes. *Cytokine Growth Factor Rev. 17*, 339–348.
29. Journeay, S., and Singh, B. (2007) EMAP-II antibody detects both proEMAP/p43 and mature EMAP-II molecules. *Acta Neuropathol. 114*, 435.
30. Mirande, M., Cirakoglu, B., and Waller, J. P. (1982) Macromolecular complexes from sheep and rabbit containing seven aminoacyl-tRNA synthetases. III. Assignment of aminoacyl-tRNA synthetase activities to the polypeptide components of the complexes. *J. Biol. Chem. 257*, 11056–11063.
31. Kaminska, M., Shalak, V., Francin, M., and Mirande, M. (2007) Viral hijacking of mitochondrial lysyl-tRNA synthetase. *J. Virol. 81*, 68–73.
32. Neupert, W., and Herrmann, J. M. (2007) Translocation of proteins into mitochondria. *Annu. Rev. Biochem. 76*, 723–749.
33. Kozak, M. (1991) An analysis of vertebrate mRNA sequences: Intimations of translational control. *J. Cell Biol. 115*, 887–903.
34. Kozak, M. (2005) Regulation of translation via mRNA structure in prokaryotes and eukaryotes. *Gene 361*, 13–37.
35. Kaminska, M., Havrylenko, S., Decottignies, P., Le Marechal, P., Negrutskii, B., and Mirande, M. (2009) Dynamic organization of aminoacyl-tRNA synthetase complexes in the cytoplasm of human cells. *J. Biol. Chem. 284*, 13746–13754.
36. Tolkunova, E., Park, H., Xia, J., King, M. P., and Davidson, E. (2000) The human lysyl-tRNA synthetase gene encodes both the cytoplasmic and mitochondrial enzymes by means of an unusual alternative splicing of the primary transcript. *J. Biol. Chem. 275*, 35063–35069.
37. Chatton, B., Walter, P., Ebel, J. P., Lacroute, F., and Fasiolo, F. (1988) The yeast *VAS1* gene encodes both mitochondrial and cytoplasmic valyl-tRNA synthetases. *J. Biol. Chem. 263*, 52–57.
38. Natsoulis, G., Hilger, F., and Fink, G. R. (1986) The HTS1 gene encodes both the cytoplasmic and mitochondrial histidine tRNA synthetases of *S. cerevisiae*. *Cell 46*, 235–243.
39. Chang, K. J., and Wang, C. C. (2004) Translation initiation from a naturally occurring non-AUG codon in *Saccharomyces cerevisiae*. *J. Biol. Chem. 279*, 13778–13785.
40. Tang, H. L., Yeh, L. S., Chen, N. K., Ripmaster, T., Schimmel, P., and Wang, C. C. (2004) Translation of a yeast mitochondrial tRNA synthetase initiated at redundant non-AUG codons. *J. Biol. Chem. 279*, 49656–49663.

41. Duchene, A. M., Giritch, A., Hoffmann, B., Cognat, V., Lancelin, D., Peeters, N. M., Zaepfel, M., Marechal Drouard, L., and Small, I. D. (2005) Dual targeting is the rule for organellar aminoacyl-tRNA synthetases in *Arabidopsis thaliana*. *Proc. Natl. Acad. Sci. U.S.A. 102*, 16484–16489.
42. Mudge, S. J., Williams, J. H., Eyre, H. J., Sutherland, G. R., Cowan, P. J., and Power, D. A. (1998) Complex organisation of the 5′-end of the human glycine tRNA synthetase gene. *Gene 209*, 45–50.
43. Lazard, M., and Mirande, M. (1993) Cloning and analysis of a cDNA encoding mammalian arginyl-tRNA synthetase, a component of the multisynthetase complex with a hydrophobic N-terminal extension. *Gene 132*, 237–245.
44. Zheng, Y. G., Wei, H., Ling, C., Xu, M. G., and Wang, E. D. (2006) Two forms of human cytoplasmic arginyl-tRNA synthetase produced from two translation initiations by a single mRNA. *Biochemistry 45*, 1338–1344.
45. Edvardson, S., Shaag, A., Kolesnikova, O., Gomori, J. M., Tarassov, I., Einbinder, T., Saada, A., and Elpeleg, O. (2007) Deleterious mutation in the mitochondrial arginyl-transfer RNA synthetase gene is associated with pontocerebellar hypoplasia. *Am. J. Hum. Genet. 81*, 857–862.
46. Morales, A. J., Swairjo, M. A., and Schimmel, P. (1999) Structure-specific tRNA-binding protein from the extreme thermophile *Aquifex aeolicus*. *EMBO J. 18*, 3475–3483.
47. Helm, M., Brule, H., Friede, D., Giegé, R., Putz, D., and Florentz, C. (2000) Search for characteristic structural features of mammalian mitochondrial tRNAs. *RNA 6*, 1356–1379.
48. Mirande, M. (2007) The ins and outs of tRNA transport. *EMBO Rep. 8*, 547–549.
49. Tarassov, I., Entelis, N., and Martin, R. P. (1995) Mitochondrial import of a cytoplasmic lysine-tRNA in yeast is mediated by cooperation of cytoplasmic and mitochondrial lysyl-tRNA synthetases. *EMBO J. 14*, 3461–3471.
50. Rinehart, J., Krett, B., Rubio, M. A. T., Alfonzo, J. D., and Söll, D. (2005) *Saccharomyces cerevisiae* imports the cytosolic pathway for Gln-tRNA synthesis into the mitochondrion. *Genes Dev. 19*, 583–592.

ВИСНОВКИ

У дисертаційній роботі встановлено просторову організацію факторів елонгації трансляції, які утворюють мультибілковий комплекс eEF1H, зокрема eEF1A2 (кристалічна структура), eEF1Bα, eEF1Bβ і eEF1Bγ та їх три-гетеротримерний комплекс eEF1B$(\alpha\beta\gamma)_3$ (у розчині). Також визначені важливі функціональні особливості цих факторів і білка p43 комплексу аміноацил-тРНК синтетаз, як пов'язані, так і не пов'язані із білковим синтезом. Отримані дані є значним фундаментальним внеском у розуміння структурної організації і функціонування дорибосомного етапу елонгації трансляції у ссавців.

1. За допомогою метода малокутового розсіювання нейтронів встановлено, що фактор елонгації eEF1A1 в ГДФ-зв'язаній формі має видовжену конформацію в розчині. Його радіус гірації становить 5.2±0.2 нм, що в два рази більше, ніж радіус гірації бактеріального і дріжджового аналогів.

2. Отримано кристалографічну структуру фактора елонгації трансляції eEF1A2 в комплексі з ГДФ. Показано, що цей білок має тридоменну будову і, на відміну від eEF1A1, близьку до сферичної просторову конформацію з розрахованим радіусом гірації 2.44 нм. Встановлено, що іони Mg^{2+} не впливають на реакцію обміну гуанінового нуклеотиду на молекулі eEF1A2, що контрастує з бактеріальним фактором елонгації трансляції.

3. Показано, що eEF1A1 у ГДФ-зв'язаній формі може утворювати неканонічний потрійний комплекс з деацильованою тРНК і четвертинний комплекс з тРНК і фенілаланіл-тРНК синтетазою, а також збільшує початкову швидкість реакції, яку каталізує метіоніл-тРНК синтетаза.

4. Встановлено, що трансляційно-контрольований білок пухлин (TCTP) взаємодіє з факторами eEF1A1 і eEF1Bβ. Зв'язування TCTP з цими білками призводить до зниження швидкості реакції як спонтанного, так і eEF1Bβ-опосередкованого обміну гуанінового нуклеотиду на молекулі eEF1A1.

5. Встановлено структурну організацію трансляційних факторів eEF1Bα, eEF1Bβ і eEF1Bγ. Показано, що всі білки мають в своєму складі як

компактно згорнуті структурні домени, так і довгі неструктуровані ділянки. eEF1Bα є мономерним білком, eEF1Bβ утворює гомотример сильно видовженої форми, тоді як eEF1Bγ, в залежності від концентрації, може утворювати димери і мультмери більш високого порядку. Розкрито механізм стимуляції активності eEF1Bα субодиницею eEF1Bγ: взаємодія N-кінцевих доменів eEF1Bα і eEF1Bγ усуває аутоінгібіторний ефект N-кінцевого домену eEF1Bα, який частково перешкоджає взаємодії eEF1A з GEF-доменом.

6. Визначено сайти взаємодії між субодиницями eEF1Bα і eEF1Bγ, eEF1Bβ і eEF1Bγ, які знаходяться на N-кінцевих ділянках цих білків. Встановлено, що структурний мотив «лейцинова застібка» відповідає за тримеризацію eEF1Bβ, а також всього комплексу eEF1B, який, відповідно, має структурну організацію типу $(\alpha\beta\gamma)_3$. Показано, що eEF1B$(\alpha\beta\gamma)_3$ здатен зв'язувати до шести молекул eEF1A2, відповідно до кількості GEF-доменів в ньому.

7. Встановлено, що N-кінцевий домен білка p43 макромолекулярного комплексу аміноацил-тРНК синтетаз взаємодіє з аргініл-тРНК синтетазою. Показано, що p43 не впливає на каталітичні параметри аргініл-тРНК синтетази і не збільшує її спорідненість до відповідної тРНК. Отже, білок p43 не є кофактором для цього ферменту.

8. Доведено, що інкубація макромолекулярного комплексу аміноацил-тРНК синтетаз з каспазою 7 *in vitro* призводить до розщеплення його p43 компоненту на два фрагменти. Його С-кінцевий фрагмент, який вивільняється з комплексу, є ідентичним EMAPII і здатен викликати хемотаксис моноцитів. Розщеплення p43 призводить до втрати його тРНК-зв'язувальної властивості.

9. Вперше виявлено, що індукція апоптозу в клітинах U937 призводить до появи і вивільнення з клітин іншого ніж EMAPII протеолітичного фрагменту білка p43. Цей фрагмент, названий p43(ARF), має найвищу афінність до тРНК в порівнянні з повнорозмірним p43 і EMAPII. Встановлено, що повнорозмірний p43 викликає активацію ендотеліальних клітин, тоді як

p43(ARF) і EMAPII не мають такого ефекту. Це свідчить на користь ролі білка p43 в якості прозапального цитокіну.

10. Вперше ідентифіковано новий трансляційний продукт гена, який кодує білок p43. Цей продукт має мітохондріальну локалізацію завдяки 9 додатковим N-кінцевим амінокислотним залишкам, і його вміст становить приблизно 2% від загальної кількості p43 в клітині.

ДОДАТОК 1.

СПИСОК ПУБЛІКАЦІЙ ЗА ТЕМОЮ ДИСЕРТАЦІЇ

1. Budkevich TV, Timchenko AA, Tiktopulo EI, Negrutskii BS, **Shalak VF**, Petrushenko ZM, Aksenov VL, Willumeit R, Kohlbrecher J, Serdyuk IN, El'skaya AV. (2002). Extended conformation of mammalian translation elongation factor 1A in solution. *Biochemistry*. 41(51):15342-9. doi:10.1021/bi026495h. (*Дисертантом особисто проведено очищення препаративних кількостей фактора елонгації трансляції eEF1A1 і визначено його функціональну активність in vitro різними тестами*).
2. Crepin T, **Shalak VF**, Yaremchuk AD, Vlasenko DO, McCarthy A, Negrutskii BS, Tukalo MA, El'skaya AV. (2014). Mammalian translation elongation factor eEF1A2: X-ray structure and new features of GDP/GTP exchange mechanism in higher eukaryotes. *Nucleic Acids Res*. 42(20):12939-48. doi:10.1093/nar/gku974. (*Дисертантом особисто проведено частину експериментальних досліджень, зокрема підготовку білка для кристалізації, експерименти по обміну гуанінового нуклеотиду, аналіз та інтерпретування отриманих результатів та їх підготовку до публікації*).
3. Petrushenko ZM, Budkevich TV, **Shalak VF**, Negrutskii BS, El'skaya AV. (2002). Novel complexes of mammalian translation elongation factor eEF1A*GDP with uncharged tRNA and aminoacyl-tRNA synthetase. Implications for tRNA channeling. *Eur J Biochem*. 269(19):4811-8. doi:10.1046/j.1432-1033.2002.03178.x. (*Дисертантом особисто проведено очищення препаративних кількостей фактора елонгації трансляції eEF1A1 і фенілаланіл-тРНК синтетази і визначено їх функціональну активність in vitro*).
4. Kaminska M, **Shalak V**, Mirande M. (2001). The appended C-domain of human methionyl-tRNA synthetase has a tRNA-sequestering function. *Biochemistry.* 40(47):14309-16. doi:10.1021/bi015670b. (*Дисертантом особисто отримано високо очищений препарат фактора елонгації трансляції eEF1A1 проведено серію експериментів по взаємодії цього білка з метіоніл-тРНК синтетазою*).

5. Cans C, Passer BJ, **Shalak V**, Nancy-Portebois V, Crible V, Amzallag N, Allanic D, Tufino R, Argentini M, Moras D, Fiucci G, Goud B, Mirande M, Amson R, Telerman A. (2003). Translationally controlled tumor protein acts as a guanine nucleotide dissociation inhibitor on the translation elongation factor eEF1A. *Proc Natl Acad Sci U S A.* 100(24):13892-7. doi:10.1073/pnas.2335950100. (*Дисертантом особисто проведено частину експериментальних досліджень, зокрема експерименти по обміну гуанінового нуклеотиду, білок-білкові взаємодії (pull-down) аналіз та імуноблотинг, інтерпретування отриманих результатів та їх підготовку до публікації*).
6. Trosiuk TV, **Shalak VF**, Szczepanowski RH, Negrutskii BS, El'skaya AV. (2016). A non-catalytic N-terminal domain negatively influences the nucleotide exchange activity of translation elongation factor 1Bα. *FEBS J.* 283(3):484-97. doi:10.1111/febs.13599. (*Дисертант керував виконанням загального обсягу експериментальних досліджень, а також особисто виконав частину експериментальної роботи, аналіз та інтерпретування отриманих результатів, оформлення статті*).
7. Bondarchuk TV, Lozhko DM, **Shalak VF**, Fatalska A, Szczepanowski RH, Dadlez M, Negrutskii BS, El'skaya AV. (2019). The protein-binding N-terminal domain of human translation elongation factor 1Bβ possesses a dynamic α-helical structural organization. *Int J Biol Macromol*. 126:899-907. doi:10.1016/j.ijbiomac.2018.12.220 (*Дисертант керував виконанням загального обсягу експериментальних досліджень, а також особисто виконав частину експериментальної роботи, аналіз та інтерпретування отриманих результатів, оформлення статті*).
8. Bondarchuk TV, **Shalak VF**, Lozhko DM, Fatalska A, Szczepanowski RH, Liudkovska V, Tsuvariev OY, Dadlez M, El'skaya AV, Negrutskii BS. (2022). Quaternary organization of the human eEF1B complex reveals unique multi-GEF domain assembly. *Nucleic Acids Res.* 50(16):9490-9504. doi: 10.1093/nar/gkac685. (*Дисертант керував виконанням загального обсягу експериментальних досліджень, а також особисто виконав частину експериментальної роботи, аналіз та інтерпретування отриманих результатів, оформлення статті*).

9. Guigou L, **Shalak V**, Mirande M. (2004). The tRNA-interacting factor p43 associates with mammalian arginyl-tRNA synthetase but does not modify its tRNA aminoacylation properties. *Biochemistry*. 43(15):4592-600. doi10.1021/bi036150e. (*Дисертантом особисто проведено частину експериментальних досліджень*, з*окрема, очищення ферментів і вимірювання їх каталітичних характеристик, аналіз та інтерпретування отриманих результатів*).
10. **Shalak V**, Kaminska M, Mitnacht-Kraus R, Vandenabeele P, Clauss M, Mirande M. (2001). The EMAPII cytokine is released from the mammalian multisynthetase complex after cleavage of its p43/proEMAPII component. *J Biol Chem*. 276(26):23769-76. doi:10.1074/jbc. (*Дисертантом особисто проведено основні експериментальні дослідження з мультисинтетазним комплексом мишей, рекомбінантним білком p43 мишей і людини*, *аналіз результатів та їх підготовку до публікації*).
11. **Shalak V**, Guigou L, Kaminska M, Wautier MP, Wautier JL, Mirande M. (2007). Characterization of p43(ARF), a derivative of the p43 component of multiaminoacyl-tRNA synthetase complex released during apoptosis. *J Biol Chem.* 282(15):10935-43. doi:10.1074/jbc.M611737200 (*Дисертантом особисто проведено основну частину експериментальних досліджень*, *зокрема всю роботу з культурами клітин, імуноблотинг, взаємодію білків з тРНК, активацію ендотеліальних клітин, аналіз та інтерпретування отриманих результатів та їх підготовку до публікації*).
12. **Shalak V**, Kaminska M, Mirande M. (2009). Translation initiation from two in-frame AUGs generates mitochondrial and cytoplasmic forms of the p43 component of the multisynthetase complex. *Biochemistry.* 48(42):9959-68. doi:10.1021/bi901236g (*Дисертантом особисто проведено більшу частину експериментальних досліджень*, *зокрема створення ДНК конструкцій, трансфекцію клітин і конфокальну мікроскопію, субклітинне фракціонування, аналіз та інтерпретування отриманих результатів та їх підготовку до публікації*).

Апробація матеріалів дисертації:

1. **V. Shalak,** J.C. Robinson, P. Vandenabeele and M. Mirande. The p43 component of the multisynthetase complex is a precursor of the EMAP II cytokine. 18th International tRNA Workshop - "tRNA 2000". 2000. April 8-12. Queen's College, Cambrige, UK. *Публікація тез, постерна доповідь.*
2. M. Kaminska, **V. Shalak,** J.C. Robinson, P. Kerjan and M. Mirande. From protein synthesis to apoptosis. The p43 component of the multisynthetase complex: a molecular switch. 18th International tRNA Workshop - "tRNA 2000". 2000. April 8-12, Queen's College, Cambrige, UK. *Публікація тез, усна доповідь.*
3. M. Kaminska, **V. Shalak** and M. Mirande. Human methiony-tRNA synthetase is a processive enzyme. Asilomar Conference on Aminoacyl-tRNA synthetases in Biology, Medicine & Evolution. 2002. January 13-18. Pacific grove, CA, USA. *Публікація тез, постерна доповідь.*
4. M. Kaminska, M. Francin, **V. Shalak** and M. Mirande. Role of the general RNA-binding domains appended to mammalian aminoacyl-tRNA synthetases. 19th International tRNA Workshop. 2002. April 6-1. Shanghai, China. *Публікація тез, усна доповідь.*
5. **Vyacheslav Shalak**, Ludovic Guigou and Marc Mirande. The p43 subunit of the multi-aminoacyl-tRNA synthetase complex: structure and function. 20th International tRNA Workshop. 2003. October 2-7. Banz, Germany. *Публікація тез, постерна доповідь.*
6. **V. Shalak**, M.-P. Golinelli-Cohen, Ludovic Guigou and Marc Mirande. La machinerie traductionnele et l'apoptose: function duale d'un cofacteur des aminoacyl-tRNA synthetases. 5éme Rencontre sifrARN "ARN, le nouveau monde". 2004. Octobre 10 - 13. Arcachon, France. *Публікація тез, усна доповідь.*
7. **V. F. Shalak**, A.V. El'skaya, M. Mirande. The multi-aminoacyl-tRNA synthetase complex: link between protein synthesis and apoptosis. 5th Parnas Conference "Molecular mechanisms of Cellular Signaling". 2005. April 26-29. Kyiv. Ukraine. *Публікація тез, усна доповідь.*
8. M. Kaminska, **V. Shalak**, S. Havrylenko, L. Guigou, R. Freguja and M. Mirande. Human aminoacyl-tRNA synthetases: role of the eukaryotic-specific, protein-

protein and protein-RNA interaction domains. aaRS2008. International conference on aminoacyl-tRNA synthetase: from basic mechanisms to systems biology. September 7-11. 2008. Veyrier du Lac, France. *Публікація тез, постерна доповідь.*

9. V. V. Liudkovska, **V.F. Shalak**. Complex of translation elongation factors (eEF-1H): in vitro reconstitution from recombinant proteins. International life sciences' students' conference. August 19-23. 2009. Kyiv, Ukraine. *Публікація тез, усна доповідь.*
10. **V. Shalak**, V. Liudkovska, A. Timchenko, B. Negrutskii. Interaction between subunits of translation elongation factor 1B: two approaches to study their complexes in vitro. X Український біохімічний з'їзд. 13-17 вересня. 2010. м. Одеса, Україна. *Публікація тез, усна доповідь.*
11. Trosiuk T.V**., Shalak V. F.** Construction and expression of deletion mutants of translation elongation factors eEF1Bα, eEF1Bβ, eEF1Bγ. VII conference of Young Scientists of the Institute of Molecilar Biology and Genetics NAS of Ukraine. 28-29 May 2013. Kyiv, Ukraine. *Публікація тез, усна доповідь.*
12. Trosiuk T.V., **Shalak V. F.** The interaction of truncated forms of translation elongation factor eEF1Bγ with eEF1Bα and eEF1Bβ. VIII Conference of Young Scientists of Molecular Biology and Genetics NAS of Ukraine Dedicated to 90th anniversary of P.G. Kostyuk. 20-21 May 2014. Kyiv, Ukraine. *Публікація тез, усна доповідь.*
13. Trosiuk T.V., **Shalak V. F.** Dissection of translation elongation factor eEF1Bγ: creation of deletion mutants to study its interaction with protein partners in vitro. XI Український біохімічний конгрес. 6-10 жовтня 2014 р. м. Київ. *Публікація тез, усна доповідь*.
14. **V. Shalak**, R. Szczepanowski, L. Kapustian, J. Debski, L. Porubleva, T. Trosiuk, A. Nehelia, I. Shrubkovskij, M. Dadlez, M. Bochtler, B. Negrutskii. COMBIOM in research of translation elongation factors. Combiom Final Scientific Meeting. 16-17 April 2015. Kyiv, Ukraine. *Публікація тез, усна доповідь.*
15. Bondarchuk T.V., **Shalak V.F.** Leucine-zipper motif is responsible for the multimerization of translation elongation factor 1Bβ. International Conference for the

Young Scientists (CYS-2015), 21-25 September 2015, Kyiv, Ukraine. *Публікація тез, усна доповідь.*

16. Bondarchuk T. V., **Shalak V.F.** Structural and functional features of translation elongation factor 1B alpha. 41st FEBS congress "Molecular and systems biology for a better life", September 03-08, 2016, Ephesus/Kusadasi, Turkey. *Публікація тез, постерна доповідь.*
17. **В'ячеслав Шалак**, Тетяна Бондарчук. Неглобулярні білки з неструктурованими ділянками: точне визначення молекулярної маси, агрегатного стану і локалізації неструктурованих ділянок. XII Відкрита конференція молодих вчених ІМБГ НАН України. 15-16 травня 2018 року. м. Київ. *Публікація тез, ключова доповідь*.
18. T.V. Bondarchuk, **V.F. Shalak**, A. Fatalska, D.M. Lozhko, R.H. Shchepanovskyi, M. Dadlez, B.S. Negrutskii, A.V. El'skaya. The new model of structural organization of the human translation elongation complex eEF1B. XII Український біохімічний конгрес. 30 вересня-4 жовтня 2019 р. м. Тернопіль. Україна. *Публікація тез, усна доповідь.*